50272-101

REPORT DOCUMENTATION PAGE	1. REPORT NO. NCEER-94-0009	2.	PB94-195815

4. Title and Subtitle Proceedings of the Third U.S.-Japan Workshop on Earthquake Protective Systems for Bridges	5. Report Date March 31, 1994 6.
7. Author(s) I. Buckle and I. Friedland	8. Performing Organization Rept. No.
9. Performing Organization Name and Address National Center for Earthquake Engineering Research State University of New York at Buffalo Red Jacket Quadrangle Buffalo, New York 14261	10. Project/Task/Work Unit No. 11. Contract(C) or Grant(G) No. (C) NSF - BCS 94-03743 (G) NIST & FHWA - DTF H61-92-C-00106
12. Sponsoring Organization Name and Address National Center for Earthquake Engineering Research State University of New York at Buffalo Red Jacket Quadrangle Buffalo, New York 14261	13. Type of Report & Period Covered Technical report 14.

15. Supplementary Notes This workshop was conducted in Berkeley, California. It was supported by the National Science Foundation, the National Institute of Standards and Technology, and the Federal Highway Administration of the United States Department of Transportation.

16. Abstract (Limit: 200 words)

This report presents the results of a workshop which addressed both American and Japanese developments in earthquake protective systems for bridges. Also explored was the potential for future cooperation between the two countries in the design and application of intelligent systems for the protection of bridges. The volume includes thirty-four technical papers and two state-of-the-art reports. Six of the technical papers concern passive bridge protection systems, such as various types of base isolation bearings, damping devices and sliding isolation systems. Seven papers treat hybrid protective systems, including active mass drivers, variable stiffness control, and the use of electrorheological fluids for variable dampers. A variety of design issues and examples, such as the critical loads of elastomeric bearings, the design of a Menshin bridge on soft soil, the seismic rehabilitation of the Golden Gate Bridge, CALTRANS's analytical procedures for base isolated bridges, etc, are the focus of another thirteen papers. Eight additional papers review the results of a variety of experimental test programs and field observations. An appendix provides an outline of the workshop program, a list of participants, etc.

17. Document Analysis a. Descriptors

b. Identifiers/Open-Ended Terms

Base isolation. Sliding isolation systems. Cable stayed bridges. Highway bridges. High damping rubber bearings. Pier uplift. Hybrid control systems. Field tests. Menshin bridges. Design methods. Experimental tests. Case studies. Seismic performance. Earthquake engineering.

c. COSATI Field/Group

18. Availability Statement	19. Security Class (This Report)	21. No. of Pages
Release unlimited	Unclassified	616
	20. Security Class (This Page) Unclassified	22. Price

NOTICE

This report was prepared by the National Center for Earthquake Engineering Research (NCEER). Neither NCEER, associates of NCEER, its sponsors, nor any person acting on their behalf:

a. makes any warranty, express or implied, with respect to the use of any information, apparatus, method, or process disclosed in this report or that such use may not infringe upon privately owned rights; or

b. assumes any liabilities of whatsoever kind with respect to the use of, or the damage resulting from the use of, any information, apparatus, method or process disclosed in this report.

Any opinions, findings, and conclusions or recommendations expressed in this publication are those of the author(s) and do not necessarily reflect the views of the National Science Foundation, the National Institute of Standards and Technology, the Federal Highway Administration of the U.S. Department of Transportation, or other sponsors.

PB94-195815

Proceedings of the Third U.S. - Japan Workshop on Earthquake Protective Systems for Bridges

Held in
Berkeley, California
January 24-25, 1994

Technical Report NCEER-94-0009

Edited by I. Buckle[1] and I. Friedland[2]
March 31, 1994

NCEER Task Number 106-F-5.1.1

NSF Award Number BCS 94-03743

National Institute of Standards and Technology

and

FHWA Contract Number DTF H61-92-C-00106

1 Deputy Director, National Center for Earthquake Engineering Research
2 Assistant Director for Bridges and Highways, National Center for Earthquake Engineering Research

NATIONAL CENTER FOR EARTHQUAKE ENGINEERING RESEARCH
State University of New York at Buffalo
Red Jacket Quadrangle, Buffalo, NY 14261

BACKGROUND

This report presents the Proceedings of the Third U.S.-Japan Workshop on Earthquake Protective Systems for Bridges, which was held in Berkeley, California on January 24 and 25, 1994. The workshop addressed current developments in both the United States and Japan, and explored the potential for future cooperation in the design and application of intelligent systems for the protection of bridges from earthquake effects.

The first U.S.-Japan Workshop on Earthquake Protective Systems for Bridges was organized by the National Center for Earthquake Engineering Research (NCEER) and was held in Buffalo, New York, on September 4 and 5, 1991. Held under the auspices of Task Committee G on "Passive, Active, and Hybrid Control Systems" (since renamed as "Structural Control and Intelligent Materials Systems") in cooperation with Task Committee J on "Wind and Earthquake Engineering for Transportation Systems" of the UJNR Panel on Wind and Seismic Effects, it was attended by 35 Japanese and 28 U.S. participants. This first workshop provided a forum for discussions and the exchange of technology on a wide range of topics including the state-of-practice in seismic isolation hardware, testing of seismically isolated bridges and components, active control and hybrid systems, design issues and applications, long span bridges, seismic retrofit, and new construction. The workshop Proceedings have been published as NCEER Technical Report 92-0004. In conjunction with the workshop, the Japanese participants undertook an extensive study tour of isolated bridges in the United States. Eleven bridges in six states (Missouri, Illinois, New York, New Jersey, Pennsylvania, and California) were visited over a period of six days.

One significant result of this first workshop was the desire to formalize the exchange of information, in order to allow both countries to cooperate in the development of, and benefit from, advances in the technology of earthquake protective systems.

A second workshop was therefore organized by the Public Works Research Institute (PWRI) of the Japan Ministry of Construction. It was held in Tsukuba, Japan, on December 7 and 8, 1992, and was attended by 93 Japanese, 13 U.S., and 1 New Zealand participants. This meeting continued the discussions and presentations made at the first workshop in the areas of isolation hardware and testing, active control and hybrid systems, seismic retrofit and new design issues. It also expanded the discussions into new areas including movement joint design, displacement restraint devices, and the durability of isolation hardware in the field. This workshop was also held under the auspices of Task Committees G and J of the UJNR Panel on Wind and Seismic Effects. The Proceedings of this workshop were published by PWRI Technical Report No. 3196 in 1993.

THE THIRD U.S.-JAPAN WORKSHOP ON EARTHQUAKE PROTECTIVE SYSTEMS

Due to the continued advancement in earthquake protective systems technology and a high level of interest in both the U.S. and Japan, a third workshop was organized by NCEER in cooperation with PWRI, and again held under the auspices of Task Committees G and J of the UJNR Panel on Wind and Seismic Effects. The workshop was attended by 45 U.S. and 32 Japanese participants. In addition, one participant each from New Zealand and Canada, and two from Taiwan, also attended. U.S. financial sponsorship for the workshop was provided by the National Science Foundation, the National Institute of Standards and Technology, and the Federal Highway Administration of the U.S. Department of Transportation. The Public Works Research Institute of the Japan Ministry of Construction organized the Japan side of the meeting.

The third workshop consisted of presentations and discussions of 14 U.S. and 18 Japanese papers with a focus on research and the application of technology, rather than state-of-the-art reviews. The papers covered a wide range of topics including seismic isolation hardware, testing of isolated bridges and components, active control and hybrid systems, design issues and applications, long span bridges, seismic retrofitting, and new construction. Of continuing interest is the difference in philosophy between "menshin" design in Japan and seismic isolation as practiced in the United States. Participants also showed great interest in hybrid and active systems for bridges, as well as special applications of passive systems; e.g., the design of very long bridges on soft soils.

The workshop was held the week following the January 17, 1994, Northridge (California) earthquake. Many of the workshop participants were concerned with the impact of the earthquake on the region in and around the city of Los Angeles including, but not limited to, the performance of various seismically-isolated buildings and bridges in the region. This earthquake, along with the Loma Prieta earthquake of 1989 and the Kushiro-oki and Hokaido Nansei-oki earthquakes of 1993, demonstrated the fragility of existing urban infrastructure and its importance to public commerce and regional economies. The participants recognized these issues and agreed that further research efforts should be directed towards the development of new intelligent systems and protective measures. It was agreed that the future emphasis should be placed on a systems approach to studying the transportation infrastructure and should include consideration of not only safety but also performance, maintenance, and operational efficiency.

A study tour of seismically isolated bridges in the San Francisco Bay area was undertaken by both the U.S. and Japanese participants on Saturday and Sunday, January 22 and 23, 1994. This tour was performed jointly with participants from the Second U.S.-Japan Workshop on Seismic Retrofit of Bridges, which was organized by the University of California at Berkeley and was held on January 20 and 21, 1994, at the same location. A number of the Japanese participants also visited areas damaged by the Northridge earthquake both prior to and immediately after the Protective Systems workshop.

RESOLUTIONS

The participants agreed that the workshop was successful and that it led to a greater understanding of many of the issues involved in earthquake protective systems for bridges. While much information has already been developed on these important issues, the participants agreed that many problems remain unresolved and that additional research and studies are still needed.

The participants suggested that increased cooperation between the U.S. and Japan would be beneficial to both countries for improving the technology and the state-of-practice for earthquake protective systems. As a result, four resolutions were developed and approved during the meeting, as follows:

1. There are many topics of common interest related to the development and implementation of earthquake protective systems for bridges. It is therefore resolved that continued cooperation between researchers and bridge engineers in both countries be actively encouraged. The free exchange of research and design experience, in both the laboratory and field, will facilitate the advancement of this technology and its practical implementation in both countries.

2. In view of the success of this workshop, the importance of this technology, and the rapidly advancing state-of-the-art, it is resolved that the Fourth U.S.-Japan Workshop on Earthquake Protective Systems for Bridges be held in two years in Japan.

3. It is resolved that in the intermediate year, specialist group meetings be arranged to focus on single topics, such as design details, practical implementation issues related to hybrid control, comparative performance of different hardware, and so on. As a consequence, the meetings are expected to adopt a working format in order to facilitate the exchange of design details and philosophies.

4. It is resolved that the fourth workshop be oriented towards research and application rather than state-of-the-art reviews. Topics to be covered should include: (1) innovative protective systems; (2) design methods for seismically isolated/menshin bridges; (3) full-scale verification of performance; and (4) comparative design examples. As passive protective systems have begun to be implemented in both countries, increased emphasis on active and hybrid systems and on the use of smart and high-performance structural materials and systems will be made in this workshop.

ACKNOWLEDGEMENTS

The workshop was jointly organized by the National Center for Earthquake Engineering Research in the United States and the Public Works Research Institute of the Ministry of Construction, Japan. The program coordinators for the workshop were Dr. Ian G. Buckle, professor of civil engineering at the State University of New York at Buffalo, and Dr. Kazuhiko Kawashima, Head of Earthquake Engineering Division of the Public Works Research Institute. A Steering Committee consisting of Ian G. Buckle, Masanobu Shinozuka, Stephen A. Mahin, and Ian M. Friedland arranged the workshop on behalf of the participants.

Organizational support for the workshop was provided on the Japan side by the Public Works Research Institute. As noted earlier, support for the U.S. side was provided by the National Science Foundation, the National Institute of Standards and Technology, and the Federal Highway Administration of the U.S. Department of Transportation. The continuing support of Dr. S. C. Liu, Dr. H. S. Lew, and Mr. James D. Cooper is hereby acknowledged.

Participants at the Third U.S. - Japan Workshop on Earthquake Protective Systems for Bridges

Table of Contents

JAPANESE AND U.S. STATE-OF-THE-ART SUMMARY PAPERS

Menshin Design of Highway Bridges in Japan

Seismic Isolation of Bridges in the USA

NIST

U.S. Department of Transportation
Federal Highway Administration

NATIONAL CENTER FOR EARTHQUAKE ENGINEERING RESEARCH

MENSHIN DESIGN OF HIGHWAY BRIDGES IN JAPAN

Kazuhiko Kawashima[1] and Shigeki Unjoh[2]

1) Head, Earthquake Engineering Division, Public Works Research Institute, Ministry of Construction, Tsukuba Science City, Japan
2) Senior Research Engineer, ditto

ABSTRACT

This paper presents the back ground of seismic isolation of highway bridges in Japan. The Menshin Design which emphasis to reduce deck response by increasing energy dissipating capability and to distribute seismic lateral force of deck to as many substructures as possible is presented. Design guidelines for the Menshin Design and its implementation are described. A new joint research program on Development of New Materials and Passive and Active Control of Long-span Bridges is introduced.

INTRODUCTION

The technology for reducing bridge response has been adopted for long time in Japan (Ref. 1). It has been used from short and medium size bridges to long span bridges. Viscous damper is one of the most typical examples of such technologies (Refs. 2 and 3). It has been successfully adopted to distribute the lateral force to several substructures. The viscous damper provides a resistive force when subjected to a high-velocity motion such as the one encountered during an earthquake, while it does not offer the resistive force to low-velocity motion such as the deck motion caused by temperature change. Hence, by providing the viscous damper the seismic lateral force can be more evenly carried by many columns without constraining deck elongation and shrinkage due to temperature change.

The SU Damper is also an outcome of technical development for reducing bridge response (Ref. 4). It consists of friction bearing and prestressed strand connecting columns and a deck. By adjusting the prestressing of the strand, natural period of the deck is controlled. The strand also prevents the excessive relative displacement of the deck. The friction bearing dissipates the energy so as to increase the damping of the bridge.

Various dampers have also been developed for long span bridges. A special type of vane-damper was adopted to Higashi Kobe Bridge (Ref. 5) and Tsurumi Fairway Bridge

(cable stayed bridges). A device to control the natural period and to increase energy dissipation was adopted at Hituishi–Iwaguro bridge (cable stayed bridge) of the Honshu–Shikoku Bridge (Ref. 6).

Base isolation (Refs. 7–10) has been highlighted in Japan as a new technology to reduce seismic response of structures. Special interest was due to the fact the energy dissipation is made by bearings and that compact ruminated rubber bearing such as LRB is available. Various high damping rubber bearings (HDR) have also been developed. Although various dampers have been successfully adopted for long time as describe above, it requires to install dampers in addition to bearings. Maintenance of dampers requires some special attention in addition to the usual maintenance. Some space on the pier crest is also occupied by the dampers. It is good from such maintenance and space point of view to adopt the compact type of bearings with energy dissipating capability such as LRB and HDR. Furthermore, it matches with the trend that rubber bearings should be more used. Existing steel bearings cause problem due to corrosion.

One more important motivation to adopt the seismic isolation is that it becomes possible to construct multi–span continuous bridges. The expansion joints cause vibration and noise pollution, and are not comfortable to drivers. They need to be replaced frequently, and this often causes traffic congestion. Therefore although simply supported girder bridges or two and three span continuos girder bridges have been frequently constructed, such trend needs to be changed. Super multi–span continuous bridges with as long continuos deck as possible are required. For such purpose, LRB and HDR are effective. Because the lateral stiffness of LRB and HDR is small, it absorbs the deck elongation and shrinkage due to temperature change.

Based on those considerations, the seismic isolation is considered promising for highway bridges. However, there are various unique environmental and natural conditions that the occurrence of an earthquake with magnitude over 8 is much frequent and the ground is generally much softer in Japan as compared with in New Zealand, U.S.A. and Italy where many seismic isolated bridges have been constructed, specific researches and technical developments are required in Japan. Based on such technical development, the Menshin Design which is slightly different with the seismic isolation was developed, and is being adopted.

This paper describes the history of the technical development in seismic isolation of highway bridges, and the state of the art of the Menshin Design and its implementation.

PAST TECHNICAL DEVELOPMENT FOR SEISMIC ISOLATION

Guidelines for Seismic Isolation Design of Highway Bridges

For studying the application of seismic isolation to highway bridges, a committee chaired by Professor Tsuneo Katayama, University of Tokyo, was formed through 1986 to 1989 at the Technology Research Center for National Land Development, which was the first major activity to study the seismic isolation of highway bridges in Japan. Three programs were studied in the committee, i.e., 1) survey of seismic isolation devices which can be used for highway bridges, 2) study on the key points of the seismic isolation design of highway bridges, and 3) trial designs of seismic isolated highway bridges. As the final accomplishments of the three year study, "Guidelines for Seismic Isolation Design of Highway Bridges" was published in 1989 (Ref. 11).

Pilot Construction Program of Menshin Bridges

Five highway bridges were constructed as a pilot program under the supervision of the Ministry of Construction to verify the effectiveness and performance of the seismic isolation (Ref. 1). A working group was formulated in the Ministry of Construction to supervise the design and construction. Because the Menshin Design was being developed by the Joint Research which will be described later, it was adopted in the design. Miyagawa Bridge in Shizuoka-ken was completed in March 15, 1991 as the first Menshin highway bridge in Japan (Ref. 12).

Joint Research on Menshin Bridges between PWRI and 28 Companies

A three-year joint research program on the Menshin Design of Highway Bridges was made between Public Works Research Institute and twenty eight companies since July 1989. The goal of the program was to develop the Menshin Design method and the new Menshin devices for highway bridges. Table 1 shows the research items and the contribution of each organization.

There were four research topics in the joint program:

1)Development of new Menshin devices

The Menshin devices for highway bridges need to be compact and weather-proof since they are installed at narrow pier crests exposed to weathering condition. Ten new devices in total were developed in the program. Among them, 4 high damping rubber bearings (HDR) (Ref. 13), 2 sliding Menshin devices with HDR (Ref. 14), and a roller Menshin device with HDR (Ref. 15) seem promising for application. All Menshin devices developed were tested with use of the dynamic loading system at PWRI under the same loading conditions developed in the program (Ref. 16).

2)Development of expansion joints and restrainers

A knock−off mechanism at an abutment to reduce the impact force induced by the collision between a deck and an abutment (Ref. 17), and a finger expansion joint which is distinguished from the regular finger joints by the transverse movement (Ref. 18), were developed. A special restrainer which absorbs the energy and allows the deck to move in two lateral directions was developed (Ref. 19).

3)Development of Menshin Design method

Taking into account the high seismic activity and the soft soil condition, the Menshin Design method was developed as will be described later.

4)Application of Menshin design

It was found that the Menshin Design can be effectively used to construct super−multi−span continuous bridges with deck length of 1 km (Ref. 20). Connection of existing simple supported girders to reduce the number of expansion joints, and retrofitting of existing bridges to increase the seismic safety by using Menshin Design were studied (Ref. 21).

The final accomplishment of the program was complied in March 1992 as the " Manual of Menshin Design of Highway Bridges" (Refs. 22 and 23).

MENSHIN DESIGN

Although the elongation of natural period and the increase of energy dissipation capability of a structure are key factors in seismic isolation, the elongation of fundamental natural period is not easily achieved for bridges in Japan from various reasons.

First reason is the soft soil condition. Because most of the populated areas are located on alluvial fan deposits, soils are very weak. Second reason is the high seismicity accompanying earthquakes with magnitude over 8 (Ref. 24). Large earthquakes in magnitude produce a ground motion predominant in long period (Ref. 25). Reflecting these environmental and natural conditions, the conservative lateral force coefficients as shown in **Figs. 1 and 2** have been adopted in seismic design of highway bridges (Ref. 26).

Third reason is difficulty to widen the clearance between decks, and between the deck and abutment. The increase of natural period produces a large relative displacement between the deck and the substructures, and requires special expansion joints which absorb large relative displacement. From the demand of driving comfort, maintenance problems and noise and vibration pollution, every efforts are now directed to reduce the clearance at

expansion joints. Because even regular expansion joints currently used cause considerable problem, the increase of gap clearance can not be incorporated.

Fourth reason is the evaluation on collision developed either between abutment and deck or between adjacent decks. When enough clearance is not provided, collision would take place. In fact, collision took place in the past earthquakes (Ref. 27). It is known from these past experiences that collision did not cause critical structural problems although expansion joints were often badly damaged (Ref. 28 and 29). On the contrary, collision dissipates energy. From experiment and analysis, it is effective to constrain the deck response by collision at small deck displacement (Ref. 30). From these reasons, it is superior not to provide a large gap so as to allow the large relative displacement of deck. A little bit larger gap than the normal gap.

Based on these considerations, it seems preferable not to intentionally increase natural period and not to widen the gap clearance at joints. Instead of intentional increase of natural period, combination of increase of energy dissipating capability and distribution of seismic lateral force to as many substructures as possible is preferred in highway bridges. It may be effective to adjust the natural period of bridges so as to avoid the resonance with ground motion. This is an extension of the existing seismic design approach which has been adopted in highway bridge in Japan. The design concept in which bridges are designed taking advantage of the increase of energy dissipating capability and the distribution of seismic lateral force is proposed to be referred as "Menshin Design(免震)" (Refs. 22 and 1).

Followings are the basic principles of Menshin Design for highway bridges with ordinary span length:

1) Seismic lateral force should be distributed to as many substructures as possible. The seismic lateral seismic force should be reduced by increasing the energy dissipating capability with use of Menshin bearings.

2) The natural period of bridges should be not be forcibly elongated, but adjusted so as to avoid the resonance with a ground motion.

3) Gap at expansion joints should not be so widened.

4) The Menshin Design should be adopted only at the site with stable soil behavior. The site vulnerable to soil liquefaction and other type of failure should be avoided.

5) The Menshin Design is encouraged to construct super-multi-span continuous bridges.

MENSHIN DESIGN METHOD

Manual of Menshin Design

The Manual for Menshin Design of Highway Bridges was developed as the final accomplishment of the 3 year joint research program between the Public Works Research Institute and 28 companies (Ref. 22). Although this is not the mandate specifications, it is recommended to consider the basic requirements of the Manual in addition to the Design Specifications of Highway Bridges (Ref. 26). The Manual consists of 9 chapters and 10 appendices. The table of contents is presented in the appendix.

The mandate specification for Menshin Design is being formulated at the Menshin Design Working Group, the Seismic Design Subcommittee of the Bridge Committee, Japan Road Association, based on the Manual of Menshin Design of Highway Bridges. Because seismic performance of Menshin bridges has not yet fully confirmed through seismic experience in the past earthquakes, at the design seismic lateral force is not allowed to reduce from the value specified by the Design Specifications of Highway Bridges. Since various data are being accumulated on the seismic performance of the Menshin bridges, it is expected to reduce the seismic lateral force in the new specifications.

Idealization

In Menshin Design, bridges are designed by following the standard static design method (static frame analysis). Precise evaluation of seismic safety is made by the dynamic response analysis. In such analysis, the Menshin devices are idealized by as a set of equivalent linear springs. Equivalent stiffness and the equivalent damping ratio of the isolator and damper are the major parameters used in the analysis. In the static frame analysis, natural period of the bridge can be computed for each seismic design structural unit as :

$$T = 2.01\sqrt{\delta} \tag{1}$$

$$\delta = \frac{\int w_i \cdot u_i^2}{\int w_i \cdot u_i} \tag{2}$$

where

T : natural period (sec)

w_i : dead weight (tf/m) of the seismic design structural unit (superstructure and substructure above the ground surface assumed in seismic design) at point "i"

u_i : lateral displacement (m) developed in the seismic design structural unit at point "i" when subjected to w_i in the direction considered in design

Damping ratio of the bridge is computed as

$$\left.\begin{aligned} h &= \frac{\sum K_{Bi} \cdot u_{Bi}^2 \cdot c_{hi}}{\sum K_{Bi} \cdot u_{Bi}^2 \cdot c_i} \\ c_{hi} &= h_{Bi} + \frac{h_{Pi}}{K_{Pi}} + \frac{h_{Fui}}{K_{Fui}} + \frac{h_{F\theta i} \cdot H^2}{K_{F\theta i}} \\ c_i &= 1 + \frac{K_{Bi}}{K_{Pi}} + \frac{K_{Bi}}{K_{Fui}} + \frac{K_{Bi} \cdot H^2}{K_{F\theta i}} \end{aligned}\right\} \quad (3)$$

where

h : modal damping ratio of bridge
h_{Bi} : damping ratio of i−th damper
h_{Pi} : damping ratio of i−th pier/abutment
h_{Fui} : damping ratio of i−th foundation associated with translational movement
$h_{F\theta i}$: damping ratio of i−th foundation associated with rotation
K_{Pi} : equivalent stiffness of i−th pier/abutment
h_{Fui} : translational stiffness of i−th foundation
$K_{F\theta i}$: rotational stiffness of i−th foundation
u_{Bi} : design displacement of i−th menshin device
H : height from the bottom of pier to the gravity center of deck

Eq.(3) gives the approximate estimation of the damping ratio of a bridge. When mode shapes are computed, the modal damping ratio may be computed as

$$h = \frac{\sum_{j=1}^{n} \phi_{ij}^T \cdot h_j \cdot k_j \cdot \phi_{ij}}{\phi_i^T \cdot K \cdot \phi_i} \quad (4)$$

where

ϕ_{ij} : mode vector of j−th structural component for i−th mode
h_j : damping ratio of j−th structural component
k_j : stiffness matrix of j−th structural component
ϕ_{iT} : mode vector of bridge for i−th mode
K : stiffness matrix of bridge.

Table 2 shows the damping ratio recommended for structural component Eqs.(3) and (4).

Design Force

Menshin devices are designed by the seismic coefficient method (SCM) and the bearing capacity method (BCM). The allowable stress approach is adopted in the seismic coefficient method, while the bearing capacity approach is adopted in the bearing capacity method. Bridges are designed by the seismic coefficient method, and then the ductility of reinforced concrete piers is checked by the bearing capacity method.

In the seismic coefficient method, the design lateral force coefficient is given as

$$k_h = c_z \cdot c_G \cdot c_I \cdot c_T \cdot c_E \cdot k_{h0} \geq 0.1$$
$$c_T \cdot c_E \geq 0.8 \qquad (5)$$

where

c_z : modification factor for zone (refer to **Fig. 3**)
c_G : modification factor for ground condition (refer to **Table 3**)
c_I : modification factor for importance (refer to **Table 4**)
c_T : modification factor for structural response (refer to **Table 5**)
c_E : modification factor for energy dissipation capability (refer to **Table 6**)
k_{h0} : standard design horizontal seismic coefficient (=0.2)

The modification factors c_z, c_G, c_I and c_T are specified in the Design Specifications of Highway Bridges (Ref. 26). The modification factor c_E takes a value shown in **Table 6** depending on the modal damping ratio of the bridge in the fundamental mode. The design lateral force is reduced as large as **20%**.

In the bearing capacity method, the lateral force coefficient khc and the equivalent lateral force coefficient khe are given as

$$k_{he} = \frac{k_{hc}}{\sqrt{2\mu - 1}} \qquad (6)$$

$$k_{hc} = c_z \cdot c_I \cdot c_R \cdot c_E \cdot k_{hc0} \geq 0.3 \qquad (7)$$

where

c_z : modification factor for zone (refer to **Fig. 3**)
c_I : modification factor for importance (refer to **Table 4**)
c_R : modification factor for structural response (refer to **Table 7**)
c_E : modification factor for energy dissipation capability (refer to **Table 8**)
k_{hc0} : standard lateral force coefficient for bearing capacity method (=1.0)
μ : allowable ductility factor of reinforced concrete piers

The modification factors c_z, c_I, and c_R are specified in the Seismic Design

Specifications of Highway Bridges. The modification factor c_E depends on the modal damping ratio of the bridge, and takes a value of **Table 8**. The design force is reduced as large as 30%.

Design of Isolators and Energy Dissipators

In design of isolators and energy dissipators, the design displacement of menshin device u_B, the equivalent stiffness K_B and the equivalent damping ratio h_B of the Menshin device are the key factors.

The design displacement of Menshin device u_B is evaluated as

$$u_B = \frac{k_h \cdot W_u}{K_B} \quad \text{(S.C.Method)} \tag{8}$$

$$u_B = \frac{k_{hc} \cdot W_u}{K_B} \quad \text{(B.C.Method)} \tag{9}$$

where

k_h : lateral force coefficient by Eq.(5)
k_{hc} : lateral force coefficient by Eq.(7)
K_B : equivalent stiffness (tf/m) of Menshin device
W_u : weight of the superstructure (tf) supported by the Menshin device

Requirements for Dynamic and Static Load

Various requirements for the devices against static load and dynamic load are described in the Manual. It is unique that precise loading test procedures for both dynamic and static loads are described in the Manual. Some of the important requirements for dynamic load is as:

1) Menshin devices have to be designed and fabricated so that their equivalent stiffness k_B and equivalent damping ratio h_B be within $\pm 20\%$ of the design values.

2) Menshin devices have to be stable against 50 cycles of harmonic loading with design displacement of u_B given by Eq.(9).

3) Deck should return to the rest position even after it was subjected to a large earthquake. The residual displacement u_{BR} developed in menshin devices after it is smoothly released from the deformed displacement of given by Eq.(9) needs to satisfy.

$$u_{BR} \leqq 0.1 \cdot u_B \qquad (10)$$

4) The equivalent stiffness and the equivalent damping ratio of menshin devices need to be stable against the change of load condition at normal time, change of natural environment such as the temperature change and earthquake-induced cyclic loading. Stability has to be examined for 1) cyclic loading associated with the elongation and shrinkage of deck due to temperature change and traffic load, 2) effect of loading hysteresis, 3) variation of vertical loading, 4) effect of loading rate, 5) effect of pre-deformation due to creep and shrinkage, 6) direction of excitation, and 7) change of the equivalent stiffness and the equivalent damping ratio depending on the temperature change.

On the other hand, major requirements for static load include :

1) Materials and mechanism of the menshin devices need to give credit to long term use. They need to be stable against the daily and annual cyclic elongation and shrinkage of deck due to the temperature change.

2) The menshin devices need to be stable against local shear strain. Check of the local shear strain needs to be made in accordance with the Design Guidelines of Bearings (Ref. 35).

3) In the rubber-type menshin devices, the creep of rubber which would be developed for the life time of bridges in vertical direction due to the dead weight of superstructure needs not to exceed 5% of the total thickness of rubber.

4) The equivalent stiffness of menshin device at $-10℃$ need not to exceed 1.5 time the equivalent stiffness at $40℃$.

IMPLEMENTATION OF MENSHIN DESIGN

Table 9 shows the directory of Menshin bridges which were completed or are under construction. There are over 30 bridges under design and planning stage. It should be noted that as describe above because the seismic lateral force is not allowed at this stage to reduce from the value specified in the Design Specifications of Highway Bridges, some bridges which merely adopted Menshin bearings are included in **Table 9**. From the same reason, Menshin bearings have been adopted for most of existing bridges as a tool which enables to make simply supported girders continuous. Although the seismic retrofit was not the official reason for adopting the Menshin bearings, the seismic retrofit effect is of course expected in addition to make the deck continuous.

The Road Bureau of the Ministry of Construction compiled in June 1993 a technical development program which is required to challenge toward 21 century (Ref. 34). Seventy four technologies were identified as essential, and the further development of the Menshin Design is included as a technology required to mitigate road environment. Obviously effectiveness of constructing super-multi-span bridges to reduce noise and vibration pollution is highly expected in the Menshin Design. The Ministry of Construction is now intending to effectively use the Menshin Design technology which enables to construct super-multiple-continuous bridges which are advantageous for road environment and enough seismic safety.

Typical implementation of the Menshin Design is as follows. The first Menshin bridge in Japan is Miyagawa Bridge as shown in **Photos 1** and **2**, Shizuoka-ken. It was completed in March 1991. A series of forced excitation tests using an eccentric mass-shaker and quick-release hydraulic jacks were conducted as shown in **Photos 1** and **2** to verify the design. Strong motion observation has been made since the completion, and an analysis of the first data was made (Ref. 31).

Photo 3 shows Yama-age Bridge in Tochigi-ken (Ref.32). This was the first Menshin bridges utilizing high damping rubber bearings. Superstructure is of 6-span post-tensioning prestressed concrete box girder with deck length of 246.3m. Forced excitation tests using an eccentric mass-shaker and quick-release hydraulic jacks were made.

Photo 4 shows On-netoh Bridge on National Highway No.44 in Hokkaido. this bridge experienced a significant shaking during the Kushiro-oki Earthquake in January 1993. The peak acceleration of about 360 cm/sec^2 was induced on the ground surface near the bridge. No damage was developed due to the earthquake. The relative displacement at the bearings in longitudinal direction was only 2 to 2.5 cm. This earthquake provided as important data on the response of a Menshin bridge in cold area. Because temperature dependence of LRB was precisely investigated in laboratory (Ref. 33), a precise analysis is expected.

Photos 5 and **6** show Higashi-ohgi-shima Viaduct with 9-span continuous prestressed concrete girder on Metropolitan Expressway and Matsuno-hama Viaduct with 4-span continuous steel box girder on Hanshin Expressway, respectively. The forced excitation tests were also made for these bridges and the dynamic characteristics of Menshin bridges were investigated.

A unique application of Menshin Design is the O-hito Viaduct which is under construction in Shizuoka-ken as a part of the Izu Crossing Highway. The bridge is of 29-span

continuous prestressed concrete girder with deck length of 725m.

Menshin design has been applied for the jointless system and seismic strengthening of existing simply-supported girder bridges. Photo 7 shows the replacement of existing steel bearings by LRB.

A NEW JOINT RESEARCH PROGRAM ON SEISMIC CONTROL OF LONG-SPAN BRIDGES

A new three-year joint research program on "Development of Seismic Control Systems of Long-Span Bridges" was initiated from October 1993. This research is being made jointly between the Public Works Research Institute, Public Works Research Center and 19 companies. The Public Works Research Center is a foundation belonging to the Public Works Research Institute.

This research is directed to develop a new passive and active control technologies and to use intelligent materials for long-span bridges. As the post Honshu-Shikoku Bridge Project, new bridge construction with center span length over 2 km is being considered. In the technical development program of the Road Bureau of the Ministry of Construction, development of seismic design method for long-span bridge is included as one of the 74 key technologies. Passive and active control technologies for new types of structures are the key issue. The joint research is intended to support this technical development.

The research program includes the following three topics.

1) Development of New Materials and Passive and Active Control
   It is intended to effectively use new materials such as super low-yield strength metals, super plastic rubbers, super high damping rubbers and rheological fluid. They may be used to produce energy dissipators for various purpose. Intelligent dampers, a tuned liquid damper and an intelligent knock-off device are to be developed.

2) Development of New Control Design Method
   Depending on new materials and passive and active control developed in 1), new controlling methods need to be developed. Accurate evaluation method of damping of structure which use new materials and controlling devices, and optimum control points are to be investigated.

3) Application to Bridges
   Various application of the new materials and controlling systems can be considered. Application of the controlling systems to substructures, high piers, suspended slabs,

cable stayed bridges and suspension bridges are studied. Application of active control of bridges during construction stage is promising.

Table 10 shows the research objectives and the contribution of each organization. The 19 companies include material makers, bearing supports fabricators, consulting engineering companies, steel bridge fabricators and general contractors.

CONCLUDING REMARKS

Seismic isolation expanded the freedom of design and construction practice of highway bridges. It has been used as a tool to construct super-multi-span continuous bridges, curved and skewed bridges capable to move in two horizontal directions and seismic strengthening. Data on bridge response through forced excitation tests, shaking table tests, loading tests of energy dissipators and isolators, strong motion observation and seismic excitation are being accumulated. It was very important that On-netoh bridge located close to the fault of Kushiro-oki Earthquake in January 1993 behaved quite well. Through the analysis of those data, the seismic response of Menshin bridges is being verified.

Implementation of the Menshin Design is being made throughout the country. The Menshin Design was applied to 15 new bridges and 8 existing bridges. A number of bridges are being designed and planned.

A new three-year joint research was initiated among PWRI, PWRC and 19 companies to develop new materials and passive and active control systems for long-span bridges. New innovative materials and systems are studied in the program. It is expected to develop new materials, dampers, controlling algorithm and application.

REFERENCES

1) Kawashima, K., Hasegawa, K., and Nagashima, H. : A Perspective of Menshin Design for Highway Bridges in Japan, Proc. 1st U.S.-Japan Workshop, September 1991
2) Oseki, J. : Shear Viscous Damper – Application to Design of Multi-span Continuous Bridges –, Bridges and Foundation, 1980 (in Japanese)
3) Fukuoka, S. : Design of Multi-span Continuous Highway Bridges with Use of Shear Viscous Damper, Bridges and Foundations, 1980 (in Japanese)
4) Okamoto, S. and Uemae, Y. : Aseismic Bridge Structure by Elastic Supports Using Tie Members (SU Damper Method), Proc. Symposium on New Ideas in Structural Design, Japan Society of Civil Engineers and Architectural Institute of Japan, 1963 (in Japanese)
5) Kitazawa, M., Ishizaki, H., Emi, S. and Nishimori, K. : Characteristics of Earthquake Responses and Design of Aseismic Design on the Long-period Cable-stayed Bridge

(Higashi−Kobe Bridge) with All Movable Shoes in Longitudinal Direction, Proc. Japan Society of Civil Engineers, No. 422/I−14, October 1990 (in Japanese)
6) Kanemitsu, H. and Higuchi, K. : Displacement Control of Bridges with Suspended Girder, Technical Report of the Honshu−Shikoku Bridge Authority, 1981 (in Japanese)
7) Buckle, I. G. and Mayes, R. L. : Seismic Isolation:History, Application and Performance −A World View, Earthquake Spectra, Vol. 6, No. 2, May 1990
8) McKay, G. R., Chapman, H.E. and Kirkcaldie, D. K. : Seismic Isolation : New Zealand Application, Earthquake Spectra, Vol. 6, No. 2, May 1990
9) Skinner, R. I., Tyler, R. G., Heine, A. J. and Robinson, W. H. : Hysteresis Dampers for the Protection of Structures from Earthquakes, Proc. New Zealand − Japan Workshop on Base Isolation of Highway Bridges, Wellington, New Zealand, December 1987
10) Billings, I. J. and Kirkcaldie, D. K. : Base Isolation of Bridges in New Zealand, Proc. New Zealand − Japan Workshop on Base Isolation of Highway Bridges, Wellington, New Zealand, December 1987
11) Technology Research Center for National Land Development : Guidelines for Design of Base−isolated Highway Bridges, Final Report of Base Isolation to Seismic Design of Highway Bridges (Chairperson : Professor T. Katayama), March, 1989 (in Japanese)
12) Matsuo, Y., and Hara, K.: Design and Construction of Miyagawa Bridge, 1st U.S.−Japan Workshop, September 1991.
13) Suizu, Y. and Sudoh, C. (Part 1), Kawashima, K., Koshitoge, M., Endo, K., Yamada, C., and Nishimoto, T. (Part 2), and Nishikawa, I., Katoh, M., Itoh, M., and Muramatsu, Y. (Part 3): Development of High Damping Rubber Bearing for Menshin Design, 1st U.S.−Japan Workshop, September 1991
14) Iguchi, T.: Development of a Sliding Friction Damper, 1st U.S.−Japan Workshop, September 1991
15) Takaku, T., Shimada, M., Tsumura, N. and Izuma, S. : Development of Roller Type Bearing for Menshin Bridges, 1st U.S.−Japan Workshop, September 1991
16) Kawashima, K., Makiguchi, K., Suizu Y., and Endo, K. : Approving Test Procedure for Menshin Devices, 2nd U.S.−Japan Workshop, December 1992
17) Goto, Y., Kikuchi, T., Kimishima, T., Matsumoto, F., Ozaki, D., and Tsukamoto, A. : Development of Expansion Joint, Stopper and Knock−off Abutment for Menshin Bridges, 2nd U.S.−Japan Workshop, December 1992
18) Kimishima, T., Harada, H., and Ozaki, D.: Development of Finger Joint Movable in Horizontal Directions for Menshin Bridges, 1st U.S.−Japan Workshop, September 1991
19) Ozaki, D., and Matsumoto, F.: Development of Falling−off Prevention Devices for Menshin Bridges, 1st U.S.−Japan Workshop, September 1991
20) Goto, Y., Tokunaga, M., Yoshimura, T., and Sintaku, M.: Seismic Response of Multi−span Continuous Bridge with Deck Length of 1 km, 1st U.S.−Japan Workshop, September 1991
21) Yamaguchi, M., Makiguchi, Y., Kawasaki, I.: Application of Menshin Design to Seismic

Retrofit of Existing Bridges by Connecting Concrete Slabs of Adjacent Girders, 1st U.S.–Japan Workshop, September 1991
22) Public Works research Institute and 28 Companies: Manual of Menshin Design of Highway Bridges, March 1993, Technical Note, No. 60, Public Works Research Institute (in Japanese)
23) Kawashima, K. : Manual for Menshin Design of Highway Bridges, Proc. 2nd U.S.–Japan Workshop, December 1992
24) Arakawa, T. and Kawashima, K.: Seismicity and Maximum Possible Earthquake around Japan for Application to Seismic Risk Analysis, Technical Memorandum, Vol. 2098, Public Works Research Institute, March 1984 (in Japanese)
25) Kawashima, K., Aizawa, K. and Takahashi, K. : Attenuation of Peak Ground Motions and Absolute Acceleration Response Spectra, Report of PWRI, Vol. 166, Public Works research Institute, September 1985 (in Japanese)
26) Japan Road Associations : Design Specifications for Highway Bridges – Part V Seismic Design –, February 1990 (in Japanese)
27) Public Works Research Institute : Report on the Disaster Caused by the Miyagi–ken–oki Earthquake of 1978, Vol. 159, March 1983 (in Japanese)
28) Williams, D. and Godden, W. G. : Experimental Model Studies on the Seismic Response of High Curved Overcrossings, Report No. EERC 76–18, Earthquake Engineering Research Center University of California, Berkeley, 197
29) Kawashima, K. and Penzien, J. : Correlative Investigation on Theoretical and Experimental Dynamic Behavior of A Model Bridge Structure, Report No. EERC 76–26, Earthquake Engineering Research Center, University of California, Berkeley, 1976
30) Kawashima, K., Hasegawa, K. and Nagashima, H. : Experiment and Analysis on Seismic Response of Menshin Bridges, 1st U.S.–Japan Workshop, September 1991
31) Kawashima, K., Nagashima, H., Masumoto, S. and Hara, K.: Response Analysis of Miyagawa Bridges based on a Measured Acceleration Record, 2nd U.S.–Japan Workshop, December 1992
32) Uzuka, T., Kawakami, K., Kumakura, K. and Tani, H.: Menshin Design and Construction of Multi–span Continuous Prestressed Concrete Bridge, 2nd U.S.–Japan Workshop, December 1992
33) Nakano, O., Nishi, H., Shiroi, T. and Kumagai, K. : Temperature Dependency of Base Isolated Bearings, 2nd U.S.–Japan Workshop, December 1992
34) Road Bureau of Ministry of Construction: Five–year Technical Development Program–Challenge to New Possibility toward 21th Century–, June 1993 (in Japanese)
35) Japan Road Association : Guide–Specification of Design of Bearings, July 1991 (in Japanese)

Note

1) 1st U.S.–Japan Workshop : Proc. 1st U.S.–Japan Workshop on Earthquake Protective Systems of Bridges, Buffalo, New York, U.S.A., September 1991, Technical Report NCEER 92–0004, National Center for Earthquake Engineering Research, State University of New York at Buffalo, February 1992
2) 2nd U.S.–Japan Workshop: Proc. 2nd U.S.–Japan Workshop on Earthquake Protective Systems of Bridges, Tsukuba, Japan, Technical Memorandum, No. 3196, Public Works Research Institute, December 1992

APPENDIX

TABLE OF CONTENTS OF MANUAL FOR MENSHIN DESIGN OF HIGHWAY BRIDGES

Table 1 Research Theme and Organizations of Joint Research Program between the Public Works Research Institute and 28 Private Firms for Developing Menshin Design Method of Highway Bridges

Research Theme	P	Ka	Si	Ob	Ku	Tn	H	Ni	Su	M	G	Or	Ti	I	Nk	Ko	Ns	Ol	Y	To	Bs	Bb	Se	Sh	Pc	J	N	Chief	Sub-Chief
1. Development of Device for Isolation																													
1.1 High Energy Absorbing Rubber Bearing								○					○						○	○	○			○					
1.2 Friction Damper													○									○	○					Ol	Bs
1.3 Steel Damper								○							○														
1.4 Link Bearing Develop of																	○												
1.5 Viscous Damper																		○											
1.6 Test Method	○							○							○		○	◎	○	○	○	○	○	○					
2. Development of Expansion Joint and Falling-off Prevention Device for Isolated Bridge																												Tc	—
2.1 Expansion Joint				○									○																
2.2 Falling-off Prevention Device	○												○					○											
3. Development of Design Method for Isolated Bridge																													
3.1 Design Philosophy	○	○	○	○		○		○				○	◎					○							○	○	○		
3.2 Dynamic Responce Analysis Method	○		○		○	◎		○			○			○					○	○	○	○	○				Ka	Pc
3.3 Design Method of Device for Isolation	○						○	○				◎	○		○		○	○	○	○	○	○	○	○				
3.4 Simplified Design Method	○	○	◎		○	○					○	○																	
3.5 Design Method of Expansion Joint and Falling-off Prevention Device	○			○			○								○			○							◎				
4. Application of Base Isolation to Bridge																													
4.1 Application to Prestressed Concrete Bridge	○	◎							○	○			○														○		
4.2 Application to Steel Bridge	○													○	○	○											◎	Ob	J
4.3 Application to Multiple Super-long Bridge	○			◎					○							○									○	○	○		
4.4 Application to Seismic Retrofit	○									○				○				○								◎			

P: Public Works Research Institute, Ka: Kajima, Si: Shimizu, Ob: Ohbayashi, Ku: Kumagai, Tn: Takenaka Doboku + Takenaka, H: Hazama, Ni: Nishimatsu, Su: Sumitomo, M: Mitsui, G: Goyoh, Ok: Okumura, Ti: Taisei + Tokyo Fablic + Nippon Chuzo, I: Ishikawajima Harima, Nk: NKK + Nippon Chuzo, Ko: Kobe Steel, Ns: Nippon Seiko, Oe: Oiles, Y: Yokohama Rubber, To: Toyo Rubber, Bs: Bridgestone, Bb: BBM, Se: Seibu Polymer, Sh: Showa Densen, Pc: Pacific Consultants, J: Japan Engineering Consultant, N: New Structural Engineering Consultants.

Table 2 Damping Ratio Recommended for Structural Components

Structural Components	Steel	Concrete
Super Structures	0.02～0.03	0.03～0.05
Menshin Device	Damping Ratio	
Pier/Columns	0.03～0.05	0.05～0.1
Footing	0.1～0.3	

Table 3 Modification Factor for Ground Condition C_G

Ground Group	I	II	III
C_G	0.8	1.0	1.2

Table 4 Modification Factor for Importance C_I

Group	C_I	Definition
1st class	1.0	Bridges on expressway (limited access highways), general national road and principal prefectural road. Important bridges on general prefectural road and municipal road.
2nd class	0.8	Other than the above

Table 5 Modification Factor for Structural Response C_T

Ground Group	Structural Response Coefficient C_T		
Group I	$T<0.1$ $C_T=2.69T^{1/3}\geqq 1.00$	$0.1\leqq T<1.1$ $C_T=1.25$	$1.1<T$ $C_T=1.33T^{-2/3}$
Group II	$T<0.2$ $C_T=2.15T^{1/3}\geqq 1.00$	$0.2\leqq T<1.5$ $C_T=1.25$	$1.3<T$ $C_T=1.49T^{-2/3}$
Group III	$T<0.34$ $C_T=1.80T^{1/3}\geqq 1.00$	$0.34\leqq T<1.5$ $C_T=1.25$	$1.5<T$ $C_T=1.64T^{-2/3}$

Table 6 Modification Factor for Modal Damping Ratio of Bridge C_E
(Seismic Coefficient Method)

Damping Ratio h	Modification Factor C_E
$h < 0.1$	1.0
$h \geq 0.1$	0.9

Table 7 Modification Factor for Structural Response C_R

Ground Group	Structural Response Coefficient C_R		
Group I	$T \leq 1.4$ $C_R = 0.7$		$1.4 < T$ $C_R = 0.876T^{-2/3}$
Group II	$T < 0.18$ $C_R = 1.15T^{1/3} \geq 0.7$	$0.18 \leq T \leq 1.6$ $C_R = 0.86$	$1.6 < T$ $C_R = 1.16T^{-2/3}$
Group III	$T < 0.29$ $C_R = 1.15T^{1/3} \geq 0.7$	$0.29 \leq T \leq 2.0$ $C_R = 1.00$	$2.0 < T$ $C_R = 1.59T^{-2/3}$

Table 8 Modification Factor for Modal damping Ratio of Bridge C_E
(Bearing Capacity Method)

Damping Ratio h	Modification Factor C_E
$h < 0.1$	1.0
$0.1 \leq h < 0.12$	0.9
$0.12 \leq h < 0.15$	0.8
$0.15 \leq h$	0.7

Table 9 Directory of Menshin Bridges in Japan
(a) New Constructions

Bridge	Location	Deck Length	Administrator	Year Constructed	Super-Structure Type	Bearing Type
Onnetoh Bridge	Hokkaido	102.2m	Hokkaido Development Bureau	1993	4-Span Continuous Steel Plate Girder	LRB
Nagakigawa Bridge	Akita	97m	Noshiro Construction Office, MOC	Under Construction (1993)	3-Span Continuous Steel Plate Girder	LRB
Maruki-bashi Bridge	Iwate	92.5m	Iwate-ken	1992	3-Span Continuous Prestressed Concrete Box Girder	LRB
Yama-age Bridge	Tochigi	250m	Tochigi-ken	1993	6-Span Continuous Prestressed Concrete Box Girder	HDR
Miyagawa Bridge	Shizuoka	110m	Shizuoka-ken	1991	3-Span Continuous Steel Plate Girder	LRB
O-hito Viaduct	Shizuoka	725m	Shizuoka-ken	Under Construction	29-Span Continuous Prestressed Concrete Slab	LRB
Hirao Bridge	Yamaguchi	350m	Yamaguchi-ken	Under Construction (1993)	5-Span Continuous Prestressed Concrete Box Girder	HDR
Uehara Bridge	Nagoya	65m	Nagoya City	1991	2-Span Continuous Steel Plate Girder	LRB
Route #12 Interchange Bridge	Tokyo	136.6m	Metropolitan Expressway Public Corp.	1991	6-Span Continuous Prestressed Concrete Slab	LRB
Bay Shore Route	Tokyo	417.6m	Metropolitan Expressway Public Corp.	Under Construction (1994)	9-Span Continuous Prestressed Concrete Box Girder	LRB
Matsunohama Bridge	Osaka	211.5m	Hanshin Expressway Public Corp.	Under Construction	4-Span Continuous Steel Box Girder	LRB
Izumisano Bridge	Osaka	318m	Hanshin Expressway Public Corp.	Under Construction	6-Span Continuous Steel Box Girder	LRB
Trans Tokyo Bay	Tokyo	910m	Trans Tokyo Bay Highway Corp.	Under Construction (1994)	11-Span Continuous Steel Box Girder	HDR
Trans Tokyo Bay	Tokyo	800m	Trans Tokyo Bay Highway Corp.	Under Construction (1994)	10-Span Continuous Steel Box Girder	LRB
Karasaki Bridge	Fukushima	76.95m	Soma Kyodo Power Company Ltd.	1991	2-Span Continuous Prestressed Concrete Box Girder	HDR

Note) LRB: Load Rubber Bearing, HDR: High Damping Rubber Bearing

(b) Existing Bridges

Bridge	Location	Deck Length	Administrator	Year Constructed	Super-Structure Type	Bearing Type
Komatsukawa Route	Tokyo	120m	Metropolitan Expressway Public Corp.	Under Construction	Interconnection of Simply-Supported Girder (3-Spans)	LRB
Komatsukawa Route	Tokyo	120m	Metropolitan Expressway Public Corp.	Under Construction	Interconnection of Simply-Supported Girder (3-Spans)	LRB
Route #6	Tokyo	80m	Metropolitan Expressway Public Corp.	1992	Interconnection of Simply-Supported Girder (4-Spans)	LRB
Route #6	Tokyo	80m	Metropolitan Expressway Public Corp.	1992	Interconnection of Simply-Supported Girder (4-Spans)	LRB
Route #6	Tokyo	80m	Metropolitan Expressway Public Corp.	1992	Interconnection of Simply-Supported Girder (4-Spans)	LRB
Moriguchi Route	Osaka	90m	Hanshin Expressway Public Corp.	1991	Interconnection of Simply-Supported Girder (2and3-Spans)	LRB
Moriguchi Route	Osaka	90m	Hanshin Expressway Public Corp.	1991	Interconnection of Simply-Supported Girder (2and3-Spans)	LRB
Sakai Route	Osaka	89.5m	Hanshin Expressway Public Corp.	1993	Interconnection of Simply-Supported Girder (4-Spans)	LRB

Table 10 Research Theme and Organizations of New Joint Research Program on Seismic Control of Long-Span Bridge

Research Theme		Research Group																			
				Material Makers				Bridge Fabricaters		General Contractors							Consulting Firms				
		P	PC	OI	BS	YG	NJ	IH	KH	OB	OR	KA	KU	SU	TA	PS	OC	KC	KG	NG	PA	YE
Development of New Materials and Passive and Active Control	Application of Super Low Yield Strength Metals	○	○	○			○															
	Development of Super Plastic Rubber Dampers	○	○		○																	
	Development of Super High Damping Rubber Bearings	○	○			○																
	Development of Electro Rheological Fluid Dampers	○	○	○																		
	Development of Intelligent Knock-off Devioces	○	○							○												
	Development of Intelligent Dampers	○	○	○								○	○									
	Application of Tuned Liquid Dampers	○	○									○										
Development of New Control Design Method	Development of Evaluation Method of Damping Characteristics	○	○					○		○		○					○		○		○	○
	Optimal Control Points by Dampers	○	○					○	○						○			○			○	○
Application to Bridges	Seismic Responce Control during Construction	○	○								○											
	Development installed in Damping Materials Pavement, Curb and Handrails	○	○				○					○		○		○						
	Application to Substructures	○	○														○					
	Application to Bridges with High Pier	○	○					○	○											○		○
	Application to Suspended Slab Bridges	○	○											○		○						
	Application to Cable-Stayed Bridges	○	○							○						○		○				
	Application to Suspension Bridges	○	○																○			

P: Public Works Research Institute, PC: Public Works Research Center, OI: Oiles, BS : Bridgestone, YG: Yokohama Rubber, NJ: Shin-Nippon Steel,
IH: Ishikawajima Harima, KH: Kawasaki Heavy Industry, OB: Ohbayashi, OR: Oriental, KA: Kajima, KU: Kumagai, SU: Sumitomo, TA: Takenaka,
PS: PS, OC: Oriental Consultant, KC: Kaihatsu Consultant, KG: Kensetsu Gijutsu Consultant, NG: Nihon-Gijutsu Kaihatsu Consultant,
PA: Pacific Consultant, YE:Yachiyo Engineering Consultant

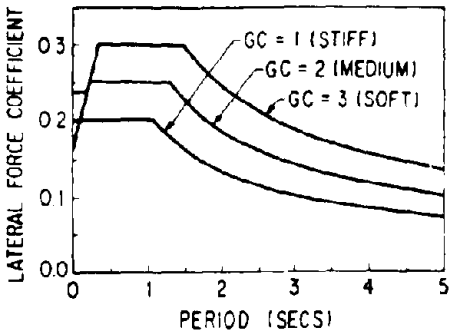

Fig. 1 Lateral Force Coefficient for Seismic Coefficient Method ($c_z = c_I = 1.0$)

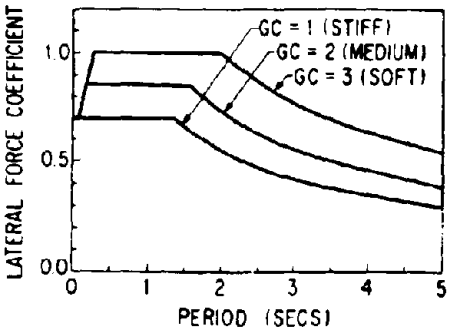

Fig. 2 Lateral Force Coefficient for Bearing Capacity Method ($c_z = c_I = 1.0$)

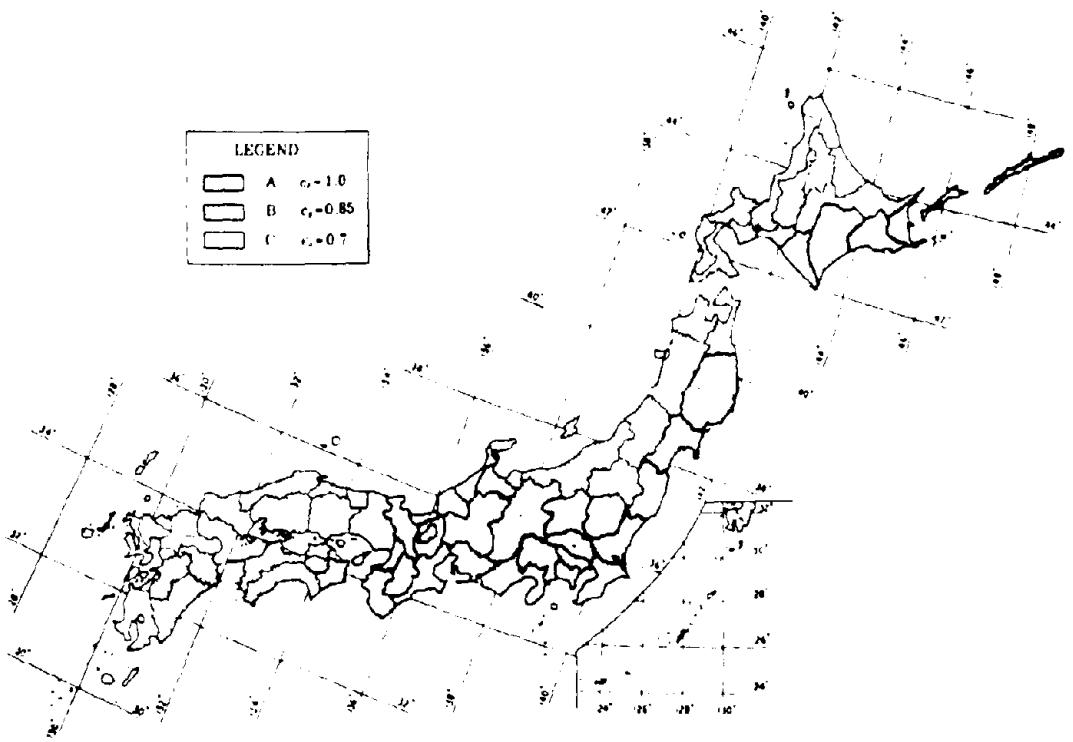

Fig. 3 Modification Factor for Zone C_z

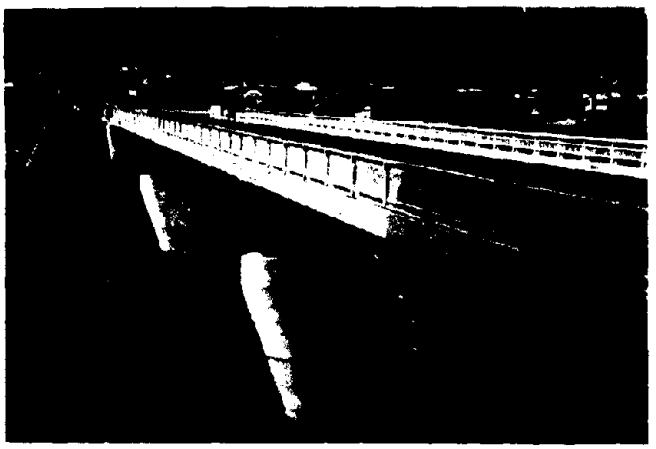

Photo 1 Miyagawa Bridge (Shizuoka−ken)

Photo 2 LRB used for Miyagawa Bridge

Photo 3 Yama–age Bridge (Tochigi–ken)

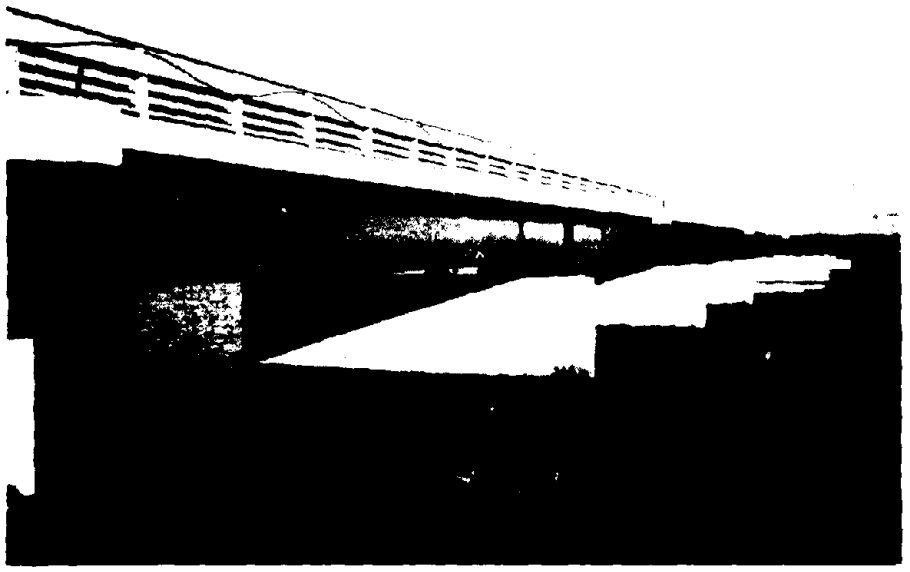

Photo 4 On–netoh Bridge (Hokkaido Development Bureau)

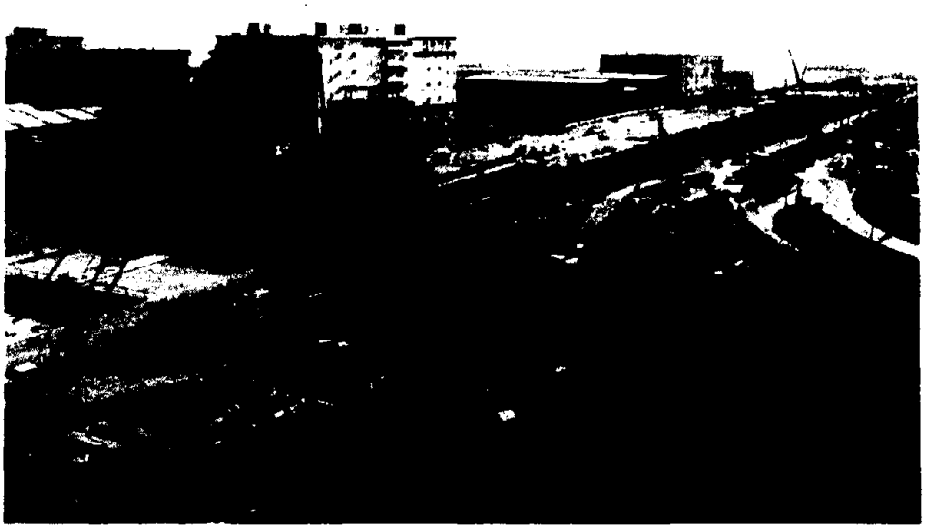

Photo 5 Higashi-ohgi-shima Viaduct (Metropolitan Expressway)

Photo 6 Matsuno-hama Viaduct (Hanshin Expressway)

(a) Removal of Existing Bearings

(b) Set–up of LRB

Photo 7 Jointless System of Existing Bridges (Hanshin Expressway)

SEISMIC ISOLATION OF BRIDGES IN THE U.S.A.

Dr. Ronald L. Mayes[1]

Seismic isolation is an alternative strategy for protecting bridges from earthquake damage. It focuses on the demand side of the equation – reducing seismic forces with the goal of limiting them to the elastic capacity of new or existing structures, thereby minimizing or avoiding inelastic deformation and damage to the foundation and columns. In addition to reducing the seismic forces, the unique bilinear force-deflection characteristics of seismic isolation systems also permit the engineer to control – within limits – the distribution of lateral loads.

The paper will provide an overview of the new AASHTO seismic-design requirements, the force-redistribution concept, and the benefits of seismic isolation in retrofit applications. A summary of the key features of the almost 50 U.S. bridge applications to date will also be provided.

INTRODUCTION

Prior to the Loma Prieta earthquake of October 17, 1989, awareness of seismic risk outside of California seemed to be increasing. Further impetus was provided in 1990 when the AASHTO Bridge Committee adopted the 1983 Guide Specifications as Standard (AASHTO, 1991) and approved a new *Guide Specifications for Seismic Isolation Design* (Mayes, et al., 1992).

Since 1990, seismic isolation has gained rapid acceptance in low and moderate seismic zones. There are several reasons for this. First, the seismic load case is often eliminated as a governing load case in low-to-moderate seismic zones. Second, besides lowering the overall seismic force on the structure, isolation design makes it possible to distribute the seismic and nonseismic lateral forces among the substructures in a way that benefits the global design (Mayes et al., 1991). In new construction, this capability can be a source of significant cost savings in foundations. In retrofit situations, it may facilitate the reduction of the lateral forces to levels within the elastic capacities of the weaker existing substructures and foundations, thus avoiding costly strengthening of these components, while solving the other two seismic-retrofit problems, i.e., vulnerable bearings and inadequate girder support lengths. Third, AASHTO's adoption of the *Guide Specifications for Seismic Isolation Design* has filled a void in the code which often served as an impediment to the implementation of seismic isolation in bridges.

The basic concepts and applications of seismic isolation to U.S. bridges can be found in the references by Buckle et al., 1986, 1987 and 1990; Kelly and Jones, 1991; Mayes et al., 1992;

---

[1] President, Dynamic Isolation Systems, Inc., 2855 Telegraph Avenue, Suite 410, Berkeley, California 94705

and Dynamic Isolation Systems, 1992. The concept of lateral force distribution can be found in Mayes et al., 1991, and O'Connor and Mayes, 1992.

AASHTO CODE REQUIREMENTS

One of the major impediments to the implementation of seismic isolation has been the lack of code requirements. With liability issues being a major concern to design professionals in today's litigious society, many firms have been unwilling to use the technology without the protection of professionally-acceptable code provisions. Thus, the October 1990 adoption of Seismic Isolation Design Requirements by AASHTO (AASHTO, 1991; Mayes et al., 1992) was a key step forward in the more-widespread use of seismic isolation.

Seismic isolation provides a significant reduction in the elastic seismic forces the bridge must resist when compared to conventional fixed-base design (Buckle et al., 1986, 1989, 1990). As a consequence, there are 2 possible design philosophies that can be used and both are included in the AASHTO *Guide Specifications*. The first is to take advantage of the reduced forces and provide the most economical bridge design. This option utilizes the same Response Modification Factors (R-Factors) as the recently adopted AASHTO Standard Specifications and, thus, provides the same level of seismic safety as conventional design. The advantage of this design option is that if seismic forces are governing the design of the bridge, cost savings up to approximately 10% of the total bridge cost can be realized (Billings, 1985; Thorkildsen, 1991; O'Connor and Mayes, 1992).

The second design option is to provide a bridge with much better seismic-performance characteristics than that of a conventional design using the AASHTO Standard Specifications. The intent of this design option it to eliminate or significantly reduce damage (inelastic deformation) to the substructure and abutments. In this case, an R-Factor in the range of 1 to 1.5 will ensure essentially elastic response by eliminating the ductility demand on the substructure. In bridges, this design option can generally be achieved for similar or less cost than a conventional design.

FORCE-DISTRIBUTION CHARACTERISTICS

The primary purpose of seismic isolation bearings is to provide a significant reduction in earthquake forces. A second, but equally important design option, is to control the distribution of not only the seismic forces but other lateral loads as well (Mayes et al., 1991). The bilinear force-deflection characteristics of seismic isolation bearings provides some alternate design options for the resistance of lateral-load effects due to wind, braking, centrifugal, and seismic loads.

There are distinct changes that occur in the response of a bridge that incorporates seismic isolation bearings (O'Connor and Mayes, 1992). In an isolated bridge, elastic restraint is provided in both the longitudinal and transverse directions at each support. The distribution of lateral loads is then a function of the bilinear force-deflection characteristics of the isolation bearings, unless the columns are very flexible, in which case the combined stiffness of the bearings and columns will control the distribution of lateral loads.

APPLICATIONS

There are now over 60 bridges in the U.S. that are either complete or under construction. Table 1 provides a summary of the key features of each of the projects. The table does not include the details of two additional bridges: one in Oregon using the FIP system and the other in Indiana using the Eradiquake system. Detailed examples of cost savings on new construction can be found in Thorkildsen, 1991, and O'Connor and Mayes, 1992. For seismic retrofit, there are 3 global alternatives available to a designer:

- Increase ductility and/or capacity of columns, such that the combination is sufficient to resist the demand. This is the conventional approach.

- Decrease demand and/or increase capacity until capacity exceeds the demand. This is the isolation approach.

- Get as much capacity and/or ductility and/or demand reduction as practical and accept the risk. This means some damage in a future event will occur, but this risk may be judged to be acceptable, from an economic viewpoint.

Seismic isolation, when applicable, is an attractive alternative since replacement of vulnerable rocker/roller bearings with isolation bearings may prevent column- and foundation-strengthening work to be performed. To date, about 50% of the U.S. seismic isolation applications are retrofit projects.

REFERENCES

AASHTO (1991), *Standard specifications for highway bridges*, American Association for State Highway and Transportation Officials (AASHTO)., 15th Edition, 1989, and Interim Specifications, 1990, 1991.

Billings, I.J., and Kirkcaldie, D.K. (1985), "Base isolation of bridges in New Zealand," Proceedings US-NZ Workshop on Seismic Resistance of Highway Bridges, *Report No. 12-1*, Applied Technology Council.

Buckle, I.G., Mayes, R.L., and Button, M.R. (1986), *Seismic design and retrofit manual for highway bridges*, Computech Engineering Services, Berkeley, CA. Also published by Federal Highway Administration as Report FHWA/RD-86/006, 1987.

Buckle, I.G., and Mayes, R.L. (1987), "The application of seismic isolation to bridges," *Proceedings*, ASCE Structures Congress: Seismic Engineering - Research and Practice, 633-642, May 1990.

Buckle, I.G., and Mayes, R.L. (1990), "Seismic isolation: history, application and performance - a world view," *Earthquake Spectra Journal*, EERI, 6:2.

CSMIP (1992), "CSMIP strong motion records from the Petrolia, California earthquake of April 25-26, 1992," California Strong Motion Instrumentation Program (CSMIP) *Report No. OSMS 92-05.*

Dynamic Isolation Systems (1992), *AASHTO design procedures for seismically isolated bridges*, Seminar Notes.

Kelly, T.E., and Jones, D.M. (1991), *Case studies of seismically isolated bridges*, ASCE Structures Congress.

Mayes, R.L., Jones, D.M., Kelly, T.E., and Knight, R.P. (1991), "An alternate approach to the distribution of lateral loads in bridges," *Proceedings*, ACI 3rd World Congress on Joints and Bearings.

Mayes, R.L., Buckle, I.G., Kelly, T.E, and Jones, L.R. (1992), "AASHTO seismic isolation design requirements for highway bridges," *ASCE Journal of Structural Engineering*, 118:1.

O'Connor, T.F., and Mayes, R.L. (1992), "Controlling lateral load distribution in bridges to achieve overall economy," *Proceedings*, 9th International Bridge Conference.

Thorkildsen, E. (1991), "The use and subsequent reuse of seismic isolation bearings on a California interchange," *Proceedings*, 8th International Bridge Conference.

TABLE 1: SEISMICALLY ISOLATED BRIDGES IN NORTH AMERICA

Structure / Year	Geometry	Equiv. Design Spectrum	Superstructure Type	Remarks
1. **Santa Ana River Bridge** *(Retrofit)* 1986	Length = 1010' (308 m) 13 spans, max span 180' (55 m)	ATC A = 0.4g Soil Profile Type II	3 - 180' (55 m) simple span through trusses; 10 steel girder approach spans	Replacement of vulnerable steel bearings reduced elastic forces to levels within the elastic capacity of the existing concrete wall piers and certain truss members that were overstressed.
2. **Sierra Point Overhead** *(Retrofit)* 1986	Length = 616' (188 m) Width = 117' (36 m) 10 simple spans, max. span 100' (31 m)	Caltrans A = 0.6g 0 - 10' alluvium	Longitudinal steel plate girders; transverse steel plate girder bent caps	3' diameter, 25' tall columns were protected by reducing elastic seismic forces, by a factor of 6, to levels well within their elastic capacity.
3. **Main Yard Vehicle Access Bridge** *(Retrofit)* 1987	Length = 256' (78 m) Width = 32' (10 m) 2 equal simple spans 58° skew	Caltrans A = 0.5g 10 - 80' alluvium	2 - 128' (39 m) simple span steel through plate girders; steel floor beams, concrete deck	Replacement of vulnerable steel bearings eliminated the potential for shear failure in the columns of the 2-column bent with infill wall. Forces on the tall abutments were also reduced.
4. **Eel River Bridge** *(Retrofit)* 1987	Length = 606' (185 m) Width = 26' (8 m) 2 equal simple spans	Caltrans A = 0.5g >150' alluvium	2 - 300' (92 m) steel through truss simple spans	Replacement of vulnerable steel bearings provided protection for the nonductile wall piers.
5. **All-American Canal Bridge** *(Retrofit)* 1988	Length = 410' (125 m) Width = 41' (13 m) 3 continuous spans	Caltrans A = 0.6g >150' alluvium	Continuous steel plate girders (replacing former steel deck trusses)	Use of isolation on the superstructure replacement eliminated the need to replace the columns and foundations or strengthen them under water.
6. **Sexton Creek Bridge** *(New)* 1990	Length = 394' (120 m) Width = 40' (12 m) Max. span 154' (47 m) Slight horizontal curvature	AASHTO A = 0.2g Soil Profile Type III	3-span continuous steel plate girders	Overall seismic force input was reduced by a factor of 3, and the isolation design redistributed much of the lateral seismic and nonseismic forces from the wall piers and piled foundations to the abutments.
7. **Toll Plaza Road Bridge** *(New)* 1990	Length = 176' (54 m) Width varies, 150' to 210' (46 m to 64 m) Single span	AASHTO A = 0.1g Soil Profile Type II	176' (54 m) simple span composite steel plate girder	Some overall seismic benefit, plus transverse thermal capability of isolation bearings on such a very wide bridge was an important consideration.
8. **Dean Slough Bridge** *(Retrofit)* 1990	Length = 320' (98 m) Width = 58' (18 m) 3 spans, max. span 140' (43 m) 38° skew	AASHTO A = 0.2g Soil Profile Type III	3-span continuous riveted haunched steel plate girders	An isolation design focusing on redistribution of lateral forces away from the fixed pier made it possible to accomplish seismic upgrade by replacing the bearings.
9. **UMSL Garage Bridge** *(New)* 1991	Dual Structures (one per track) Length = 286' (87 m) 3 spans, max. span 100' (31 m)	AASHTO A = 0.1g Soil Profile Type I	3-span continuous haunched concrete box girder	(See SB I-170/EB I-70)
10. **Springdale Bridge** *(New)* 1991	Dual Structures (one per track) Length = 221' (67 m) 3 spans, max. span 85' (26 m) 31° skew	AASHTO A = 0.1g Soil Profile Type I	3-span continuous haunched concrete box girder	(See SB I-170/EB I-70)
11. **Ramp 26 Bridge** *(New)* 1991	Dual Structures (one per track) Length = 292' (89 m) 4 spans, max. span 81' (25 m) 50° skew	AASHTO A = 0.1g Soil Profile Type I	4-span continuous haunched concrete box girder	(See SB I-170/EB I-70)
12. **NB I-170 Bridge** *(New)* 1991	Dual Structures (one per track) Length = 288' (88 m) 4 spans, max. span 114' (35 m)	AASHTO A = 0.1g Soil Profile Type I	2-span continuous steel box girder flanked by short simple span steel box girders	(See SB I-170/EB I-70)

Structure / Year	Geometry	Equiv. Design Spectrum	Superstructure Type	Remarks
13. **West Street Overpass** *(Retrofit)* 1991	Length = 172' (52 m) Width = 33' (10 m) 4 spans, max. span 54.5' (17 m)	AASHTO A = 0.19g Soil Profile Type III	4 simple-span steel beam structures	Replaced vulnerable steel bearings in 2 center spans over thruway traffic lanes to prevent collapse and relieve forces on center pier.
14. **Pequannock River Bridge** *(New)* 1991	Dual Structures Length = 854' (260 m) Width = 63' (19 m) 8 spans, max. span 123' (38 m) Slight horizontal curvature	AASHTO A = 0.12g Soil Profile Type II	Three continuous steel plate girder units of 2, 3, and 3 spans	Isolation design reduced overall seismic force input and mitigated disparity in pier stiffnesses by redistributing lateral forces.
15. **Geiger Road Bridge** *(New)* 1991	Dual Structures (one per track) Length = 832' (254 m) 8 spans, max. span 115' (35 m)	AASHTO A = 0.1g Soil Profile Type I	Equal continuous units; one tangent, one curved; each 416' (127 m) long, 4-span haunched concrete box girder	(See SB I-170/EB I-70)
16. **East Campus Drive Bridge** *(New)* 1991	Dual Structures (one per track) Length = 417' (127 m) 4 spans, max. span 114' (35 m) Slight horizontal curvature	AASHTO A = 0.1g Soil Profile Type I	4-span continuous haunched concrete box girder	(See SB I-170/EB I-70)
17. **SB I-170/EB I-70 Bridge** *(New)* 1991	Dual Structures (one per track) Length = 910' (278 m) Width = 12' (4 m) per track 7 spans, max. span 196' (60 m) Partially curved	AASHTO A = 0.1g Soil Profile Type I	Span 1: 120' (37 m) simple span steel box girder; Spans 2-4: 280' (85 m) 3-span continuous haunched concrete box girder; Spans 5-7: 510' (156 m) 3-span continuous curved steel box girder	Isolation design facilitated distribution of longitudinal forces among the substructures for optimum economy while providing some seismic benefit.
18. **Cache River Bridge** *(Retrofit)* 1991	Length = 280' (85 m) Width = 35' (11 m) 3 spans, max. span 108' (33 m) 21° skew	AASHTO A = 0.2g Soil Profile Type III	3-span continuous steel plate girders	Seismic isolation/force-redistribution design enabled re-use of the existing pier in this superstructure replacement project.
19. **Wabash River Bridge** *(New)* 1991	Dual Structures Length = 880' (268 m) Width = 41' (13 m) 7 spans, max. span 150' (46 m)	AASHTO A = 0.1g Soil Profile Type II	7-span continuous steel plate girders	Isolation design maximized seismic protection at least cost for the hammerhead wall piers and piled foundations.
20. **Route 161 Bridge** *(New)* 1991	Dual Structures Length = 356' (109 m) Width = 46' (14 m) 4 spans, max. span 96' (29 m) 26° skew	AASHTO A = 0.14g Soil Profile Type III	4-span continuous steel plate girder	Isolation reduced overall seismic force input and mitigated disparity in pier stiffnesses by redistributing lateral forces.
21. **Lacey V. Murrow Bridge - West Approach** *(Retrofit)* 1992	Length = 1128' (344 m) Width = 55' (17 m) 8 spans, max. span 195' (59 m)	AASHTO A = 0.25g Soil Profile Type II	3-span continuous concrete box girders; 3-span continuous deck trusses; simple span tied arch (similar tied arch span at east end also retrofitted)	Seismic isolation saved the existing piers and foundations, thus avoiding the need to replace the whole structure.
22. **Dog River Bridge** *(New)* 1992	Dual Structures Length = 462' (141 m) Width = 37' (11 m) 3 spans, max. span 180' (55 m)	AASHTO Category A	3-span continuous steel plate girders	Isolation design selected to take advantage of force redistribution and low maintenance features.
23. **Clackamas Connector** *(New)* 1992	Length = 1005' (307 m) Width = 36' (11 m) 8 spans, max. span 135' (41 m) 12.5° Horizontal curve through 80° central angle	AASHTO A = 0.29g Soil Profile Type III	8-span continuous post-tensioned concrete trapezoidal box girder	Isolation design resulted in a net savings of $400,000 (12%) due to reduction in foundation size and will protect the tapered single column bents from damage in an earthquake.
24. **Blackstone River Bridge** *(New)* 1992	Length = 1000' (305 m) Width = 86' (26 m) 4 spans, max. span 280' (85 m)	AASHTO A = 0.1g Soil Profile Type II	4-span continuous composite steel plate girders	Isolation design reduced overall seismic force input and mitigated disparity in pier stiffnesses.

Structure / Year	Geometry	Equiv. Design Spectrum	Superstructure Type	Remarks
25. **Ompompanoosuc River Bridge** *(Retrofit)* 1992	Length = 251' (77 m) Width = 31' 9 m) 3 equal spans 45° skew	AASHTO A = 0.10g Soil Profile Type III	3-span continuous steel plate girders	Seismic forces were reduced by a factor of 2.5 and then redistributed to minimize the forces on the piers.
26. **Providence Viaduct** *(Retrofit)* 1992	Dual structures Length = 1290' (393 m) Width = 45' (14 m) 8 spans, max. span 210' (64 m)	AASHTO A = 0.32g Soil Profile Type III	2 steel plate girder simple spans and 2 3-span continuous haunched steel plate girder units	2-level criteria calling for serviceability after an A = 0.16g event and no collapse in an A = 0.32g event. Isolation was the cost-effective solution, and the viaduct will remain n service after the higher level event.
27. **I-80 Bridges B764E & W** *(Retrofit)* 1992	Dual Structures Length = 443' (135 m) Width = 43' (13 m) 6 spans, max. span 101' (31 m) Slight horizontal curvature	AASHTO A = 0.37g Soil Profile Type I	Simple span, composite steel plate girders or rolled beams	Isolation and force-redistribution design reduced seismic forces to within the elastic capacity of the 3 column bents and mitigated the disparity in pier stiffnesses. Simple spans were tied together to make superstructure respond as a diaphragm.
28. **Carlson Blvd. Bridge** *(New)* 1992	Length = 153' (47 m) Width = varies 49' to 57' (15 m to 17 m) Single span 45° skew	Caltrans A = 0.7g 80 - 150 ft. alluvium	Simple span multi-cell concrete box girder	Isolation design reduced the elastic force coefficient to 0.45 (factor of 3 from peak), a design advantage for the wall abutments.
29. **Squamscott River Bridge** *(New)* 1992	Length = 874' (267 m) Width = 52' (16 m) 6 spans, max. span 156' (48 m)	AASHTO A = 0.15g Soil Profile Type III	6-span continuous steel plate girders	Isolation and force-redistribution design resulted in a net savings of $160,000.00 (4%) in the overall cost of the bridge due to reduction in the size of the "fixed" pier and the number of piles.
30. **Relocated NH Rte. 85 over NH Rte. 101** *(New)* 1992	Length = 170' (52 m) Width = 76' (23 m) 2 equal spans 16° skew	AASHTO A = 0.15g Soil Profile Type I	2-span continuous steel plate girders	Seismic forces were reduced by a factor of 4.5 and then redistributed to further reduce the forces on the 34' high wall abutments.
31. **US 51 over Minor Slough** *(New)* 1992	Length = 371' (113 m) Width = 47' (14 m) 3 equal spans 45° skew	AASHTO A = 0.25g Soil Profile Type II	3 - 121' (37 m) simple span prestressed concrete I-girders with continuous deck	Seismic forces were reduced by a factor of 3.5 and then redistributed to minimize the forces on the piers.
32. **Poplar St. East Approach Bridge #082-0005** *(Retrofit)* 1992	Length = 856' (261 m) Width varies 112' to 165' (34 m to 50 m) 6 spans, max. span 161' (49 m)	AASHTO A = 0.12g Soil Profile Type III	2 dual steel plate girder units (5-span continuous and 1 simple span); supported on multi-column or wall piers; piled foundations	Isolation as a seismic upgrade was implemented by change order to an existing rehabilitation contract.
33. **Cedar River Bridge** *(New)* 1992	Dual Structures Length = 521' (159 m) Width varies 72' to 86' (22 m to 26 m) 4 spans, max. span 196' (60 m) Horizontal curve	AASHTO A = 0.25g Soil Profile Type II	4-span continuous steel plate girders	Isolation used for initial economy and assurance of serviceability after an earthquake.
34. **Main Street Bridge** *(Retrofit)* 1993	Length = 96' (29 m) Width = 52' (16 m) 2 equal spans	AASHTO A = 0.17 Soil Profile Type I	2-span continuous steel beams with concrete deck	Replaces badly deteriorated simple-span superstructure. Isolation reduced seismic forces by a factor greater than 4, and was the most economical solution, enabling re-use of the center pier.
35. **Aurora Expressway Bridge** *(Retrofit)* 1993	Length = 201' (61 m) Width = 48' (15 m) 3 spans, max. span 86' (26 m) 1° curve	AASHTO A = 0.19 Soil Profile Type III	Continuous steel beams with concrete deck.	Seismic upgrade part of general rehabilitation project. Isolation reduced forces by a factor of 3, and design was adjusted to minimize forces on piers. Scheduled for full-scale testing by SUNY Buffalo.

Structure / Year	Geometry	Equiv. Design Spectrum	Superstructure Type	Remarks
36. **Foundry Street Overpass** *(Retrofit)* 1993	Dual Structures Length = 204' (62 m) Width = 85' and ±130' (26 m and ±40 m) 3 spans, max. span 73' (22 m) 3600' (1098 m) radius curve	AASHTO A = 0.18 Soil Profile Type II	Simple span steel beams supporting concrete deck.	Part of the NJTPA widening project. Isolation chosen to guarantee serviceability of facility after a seismic event.
37. **Bridge over County Road 3** *(New)* 1993	Length = 456' (139 m) Width = 66' (20 m) 5 spans, max. span 100' (31 m) 9.3% grade	AASHTO A = 0.1g Soil Profile Type II	Continuous welded steel plate girders with concrete deck.	Designed for heavy coal-hauling vehicles. Isolation design was the most economical overall solution and ensures serviceability after a seismic event.
38. **Burrard Bridge - Main Spans** *(Retrofit)* 1993	Length = 1080' (329 m) Width = 43' (13 m) 5 simple spans, max. span 294' (90 m)	AASHTO A = 0.2g Soil Profile Type I	Side spans are simple span deck trusses. Center span is a Pratt through truss	Isolation reduced seismic force demand by a factor of 4 to levels within the capacity of the existing substructures.
39. **Foundry Street Overpass 106.68** *(Retrofit)* 1993	Dual Structures Length = 204' ((62 m) Width = 85' and ±130' (26 m and 40 m) 3 spans, max. span 73' (22 m) 3600' (1098 m) radius curve	AASHTO A = 0.18 Soil Profile Type II	Simple-span steel beams supporting concrete deck	Part of the NJTPA widening project. Isolation chosen to guarantee serviceability of facility after a seismic event.
40. **West Fork River Bridge** *(New)* 1994	Length = 612' (187 m) Width = 66' (20 m) 3.4% grade	AASHTO A = 0.1g Soil Profile Type II	Continuous welded steel plate girders with concrete deck.	Designed for heavy coal-hauling vehicles. Isolation design was the most economical overall solution and ensures serviceability after a seismic event.
41. **South Boston Bypass Viaduct** *(New)* 1994	Length = 1940' (592 m) Width = varies 32' to 60' (10 m to 18 m) 11 spans, max. span 200' (61 m) Reverse curvature	AASHTO A = 0.17 Soil Profile Type III	Concrete deck supported by 120' simple span with 3 trapezoidal steel box girders, plus 1820' 10-span continuous unit with 2 curved trapezoidal steel box girders	Isolation design was most cost effective globally. Serviceability after a seismic event is ensured for this important segment of the Central Artery Project.
42. **Poplar Street East Approach, Roadway B** *(New)* 1994	Dual Structures Length = 2992' (913 m) Width = varies 33' to 43' (10 m to 13 m) 24 spans, max. span 138' (42 m) Curved partially	AASHTO A = 0.12 Soil Profile Type III	3-, 4- and 5-span continuous, curved steel plate girder units	Replaces existing main line structure. Isolation provides the serviceability – not just survival demanded by this critically-important route after a seismic event.
43. **Mohawk River Bridge** *(Retrofit)* 1994	Dual Structures Length = 1000' ((305 m) Width = 56' (17 m) 9 spans, max. span 215' (66 m) Curved, skewed	AASHTO A = 0.19 Soil Profile Type II	Main 3-span unit is haunched, riveted steel plate girders. Approach units are simple span riveted steel plate girders or rolled beams.	Major rehabilitation and strengthening project which includes seismic upgrade. Isolation design avoided costly strengthening of columns and foundations and will keep the structures in service after an earthquake.
44. **Conrail Bridge** *(New)* 1994	Dual Structures Length = 733' (224 m) Width = 56' (17 m) 4 spans, max. span 274' (84 m)	AASHTO A = 0.19 Soil Profile Type II	4-span continuous, curved, haunched, welded steel plate girders with concrete deck.	Replacement of original structure. Isolation was most economical overall design and will keep the structures in service after an earthquake.
45. **Queensborough Bridge** *(Retrofit)* 1994	Length = n/a Width = n/a 3 spans, max. span n/a	AASHTO A = 0.21g Soil Profile Type I	High level bridge. 3-span continuous, haunched, steel plate-girders. 2-girder system with floor beams	Seismic forces reduced by a factor of 1.5. Force distribution favors end piers.
46. **Alemany Interchange** *(Retrofit)* 1994	Length = 2470' (753 m) Width = varies 34' to 68' (10 m to 21 m), max. span 105' (32 m) Partially curved	Caltrans A = 0.5g 10' to 80' alluvium	Single and double deck viaduct. R/C box girders and columns. 7 continuous units.	Complex seismic retrofit. Isolation bearings used at certain bents to obtain specific force-deflection characteristics.

Structure / Year	Geometry	Equiv. Design Spectrum	Superstructure Type	Remarks
47. **Saugatuck River Bridge** *(Retrofit)* 1994	Dual Structures Length = 1210' (369 m) Width = 59' (18 m) 10 spans, max. span 129' (39 m)	AASHTO A = 0.16 Soil Profile Type II	3 continuous, steel plate-girder units of 3, 4 and 3 spans	New, widened superstructure replaces old simple spans as proposed by contractor. Cost of removing lead paint from existing superstructure was prohibitive. Isolation and force-redistribution design enabled use of existing piers and foundations.
48. **Chain-of-Rocks Road over FAP 310** *(New)* 1994	Length = 479' (146 m) Width = 47' (14 m) 4 spans, max. span 148' (45 m) 5° horizontal curve	AASHTO A = 0.13 Soil Profile Type III	4-span, continuous, curved, steel plate-girders	Isolation design provided even distribution of lateral forces among the substructures and multi-directional response to lateral forces on the curved superstructure. Overall seismic force was reduced by a factor greater than 2.
49. **Clays Ferry Bridge** *(Retrofit)* 1995	Length = 1713' (522 m) Width = 126' (38 m) 5 spans, max. span 448' (137 m) 3% grade	AASHTO A = 0.1g Soil Profile Type I	5-span, continuous deck truss, haunched at center 2 piers	Widening and seismic upgrade. Seismic forces reduced by a factor of 2.
50. **Neponset River Bridge** *(New)* 1994	Length = 1188' (362 m) Width = 35' (11 m) 10 equal spans	AASHTO A = 0.15 Soil Profile Type III	Simple-span, steel through-girders, double-track ballasted deck	Global design based on seismic isolation. Seismic forces were reduced by a factor of 2
51. **Pine Hill Road over Everett Turnpike** *(New)* 1994	Length = 241' (74 m) Width = 39' (12 m) 2 spans, max. span 123' (38 m) 33° skew	AASHTO A = 0.15 Soil Profile Type I	2-span, continuous, steel plate-girders	Overall seismic forces were reduced by a factor of approx. 2.5 and were then redistributed to favor the abutments slightly.
52. **Wilson Avenue Overpass 105.79SO** *(Retrofit)* 1994	Length = 156' (48 m) Width = 60' (18 m) 3-spans, max. span 80' (24 m) Skewed	AASHTO A = 0.18g Soil Profile Type I	Steel beams, 3 simple spans	Part of the NJTPA widening project. Isolation chosen to guarantee serviceability of facility after a seismic event.
53. **Conrail Newark Branch Overpass E106.57** *(Retrofit)* 1994	Length = 306' (93 m) Width = 85' (26 m) 4 spans, max. span 120' (37 m) Slight skew & curve	AASHTO A = 0.18g Soil Profile Type II	Steel plate-girders, 4 simple spans	Part of the NJTPA widening project. Isolation chosen to guarantee serviceability of facility after a seismic event.
54. **Wilson Avenue Overpass E105.79SO** *(Retrofit)* 1994	Length = 156' (48 m) Width = 71' (22 m) 3 spans, max. span 81' (25 m) Skewed	AASHTO A = 0.18g Soil Profile Type I	Steel beams, 3 simple spans	Part of the NJTPA widening project. Isolation chosen to guarantee serviceability of facility after a seismic event.
55. **Relocated E-NSO Overpass E106.26A** *(New)* 1994	Length = 1485' (453 m) Width = 47' (14 m) 9 spans, max. span 190' (58 m)	AASHTO A = 0.18g Soil Profile Type II	Steel plate-girders, continuous units of 5 and 4 spans	Part of the NJTPA widening project. Isolation chosen to guarantee serviceability of facility after a seismic event.
56. **Moodna Creek Bridge** *(Retrofit)* 1994	Dual Structures Length = 201' (61 m) Width = 56' (17 m) 3 spans, max. span 104' (32 m)	AASHTO A = 0.15g Soil Profile Type II	3 simple spans; steel plate-girder center span; rolled beam side spans	Seismic upgrade. Forces reduced by a factor of 3.
57. **Coldwater Creek Bridge No. 11** *(New)* 1994	Length = 492' (150 m) Width = 3 ' (10 m) 3 spans, max. span 190' (58 m) Curved, 4.5% grade	AASHTO A = 0.55g Soil Profile Type I	3-span continuous steel plate-girders	Seismic forces reduced by a factor greater than 6. Forces minimized at abutments.

Structure / Year	Geometry	Equiv. Design Spectrum	Superstructure Type	Remarks
58. **East Creek Bridge No. 14** *(New)* 1994	Length = 510' (156 m) Width = 34' (10 m) 3 spans, max. span 230' (70 m) Curved, 7% grade	AASHTO A = 0.55g Soil Profile Type I	3-span continuous steel plate girders	Seismic forces reduced by a factor greater than 6. Forces minimized at abutments.
59. **Berry's Creek Bridge** *(Retrofit)* 1995	Dual Structures Length = 1017' (310 m) Width = 69' (21 m) 13 spans, max. span 120' (37 m)	AASHTO A = 0.18g Soil Profile Type II	Continuous steel plate-girders, units of 3, 4, 3 and 3 spans	Staged construction. New superstructure on existing substructures. Overall seismic force reduced by a factor of 3, thus enabling use of existing columns.
60. **Poplar Street East Approach, Roadway C** *(New)* 1995	Length = 3080' (939 m) Width = varies 33' to 43' (10 m to 13 m) 28 spans, max. span 138' (42 m) Partially curved	AASHTO A = 0.12g Soil Profile Type III	3-, 4- and 5-span, continuous, curved steel plate-girder units	Replaces existing main line structure. Isolation provides the serviceability demanded by this critically important route after a seismic event.
61. **Conrail Newark Branch Overpass W106.57** *(Retrofit)* 1995	Length = 413' (126 m) Width = 73' (22 m) 6 spans, max. span 97' (30 m) Skewed	AASHTO A = 0.18g Soil Profile Type I	Steel beams, 6 simple spans	Part of the NJTPA widening project. Isolation chosen to guarantee serviceability of facility after a seismic event.

PASSIVE PROTECTIVE SYSTEMS

Application of Base Isolation Bearings for Lateral Force Distribution

Shaking Table Tests on Base-Isolated Bridge with Sliding System

Development of New Type Damper for Cable Stayed Bridge

Experimental Study of a Class of Bridge Sliding Seismic Isolation Systems

Recovery Characteristics of Dynamic Properties of High Damping Rubber Bearings

Effects of Pier Uplift and Sliding Isolation on Seismic Performance of Highway Bridges

NIST

U.S. Department of Transportation
Federal Highway Administration

APPLICATION OF BASE ISOLATION BEARINGS FOR LATERAL FORCE DISTRIBUTION

by Tatumasa Takaku [1], Teruo Kimishima [2], Shinichi Izuma [2], and Kazuo Endou [3]

1 Bridge Construction and Engineering Department, NKK Corporation, Tsurumi-ku, Yokohama, Japan
2 Engineering Design Department, Japan Casting Co., Ltd., Kawasaki-ku, Kawasaki, Japan
3 The Yokohama Rubber Co., Ltd., Hiratsuka, Kanagawa, Japan

ABSTRACT

In multi-span continuous bridges, problems of (1) the distribution of seismic forces and (2) large movements due to temperature are significant. An effective method for distributing seismic forces is to join the superstructure and substructure by a hinge connection, which distributes lateral seismic force to multiple substructures. The NKK Group (comprising the NKK Corporation, Japan Casting Co., Ltd., and the Yokohama Rubber Co., Ltd.) developed a roller-type base isolation bearing and extended the technology to bearings for lateral force distribution. Two types of bearings were developed: a roller type and a laminated rubber type. The roller bearing is suitable for bridges that are subjected to large bearing forces and movements. The laminated rubber bearings are suitable for medium span bridges because of their simple construction. Trial design of the roller type was carried out to study structural details and mechanical properties. The laminated rubber type bearing was applied to a highway bridge modification for making existing simple span bridges continuous. The result of this work is reported in this paper. In addition, property tests of high-damping rubber were carried out to clarify any differences between large-lot production for construction and small-lot production for experimental work. These test results are also described in this report.

INTRODUCTION

Recent demands in the construction of multi-span continuous highway bridges have focused on: 1) no joints and 2) a maintenance-free flat road surface. These bridges are more earthquake-resistant because of their greater redundancy than simple supported span bridges. The distribution of lateral forces in multi-span continuous bridges is crucial for substructures to avoid the concentration of seismic forces at a single fixed point; otherwise, a single substructure with fixed conditions would become extremely large in size. The lateral forces are commonly distributed to the substructures using rubber bearings. The lateral stiffness of the rubber bearing can be easily determined to transmit the seismic forces to each substructure in proportion to its resistive capacity. If movements become larger, such as in case of long spans, roller-type bearings become more useful than rubber bearings. The inertial force distributed to pier i of the continuous girder shown in Fig. 1 is determined by Eq. (3):

$$\Sigma Km = \frac{1}{\frac{1}{\Sigma Ks} + \frac{1}{\Sigma Kp}} \quad \text{(tf/cm)} \qquad (1)$$

$$\delta e = \frac{\Sigma H}{\Sigma Km} \quad \text{(cm)} \qquad (2)$$

$$Hi = \delta e \cdot Kmi \quad \text{(tf)} \qquad (3)$$

where,

δe: displacement of the superstructure due to earthquake (cm)
H: inertial force (tf)
Ks: shear stiffness of the bearing for lateral force distribution (tf/cm)
Kp: shear stiffness of the substructure (tf/cm)
Km: combined shear stiffness of the bearing for lateral force distribution and substructure (tf/cm)

ROLLER-TYPE AND LAMINATED RUBBER TYPE BEARING FOR LATERAL FORCE DISTRIBUTION

Roller-type bearing for lateral force distribution

The roller-type bearing for lateral force distribution was an improvement of the roller-type base isolation bearing that was published in the proceedings of the First U.S.-Japan Workshop on Earthquake Protective Systems for Bridges. Fig. 2 shows the construction of the bearing. Ordinary bearing functions, such as the bearing for vertical force, are provided by a roller with high hardness, as has been used in many highway bridges. For distribution of the inertial force to the substructure, the bearing uses the shear stiffness of the restoring rubber. Chloroprene synthetic rubber (CR), natural rubber (NR), and high-damping rubber can be used for the restoring rubber.

Features:

(a) The shear stiffness can be set regardless of the vertical force. Therefore, the distribution of inertial force to the substructures can be easily adjusted.
(b) Super-high vertical forces can also be accommodated.
(c) The use of high-damping rubber as the restoring rubber results in a bearing that can provide damping.

Laminated rubber type bearing for lateral force distribution

The bearing functions, such as bearing for vertical force and absorption of superstructure deflection, are provided by laminated rubber. The bearing uses the shear stiffness of laminated rubber to distribute inertial force to the substructures. The bearing can be moved in all directions. The general construction of this bearing is shown in Fig. 3. Chloroprene synthetic rubber (CR), natural rubber (NR), and high-damping rubber can be used for restoring rubber. This type of bearing is used for lateral force distribution, which is most common in Japan at present. These bearings have been increasingly used not only for newly-built bridges, but also for work connecting existing simple span bridges. They distribute the inertial force as a continuous bridge and improve seismic safety and running properties.

Features:

(a) Bearing construction is simple.
(b) Low to high vertical forces can be accommodated.
(c) The bearing can move in all directions.

TRIAL DESIGN OF ROLLER-TYPE BEARING ROR LATERAL FORCE DISTRIBUTION

Based upon a bridge model, trial design was carried out to determine whether the developed roller-type bearing for lateral force distribution can be used for the superstructure and substructure in an actual bridge. Also, the displacement and dimensional changes of the restoring rubber due to an earthquake were quantified.

Bridge model

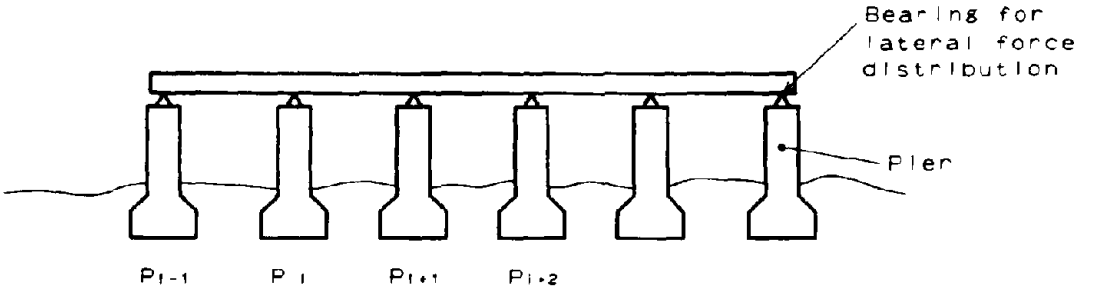

Fig. 1 Multi-span Continuous Bridge for distribution of seismic forces

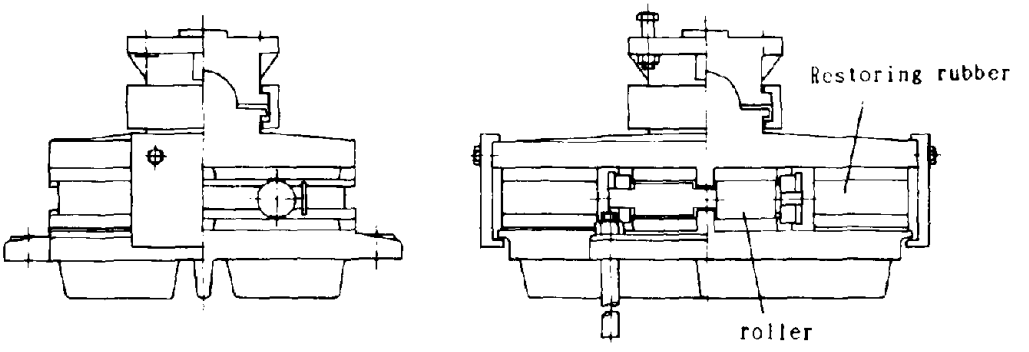

Fig. 2 Roller-type bearing for lateral force distribution

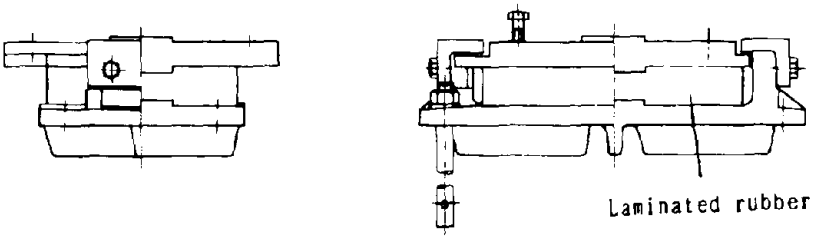

Fig. 3 Laminated rubber-type bearing for laterel force distribution

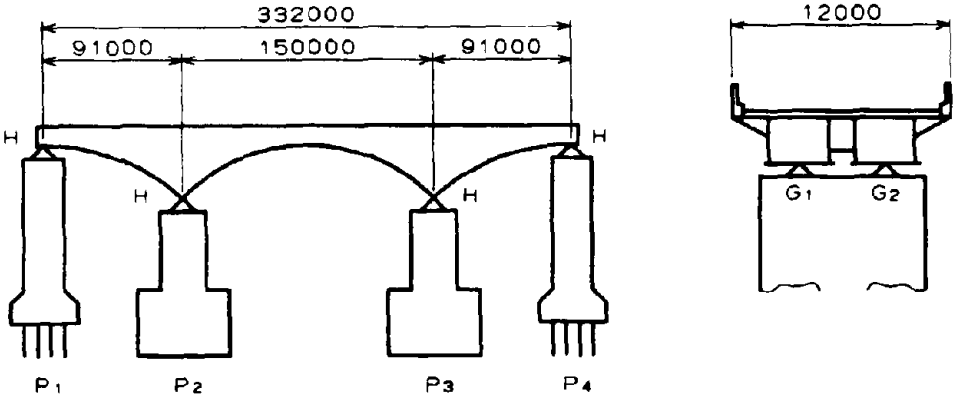

Fig. 4 Generel view of a proto-type bridge for trial design

Table 1 Reactions for design of roller-type bearing

(tf)

	P1		P2		P3		P4		total
	G1	G2	G1	G2	G1	G2	G1	G2	
Reaction due to dead load	133	134	776	720	780	715	122	120	3500
Total reaction	264	276	1207	1140	1215	1130	242	240	5714

Table 2 Behavior of roller-type bearings

Bearing	Lateral displacement due to earthquake	seismic inertia force
P1, P4	± 146 mm	33 tf
P2, P3	± 146 mm	185 tf

Table 3 Dimensions of roller-type bearings

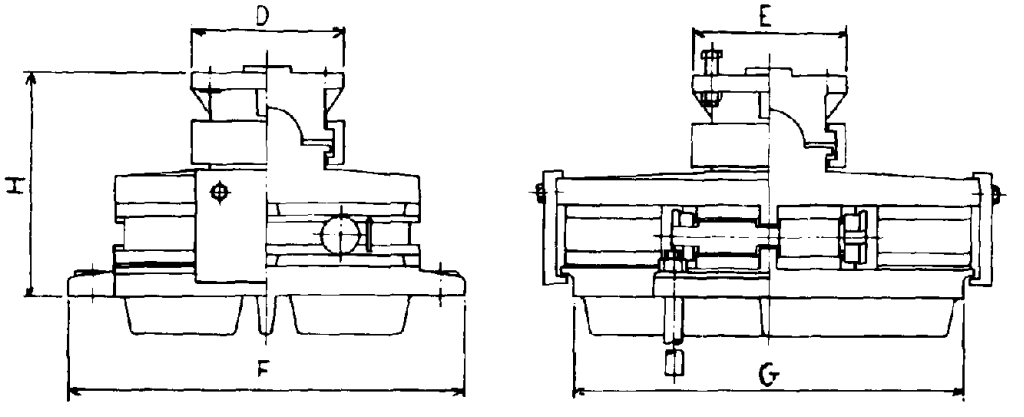

Bearing / mm	D	E	F	G	H
P1, P4	370	370	830	1150	595
P2, P3	700	700	1800	2280	1100

Teble 4 Dimensions of HDR used for roller-type bearing

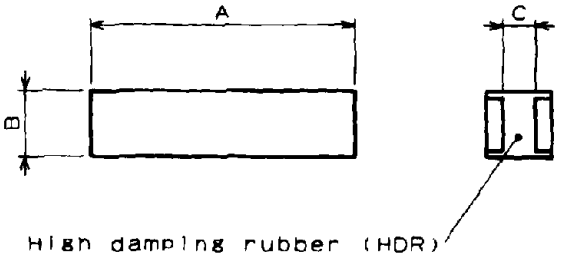

Bearing \ mm	A	B	C
P1, P4	660	234	108
P2, P3	1740	498	108

Table 5 Design conditions of laminated rubber-type bearing

Total reaction	40.4 tf
Reaction due to dead load	20.2 tf
Up lift	2.1 tf
Design lateral force coefficeint	0.25

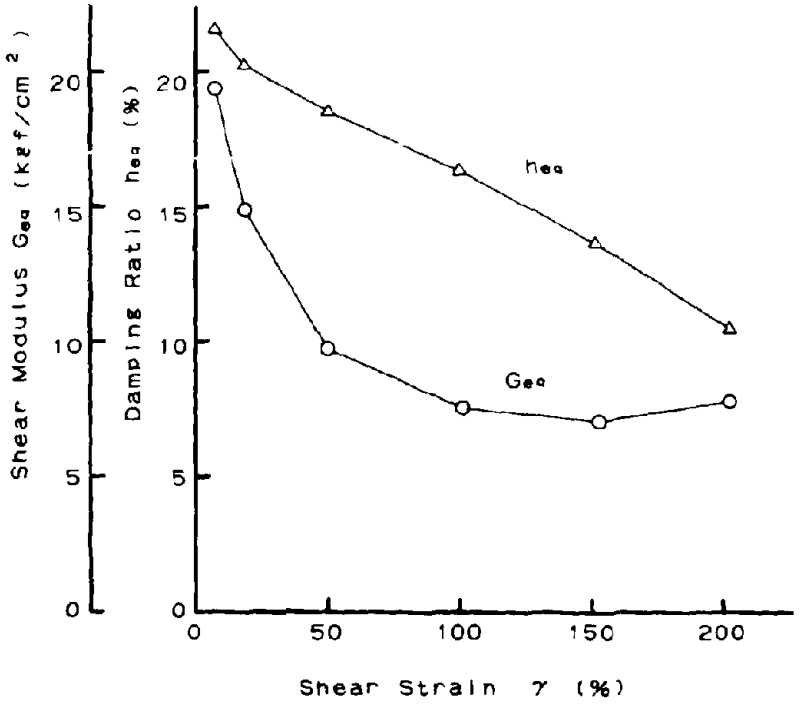

Fig.5 Shear modulus and damping ratio of a high damping rubber(HDR)

The model bridge has three continuous steel deck-type box girders. Fig. 4 shows a schematic of the bridge.

Design conditions of bridge:

Bridge grade: first class bridge
Span length: 332m
Width: 10.8m
Skew angle: 90°
Bridge type: 3 continuous steel deck-type box girder bridge
Design load: TL-20
Temperature change: ±25°C
Design lateral force coefficient: 0.25
Substructure
P1, P4: footing foundation
P2, P3: pile foundation
Weight of superstructure: 3500 tf
Total inertial force: 875 tf

Trial design

One type of bearing was used for P1 and P4, and another type was used for P2 and P3. The design was made to distribute the inertial force in proportion to the dead load of each bearing. Table 1 gives the dead load of the bearings.

(1) Restoring rubber

High-damping rubber was used as the restoring rubber material. This rubber was developed under the "Joint Research Program for Developing Menshin Systems for Highway Bridges." and the details were published in the Proceedings from the First U.S.-Japan Workshop on Earthquake Protective Systems for Bridges. Fig. 5 shows the shear modulus and effective damping ratio for the high-damping rubber. As shown in Fig. 5, the shear modulus of high-damping rubber varies with the shear strain. Therefore, the restoring rubber was designed by setting the shear modulus to be 8kgf/cm^2, assuming the shear strain of the rubber to be 135%.

(2) Size of bearing and restoring rubber

The design was made using established design conditions. The calculated bearing is given in Table 2, the size of the bearing in Table 3, and the size of the restoring rubber in Table 4.

(3) Results

The size of the trial-designed bearing permitted it to be set smoothly between the superstructure and substructure. The height of the bearing was nearly the same as that of the standard roller bearing. The displacement of the superstructure due to earthquakes did not reach a level that could cause problems in designing the expansion joints.

APPLICATION OF LAMINATED RUBBER-TYPE BEARING TO THE EXISTLING BRIDGES FOR LATERAL FORCE DISTRIBUTION

Outline of girder connecting work for the Senkawa Viaducts

The Senkawa Viaducts, completed in 1976, on the Chuo (Central) Expressway of the Japan Highway Public Corporation have a total length of 1282m. The viaducts are composed of about 70 units of simple composite I-girders, simple non-composite I-girders, and cantilever type Rhamen RC piers for each vertical line.

In this work, six simple composite I-girders were connected into a continuous bridge to eliminate expansion joints, which are the main sources of noise and vibration. The bearings were not a Menshin design due to the restriction on bearing

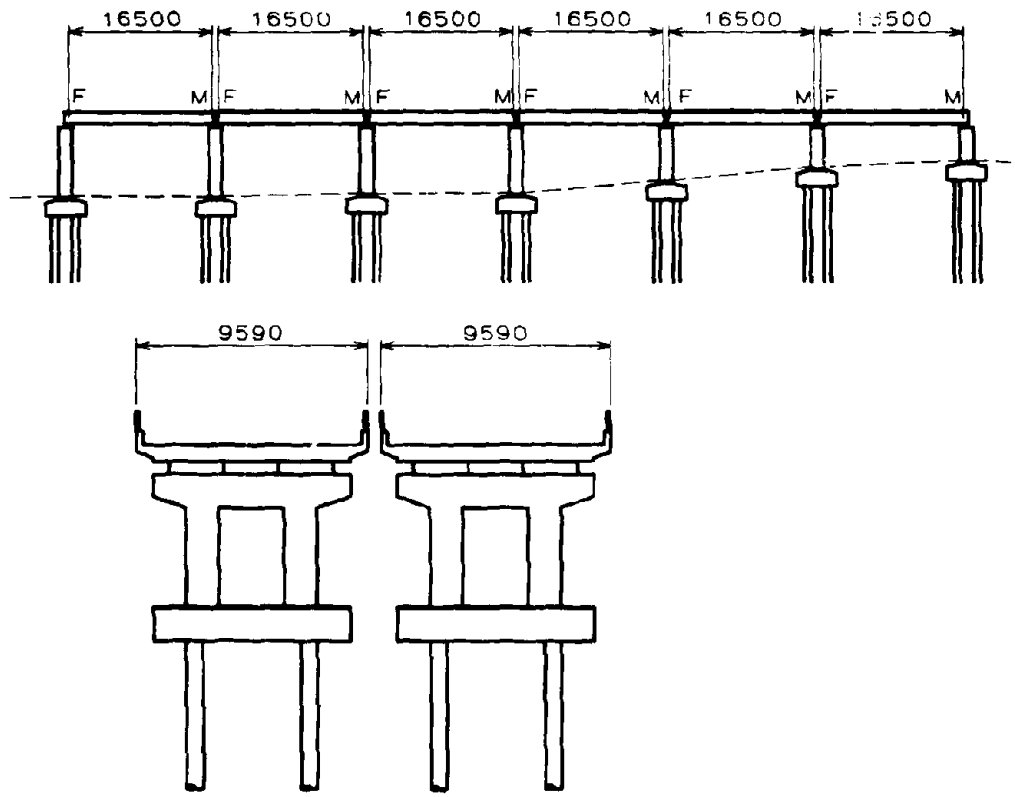

Fig. 6 General view of the Senkawa viaducts

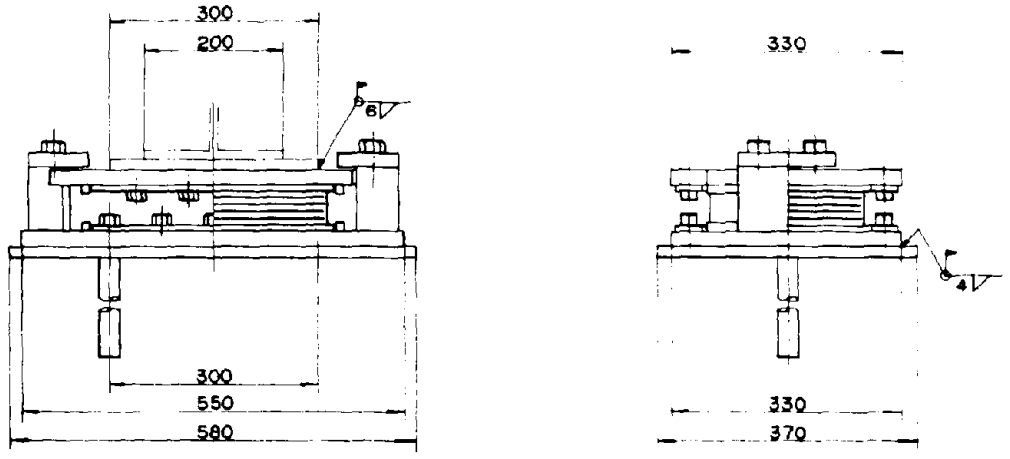

Fig. 7 Laminated rubber-type bearing used at the Senkawa Viaducts

Photo 1 Senkawa viaducts

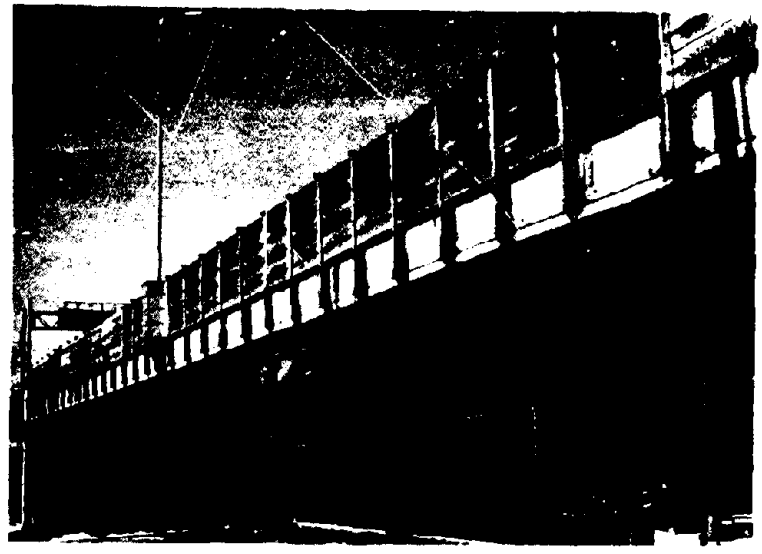

Photo 2 Bearings being renewed at site

Photo 3 Bearings assembled at yard

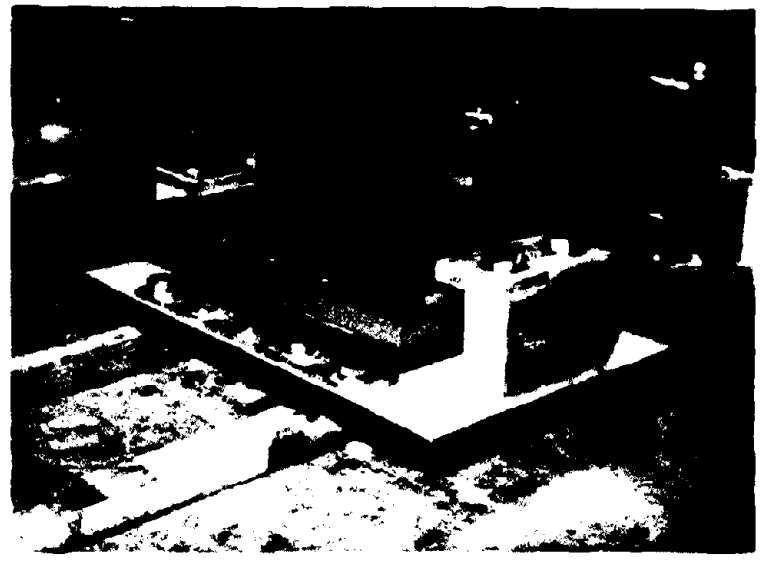

height but were made by the lateral force distribution method, with reference to the "Manuals for Menshin Design for Highway Bridges (draft)."

Both movable and fixed existing bearings were line bearings. Jacking up was performed on both movable and fixed sides of one pier at the same time, and the existing bearings were replaced with laminated rubber bearings for lateral force distribution.

Photo 1 shows a part of the viaduct, Photo 2 shows the bearing being renewed at site. A schematic view of the viaducts is shown in Fig. 6.

Design conditions of bridge:

Bridge grade: first class bridge
Width: 8.5m x 2
Span length: 6 x 16.5m
Skew angle: 90°
Bridge type: 6-continuous composite H-type bridge
Design load: TL-20
Temperature change: ±30°C
Design lateral force coefficient: 0.25

Design of laminated rubber type bearing for lateral force distribution

Since the bearings were designed by the lateral force distribution method, reduction in seismic forces was not considered. Actually, however, reduction in seismic forces can be expected because high-damping rubber is used.

The bearing has a simple construction in which steel plates are arranged over and under the high-damping rubber. A total of 112 sets of bearings were produced.

Table 5 gives the design conditions for the bearings, Fig. 7 shows their construction, and Photo 3 shows the bearing assembly.

PROPERTIES TESTS OF HIGH-DAMPING RUBBER BEARING

Outline of test

Twenty high-damping rubber bearings were produced along with the large lot of bearings for the Senkawa Viaducts. These were subjected to lateral loading, endurance, and low rate loading tests to determine whether the physical properties obtained in small experimental lots can be reproduced. The facilities for refining and rolling rubber sometimes differs between small experimental lots and large mass-production lots. In this case, a difference in the physical properties due to a simple difference in the mixing conditions of the rubber was postulated. The tests were carried out to confirm this and, at the same time, to investigate variations in physical properties, which could not be investigated during the development stage. The high-damping rubber used was developed under the Joint Research Program between PWRI (Public Works Research Institute, the Ministry of Construction) and 28 private firms. Its basic physical properties are given in Table 6. Figure 8 and Photo 4 show the shape of the model, and Photo 5 shows the status of the tests. The experimental results obtained were almost as expected, and the physical properties obtained at the development stage were reproduced. Details of the tests are described below.

Test method

(1) Lateral loading test

A lateral loading test was used to investigate the variations in shear stiffness. Table 7 gives the test conditions. The effective stiffness (shear modulus) and the effective damping ratio were determined from the relationship between the lateral reaction and lateral displacement. The test was performed under the two conditions of ±50% and ±100% shear strain because of the capacity of the testing machine.

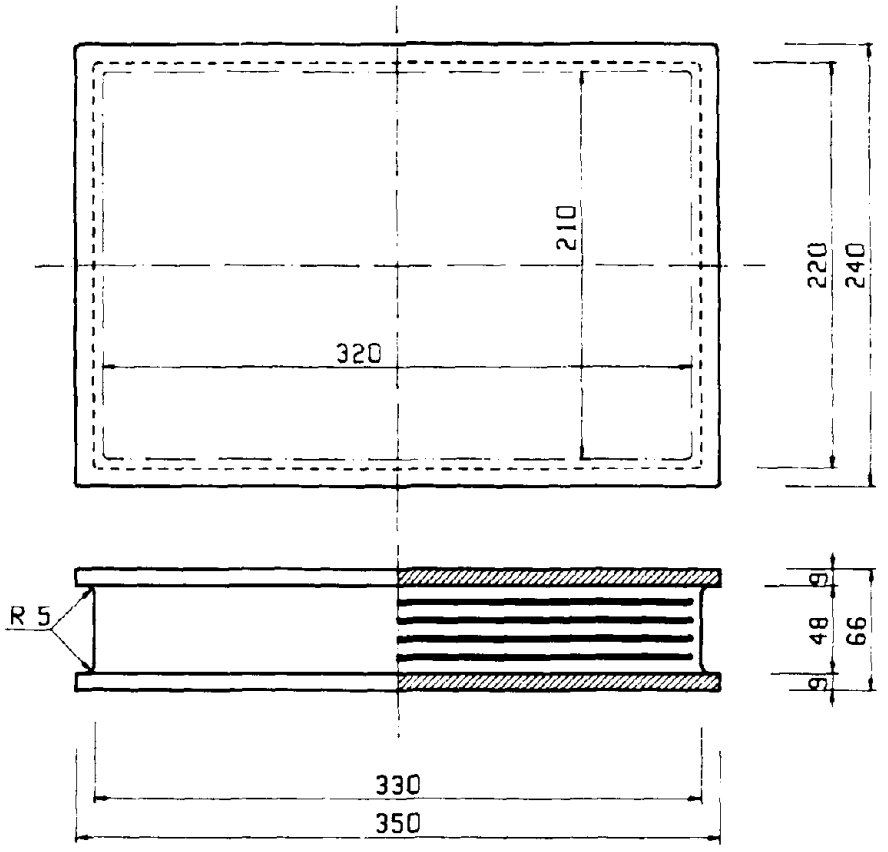

Rubber Layer 8 mm X 5 = 40 mm
Steel Plate 2 mm X 4 = 8 mm

Fig.8 Full scale model of laminated high damping rubber(HDR) for properties tests

Photo 4 A model of laminated high damping rubber(HDR)

(2) Endurance test

Fifty-cycle endurance tests were performed at ±100% shear strain on four models to investigate the change of shear stiffness and the presence of flaws. The "Manuals for Menshin Design for Highway Bridges (draft)" states that the test should be performed at ±150% shear strain. However, the test was actually performed at ±100% shear strain because of the capacity of the testing machine. The detailed test conditions are given in Table 7.

(3) Low rate loading test

A slow loading test was carried out on two models in accordance with the extrapolation method in the "Manuals for Menshin Design for Highway Bridges (draft)." The loading test of ±50% shear strain was performed under four vibration frequencies in the range of 0.001Hz to 0.5Hz. The relationship between strain velocity and shear modulus was determined, and the normal slow-speed physical properties were estimated by extrapolation from this relationship. The detailed test conditions are given in Table 7.

Test results

(1) Lateral loading test

(a) Figs. 9 shows an example of the hysteresis curves obtained from 10 cycles of continuous loading at ±50% and ±100% shear strain, respectively. The shear stiffness tends to decrease due to cyclic loading but is stable after the third cycle.

(b) Table 8 gives a comparison of the effective stiffness and the effective damping ratio determined from the third-wave hysteresis curve to the target value determined from experimental results obtained by the joint research carried out by PWRI and the private firms. This table indicates that the results obtained were nearly as expected. Fig. 10,11 shows the frequency distribution of 20 characteristic physical properties.

(c) Summary

This test confirmed that the shear stiffness of the high-damping rubber bearing used in the actual bridges is in good agreement with the characteristic physical properties obtained during the development stage. The range of spring constant variations is slightly high, being ±8% when the mean value was set to be 1.0. We hope to reduce this value to ±5%.

(2) Endurance test

(a) Fifty cycles of continuous loading were applied at ±100% shear strain, and no abnormality was found on the model. An example hysteresis curve in this test is shown in Fig. 12.

(b) Fig. 13,14 shows the relationship between the number of cycles and the shear modulus and damping ratio obtained from the hysteresis curve.

(c) Summary

The shear modulus and damping ratio tend to gradually decrease with increasing numbers of cycles. Taking the mean value at four to ten cycles as 1, the decreasing ratios of the shear modulus and damping ratio at the fiftieth cycle are 0.92 and 0.90, respectively. This is in good agreement with the value obtained in the development stage. The tests confirmed that even if 50 cycles of continuous loading are applied, no abnormality is found on the model.

(3) Low rate loading test

Table 6 Summary of physical properties of HDR

Tensile strength	210kgf/cm²
Elongation	680%
Tensile stress at 100% strain	20.0kgf/cm²
Hardness(IRHD)	68

Table 7 Testing method for laminated high damping rubber bearings used at the Senkawa viaducts

	Lateral loading test	Endurance test	Low rate loading test
Specimens	No.1 ~ 20	No.1 ~ 4	No.1 ~ 2
Axial load	20.2 tf	20.2 tf	20.2 tf
Shear strain	± 50%, ± 100%	± 100 %	± 50 %
Frequency(Hz)	0.5	0.5	0.001, 0.01, 0.1, 0.5
Loading cycle	Each 10 cycles	50 cycles	Each 3 cycles
Temperature	20℃	20℃	20℃

Teble 8 Results of lateral loading test

		Shear strain 50%		Shear strain 100%	
		Effective stiffness keq	Effective damping ratio heq	Effective stiffness keq	Effective damping ratio heq
Target		2505 Kgf/cm	16.4%	1800Kgf/cm	14.0%
Actual	Average	2436.9(0.97)	16.6(1.01)	1777.0(0.99)	13.9(0.99)
	Range	2274.6~2618.0 (0.91~1.05)	16.3~16.9 (0.99~1.03)	1629.8~1919.9 (0.91~1.07)	13.5~14.5 (0.96~1.04)

Notes 1. Target is determined by proto-type test

2. ( ) expresses [Actual/Target]

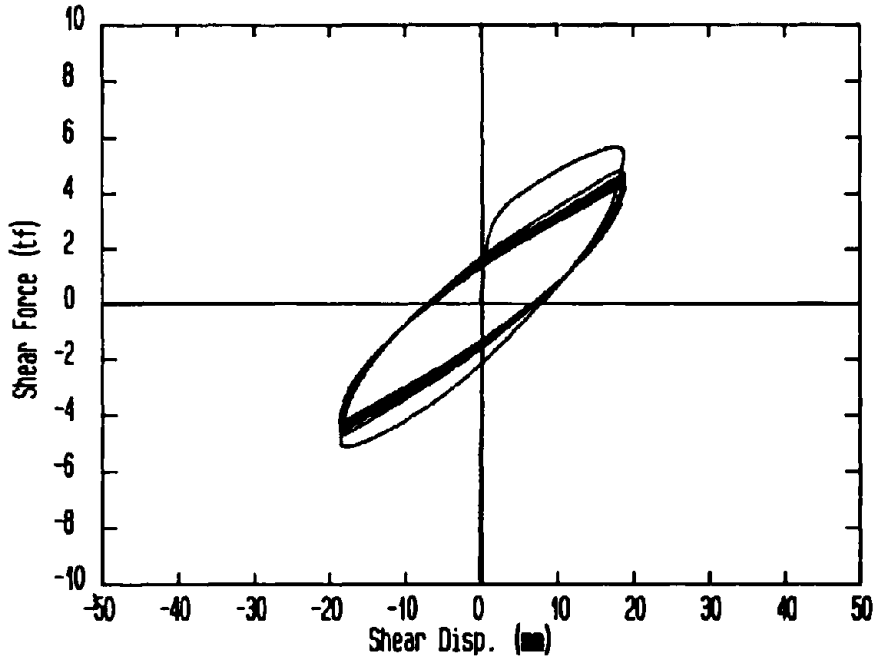

(a) Shear strain 50%

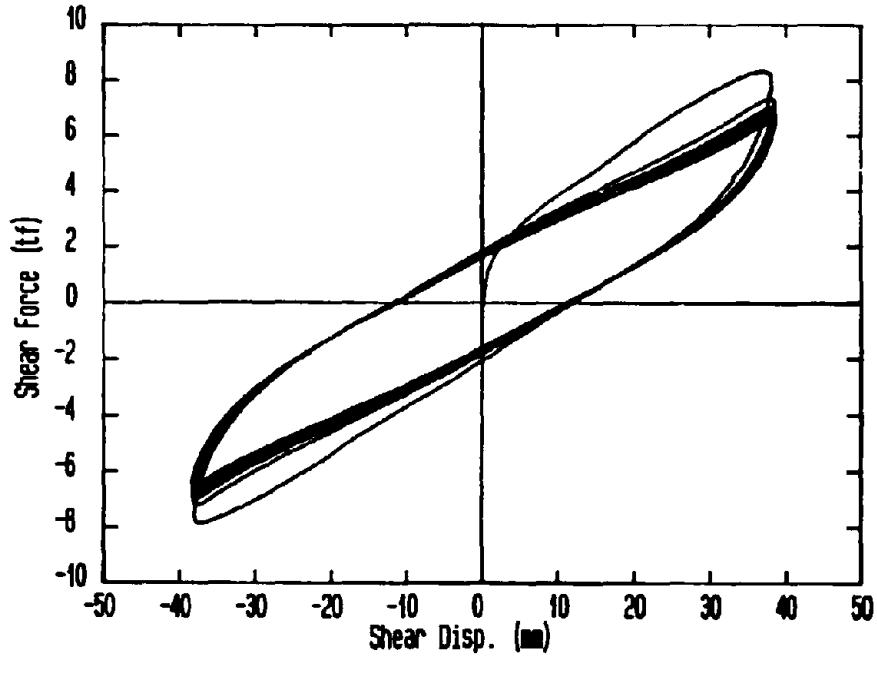

(b) Shear strain 100%

Fig. 9 Hysteresis curves of HDR

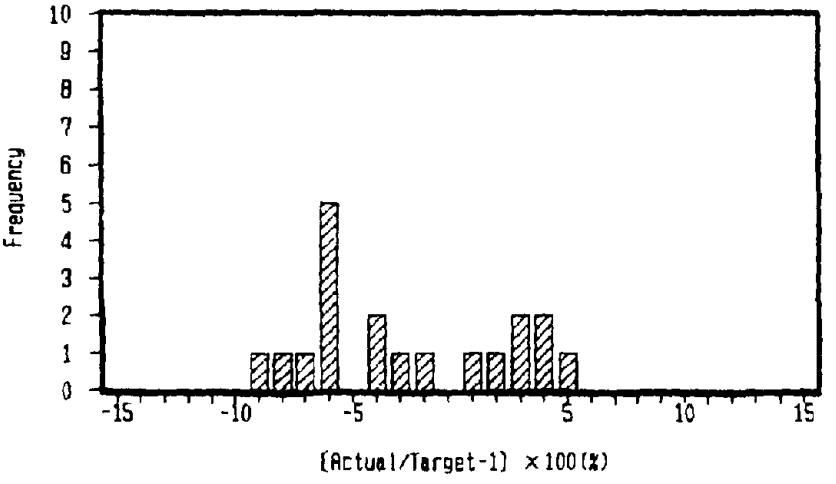

(a) Effective stiffness

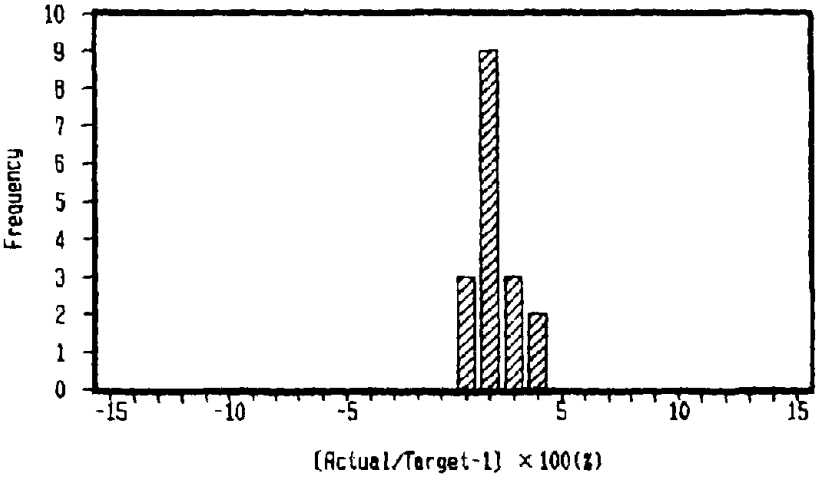

(b) Effective damping ratio

Fig.10 Frequency distribution of HDR at shear strain 50%

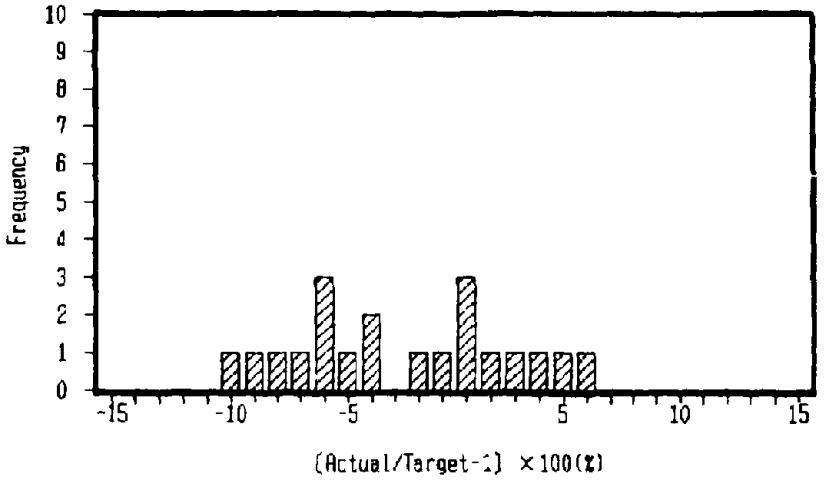

(a) Effective stiffness

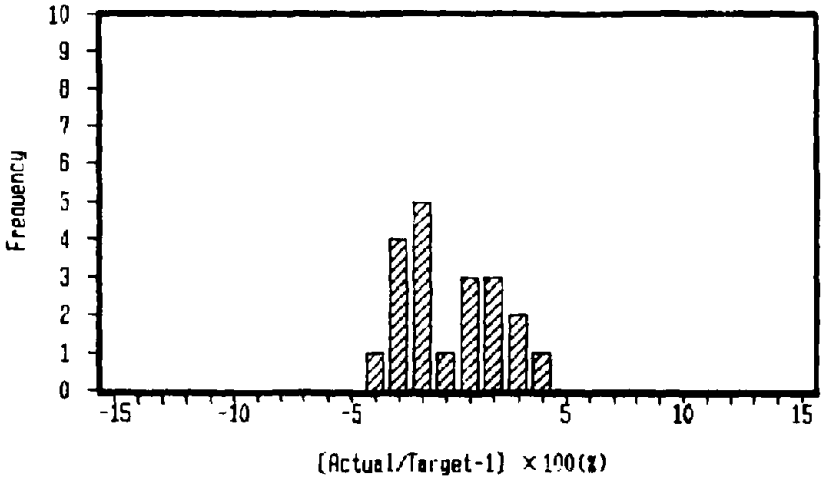

(b) Effective damping ratio

Fig. 11 Frequency distribution of HDR at shear strain 100%

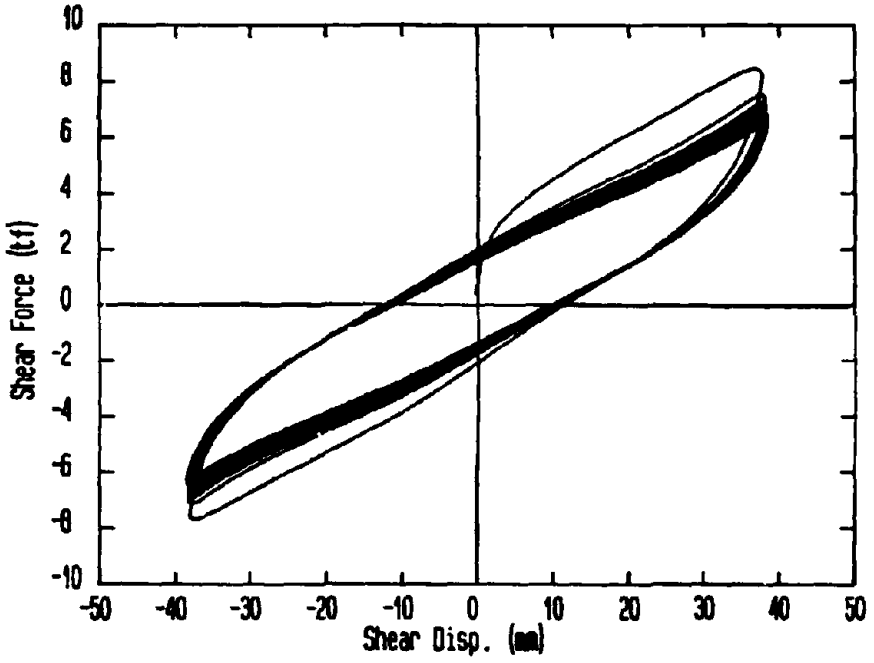

Fig. 12 Hysteresis curves of HDR by endurance test, 50 cyclic loadings

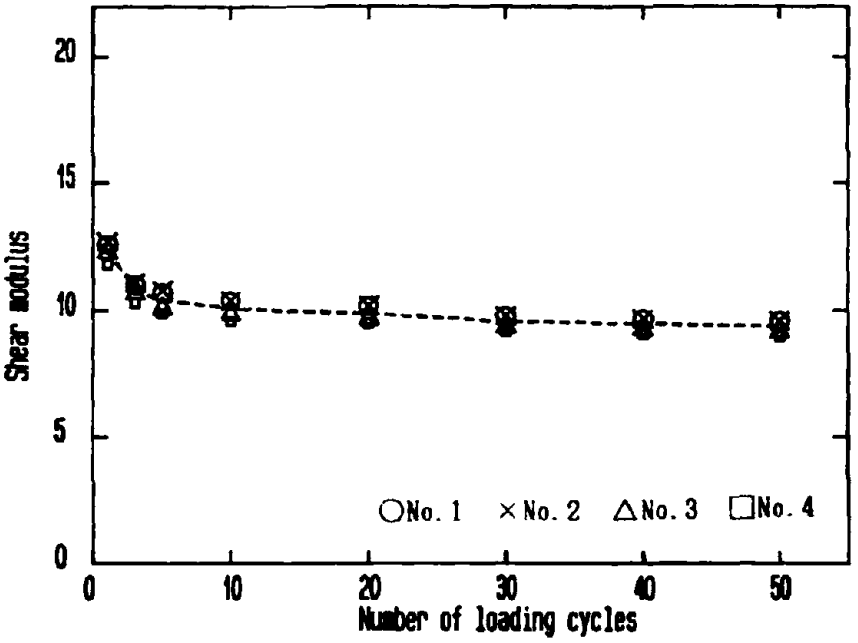

Fig. 13 Behavior of shear modulus of HDR by endurnce test

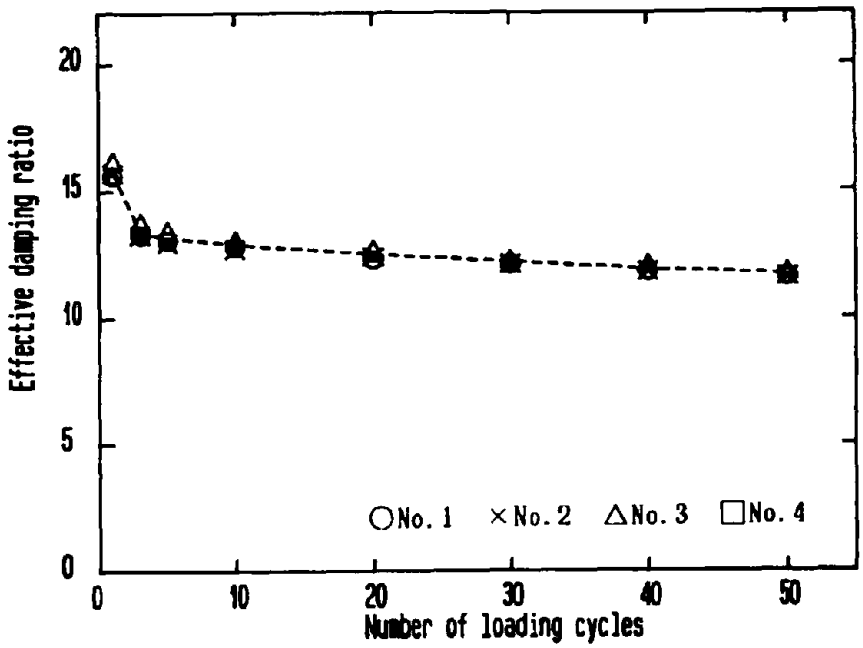

Fig. 14 Behavior of effective damping ratio of HDR by endurance test

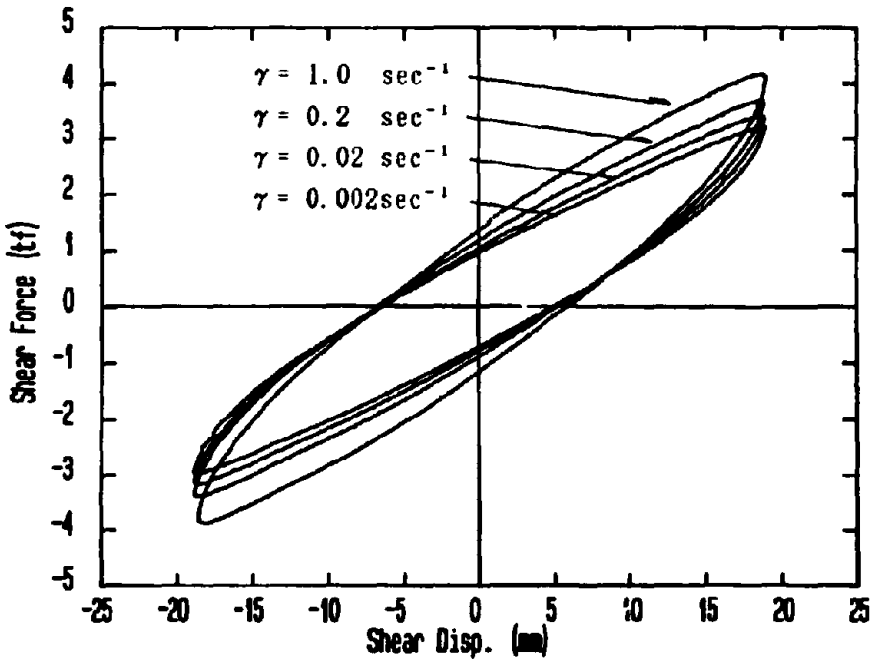

Fig 15. Hysteresis curves of HDR by low rate loading test

with displacement amplitude of 50% shear strain

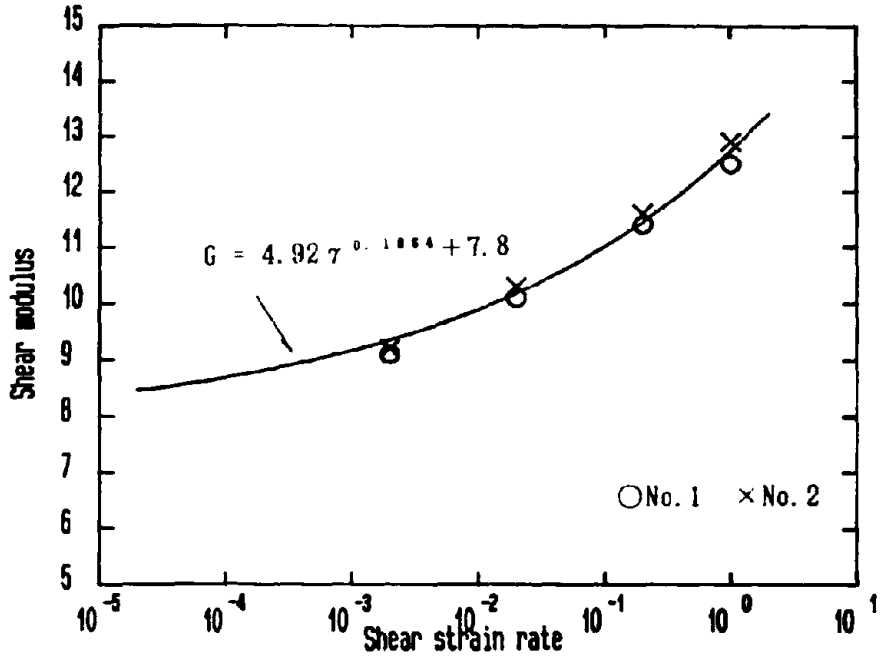

Fig. 16 Shear strain rate dependence of shear modulus of HDR evaluated by extrapolation method

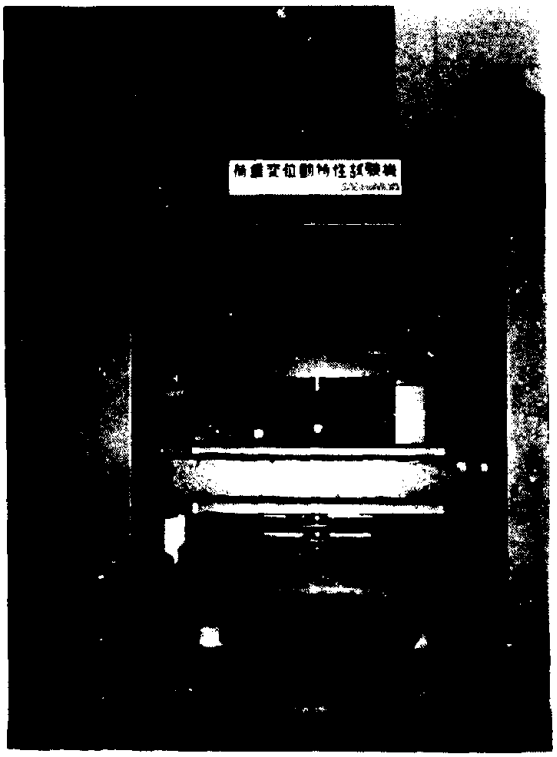

Photo 5 Testing rig

(a) Fig. 15 shows an example hysteresis curve obtained when the vibration frequency at ±50% shear strain is changed.

(b) Fig. 16 shows the relationship between the strain velocity and the shear modulus obtained from the hysteresis curve of the third cycle.

(c) Summary

As was found during development, the shear modulus tends to decrease as the frequency decreases. The decreasing ratio is also in good agreement with the value obtained in the development stage. The relationship between shear modulus Gs and strain velocity $\dot{\gamma}$ is expressed by Eq. (4).

$$Gs = 4.92\dot{\gamma}^{0.1864} + 7.8 \quad (4)$$

Thus, Gs of 8.5kgf/cm^2 can be obtained by extrapolating the static physical properties at a normal strain rate of 2.3 x 10^{-5}/sec (= 50%/6 hours). This shear modulus is about 40% lower than that for a strain velocity of 3sec (= 150%/(1/4sec)) during an earthquake. This value is in good agreement with the value obtained in the development stage.

The results of the lateral loading test on the high-damping rubber bearing confirmed that the bearings produced in a high volume lot provide almost the same performance as those produced in a small experimental lot.

CONCLUSIONS

(1) Recent bridges reflect a change from simple girders to multi-span continuous girders. The reasons for this change are 1) improvement in the running property, 2) reduction in noise and vibration, and 3) improvement in maintenance due to jointless construction.

(2) Problems of the multi-span continuous bridge are 1) distribution of seismic forces and 2) large movements due to temperature. The use of bearings designed using part of the Menshin bearing functions for lateral force distribution are effective in solving these problems.

(3) Roller-type bearings for lateral force distribution are suitable for bridges that are subjected to large bearing forces and large movements. On the other hand, laminated rubber-type bearings for lateral force distribution are suitable for medium span bridges because of their simple construction that takes advantage of the properties of the rubber.

(4) Laminated rubber bearings were used for the Senkawa Viaducts connecting work. As a result, their effectiveness was verified.

(5) Property tests of high-damping rubber were carried out. The results confirmed that bearings produced in a high volume lot provide almost the same performance as those produced in a small experimental lot.

ACKNOWLEDGMENTS

The bearing for lateral force distribution developed by NKK Group is an improvement of the roller-type Menshin bearing (R + HDR) developed under the Joint Research Program on "Development of Menshin Systems of Highway Bridges." That program was carried out for three years from 1989 by the Public Works Research Institute (PWRI) and the NKK Group.

The property tests for the high-damping rubber were carried out at the Hiratsuka Plant of the Yokohama Rubber Co., Ltd.

Genial guidance was provided by the personnel concerned with the Senkawa Viaducts connecting work in the Japan Highway Public Corporation, Tokyo No. 3 Operation Bureau, Hachiouji Operation Office, and in Choudai Co., Ltd., a consulting firm. Their guidance is gratefully acknowledged.

REFERENCE

1) Takaku, T., Shimada, M., Tsumura, N., Izuma, S., "Development of Roller-type Bearing for Menshin Bridges," Proceedings from the First U.S.-Japan Workshop on Earthquake Protective Systems for Bridges, Technical Report NCEER-92-0004, Feb. 1992.

2) PWRI and 28 Private Firms:Manual for Menshin Design of Highway Bridges, 1992.

Shaking Table Tests on Base-Isolated Bridge with Sliding System

Maria Q. Feng
Assistant Professor
Department of Civil Engineering
University of California, Irvine
Irvine, CA 92717

Susumu Okamoto
Research Engineer
Earthquake and Wind Engineering Research Group
Technology Research Center, Taisei Corporation
Yokohama, Japan

ABSTRACT

A shaking table test was performed for a model bridge isolated by a sliding system at PWRI (Public Works Research Institute), Ministry of Construction, Japan, under the joint research project between NCEER (National Center for Earthquake Engineering Research) and PWRI. This paper describes the results of experimental testing and related numerical studies both for the tested model bridge and an actual bride. The model bridge used for the shaking table test has flexible piers and was previously used for testing the base isolation performance of lead rubber bearings (LRB) and high damping rubber bearings (HDR). A numerical model that can be efficiently used for the analysis and numerical simulation of the seismic response of the bridge isolated by a sliding system is proposed and utilized. The shaking table testing and numerical simulation study demonstrate the effectiveness of the sliding isolation system for protecting bridges with flexible piers from earthquakes, especially large earthquakes.

INTRODUCTION

A shaking table test of a bridge model, designed by the Japanese standard specification for bridges, was conducted at PWRI, Japan, in the Fall of 1993. The sliding isolation system used here is composed of sliding bearings with relatively high friction coefficient (20% in high velocity range) and rubber restoring force devices. The same bridge model, also with the same flexible piers, was previously used for the shaking table test of the isolation systems with LRB and HDR[1]. Several earthquake records and design earthquakes with different intensities and frequency contents were used as input motions in the test. Unfortunately it was not possible to use the input motions with large intensities due to the displacement limitation of the shaking table. Therefore the behavior of the bridges under such large intensity earthquakes was analyzed by numerical simulation. Such numerical simulation makes use of the dynamic characteristics of the sliding system identified by an identification test performed prior to the shaking table test and confirmed by the shaking table test carried out at the level of earthquake intensity that the table was able to tolerate.

To be able to numerically simulate with satisfactory accuracy the response of actual bridges equipped with sliding isolation systems is also important for the design of bridges with such isolation systems. In this respect, M. Constantinou proposed an analytical procedure using Y.K. Wen's model[2]. The model provides a convenient analytical tool to solve relatively simple problems. However, for the design of more complicated bridges such as a continuous bridge supported by multiple piers with sliding systems, a simpler model is much more preferable for computational ease. For this purpose, a simple numerical model based on the direct integration method is proposed and utilized throughout this paper. The model is idealized in terms of an explicit mathematical expression[3], instead of the usual algorithm that describes the stick-slip model of sliding. The accuracy of the numerical procedure is confirmed by the comparison of results between the shaking table test and the numerical simulation performed on the bridge model.

The effectiveness of the sliding isolation system is demonstrated here not only by the shaking table test but also by means of numerical simulation performed on the model bridge as well as on an actual bridge.

SHAKING TABLE TEST

Experimental Setup

A simple girder bridge model with two flexible piers was used in this test as shown in Fig.1. The bridge span, the pier height, and the deck weight are 6.0m, 2.5m, and 390 kN respectively. The fundamental natural period of the bridge is 0.48 seconds when the girder is supported by piers through a fixed bearing on one end and a roller bearing on the other.

The sliding type isolation system developed by NCEER[3] is used in this test. Two sliding bearings and a rubber restoring device were installed on each pier with the rubber device located in the middle of two sliding bearings. In total, therefore, four sliding bearings and two rubber restoring devices were used for the model.

As shown in Fig. 2, the sliding bearing consists of a stainless steel plate attached to the deck and a circular Teflon plate (diameter = 10 cm) fixed on the pier through a bearing plate. The bearing plate has a semi-spherical surface which can rotate freely from the pier deformation to keep the Teflon plate in horizontal and in perfect contact with the steel plate. A load cell is installed between the bearing and the pier to measure the vertical load on the bearing. The pressure on the sliding surface of the Teflon plate is evaluated as 12.4 MPa.

Figure 3 shows a typical relationship between the friction coefficient and the sliding displacement observed during an parameter identification test carried out prior to the shaking test. Figure 4 illustrates the relationship between the friction coefficient and the sliding velocity during the shaking table test using the Kaihoku earthquake record. The friction coefficient increases as the sliding velocity increases. The solid line in the figure indicates the approximation formula proposed by M. Constantinou et al[3]. The average friction coefficient at low velocity range and high velocity range of the bearing were found to be 8% and 20% respectively.

Figure 5 depicts the rubber restoring force device, which consists of a rubber block and an anchor bar. Figure 6 indicates the force-displacement relationship of the rubber restoring force device obtained from the identification test. The device works as a horizontal spring within a small displacement range, and serves as a displacement restrainer when the displacement approaches a certain limit. However, the device did not reach the limiting displacement during the present shaking table test. The natural period

evaluated from the weight of the deck (390 kN) and the stiffness of the device (1.32 kN/cm) is 2.44 seconds.

Two earthquake records (Kaihoku and Hachirougata) and two artificial design motions (Japanese Level 1 and level 2 earthquake motions on ground condition II - stiff soil) were used in the test. As shown in their response spectra in Fig. 7, these motions have different intensities and frequency contents. Due to the limited displacement capacity of the shaking table, however, it was not possible to use the earthquake motions with large intensities for the shaking table test. Therefore, the Hachirougata and Level 2 motions were used after scaling them down linearly by a factor of approximately 1/2 to 1/3 respectively. The shaking was applied only in the longitudinal direction.

Test Results

Table 1 lists the maximum values of the normalized shear force, deck acceleration, bearing displacement and permanent displacement of the model bridge under different earthquake motions. Permanent displacements were observed only under the Kaihoku and Hachirougata motions. Maximum response except for the permanent displacement occurred under the Kaihoku 0.544g input motion. Figure 8 plots a typical set of time histories of various responses and the force-displacement relationship of the isolation system under the Kaihoku 0.544g motion. The maximum deck acceleration is 0.244g which is much smaller than the table acceleration (0.544g) due to the isolation effect. The pier acceleration reaches a maximum value of 1.158g because of the pier reaction to the initiation of sliding, but this does not affect the pier shear force. In fact the corresponding shear force normalized by the deck weight is only 0.254 which is almost equal to the normalized inertia force of the deck. The maximum sliding displacement is 3.43 cm, but the permanent displacement in this case is almost zero. The maximum permanent displacement of 0.379 cm occurred under the Kaihoku 0.184g motion.

Figure 9 shows the maximum values of the pier acceleration, deck acceleration, normalized shear force of the pier, and bearing displacement as functions of the maximum table acceleration. The pier acceleration and bearing displacement become larger as the table acceleration increases. However, the deck acceleration and normalized shear force of the pier remain constants at their respective maximum values beyond the table acceleration of 0.2g, regardless of the increase of table acceleration. This is the unique and significant advantage of the sliding base isolation system as applied to bridges. The maximum deck acceleration is 0.22g corresponding to the friction force plus the restoring force.

SIMULATION OF SHAKING TABLE TESTS

Analytical Model

The analytical model depicted in Fig. 10 is used to simulate the shaking table test. The discontinuous function $sgn(\dot{u}_d)$ in the governing equations of motion (1) and (2) is replaced by the analytical expression (3)[4] for approximation,

$$m_d(\ddot{z} + \ddot{u}_p + \ddot{u}_d) + c_d\dot{u}_d + k_d u_d = -sgn(\dot{u}_d)\mu m_d g \quad (1)$$

$$m_p(\ddot{z} + \ddot{u}_p) + c_p\dot{u}_p + k_p u_p - c_d\dot{u}_d - k_d u_d = sgn(\dot{u}_d)\mu m_d g \quad (2)$$

where $\ddot{z}$ is the ground acceleration (table acceleration), u_p is the displacement of pier relative to ground, u_d is the displacement of deck relative to pier (bearing displacement), and μ is the friction coefficient.

$$sgn(\dot{u}_d) = \frac{1 - \exp(-\delta \dot{u}_d)}{1 + \exp(-\delta \dot{u}_d)} \tag{3}$$

where δ is a parameter to define the shape of the function $sgn(\dot{u}_d)$ in approximation (4.0 sec/cm is used in this analysis).

The friction coefficient μ is evaluated in Eq. (4) as a function of the sliding velocity $\dot{u}_d$.

$$\mu = \mu_{max} - (\mu_{max} - \mu_{min}) \cdot \exp(-a \cdot |\dot{u}_d|) \tag{4}$$

where a is a parameter defining the relationship between the friction coefficient and sliding velocity as shown in Fig. 4 (0.2 sec/cm in this analysis), μ_{max} is the friction coefficient in low velocity range (8% in this analysis, and μ_{min} is the friction coefficient in high velocity range (20% in this analysis).

Simulation Results

Newmark's β method is used in the dynamic response simulation. Figure 11 compares the time histories obtained from the simulation and the test. These time histories represent sliding displacement and deck acceleration, together with the force-displacement relationship of the isolation system under the Kaihoku and Hachirougata ground motions. In both cases, the simulation and the test produced almost the same peak response values and similar time histories. Table 2 compares these peak response values. It is important to observe that both peak deck acceleration and peak bearing displacement are very similar, since this means that the proposed analytical model represented by Eqs. (1) - (4) can be reliably used in evaluating the maximum values of the key response quantities, thus it is useful in the design procedure of bridges with sliding isolation systems.

SIMULATION OF ACTUAL BRIDGE

Bridge Model

Response of bridges to large earthquakes are analyzed through the numerical simulation. The Miyagawa bridge is the first isolated bridge in Japan. This bridge is base-isolated with LRB and is chosen for this study. The simulated response of this bridge hypothetically equipped with the sliding system is compared with that of the same bridge as isolated by LRB. For this numerical simulation, the characteristics of LRB are evaluated from the available experimental data[5]. On the other hand, the characteristics of the sliding system are so assumed that they produce a large isolation effect with a limited bearing displacement under Level 2 motion.

The Miyagawa bridge has two flexible piers and two abutments. Hence, for accurate analysis, two piers should be considered in the analytical model. In the current analysis, however, the one pier model shown in Fig. 10 was used to evaluate the

fundamental characteristics of the bridge under a design earthquake. This simplified model is believed to produce the result with good accuracy.

The characteristics of the pier and the deck are defined based on the data of Miyagawa bridge[5] as follows:

Deck weight	4910 kN
Pier weight	1117 kN
Pier stiffness	1382 kN/cm
Pier damping	2%

The fundamental period when the bearing is fixed is evaluated as 0.41 seconds.

The same Teflon and stainless steel plates as used in the shaking table test are used in the model. The friction coefficient is defined as 8% at low velocity range and 20% at high velocity range. The stiffness of the rubber restoring force device is chosen so as to obtain the natural period of 1.5 seconds after sliding.

Level 1 and Level 2 design motions on ground condition II are used in this analysis. The pier is assumed to be linear in this analysis even for the Level 2 motion.

For comparison, the behavior of the bridge isolated with LRB is also simulated. The post-yielding stiffness of LRB is selected so as to have the natural period of 1.0 second. The yield force normalized by the deck weight is equal to 12%.

Simulation Results

Table 3 and Fig. 12 compare the simulation results for the bridge isolated by sliding bearings with those for the bridge not isolated. For Level 1 motion, the deck acceleration and the deck displacement relative to the ground for the isolated bridge are respectively smaller than those for the bridge not isolated. For Level 2 motion, the deck acceleration for the isolated bridge is smaller than that of the not isolated bridge, but the deck displacement relative to the ground for the isolated bridge is larger than that for the bridge not isolated.

Also, in Table 3 and Fig. 12, comparisons are made between the simulation results for the bridges isolated by sliding bearings and by LRB. For Level 1 motion, the deck acceleration of the bridge with the sliding system is a little larger than that with the LRB system. However, the bearing displacement of the bridge with the sliding system is smaller than that of the bridge with LRB system.

For more intensive Level 2 motion, the situation is reversed: The bearing displacement of the bridge with the sliding system is a little larger than that of the bridge with the LRB system, but more importantly, the deck acceleration of the bridge isolated by the sliding system is 80% of that isolated by LRB.

Additional analysis including the comparison of the isolation performance between the sliding system and HDR system is currently under way and its results will be published as they become available.

CONCLUSIONS

A shaking table test and analytical study of bridges with sliding isolation systems have been performed. The following observations are made.

1) The deck acceleration of the bridge isolated by the sliding system is limited to a constant value regardless of input acceleration, even when the deck is supported by flexible piers.
2) An analytical method based on the direct integration procedure using the continuous mathematical formula representing sliding behavior is proposed and utilized. The accuracy of this procedure is confirmed through the comparison between experimental results and analytical simulation.

3) Numerical simulation of an actual bridge shows better isolation performance in terms of deck response acceleration of the sliding system than that of the LRB system under large earthquakes.

ACKNOWLEDGMENT

The shaking table test was performed at PWRI as a joint research project between NCEER and PWRI under the auspices of the Paneal of Wind and Seismic Effects, US/Japan Natural Resource (UJNR) Program. The authors gratefully acknowledge the support and encouragement of Dr. K. Kawashima and Mr. K Unjou of the Earthquake Engineering Division, PWRI. They also wish to express their gratitude to Professor M. Shinozuka of Princeton University for his guidance and valuable comments. The first author was supported by NSF under Contract BCS-9223234 and NCEER under Contract DTFH61-92-c-00106. The support of NSF Program Director M. P. Singh is acknowledged. The second author expresses his gratitude to Taisei Corporation for its support throughout this study.

REFERENCES

1) Kawashima, K., Hasegawa, K., Nagashima, H., "Experiment and Analysis on Seismic Response of Menshin Bridges", Proceedings from the first U.S.-JAPAN workshop on earthquake protective systems for bridges, pp. 273-298, NCEER-92-0004, 1992.

2) Mokha, A., Constantinou, M., and Reinhorn, A., "Teflon Bearing In Aseismic Base Isolation: Experimental Studies and Mathematical Modeling", Technical Report NCEER-88-0038, December 5, 1988.

3) Okamoto, S., Constantinou, M., Tsopelas, P., Fujii, S., Osaka, D., "Shake Table Test of A Model Bridge with Sliding Isolation System", Proceedings of the second U.S.-JAPAN workshop on earthquake protective systems for bridges, pp. 89-112, Technical Memorandum of PWRI No. 3196, 1992.

4) Feng, Q., Shinozuka, M., Fujii, S., Fujita, T., "A Hybrid sliding isolation system for bridges", Proceedings from the first U.S.-JAPAN workshop on earthquake protective systems for bridges, pp. 323-336, NCEER-92-0004, 1992.

5) Matsuo, Y., Hara, K., "Design And Construction of Miyagawa Bridge (First Menshin Bridge in Japan)", Proceedings from the first U.S.-JAPAN workshop on earthquake protective systems for bridges, pp. 389-405, NCEER-92-0004, 1992.

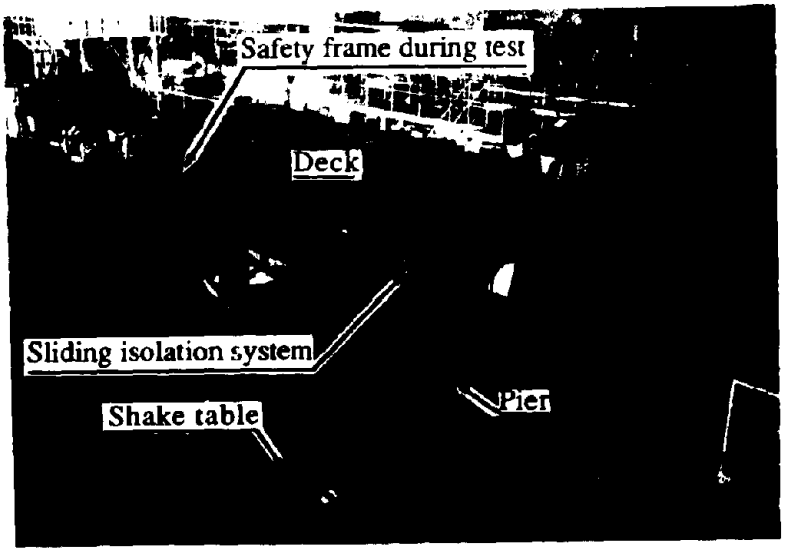

Figure 1 Bridge model

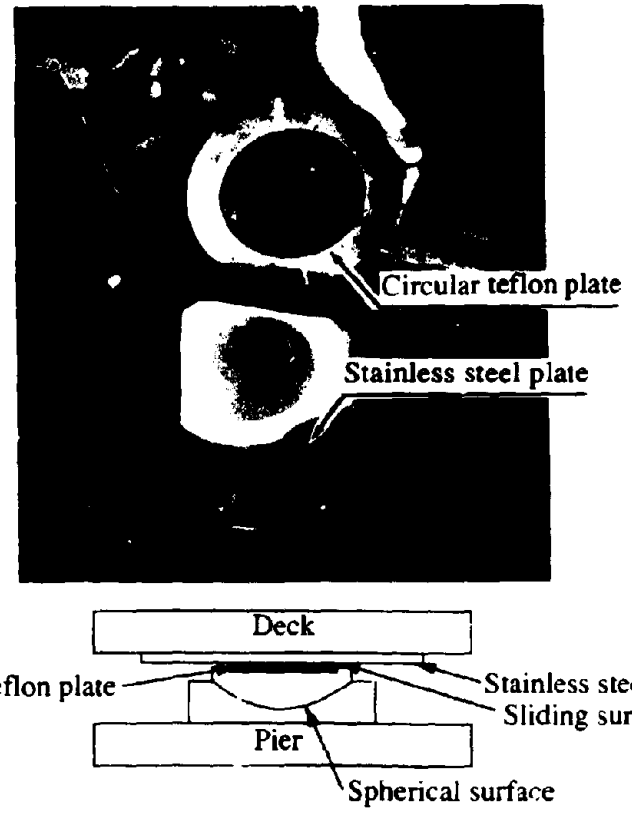

Figure 2 Detail of sliding bearing

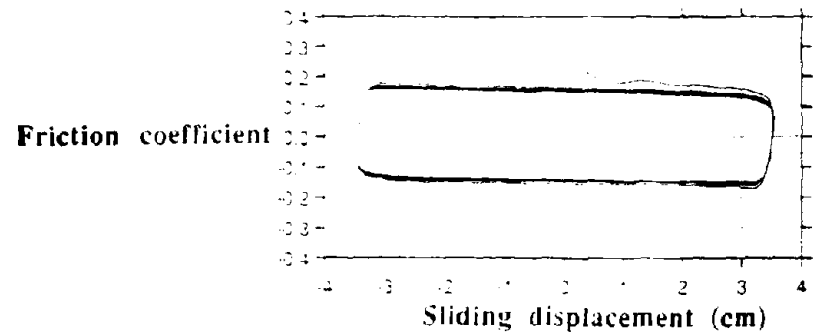

Figure 3 Example of identification test
(Maximum sliding velocity : 20cm/sec)

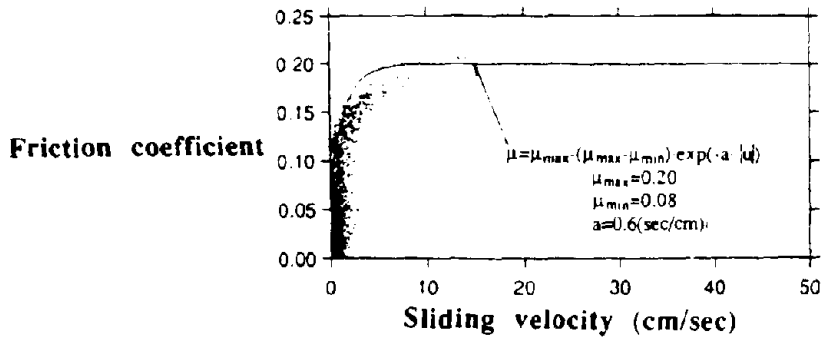

Figure 4 Realtionship between sliding velocity and friction coefficient

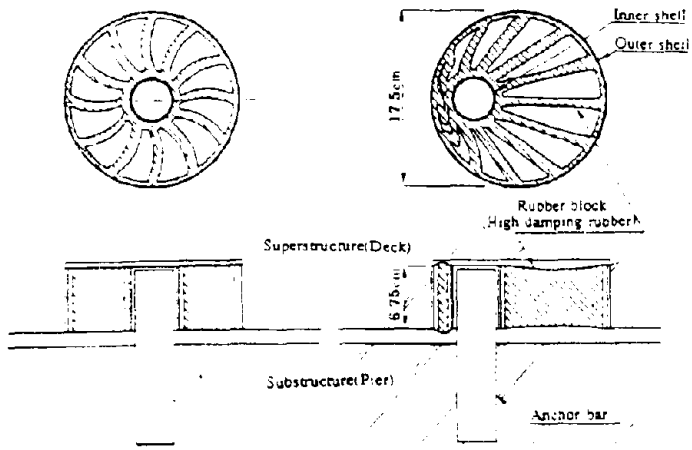

Numbers in this figure indicate size of rubber restoring force device used in the test

(a) Configuration of rubber device (b) Deformed rubber device

Figure 5 Rubber restoring force device

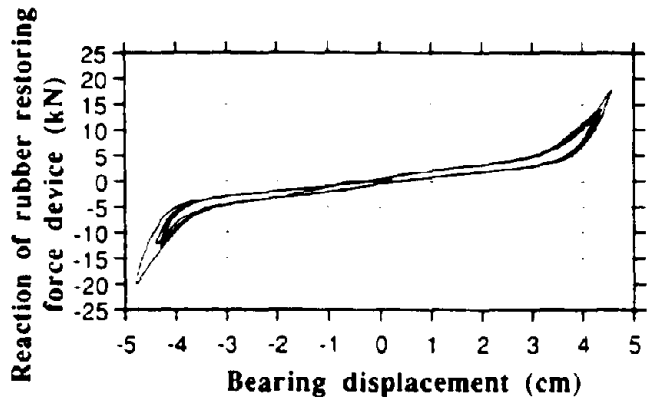

Figure 6 Force displacement relationship of rubber restoring force device

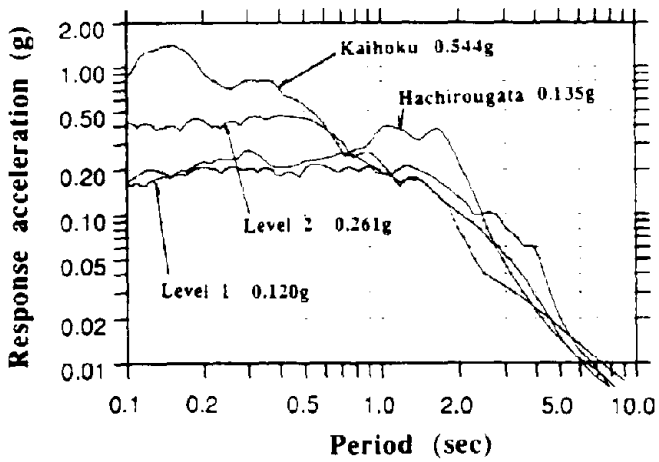

Figure 7 Resoponse spectra of input motions

Table 1 Maximum responses of model bridge during shake table test

Input Motion	Table Acceleration (g)	Normalized Shear Force	Deck Acceleration (g)	Bearing Displacement (cm)	Permanent Displacement (cm)
Kaihoku	0.087	0.116	0.126	0.120	0.077
	0.184	0.208	0.203	0.546	0.379
	0.183	0.178	0.190	0.600	0.242
	0.255	0.230	0.217	1.041	0.150
	0.250	0.207	0.212	0.970	0.044
	0.432	0.254	0.220	2.636	0.214
	0.428	0.245	0.216	2.741	0.060
	0.426	0.254	0.217	2.780	0.055
	0.489	0.247	0.218	3.027	0.091
	0.543	0.248	0.220	3.341	0.065
	0.544	0.254	0.224	3.425	0.003
Hachirougata	0.043	0.056	0.065	0.040	0.008
	0.084	0.120	0.130	0.095	0.006
	0.115	0.156	0.161	0.241	0.036
	0.135	0.181	0.181	0.487	0.105
Level 1 Ground Condition II	0.078	0.152	0.158	0.151	—
	0.121	0.185	0.187	0.345	—
	0.120	0.152	0.166	0.338	—
Level 2 Ground Condition II	0.180	0.215	0.206	1.035	—
	0.270	0.231	0.207	1.326	—
	0.265	0.223	0.216	1.286	—
	0.261	0.222	0.214	1.502	—

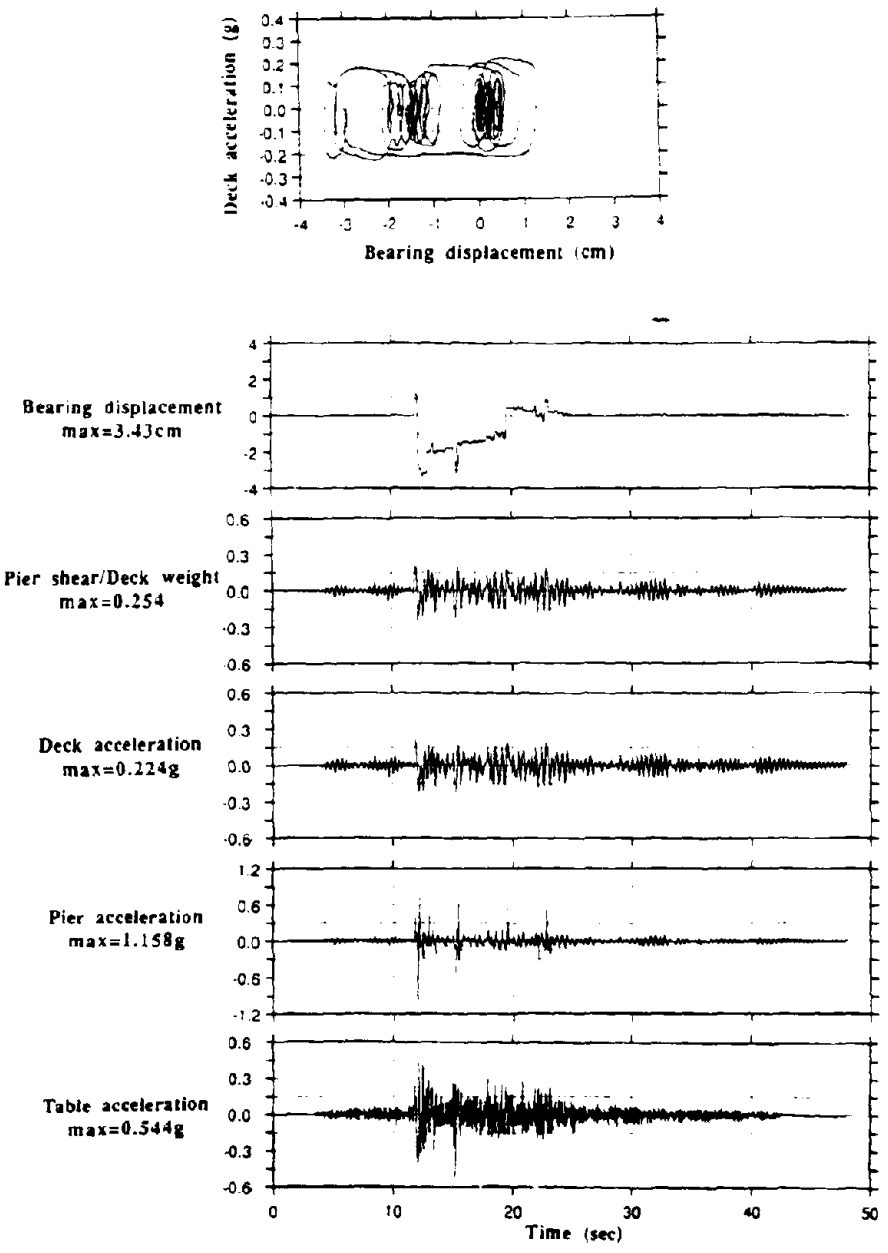

Figure 8 Response of base-isolated bridge with sliding system (Input motion : Kaihoku 0.544g)

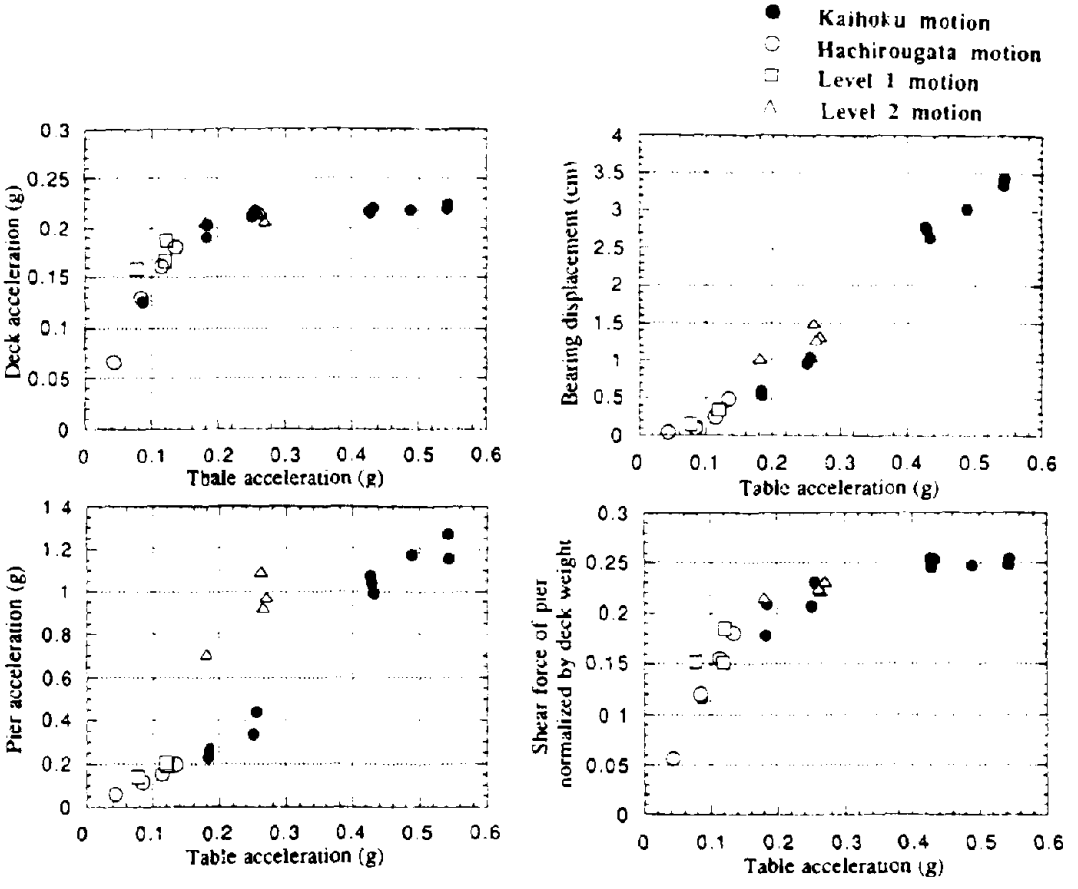

Figure 9 Maximum response of model bridge

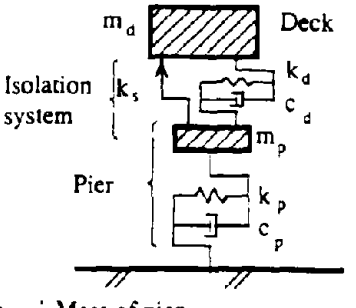

m_p : Mass of pier
m_d : Mass of deck
k_p : Linear spring of pier
k_d : Linear spring of isolation system
c_p : Dashpot of pier
c_d : Dashpot of isolation system
k_s : Non-linear spring of the sliding bearing

Figure 10 Simulation model

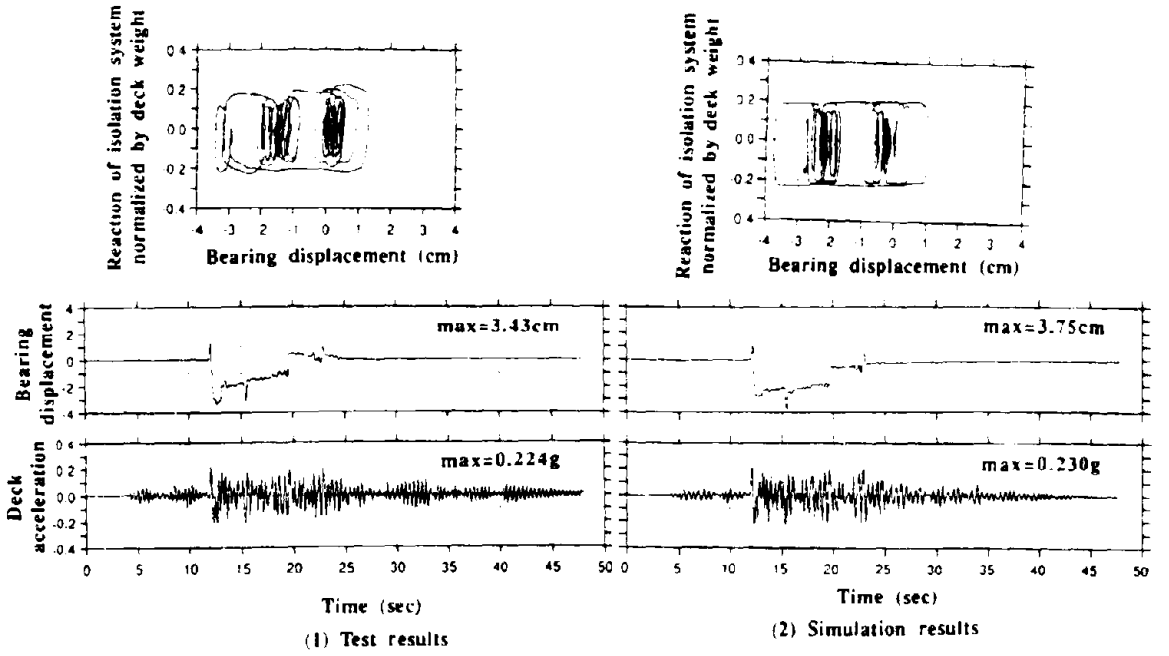

(a) Input motion : Kaihoku 0.544g

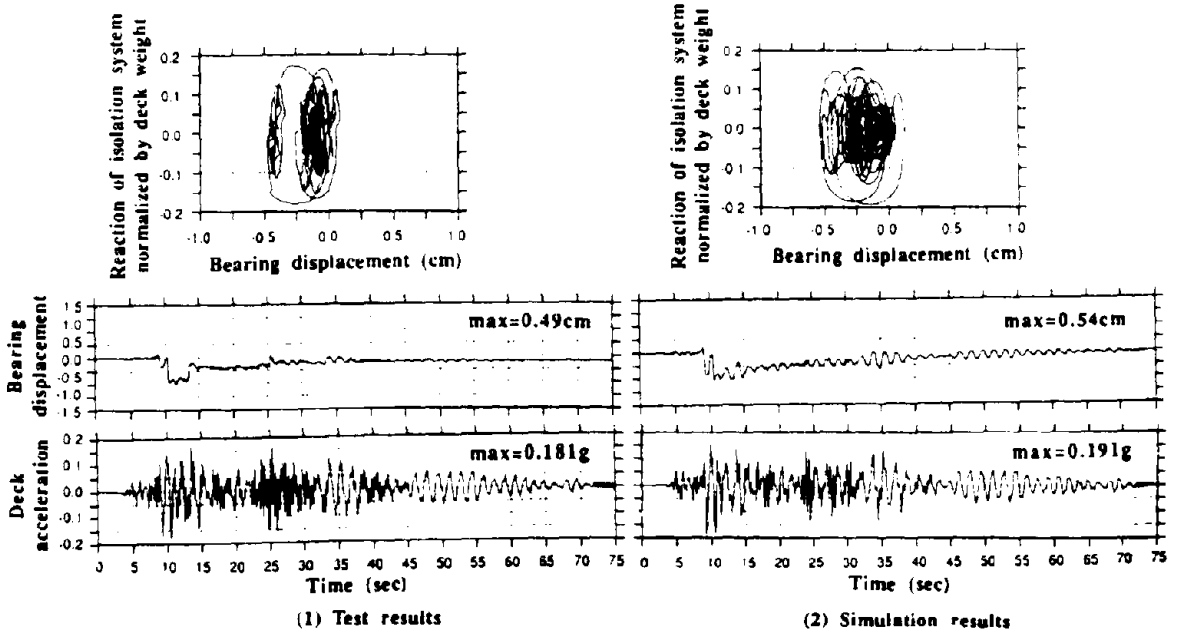

(b) Input motion : Hachirougata 0.135g

Figure 11 Results of simulation

Table 2 Comparison of simulation results with test results

Input Motion	Table Acceleration (g)	Deck Acceleration (g)			Bearing Displacement (cm)		
		Test Results	Simulation Results	Simulation / Test	Test Results	Simulation Results	Simulation / Test
Kaihoku	0.087	0.126	0.116	0.92	0.120	0.057	0.48
	0.184	0.203	0.202	0.99	0.546	0.389	0.71
	0.183	0.190	0.202	1.06	0.600	0.392	0.65
	0.255	0.217	0.210	0.97	1.041	1.086	1.04
	0.250	0.212	0.210	0.99	0.970	1.083	1.12
	0.432	0.220	0.221	1.00	2.636	2.782	1.06
	0.428	0.216	0.221	1.02	2.741	2.801	1.02
	0.426	0.217	0.221	1.02	2.780	2.777	1.00
	0.489	0.218	0.226	1.03	3.027	3.311	1.09
	0.543	0.220	0.230	1.05	3.341	3.733	1.12
	0.544	0.224	0.230	1.02	3.425	3.754	1.10
Hachirougata	0.043	0.065	0.064	0.98	0.040	0.051	1.28
	0.084	0.130	0.133	1.02	0.095	0.130	1.37
	0.115	0.161	0.165	1.03	0.241	0.249	1.03
	0.135	0.181	0.191	1.06	0.487	0.544	1.12
Level 1 Ground Condition II	0.078	0.158	0.156	0.99	0.151	0.145	0.96
	0.121	0.187	0.202	1.08	0.345	0.450	1.30
	0.120	0.166	0.201	1.21	0.338	0.458	1.36
Level 2 Ground Condition II	0.180	0.206	0.208	1.01	1.035	0.923	0.89
	0.270	0.207	0.211	1.02	1.326	1.546	1.17
	0.265	0.216	0.211	0.98	1.286	1.555	1.21
	0.261	0.214	0.211	0.99	1.502	1.517	1.01
			Average	1.02		Average	1.05

Table 3 Simulation results of actual bridge

Input Motion		Deck Acceleration (g)	Bearing Displacement (cm)	Deck Relative Displacement (cm)
Level 1	Non-Isolated	0.484		2.12
	Sliding System	0.190 (0.393)	0.31	0.92 (0.43)
	LRB	0.184 (0.380)	1.50	2.04 (0.96)
Level 2	Non-Isolated	1.945		8.51
	Sliding System	0.393 (0.202)	10.83	12.36 (1.45)
	LRB	0.505 (0.260)	9.97	11.91 (1.40)

( ) indicates the ratio versus the value of non-isolated bridge

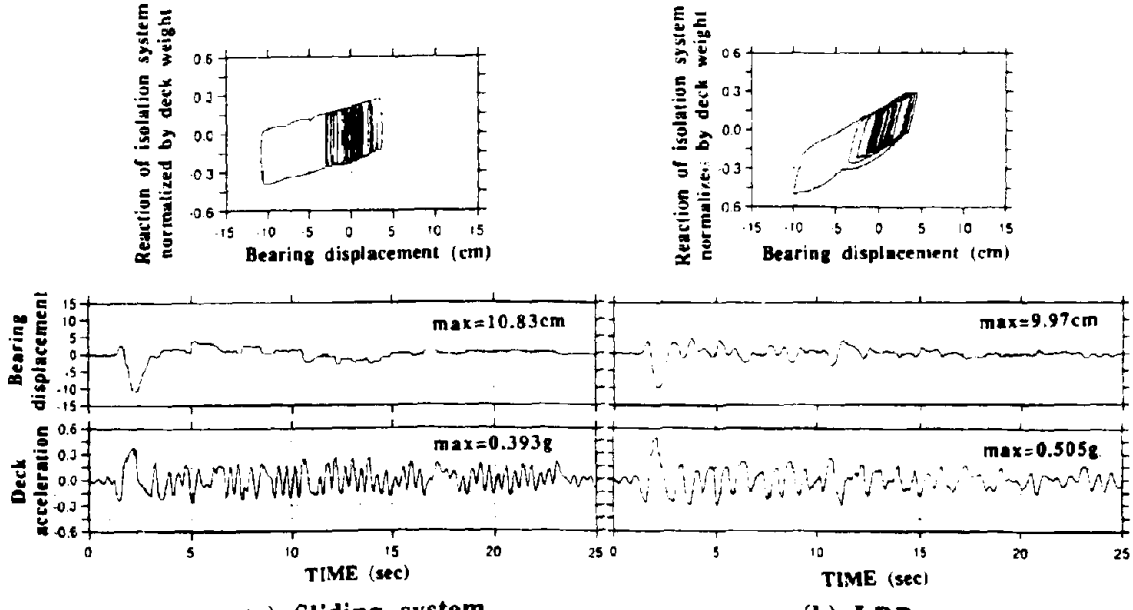

(a) Sliding system (b) LRB

Figure 12 Simulation results of actual bridge (Input motion : Level 2 0.367g)

DEVELOPMENT OF NEW TYPE DAMPER FOR CABLE STAYED BRIDGE

Masahiko KITAZAWA[*1], Jiro ISEKI[*2], and Ikuo SHIMODA[*2]
[*1] Kobe Construction Division, Hanshin Expressway Public Corp. Kobe, Japan
[*2] Technical Div. 2, Oiles Corporation, Tokyo, Japan

ABSTRACT

Presented are development of a new type damper and its application for a long span cable stayed bridge in Japan. Vane type damper was developed and the dynamic characteristics obtained through dynamic loading tests were presented. It was found that the performance of the damper is obtained as demanded, and when applied for a long span cable stayed bridge with a long natural period, the displacement of the bridge caused by earthquake decreases as required.

INTRODUCTION

Among several supporting systems for cable stayed bridge in the longitudinal direction "all free" system, where the main girder is supported by towers via cables, gives the bridge a longer natural period in the longitudinal direction and therefore reduces earthquake forces to the towers and foundations considerably. The longitudinal displacement of girder, however, becomes quite large, which might cause several unfavorable effects to the bridge at the time of an earthquake. Therefore installation of some kind of energy dissipating system is needed.

At the construction of the Higashi-Kobe Bridge with center span of 485m as shown in Fig.1, adopting "all free" system, the vane type damper is developed and installed between girder and piers to sufficiently decrease relative displacement at earthquake.

DEVELOPMENT OF VANE DAMPER

Outline of Vane Damper

Fig. 2 and Photo 1 show a design plan and a view of Vane Damper.

The model is designed so that the maximum damping force be 180tf at the maximum relative velocity of 100cm/sec. Maximum relative displacement of damper is $\pm$90cm. When the damper acts, oil in the drum passes from one compartment to the other through an orifice in the partition, generating the difference of the oil pressure between two compartments in the drum. The

difference of the oil pressure produces the damping force, which is theoretically proportional to the square of oil flow velocity. This means damping force to be proportional to the square of the velocity of motion.

Dynamic Loading Tests on the 1/2-scale Model of Vane Damper

Photo 2 shows the set-up of the dynamic loading tests on the 1/2-scale model.

The tests were conducted with different movement velocities up to 50cm/sec, different displacement up to 25cm and with different orifice sizes. The loading was assumed as harmonic and repeated by 5 cycles for each testing case.

Fig.3 shows the relation between the damping force and movement velocity obtained from dynamic loading tests. It was found that the damping force is controlled as demanded through controlling the orifice size from outside of damper and agree with theoretical value well.

APPLICATION OF THE VANE DAMPER FOR A LONG SPAN CABLE STAYED BRIDGE

Outline of the Higashi-Kobe Bridge

The Higashi-Kobe Bridge is a three-span cable-stayed bridge 885 meters long. Its center span of 485 meters will make it one of the longest cable stayed bridges in the world. It has double decks, the upper and lower roadways having three lanes each. The features of the bridge can be summarize as follows:

- Center span length -- 485m
- Width of bridge -- 13.5m (3 lanes for upper and lower decks)
- Main girder -- 9m high Warren truss with no vertical chords
- Tower -- H-shaped tower with 146.5m high columns and curved cross beams tied at relatively low positions

Seismic Design

The design acceleration response spectrum was provided with a relatively large safety margin in the long period range. This is because the Higashi-Kobe bridge has an unprecedented long natural period of 4.4 sec. in the longitudinal sway mode oscillation. The design spectrum range around the natural period plays a critical role in determining the structure response to earthquake. Fig. 4 shows the design response spectrum determined after several studies.

The design acceleration at 4.4 sec. which corresponds to the natural period of longitudinal oscillation of the bridge becomes 120 gal, which is nearly 1/3 of that in conventional bridges in

Japan. At the design of the damper, an earthquake 1.4 times stronger than that for the seismic design of bridge is assumed. Using the characteristics of the vane damper, non-linear time history earthquake response analysis was conducted using 1.4 times stronger earthquake wave. The results are given in Table 1 and can be summarized as follows.

(1) If an earthquake 1.4 stronger than the design spectrum occurs on the bridge without the dampers (structural damping ratio of 1% is assumed), the displacement of the girder will be 72 × 1.4 = 102 cm. This will be over critical displacement of 74 cm at which the tower may cause buckling.

(2) When dampers are installed, the girder displacement will be reduced to 64 cm, which is in the range of the design displacement of 61 cm. This is below the critical displacement for the tower to buckle. In this case, equivalent damping constant due to the damper is calculated to be approximately 6% based on the displacement response.

Verification of Dynamic Behavior of the Bridge by Shaking Table tests

The appropriateness of the method adopted to evaluate the bridge response to the earthquake and the effectiveness of the damper were confirmed by vibration rests using a three-dimensional 1/100-scale elastic model. The model was made of steel satisfying the similarity of stiffness and weight. The natural frequency and mode shapes of the model in several low modes agreed well with the analytically predicted ones. The structural damping of the model without the damper is adjusted to 1~ 2%, reflecting fairly light damping of a large flexible structure. An electro-magnetic damper is attached to the girder of the model to substitute the vane-type oil damper.

Modified long-period predominant and short-period predominant earthquake recorders were used for input earthquake ground motion. Results are shown in Table 2. All values are converted to the prototype for comparison. Displacement response due to the short period predominant earthquake (El Centro NS, 1940) record is found to be much less than the design values.

Displacement response at the top of the tower due to the long period predominant earthquake motion without the damper is observed to be nearly equal to the design values. However, the energy dissipation of the damper suppressed the response fairly well to the design values. Close agreement of the experimental and numerically calculated results verifies both methods.

CONCLUSIONS

The dynamic characteristics and applicability of the vane damper developed for reducing seismic response of long span cable-stayed bridge are experimentally and analytically studied.

According to the above investigation, the following conclusions may be deduced. Based on the dynamic loading tests of the vane damper, the relation between velocity and damping force is obtained as designed, and the effectiveness of the damper on the whole bridge structure were confirmed by dynamic tests and earthquake response analysis.

ACKNOWLEDGEMENT

The authors would like to express their sincere appreciation to Prof. Yoshikazu Yamada and Prof. Kenzo Toki (Kyoto University) for their valuable contributions to this study.

REFERENCES

Toki and Nakase 1986. Reliability of long period component of SMAC accelerograms. Proc., 7th Japan Earthquake Engineering Symposium.

Kitazawa, Ishizaki, Emi, and Nishimori, 1990. Characteristics of earthquake response and aseismic design of the long-period cable-stayed bridge (Higashi-Kobe bridge) with all movable shoes in longitudinal direction. Proc., Japan Society of Civil Engineers, 422(10).

Yamada, Shiraishi, Toki, Matsumoto, Matsuhashi, Kitazawa, and Ishizaki 1991. Earthquake resistant and wind-resistant design of the Higashi-Kobe bridge. Int'l Sem. on Cable-Supported Bridges.

Kitazawa, Nishimori, Noguchi, and Shimoda 1992, Earthquake resistant design of a long-period cable-stayed bridge. Proc., 10th World Conference on Earthquake Engineering.

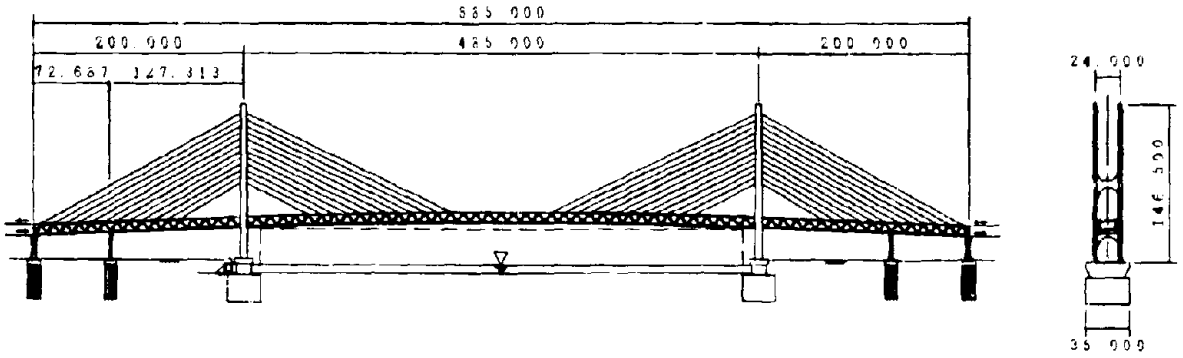

Fig.1 The Higashi-Kobe Bridge

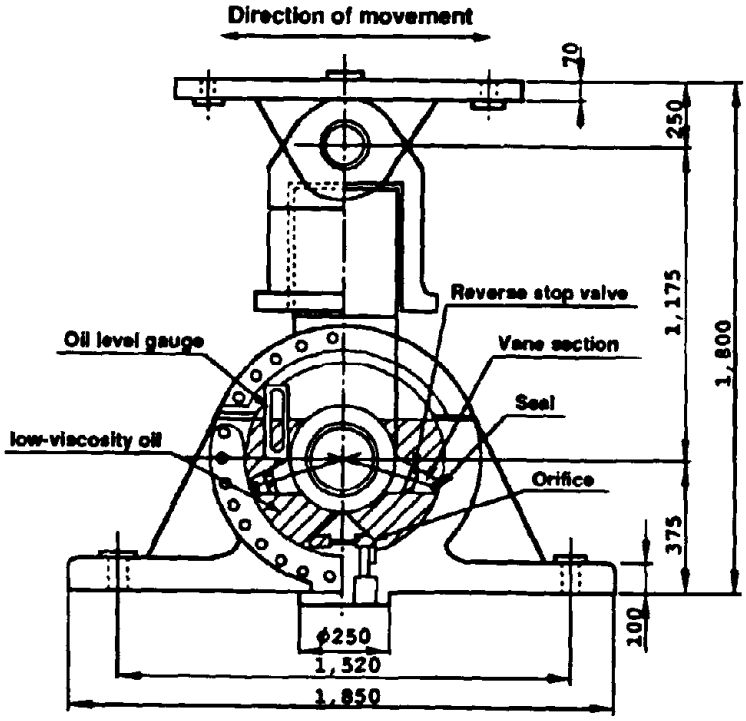

Fig.2 Vane-type oil damper

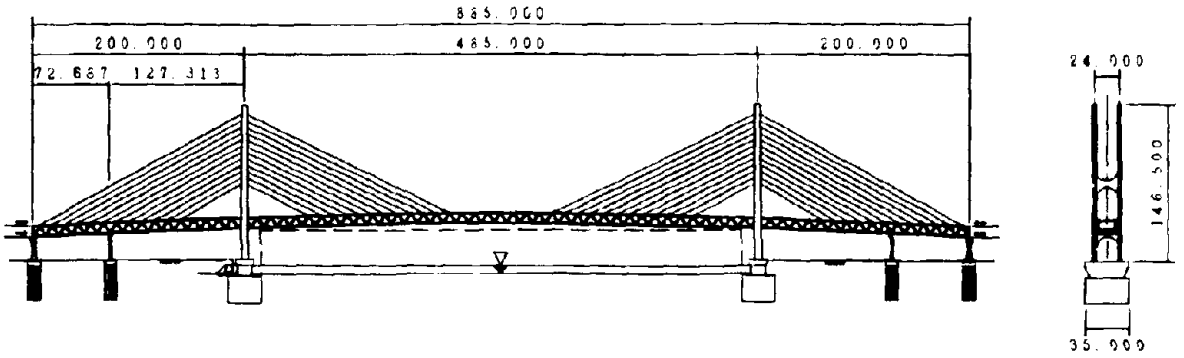

Fig.1 The Higashi-Kobe Bridge

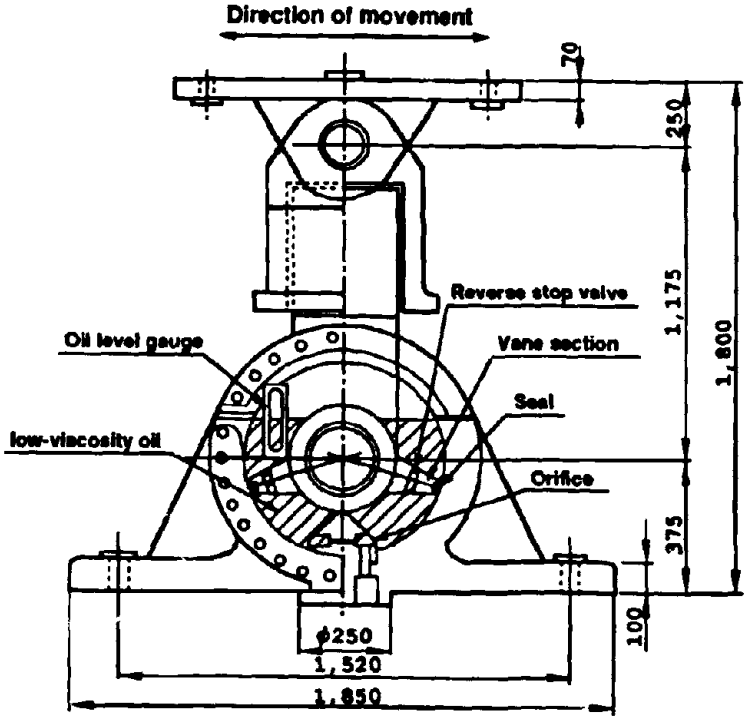

Fig.2 Vane-type oil damper

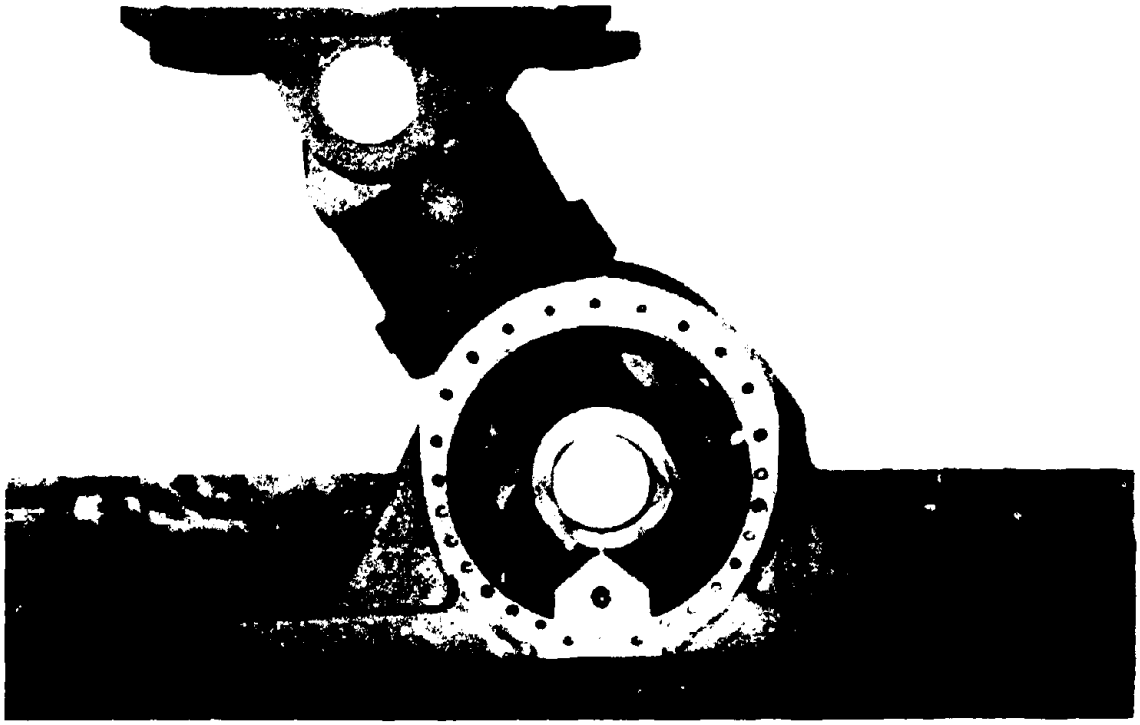

Photo 1 The Vane-type oil damper showing the Vane

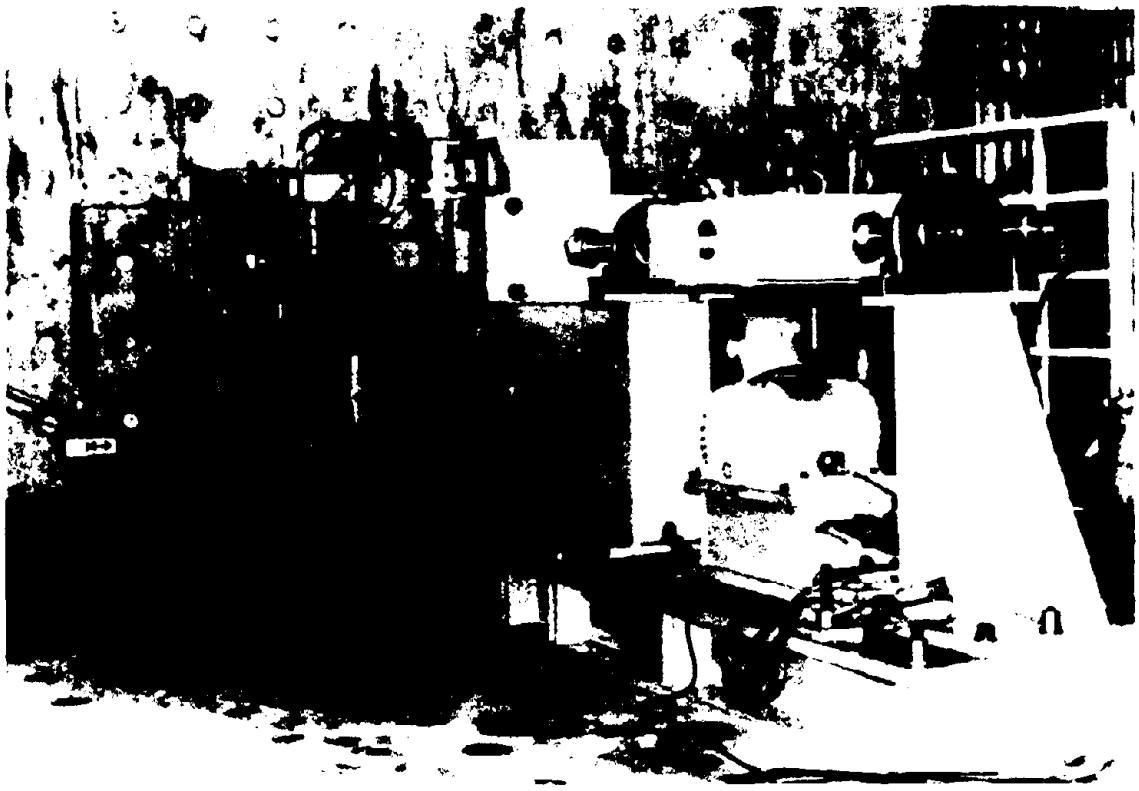

Photo 2 Dynamic loading tests on the damper of 1/2 scale model

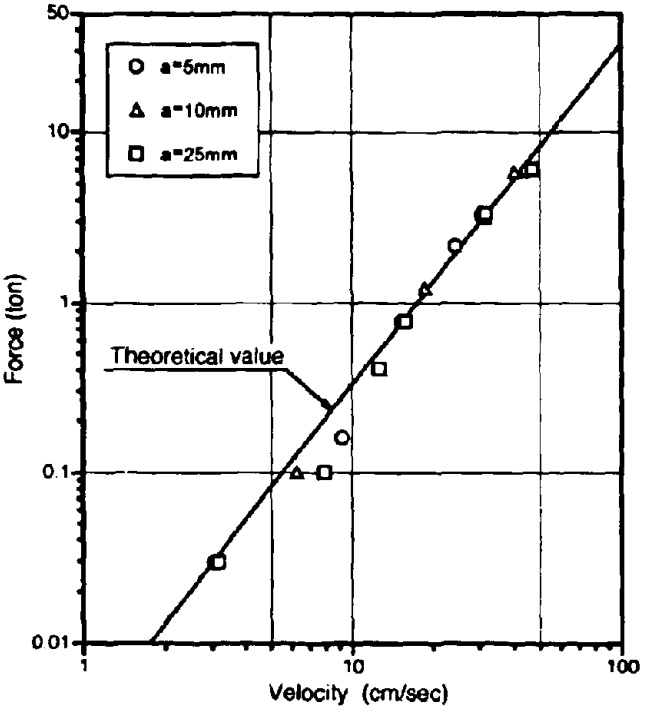

Fig.3 Force-Velocity characteristics of the 1/2 scale model

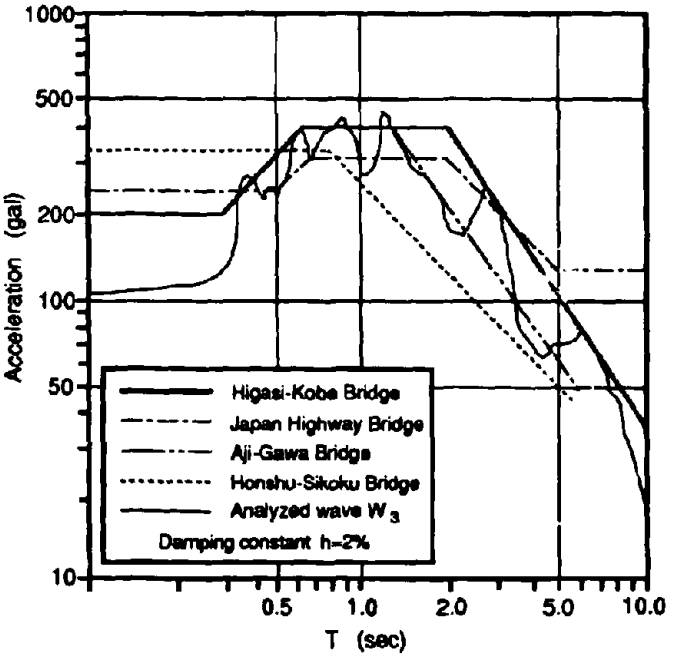

Fig.4 Design response spectrum

Table 1 Effect of Vane-type Damper on Girder displacement

Earthquake Level	Damping Constant (%)	Relative Girder displacement (cm)	Maximum Response Velocity (cm/sec)	Damper Reaction (kN)
whole structure design level (1.0EQ)	2*	61	-	-
	1	72		-
	2	61	98	-
girder stopping device design levele (1.4EQ)	1	102	231	-
	1+6.2**	64	99	3620

Remarks: - Values marked with * were obtained using the design spectrum
- Damping constant marked with ** indicates damping of the whole structure plus damping due to the damper

Table 2 Maximum displacement response obtained from shaking table tests

Input Earthquake		Input Along Long'l Axis	
		No Damper	With Damper
Long Period	Izu-oki EQ. (synthesized)	64.0	50.0 (53.9)
	Chiba-oki EQ. (corrected)	63.0	52.0 (51.6)
short period	El Centro EQ.	18.5	17.0
Design Value by Response spectra		60.4	-

N.B. - Viscous damping coefficient of 2% is assumed for cases without damper
- Values ( ) are those calculated from time history response analysis

EXPERIMENTAL STUDY OF A CLASS OF BRIDGE SLIDING SEISMIC ISOLATION SYSTEMS

M.C. Constantinou, P. Tsopelas
Department of Civil Engineering, State University of New York at Buffalo

S. Okamoto
Technology Research Center, Taisei Corporation, Yokohama, Japan

ABSTRACT

In 1991, the University at Buffalo and Taisei Corporation began a collaborative research program on the experimental study of advanced sliding seismic isolation systems for bridges. The project had the objectives of producing and experimentally verifying a class of sliding isolation systems by modifying and/or adapting existing technology. Particular emphasis was given to the adaptation and use of aerospace and military hardware. Furthermore, the project included the study of established sliding isolation systems such as the Friction Pendulum (or FPS) system [1] which has been used in a number of building and other, but not bridge, applications in the United States, and the lubricated sliding bearing/hysteretic steel damper system used in a large number of bridges in Italy [2].

This paper presents a description of the experimental program and representative results.

INTRODUCTION

A significant number of bridges are seismically isolated in various parts of the world. The total length of isolated bridge deck exceeds 200 km, of which nearly 150 km are located in Italy and supported by some form of sliding system. Applications of bridge seismic isolation systems in the U.S. have been primarily with lead-rubber bearings, and few with sliding bearings. Currently, 56 isolated bridges in the U.S. of total deck length exceeding 11 km, are completed, or they are in the construction or in the design stage. Interestingly, only 8 of these bridges are located in California [3]. Japan recently moved towards a cautious implementation of modern isolation systems in bridges, having previously used an early form of a sliding bearing-viscous damper isolation system in over 100 bridges of the Shinkansen [4,5]. So far the application is restricted to only longitudinal isolation using elastomeric systems.

Despite the wide implementation of sliding isolation systems in bridges, the authors are aware of only one previous evaluation of sliding systems by large scale shake table testing [6]. Furthermore, a number of sliding isolation systems have been implemented in buildings but not evaluated for bridge application, while other systems have been proposed but not experimentally evaluated. The experimental study reported in this paper has been conducted in order to evaluate these sliding isolation systems. For this purpose, a 160 kN, quarter length scale bridge model was

utilized. The bridge model featured flexible piers and it could be configured to resemble either a non-isolated multiple-span bridge , or single- , two- and multiple-span isolated bridges

The tested isolated systems included three different types

(a) Systems consisting of flat sliding bearings and restoring force devices in the form of rubber springs, wire rope springs and fluid stiffness/damping devices,

(b) Spherically shaped (or FPS) sliding bearings, and

(c) Lubricated sliding bearings with yielding steel dampers

All systems were configured for areas of strong seismic loading such as California and Japan. All were characterized by significant energy absorption capability. However, the design criteria were different in the three basic types. In systems type (a), the design criteria were to reduce the transmission of force to the bridge substructure while restricting bearing displacements to less than 200 mm (8 in) in prototype scale. In systems type (b) and (c), the design criteria were to minimize the transmission of force to the bridge substructure without restricting the bearing displacements.

This paper presents results for the non-isolated and isolated bridge in only the multiple-span configuration, that is, a bridge deck supported by two flexible piers. Furthermore, results for only one of the tested isolation system configurations of each of the three basic types are presented. The interested reader is referred to the reports of Constantinou [7] and Tsopelas [8] for more results and details of the testing.

BRIDGE MODEL AND ISOLATION SYSTEM

The bridge model is shown in Figure 1. At quarter length scale, it had a clear span of 4.8 m (15.7 feet), height of 2.53 m (8.3 feet) and total weight of 160.8 kN (36 kips). The deck itself weighted 143 kN (32 kips). Each pier consisted of two steel square tube columns with top made of a channel section. The columns transferred the gravity load to the overhangs of the concrete extension of the shake table at a point located 0.57 m (1.87 feet) beyond the edge of the shake table. This resulted in significant vertical motion of the two overhangs, which increased the severity of testing.

In its non-isolated configuration, that is with the deck pinned to the flexible piers, the bridge had a fundamental period of 0.26 secs (or 0.52 secs in prototype scale) and damping ratio in the range of 0.04 to 0.08 of critical. The damping was result of hysteretic action, not in the columns of the model, but in the overhangs of the concrete extension. Thus while the columns remained elastic, the pier system displayed realistic hysteretic action.

A total of 25 isolation system and bridge configurations were tested. Of these, three configurations are described in this paper. All three had both piers flexible as shown in Figure 1. The isolation systems were:

(a) A system consisting of four flat sliding bearings (unfilled PTFE-stainless steel interfac with coefficient of friction at high velocity of sliding $f_{max} = 0.150$. Restoring force was developed by two rubber springs, each of which provided an effective stiffness 112.3 kN/m (0.64 kip/in) at displacement of 35 mm (1.38 in). Beyond this displacement, the devices exhibited increased stiffness and acted as displacement restrainers. They had a maximum displacement capacity of 50 mm (2 in). The effective period of the isolation system at displacements below the limit of 35 mm (1.38 in) was 1.60 secs (or 3.20 secs in prototype scale)

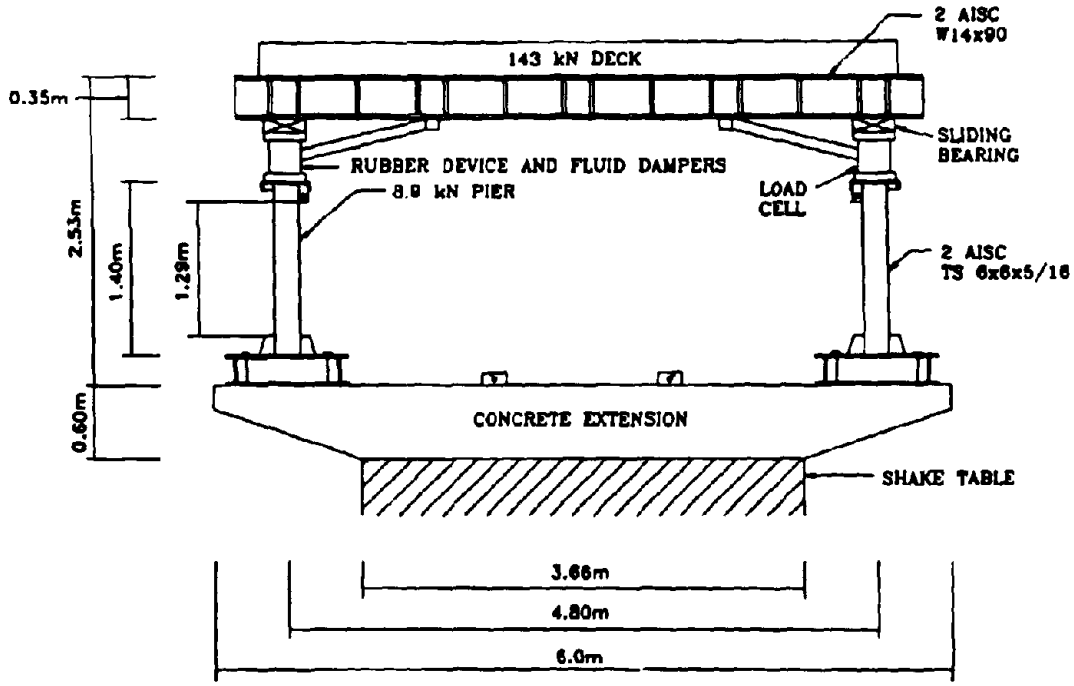

FIGURE 1: QUARTER LENGTH SCALE BRIDGE MODEL

In a number of tests the isolation system was enhanced by four linear viscous fluid dampers with displacement capacity of 50 mm (2 in) and combined damping constant equal to 61.7 kN-s/m (0.352 kip-s/in). The dampers were identical to those reported in [9] and provided a damping ratio to the isolation system of nearly 54% of critical at the temperature of 25 °C. The damping ratio was estimated from experimental results to be at 41% of critical at the temperature of 50 °C and at 78% of critical at the temperature of 0 °C.

(b) A system consisting of four spherical sliding (or FPS) bearings with a radius of curvature equal to 558.8 mm (22 in) and coefficient of friction f_{max} = 0.120. The bearings were constructed of polished stainless steel and PTFE-composites. The bearings had displacement capacity of 88.9 mm (3.5 in). The period of the isolation system was 1.50 secs (or 3.0 secs in prototype scale).

(c) A system consisting of four lubricated flat PTFE-stainless steel bearings, each equipped with two mild steel E-shaped dampers. Friction in the bearings was about 0.01 to 0.02. The mild steel dampers were detailed to fully yield at a displacement of 5 mm and force of 3.5 kN (0.79 kips) or 0.2 times the deck weight. The system lacked restoring force capability. The bearings successfully sustained during testing about 50 cycles of displacement with amplitude exceeding 50 mm (2 in), for which the maximum strain in the steel was approximately equal to 0.03 and the global ductility was equal to 10.

Various components of the tested isolation systems are shown in Figure 2. The rubber springs were installed with their outer steel cylinder connected to the pier and their inner steel cylinder connected to the deck by a run-through rod. Spring action developed by extension of the radial rubber elements.

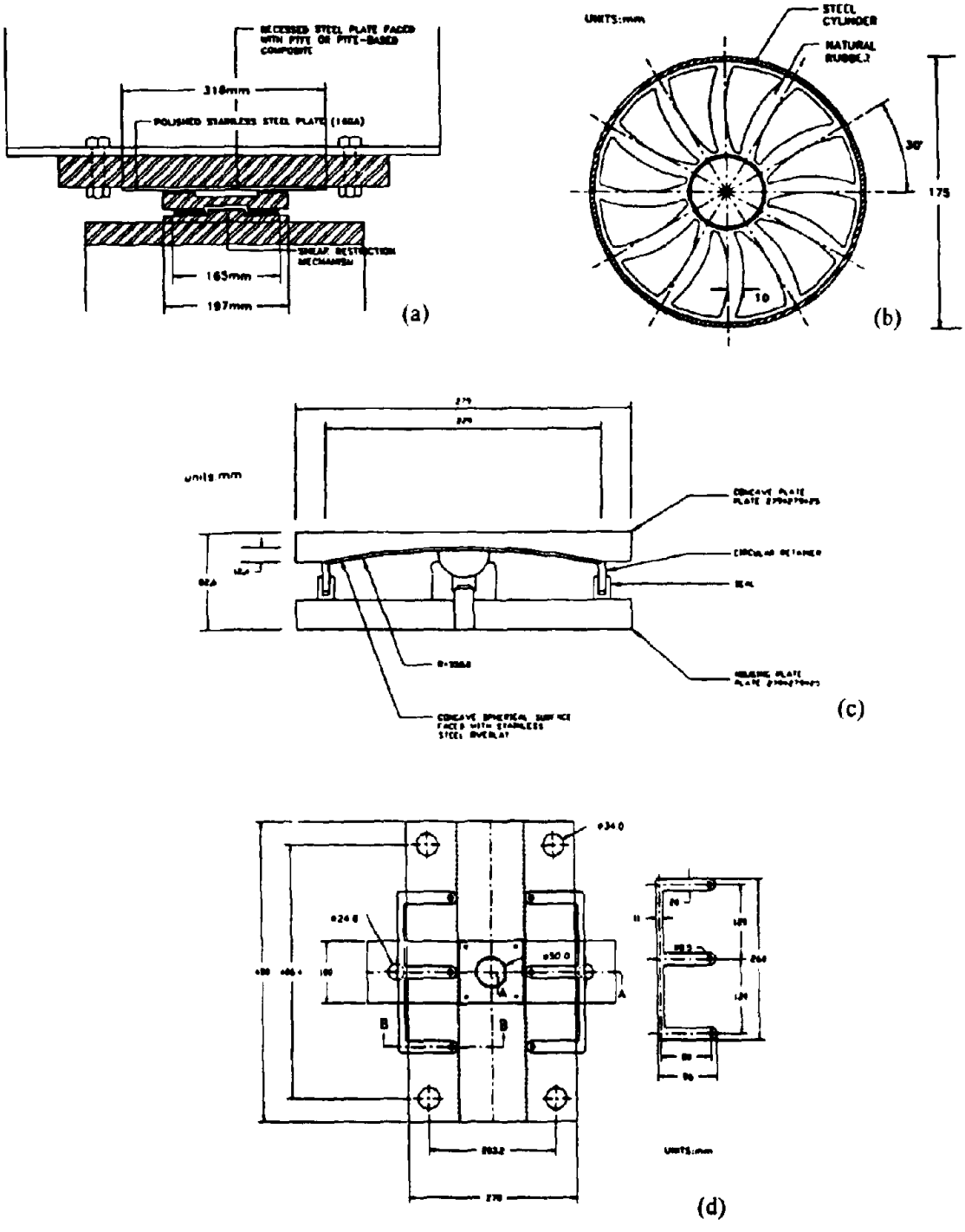

FIGURE 2: ELEMENTS OF ISOLATION SYSTEMS (a) FLAT SLIDING BEARING (b) RUBBER SPRING (c) FPS BEARING (d) LUBRICATED SLIDING BEARING WITH E-SHAPED STEEL DAMPERS

EXPERIMENTAL RESULTS

A total of 643 earthquake simulation tests were performed using 24 recorded and artificial motions. Herein only a representative portion of the obtained test results is presented. Table 1 lists some of the earthquake motions and their characteristics. In certain tests these motions were combined with their vertical counterparts. The response spectra of the Japanese Level 2 bridge design motions are shown in Figure 3. The difficulties in achieving effective seismic isolation for these motions are apparent. For example, the spectrum for Ground Condition 3 (deep cohesionless soil) extends to a period of 2 secs with a spectral value of 1g. To obtain effective isolation it is required that the period is shifted to a value beyond 3 secs, which for typical light weight bridges is only possible with sliding systems.

TABLE 1: EARTHQUAKE MOTIONS USED IN TEST PROGRAM AND CHARACTERISTICS IN PROTOTYPE SCALE

Notation	Record	Peak Acc. (g)	Peak Vel. (mm/sec)	Peak Dis. (mm)
El CentroS00E	Imperial Valley, May 18 1940, Component S00E	0.34	334.5	108.7
Taft N21E	Kern County, July 21,1952, Component N21E	0.16	157.2	67.1
Pacoima S16E	San Fernando, February 9, 1971, Component S16E	1.17	1132.3	365.3
Pacoima S74W	San Fernando, February 9, 1971, Component S74E	1.08	568.2	108.2
Hachinohe N-S	Tokachi, Japan, May 16, 1968 Hachinohe, Comp N-S	0.23	357.1	118.9
JP. L2G1	Artificial Compatible with Japanese Level 2 Gr. Cond. 1	0.37	864.0	526.0
JP. L2G2	Artificial Compatible with Japanese Level 2 Gr. Cond. 2	0.43	998.0	527.0
JP. L2G3	Artificial Compatible with Japanese Level 2 Gr. Cond. 3	0.45	1121.0	700.0
CalTrans A2	Art.Comp. with CalTrans 0.6g 80'-150'Alluvium Spect.	0.60	836.4	282.9
CalTrans S3	Art. Comp. with CalTrans 0.6g 10'-80'Alluvium Spect.	0.60	778.0	438.9
CalTrans R3	Art. Comp. with CalTrans 0.6g Rock Spect.	0.60	571.0	342.4

Table 2 presents the recorded response of the non-isolated bridge. In this case all earthquake motions were reduced to only a portion of their actual intensity (e.g. El Centro S00E 25% indicates a motion with approximately 1/4 the intensity of the actual motion - see Table 1). We observe that for these weak motions, with peak acceleration not exceeding 0.12g, the bridge substructure is subjected to considerable forces, which are in the range of 0.2 to 0.35 times the bridge weight.

Table 3 presents the recorded response of the isolated bridge with the sliding bearing-rubber restoring force device system. Only the response in strong seismic excitation is presented. Concentrating first on the system without fluid dampers, we observe that in the strongest motions (i.e. the Japanese Level 2 and Pacoima S16E) the isolation system develops

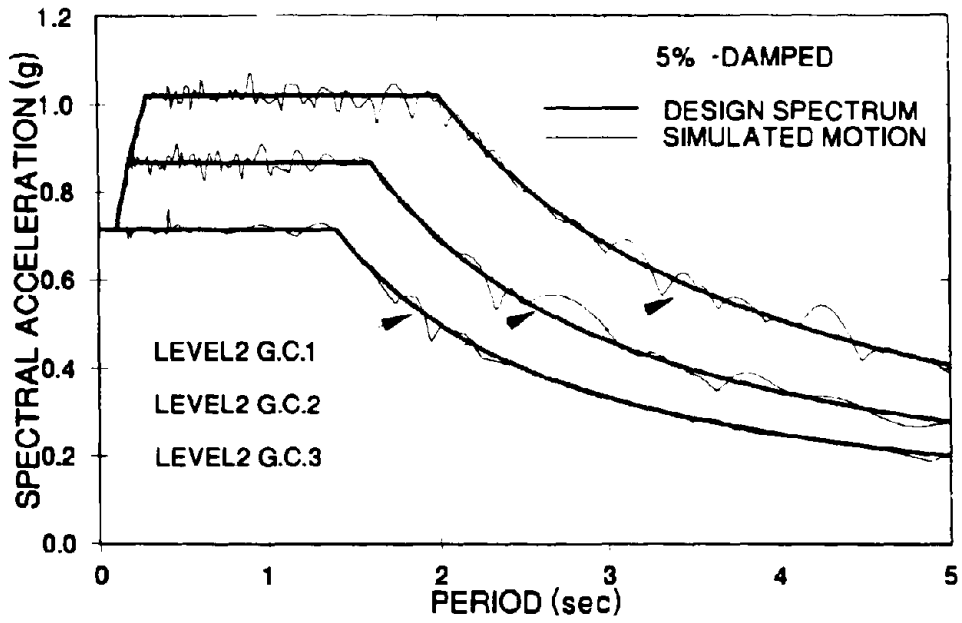

FIGURE 3 RESPONSE SPECTRA OF JAPANESE LEVEL 2 BRIDGE MOTIONS

TABLE 2: RECORDED RESPONSE OF NON-ISOLATED BRIDGE PIER DRIFT RATIO = PIER DRIFT / PIER HEIGHT (=1290 mm).

Excitation	Peak Pier Drift Ratio (%)	Peak Pier Shear Force / Carried Weight
El Centro S00E 25%	0.381	0.271
Taft N21E 75%	0.385	0.278
Pacoima S74W 13%	0.346	0.214
Pacoima S16E 13%	0.275	0.186
Hachinohe NS 50%	0.311	0.198
JP. L2 G1 25%	0.301	0.181
JP. L2 G2 25%	0.365	0.225
JP. L2 G3 25%	0.497	0.283
CalTrans R3 20%	0.389	0.234
CalTrans S3 20%	0.565	0.345
CalTrans A2 20%	0.475	0.298

large enough displacements to engage the displacement restrainer. This results in large substructure forces. Elimination of this event is accomplished with the introduction of fluid dampers. This enhanced isolation system could sustain the severe long period Japanese Level 2 bridge design motions with bearing displacements less than 200 mm (8 in) and substructure forces of 0.33 to 0.38 times the weight. In this respect we note that current Japanese bridge design procedures [10] require that bridge piers are designed for a lateral force not less than 0.3 times the weight, even when seismic isolation and pier ductility are utilized for reduction of forces.

TABLE 3: RECORDED RESPONSE OF ISOLATED BRIDGE WITH SLIDING BEARING-RUBBER RESTORING FORCE DEVICE-FLUID DAMPER SYSTEM (COEFFICIENT OF FRICTION f_{max} = 0.150, PERIOD IN PROTOTYPE SCALE=3.2 secs)

Excitation	Peak 1 Bearing Displ. (mm)	Permanent 1 Bearing Displ. (mm)	Peak Pier Drift Ratio (%)	Peak Pier Shear Force / Carried Weight	Fluid Dampers (No.)
El Centro S00E 200%	103.2	5.6	0.340	0.265	0
2 El Centro S00E+V 200%	105.6	4.0	0.360	0.275	0
Taft N21E 400%	130.8	6.4	0.350	0.267	0
2 Taft N21E+V 400%	112.8	6.8	0.360	0.271	0
Hachinohe NS 300%	144.4	8.8	0.360	0.273	0
Pacoima S74W 100%	146.0	14.8	0.390	0.306	0
Pacoima S16E 75%	184.4	7.2	0.570	0.448	0
JP. L2 G1 100%	234.0	35.2	0.550	0.509	0
JP. L2 G2 75%	138.0	9.6	0.330	0.240	0
JP. L2 G3 75%	128.8	3.6	0.320	0.263	0
CalTrans R3 100%	108.0	18.8	0.360	0.291	0
CalTrans S3 100%	154.0	4.0	0.430	0.331	0
CalTrans A2 100%	178.0	34.8	0.430	0.331	0
El Centro S00E 200%	94.4	2.0	0.440	0.356	4
Pacoima S16E 100%	176.8	2.8	0.560	0.461	4
JP. L2 G1 100%	158.8	5.6	0.420	0.332	4
JP. L2 G2 100%	154.8	2.0	0.450	0.375	4
JP. L2 G3 100%	189.2	10.0	0.440	0.360	4
CalTrans A2 100%	130.8	30.4	0.420	0.337	4

1 In prototype scale

2 Combined horizontal and vertical motion

Vivid illustration of the effectiveness of fluid dampers is presented in Figure 4. The top two figures present the isolation system hysteresis loop and pier hysteresis loop of the system without fluid dampers in the Japanese Level 2, Ground Condition 1 motion. The use of fluid dampers in the same motion reduced bearing displacements and substructure forces by nearly 35%. Moreover, the peak response of the system with fluid dampers in the Ground Condition 2 and 3 motions is nearly the same as that in Ground Condition 1 motion. This demonstrates a marked insensitivity of the response of the combined sliding-viscous damper system to the frequency content of these long period motions. Very interestingly, this significant improvement in the behavior of the system was accomplished with the use of four dampers with a combined weight of 40 N (9 lb), whereas the bridge weight was 160800 N (36000 lbs).

For excitations less severe than the Japanese Level 2 motions, the isolation system without fluid dampers provided a considerable degree of protection. While maintaining displacements below the limit of 200 mm (8 in), the system allowed the development of substructure forces which were comparable to those of the non-isolated bridge (see Table 2), except that the excitation was about five times stronger.

An example is provided in Figure 5 which shows the response of the isolated bridge in the simulated CalTrans A2 motion (100% level) and the response of the non-isolated bridge in the same motion at only 20% of full level. Evidently, the substructure response is nearly the same, whereas the input differs by a factor of five.

Table 4 presents the recorded response of the isolated bridge with the FPS system. This system affords a better degree of isolation than the previous system, which is characterized by more ability to dissipate energy than the FPS system. This better isolation capability of the FPS system is produced at the expense of larger bearing displacements, which for the Japanese Level 2 motions are about 350 mm (14 in). However for the motions which are representative of California, the demand for displacement is less while the bridge substructure forces are about 0.25 times the bridge weight.

A very interesting observation made during the testing of the FPS system was the exceptional stability of the frictional properties of the bearings. Figure 6 shows recorded force-displacement loops of the FPS bearings in identification tests conducted on the shake table. The bearings underwent five cycles of harmonic motion of 0.4 Hz frequency and 75 mm amplitude. The peak velocity of sliding was 188 mm/s. One test was conducted prior to seismic testing. The other identical test was conducted after 58 seismic tests. It may be observed that the loops prior and following the 58 seismic tests are identical. The friction coefficient remained unchanged after at least 30 cycles at approximately the displacement capacity of the bearings and over 100 cycles at lower displacement.

The results for both the FPS and sliding bearing-rubber device-fluid damper systems demonstrate a very small effect of the vertical ground motion. Furthermore, both systems resulted in permanent displacements, which were not cumulative. That is, in none of the tests in Tables 3 and 4 the bridge was re-centered prior to each test. Rather, the isolation systems had the tendency to re-center themselves on initial movement.

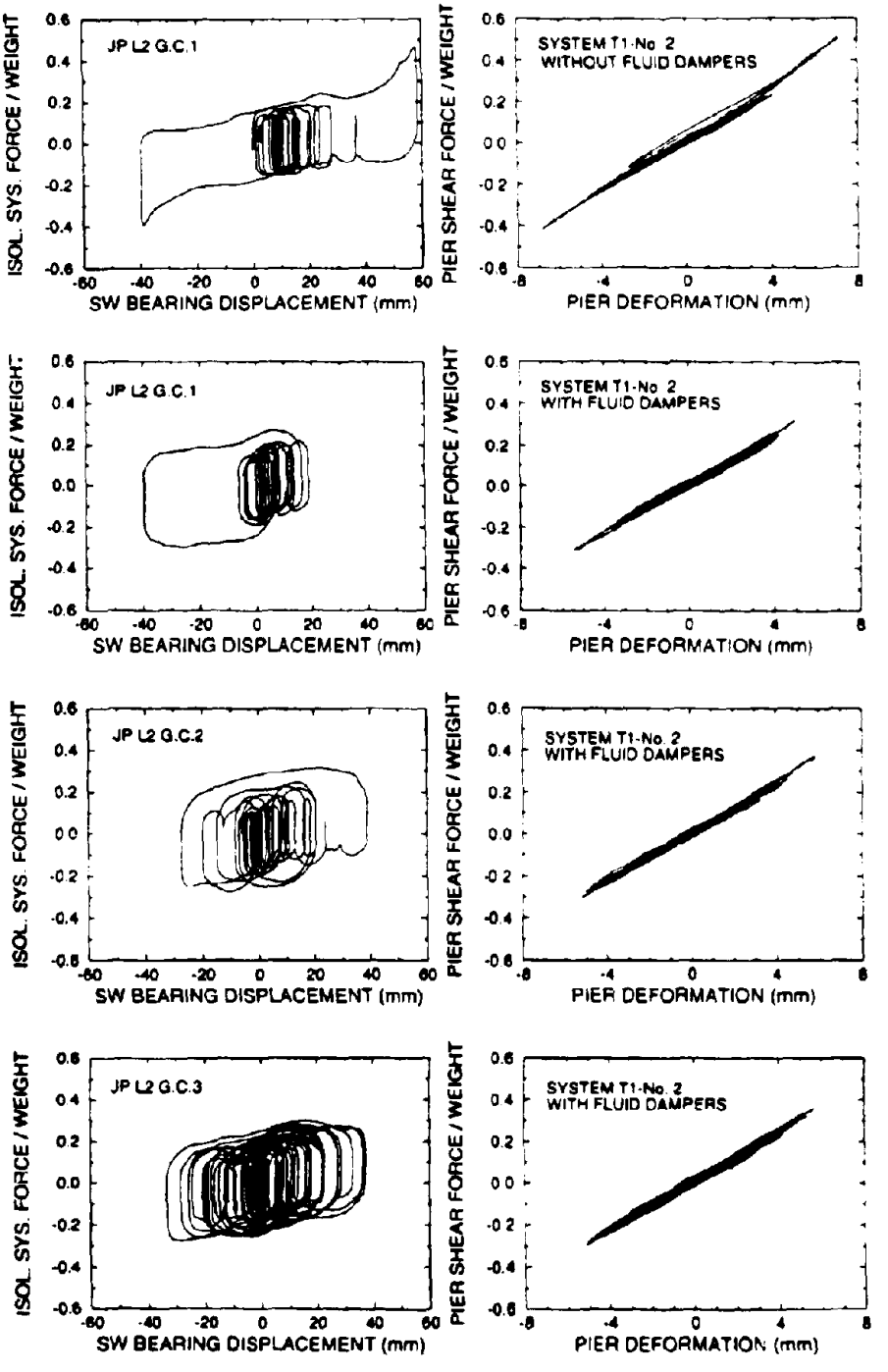

FIGURE 4: RESPONSE OF ISOLATED BRIDGE (FLAT SLIDER AND RUBBER SPRING SYSTEM) WITHOUT FLUID DAMPERS IN THE JAPANESE LEVEL 2, G.C. 1 MOTION (TOP TWO FIGURES) AND WITH FLUID DAMPERS IN ALL THREE GROUND CONDITIONS OF JAPANESE LEVEL 2 MOTIONS

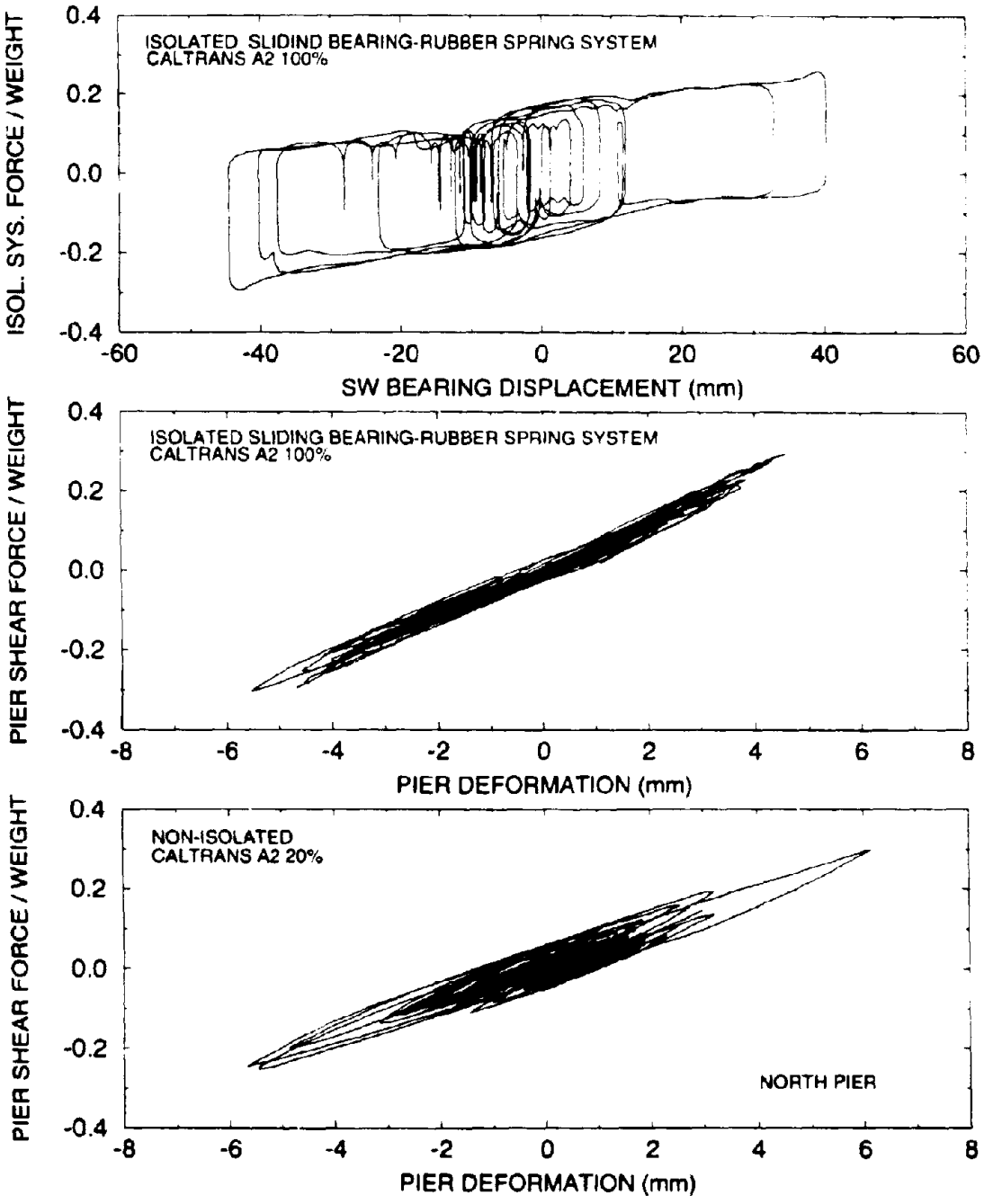

FIGURE 5: COMPARISON OF RESPONSE OF ISOLATED BRIDGE IN CALTRANS A2 MOTION TO RESPONSE OF NON-ISOLATED BRIDGE IN 20% OF CALTRANS A2 MOTION

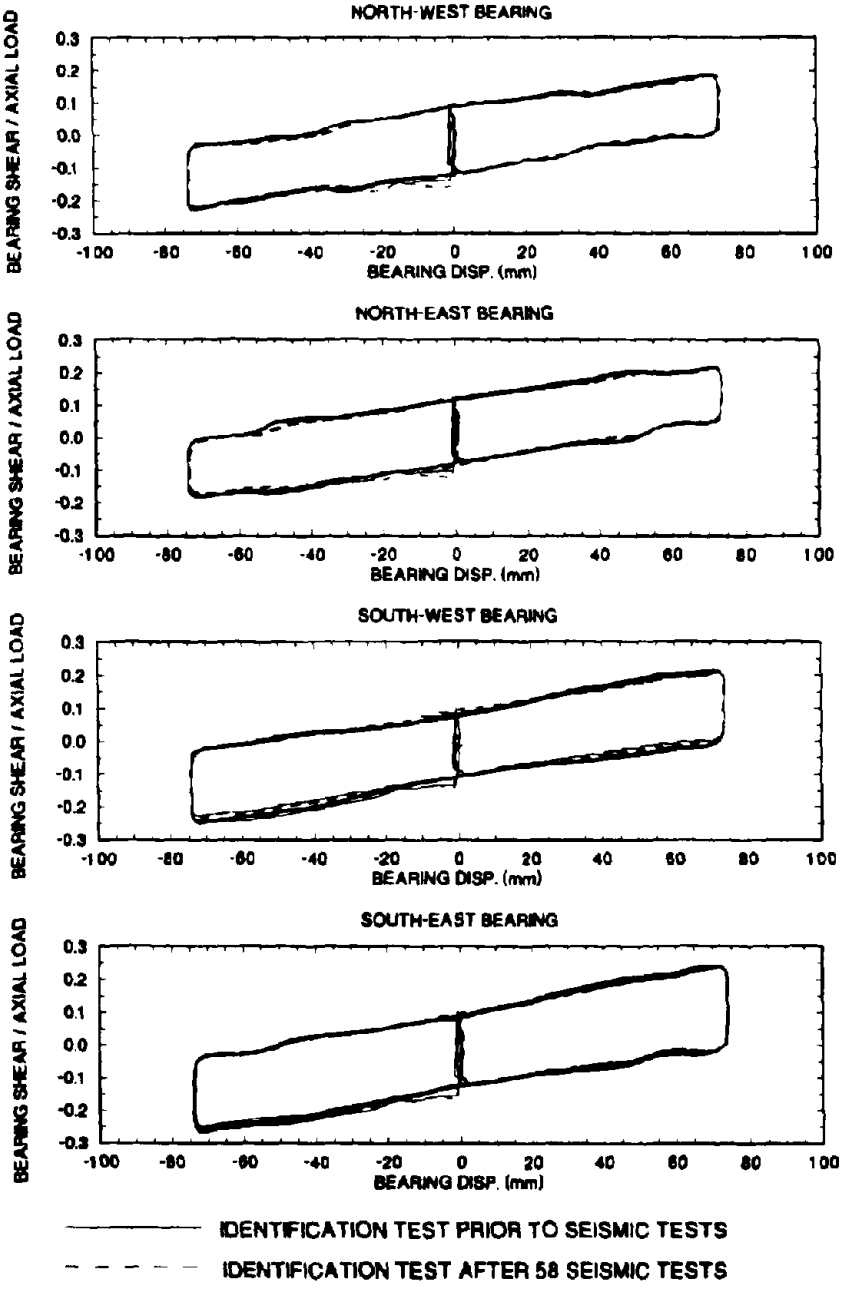

FIGURE 6: RECORDED FPS BEARING FORCE-DISPLACEMENT LOOPS FOR FIVE CYCLES OF HARMONIC MOTION PRIOR TO AND FOLLOWING 58 SEISMIC TESTS

TABLE 4: RECORDED RESPONSE OF ISOLATED BRIDGE WITH FPS SYSTEM (COEFFICIENT OF FRICTION f_{max} = 0.120, PERIOD IN PROTOTYPE SCALE= 3.0 secs).

Excitation	Peak 1 Bearing Displ (mm)	Permanent 1 Bearing Displ. (mm)	Peak Pier Drift Ratio (%)	Peak Pier Shear Force / Carried Weight
El Centro S00E 200%	127.6	18.0	0.270	0.194
2 El Centro S00E+V 200%	126.8	17.6	NA 3	0.199
Taft N21E 400%	220.0	40.4	0.300	0.203
2 Taft N21E+V 400%	216.0	38.4	NA 3	0.204
Hachinohe NS 300%	268.0	76.8	0.400	0.283
Pacoima S74W 100%	174.4	12.8	0.310	0.218
Pacoima S16E 100%	361.6	39.6	0.450	0.287
JP. L2 G1 100%	311.6	19.2	0.430	0.265
JP. L2 G2 100%	232.8	45.6	0.370	0.261
JP. L2 G3 85%	339.2	62.0	0.360	0.247
CalTrans R3 100%	116.8	8.4	0.340	0.212
CalTrans S3 100%	126.4	28.0	0.370	0.238
CalTrans A2 100%	270.8	26.0	0.390	0.265

1 In prototype scale

2 Combined horizontal and vertical motion 3 Instrument affected by vertical motion

Table 5 presents results for the isolated bridge with lubricated sliding bearings and E-shaped steel dampers. Tests were conducted with seismic input of lower intensity than the other systems because permanent displacements were large and cumulative. This was the result of the system's inability to provide re-centering force. Nevertheless, the system sustained a large number of cycles at peak strain of about 0.03 in the steel dampers and transferred forces to the substructure which were only marginally larger than the yield force of the system. It appears that this system may provide effective isolation in areas of infrequent and moderate seismic excitation.

The FPS and sliding bearing-rubber restoring force device isolation systems were very effective in strong seismic excitation. Actually, they have been configured for effectiveness in motions such as the Japanese Level 2 and CalTrans motions. Nevertheless, they proved to be also effective in weak excitation, such as the Japanese Level 1 motions. This service-type of loading has peak ground acceleration of about 0.12g , for which bridges in Japan must remain elastic. Figure 7 compares pier force-drift loops of the non-isolated and isolated (with highest friction) bridges recorded in tests with these motions. Evidently, the piers of the isolated bridge remain elastic and respond with a marked insensitivity to the significantly different content in frequency of the three motions. In contrast, the non-isolated bridge shows sensitivity and apparently

undergoes inelastic deformations. Interestingly the isolated bridge with friction coefficient at high velocity of sliding f_{max} = 0.150 provides a degree of isolation even when the peak ground acceleration is less than f_{max} g. The reason for this behavior is the velocity dependency of the coefficient of friction. At low velocity of sliding the bearings mobilize a friction coefficient much less than f_{max}, thus enabling them to provide some isolation in weak excitation

TABLE 5: RECORDED RESPONSE OF ISOLATED BRIDGE WITH LUBRICATED SLIDING BEARINGS AND E-SHAPED DAMPERS (YIELD FORCE = 0.20 x WEIGHT).

Excitation	Peak 1 Bearing Displ. (mm)	Permanent 1 Bearing Displ. (mm)	Peak Pier Drift Ratio (%)	Peak Pier Shear Force / Carried Weight
2 Taft N21E 400%	235.2	122.8	NA	NA
El Centro S00E 150%	108.8	108.8	0.320	0.227
Taft N21E 200%	176.4	116.8	0.300	0.197
Hachinohe NS 100%	166.8	118.0	0.290	0.194
JP. L2 G1 50%	202.8	99.6	0.320	0.209
JP. L2 G2 50%	99.6*	8.0	0.310	0.210
JP. L2 G3 50%	136.0	19.2	0.320	0.213
JP. L2 G3 75%	222.4	8.8	0.350	0.231

1 In prototype scale

2 Combined horizontal and vertical motion * Initial displacement

CONCLUSIONS

Sliding isolation systems, such as the FPS and sliding bearing-rubber restoring force device-fluid damper systems, may be configured for high effectiveness in strong seismic excitation. Specifically, these systems may be designed for all soil conditions in Japan to deliver bridge substructure forces at the minimum code design level while allowing bearing displacements of less than 200 mm (8 in). These systems have been experimentally shown to be also effective in weak seismic excitation.

The tested lubricating bearing-steel damper isolation system, which found numerous applications in Italy, was found to be effective in infrequent and moderate earthquakes. While the system successfully sustained a large number of cycles of motion and maintained the substructure forces at about its yield force level, it developed large and cumulative permanent displacements. This was the result of its lack of restoring force capability.

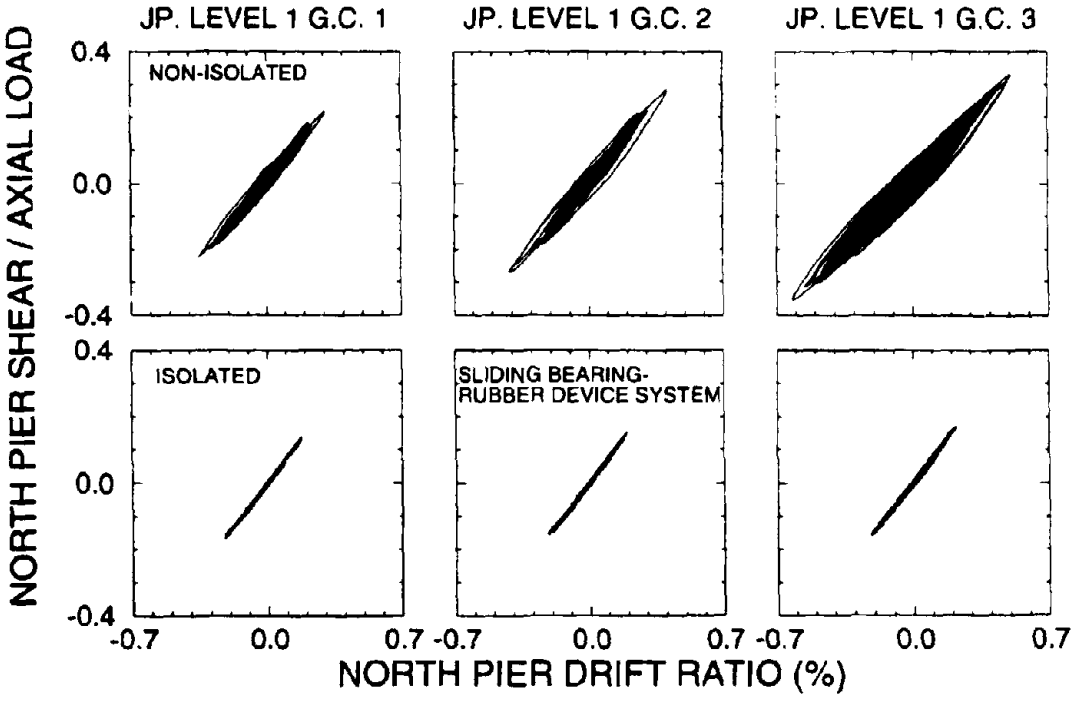

FIGURE 7: COMPARISON OF SHEAR FORCE-DRIFT LOOPS IN PIERS OF NON-ISOLATED AND ISOLATED BRIDGES FOR THE WEAK JAPANESE LEVEL 1 MOTIONS (PGA=0.12g).

ACKNOWLEDGMENTS

Financial support for this project has been provided by Taisei Corporation, Japan and the National Center for Earthquake Engineering Research. Earthquake Protection Systems, San Francisco, CA, Taylor Devices, N. Tonawanda, NY, Taisei Corp., Japan and ALGA, Italy manufactured the isolation hardware.

REFERENCES

1. Zayas, V., S.S. Low and S.A. Mahin. "The FPS Earthquake Resisting System, Experimental Report," Earthquake Engineering Research Center, Univ. of California, Report No. UCB/EERC-87/01, Berkeley, 1987.
2. Medeot, R. "The Evolution of Aseismic Devices for Bridges in Italy," Proc. 3rd World Congress on Joint Sealing and Bearing Systems 2, Torondo, Oct. 1991, pp.1295-1320.
3. Constantinou, M.C. Lecture Notes in Seismic Isolation and Passive Energy Dissipation Course in Passive and Active Structural Control in Civil Engineering. Udine (Italy) International Centre for Mechanical Sciences, 1993.
4. Buckle, I.G., and R.L. Mayes. "Seismic Isolation History, Application and Performance-A World View," Earthquake Spectra 6, May 1990, pp.161-201.
5. Kawashima, K., K. Hasegawa and Nagashima. "A Perspective of Menshin Design of Highway Bridges in Japan," 1st U.S.-Japan Workshop on Earthquake Protective Systems for Bridges, Buffalo, Sept. 1991.
6. Constantinou, M.C., A. Kartoum, A. M. Reinhorn and P. Bradford. "Experimental and Theoretical Study of a Sliding Isolation System for Bridges," National Center for Earthquake Engineering Research, Report No. NCEER 91-0027, Buffalo, NY, 1991.
7. Constantinou, M.C., P. Tsopelas, Y-S. Kim and S. Okamoto. "NCEER-TAISEI Corporation Research Program on Sliding Seismic Isolation Systems for Bridges-Experimental and Analytical Study of Friction Pendulum System," National Center for Earthquake Engineering Research, Report No. NCEER 93-0020, Buffalo, NY, 1993.
8. Tsopelas, P., S. Okamoto, M.C. Constantinou, D. Ozaki and S. Fujii. "NCEER-TAISEI Corporation Research Program on Sliding Seismic Isolation Systems for Bridges-Experimental and Analytical Study of Systems Consisting of Sliding Bearings, Rubber Restoring Force Devices and Fluid Dampers," National Center for Earthquake Engineering Research, Report No. NCEER 93-xxxx, Buffalo, NY, 1993.
9. Constantinou, M.C. and M.D. Symans. "Experimental and Analytical Investigation of Seismic Response of Structures with Supplemental Fluid Viscous Dampers," National Center for Earthquake Engineering Research, Report No. NCEER 92-0032, Buffalo, NY, 1992.
10. -----, "Temporary Manual of the Design Method for Base-Isolated Highway Bridges," Civil Engineering Research Center (CERC), Japan, 1992 (in Japanese).

RECOVERY CHARACTERISTICS OF DYNAMIC PROPERTIES OF HIGH DAMPING RUBBER BEARINGS

Nobuo MUROTA[2] , Kengo GODA[1] , Shigenobu SUZUKI[1]
Chiaki SUDO[2] , Yoji SUIZU[1]

[1] Bridgestone Corporation , Kodaira-shi , Japan
[2] Bridgestone Corporation , Yokohama-shi , Japan

ABSTRACT

Basic Dynamic Properties and Recovery Characteristics of High Damping Rubber Bearing was estimated by dynamic shear tests using full size bearing. First, basic bearing properties at an initial state were evaluated and compared with the design value. The test bearing was then vertically loaded and performance tested at intervals of 1 , 13 , 44 and 73 days. This procedure resulted in a quantitative evaluation of the Recovery Characteristics and proved that the expression of bearing properties currently being used for designing bearing, accurately predicts the recovery characteristics of the bearing.

INTRODUCTION

High damping rubber bearings (HDR) have been used for many bridges and buildings, and are recognized as one of the most popular MENSHIN devices (Refs. 1,2). One of the characteristics of HDR is dependency of its dynamic properties to its load history. When HDR experiences high strains , the stiffness will be degradated(reduced) in the smaller strain levels. This is also known as "scragging". However, as time passes , the stiffness and damping ratio gradually recover. This phenomenon is known as the "Recovery" Characteristics of HDR (Ref. 3).

These two factors , "load-history dependence" and "recovery", must be considered adequately when designing with HDR. Although there has been much research published about load-history dependency , recovery of HDR has never been studied quantitatively. In design of HDR , we have proposed polinomial expressions of shear modulus (G) and equivalent damping ratio (heq) as functions of shear strain. These polynomial expressions were developed from scale model test results and assumed the recovery value was equal to average value of G and heq before and after a high shear strain experience. (Refs.1 and 2)

In order to confirm the accuracy of these expressions, an experimental study of the recovery characteristics of HDR (by dynamic tests) was performed after several time intervals using a full scale bearing.

TEST BEARING

The HDR test bearing for this study is shown in Fig.1. The bearing has 23 layers of 3.8 mm thick rubber and 22 steel shims of 2.2 mm thick. The shim diameter is 435 mm and outer surface of bearing is covered with synthetic rubber for protection. The bearing is large enough to be used as actual isolation bearing. Its designed performance is as follows;

Application Load Range	W	: 90.0 (tf) to 150.0 (tf)
Horizontal Stiffness Kh at 100% shear strain		: 1.38 (tf/cm)
Equivalent Damping Ratio Heq		: around 15.0 (%)
Vertical Stiffness	KV	: 1770 (tf/cm)

The rubber compound used in this bearing is KL401. This compound has a shear modulus value(G) in the middle of the Bridgestone series of high damping compounds.
Fundamental mechanical properties of the compound are as follows;

Hardness	Hd	: 67±5
Elongation at Break	Eb	: ≥650 (%)
Tensile Strength	Tb	: ≥100 (kgf/cm²)
Modulus at 25%	M_{25}	: 12.0±2.0 (kgf/cm²)

*by JIS K 6301

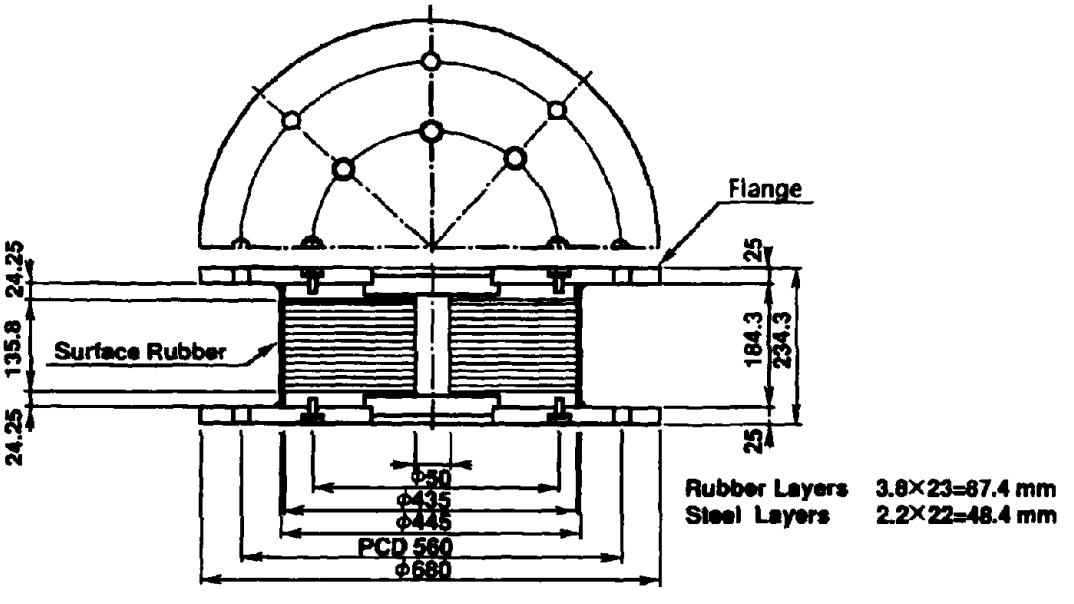

Fig.1 Test Bearing

TEST FACILITIES

1. Dynamic Test Machine

The test machine consisted of one(1) horizontal actuator which can develop a max.dynamic load of 20.0(tf) with a max.stroke of 300.0(mm) , and one(1) vertical actuator which has a max compression of 100.0(tf) and max.tension of 30.0(tf). (See Fig.2 and Table.1).

2. Pressure Device

In order to reproduce actual condition, the test bearing was vertically loaded by the pressure device shown in Fig.3. The hydraulic jack applied a load of 91.5(tf) resulting in a face pressure around p = 65.0(kgf/cm²).

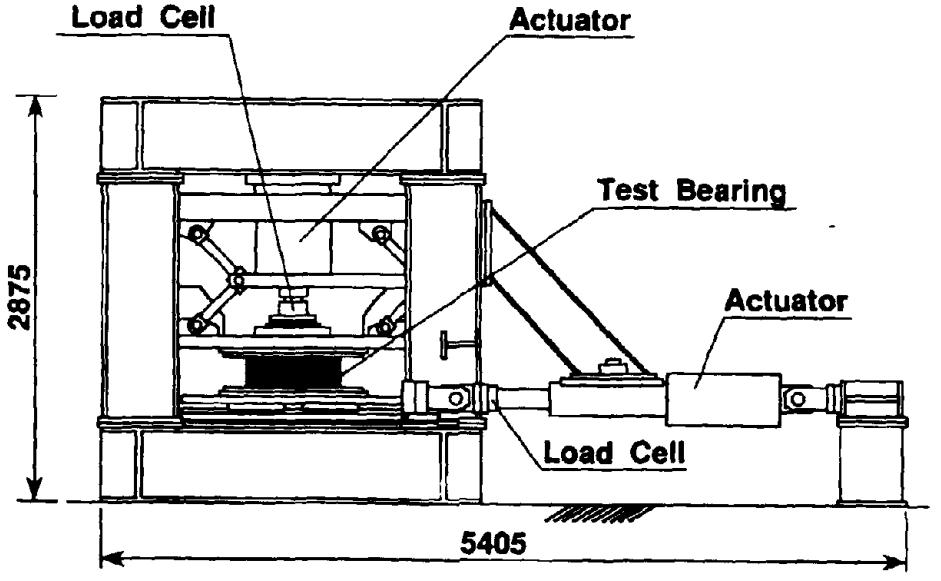

Fig.2 Dynamic Test Machine

Table1 Performance of Dynamic Test Machine

Vertical Direction		Horizontal Direction	
Dynamics	Compression 100tf Tension 30tf	Dynamic	±20tf
Stroke	±100mm	Stroke	±300mm
Max Velocity	3.14cm/sec	Max Velocity	62.8cm/sec
Frequency	0.01~5Hz	Frequency	0.01~5Hz

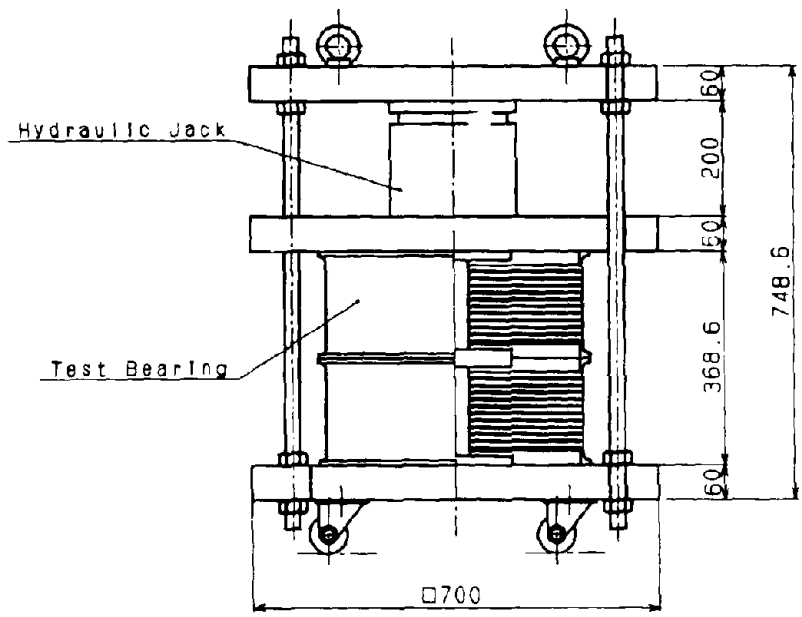

Fig.3 Pressure Device

TEST PROGRAM

Test was caried out by following procedure;

1. In order to estimate dynamic properties at initial state , the bearing was subjected to the horizontal cyclic loading test at 6 levels shear strain ;i.e. 10%,30%,50%,100%,150% and 200%. The vertical load was set at 91.5(tf). Three cycles, at a frequency of 0.5Hz were performed in rapid succession at each strain level except 200%. Because of dynamic loading capacity, testing at 200% was carried out at 0.2Hz. The series was then repeated imediately without time interval. The first series is called "STEP-1" and the second "STEP-2".
2. After the initial properties were evaluated in STEP-1 and STEP-2, the bearing was set in a Pressure Device (as mentioned in 3.2) and vertically loaded for the required number of days . The bearing was then removed from the device and horizontally tested as before. The change of properties were then established. When the test was completed, the bearing was again put under vertical load. This prosedure was repeated after intervals of 1 ,13 ,44 and 73 days (STEP-3 to STEP-6).

DETERMINATION OF DYNAMIC PROPERTIES

The dynamic horizontal properties of a bearing is represented as shear modulus (G) and equivalent damping ratio (heq). For this study, they are calculated by following equations;

Table2 Test Condition

Conditions / TEST	Shear Strain γ_t(%)	Frequency f(Hz)	Cycle (-)	Temperature (℃)
<STEP1>~<STEP6>	10(8.7mm)	0.50	3	27.0
	30(26.2mm)	0.50	3	27.0
	50(43.7mm)	0.50	3	24.5
	100(87.4mm)	0.50	3	24.7
	150(131.1mm)	0.50	3	24.0
	200(174.8mm)	0.20	3	15.0
1.Vertical Pressure		65kgf/cm²(91.5tf)		
2.Type of Wave		Sine Wave		

<STEP1>Pre-200%
<STEP2>Just after<STEP1> :Post-200%
<STEP3>1 Day after<STEP2>
<STEP4>13 Days after<STEP3>
<STEP5>44 Days after<STEP4>
<STEP6>73 Days after<STEP5>

$$Kh = \frac{F(xmax) - F(xmin)}{xmax - xmin} \quad , \quad G = \frac{Kh \cdot hr}{Aef}$$

$$heq = \frac{Wd}{2\pi \cdot Kh \cdot xmax^2}$$

where , Kh : effective horizontal stiffness
hr : total rubber height
Aef : effective supporting area(area of inner shim)
xmax,xmin : maximum or minimum displacement of loop
F(xmax),F(xmin): horizontal load at xmax or xmin
Wd : energy dissipated in one cycle

TEST RESULTS

1. Horizontal Dynamic Properties at Initial State

The relationship between shear stress(τ) and shear strain(γ) of STEP-1 and STEP-2 for all cycles are shown in Fig.4 and Fig.5. Since the restoring force of the bearing exceeded the dynamic capacity of actuator , the maximum strain of 1st and 2nd loop at each strain level did not reach the desired strain level. However in 3rd loops,the strain amplitude almost reached to the target value. Additionally in Fig.4 , the peak of loops at 200% strain was cut off and was plotted as flat line. This is because the restoring force exceeded the capacity of the horizontal actuator.
These figures show typical load-history dependent characteristics of HDR. The Hysterisys loops in STEP-1 shows sharp, higher peak values,whereas STEP-2 is more rounded with lower peaks.

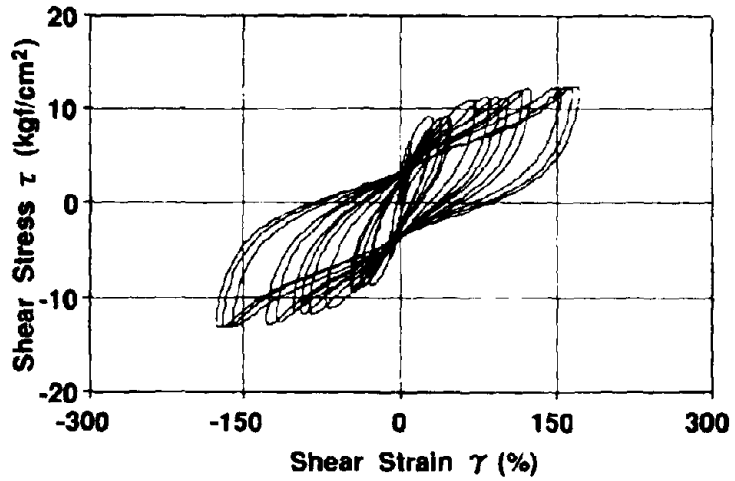

Fig.4 Restoring Force Characteristics Pre-200% <STEP1>

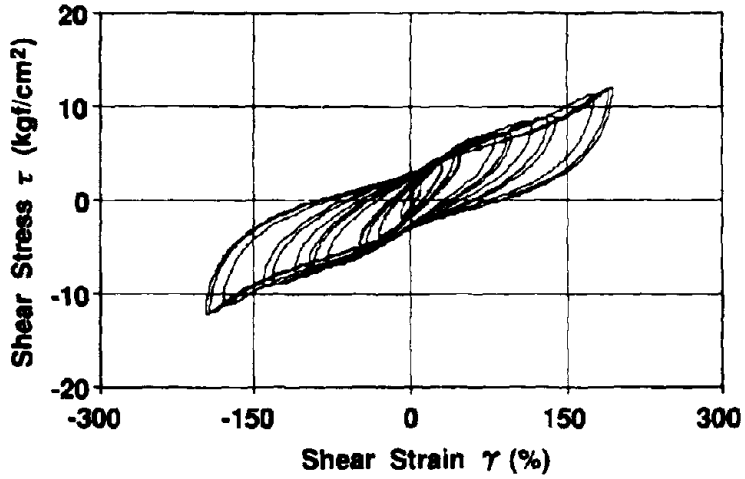

Fig.5 Restoring Force Characteristics Post-200%<STEP2>

Photo.1 shows the test bearing under the dynamic loading test.

Fig.6 compares the shear modulus (G) and equivalent damping ratio (heq) data from STEP-1 and STEP-2. The designed value is also plotted for comparison . It is indicated that just after a high strain load cycle, HDR will exhibit deterioration in shear modulus,especially in the small strain level. Heq also shows an increase in STEP-2(after high strain), but the difference is much smaller than that observed for G. The design value of G and heq is therefore determined as average value of pre-200% strain and post-200%. This corresponds to STEP-1 and STEP-2 in this test.

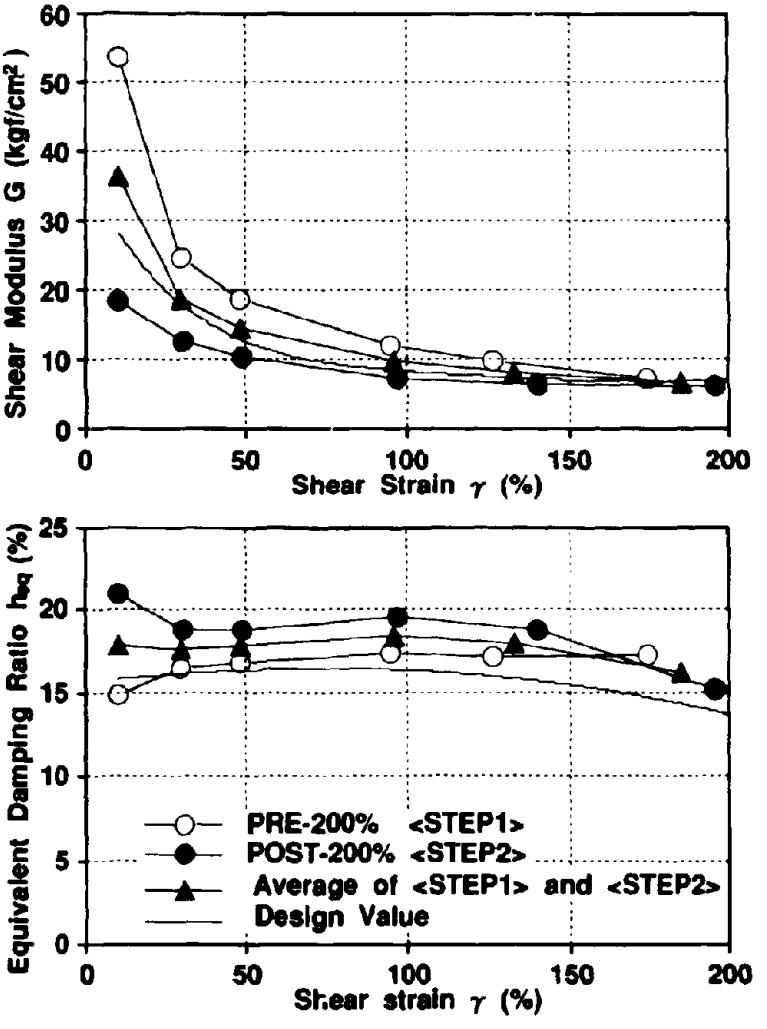

Fig.6 Horizontal Properties at Initial State

The design value of G and heq was comfirmed by dynamic test results previously caried out on scaled model bearing with a diameter of 150 to 200 mm. Large size bearing had never been tested dynamically before. These scale tests therefore provide important proof of the dynamic properties of full size bearing. The good agreement between test results and design value are shown in Fig.6. Full size bearings, which were previously tested staticaly, have therefore been shown to have the dynamic properties as designed.

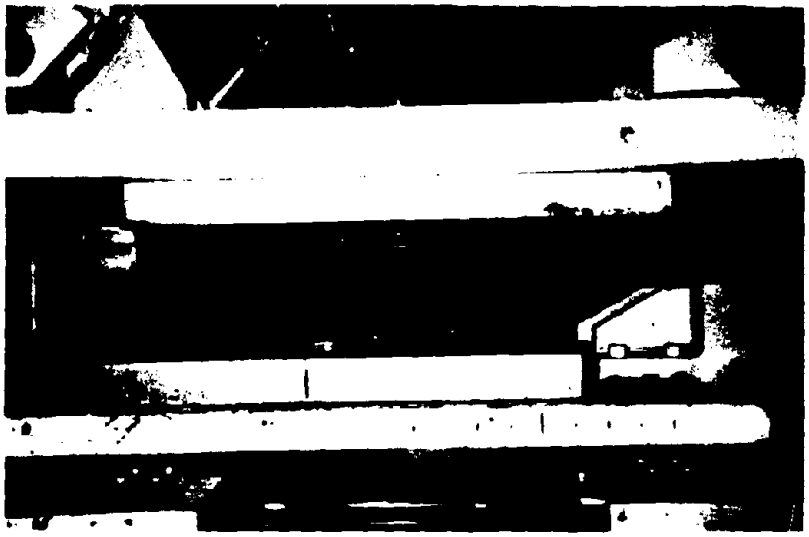

Photo.1 HDR under Dynamic Test

2. Evaluation of Recovery

Dynamic restoring force characteristics after 73 days intervals(STEP-6) are shown in Fig.7. Compared with those of STEP-1 and STEP-2 (Fig.4 and Fig.5), it is clear that restoring force has recovered to a value above STEP-2, but below the level of STEP-1. Fig.8 compares the shear modulus (G) and equivalent damping ratio (heq) calculated from 3rd cycles of each strain for STEP-1 to STEP-6. As can be seen, after STEP-2, G guradually increased, whereas heq slightly decreased with time. Fig.9-1, Fig.9-2 show the change of G and heq from STEP-1 to STEP-6. The values are calculated from 1st and 3rd cycles of 50%,100% and 200% shear strain. Digital values are also listed on Table 3. Here, the recovery ratio of STEP-2 of both G and heq was adopted in order to investigate the phenomenon. The recovery ratio shows maximum value after 1 day interval(STEP-3). Therefore, recovery occures "fast" immediately after initial loading , then gradually reduces its rate as time passes. Compared with G, the recovery of heq is small from STEP-2 through STEP-6. This result indicates that the dissipated energy(Wd) increase slightly with time. While recovery is still progressing slowly after 73 days interval, it is believed that recovery will be negligible after 100 days.

3. Verification of Design Expressions for G & heq

Fig.10 shows comparison between average value of G and heq for STEP-1 , STEP-2 and STEP-6 (73 days interval). Although there are some differences in small strain level, a good agreement is recognized.
This result indicates that the average value of before and after high

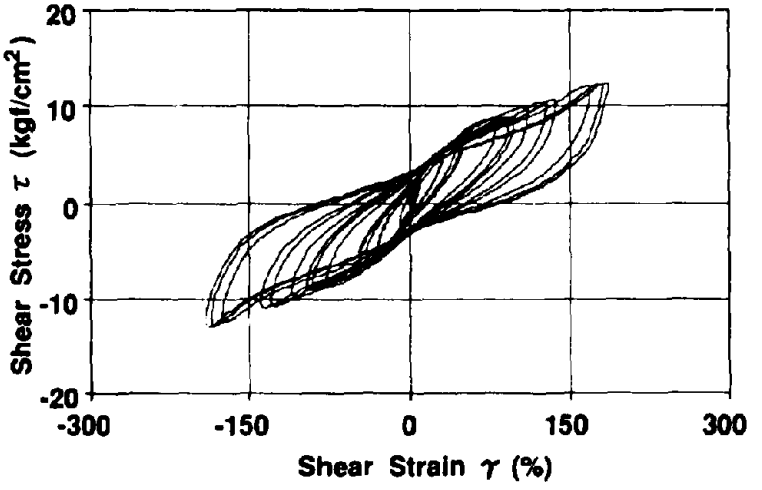

Fig.7 Restoring Force Characteristics after 73Days<STEP6>

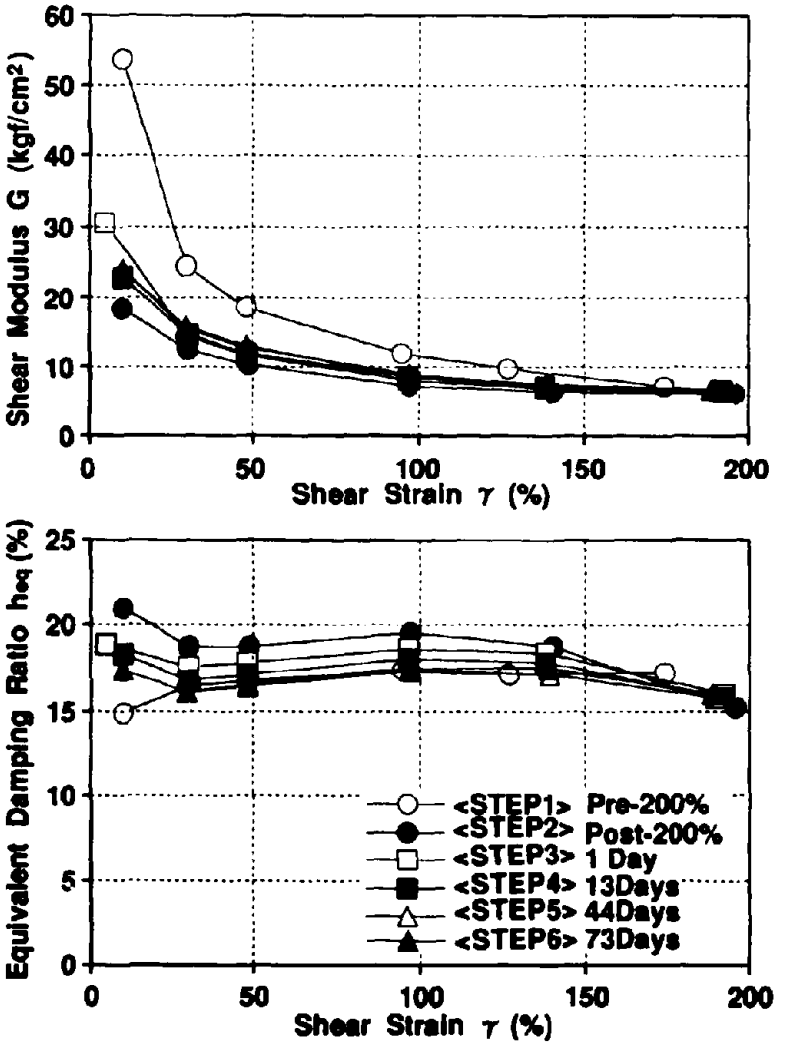

Fig.8 Recovery of Characteristics (The 3rd Cyclic Loop)

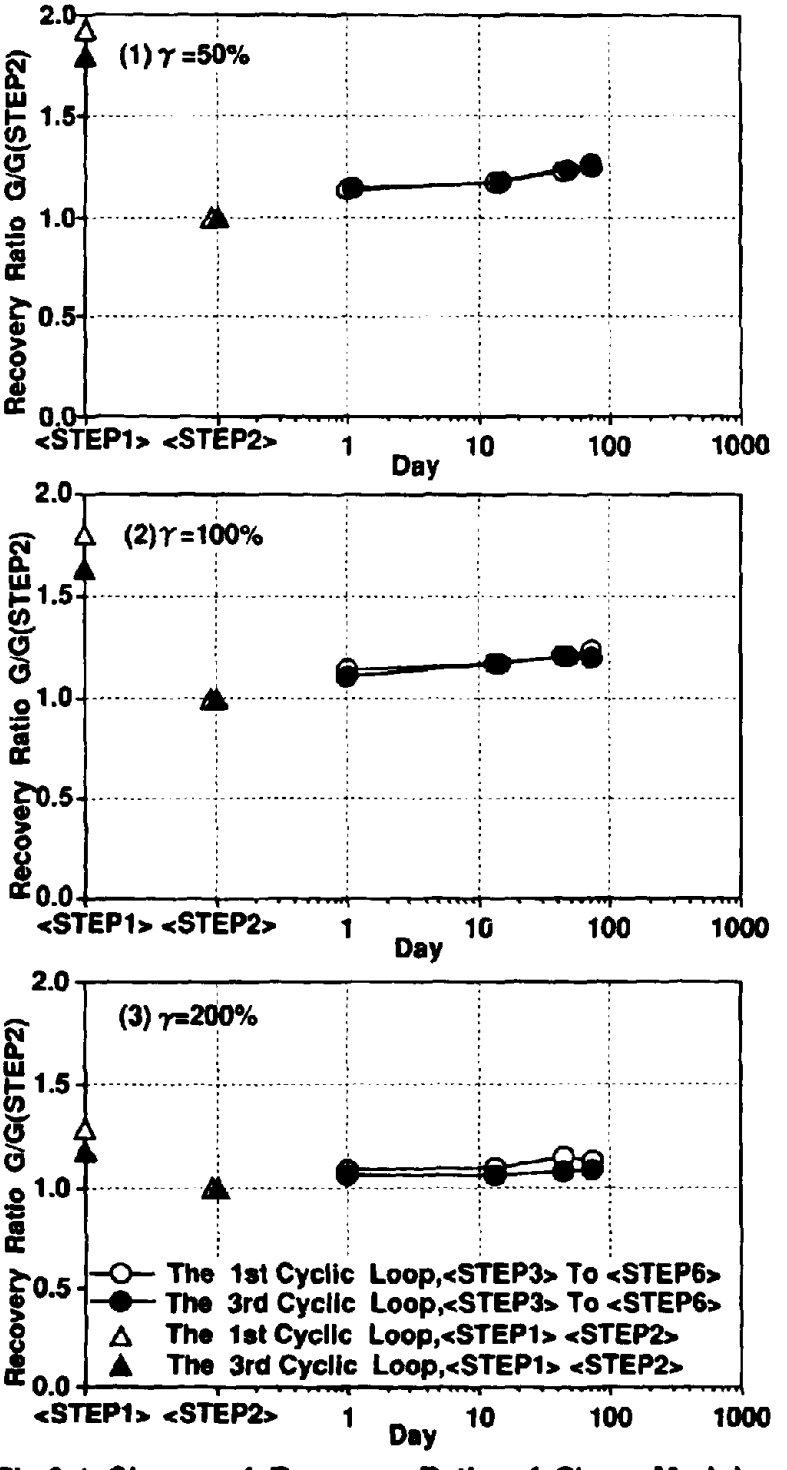

Fig.9-1 Change of Recovery Ratio of Shear Modulus

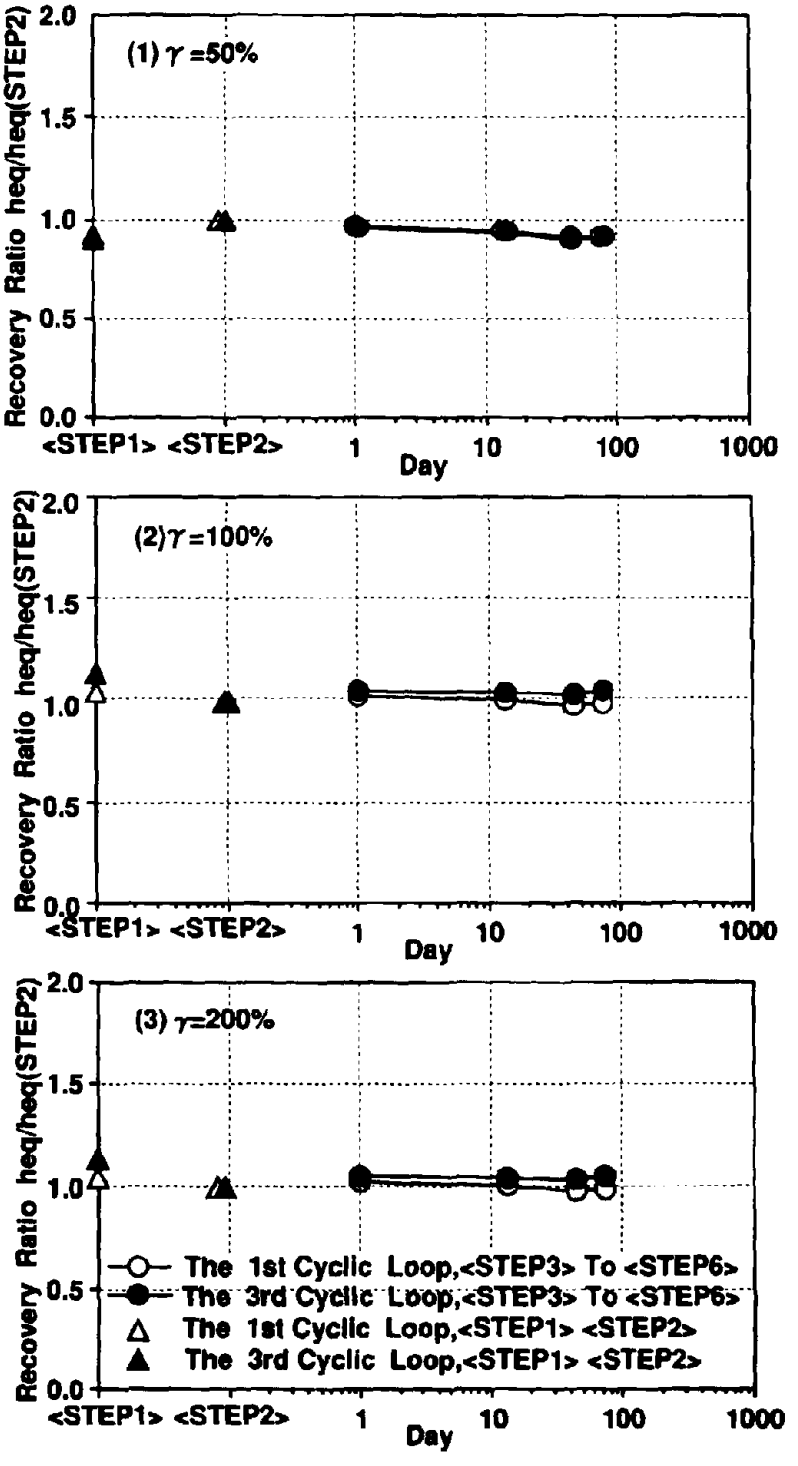

Fig.9-2 Change of Recovery Ratio of Equivalent Damping

Table3 Recovery Characteristics at γ_t=50,100,200%

(1) γ_t=50%(Target Strain γ_t)

<STEP> Days	Cycle	Shear Strain γ(%)	Shear Modulus		Damping Ratio	
			G(kgf/cm²)	G/G(STEP2)	heq(%)	heq/heq(STEP2)
STEP1 Initial	1st	38.5	22.34	1.93	16.90	0.91
	3rd	48.1	18.42	1.80	16.85	0.90
STEP2 0	1st	41.1	11.59	1.00	18.49	1.00
	3rd	48.3	10.24	1.00	18.79	1.00
STEP3 1	1st	40.9	13.18	1.14	17.57	0.95
	3rd	48.1	11.66	1.14	17.90	0.95
STEP4 13	1st	40.9	13.59	1.17	16.91	0.91
	3rd	48.1	11.99	1.17	17.20	0.92
STEP5 44	1st	41.4	14.24	1.23	16.36	0.88
	3rd	48.1	12.66	1.24	16.50	0.88
STEP6 73	1st	41.7	14.46	1.25	16.32	0.88
	3rd	48.1	12.95	1.26	16.60	0.88

(2) γ_t=100%(Target Strain γ_t)

<STEP> Days	Cycle	Shear Strain γ(%)	Shear Modulus		Damping Ratio	
			G(kgf/cm²)	G/G(STEP2)	heq(%)	heq/heq(STEP2)
STEP1 Initial	1st	70.9	15.09	1.81	17.66	0.93
	3rd	94.4	11.84	1.64	17.45	0.89
STEP2 0	1st	80.3	8.34	1.00	19.06	1.00
	3rd	97.2	7.23	1.00	19.53	1.00
STEP3 1	1st	78.8	9.52	1.14	18.52	0.97
	3rd	96.7	7.99	1.11	18.72	0.96
STEP4 13	1st	78.6	9.79	1.17	17.85	0.94
	3rd	96.7	8.44	1.17	18.10	0.93
STEP5 44	1st	79.9	10.06	1.21	17.41	0.91
	3rd	97.0	8.75	1.21	17.39	0.89
STEP6 73	1st	79.6	10.32	1.24	17.37	0.91
	3rd	97.0	8.67	1.20	17.56	0.90

(3) γ_t=200%(Target Strain γ_t)

<STEP> Days	Cycle	Shear Strain γ(%)	Shear Modulus		Damping Ratio	
			G(kgf/cm²)	G/G(STEP2)	heq(%)	heq/heq(STEP2)
STEP1 Initial	1st	157.4	7.94	1.29	17.12	1.04
	3rd	174.5	7.26	1.18	17.25	1.13
STEP2 0	1st	178.1	6.17	1.00	16.49	1.00
	3rd	195.9	6.14	1.00	15.25	1.00
STEP3 1	1st	173.8	6.69	1.08	16.85	1.02
	3rd	192.3	6.49	1.06	15.96	1.05
STEP4 13	1st	173.0	6.78	1.10	16.50	1.00
	3rd	191.6	6.51	1.06	15.82	1.04
STEP5 44	1st	172.3	7.10	1.15	16.14	0.98
	3rd	190.1	6.63	1.08	15.78	1.03
STEP6 73	1st	172.7	6.70	1.09	16.30	0.99
	3rd	188.9	6.66	1.08	16.01	1.05

shear strain (ie:200%) gives a good approximation of the recovery effect The accuracy of design expressions for G and heq is therefore verified.

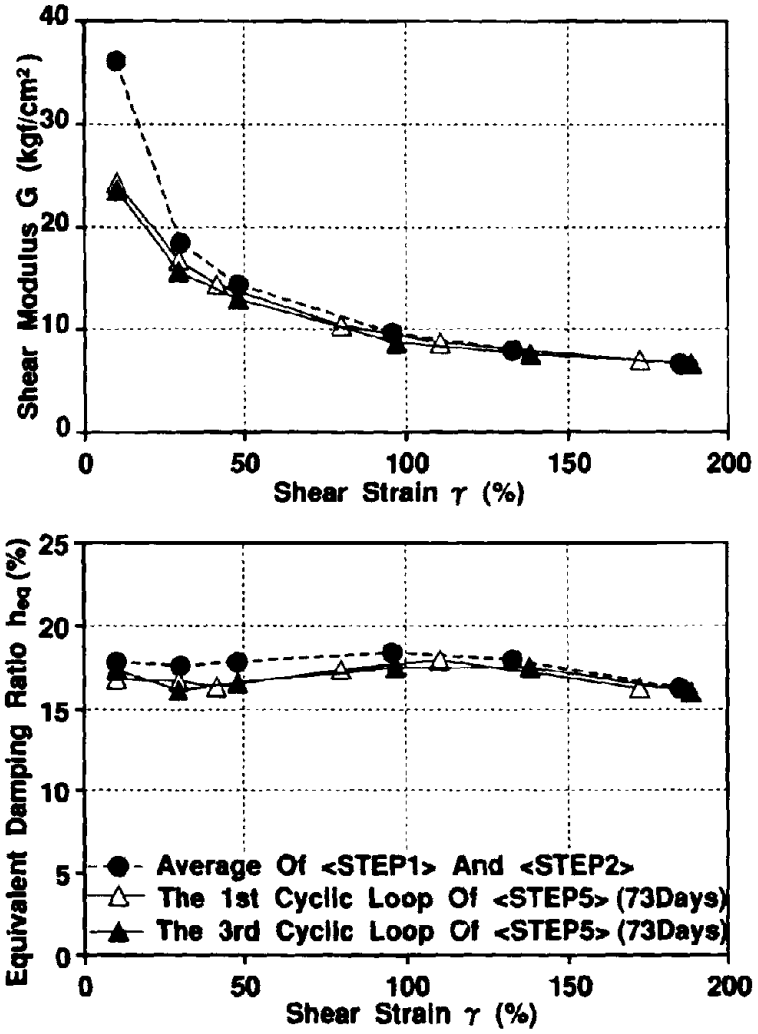

Fig.10 Comparison between Recovered Performance and Design Value

CONCLUSIONS

1. Recovery characteristics of High Damping Rubber Bearing was estimated over a 73 days interval. Shear modulus (G) and equivalent damping ratio (heq) were recovered to design level equal to the average of the values "before" and "after" high shear strain (200%) experience. The validity of design expression for G and heq that has been used in the past was verified by these results.
2. After high shear strain (200%) experience, shear modulus gradually increase, whereas equivalent damping ratio slightly decrease with time.
Recovery ratio shows maximum value after 1 day interval and minimum after 73 days interval. This results indicate that recovery occurs "fast" immediately after initial loading, then gradually reduces its rate as time passes. It is predicted that recovery will be almost finished after 100 days.
3. Dynamic properties of full scale HDR were comfirmed. There were a good agreement with design value.

REFERENCES

1. Yoji SUIZU and Chiaki SUDO:Development of High Damping Rubber Bearing for Menshin Bridges (Part 1), 1st U.S-Japan Workshop on Earthquake Protective Systems for Bridges, National Center for Earthquake Engineering Reserch, Buffalo, New York, 1991
2. Kazuhiko KAWASHIMA, Kazuo ENDO, Nobuyuki DORO, Chiaki SUDO, Ichiro NISHIKAWA: Approving Test Results on Four High Damping Rubber Bearings,2nd U.S-Japan Workshop on Earthquake Engineering Systems of Highway Bridges, Public Works Reserch Institute Tsukuba Science City, Japan, 1992
3. David M.Cho et. al.,The Los Angeles County Emergency Operations Center,on High Damping Rubber Bearings to Withstand an Earthquake Bigger than the "Big One":Proceedings of ATC-17-1 Seminar on Seismic Isolation, Passive Energy Dissipation, and Active Control, San Francisco, California, 1993

EFFECTS OF PIER UPLIFT AND SLIDING ISOLATION ON SEISMIC PERFORMANCE OF HIGHWAY BRIDGES

Xiao-Feng Wang
Department of Civil Engineering
Washington University at St. Louis

Phillip L. Gould
Department of Civil Engineering
Washington University at St. Louis

Abstract

The effects of pier uplift on sliding isolated highway bridges are studied for a symmetrical two-span continuous deck bridge. The seismic excitation uses the 1940 El Centro earthquake ground motion with a scaled peak ground acceleration $0.60g$, which is comparable to the CalTrans bridge design spectra of $0.60g$ acceleration for rock. Pier uplift is found to enhance the effectiveness of sliding isolation for a highway bridge, especially for piers with inadequate lateral strength capacity. Elastic behavior of the pier is possible, while the seismic performance of a sliding isolated highway bridge is affected minimally by the pier uplift. These benefits are achieved with a relatively small amount pier uplifting.

Introduction

The application of seismic isolation significantly improves the seismic performance of highway bridges during a severe earthquake, as earthquake energy is more reliably absorbed by energy dissipation mechanisms which are incorporated in the seismic isolation systems, rather than by the structural components, usually the piers. Hence, elastic behavior of piers under a severe earthquake may be achieved. Also, since the distribution of seismic lateral forces between the piers and abutments is easily controlled, the shear forces in the piers can be reduced greatly.

Besides applications for new highway bridges, seismic isolation has been shown to be a competitive alternative in retrofitting existing bridges that were designed and built before the implementation of modern seismic codes. The seismic deficiency commonly exhibited in these bridges is that the pier lacks adequate lateral load resistance and has very limited ductility. By using seismic isolation bearings, either

lead-rubber bearings with a low yield lead plug or Teflon sliding bearings with low friction, at the top of piers with inadequate strength, the shear forces developed may be below the capacity of these seismically deficient piers. However, there is a fundamental assumption for the calculated lateral demand, i.e., the pier base is assumed to be fixed into the foundation, which is questionable because the required uplift resistance capacity may be well below the demand for the existing bridges and the pier might lift off from the foundation. Though remedies, such as footing tiedowns, extended footings, cast-in-drilled-hole piles and drilled piers, can be applied to make up the deficiencies, it has been reported that they are among the most difficult tasks in retrofit projects (Jackson 1993).

While the uplift resistance capacity seems highly desirable, an approach dramatically different from this conventional practice was suggested in the 70's for the seismic design of the South Rangitikei Bridge in the New Zealand (Beck and Skinner 1974; Skinner, Robinson and McVerry 1993). It was believed that pier uplift not only eliminated the strict requirement of anchorage of the pier, but also made the elastic behavior of the pier possible. It was also found that energy dissipation devices were needed for reducing both the deck displacement and the amount of uplift. However, the fact that the activation of the energy dissipation devices was possible only after the uplift occurred seems to be a limitation of such practice.

For seismic isolated bridges, especially using sliding bearings, energy dissipation will occur long before, as well as after, pier uplift. Consequently, the seismic isolation first reduces the uplift force; then, as the uplift force builds up to cause the pier to lift off from the foundation, the inherent energy dissipation mechanism continues its function.

Hence, the assumption of the pier fixed to the foundation is eliminated in this study. Effects of pier uplift on seismic performance of sliding isolated highway bridges, as compared with that of a fixed pier, are examined. The model for the highway bridge is a symmetrical two span continuous deck bridge, which is consistent with a reported study for longitudinal seismic performance of a sliding isolated highway bridge with a fixed pier by Kartoum et al. (1992). The seismic excitation uses the 1940 El Centro earthquake ground motion with a scaled peak ground acceleration (PGA) 0.60g, which is comparable to the CalTrans bridge design spectra of 0.60g acceleration for rock.

Model of Highway Bridge

A symmetrical two span continuous deck bridge is shown in Figure 1a, and the corresponding analytical model is shown in Figure 1b. Sliding bearings with a lower

coefficient of friction are inserted between the top of the pier and the bottom of the deck. The other sliding bearings, with a larger coefficient of sliding friction and with re-centering devices, are located at abutment supports. The capacity of the re-centering devices is represented by a parameter T_b. The flexibility of the pier is described by a nominal period of the pier T_p. Both parameters are defined consistent with the study of Kartoum et al. (1992).

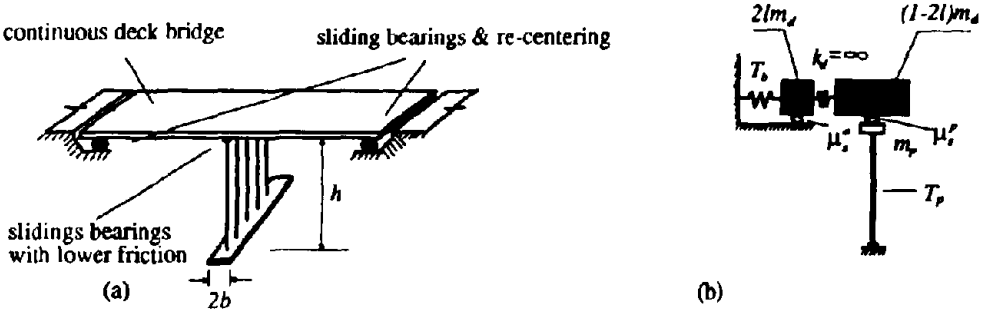

Figure 1. (a) Symmetrical two-span continuous deck bridge; (b) Analytical model

Equations of Motion

The equations of motion for the phase of pier contact with the foundation involve two variables, u_p, and u_d, i.e. the pier displacement and the deck displacement with respect to the ground, respectively.

$$m_d(\ddot{u}_d + \ddot{u}_g) + F_f^p + 2F_f^a + 2F_r^a = 0 \tag{1}$$

$$m_p(\ddot{u}_p + \ddot{u}_g) + F_b - F_f^p = 0 \tag{2}$$

where,

$$F_f^p = \mu_s^p(1-2l)m_d g z_p \tag{3}$$

$$F_f^a = \mu_s^a l m_d g z_d \tag{4}$$

$$F_r^a = k_r u_d + c_r \dot{u}_d \tag{5}$$

in which l is the ratio of the weight carried by abutment to the weight of the deck; μ_s^p, μ_s^a, are the coefficients of sliding friction, which are approximated by the equation (Mokha et al. 1988; Constantinou et al. 1990):

$$\mu_s^i = f_{max}^i - Df^i \exp(-a_i|\dot{u}_i|) \tag{6}$$

For the bearing at the pier, $i=p$, $f_{max}^i=0.070$, $Df^i=0.050$, $a^i=31.50 sec/m$ $(0.80 sec/in)$, and $u_i=u_d-u_p$, whereas, for the bearings at the abutments, $i=a$, $f_{max}^i=0.149$, $Df^i=0.093$, $a^i=23.62 sec/m$ $(0.60 sec/in)$, and $u_i=u_d$; z_p and z_d, two parameters which control the condition of separation and reattachment of the bearings, can be numerically solved from the following differential equation (Constantinou et al. 1990).

$$y\dot{z}_i = \dot{u}_i - 0.9 z_i|\dot{u}_i z_i| - 0.1\dot{u}_i z_i^2 \tag{7}$$

in which y is the shear deformation of the Teflon pad before sliding. Because of the small value of this shear deformation $0.0127 cm$ $(0.005 in)$, equation (7) is a stiff differential equation and the numerical integration of the equations of motion requires a specific numerical scheme (Nagarajaiah et al. 1991).

After the pier uplift from the foundation, the equations of motion can be written as

$$m_d(\ddot{u}_d + \ddot{u}_g) + F_f^p + 2F_f^a + 2F_r^a = 0 \tag{8}$$

$$m_p(\ddot{u}_p + \ddot{u}_g + \ddot{\chi}) + F_b - F_f^p = 0 \tag{9}$$

$$m_p(b^2 + h^2)\ddot{\theta} + m_p(\ddot{u}_p + \ddot{u}_g)h - F_f^p h \pm (m_d + m_p)gb = 0 \tag{10}$$

where, θ is the rotation from pier uplift and χ is the additional horizontal displacement at the top of the pier, so that $\chi=h\theta$.

It should be pointed out that the equations of motion for the fixed pier are the same as those for the phase of pier contact with the foundation. However, inelastic behavior of the pier is possible under a strong ground motion. The hysteresis of the pier is accounted for by using a bilinear model (Wen, 1976).

Criteria of Pier Uplift

The pier lifts off from the foundation when the overturning moment generated from a strong ground motion exceeds the overturning resistance from the gravity loads. This criterion is expressed by

$$|F_b|h \geq (m_p + m_d)gb \tag{11}$$

or in normalized form, if $f_b = F_b / m_p$

$$|f_b| \geq \frac{\alpha g}{\gamma} \tag{12}$$

where,

$$\alpha = \frac{b}{h} \tag{13}$$

$$\gamma = \frac{m_p}{m_p + m_d} \tag{14}$$

Since f_b is also related to the pier strength demand ratio f_b^p by

$$f_b^p = \frac{\gamma f_b}{1 - 2l + 2l\gamma} \tag{15}$$

f_b^p represents a shear force which is defined as the portion of the weight carried by the pier(Kartoum et al. 1992). Then, the criterion of pier uplift can also be written as

$$|f_b^p| \geq \frac{\alpha g}{1 - 2l + 2l\gamma} \tag{16}$$

Equation (16) implies that the uplifting pier will perform elastically, provided that the pier strength capacity is greater than the minimum uplift resistance supplied solely by the gravity.

The seismic response of the highway bridge is calculated by numerical integration of equations of motion. The numerical algorithm uses a semi-implicit fourth order Runge-Kutta scheme which is suitable to solve stiff differential equations.

Effects of Pier Uplift

The effects of pier uplift on the seismic performance of a sliding isolated highway bridge are investigated as compared to that of the same bridge with a fixed pier. This

highway bridge has the following characteristics, α=0.05, γ=0.10, T_p=0.4*sec*, ξ_p=0.05; and the re-centering devices incorporated at the abutments result in, T_b=2.0*sec*. Possible viscous damping is neglected, i.e. ξ_b=0. The pier strength capacity, defined as a portion of weight the pier carries, is assumed to be 0.10, which represents a pier with an inadequate lateral capacity in an existing highway bridge.

The maximum response of the highway bridge in terms of pier strength demand ratio, the lateral force distribution factor, the deck acceleration, the pier acceleration, the bearing displacement at abutments, the bearing displacement at pier, and uplift amount, calculated for the 1940 El Centro earthquake ground motion with a scaled PGA=0.60g, are listed in Table 1 for both fixed piers and uplifting piers, respectively.

Table 1. The maximum response of the sliding isolated highway bridge for the 1940 El Centro earthquake ground motion with a scaled PGA=0.60*g*

fixity of pier	f_b'	load distri. factor	deck acc. (*g*)	pier acc. (*g*)	bearing displ. @ abut *cm(in)*	bearing displ. @ pier *cm(in)*	uplift amount *cm(in)*
fixed	0.103	1.95	0.21	0.54	11.53(4.54)	6.40(2.52)	0
uplift	0.078	1.86	0.19	0.51	10.67(4.20)	4.55(1.79)	0.91(0.36)

Figure 2a,b show the pier strength demand ratio time history for a fixed pier and an uplifting pier respectively. The pier uplift reduces the maximum pier strength demand from 0.103, in the case of the fixed pier, to 0.078. Since the pier strength capacity is assumed to be 0.10, the pier is protected from the damage which will occur for the fixed pier condition.

The distribution of seismic lateral forces between the abutments and the pier in this study is examined by a distribution factor which is the ratio of the maximum lateral force resisted by one abutment to that of the pier. For seismic isolated highway bridges, this factor is in the range of 1 to 2, depending upon the relative lateral capacity of the abutment and the pier. For a weak pier, the larger factor will be selected. From the factors shown in Table 1, it can be concluded that the pier uplift has a minor effect on the distribution of lateral forces. Also, the effects of pier uplift on the maximum acceleration of the deck and the pier are insignificant.

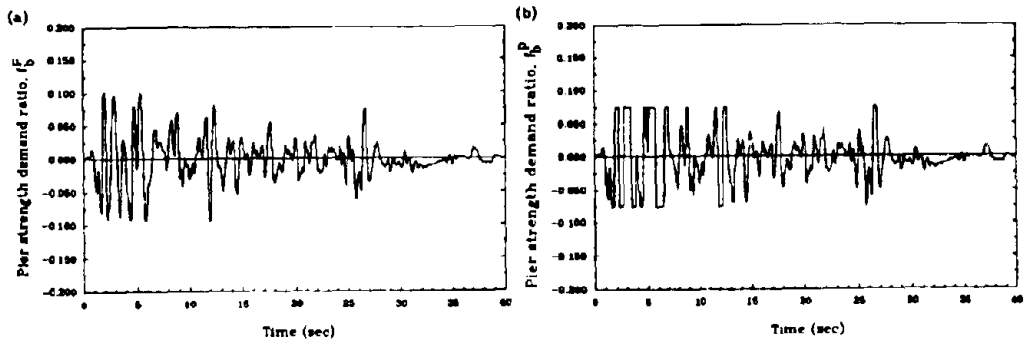

Figure 2. The pier strength demand ratio time history (a) fixed pier; (b) uplifting piers

Figure 3a shows the time history of the bearing displacement at the abutment, which is also the deck displacement time history, for fixed piers and uplifting piers. Though the time histories in the first 15 seconds have some difference, the bearing displacement at the abutments seems to be affected minimally by pier uplift.

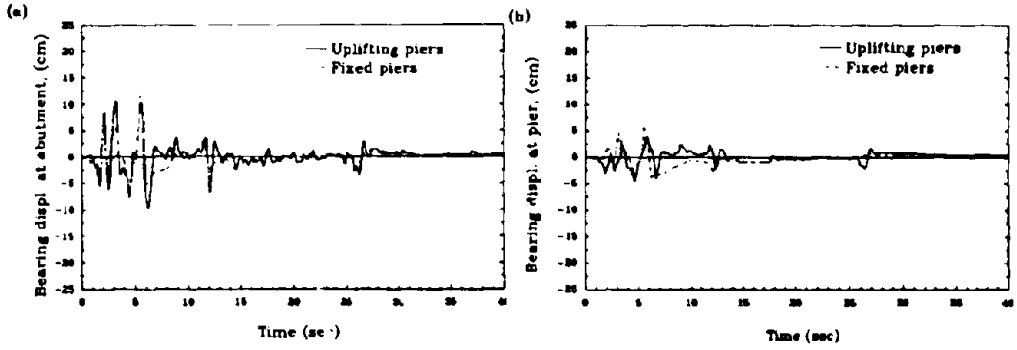

Figure 3. The time history of the bearing displacement (a) at abutment; (b) at pier

Interestingly, by comparison with the time history of the bearing displacement at the pier for fixed piers and uplifting piers, shown in Figure 3b, uplifting piers tend to reduce the maximum bearing displacement from 6.40*cm* (2.52*in*) to 4.55*cm* (1.79*in*).

Effects of T_p

It has been demonstrated that the pier strength demand ratio is reduced with increasing flexibility of the pier when the pier is fixed into the foundation (Kartoum et al. 1992). Figure 4a. shows the pier strength demand ratio with the variation of T_p from the 0.20 to 0.60*sec* and confirms this reduction for the fixed pier.

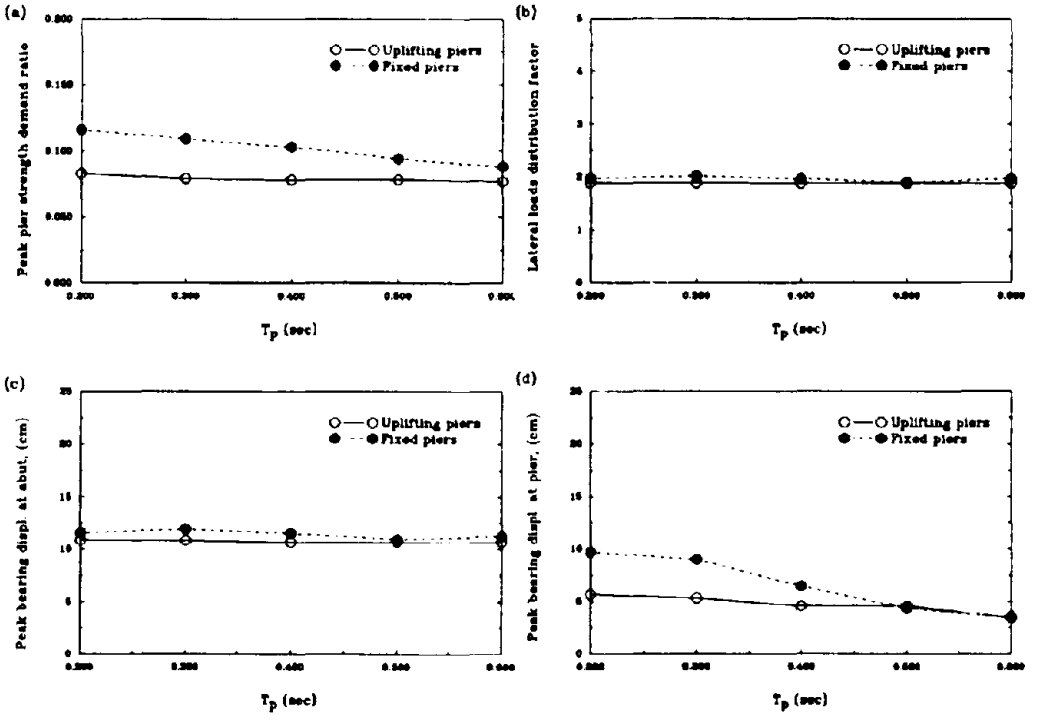

Figure 4. The maximum response with the variation of T_p for uplifting piers and fixed piers for the 1940 El Centro earthquake accelerogram with a scaled PGA=0.60g (a) Maximum pier strength demand ratio; (b) Lateral force distribution factor; (c) Maximum bearing displacement at abutments; (d) Maximum bearing displacement at pier.

Also, it shows that there is not much variation of the strength demand ratio for the uplifting pier; the maximum values are obviously less than 0.10, which implies elastic behavior of the uplifting pier. This is a result of the initial condition for the pier uplift given by equation (16). During the phase of pier uplift, the sliding bearings

provide significant energy dissipation mechanisms which highly damp the response of the uplifting pier. The pier strength demand is no longer developed but bounded around a value at the instant of initial pier uplift. For this study, this value is 0.075.

Figure 4b,c show the maximum lateral force distribution factor and bearing displacement at the abutments with the variation of T_p. For both cases the effect of the flexibility of the pier on the distribution factor and the bearing displacement is insignificant. However, the effect of pier uplift, as discussed earlier, will reduce the bearing displacements at the pier, as observed in Figure 4d.

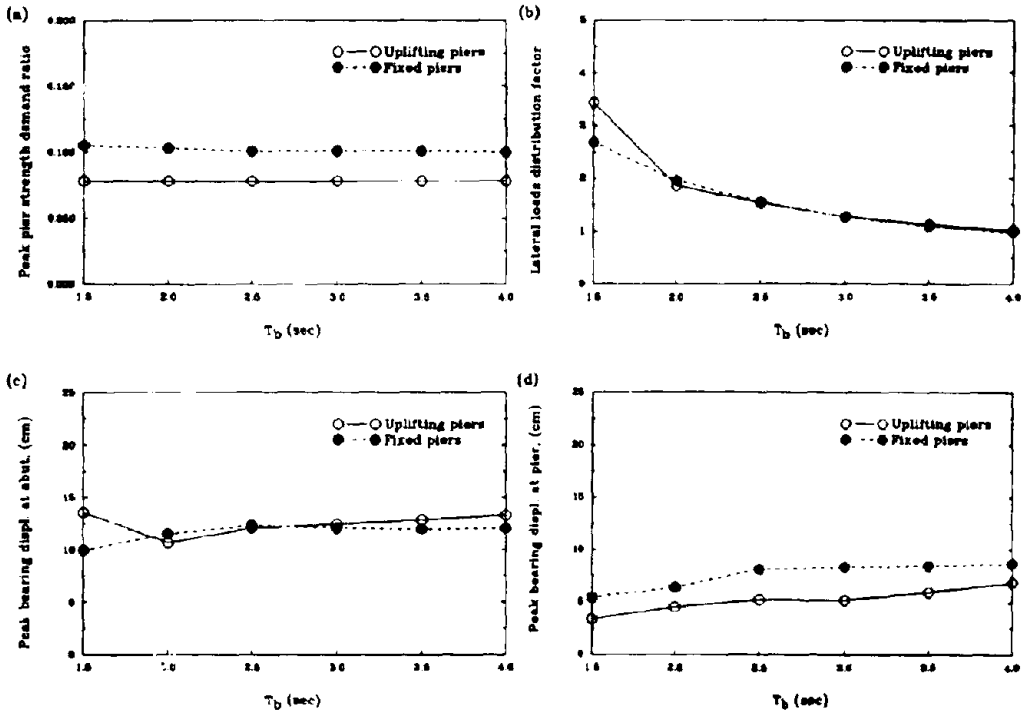

Figure 5. The maximum response with the variation of T_b for uplifting piers and fixed piers for the 1940 El Centro earthquake accelerogram with a scaled PGA=0.60g (a) Maximum pier strength demand ratio; (b) Lateral force distribution factor; (c) Maximum bearing displacement at abutments; (d) Maximum bearing displacement at pier.

Effects of T_b

The capacity of the re-centering devices is described by a parameter T_b. The larger the value of T_b, the weaker the re-centering. For the fixed pier, the effect of T_b on the strength demand ratio of the pier is not important as shown in Figure 5a. This is also consistent with the findings of the study by Kartoum et al (1992). As explained earlier, the strength demand of the uplifting pier is controlled by the condition of pier uplift. So the re-centering capacity has no effect on the pier strength demand.

However, the stronger the re-centering, the larger the force which must be resisted by the abutments. This explains the reason that the lateral force distribution factor decreases with an increase in T_b as shown in Figure 5b. Again, the effect of pier uplift does not change the distribution of lateral forces between the abutments and the pier.

Figure 5c,d show the maximum bearing displacement at the abutments and at the pier with the variation of T_b. While the effect of pier uplift on the maximum bearing displacement at the pier is beneficial as it leads to the reduction of the maximum values, such effects on the bearing displacement at the abutments are apparently mixed. However, even so, it is certainly not detrimental.

Behavior of Uplifting Pier

The seismic behavior of the uplifting pier is stable for the 1940 El Centro earthquake ground motion with a scaled PGA=0.60g, as shown by the uplift time history in Figure 6a. Figure 6b further shows the maximum uplift with the variation of intensity of the excitation. It is observed that the maximum uplift amount increases nearly linearly with an increase of PGA from 0.50g to 0.80g; even so, the maximum uplift is not large enough to be of concerned. The maximum uplift amount is also studied with the variation of T_p and T_b, as shown in Figure 6c,d, respectively. It is observed that the maximum values seems to decrease with increasing flexibility of the pier, while the effect of the capacity of re-centering is negligible.

Conclusion

Pier uplift from the foundation enhances the effectiveness of sliding isolation for highway bridges. The strength demand of the uplifting pier is less than that of the corresponding fixed pier, which might exceed the pier strength capacity. The elastic

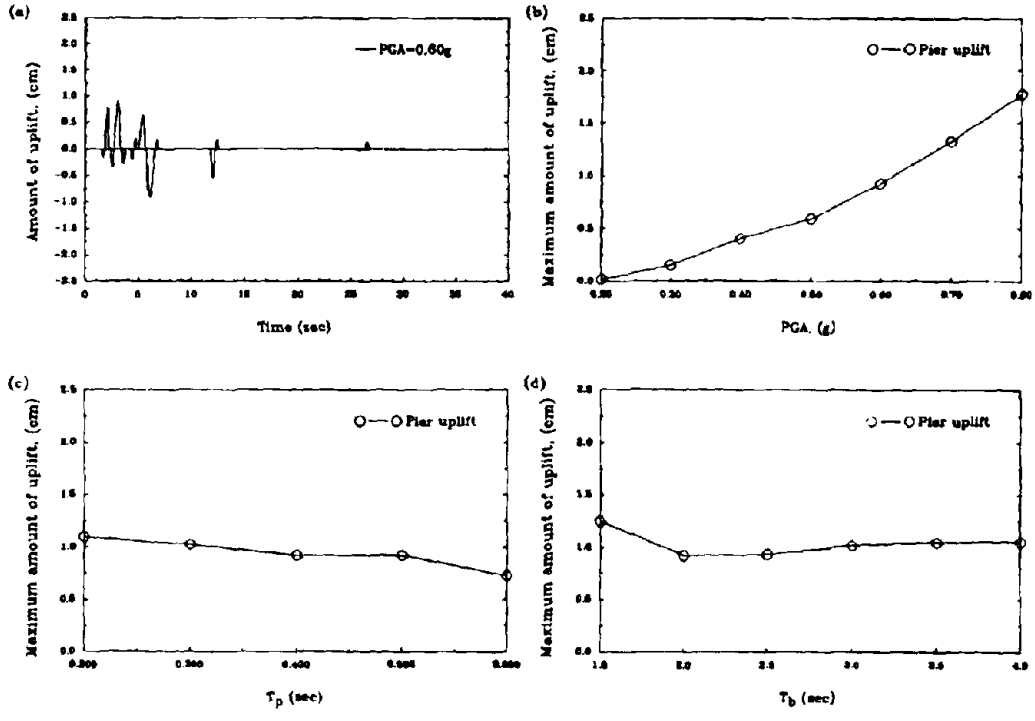

Figure 6. The behavior of uplifting pier for the 1940 El Centro earthquake (a) The uplift time history for PGA=0.60g; (b) Maximum uplift amount with the variation of intensity; (c) Maximum uplift amount with the variation of T_p, (d) Maximum uplift amount with the variation of T_b

behavior of the pier with inadequate lateral strength capacity is possible, provided that the capacity is above the strength demand to initiate pier uplift.

The distribution of lateral force between the abutments and the pier using sliding isolation is well controlled by the maximum friction of the sliding bearings and will be affected only slightly by pier uplift. The effect of uplift on the bearing displacement seems to be significant, especially at the pier.

The effects of the flexibility of the pier for the seismic response of highway bridges seem to be less significant with uplifting piers than that with fixed piers. The effects of the capacity of the re-centering is basically the same for both cases.

The behavior of an uplifting pier is stable in so far as its insensitivity to the flexibility of the pier and to the capacity of the re-centering. More importantly, the maximum amount of uplift increases only linearly with the intensity of excitation. For the maximum credible earthquake, the amount of uplift is not large enough to be of concerned.

References

Beck, J.L. and Skinner, R.I. (1974). "The seismic response of a reinforced concrete bridge pier designed to step." *Earthquake Engrg. & Struct. Dyn.*, 2(4), 343-358

Constantinou, M.C., Mokha, A. and Reinhorn, A.M. (1990) "Teflon bearing in base isolation. II: modeling." *J. Struct. Engrg.*, ASCE,116(2), 455-474.

Jackson, Thomas B. (1993). "Seismic retrofitting of highway bridges." *Bridge Inspection and Rehabilitation*, John Wiley & Sons, New York, 241-260

Kartoum, A., Constantinou, M.C. and Reinhorn, A.M. (1992). "Sliding isolation system for bridges: Analytical study." *Earthquake Spectra*, EERI, 8(3), 345-372

Mokha, A., Constantinou, M.C. and Reinhorn, A.M. (1988) "Teflon bearings in aseismic base isolation. Experimental studies and mathematical modeling." Report No. NCEER-88-0038, National Center for Earthquake Engineering Research, SUNY, Buffalo, N.Y.

Nagarajaiah, S., Reinhorn, A.M. and Constantinou, M.C. (1991a) "Nonlinear dynamic analysis of 3-D base isolated structures." *J. Struct. Engrg.*, ASCE,117(7),2035-2054.

Skinner, R.I., Robinson, W.H. and McVerry, G.H. (1993). "Applications of seismic isolation." *An Introduction to Seismic Isolation*, John Wiley & Sons, New York, 288-291.

Wen, Y.K. (1976). "Method for random vibration of hysteretic systems." *J. Eng. Mech. Div.* ASCE, 102(2), 249-263

HYBRID PROTECTIVE SYSTEMS

Seismic Response Control of Highway Bridges by Variable Stiffness Control

Use of Hybrid Dampers for Vibration Control of Structures

Application of Electro-Rheological Fluid for Variable Damper

Fuzzy Control of Bridge Vibration by Using Variable Dampers

Prediction Control of a SDOF System

Hybrid Protective Systems for Seismic-Excited Bridges

Closed-Open-Loop Control of Seismic Response of Structure with Active Mass Driver System

NIST

SEISMIC RESPONSE CONTROL OF HIGHWAY BRIDGES BY VARIABLE STIFFNESS CONTROL

Kazuhiko KAWASHIMA[1], Shigeki UNJOH[2] and Hidetoshi MUKAI[3]

1) Head, Earthquake Engineering Division, Public Works Research Institute, Ministry of Construction, Tsukuba Science City, Japan
2) Senior Research Engineer, ditto
3) Assistant Research Engineer, ditto

ABSTRACT

Presented is a concept of the variable stiffness control to control bridge response against an earthquake. The proposed concept is to shift the instantaneous natural period of bridges using the variable dampers by avoiding the resonance with ground motions. The effectiveness of the variable stiffness control through the analytical simulation is presented.

INTRODUCTION

The authors proposed variable dampers in which the damping coefficient can be variable dependent on structural response of highway bridges. Various studies including the applicability and practicability have been made at the Public Works Research Institute.[1)-9)]

Variable stiffness control is an another interesting field of extension of the variable damper. If one shifts the natural period of structures, the structural response may be significantly reduced by avoiding the resonance with the ground motion. The variable stiffness control is to shift the instantaneous natural period of bridges using the variable dampers.

This paper proposes the concept of the variable stiffness control using the variable dampers and the effectiveness of the variable stiffness control through the analytical simulation is presented.

CONCEPT OF VARIABLE STIFFNESS CONTROL

Most of bridges with an usual size have the natural period ranging from 0.3 to 1.5 second, and this natural period range corresponds to the predominant period of earthquake-induced ground motions. Thus the resonance of the bridge response with the ground motion tends to be developed during an earthquake. The bridge response can be

reduced if the resonance of bridge response with the ground motion is avoided.

Although it is hard to predict the predominant period of ground motion prior to an earthquake, it can be evaluated time by time during an earthquake. The moving window analysis may be used for evaluating the instantaneous predominant period of ground motion T^* . The resonance of bridge response with the ground motion may be avoided if the instantaneous natural period of bridges T be shifted from the instantaneous predominant period of ground motion T^* during an earthquake.

There are various methods to shift the instantaneous natural period of bridges during an earthquake. Flexibility of bearings may be changed, and active tendons/bracings may be adopted. If one provides the variable dampers for a bridge which is elastically supported by rubber bearings, the natural period of the bridge can be varied by changing the damping coefficient of the variable dampers. If one makes the damping ratio of the variable damper very large, the variable damper would acts as a damper stopper. On the other hand, if one makes the damping ratio small, the natural period of the bridge takes the value computed from the stiffness of the rubber bearings and piers. The variable dampers have various advantage for controlling the instantaneous natural period of bridges because it is more stable for long term use than the active tendons/bracing systems.

Fig. 1 shows the principal of the variable stiffness. The natural period of a bridge T is variable in the range between T_P and T_F . The periods T_P represents that when the damper acts as a damper stopper, it means that the bearing support condition is pinned. On the other hand, the period T_F represents that when the dampers do not work, i.e., the bearing support condition is free. If the instantaneous predominant period of ground motion T^* approaches the natural period of the bridge T , the bridge response becomes larger by the resonance effect. Therefore, if the natural period of the bridge T can be far from the predominant period of ground motion T^* , the bridge response can be significantly reduced.

ALGORITHM OF THE VARIABLE STIFFNESS CONTROL

Fig. 2 shows the algorithm of the variable stiffness control. The instantaneous predominant period of ground motion T^* at time t_i is computed by the moving window Fourier Spectrum. The damping coefficient of variable dampers is varied so that the instantaneous natural period of the bridge T be shifted to prevent the resonance with the ground motion.

Although several algorithm can be considered, the period shift is assumed here as

$$T_{i+1} = \alpha T_i^* \quad (\beta_1 \cdot T_i^* < T_i < \beta_2 \cdot T_i^*) \qquad (1)$$

where,

T_i : instantaneous natural period of a bridge at time t_i

T^* : instantaneous predominant period of ground motion at time t_i

α : control coefficient

β_1 , β_2 : on−off coefficient to control

The coefficient α has to be determined depending on the natural period of the bridge T and the instantaneous predominant period T^* of an ground motion. It is proposed that α is set as

$$\alpha \begin{cases} >1/2 & (T^* \leqq T) \\ <2 & (T^* > T) \end{cases} \tag{2}$$

The coefficient β represents the on−off coefficient of the variable stiffness control. When the instantaneous predominant period of the ground motion T_i^* at time t_i is far from the natural period of the bridge T , the variable stiffness does not need to work. Therefore, a certain period range to prevent the resonance is determined by the coefficient β .

EARTHQUAKE RESPONSE ANALYSIS METHOD

The equations of motion for a linear multi−degree−of−freedom system with the variable stiffness control may be written as

$$\underline{M}\,\ddot{\underline{x}} + (\underline{C} + \underline{C}_V)\,\dot{\underline{x}} + \underline{K}\,\underline{x} = -\underline{M}\,\ddot{X}_0 \tag{3}$$

in which $\underline{M}$, $\underline{C}$ and $\underline{K}$ represent mass, damping and stiffness matrices of the system, respectively. $\underline{x}$ and x_0 denote displacement vector of the system and an earthquake ground motion, respectively. $\underline{C}_V$ denotes a damping matrix of the variable dampers and is assumed as

$$\underline{C}_V = \sum_{i=1}^{n_V} \underline{c}_{ij}^{\,V} \tag{4}$$

where

$$\underline{c}_{ij}^{\,V} = \begin{bmatrix} C & -C \\ -C & C \end{bmatrix} \tag{5}$$

in which $\underline{c}_{ij}^{\,V}$ and n_V represent damping matrix of the variable dampers, which are installed between the i−th node and the j−th node, and a number of the variable dampers installed, respectively. C is the damping coefficient of an each variable damper and is given according to the control algorithm as shown in **Fig. 2.**

Although there are various methods to prescribe the damping matrix $\underline{C}$ of the structure, it is assumed here to be written as Eq.(6) assuming that the damping matrix $\underline{C}$ can be diagonalized by the modal matrix.

$$C = (\Phi)^{-1} diag[2h_k w_k] (\Phi^T)^{-1} \tag{6}$$

in which, Φ denotes a modal matrix of the system and $diag[2h_k w_k]$ denotes a diagonal matrix with elements of $2h_k w_k$ ($k = 1,2,3,\cdots$; mode number).

Since $\underline{C}_V$ is time−varying, Eq.(3) has to be solved by a direct integration method.

According to the above analytical method, a computer program "VSTIFF," which can analyze earthquake response of a multi−degree−of−freedom system with the variable

stiffness, was developed.

EFFECTIVENESS OF VARIABLE STIFFNESS CONTROL

To study the effectiveness of the variable stiffness control, a three-span continuous girder bridge, as shown in **Fig. 3**, with a span length of 90m is analyzed. The response in longitudinal direction is considered. The superstructure of the model is supported by elastic bearings, and four variable dampers with the same characteristics are installed between the deck and the piers. The weight of the superstructure and spring stiffness of the rubber bearings are assumed as 4,719KN and 6,247KN/m, respectively. The stiffness of piers is assumed so that the fundamental natural period of the bridge be about 0.5 sec when the deck support condition is hinged. The stiffness of rubber bearings is set so that the fundamental natural period of bridge be 1.0 sec. The damping ratio of the bridge without control is assumed as 0.02.

An acceleration ground motion as shown in **Fig. 4** is used as an input acceleration. The instantaneous predominant frequency ($1/T^*$) of the input acceleration is also shown in **Fig. 4**. Because the predominant period of ground motion is about 1 sec, α in Eq.(1) was assumed as 1/2.

Fig. 5 shows the dependence of the natural period/damping ratio of the bridge on the damping coefficient of variable dampers. **Fig. 6** shows the corresponding mode shapes of the bridge. When the damping coefficient C of the variable dampers is 0, the 1st mode is a rigid vibration mode of the deck in the longitudinal direction and is the most predominant mode against ground motions. The 2nd mode is the vertical vibration of the deck which does not contribute the bridge response against the horizontal ground motion. The natural periods of these modes are 1.0 sec and 0.23 sec, respectively.

If one increases the damping coefficient of the variable dampers, the natural periods of the 1st and 2nd modes increase. At the damping coefficient C of about 4,200KN·sec/m, the fundamental natural period of bridge take very large value, because this corresponds to the critical damping of the structure. Furthermore if one increases the damping coefficient of the variable dampers, the 1st and 2nd modes become overdamped modes and they do not contribute the response against a ground motion. However, a new mode as shown in **Fig. 5** appears as a predominant mode and the natural period decrease with increase of the damping coefficient of the variable dampers. The natural period of the mode gradually approaches 0.45 sec, which is the natural period when the bearing support condition is pinned, as the damping coefficient of the variable dampers increase.

Fig. 7 shows the control relation between the predominant natural period of the bridge and the damping coefficient of the variable dampers. Although the period shift may be made in the damping coefficient range of 0 to over 8,000KN·sec/m, it is assumed here that the period shift be made in the range of damping coefficient C over 4,200KN·sec/m.

Fig. 8 and **Table 1** compares the deck acceleration and displacement of the bridge

with and without control. The peak displacement and peak acceleration of deck decreases to 17% and 50% of those without control. The bending moment of pier bottom decreases to 52% of the one without control. The peak damping force required for the four variable dampers is 761KN×4=3,040KN and the peak stroke is 3.1cm.

CONCLUDING REMARKS

The concept of the variable stiffness control to control bridge response against an earthquake was presented. The effectiveness of the variable stiffness control was studied through the analytical simulation. It is demonstrated that the peak displacement and peak acceleration of deck decreases to 17% and 50% of those without control, and that the bending moment of pier bottom decreases to 52% of the one without control. The peak damping force required for the four variable dampers is 761KN×4=3,040KN and peak stroke is 3.1cm. The effectiveness of the variable stiffness control is also being studied through the shaking table tests.

Table 1 Peak Responses

	DECK		PIER BOTTOM
	DISP. (cm)	ACCEL. (gal)	BENDING MOMENT(tfm)
NO CONTROL	33.1	1,301	3,288
WITH CONTROL	5.6	653	1,701
VD	DAMPING FORCE : 77.6 tf STROKE : 3.1 cm		

REFERENCES

1) Kawashima, K. and Unjoh, S. : "Development of Hybrid Control Technology." Civil Engineering Journal, Tokyo, Japan, pp. 2–5, Vol. 32–6, 1989 (in Japanese).
2) Taguchi, J., Iwasaki, T., Adachi, Y., Sasaki, Y. and Kawashima, K. : " U.S.–Japan cooperative research program on hybrid control of seismic response of bridge structures." 22nd Joint Meeting, U.S.–Japan Panel on Wind and Seismic Effects, UJNR, Gaithersburg, Maryland, USA, May, 1990, NIST Special Publication
3) Kawashima, K., Unjoh, S., Nagashima, H. and Shimizu, H. : "Current research efforts in Japan for passive and active control of highway bridges against earthquakes." Proc. 23rd Joint Meeting, U.S.–Japan Panel on Wind and Seismic Effects, UJNR, Tsukuba, Japan, 187–209, 1991
4) Kawashima, K., Unjoh, S. and Shimizu, H. : "Earthquake response control of highway bridges by variable damper." Proc. of Colloquium on Control of Structures, Japan Society

of Civil Engineers, Part. B, pp.221−224, July, 1991 (in Japanese)
5) Kawashima, K., Unjoh, S. and Shimizu, H. : "Seismic response control of highway bridges by variable damper." 24th Joint Meeting, U.S.−Japan Panel on Wind and Seismic Effects, UJNR, Gaithersburg, May, 1992, NIST Special Publication 843
6) Kawashima, K., Unjoh, S., Iida, H. and Mukai, H. : "Effectiveness of the variable damper for reducing seismic response of highway bridges, Proc. of 2nd U.S.−Japan Workshop on Earthquake Protective Systems for Bridges, Tsukuba, Dec. 7−8, 1992, Technical Note of the Public Works Research Institute, No. 3196
7) Kawashima, K., Unjoh, S. and Mukai, H. : "Seismic response control of highway bridges by variable dampers." 25th Joint Meeting, Panel on Wind and Seismic Effects, UJNR, Tsukuba, May, 1993, Technical Note of Public Works Research Institute, No. 3217
8) Kawashima, K., Unjoh, S. and Shimizu, H. : "Earthquake Response Control of Highway Bridges by Variable Damper", Transactions of the Japan National Symposium on Active Structural Response Control, Japan Science Council, pp.311−317, March, 1992 (in Japanese)
9) Kawashima, K., Unjoh, S. and Shimizu, H. : "Experimental Study on Dynamic Characteristics of Variable Damper", Transactions of the Japan National Symposium on Active Structural Response Control, Japan Science Council, pp.311−317, March, 1992 (in Japanese)

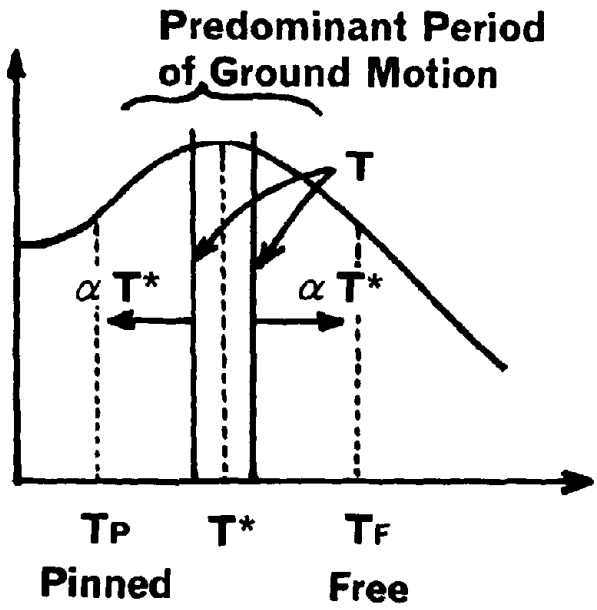

Fig. 1 Concept of Variable Stiffness

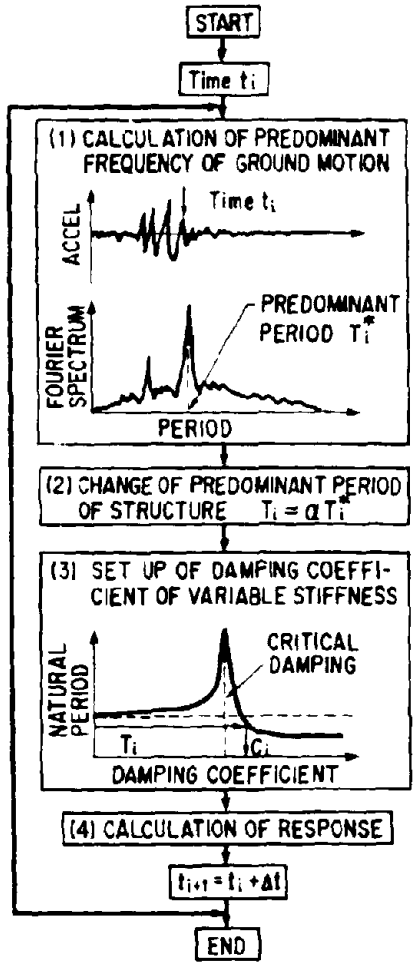

Fig. 2 Control Algorithm of Variable Stiffness

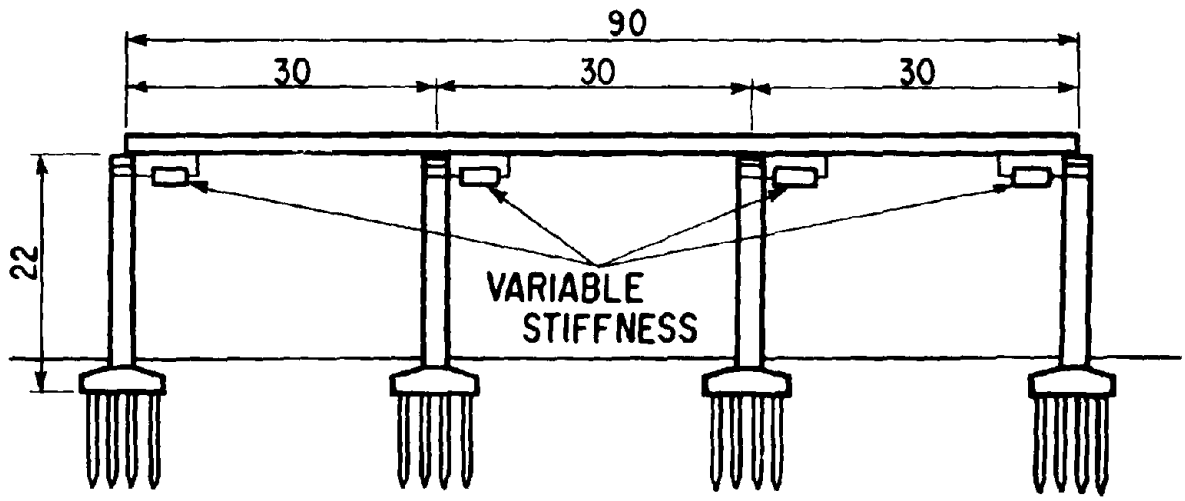

Fig. 3 Model Bridge Analysed

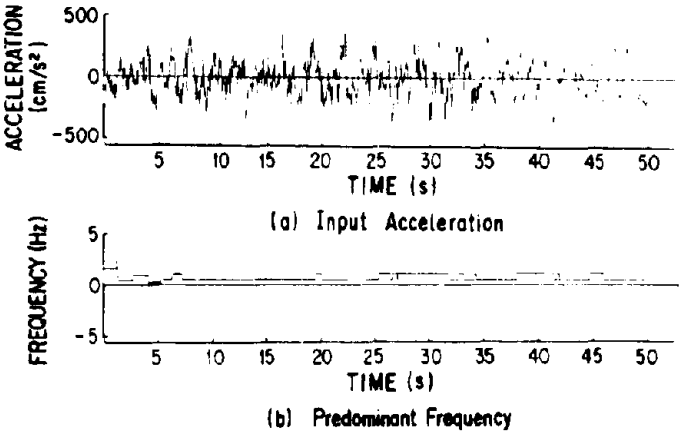

Fig. 4 Input Acceleration and the Predominant Period

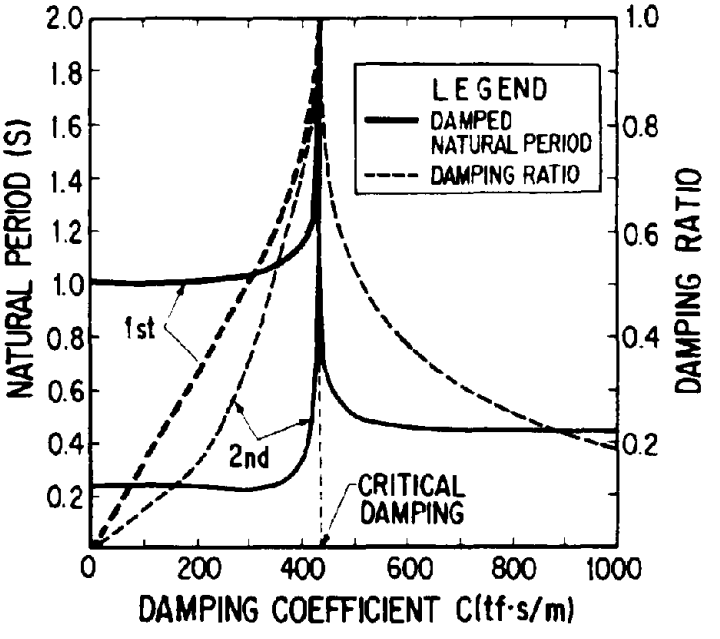

Fig. 5 Dependence of Natural Period/Damping Ratio of the Bridge on Damping Coefficient of Variable Dampers

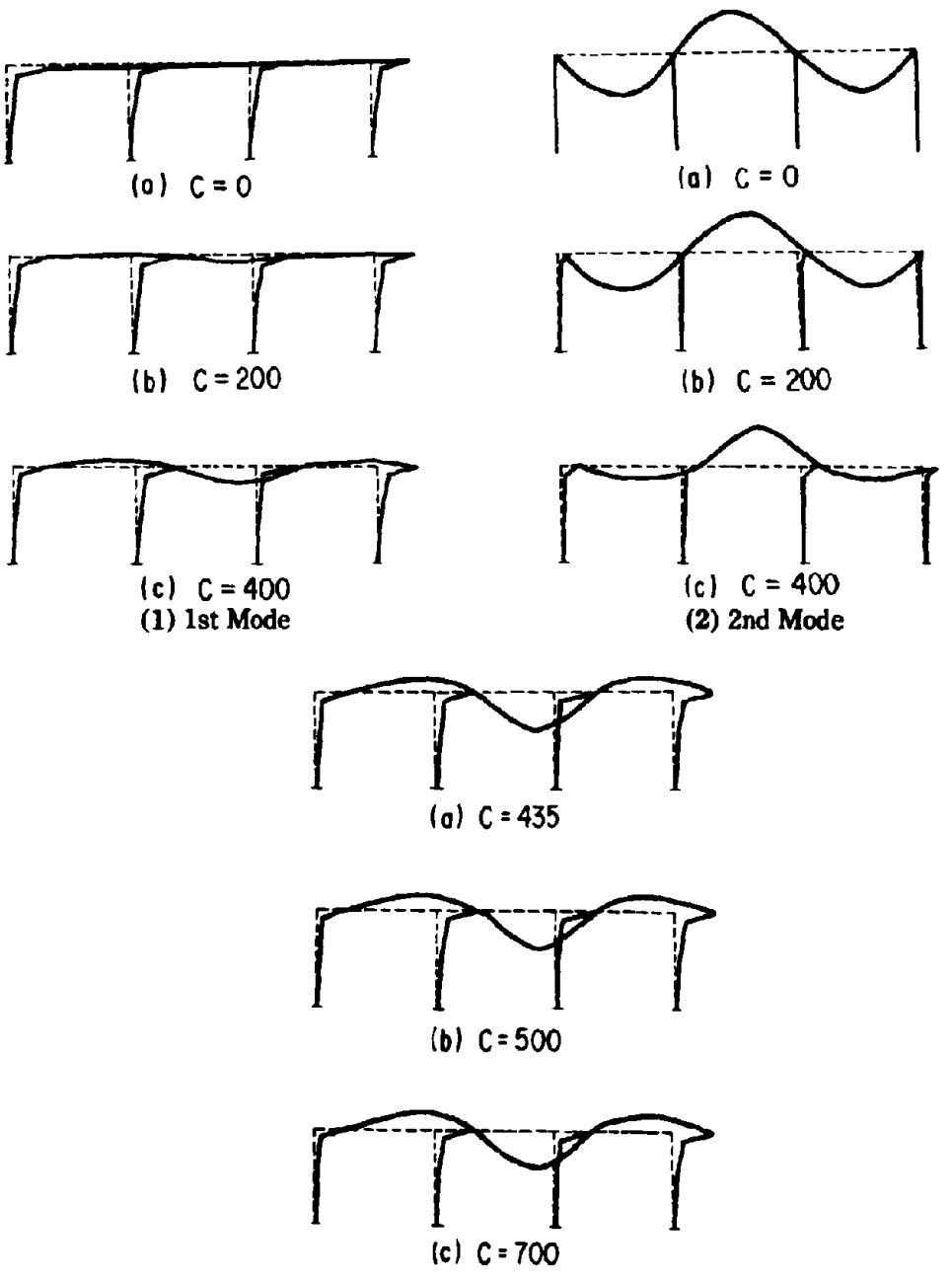

(3) Over damped Region

Fig. 6 Dependence of Natural Modes of the Bridge on Damping Coefficient of Variable Dampers

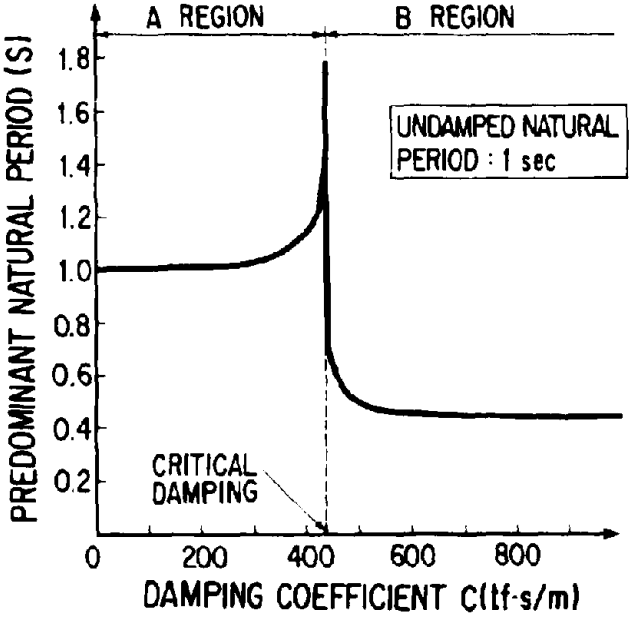

Fig. 7 Dependence of Natural Period of the Bridge on Damping Coefficient of Variable Dampers used for the Control

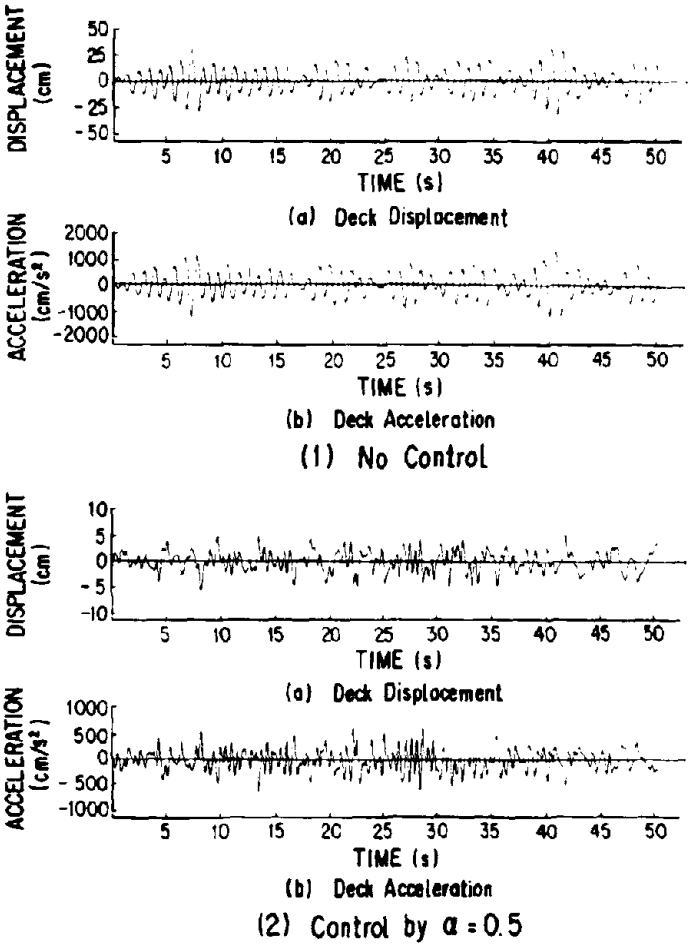

Fig. 8 Effectiveness of Variable Stiffness Control

USE OF HYBRID DAMPERS FOR VIBRATION CONTROL OF STRUCTURES

F. Gordaninejad[1], A. Ray[2] and H. Wang[3]
Department of Mechanical Engineering
University of Nevada
Reno, Nevada 89557

ABSTRACT

The feasibility of using electro-rheological (ER) fluid dampers for vibration control of structures was investigated. Prototypes of single- as well as multi-electrode ER fluid dampers were designed, built and tested to examine their performance under a forced vibration motion. Bang-bang and linear proportional control algorithms were employed to control vibration.

In the present work the problem associated with the high voltage requirement of these type of dampers was addressed. The designs were modified to reduce the required activation voltage. These modifications include increasing the electrode surface area as well as the number of electrodes, which resulted in a uniform and high intensity electric field inside the dampers. Using manual control, apparent viscosities were determined for each damper as a function of the applied voltage. Subsequently, these relations were used in the control algorithms.

The results obtained in the present investigation show that the increase in the electrode length leads to an increase in the apparent damping coefficient. An increase of the number of electrodes from 1 to 3 resulted in a sharp increase in the apparent viscosity. The use of bang-bang control with a three-electrode damper resulted in an instantaneous decrease of the amplitude of vibration.

INTRODUCTION

Winslow [1] was the first to report the electrorheological (Winslow's) effect. The rheology of the ER fluids can be changed significantly in a very short period of time (10^{-4} to 10^{-5} sec) in the presence of an electric field. The resistance of these fluids to flow increases with the increase in the applied electric field strength, and at relatively high field strengths the fluid is reported to behave as a jell-like solid [2-7]. The rapid response of the ER fluids to the applied electric field provides many design possibilities in different engineering disciplines wherein controlled suppression of undesirable

---

1 Associate Professor

2 Visiting Assistant Professor

3 Graduate Student

vibrations is necessary. ER fluid devices can be categorized as those with fixed electrodes and those with sliding electrodes [8]. Examples of fixed electrode devices include automotive suspension dampers, automatic valves and engine mounts. Those with sliding electrode include dampers, clutches, breaks and robotic devices [9-14]. However, as there can be more than one method of designing these devices, this categorization is not too strict. In addition to automotive applications, ER fluid dampers can potentially be used for the suppression of vibration in civil structures that undergo seismic and wind excitations. Large-scale civil structures such as bridges under earthquakes, strong winds and heavy traffic loads need to dissipate the considerable amount of energy produced due to vibrations and ER fluid devices can play a very important role in damping out such vibrations.

Among the above mentioned applications, ER fluid dampers [15,16] and fixed electrode ER fluid valves [17] have been designed and used in various laboratory tests. Gordaninejad *et al* [15] and Haiqing *et al* [18] reported suppression of vibration of a cantilever beam using ER fluid. Gordaninejad *et al* and Gavin *et al* [16] have reported the prototype development of ER fluid dampers. While both prototypes can be categorized as sliding electrode devices, one uses cylindrical electrodes [15] while the other uses flat electrodes [16].

The control of undesirable vibration in dynamical systems such as those mentioned above is a vital task. Currently employed techniques of vibration control in civil structures are based primarily on passive measures. Some examples include base isolations, friction and viscoelastic dampers and bracing systems. They offer limited capability to suppress the vibration of structures, while lacking in controlling motion under severe dynamic loading. The feasibility of active control systems for large structures has been demonstrated for certain cases by using variable stiffness devices (hydraulic and electromagnetic actuators) [19] and active bracing [20,21] in laboratory testing. Full-scale implementations of some active systems have begun in the U.S. and Japan [22,23]. The use of hybrid systems [24,25] is more attractive because the passive system provides a steady dissipation capability while the active system can control the transient dynamic motion. The active devices mentioned above are often costly, slow in response, and complicated. Some of the disadvantages of active control may be eliminated by using ER fluid devices (such as ER fluid dampers) because of the fast change in the rheology of these materials in the presence of an electric field.

Several control schemes have been developed in recent years that utilize the above-mentioned property of ER fluids [16,26-29]. Analytical and numerical simulations have been done by Leitmann *et al* using Lyapunov stability theory as well as fuzzy logic control concept [26,27]. Lyapunov stability theory can be viewed as one predicted on the minimization of phase velocity. Control schemes were also developed on the basis of minimizing the rate of change of the energy of the body. Due to the

nonlinear characteristic of the ER fluids, Gavin *et al* [16] modeled the control scheme assuming that a near resonance force is impressed upon the damper and that the excitation amplitude and the damping are small. An attempt has also been made at nonlinear modeling of telescopic ER fluid dampers [28]. Considering Coulomb friction and viscous friction terms separately, it has been shown that the Coulomb friction term is comparable with the viscous term when the electric field strength ranges between 1 kv/mm to 2 kv/mm [28]. At lower field strength Coulomb friction is negligible. Bang-bang control and instantaneous optimal control algorithms were developed for hybrid dampers having an active and a passive damping components [29]. Ehrgott *et al* [30,31] used a dynamic test device that consists of ER fluid between two coaxial cylinders. The outer cylinder was connected to the ground while high voltage was applied to the inner cylinder. This was a moving electrode device where the inner electrode moves with respect to the fixed outer electrode. Dynamic properties of ER fluid were evaluated by subjecting them to oscillating shear strain. Hysteresis plots for a constant electric field and different frequencies were evaluated and were used to determine the equivalent viscous damping coefficient [30]. To reduce the vibration of the structure, pulse control was implemented wherein an out-of-phase force pulse was applied to the ER damper [31]. A control law has been developed and implemented for ER fluid dampers to suppress structural vibration [32]. Both numerical simulations and experimental work have been carried out to evaluate and validate the theoretical predictions.

In the present investigation, the damping ability of small-scale ER fluid dampers with one-, two-, three- and fifteen-electrodes were tested. Dampers were used to suppress the forced vibration of the tip of a cantilever beam. Vibration data were collected using an accelerometer connected to a data acquisition board through an amplifier and a band pass filter. The amplitude of acceleration thus obtained was used to compute the apparent damping coefficient of the dampers as a function of applied voltage. These functions were subsequently used to implement bang-bang and linear proportional control algorithms.

EXPERIMENTAL SETUP

Single-, double-, triple- and fifteen-electrode ER fluid dampers were designed and built in small scale to suppress the forced vibration of the tip of a thin, aluminum, cantilever beam. The space inbetween the electrodes inside the dampers were filled with ER fluid. The fluid between the electrodes is electrically stressed by the voltage applied to the damper using a 408B Fluke High Voltage Power Supply. For the dampers used in this investigation, the electrode surface area and the inter-electrode separation were different, while their basic construction was the same.

The performance of all the ER fluid dampers were examined by the experimental setup illustrated in Figure 1. The dampers were connected to a thin, aluminum, cantilever beam with a rectangular cross-section. The beam was clamped to an All American Vibration Fatigue Testing Machine and was shaken at a frequency of 10 Hz. The vibration at the tip of the beam was measured by using an accelerometer. The signal obtained from the accelerometer was amplified and passed through a 10 Hz band pass filter. The filtered signal was fed into a Keithly Metrabyte (DAS 20) data acquisition board inside a 486 DX IBM PC.

Using the equation of motion for the present system (consisting of a mass and damper only) the following expression for the apparent viscosity, c, can be derived

$$c = m\omega\sqrt{\frac{1}{r^2} - 1} \tag{1}$$

where r is the ratio of accelerations of the tip of the cantilever beam measured with and without the damper attached to it. Using the measured values of acceleration the ratio r can be computed and used to determine the apparent viscosity as a function of the applied voltage, v. It should be noted, however, that the calculated values of viscosity consist of two parts, a constant zero-field viscosity, c_0, and a voltage dependent part, c_v, i.e., $c=c_0+c_v$. In all of the results presented below $c_v(=c-c_0)$ is plotted as a function of voltage.

The implemented bang-bang control algorithm uses the above equation to suddenly reduce the amplitude of acceleration to a specified fraction. The resulting program measures the value of the acceleration of the tip of the cantilever beam and reads the user specified fraction to which the measured value to be reduced. The program, then, computes the product of the user specified fraction and the measured acceleration and the corresponding voltage to be applied to the damper to achieve such an attenuation. If the computed voltage is more than the danger level (i.e., the breakdown voltage for the ER fluid damper), an "error message" is displayed and the maximum safe voltage is applied to the damper. Otherwise, the computed voltage is applied. The linear control algorithm uses the same expression for c as given in Eq. (1) and reduces the amplitude of acceleration gradually to the desired level. Here the voltage is incriminated in small steps.

RESULTS AND DISCUSSION

In the following, the results on the damping of a forced vibration of the tip of a cantilever beam are presented. For all the experiments, the frequency of vibration was approximately 10 Hz and the vibrating force was sinusoidal. The length of the cantilever beam was short enough to consider its motion that of a rigid body. The following results were obtained using manual control of the voltage applied to the

dampers as well as using bang-bang control and linear control algorithms. These results were used to compute the apparent viscosities of the ER fluid at different applied voltages as detailed above.

Figure 2 shows the normalized amplitude of acceleration, $\ddot{x}_n = \ddot{x}_{m(v)}/\ddot{x}_{m,v=0}$, as a function of the applied voltage for one-, two-, three- and fifteen-electrode dampers. Such a normalization distributes the data points between *0* and *1* and thus facilitates comparison. For the fifteen-electrode damper the damping is maximum, while it is minimum for the one-electrode damper. Apparent viscous coefficients were computed as detailed above and plotted as a function of the applied voltage (Fig. 3). Again to facilitate comparison, $c_v(=c-c_0)$ is plotted. It can be seen that the damping coefficient for the fifteen-electrode damper has the sharpest increase with the applied voltage. Figures 4 and 5 show the normalized acceleration and the apparent viscosity respectively of two single-electrode dampers having different electrode surface areas. The one with the longer electrode and hence greater surface area is showing a better response toward the applied electric field.

The relationships between the apparent viscosity and the voltage applied to the dampers obtained in the present investigation were subsequently used in the control algorithms. Figure 6 shows a typical acceleration-time curve obtained from a three-electrode damper using a bang-bang controller. The voltage was suddenly increased from 0 to 3 Kv, three seconds after the initiation of the experiment. As can be seen, the amplitude of acceleration has dropped, almost immediately after application of the voltage, by more than 66%. Figure 7 shows an output obtained from the same damper with a proportional controller where the applied voltage was increased gradually in increments proportional to the instantaneous acceleration.

From the above results it can be seen that the damping increases with the increase in the applied voltage and with the number of electrodes as well as with the electrode size in the damper. An increase in the voltage increases the field strength and thus increases the apparent viscosity. Increase in the number of electrodes increases the applied field strength by reducing the inter-electrode separation. In addition, it increases the total surface area of the electrodes that is in contact with the ER fluid and thereby increases the zero-field viscosity. Increase of the electrode surface area will have an additional influence on the enhancement of the apparent viscosity, as an electrode with greater surface area can more uniformly distribute the electric field throughout the bulk of the ER fluid in the damper and thus make the damping more effective by activating a greater volume of fluid.

CONCLUSIONS

In the present investigation, small-scale ER fluid dampers were designed, built and used to suppress the forced vibration of the tip of a cantilever beam. Emphasis was given on the design modification needed to improve the effectiveness of the dampers. In addition, control algorithms were designed and implemented.

Analysis of the results showed that some of the important parameters to be considered while designing an effective ER fluid damper are those which maximize the viscous damping upon application of an electric field. To increase viscous damping we may increase the voltage applied to the dampers. However, we can maximize damping at lower voltages by distributing a high-intensity electric field uniformly over the entire bulk of the ER fluid. This calls for design changes increasing the number of electrodes and modifying their sizes.

ACKNOWLEDGEMENTS

This project was funded by the US Department of Energy. Authors thank the LORD Corporation for supplying the ER fluid.

REFERENCES

1. Winslow W.M., "Induced Fibration of Suspensions", Journal of Applied Physics, Vol. 20, pp. 1137-1140, December 1949.

2. Klass D. And Martinek T. W., "Electroviscous Fluids. II. Electrical Properties", Journal of Applied Physics, Vol. 38, No. 1, pp. 75-80, 1967.

3. Zukoski C. F., And Goodwin J. W., "Toward The electrical Control of Viscosity: Optimization of Electrorheological Fluids", International Conference on Industrial Electronics, Control and Instrumentation, Published by IEEE, pp. 9-13, 1986.

4. Weiss K. D., Coulter J. P., And Carlson J. D., "Materials Aspect of Electrorheological Systems", J. Intelligent Material Systems and Structures, Vol. 4, No. 1, pp. 13-34, 1993.

5. Gast A., And Ukoski C., "Electrorheological Fluids As Colloidal Suspensions", Advances in Colloid and Interface Science, Vol. 30, pp. 153-202, 1989.

6. Block H. And Kelly P., "Electro-rheology", Journal of Physics}}, Vol. 21, No. 12, pp. 1661-1677, 1988.

7. Bares J. E, and Carlson J. D., "Electrorheological Fluid Design: An overview", Proc. Of the Second International Conference on ER Fluids, Edited by J.D. Carlson, A.F. Sprecher, and H. Conrad, pp. 93-113, 1989.

8. Duclos T. G., "Design of Devices using Electrorheological fluids", SAE Technical Paper Series, 881134, Future Transportation Technology Conference and Exposition, San Francisco, California, August 8-11, 1988.

9. Choi S. B., Gandhi M. V., And Thompson B. S., "An Experimental Investigation on Smart Composite Laminated Structures Featuring Embedded Electrorheological Fluid Domains for Vibration Control Applications", Composite Engineering, Vol. 2, pp. 543-559, 1992.

10. Coulter J. P., and Duclos T. G., "Application of Electrorheological Materials in Vibration Control", Proc. of the Second International Conference on ER Fluids, Edited by J.D. Carlson, A.F. Sprecher, and H. Conrad, pp. 300-324, 1989.

11. Brooks D. A., "Devices Using Electro-Rheological Fluids", Proc. of the Second International Conference on ER Fluids, pp. 371-401, 1989.

12. Duclos T. G., "Electrorheological Fluids and Devices", Automotive Engineering, pp. 45-48, December 1988.

13. Gandhi M. V., and Thompson B. S., "A New Generation of Revolutionary Ultra-advanced Intelligent Composite Materials Featuring Electro-Rheological Fluids", Smart Materials, Structures, and Mathematical Issues, Ed. by C. A. Rogers, Technomic Publ. Co., pp. 63-68, 1988.

14. Coulter J. P., and Miller L. R., "Application for Smart Materials in the Field of Vibration Control", Proc. of the Second International Conference on ER Fluids, Edited by J.D. Carlson, A.F. Sprecher, and H. Conrad, pp. 132-146, 1989.

15. Gordaninejad F., Ghazavi A., Ray A., Wang H., and Saiidi M., "Intelligent Electrorheological Fluids for Active Vibration Control: an Experimental Study", Proc. of the ninth international conference on composite materials, Madrid, Spain, pp. 473-480, 1993.

16. Gavin H. P., Ortiz D. S., and Hanson R. D., "Use of ER Fluid Dampers for Reduction of Seismic Structural Response", UJNR Workshop on Smart and High Performance Materials and Systems, May 10-14, 1993, Building Research Institute, Tsukuba, Japan.

17. Peel D. J., and Bullough W. A., "Effect of Flow Rate, Excitation Level and Solids Content on The Time Response In an Electro-Rheological Valve", Journal of Intelligent Material Systems and Structures, Vol. 4, pp. 54-64, January 1993.

18. Haiqing G., King L. M., and Cher T. B., "Influence of an Locally Applied Electro-Rheological Fluid Layer on Vibration of a Simple Cantilever Beam", Journal of Intelligent Material Systems and Structures, Vol. 4, pp. 379-384, July 1993.

19. Kobori T., et al., "Experimental Study on Active Variable Stiffness System", Proc. Fourth World Congress of Tall Building and Urban Habitat, Hong Kong, 1990.

20. Chung L. L., Reinhorn A.M., and Soong T. T., "Experiments on Active Control of Seismic Structures", ASCE J. Eng. Mech., Vol. 114, pp. 241-256, 1988.

21. Chung L. L., Lin R. C., Soong T. T., and Reinhorn A.M., "Experimental Study of Active Control of MDOF Seismic Structures", ASCE J. Eng. Mech., Vol. 115, pp. 1609-1627, 1989.

22. Soong T. T., Marsi S. F., and Housner G. W., "An Overview of Active Structural Control under Seismic Loads", Earthquake Spectra, Vol. 7, No. 3, pp. 483-505, 1991.

23. Kobori T., "State-of-the-Art of Seismic Response Control Research in Japan", Proc. of the U.S. National Workshop on Structural Control Research, Edited by G. W. Housner and S. F. Marsi, pp. 1-12, 1990.

24. Reinhorn A.M., Soong T. T., and Wen C. Y., "Base Isolated Structures with Active Control", Proc. ASME PVD Conf., PVP-127, pp. 413-420, San Diego, CA., 1987.

25. Kelly J. M., Leitmann G., and Soldatos A. G., "Robust Control of Base-Isolated Structures Under Earthquake Excitations", J. Optim. Th. Appl., Vol. 53, pp. 159-180, 1987.

26. Leitmann G., and Reithmeier E., "Semiactive Control of a Vibrating System by Means of Electrorheological Fluid", Dynamics and Control, Vol. 3, pp. 7-33, 1993.

27. Leitmann G., "Vibration Attenuation by Means of Semiactive Control Schemes", Submitted to Math. Modelling and Sci. Computing.

28. Stanway R., Sproston J. L., and Stevens N. G., "Non-Linear Modelling of an Electro-Rheological Vibration Damper", Journal of Electrostatics, Vol. 20, pp. 167-184, March, 1987.

29. Feng Q., and Shinozuka M., "Control of Seismic Response of Bridge Structures Using Variable Dampers", Journal of Intelligent Material Systems and Structures, Vol. 4, pp. 117-122, January 1993.

30. Ehrgott R., and Masri S. F., "Modelling the Oscillatory Dynamic Behavior of Electrorheological materials", Smart Materials and Structures, Institute of Physics, UK., Vol. 1, No. 4, pp. 275-285, 1992.

31. Ehrgott R., and Masri S. F., "Use of Electro Rheological materials in Intelligent Systems", Proceedings of the U.S.- Italy - Japan Workshop on Structural Control and Intelligent Systems, Sorrento, Italy, 13-15 July 1992, pp 87-100.

32. Wang K. W., Kim S. Y., Lee H. S., and Shea D. B., "Vibration Control of Flexible Structures via Electrorheological-fluid-based Dampers", Smart Structures and Intelligent Systems, SIPE Vol. 1917, 1993, pp 157-167.

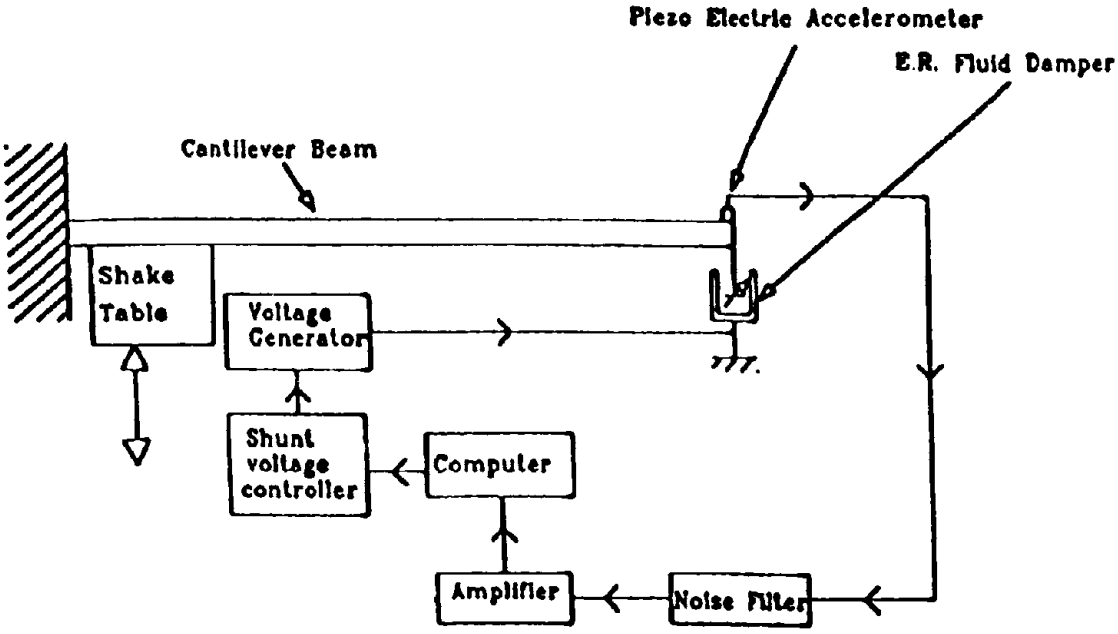

Figure 1. The experimental setup.

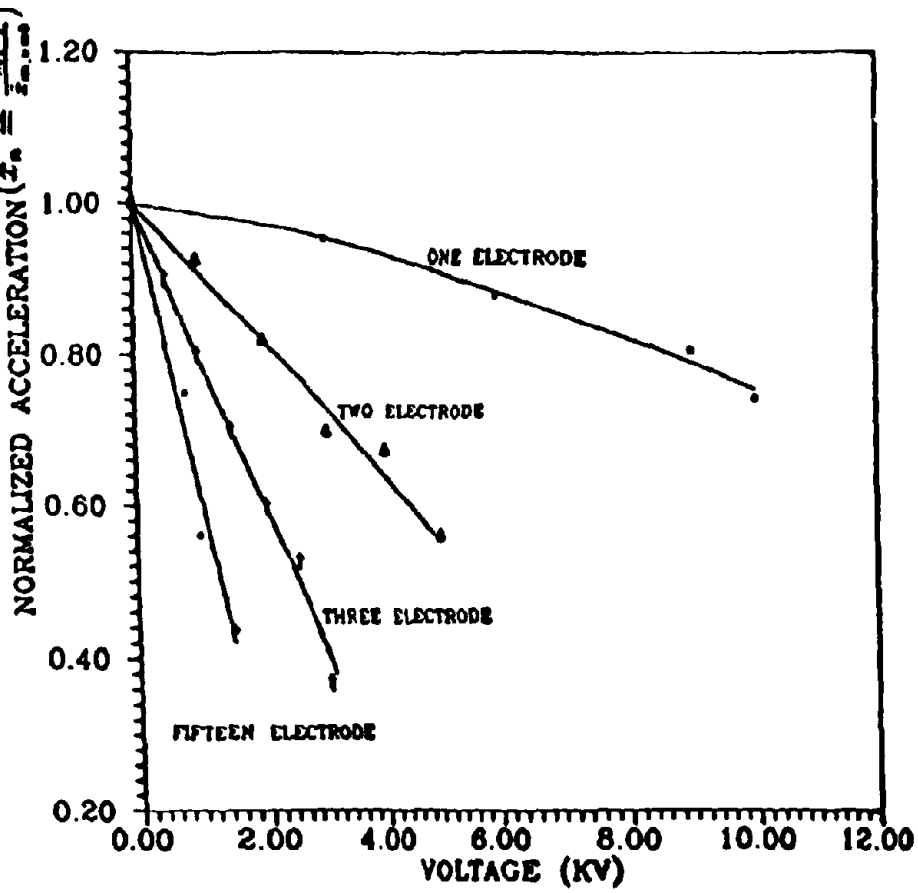

Figure 2. **Normalized acceleration as a function of the voltage applied to dampers with different number of electrodes.**

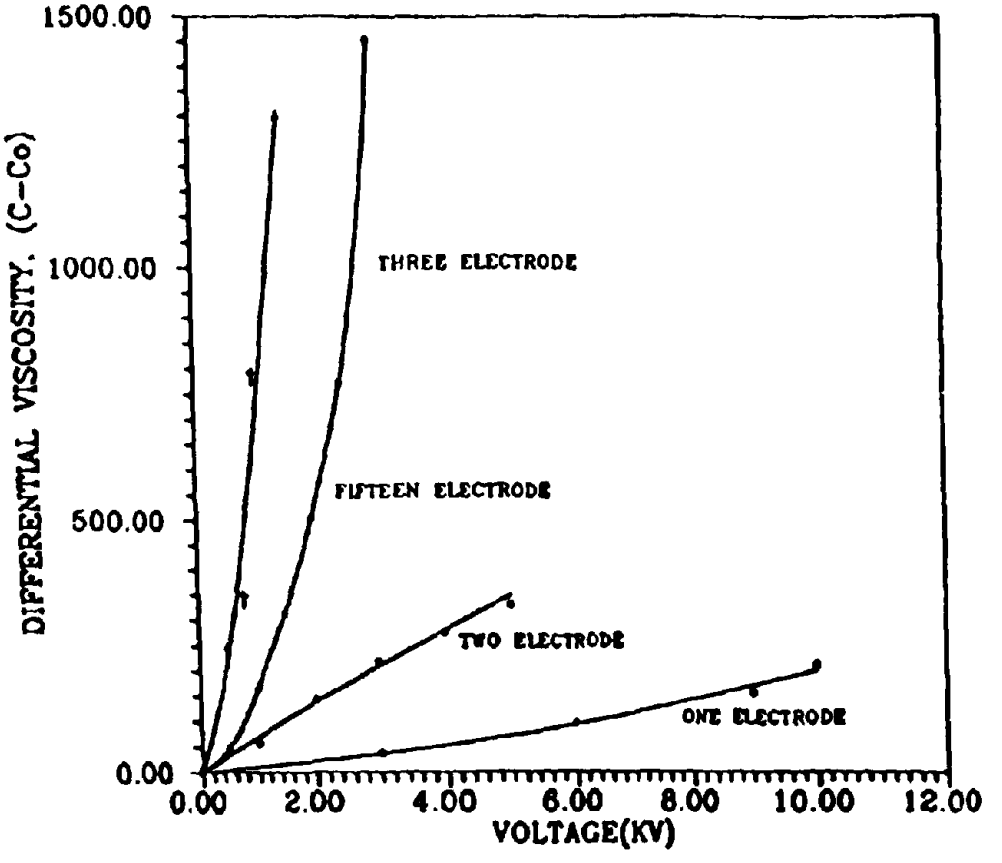

Figure 3. **Apparent viscosity as a function of the voltage applied to dampers with different number of electrodes.**

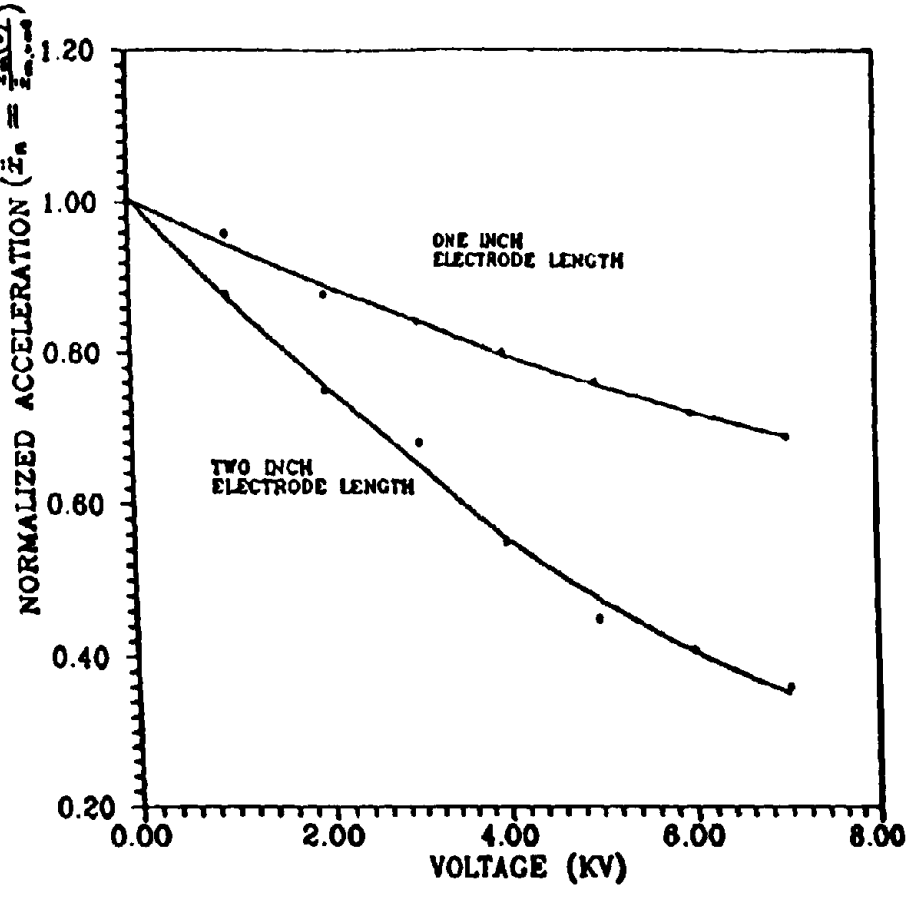

Figure 4. **Normalized acceleration as a function of the voltage applied to single-electrode dampers with different electrode lengths.**

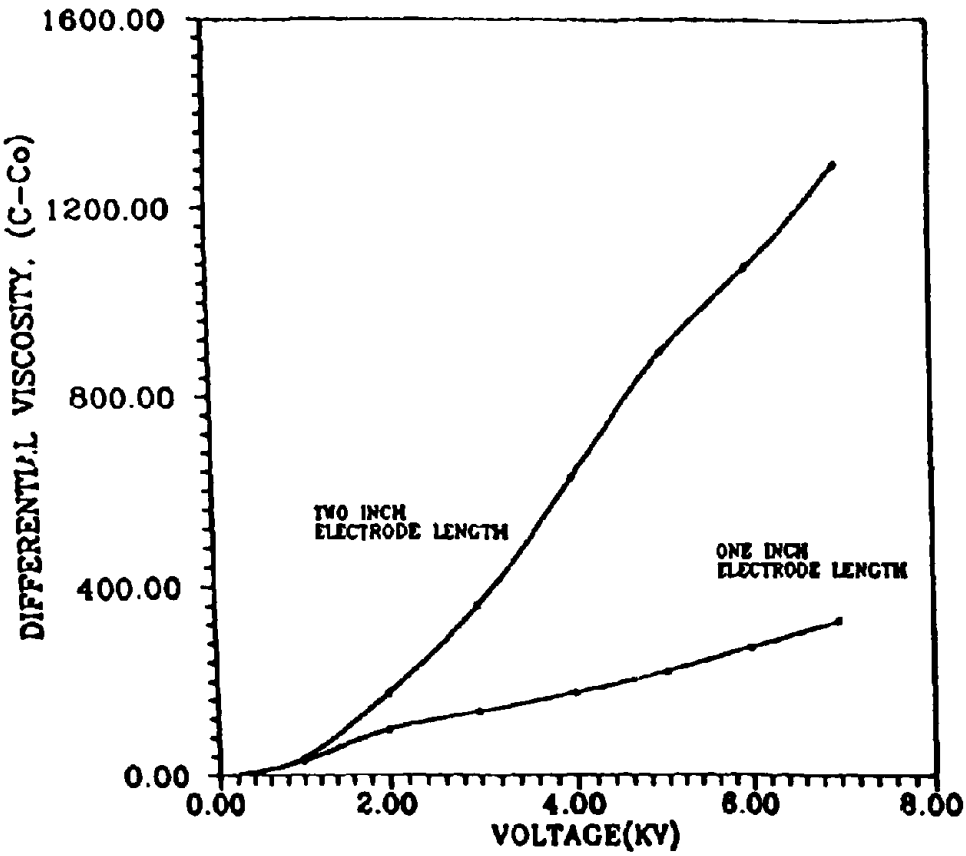

Figure 5. **Apparent viscosity as a function of the voltage applied to single-electrode dampers with different electrode lengths.**

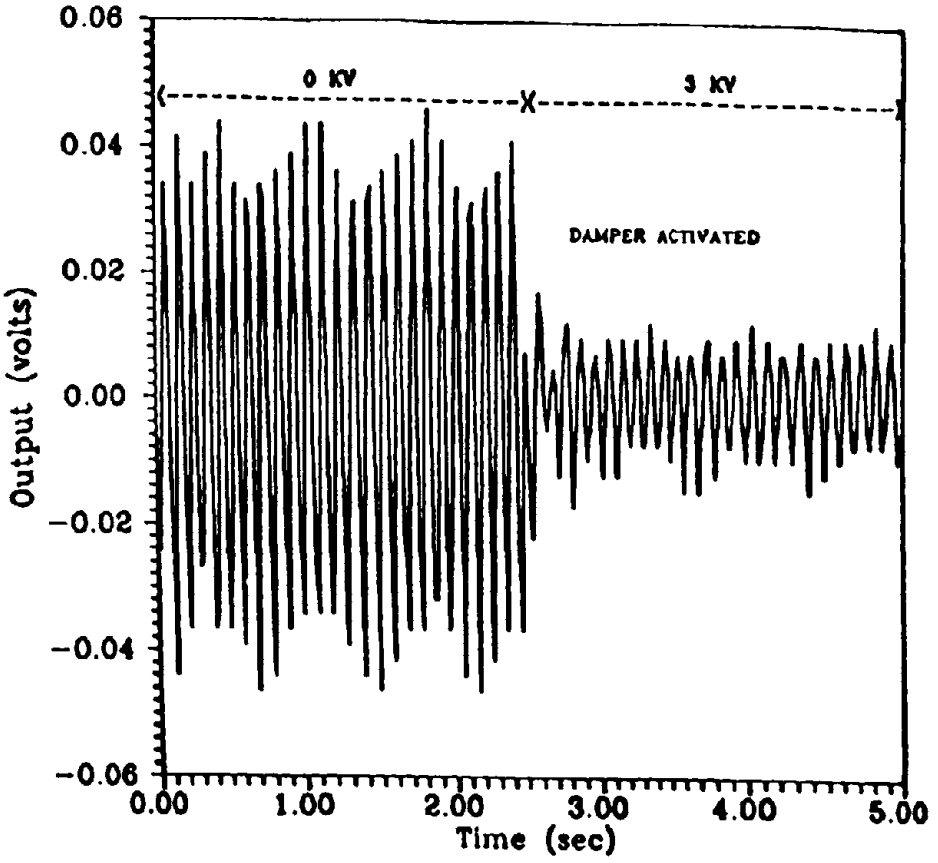

Figure 6. **Bang-bang control of forced vibration of the tip of a cantilever beam using a triple-electrode ER fluid damper.**

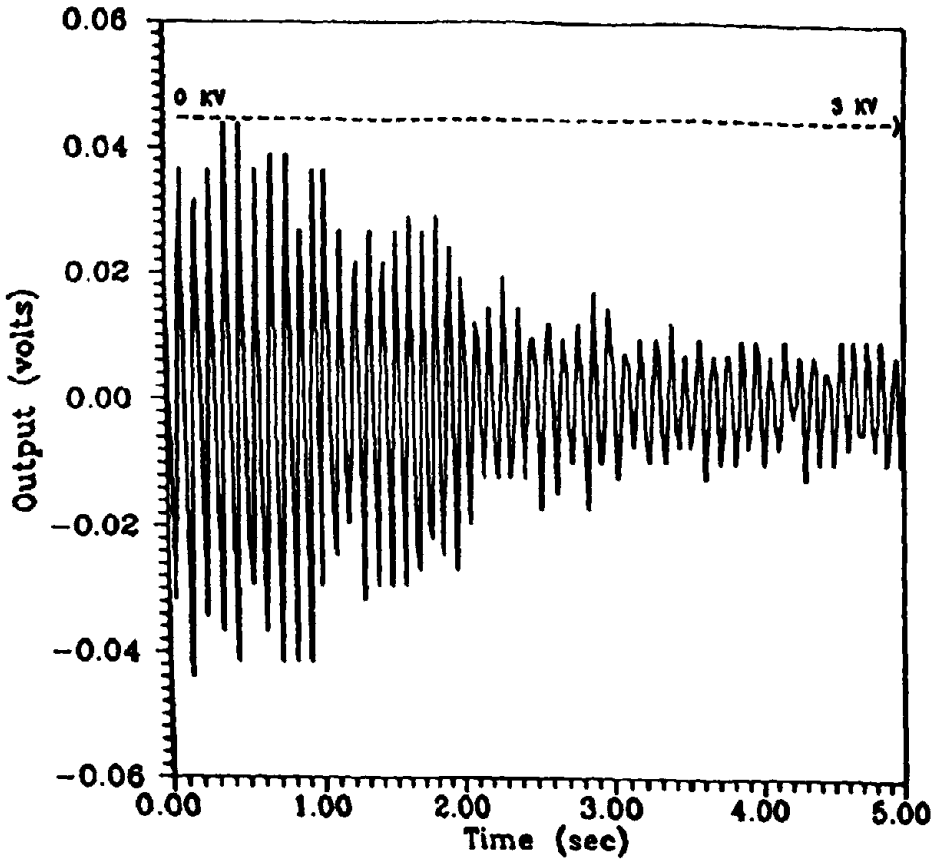

Figure 7. **Proportional linear control of forced vibration of the tip of a cantilever beam using a triple-electrode ER fluid damper.**

APPLICATION OF ELECTRO-RHEOLOGICAL FLUID FOR VARIABLE DAMPER

Kazuhiko KAWASHIMA[1], Shigeki UNJOH[2], Shigenobu SUZUKI[3] and Shigeki ENDOH[3]

1) Head, Earthquake Engineering Division, Public Works Research Institute, Ministry of Construction, Tsukuba Science City, Japan
2) Senior Research Engineer, ditto
3) Research and Development Division, Bridgestone Corporation, Ogawahigashi-cho, Kodaira-shi, Tokyo, Japan

ABSTRACT

This paper presents the potential application of electro-rheological (ER) fluid for the seismic response control of structural systems. Variable damper systems using ER fluid and the trial design are presented. The applicability of the ER damper for the seismic response control of structural systems are discussed.

INTRODUCTION

Electro-rheological (ER) fluid is the fluid in which the viscosity is variable depending on the applied electric field. Although the ER fluid has been studied for a long time, reliable ER fluid has not developed. The ER fluid which has high applicability for practical use has recently been developed and the application has begun to be made especially in mechanical structural systems.

The authors have been studied the variable damper using ER fluid (referred to ER damper hereinafter). The ER damper has the advantages that the damping characteristics is variable within a quick response (on the order of milliseconds) to the applied electric field, and that the mechanical system of ER damper can be simple without complicated valve systems. Therefore the reliability for practical use may be higher than an usual active control devices.

To control structural vibration during earthquakes, relatively larger damping force is required for the ER damper. Therefore, it is a critial issue to design the practical ER damper system which can vary a wide range of the damping force. This paper presents the parametric design study of the ER damper, and the applicability for practical use is discussed.

DESIGN OF ER DAMPER

The damping force of the ER damper may be given by the sum of the damping force developed by the fluid viscosity through an orifice and that developed by ER effects as shown in Eq.(1). Supposing a cylinder type damper system with an orifice as shown in **Fig. 1**, which may be suitable for developing a larger damping force, the damping force developed by the fluid viscosity and the ER effects may be given as Eqs. (2) and (3), respectively.

$$F = F_V + F_E \tag{1}$$

$$FV = \frac{12 \cdot L \cdot A^2 \cdot \eta}{B \cdot H^3} \cdot \upsilon \tag{2}$$

$$FE = \frac{3 \cdot L \cdot A}{H} \cdot \tau_y(E) \tag{3}$$

Where,

F : Total Damping Force developed by ER Damper
F_V : Damping Force developed by Fluid Viscosity through Orifice
F_E : Damping Force developed by ER Effects
A : Pressure Area of Piston
υ : Velocity of Piston
L ,B ,H : Length, Width and Distance of Electrodes
η : Viscosity of ER Fluid
$\tau_y(E)$: Shear Stress developed by ER Effects
E : Applied Electric Field Strength

It should be noted here that $\tau_y(E)$ is controlled by the applied electric field strength between the electrodes. Therefore, when $E=0$, i.e., no control, $\tau_y(0)=0$, on the other hand, when $E=E_{max}$ which is the maximum electric field strength applicable for the ER damper, maximum shear stress, $\tau_y(E_{max})$, is developed.

Based on the above theories, the damping force developed by the ER damper against the steady state loading with a constant displacement may be written in **Fig. 2.** As well-known, the damping force developed by the fluid viscosity is dependent on the piston velocity and it is not controllable. On the other hand, the damping force developed by the ER effects is not dependent on the loading velocity and is controlled only by the electric filed strength. In order to control a wide range of the damping force it is required to design the damping force developed by the fluid viscosity should be as small as possible than that developed by the ER effects.

APPLICABILITY OF ER DAMPER

Assuming that $D \gg D_s$, $D \gg H$ (see **Fig. 1**) for the simplicity, the pressure area, A , and the width of the electrodes, B , can be approximated as $A = \pi \cdot D^2/4$ and $B = \pi \cdot D$. Hence, Eqs. (1) to (3) may be rewritten as

$$\frac{F}{L} = \frac{F_V}{L} + \frac{F_E}{L} = \frac{3\pi \cdot D^3 \cdot \eta}{4 \cdot H^3} + \frac{3\pi \cdot D^2}{4 \cdot H} \cdot \tau_y(E) \tag{4}$$

$$0 \leqq \frac{F_E}{L} \leqq \frac{F_{Emax}}{L} = \frac{3\pi \cdot D^2}{4 \cdot H} \cdot \tau_y(E) \tag{5}$$

According to Eqs. (4) and (5), the relation between the size of the ER damper and the maximum damping forces developed by the fluid viscosity and the ER effects can be illustrated as shown in **Fig. 3**. The damping forces in **Fig. 3** are represented as the force per unit length of the electrodes. **Fig. 3** shows that the larger damping forces can be developed by increasing the diameter of the piston and length of the electrode, and also by decreasing the distance between the electrodes. Since the damping force developed by the fluid viscosity sensitively varies depending on the piston diameter and the distance of the electrodes, the damping force developed by the fluid viscosity tends to be larger than that developed by the ER effects for a larger size of the damper.

Fig. 4 shows the computed damping forces for various sizes of the damper. The damping forces are computed for the cases of the distance of the electrodes of 1, 2 and 3mm. The viscosity of the ER fluid, η , and the maximum shear stress by ER effects, τ_{ymax} , are assumed as 1.5×10^{-6} kgf·s/cm^2 and 1.5×10^{-2} kgf/cm^2 ($E = 3$ kV/mm), respectively. These values are employed as typical values based on the ER fluid which is now in practical use. Supposing the damper system with piston diameter of 300mm, length of the electrodes of 500mm and distance between the electrodes of 2mm, the maximum damping force controlled by the ER effects may be 20tf, which is applicable to the seismic response control of structures.

Since the damping force developed by the fluid viscosity is dependent on the applied piston velocity, it becomes much larger than that developed by the ER effects in some loading conditions as fast loading velocity. In order to decrease the damping force developed by the fluid viscosity, it is made by decreasing the piston diameter or by increasing the distance of the electrodes, and by increasing length of the electrodes.

DEVELOPMENT OF EXPERIMENTAL ER DAMPER

For the purpose of proving the design method and investigating the effectiveness and applicability of the ER damper, experimental model of the ER damper as shown in **Photo 1** is now being developed. This model is designed so that the maximum damping force developed by the ER effects be about 40kgf. The length of the electrode and the distance between the electrodes is designed as 134mm and 3mm, respectively. Anhydrous type ER fluid is used for the model. When the piston velocity is 300mm/sec, the damping force

developed by the fluid viscosity is about half of that developed by the ER effects.

A wide area of experiments using the model, such as load–displacement relation, velocity dependency, displacement dependency, temperature dependency, controllability, etc. is now planning.

CONCLUSIONS

The applicability of the ER damper for the seismic response control of structures is studied through the trial design of the ER damper. It is showed that the cylinder type damper with diameter of 300mm can develop the required damping force to control the seismic response of actual structures. The experimental ER damper model is also being developed and the comprehensive tests will be made in the future.

REFERENCES

1) Ushijima, T, Takano, K. and Noguchi, T. : Rheological Characteristics of ER Fluids and their Application to Anti–Vibration Devices with Control Mechanism for Automobiles, SAE paper #881787, 1988
2) Duclos, T., G. : Design of Devices Using Electrorheological Fluids, SAE Technical Paper #881134, 1988
3) Ehrgott, R., C. and Masri, S., F. : Modeling the Oscillatory Dynamic Behavior of Electrorheological Materials in Shear, Smart, Mater. Struct. 1, 1992
4) Sasada, T., Kishi, T. and Kamijo, K. : Electro Viscous Effects of Polymer and Solid Particle Solutions, Proceedings of the Japan Society of Mechanical Engineers. Vol.41, No.342, 1975
5) Sasada, T., Kamijo, K. and Kishi, T. : Electro Viscous Effects of Uni–phase Liquid, Proceedings of the Japan Society of Mechanical Engineers. Vol.41, No.343, 1975
6) Edited by Scott, D. and Yamagichi, J. : Solidifying Fluid Transforms Clutches and Flow Valves, Automotive Engineering, Vol.91, No.11, 1983

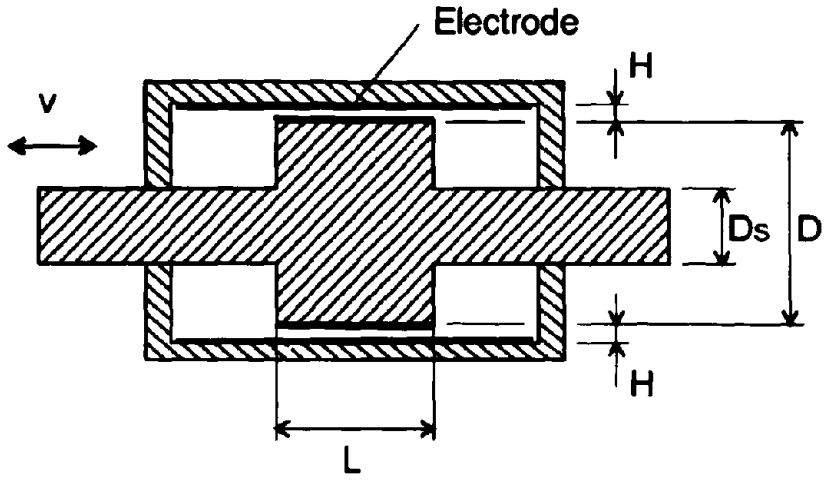

Pressure Area of Piston : $A = \frac{\pi}{4}(D^2 - Ds^2)$

Width of Electrode : $B = \pi(D + H)$

Fig. 1 Cylinder Type ER Damper

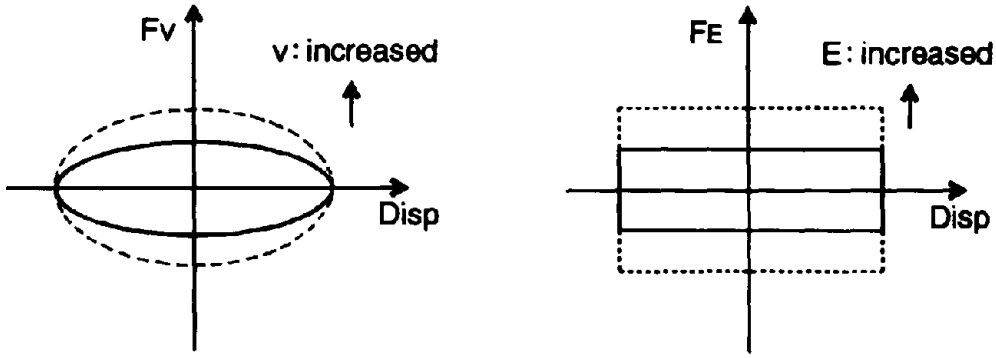

(a) Damping Force developed by the Fluid Viscosity

(b) Damping Force developed by the ER Effects

Fig. 2 Illustration of the Damping Force developed by the ER Damper

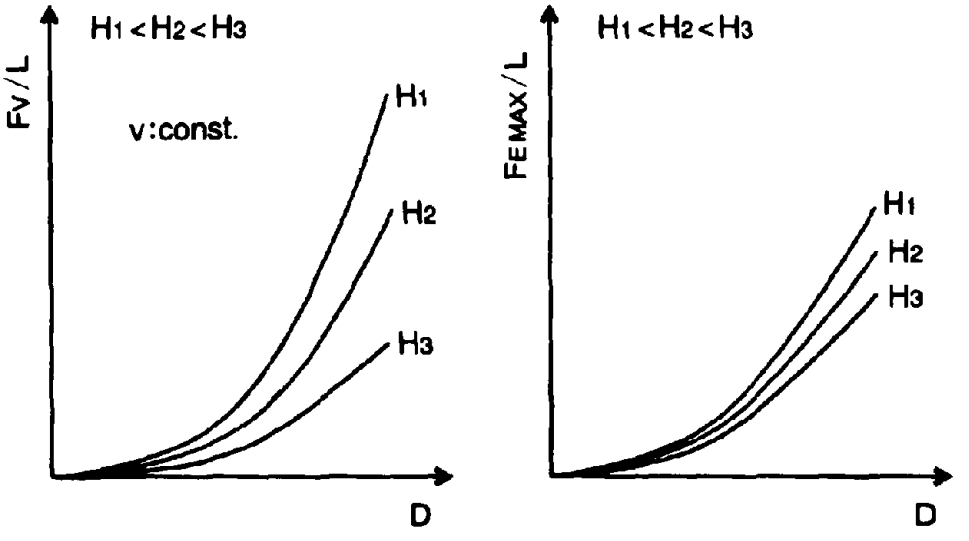

Fig. 3 Variation of the damping Force depending on the Damper Size

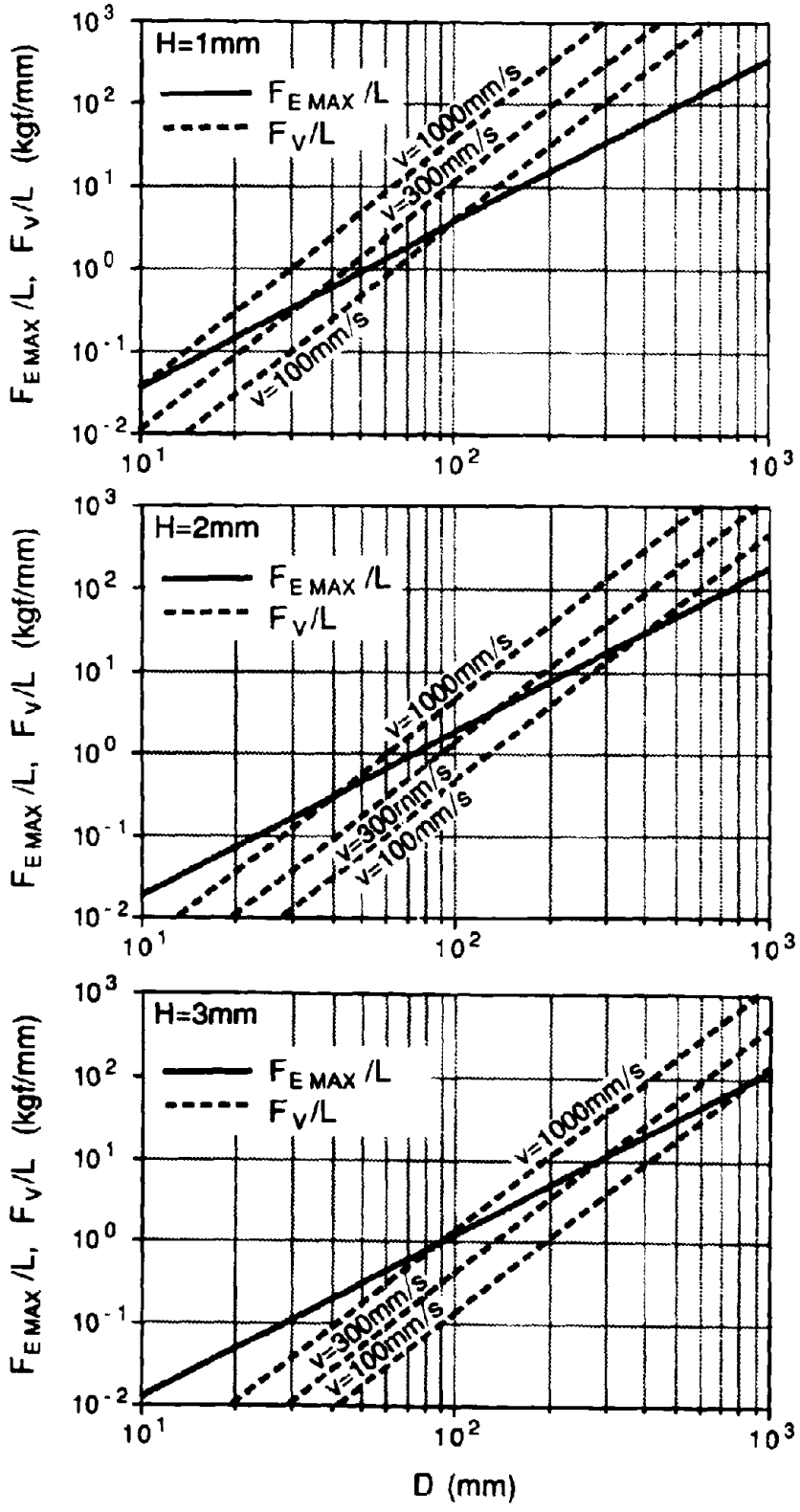

Fig. 4 Computed Damping Force with Various Size of Damper

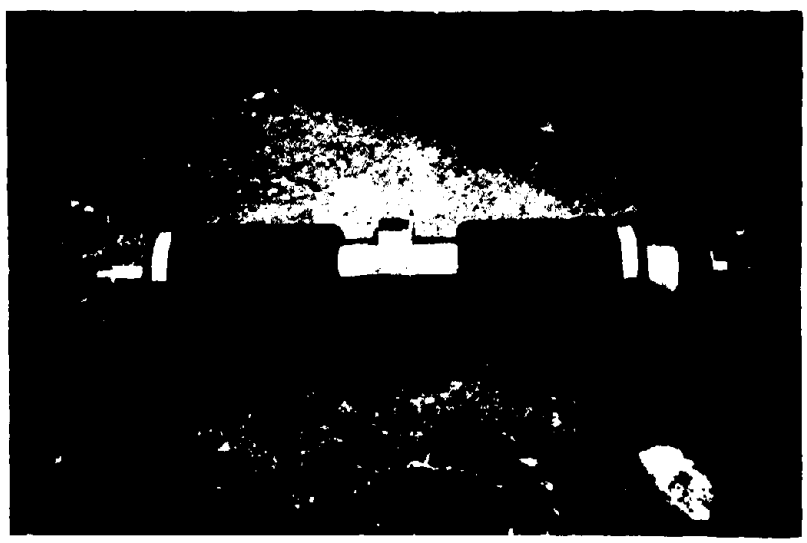

Photo 1 Experimental ER Damper

Fuzzy Control of Bridge Vibration by Using Variable Dampers

Limin SUN Dr. Eng. and Yozo GOTO Dr. Eng.
Civil Engineering Department
Technical Research Institute, Obayashi Co.
4-640 Shimokiyoto, Kiyose, Tokyo-204, Japan

ABSTRACT

This paper presents an application of fuzzy control theory to variable dampers for suppressing bridge vibrations. The bridges with long natural period, such as base-isolated or high-pier ones, may deform with medium or large displacement in longitudinal direction due to traffic-loadings or earthquakes. This may affect the serviceability of the bridge or even cause safety problems. Therefore, the suppression of such vibrations is required.

Installing dampers between bridge deck and bridge abutment is one means to reduce such vibrations. In this study, the effectiveness of variable dampers controlled by using fuzzy control theory was investigated. The variable damper used herein is a viscous oil damper with controllable damping properties. The fuzzy theory was used to infer the optimum change of the damping of the variable damper in next time step from the damping level and the damping force at present. The control algorithm is to fully display the performance of the variable damper on the condition that the bridge and the variable damper are mot destroyed. For example, when the input acceleration is small, the damper is controlled at high damping level so that the damper can produce relatively large damping force to suppress the bridge vibrations; when the input acceleration becomes large, the damping will be controlled at medium or even low level in order to keep the damping force lower than a certain desired value so that the damper and the bridge deck or abutment can be protected from damage due to the excessively large reaction force of the damper.

A bridge model with an installed variable damper, which locates between the bridge deck and the bridge abutment, is employed for analytical simulations. The simulation results show that the variable damper proposed is effective to suppress the bridge vibrations due to seismic loading providing that the rules of fuzzy control are constructed suitably. It is also found that the variable damper controlled by fuzzy theory can contribute its damping effect as much as possible corresponding to various levels of seismic loadings. The fuzzy control theory is significant to be applied for controlling the damping of the variable damper. The control rules used in this study is quite simple. The fuzzy control theory does not required the system identification and the modelling of the structure, which often cause problems when using modern control theory. The simulations show that the fuzzy control theory has high applicability.

INTRODUCTION

The bridges that have long natural period, such as base-isolated bridges and bridges having high piers, may have large longitudinal displacement during earthquake. This requires large size expansion joints, which are costly usually. On the other hand, the bridges may be easily vibrated by heavy traffic-loadings and drivers may feel uncomfortable. Such kinds of vibrations cause troubles of serviceability or even safety and, therefore, are required to be suppressed.

Applications of variable damper to suppress vibrations of buildings have been reported [1 and 2]. Control by using variable dampers, a semi-active control method, was reported to have some advantages over an active control, such as, high robustness and low energy consummation. Shinozuka et al. [3] and Kawashima et al. [4] have proposed to use variable dampers for bridge vibration control. Kawashima et al. [5] have built and tested a full-size variable damper, their variable damper is a conventional viscous oil damper with controllable orifices that is used to electrically control the damping continuously or intermittently. Several control algorithms for variable dampers have been proposed [1-4] to provide optimum damping to reduce the structural response efficiently.

In this study, variable dampers are considered to be installed in between of bridge abutment and bridge deck to reduce the longitudinal displacement of a bridge deck due to earthquake or traffic-loadings. The reason to use variable dampers is that the external loadings considered have wide range in magnitude so a conventional damper that has constant damping coefficient may not be satisfactory.

The classical control theory and the modern control theory are often used for active structural control problem. These theories assume that the system controlled is mathematically defined and the control performance index of the system can be mathematically described in terms of the parameters of the system. In the case of the large bridge with a lot of automobiles on it, however, the system becomes complicated then the identification of the system parameters is not easy. Also, it is difficult to define the control performance index in the case that the structure is nonlinear and the external input is random. So the assumptions of such control theory are hard to be fully satisfied. This often causes problems, such as unstability and so on. In the other hand, in the field of the control problem involving to human-being operation, the fuzzy control theory has been widely applied to deal with the nonlinear control problems [6]. Recently, the fuzzy control theory has been used for active structural control in civil engineering field [7 and 8]. This paper presents an application of the fuzzy control theory for variable damper for controlling bridge vibration. The feasibility of fuzzy control theory and the effectiveness of the variable damper are shown by the simulations.

BRIDGE MODEL

The model bridge used for the simulations in this study is a high-pier highway bridge as shown in Fig. 1. The bridge is symmetric and has 3 spans, the main span is 150m and the two side spans are 85m. Two piers are 70m high. The bridge is considered to be built over a valley in a mountain area. So the abutments of such kind of bridge can provide large reaction force. The variable dampers are considered to be installed between the bridge decks and the abutments at the two ends to suppress the bridge vibration in longitudinal direction.

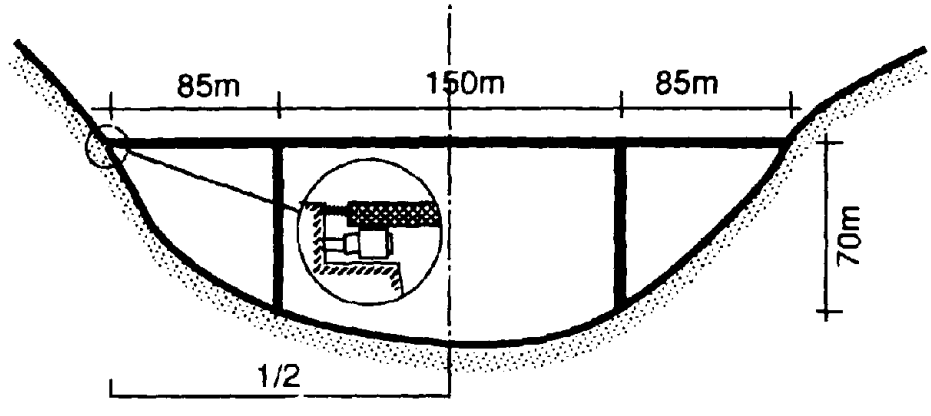

Figure 1 High-pier highway bridge with installed variable damper

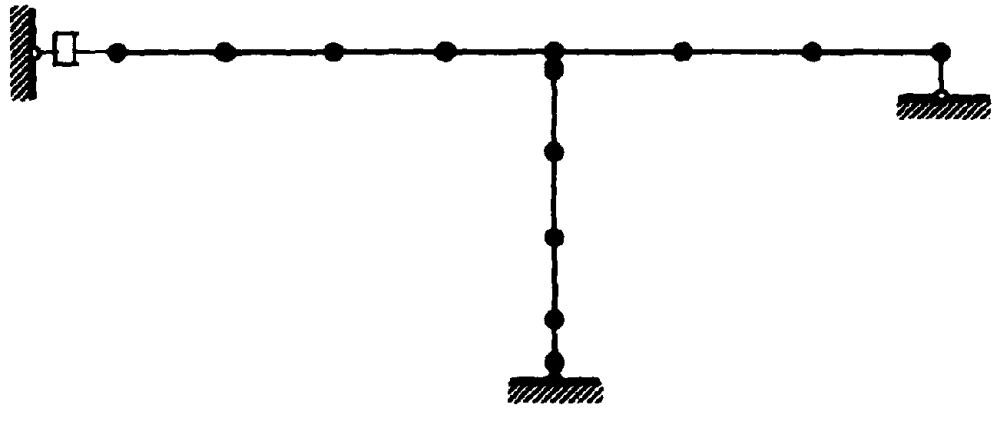

Figure 2. Multi-degree-of-freedom bridge model for complex modal analysis

Before investigating the effectiveness of the variable damper, it is necessary to verify the feasibility of the suppression method we considered, because that the use of the variable damper may cause the changes of the structural mode

shapes, indicating that the stress distribution in the structural members may change. The half of the bridge was modelled as a multiple-degree-of-freedom system because of its symmetrization, a damper was included in the model (Fig. 2). The complex modal analysis [9] of the system was carried out with various constant damping coefficients of the damper. The mode frequencies, the mode damping and the mode shapes of the first five modes are shown in Figs. 3-5.

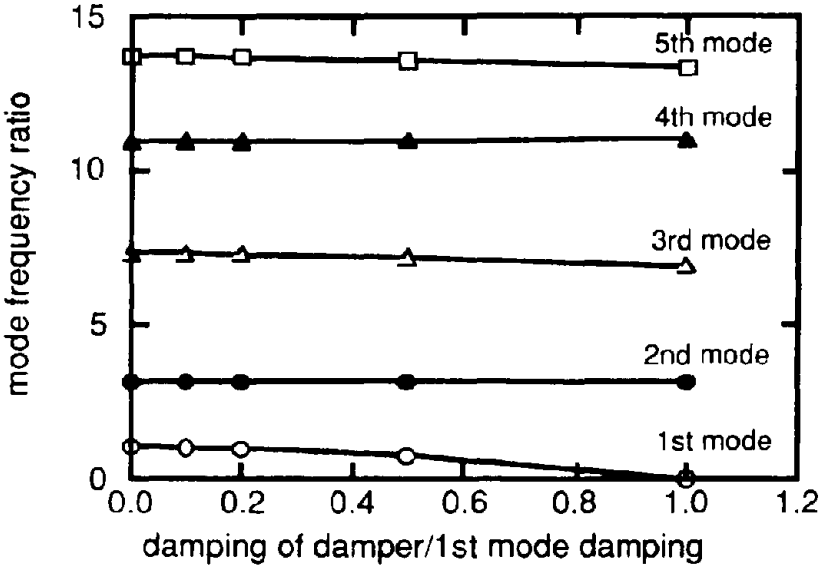

Figure 3. Mode frequencies of bridge

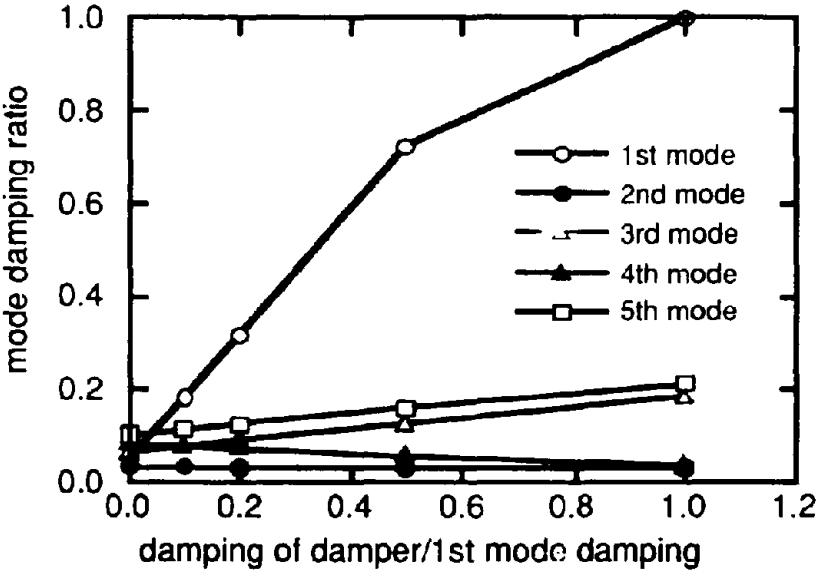

Figure 4. Mode dampings of bridge

The horizontal axes in Figures 3 and 4 are the damping coefficient of the damper nondimensionalized by the first mode damping of the system. It is found that, when the damping of the damper increases, the mode frequencies of the system become low, a little bit for the second to fifth modes and a lot for the first mode (Fig. 3). The mode damping ratios increase when the damping of the damper increases, especially, the first mode damping ratio can be large as 100%, i.e., over damping, indicating that the damper installed in the way we considered can contribute very high damping to the first mode of the bridge (Fig. 4). Figure 5 shows the mode shapes of the first to the fifth modes of the bridges. For simplicity, the amplitudes of the complex mode at each node are plotted. In this example, the damping ratio of the damper is 50% of the first mode damping of the bridge. The first, third and fifth modes have horizontal displacement while the second and the fourth do not have at the node

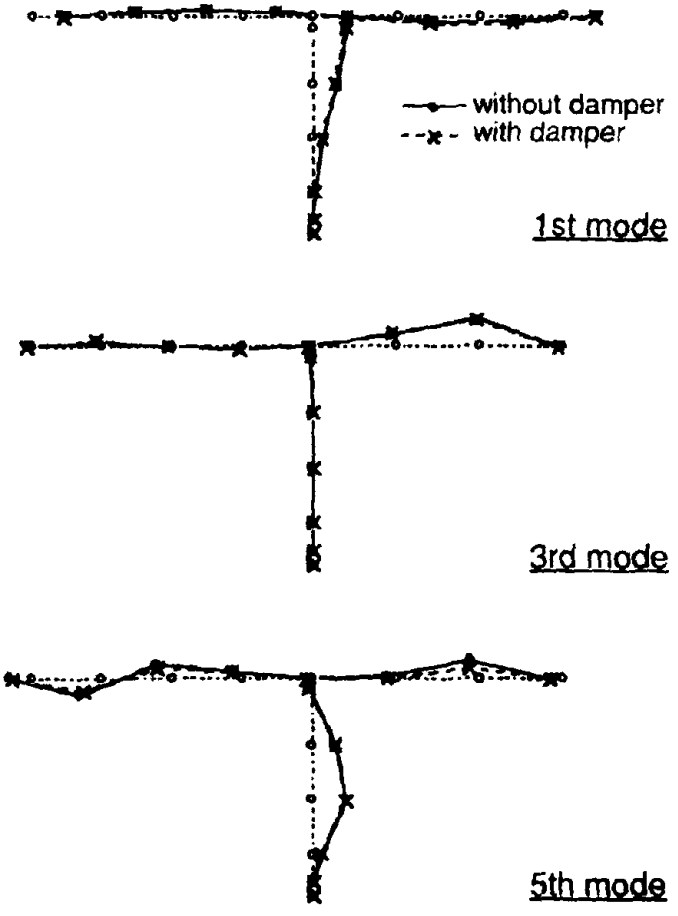

Figure 5. Mode shapes of bridge

connecting to the damper. The results of complex modal analysis show that the mode shapes are less affected by the damper installed. Some minor changes can be found in the case of the fifth mode, but the position where the maximum displacement occurs does not change. It can be said that the installing variable dampers in between of the bridge deck and the bridge abutment will not cause side effects on the stress distribution of the bridge.

The half of the bridge and a variable damper are modelled as a single-degree-of-freedom system as shown in Fig. 6, since the displacement of the bridge deck in its longitudinal direction is mainly due to the first mode of

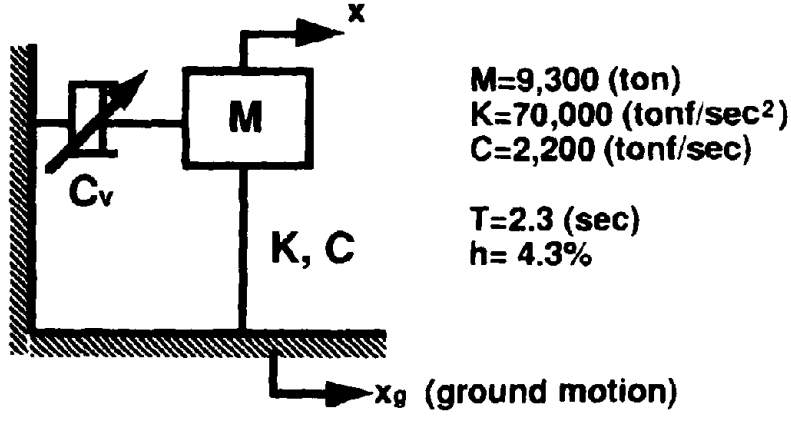

Figure 6. Single-degree-of-freedom bridge model

vibration. The first mode mass is about 9,300ton and the first natural period is 2.3sec. The structural damping ratio is about 4.3%. In this study, we consider that the ground motion at the foundation of the piers and that of the abutment are the same. So the equation of motion is written as

$$M\ddot{x} + C\dot{x} + C_v\dot{x} + Kx = - M\ddot{x}_g \qquad (1)$$

where C_v = the damping coefficient of the variable damper and $\ddot{x}_g$ = the ground acceleration. The damping force of the variable damper is

$$F_d = C_v\dot{x} \qquad (2)$$

The total damping ratio of the system, including the structure and the variable damper, is

$$h_t = h + h_v \qquad (3)$$

where $h_v = C_v/(2\omega M)$, ω = the circular natural frequency of the bridge.

FUZZY CONTROL RULES

The several fuzzy control algorithms have been proposed [7 and 8]. The discussion in the last chapter showed that the suppression method we proposed is feasible and effective. From Fig. 6 we know that the better suppression efficiency can be obtained if the damper with higher damping coefficient of the variable damper is used. In practice, however, the variable damper, the bridge deck and the bridge abutment have limitations in their capacities. Too large reaction force may destroy the members of the bridge or the variable damper itself if the damping of the variable damper is too high and the external loadings are strong. In this study, this practical limitation is always taken into account when we design fuzzy control rules.

The control algorithm we proposed is to fully display the performance of the variable damper to suppress the bridge vibration under various levels of external excitations, from low level such as traffic-loadings to high level such as strong earthquake. The control algorithm can be described as following:

1) The damping coefficient of the variable damper will be set at high level to be efficient if the damping force of the damper F_d does not exceed a certain level pre-set according to the capacities of the bridge and the variable damper;

2) The damping coefficient of the variable damper will be reduced to keep the damping force F_d smaller than the pre-set level, only when the F_d intends to exceed the pre-set level due to large external excitation. So the bridge deck, abutment and the variable damper can be protected from damage.

Table 1. Fuzzy control rules

Δh_v		F_d				
		NB	NM	ZO	PM	PB
h_t	PB	NB	NB	ZO	NB	NB
	PM	NB	ZO	PB	ZO	NB
	ZO	ZO	PB	PB	PB	ZO

Antecedent: F_d & h_t

Consequent: Δh_v

Fuzzy numbers: NB = Negative Big; NM = Negative Medium;
ZO = Zero;
PM = Positive Medium; PB = Positive Big.

The control rules constructed are shown in Table 1. For example:

Rule: IF F_d = PB & h_t = PB; THEN Δh_v = NB means

if F_d is positive big and h_t is positive big, then let Δh_v be negative big,

i.e., reduce the damping of the damper sharply;

Rule: IF F_d = PB & h_t = ZO; THEN Δh_v = ZO means

if F_d is positive big and h_t is zero, then let Δh_v be zero,
i.e., keep the damping of the damper unchanged;

Rule: IF F_d = OZ & h_t = PM; THEN Δh_v = PB means

if F_d is zero and h_t is positive medium, then let Δh_v be positive big,
i.e., increase the damping of the damper sharply;

Rule: .....

Totally 25 rules are constructed.

The max-min-height method [10] is employed for the fuzzy inference. The antecedent parts of the control are the damping force of the variable damper, F_d and the total damping ratio of the system, h_t. The consequent part is the change of the damping ratio of the variable damper, Δh_v. The membership functions of the fuzzy numbers, F_d, h_t and Δh_v are shown in Fig. 7.

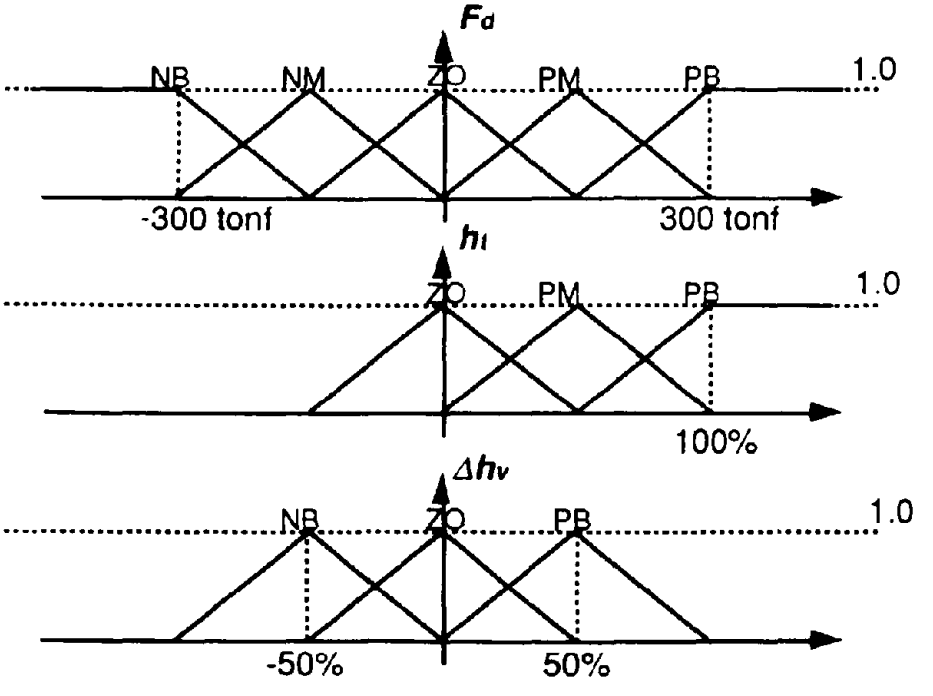

Figure 7. Membership functions of fuzzy numbers

In the simulation, we used that

PB of Δh_v to = 50%;

PB of h_t = 100%.

The El Centro NS (1940) earthquake waves, with various maximum accelerations ranged from 50gal to 300gal, were used. The maximum allowable damping force of the variable damper was set as 300tonf.

SIMULATION RESULTS

Effectiveness of a variable damper

The seismic response of the bridge model was computed with a time interval of 0.02sec. The input earthquake El Centro NS (1940) wave is shown in Fig. 8.

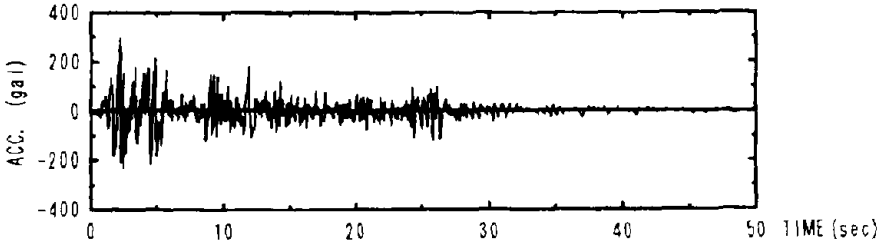

Figure 8. Input earthquake wave: El Centro NS (1940)

The time histories of the response of the bridge under the earthquake with the maximum acceleration of 100gal are shown in Fig. 9. Without the variable damper (Fig. 9(a)), the bridges have the maximum displacement of 8.2cm in its longitudinal direction and this is quite large because the structural damping is quite low. This can be reduced to 3.5cm after the variable damper is installed (Fig. 9(b)). It is shown that the variable damper is significant to suppress the response of the bridge. During 50sec of the earthquake time, the magnitude of the earthquake is strong in the first part (about 0-30sec) and becomes weak in the last part (about 30-50sec). Corresponding to this change, the variable damper provides low level damping first to reduce the damping force then gives high level damping at the last part, where the excitation level becomes small, to suppress the displacement efficiently. The variation of the damping ratio of the variable damper ranges from about 12% to 100%.

Comparison with a conventional damper having constant damping coefficient

To compare the effectiveness of the variable damper with that of conventional one that has constant damping coefficient, the simulations were carried out by using a damper with constant damping ratios of 12% and 100%, which is the lowest and the highest value of the variable damper, respectively. The results are shown in Fig. 9(c) and (d). When using the damper with low damping ratio, i.e., 12%, the damping force is relatively small and the maximum displacement of the bridge can only be reduced to 6.0cm. While using the damper with a high damping ratio, i.e., 100%, no doubt the response of the bridge can be suppressed significantly (lower than 1.3cm), however, the maximum damping force becomes large as 432tonf, which may destroy the bridge or exceed the capacity of the damper device in practice. By using the variable damper, it is possible to fully display the performance of the variable damper corresponding to various acceleration levels of the input.

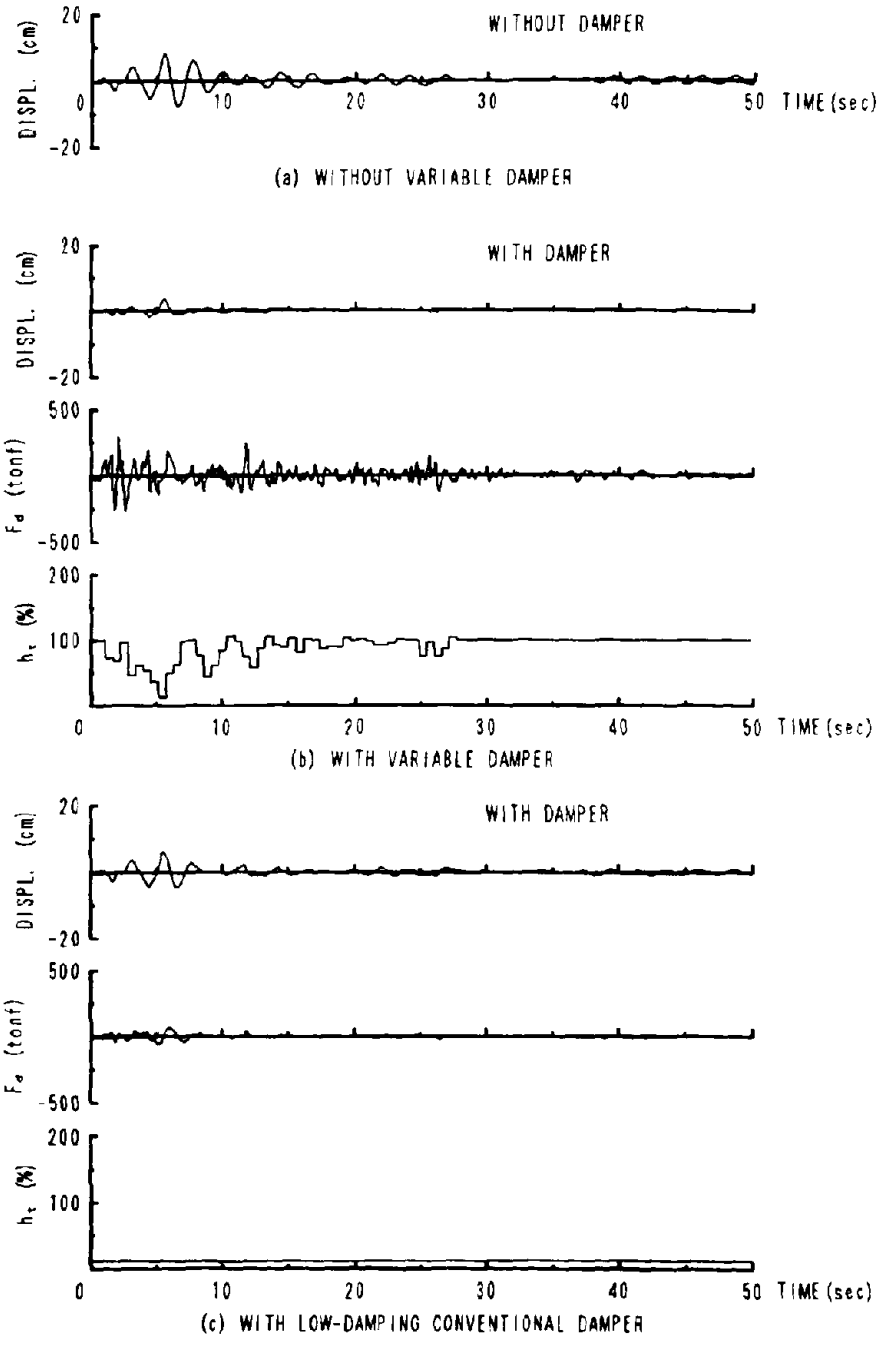

Figure 9. Effectiveness of variable damper and comparisons with conventional damper

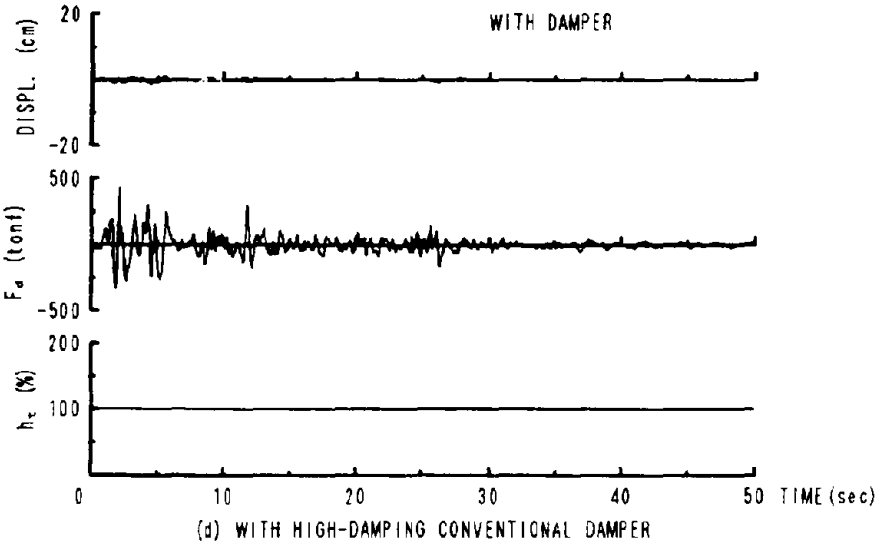

Figure 9. (Continued)

Adaptability to various levels of input

The effectiveness of the variable damper was also assessed by computing the responses of the bridge under the earthquakes with the maximum accelerations of 50gal, 100gal and 300gal, respectively. As shown in Fig. 10, by using the variable damper, the maximum displacement of the bridge was reduced from 4.1cm to 1.0cm, from 8.2cm to 3.5cm and from 24.6cm to 10.0cm, respectively. When the magnitude of the earthquake is small (Fig. 10(a)), the damping ratio of the variable damper is kept at high level (even so the maximum damping force will not exceed the value we set, 300tonf since the input acceleration is small). The variable damper is quite efficient for this case. When the magnitude of the earthquake is large (Fig. 10(c)), the damping ratio of the variable damper decreases to avoid the exceeding of the damping force over the pre-set level though the efficiency of the damper falls down with some degree comparing with the case of the small magnitude earthquake. For all the three cases, the damping of the variable damper is settled at high damping level at the last parts of the earthquakes because the input acceleration levels there become low. The simulation results show that the variable damper is adequate to various magnitudes of earthquakes. Though the suppression efficiency of the damper is not the same for various magnitude earthquakes, the performance of the variable damper has been fully displayed.

In the simulation case shown in Fig. 10(c), it can be found that the maximum damping force exceeds the value we set, 300tonf. This is because that the response of the damping force depends on not only the damping ratio of the variable damper but also the acceleration of earthquake. While in this study,

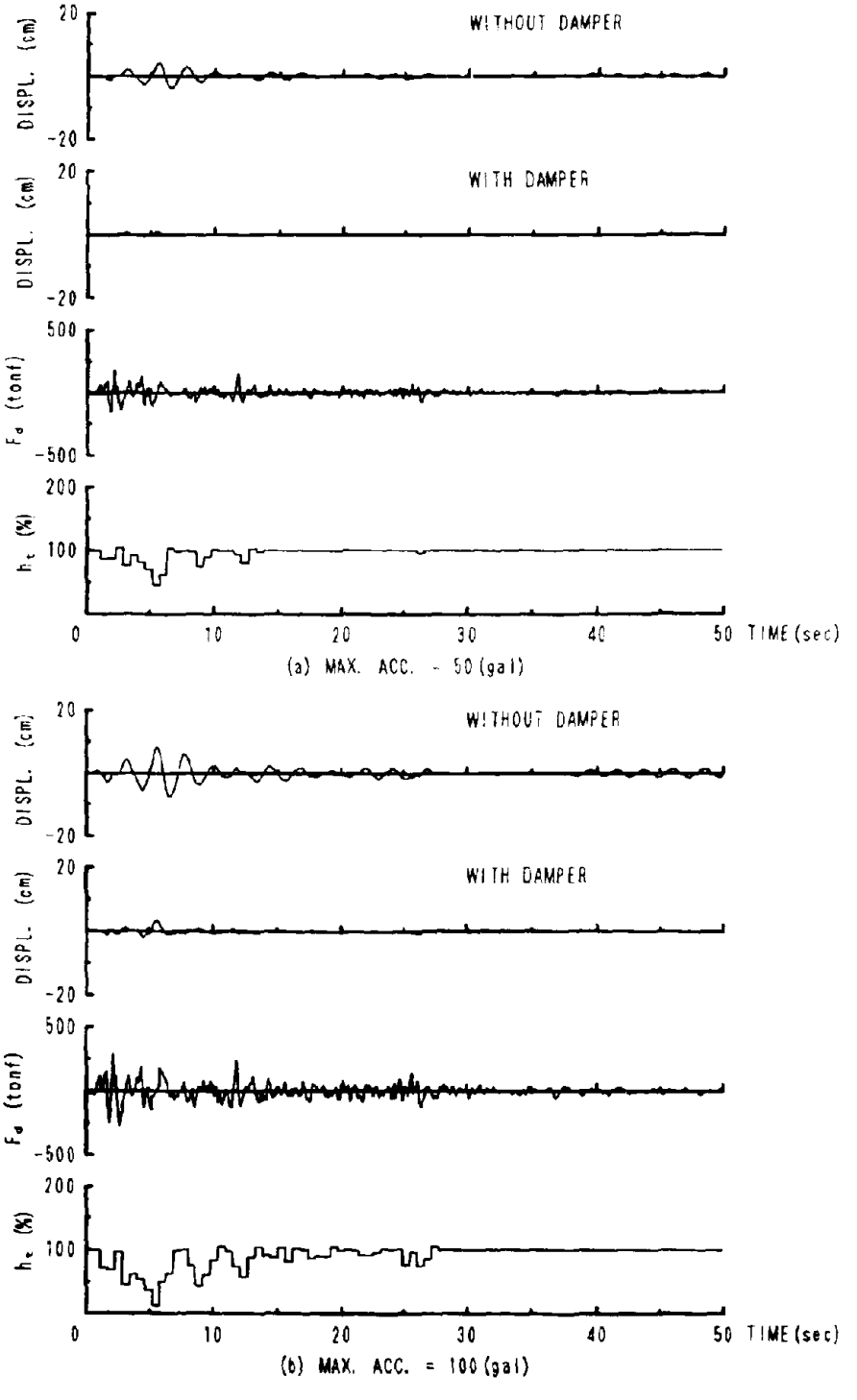

Figure 10. Responses to various levels of input

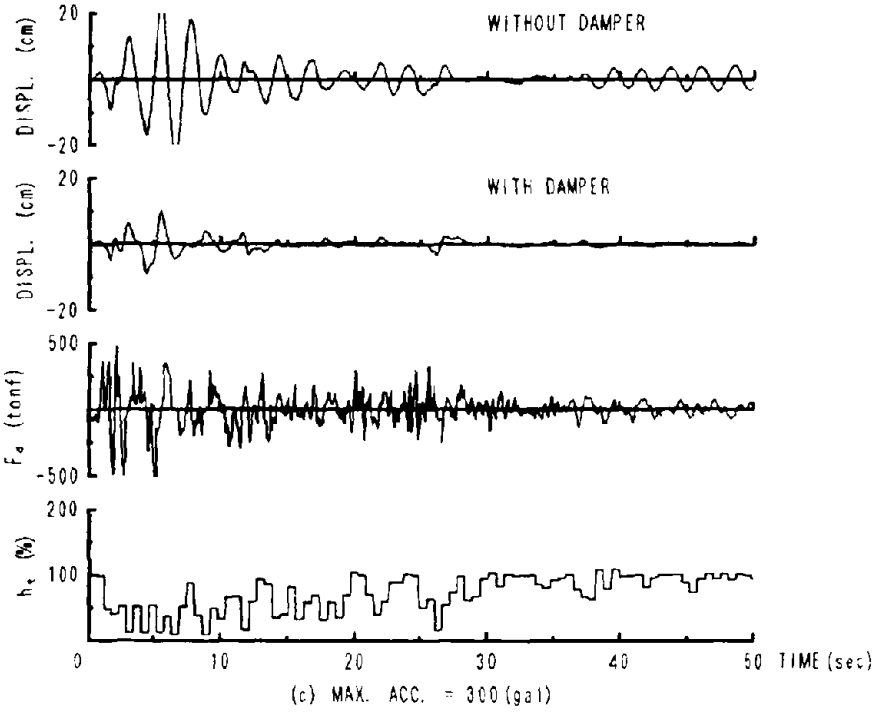

Figure 10. (Continued)

the effect of the acceleration of earthquake is not considered in the fuzzy control rules. This should be improved when constructing the fuzzy control rules in the future. If the variable damper installed has good responsibility, it is also possible to avoid the exceeding of the damping force by using small time interval for varying the damping as discussed in the next subsection.

Suitable time interval for varying damping

The time interval for varying the damping ratio of the variable damper used in the simulation cases shown in Figs. 9 and 10 is 1/4 of the natural period of the bridge, 1/4×2.3sec = 0.58sec. It is useful to investigate that how the time interval, ΔT_v affects the performance of the variable damper. In practice, using large time interval indicates that the variable damper device is easy to be built and the energy used for varying the damping can be low. However, too large time interval may cause problems such as poor responsibility, namely may cause over large damping force when the excitation becomes large suddenly and the change of the damping ratio of the variable damper can not follow. The simulations were carried out by using the time intervals of 1/4, 1/2 and 1 of the natural period of the bridge, i.e., 0.58sec, 1.16sec and 2.30sec, respectively (Fig. 11), and the maximum input acceleration is 300gal. The simulation results

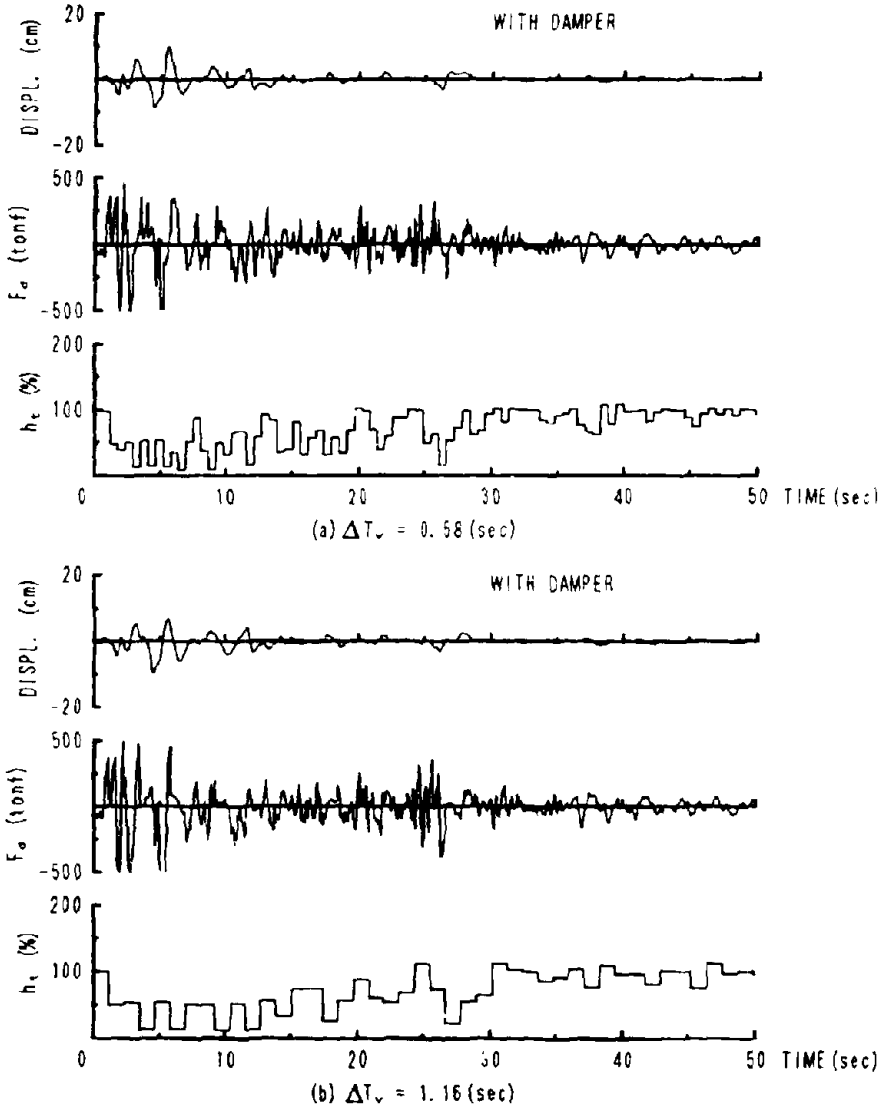

Figure 11. Responses using various time intervals for varying damping

show that the time interval ΔT_v = 1/4-1/2T is suitable (Fig. 11(a) and (b)). It is too large to use ΔT_v = T (Fig. 11(c)), because the maximum damping force is about 1,295tonf, which is much larger than the value we set.

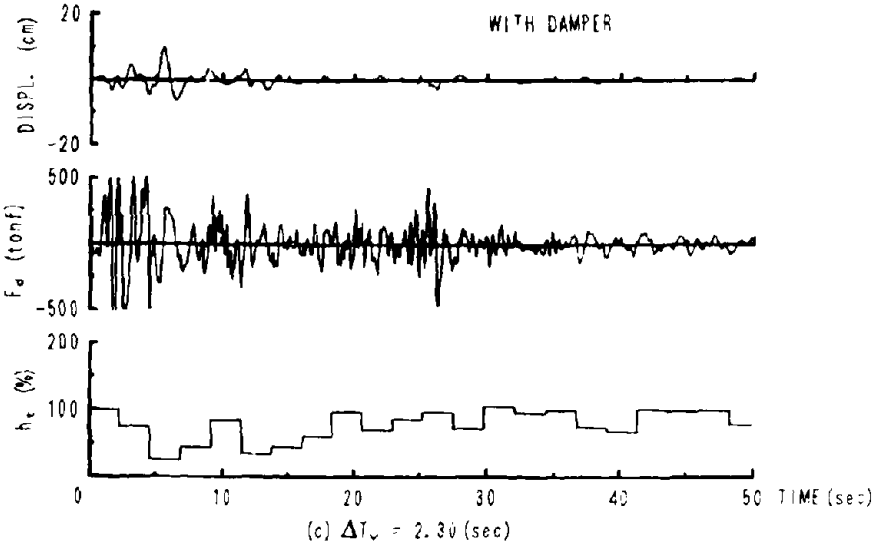

Figure 11. (Continued)

CONCLUSIONS

Concluding remarks

The simulation studies showed that, by using the variable damper, the longitudinal displacement of the bridge deck can be efficiently reduced so the sizes of expansion joint devices can be reduced. By varying the damping ratio of the variable damper, the capacity of the damper can be fully display on the condition that the damping force, i.e., the reaction force acting on the variable damper, does not exceed a certain pre-set value.

Fuzzy control theory is feasible to be u ed to control the variable damper. The control algorithm constructed based on common knowledge is simple and clear, the goal can be easily achieved if proper control rules are constructed. Furthermore, the fuzzy control theory does not need the modelling of the complicated structure and the computation for the controller is quite simple and can be easily carried out by using a simple micro chip. It can be said that the applicability of the fuzzy control theory is high. In this study, the antecedent parts of the fuzzy controller are the damping force and the damping ratio of the variable damper, their allowable values are easily to be determined according to the capacity of the variable damper.

When using the variable damper, the response is reduced and part of the horizontal seismic force is sheared by the variable damper, the horizontal shear force of the piers can also be reduced. So, it is also possible to design a bridge with low cost.

Future studies

Fuzzy control theory has been applied to deal with the control problem involving to the human-being operation. In that case, the control rules are usually constructed on the knowledge base of operators. In civil engineering field, however, there is no knowledge base on structural control, the constructions of fuzzy control rules encounter to difficulties. It is considerable to construct fuzzy control rules in following approaches: (1) by using try-and-error approach based on experimental data or numerical simulations; (2) by introducing neural network approach, so called neural fuzzy control theory, which can learn knowledge and construct control rule.

Though the fuzzy control theory can deal with nonlinear performance index function of the structural control problem well, its weak point is having low control accuracy. The combination of the fuzzy control theory and other conventional control theories, i.e., hybrid control theory, should also be investigated in the future.

REFERENCES

[1] Fujita, T. and Kabeya, K. et al. Semi-active Isolation System Using Controllable Friction Damper, Proc. of JSME, Vol.57, No. 536, p48-54, 1991 (in Japanese).

[2] Kobori, T., et al. Research on Active Seismic Response Control System with Variable Structure Characteristics -Basic Property of Variable Stiffness and Damping Mechanism and Fundamental Experiment by Shaking Table-, J. struct. eng. JSCE, Vol.37B, p183-192, 1991 (in Japanese).

[3] Shinozuka, M. and Ghanem, R. Use of Variable Dampers for Earthquake Protection of Bridges, Proc. 2nd US-Japan Workshop on Earthquake Protective Systems for Bridges, Tsukuba, Japan, p507-516, Dec., 1992.

[4] Kawashima, K., Unjoh, S. and Shimizu, H. Earthquake Response Control of Highway Bridges by Variable Damper, Transactions of the Japan National Symposium on Active Structural Response Control, Tokyo, p311-318, March 1992 (in Japanese).

[5] Kawashima, K. and Unjoh, S. et al. Effectiveness of the variable damper for reducing seismic response of highway bridge, Proc. 2nd US-Japan Workshop on Earthquake Protective Systems for Bridges, Tsukuba, Japan, p479-494, Dec., 1992.

[6] Pedrycz, W. Fuzzy Control and Fuzzy Systems. second, extended edition, Research Studies Press, 1993.

[7] Furuta, H. et al. Application of Fuzzy Control to Structural Vibration Control, Transactions of the Japan National Symposium on Active Structural Response Control, Tokyo, p101 108, March 1992 (in Japanese).

[8] Miyakoshi, J. et al. Application of Fuzzy Control Theory to Active Vibration Control, Transactions of the Japan National Symposium on Active Structural Response Control, Tokyo, p79-86, March 1992 (in Japanese).

[9] Velesos, A. S. and Ventura, C. E. Modal analysis of non-classically damped linear systems. Earthq. Eng. & Struct. Dyns., Vol.14, p217-243, 1986.

[10] Mizumoto, M. Fuzzy Inference and Fuzzy Control, Computrol, No.28, p32-45, KORONA, Oct. 1989 (in Japanese).

PREDICTION CONTROL OF A SDOF SYSTEM

Masaru HOSHIYA[1] and Yoshihito SAITO[2]

1. Professor, Department of Civil Engineering, Musashi Institute of Technology.
2. Research Associate, Department of Civil Engineering, Musashi Institute of Technology; on leave from Technical Research and Development Division, Maeda Corporation.

SUMMARY

General discussions are presented on an instantaneous optimal control of a single degree of freedom system which is subjected to earthquake ground motion. First, a method of identification of the dynamic properties of the system which is modeled by a multi-variate ARMA model is investigated with the responses of the system excited by an active control device. Then, general modes of an instantaneous optimal prediction control rule are formulated in terms of the identified components of the coefficient matrix of the ARMA model and the weights included in the control performance index.

INTRODUCTION

In the optimal regulator design, control force is traditionally evaluated such that a quadratic performance index becomes minimum. However, this regulator design can not be directly applied to civil engineering structures under earthquake excitation or strong wind turbulence force, since these excitations are not predictable beforehand, and there arise the following critical issues.

(1) Since excitation forces and corresponding responses are unknown beforehand, the control rule must be a time variant instantaneous optimal control which is relevant to the problems.

(2) Time delay of control force must be avoided that may be attributed to the time required to sense and to gather the information and the computation time for determining the proper action. To circumvent the delay, prediction of input and responses is necessary in the on-line real time process.

(3) Structural uncertainties must be taken into account so that the robustness of the control should be maintained.

Although the classical control procedures are well established within the scope of optimal regulator problem, instantaneous optimal control remains unsolved for basic matters on system identification and prediction, and on clarification of mutual relationship of different control rules that meet with the above mentioned requirements.

This study addresses itself to the abovementioned issues and investigates a single degree of freedom linear system excited by earthquake ground motion and controlled by an actuator installed on the system. First, the system is represented by an ARMA model and a theoretical formulation is derived to identify the dynamic properties of the system by exciting the system by the actuator. Then, with the identified ARMA model, together with an AR representation of earthquake excitation, response displacement and velocity of the system as well as the earthquake excitation are predicted in recursive forms so that a procedure of identification, prediction and control is established on the basis of an instantaneous optimal control rule by Yang et al.(Refs 1,2). Finally, a sensitivity analysis is carried out for the effect of identification and prediction errors on the system control.

IDENTIFICATION

A multi-variate ARMA model is used to represent a SDOF linear system, which is to be identified with observed responses of the system when excited by an actuator. Since the coefficient matrices of the ARMA model are theoretically related with physical parameters such as mass, spring constant and viscous damping coefficient, once they are identified, then all structural properties are to be identified.

The state vector equation of the SDOF system which is subjected to earthquake excitation and control force may be c..pressed as

$$\dot{X}(t) = AX(t) + B[u(t) - m\ddot{g}(t)] \tag{1}$$

where

$X^T(t) = [x(t)\ \dot{x}(t)]$

$A = \begin{bmatrix} 0 & 1 \\ -k/m & -c/m \end{bmatrix} \quad B = \begin{bmatrix} 0 \\ -1/m \end{bmatrix}$

$x(t)$: displacement response

$\dot{x}(t)$: velocity response

m : mass

k : spring constant

c : viscous damping coefficient

$u(t)$: control force

$\ddot{g}(t)$: earthquake acceleration

Discretization of eq(1) with time interval Δ leads to the following multi-variate ARMA equation.

$$X_{k+1} = \Phi X_k + \Gamma[u_k - m\ddot{g}_k] \tag{2}$$

where k stands for discrete time $t=k\Delta$.

and

$$\Phi = I + A\Delta + \frac{1}{2!}A^2\Delta^2 + \ldots + \frac{1}{r!}A^r\Delta^r + \ldots = \begin{bmatrix} \Phi_{11} & \Phi_{12} \\ \Phi_{21} & \Phi_{22} \end{bmatrix}$$

$$\Gamma = (I + \frac{1}{2!}A\Delta + \frac{1}{3!}A^2\Delta^2 + \ldots + \frac{1}{r!}A^{r-1}\Delta^{r-1} + \ldots)B\Delta = \begin{bmatrix} \Gamma_1 \\ \Gamma_2 \end{bmatrix}$$

It is proved that eigenvalues Λ and eigenvector Z of matrix A and eigenvalues Λ^* of matrix Φ are mutually related with following equations (Ref.3).

$$AZ = Z\Lambda \quad \Phi Z = Z\Lambda^* \quad \Lambda^* = \exp(\Lambda\Delta) \tag{3}$$

So if Φ is identified, matrix A is determined from solving the eigenvalue ploblem of Φ. If vector Γ is also identified, then matrix B is determined by the following equation.

$$B = A(\Phi - I)^{-1}\Gamma \tag{4}$$

It is noted that since matrices A and B include physical parameters such as m, k and c, all necessary properties of the system are determined when A and B are estimated.

The following stationary state vector equation (5) and observation vector equation (6) are formulated on which the Kalman filter by Kalman(Ref.4), Kalman et al.(Ref.5), Jazwinski(Ref .6), and Hoshiya et al.(Refs 7,8), is applied in order to identify Φ and Γ.

$$[\Phi_{11}\ \Phi_{12}\ \Gamma_1\ \Phi_{21}\ \Phi_{22}\ \Gamma_2]^T_{k+1} = [\Phi_{11}\ \Phi_{12}\ \Gamma_1\ \Phi_{21}\ \Phi_{22}\ \Gamma_2]^T_k \tag{5}$$

and

$$\begin{bmatrix} x_{k+1} \\ \dot{x}_{k+1} \end{bmatrix} = \begin{bmatrix} x_k & \dot{x}_k & u_k & 0 & 0 & 0 \\ 0 & 0 & 0 & x_k & \dot{x}_k & u_k \end{bmatrix} [\Phi_{11}\ \Phi_{12}\ \Gamma_1\ \Phi_{21}\ \Phi_{22}\ \Gamma_2]^T_k + W_k \tag{6}$$

It is noted that equation(6) is obtained from eq(2) putting that $\ddot{g}_k=0$ and W_k is a white noise vector.

PREDICTION CONTROL

The following performance index is employed for the instantaneous optimal control on the

discrete system expressed by eq(2).

$$J_k = \frac{1}{2}\left[X^T_{k+1} Q X_{k+1} + r u^2_k + 2\left(-m\ddot{g}_k\right) L^T P X_{k+1}\right] \tag{7}$$

where

$$L = \begin{bmatrix} 0 \\ 1 \end{bmatrix} \qquad P = \begin{bmatrix} 0 & 0 \\ 0 & \alpha \end{bmatrix} \qquad Q = \begin{bmatrix} k & 0 \\ 0 & m \end{bmatrix}$$

This performance index is basically identical to such an index as proposed by Sato et al.(Ref.9) that includes an additional term of effective input energy in the index of an open-closed loop control suggested by Yang et al.(Refs 1,2). In the equation(7), Q, r and P represent respectively the weighting coefficients to keep the balance of energy distribution among the first term of kinetic and potential energy, the second term of control force energy and the third term of effective input energy. The control force may be determined such that the performance index becomes minimum under a constraint equation(2). So doing, we obtain the following control force consisting of feed back and feed forward terms.

$$u_k = G_{FB} X_k + G_{FF} \ddot{g}_k \tag{8}$$

and

$$G_{FB} = -\left[r + \Gamma^T Q \Gamma\right]^{-1} \Gamma^T Q \Phi \tag{9}$$

$$G_{FF} = \left[r + \Gamma^T Q \Gamma\right]^{-1} \Gamma^T \left[Q\Gamma + P^T L\right] m \tag{10}$$

Equations(9) and (10) indicate that the feed back gain G_{FB} and the feed forward gain G_{FF} may be evaluated beforehand if the system is identified by the method as described in the preceding section. However, in order to determine the control force u_k at time $t=k\Delta$, we must know the responses X_k and input $\ddot{g}_k$ at the stage of $t=(k-1)\Delta$, and they are predicted in the following manner.

As for X_k, we use equation(2) as

$$X_k = \Phi X_{k-1} + \Gamma\left[u_{k-1} - m\ddot{g}_{k-1}\right] \tag{11}$$

The prediction of $\ddot{g}_k$ is carried out by modeling the input acceleration by an AR representation (Ref. 10) as

$$\ddot{g}_k = \alpha_1 \ddot{g}_{k-1} + \alpha_2 \ddot{g}_{k-2} + \alpha_3 \ddot{g}_{k-3} + \alpha_4 \ddot{g}_{k-4} + v_k \tag{12}$$

where v_k is a white noise.

The unknown coefficients α_i are to be evaluated recursively during the control process by applying the Kalman filter on the following state vector equation and the observation equation respectively.

$$\left[\alpha_1\ \alpha_2\ \alpha_3\ \alpha_4\right]^T_{k-1} = \left[\alpha_1\ \alpha_2\ \alpha_3\ \alpha_4\right]^T_{k-2} \tag{13}$$

and

$$\ddot{g}_{k-1} = \left[\ddot{g}_{k-2}\ \ddot{g}_{k-3}\ \ddot{g}_{k-4}\ \ddot{g}_{k-5}\right]\left[\alpha_1\ \alpha_2\ \alpha_3\ \alpha_4\right]^T_{k-1} + v_{k-1} \tag{14}$$

where v_{k-1} is a white noise.

In equation(14), $\ddot{g}_{k-1}$ to $\ddot{g}_{k-5}$ are already observed at time $(k-1)\Delta$, and once α_i are identified, $\ddot{g}_k$ at time $k\Delta$ is predicted from equation(12).

A special case is emphasized in which the mass of the system is a known constant. Then, excitation terms $u_{k-1} - m\ddot{g}_{k-1}$ in equation(11) are to be known at time $(k-1)\Delta$. Therefore, using them as the excitation, the remaining parameters k and c may be identified in a manner similar to the procedure of the preceding section. If this process is integrated into the sequential real time control algorithm, we can deal with a case in which the structural stiffness and damping are time dependent. The adaptive algorithm to determine the control force u_k at time $k\Delta$ based on the identification of the system at time $(k-1)\Delta$ and on the prediction of X_k and $\ddot{g}_k$ is schematically illustrated in Fig. 1. Fig. 1 shows that at the stage of $t=(k-1)\Delta$, the responses X_k and input $\ddot{g}_k$ are predicted by eq.(11) and (12), and the feed back gain G_{FB} and the feed forward gain G_{FF} are determined from the Φ and Γ which are identified using the observations. Therefore, the control force u_k at time $k\Delta$ are determined from the prediction and identified values.

The proposed procedure may be also interpreted as an equivalent neural network model as in Fig. 2.

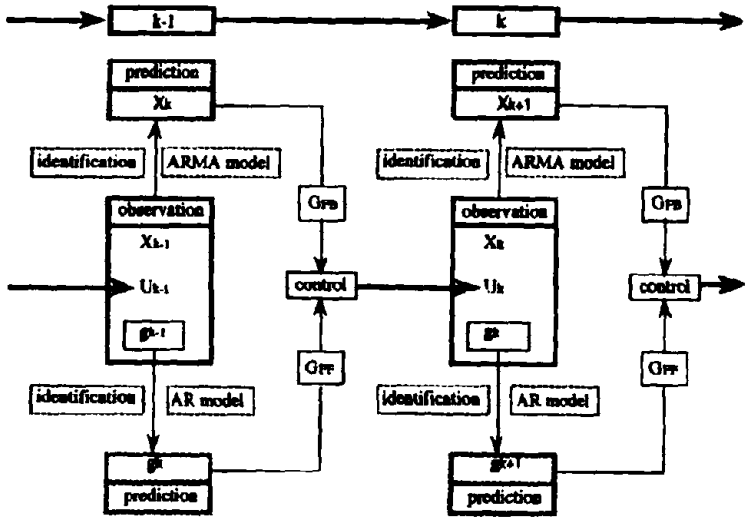

Fig. 1. Schematical Procedure of Identification, Prediction and Control

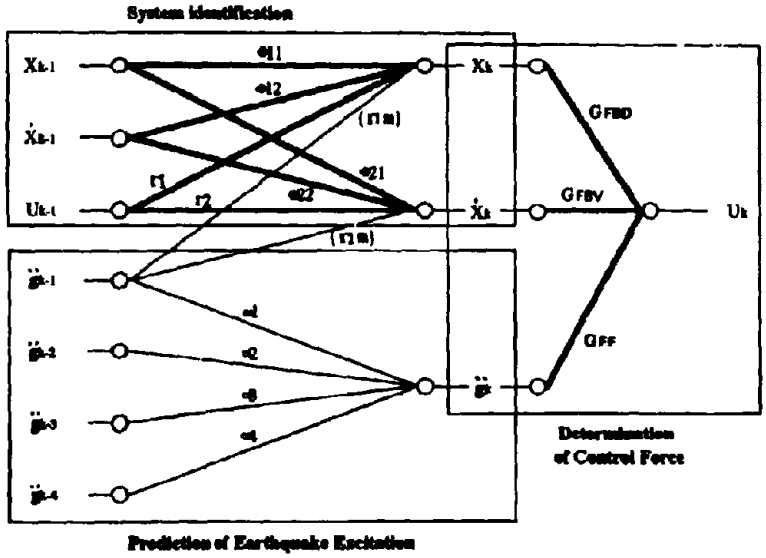

Fig. 2. An Equivalent Neural Network

DIFFERENT CONTROL RULES

If equation (8) is expressed in terms of components, the control force is given by

$$u_k = \frac{-1}{\Gamma + k\Gamma_1^2 + m\Gamma_2^2}\left[\left(\Gamma_1 k\Phi_{11} + \Gamma_2 m\Phi_{21}\right)x_k + \left(\Gamma_1 k\Phi_{12} + \Gamma_2 m\Phi_{22}\right)\dot{x}_k - \left(k\Gamma_1^2 + m\Gamma_2^2 + \alpha\Gamma_2\right)m\ddot{g}_k\right] \quad (15)$$

This equation indicates that the control force u_k consists of the first and second terms

representing the feed back force, and the third term the feed forward force. It is clear that the weighting coefficient α which appears in the third term in the numerator regulates the feed forward gain relatively against the feed back gain of the first and second terms. The weighting coefficient r for the control force energy that appears in the denominator regulates the magnitude of the control force. It is also clear that the instantaneous optimal control rule has two degree of freedom α and r in order to determine the control force.

Introducing a parameter β to relate α and r as

$$\alpha = \beta r / \Gamma_1 \tag{16}$$

different control rules will be discussed in the following paragraphs.

If the third term is dropped out, equation(15) becomes (a)the closed loop control by Yang (Refs 1,2), whereas if $\beta = 0$, it becomes (b)the open-closed loop control proposed again by Yang (Refs 1,2). The latter case(b) means that the ratio of the feed back gain and the feed forward gain is fixed. By varying the value of α in equation(15), different control rules are designed which are namely (c)hybrid feed back and feed forward controls. If $\beta = 1$, it indicates that the third term of the feed forward control force is always same to the input excitation force. In this control(d), the excitation force is perfectly counterbalanced with the feed forward control force and no response will be expected. So there arises no feed back control force. As r becomes smaller, however, the value of the feed back gain increases. Finally, if $\beta = (r - k \Gamma_1^2 - m \Gamma_2^2) / 2 r$, the feed forward term of equation(15) becomes half of the input excitation force. This is (e)a control rule that counterbalances with half of input force.

PULSE FREQUENCY TRANSFER FUNCTIONS

In order to discuss frequency properties and mutual relationships between different control rules (a) to (e), pulse frequency transfer functions of response velocity and of control force are derived against input $\ddot{g}$.

They are calculated for a system given in Table1. Figs.3 to 7 show the pulse frequency transform functions of response velocity against $\ddot{g}$, and Figs.8 to 12 show those of u against $\ddot{g}$ where the values of weighting coefficient r in the performance index are used as shown in Table2. And control (c) employs α =1.0 in the calculation.

Table 1. A SDOF System

mass	(m)	1.0	(lb sec²/cm)
stiffness	(k)	39.478	(lb/cm)
natural period	(T)	1.0	(sec)
damping coefficient		2.0	(%)

Table 2. Values of r for Pulse Frequency Transform Functions

increases ↑ / control force / ↓ decreases	decreases ↑ / r / ↓ increases	values of r	symbols
		1.00E-6	—■—
		5.00E-4	—□—
		1.98E-3	—◆—
		5.00E-3	—◇—
		9.90E-3	—▲—
		1.98E-2	—△—
		3.96E-2	—●—
		1.00E+1	—○—

It is observed that since the closed loop control(a) is depentent upon only the state vector **X**, the peaks of the frequency transform functions of control force appear around the predominant frequency(1.0Hz) of the system(Fig.8). Even if r decreases, control force can not be counterbalanced with the input force in the all domain of frequency as indicated by the curve(— ■ —)in Fig.8. But as for the open-closed loop control(b), when r is very small, control force can be counterbalanced with the input force in the all domain of frequency in Fig.9. And consequently the frequency transform functions of the response velocity becomes zero in Fig.4.

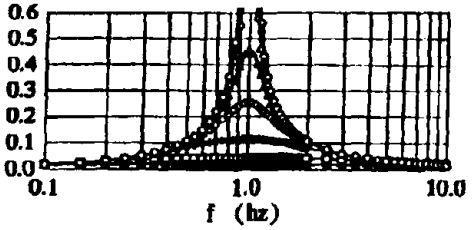

Fig.3. Pulse frequency transform function of response velocity (control (a))

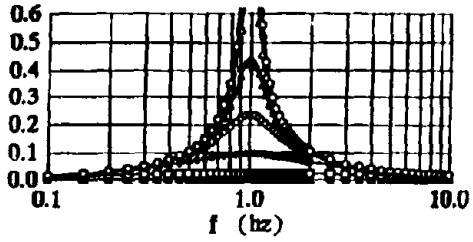

Fig.4. Pulse frequency transform function of response velocity (control (b))

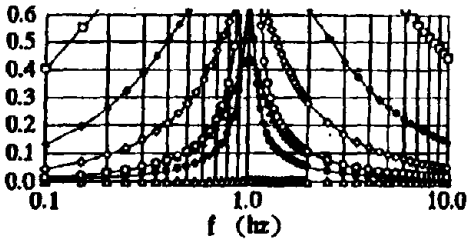

Fig.5. Pulse frequency transform function of response velocity (control (c))

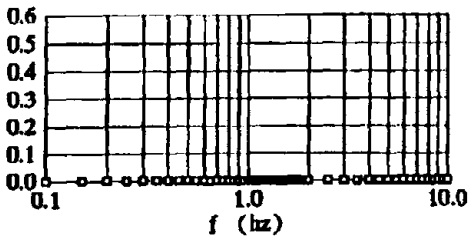

Fig.6. Pulse frequency transform function of response velocity (control (d))

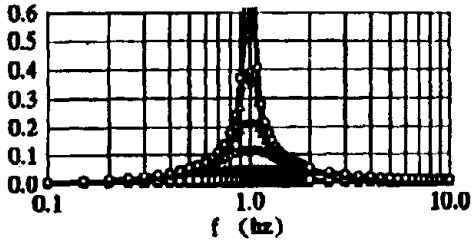

Fig.7. Pulse frequency transform function of response velocity (control (e))

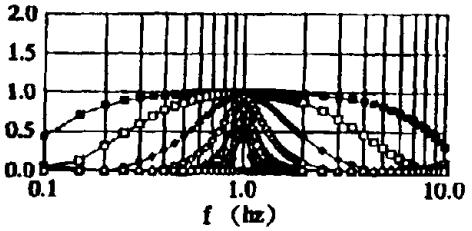

Fig.8. Pulse frequency transform function of control force (control (a))

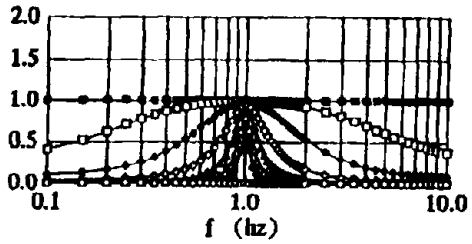

Fig.9. Pulse frequency transform function of control force (control (b))

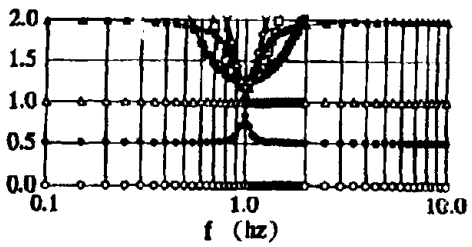

Fig.10. Pulse frequency transform function of control force (control (c))

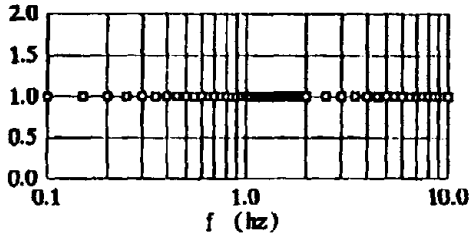

Fig.11. Pulse frequency transform function of control force (control (d))

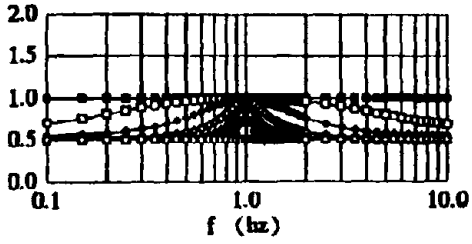

Fig.12. Pulse frequency transform function of control force (control (e))

Curves in the hybrid feed back and feed forward control (c) in Figs 5 and 10 aproach to the curve of the control(d) when r decreases, and when r satisfies with equation (16), it becomes the same as control (d). However, as r furthermore decreases, the frequency transform function of response velocity becomes larger because the control force reaches surplus. On the contrary, control(d) is always satisfied with equation (16) , and therefore the frequency transform function of the response velocity is always zero in Fig.6. So feed back control force does not arise.

Figs 7 and 12 indicate that control(e) is always counterbalanced with the half of input force, and when r decreases, feed-back control force becomes larger and aproaches to control(d).

NUMERICAL ANALYSES

In order to visualize the mutual relationships between different control rules (a) to (e), numerical analyses are carried out for a system given in Table 1 and excited by an El Centro earthquake-NS component acceleration record (Table3).

The results are shown in Figs 13 to 18 where maximum values of the control force u_s and maximum response displacement are comparatively given as functions of γ . Figs 13 and 14 shows results based on known input and responses whereas all other figures are obtained based on the prediction of input force. The symbols used are summarized in Table 4.

Table 3. Input Acceleration Wave

discrete time (△)	0.02 (sec)
time duration (T)	50.0 (sec)
maximum value (max)	341.7 (gal)

Table 4. Different Control Rules

Control Rules	Symbols
(a)closed loop by Yang	—■—
(b)open-closed loop by Yang	—◆—
(c)hybrid feed back and feed forward control	—◇—(α=0.1)
	—▲—(α=0.5)
	—△—(α=1.0)
	—●—(α=2.0)
(d)feed forward control fixed for β=1.0	—□—
(e)feed forward control fixed for $\beta=(r-k\Gamma_1^2-m\Gamma_2^2)/2r$	—○—

It is observed that since the closed loop control(a) is dependent upon only the state vector X_s , it is naturally not influenced by the prediction errors of input force (compare the curves(— ■ —) in Figs 13 and 15, and in Figs 14 and 16). The open-closed loop control(b) approaches to the closed loop control as γ increases, and to the control rule(d) as γ decreases (see the curves(— ◆ —)). In the hybrid feed back and feed forward control(c) curves become the open-closed loop control(b) when γ is large, but they approach to the control(d) when γ decreases. When γ satisfies with $\gamma = \alpha \Gamma_2$, this control rule coincides with the control(d). If γ furthermore decreases beyond this critical point, the control will diverge. As for the control(d), the response is always zero if no prediction error is involved. However , if some errors exist in the input prediction, the input force can not be counterbalanced with the feed forward control force and the difference will be taken up by the feed back control. The control(e) is always between the open-closed loop control (b) and the control(d).

Figs 17 and 18 show results in the case that the control device has an upper bound constraint on the control capability with 150tf. So it is observed that the maximum values of the control force are always less than or equal to 150tf (see Fig.17). On the contrary, the maximum values of the response displacements increases greater than those in the case of having no constraint on the control force capacity (compare Figs 16 and 18). As for the hybrid feed back and feed forward

control(c), however, the responses caused by the surplus control force are apt to be restrained (see Fig. 18).

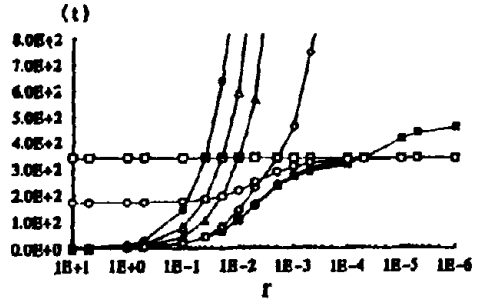

Fig. 13. Maximum Control Force (Known Input)

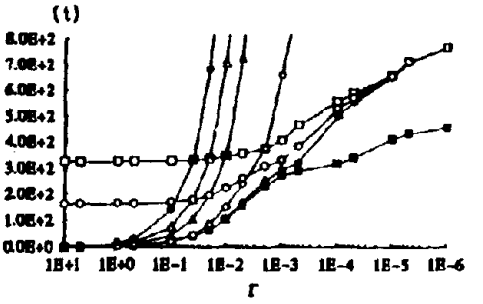

Fig. 15. Maximum Control Force (Predicted Input)

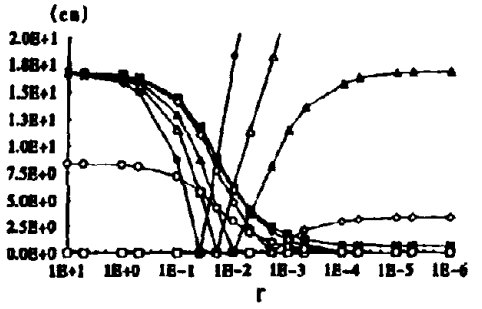

Fig. 14. Maximum Response Displacement (Known Input)

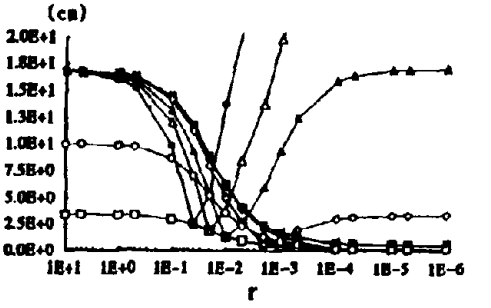

Fig. 16. Maximum Response Displacement (Predicted Input)

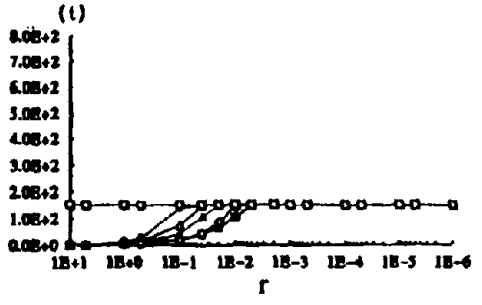

Fig. 17. Maximum Control Force (Predicted Input and Constraint of Control Force)

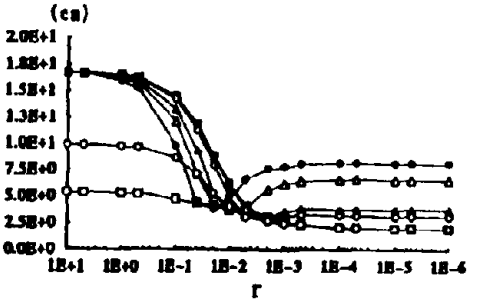

Fig. 18. Maximum Response Displacement (Predicted Input and Constraint of Control Force)

Figs 19 to 22 show results when we have identification error for the mass. They are obtained based on the known input in order to observe the effect of only identification error. First, the error of $\pm$ 50% of the mass is considered in the analysis. As for the closed-loop control(a), since the control forces increase in the case of +50% error, the responses decrease compared to the case of no prediction error(see the curves(– ■ –) in Figs 13,14 and 19,20). In the case of -50% error, the responses increase as the control forces decrease(see the curves(– ■ –) in Figs 13,14 and 21,22). The critical points of the control(c) where the responses become minimum shift to the left hand side in the case of +50% error and to the right hand side in the case of -50% error (see Figs 20 and 22). The control(d) and the control(e) are naturally influenced greatly by the identification error for the mass, because the feed forward control force is influenced by the error, even if the

input acceleration is true.

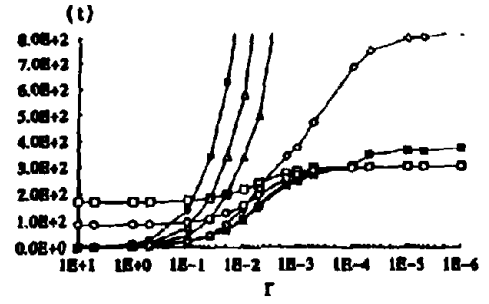

Fig. 19. Maximum Control Force (Known Input and +50% error of the mass)

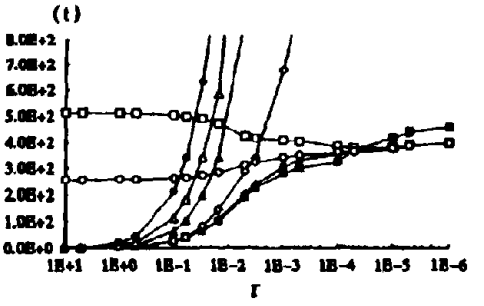

Fig. 21. Maximum Control Force (Known Input and -50% error of the mass)

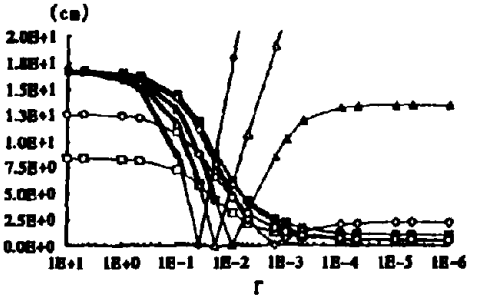

Fig. 20. Maximum Response Displacement (Known Input and +50% error of the mass)

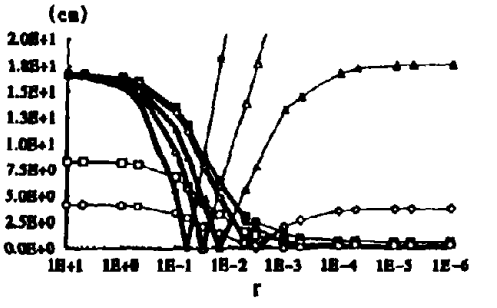

Fig. 22. Maximum Response Displacement (Known Input and -50% error of the mass)

Similar analyses are carried out on the effect of identification errors for the spring constant and the viscous damping coefficient, and it is found that their errors scarcely influence the effect of control. This is mainly due to the fact that these parameters have no connection with the input force, and furthermore the prediction of the state vector is not influenced by them as far as the error is within the range of $\pm 50\%$ of the true values.

FINAL REMARKS

This study is performed by the second author, incorporated with theoretical suggestion by the first author.

REFERENCES

1)Yang, J. N. (1982). "Control of tall Buildings under earthquake excitation." J. Engrg. M., ASCE, 108(5), Oct. pp.833-849

2)Yang,J. N., Akbarpour,A., and Ghaemmaghami,P. (1987). "New optimal control algorithms for structural control." J. Engrg. Mech., ASCE, 113(9), Sep. pp.1369-1386

3) Pl,Y.L. and Mickleborough, N.C., Time domain Modal Identification of a Linear Vibrating Structure. UNICIV Report No.R-249,The University of New South Wales, Apr., 1988.

4)Kalman, R. E. (1960). "A new approach to linear filtering and prediction problems." J. Basic Engrg., 82(1), pp.35-45.

5)Kalman, R. E. and Bucy, R. S. (1961). "New results in linear filtering and prediction theory. " J. Basic Engrg., 83(1), pp.95-108.
6)Jazwinski, A. H. (1976). "Stochastic process and filtering theory." Academic Press, New York, N.Y.
7)Hoshiya, M., and Saito, E. (1984a). "Identification of dynamic properties of a building by the EK-WGI method on microtremor records." Proc., Japan Society of Civil Engineers, No.350, Oct. pp.263-270 (in Japanese)
8)Hoshiya, M., and Saito, E. (1984b). "Structual identification by extended Kalman filter." J. Engrg. Mech., ASCE, 110(12), pp.1757-1770
9)Sato,T., Toki,K., and Sugiyama,K. (1990). "Optimal control of seismic response of structure." Proc. Japan Society of Civil Engineers, No.416, Apr. pp.191-200
10) Sato,T., Toki,K. and Hashimoto,M. (1991). "Predictive control of seismic response of structure with time delay." Proc. Japan Society of Civil Engineers, No.428,Apr. pp.193-202 (in Japanese)

HYBRID PROTECTIVE SYSTEMS FOR SEISMIC-EXCITED BRIDGES

by

J. N. Yang, Z. Li and J. C. Wu
Department of Civil and Environmental Engineering
University of California, Irvine, CA, U.S.A.

K. Kawashima and S. Unjoh
Earthquake Engineering Division, Public Works Research Institute, Japan

ABSTRACT

Recently, several hybrid protective systems have been explored for applications to seismic-excited bridge structures. In particular, two types of aseismic hybrid protective systems have been shown to be quite effective: (i) rubber bearings and variable dampers (or actuators), and (ii) sliding bearings and actuators. In this paper, control methods are presented for these hybrid protective systems. The control methods are based on the theory of variable structure system (VSS) or sliding mode control (SMC). Emphasis is placed on the direct output feedback controllers using only a few sensors. Sensitivity studies are conducted to evaluate and compare the effectiveness of passive sliding isolators and hybrid protective systems for reducing the response of seismic-excited bridge structures. The advantages of each protective system are demonstrated by simulation results for a wide range of earthquake intensities.

INTRODUCTION

Aseismic hybrid protective systems, consisting of a combination of active devices and passive isolation systems, have been shown to be quite effective for reducing the bridge response subjected to strong earthquakes. The idea of hybrid systems is to utilize the passive isolation system to reduce the ground motion transmitted to the bridge girder, whereas the active control devices are used to further reduce the bridge response. Variable viscous dampers, in which the damping coefficient can be adjusted by regulating the opening of the valves for the oil flow, have been developed and tested by Kawashima et al (1991, 1992). A hybrid protective system consisting of rubber bearings and variable dampers have been demonstrated to be quite effective for protecting seismic-excited bridge structures (Kawashima et al 1991, 1992, Feng et al 1990, Yang, et al 1993a). Structural control using variable dampers belongs to the category of parametric control and control algorithms have been investigated for SDOF structures [Feng et al 1990, Yang et al 1993a] and MDOF structures [Yang et al 1993b].

Another type of hybrid protective system, consisting of frictional-type sliding bearings and actuators, has been investigated for applications to reduce the response of seismic-excited bridges by NCEER researchers (Nagarajaiah et al 1992). The sliding bearings, made of the Teflon/stainless steel plates, allow the girder to slide during strong earthquakes thus reducing the acceleration of bridge girders. The actuator is used to further reduce not only the bridge response but also the

sliding displacement of the girder. Shaking table tests for this type of hybrid protective system have been conducted and excellent performance has been observed. Various algorithms for control of sliding isolated structures have also been studied by [e.g., Nagarajaiah et al 1992, Reinhorn et al 1993, Yang et al 1992, 1993c].

Based on the theory of variable structure system (VSS) or sliding mode control (SMC), control methods are presented in this paper for applications of aseismic hybrid protective systems described above for bridge structures. The idea of the theory of sliding mode control (SMC) is to design the controller to drive the response trajectory into the sliding surface (or switching surface) and maintain it there, whereas the motion of the structure on the sliding surface is stable. Direct output feedback controllers using only a few sensors are presented. The performance of the control methods are demonstrated by simulation results. Parametric studies are conducted to evaluate and compare the effectiveness of (i) hybrid protective systems, and (ii) a passive sliding isolation system for reducing the seismic response of bridge structures. The advantages and performance of each protective system are demonstrated by numerical simulation results for a wide range of earthquake intensities.

CONTROL OF RUBBER-BEARING ISOLATED BRIDGES

Consider a bridge structure in which rubber bearings and variable dampers are installed between the girder and piers as shown in Figure 1(a). The bridge is discretized by an n degree-of-freedom lumped mass system as shown in Figure 1(b). Let $\xi_1(t),\xi_2(t),\ldots,\xi_r(t)$ be the damping coefficients of r variable dampers installed in the bridge. The capacity of each variable damper is bounded by a minimum value and a maximum value, i.e., $\xi_{imin} \le \xi_i(t) \le \xi_{imax}$ with $\xi_{imin} \ge 0$. For simplicity of presentation, rubber bearings are assumed to behave linearly. The vector equation of motion of the entire bridge structure subjected to a one-dimensional horizontal ground acceleration $\ddot{x}_0(t)$ can be expressed as

$$M\ddot{X}(t) + C\dot{X}(t) + KX(t) = H^*(\dot{X})\,\xi(t) + \eta\,\ddot{x}_0(t) \tag{1}$$

in which $X(t)=[x_1,x_2,\ldots,x_n]'$ is an n-vector with $x_i(t)$ being the deformation of the ith element; M, C and K are (nxn) mass, damping and stiffness matrices, respectively; $\eta=-[m_1,m_2,\ldots,m_n]'$ is a mass vector with m_i being the mass at the ith nodal point; and the prime indicates the transpose of either a vector or a matrix. In Eq. (1), $H^*(\dot{X})$ is a (nxr) matrix which is a function of the velocity vector $\dot{X}(t)$, and $\xi(t)$ is a r-dimensional control vector denoting the damping coefficients of r variable dampers, i.e., $\xi(t)=[\xi_1(t), \xi_2(t), \ldots, \xi_r(t)]'$. The vector equation of motion, Eq. (1), can also be written as

$$M\ddot{X}(t) + C\dot{X}(t) + KX(t) = HU(t) + \eta\,\ddot{x}_0(t) \tag{2}$$

where H is a (nxr) constant matrix denoting the locations of r variable dampers and U(t) is a r-dimensional control vector $U(t)=[u_1(t),u_2(t),\ldots,u_r(t)]'$ with

$$u_i(t) = \xi_i(t)\dot{x}_k(t) \tag{3}$$

in which the ith variable damper is attached to the kth element of the structure. In the state space, the state equations for Eqs. (1) and (2) become, respectively,

$$\dot{Z}(t) = AZ(t) + B^*(Z)\xi(t) + E(t) \tag{4}$$

and

$$\dot{Z}(t) = AZ(t) + BU(t) + E(t) \tag{5}$$

where $Z(t) = [\, X(t)', \dot{X}(t)' \,]'$ is a 2n state vector and other matrices are defined appropriately.

Instead of variable dampers, actuators can be installed at the same locations as variable dampers. In this case, the state equation of motion is given by Eq. (5) with $u_i(t)$ being the active control force from the ith actuator (controller). Thus, Eq. (5) holds for both cases using either variable dampers or actuators.

Design of Sliding Surface

The first step in the sliding mode control method is to design the sliding surface (or switching surface) on which the response is stable. In the design of sliding surface, the external excitation E(t) is neglected; however, it is taken into account in the design of controllers. Let the r-dimensional sliding surface, S=0, be a linear combination of the state vector

$$S = PZ = 0 \tag{6}$$

in which P is a (rx2n) matrix to be determined such that the motion on the sliding surface is stable. The state equation given by Eq. (4) indicates that the coefficient, $B^*(Z)$, of the control vector, $\xi(t)$, is a function of the state vector Z(t). The procedures for determining the sliding surface for the state equation, in which the coefficient of the control vector is a function of the state vector Z, have been described in (Utkin, 1992). Using the particular functional form of $B^*(Z)$ given by Eqs. (1) and (4), and following the procedures described in (Utkin, 1992), we find that the resulting regular form for determining the sliding surface is identical to that for Eq. (5), in which U(t) is considered

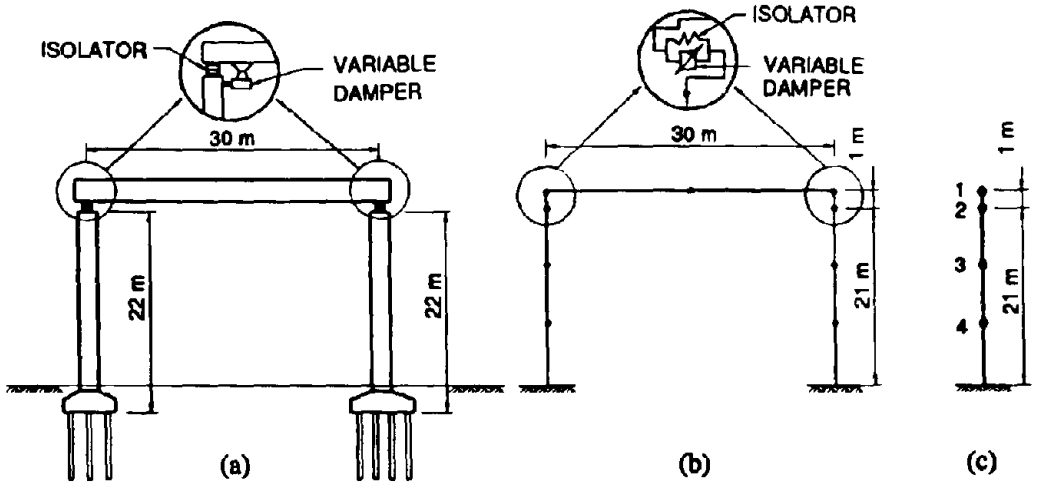

Fig.1 : Bridge Model; (a) Actual Bridge, (b) Lumped Mass System and (c) Four-Degree-of-Freedom System

a control vector and B is a constant matrix. Consequently, for the convenience of derivations, Eq. (5) can be used for the determination of the sliding surface.

One systematic approach for the determination of the P matrix is to convert Eqs. (5) and (6) into the regular form as described in (Utkin, 1992). Then, either the method of LQR or the pole assignment method can be used to determine the P matrix. In the case of LQR, the sliding surface is determined by minimizing the objective function

$$J = \int_0^\infty Z'(t)QZ(t)dt \tag{7}$$

in which Q is a (2nx2n) positive definite weighting matrix. Details for the design of the sliding surface P are described in (e.g., Utkin, 1992; Yang, Li, Wu and Young, 1993b, 1994).

Design of Controller Using Lyapunov Direct Method

To design the controller, the following Lyapunov function is considered

$$L = 0.5S'S = 0.5Z'P'PZ \tag{8}$$

The sufficient condition for the sliding mode to occur is given by

$$\dot{L} = S'\dot{S} < 0 \tag{9}$$

Substituting S=PZ into Eq. (9), taking the derivative and using both Eqs. (3) and (5), one obtains

$$\dot{L} = \sum_{i=1}^{r} \lambda_i(\xi_i z_{n+k,i} - G_i) \tag{10}$$

in which $z_{n+k,i} = \dot{x}_k$ is the velocity of the kth element of the structure on which the ith variable damper is installed as shown by Eq. (3). In Eq. (10), λ_i and G_i are the i^{th} elements of the row vector λ and the column vector G, respectively,

$$\lambda = S'(PB) \;\; ; \;\; G = -(PB)^{-1}P(AZ + E) \tag{11}$$

where the dimension of both λ' and G is r. Due to the limitation of the capacity of variable dampers, it is not possible to guarantee the condition $\dot{L} < 0$ for all time t. However, the condition $\dot{L} < 0$ is a conservative one. The criterion to be used in the following is to compensate (or reduce) $\dot{L}$ at every time instant as much as possible, realizing that the original structure without compensation (or control) is stable.

One possible controller is obtained by minimizing $\dot{L}$ in Eq. (10); with the result

$$\xi_i(t) = \begin{cases} \xi_{i\min}; & \text{if } \lambda_i z_{n+k,i} > 0 \\ \xi_{i\max}; & \text{if } \lambda_i z_{n+k,i} < 0 \end{cases} \tag{12}$$

The controller in Eq. (12) was first proposed in (Yang, Li, Wu and Young 1993b). This is a two-state variable damper in which the damping switches back and forth between the maximum and minimum values. This type of damper is the simplest to design and it is most reliable. Another possible controller is the classical sliding mode controller, in the sense that $\dot{L}$ is compensated up to the gain margin $\delta_i > 0$, i.e., $\dot{L} = -\Sigma|\lambda_i z_{n+k,i}|\delta_i$,

$$\xi_i^*(t) = \begin{cases} (G_i / z_{n+k,i}) - \delta_i & ; \quad \text{if } \lambda_i z_{n+k,i} > 0 \\ (G_i / z_{n+k,i}) + \delta_i & ; \quad \text{if } \lambda_i z_{n+k,i} < 0 \end{cases} \tag{13}$$

Since the capacity of variable dampers is limited, the final controller is obtained as

$$\xi_i(t) = \begin{cases} \xi_{imax} & ; \quad \text{if } \xi_i^* \geq \xi_{imax} \\ \xi_i^*(t) & ; \quad \text{if } \xi_{imin} < \xi_i^*(t) < \xi_{imax} \\ \xi_{imin} & ; \quad \text{if } \xi_i^* \leq \xi_{imin} \end{cases} \tag{14}$$

In Eq. (13), overflow may occur for $(G_i / z_{n+k,i})$ if $z_{n+k,i}$ is very small. This situation can be circumvented by setting $\xi^*_i(t) = \xi^*_{max} \text{sign}(G_i z_{n+k,i})$, for $|z_{n+k,i}| < \epsilon$ with ξ^*_{max} and ϵ being a large positive number and a small positive number, respectively. For the two-state controller in Eq. (13), $\dot{L}$ is always compensated (or reduced) up to the capacity of the variable dampers; however, it does not provide design parameters to be adjusted for the performance. The following controller that possesses the desirable properties is presented. Let $\xi_i(t) \in [\, 0, \Delta\xi_i = \xi_{imax} - \xi_{imin} \,]$ be a new control variable that varies from 0 to $\Delta\xi_i$, i.e., $\bar{\xi}_i(t) = \xi_i - \xi_{imin}$ or $\xi_i = \xi_{imin} + \bar{\xi}_i(t)$. Then, Eq.(10) becomes

$$\dot{L} = \sum_{i=1}^{r} \lambda_i z_{n+k,i} \, [\bar{\xi}_i(t) - \bar{G}_i] \quad ; \quad \bar{G}_i = (G_i / z_{n+k,i}) - \xi_{imin} \tag{15}$$

Hence, the following controller, $\xi^*_i(t)$, will satisfy the condition $\dot{L} < 0$

$$\xi_i^*(t) = \begin{cases} \bar{G}_i - \delta_i & ; \text{ if } \lambda_i z_{n+k,i} > 0 \;,\; \bar{G}_i < 0 \\ \bar{G}_i + \delta_i & ; \text{ if } \lambda_i z_{n+k,i} < 0 \;,\; \bar{G}_i > 0 \\ \Delta_i & ; \text{ if } \lambda_i z_{n+k,i} < 0 \;,\; \bar{G}_i < 0 \\ 0 & ; \text{ if } \lambda_i z_{n+k,i} > 0 \;,\; \bar{G}_i > 0 \end{cases} \tag{16}$$

in which $0 \leq \Delta_i \leq \Delta\xi_i$ is a design parameter for i=1,2,...,r. Finally, due to the capacity limitations of variable dampers, the controller is obtained as

$$\bar{\xi}_i(t) = \begin{cases} \Delta\xi_i & ; \quad \text{if } \xi_i^*(t) \geq \Delta\xi_i \\ \xi_i^*(t) & ; \quad \text{if } 0 < \xi_i^*(t) < \Delta\xi_i \\ 0 & ; \quad \text{if } \xi_i^*(t) \leq 0 \end{cases} \tag{17}$$

Similar to the controller in Eq. (13), if $|z_{n+k,i}| < \epsilon$, $\bar{G}_i = \xi^*_{max} \text{sign}(G_i z_{n+k,i})$ should be used in Eq. (15) for numerical computations. As observed from Eqs. (16) and (17), the action of variable dampers is always compensating $\dot{L}$ within its capacity, but the extent of compensation is not as strong as the two-state damper in Eq. (12).

Direct Output Feedback

The controllers presented above require a full-state feedback either through measurements or an observer. A control method using the direct output feedback is presented in the following.

Let $\bar{Z}_m$ be a 2n-dimensional observation (output) vector consisting of m measured (output) state variables and zero elements for those state variables that are not measured. In other words, $\bar{Z}_m$ is obtained from Z by setting zeros for those variables that are not measured. Then, the sliding surface can be expressed as

$$S = \bar{H}\bar{Z}_m = 0 \tag{18}$$

and the controller can be designed based on $\bar{Z}_m$ rather than the state vector Z. The design of the sliding surface $\bar{H}$ using the method of pole assignment has been described in (Yang, Li, Wu and Young, 1993b). In a similar manner, three controllers given by Eqs. (12) to (14) and (16) to (17) can be used except that Z and P should be replaced by $\bar{Z}_m$ and H, respectively. It is mentioned that for the method of the direct output feedback, collocated velocity sensors are needed, see (Yang, Li, Wu and Young, 1993b).

Hybrid System Using Rubber Bearings and Actuators

Controllers presented above are for the hybrid system consisting of rubber bearings and variable dampers. For the hybrid system consisting of rubber bearings and actuators, the state equation is given by Eq. (5) with $u_i(t)$ being the control force from the ith actuator (or controller). The design of the sliding surface has been described previously. The design of controllers is presented as follows. Using the state equation given by Eq. (5), the derivative of the Lyapunov function given by Eq. (9) becomes

$$\dot{L} = \sum_{i=1}^{r} \lambda_i (u_i - G_i) \tag{19}$$

For $\dot{L} < 0$, two possible controllers are given in the following [Yang, Li & Wu 1994]

$$u_i(t) = \begin{cases} G_i - \delta_i H(\bar{J} - J_0) & ; \ \text{if } \lambda_i > 0 \\ G_i + \delta_i H(\bar{J} - J_0) & ; \ \text{if } \lambda_i < 0 \end{cases} \tag{20}$$

and

$$u_i(t) = \begin{cases} G_i - \delta_i H(\bar{J} - J_0) & ; \ \text{if } \lambda_i > 0 \ , \ G_i < 0 \\ G_i + \delta_i H(\bar{J} - J_0) & ; \ \text{if } \lambda_i < 0 \ , \ G_i > 0 \\ 0 & ; \ \text{otherwise} \end{cases} \tag{21}$$

in which $\delta_i > 0$ is the gain margin and $H(\bar{J}-J_0)$ is a unit step function, i.e., $H(\bar{J}-J_0)=0$ for $\bar{J} < J_0$ and $H(\bar{J}-J_0)=1$ for $\bar{J} \geq J_0$. In Eq. (20), $\bar{J}=\bar{J}(t)=Z'Q^*Z$ is a measure of the system response with Q^* being a positive semi-definite matrix and J_0 is a specified small value. $H(\bar{J}-J_0)$ is introduced in Eqs. (20) and (21) to turn off the control force when the system response is reduced to a satisfactory level.

A saturated controller, denoted by $u_i^*(t)$, is obtained from Eq. (21) by imposing a maximum control force $\bar{u}_{imax}$, i.e.,

$$u_i^*(t) = \begin{cases} u_i(t) & ; \ \text{if } |u_i(t)| \leq \bar{u}_{imax} \\ \bar{u}_{imax} sgn[u_i(t)] & ; \ \text{if } |u_i(t)| > \bar{u}_{imax} \end{cases} \tag{22}$$

where $\bar{u}_{imax}$ can be considered a design parameter. Finally, the method of direct output feedback described in the previous section for variable dampers holds for the present case in which actuators are used.

CONTROL OF SLIDING-ISOLATED BRIDGES

Instead of rubber-bearing isolators and variable dampers, frictional-type sliding-bearing isolators and actuators can be installed between the piers and the deck. In this case, the equation of motion of the bridge deck is given by

$$m_1 \ddot{x}_{1a} + f(t) = u(t) \tag{23}$$

in which x_{1a} is the absolute displacement of the bridge deck, and u(t) is the control force from the actuator. In Eq. (23), f(t) is the frictional force from the sliding bearings modeled by [Yang et al 1992]

$$f(t) = \mu m_1 g \nu_1(t) \tag{24}$$

where $m_1 g = w_1$ is the weight of the bridge deck, μ is the coefficient of friction and $\nu_1(t)$ is the hysteretic component given by

$$\dot{\nu}_1(t) = D_y^{-1} \left\{ a\dot{x}_1 - \beta |\dot{x}_1| |\nu_1|^{n_1 - 1} \nu_1 - \gamma \dot{x}_1 |\nu_1|^{n_1} \right\} \tag{25}$$

In Eq. (25), D_y is the yield deformation and a, β, γ and n_1 are parameters defining the characteristics of the hysteresis loop. The coefficient of friction, μ, in the sliding isolation system may be velocity-dependent. An approximate expression for the frictional coefficient in the sliding bearings using Teflon/stainless steel was obtained experimentally as [Reinhorn et al 1993]

$$\mu = \mu_m - \mu_f e^{-a_\mu |\dot{x}_1|} \tag{26}$$

where μ_m is the coefficient of friction at a large velocity, μ_f is the difference between μ_m and the coefficient of friction at a small velocity, and a_μ is a constant that depends on the surface condition of the sliding bearings.

Combining the equations of motion for the pier and the equation of motion for the bridge deck, Eq. (23), one obtains the state equation of motion of the entire bridge

$$\dot{Z}(t) = AZ(t) - Bf(t) + Bu(t) + E(t) \tag{27}$$

in which the first element, x_{1a}, of Z is the absolute displacement of the bridge deck rather than the relative displacement x_1, i.e., $Z = [x_{1a}, x_2, \ldots, x_n, \dot{x}_{1a}, \dot{x}_2, \ldots, \dot{x}_n]'$. In Eq.(27), A and B are suitable (2nx2n) matrix and 2n vector, respectively. The base shear force of the pier is essentially contributed by the acceleration of the heavy bridge deck (or girder). Hence, to protect the safety of the piers, it is important to reduce the acceleration of the bridge deck. Since the technique of sliding mode control is to reduce the state variables, the absolute displacement and velocity of the deck, x_{1a} and $\dot{x}_{1a}$, are used as the state variables instead of the drift and velocity, x_1 and $\dot{x}_1$.

Since the coefficient vector for f(t) and u(t) is identical, i.e., B, the design of the sliding surface, Eq. (6), can be made in an identical manner as described previously. The controllers can

be established using the same Lyapunov function given by Eq. (8). The resulting derivative of the Lyapunov function is given by

$$\dot{L} = \lambda(u - G) \tag{28}$$

in which λ and G are scalars defined by

$$\lambda = S(PB) \; ; \; G = -(PB)^{-1}P(AZ - Bf + E) \tag{29}$$

one possible controller is given by

$$u = \begin{cases} G - \delta H(\bar{J} - J_0) \; ; \; \text{if } \lambda > 0 \\ G + \delta H(\bar{J} - J_0) \; ; \; \text{if } \lambda < 0 \end{cases} \tag{30}$$

in which $\delta > 0$ is the gain margin.

Direct Output Feedback

For the method of direct output feedback with the measurement of x_{1a} and $\dot{x}_{1a}$, the sliding surface is expressed as

$$S = p_1 x_{1a} + \dot{x}_{1a} = 0 \tag{31}$$

in which $p_1 > 0$ is a positive number to guarantee the stability of the motion on the sliding surface. It follows from Eq. (27) and (30) that the controller becomes

$$u(t) = \begin{cases} -m_1 p_1 \dot{x}_{1a} + f(t) - \delta H(\bar{J} - J_0) \; ; \; \text{if } S > 0 \\ -m_1 p_1 \dot{x}_{1a} + f(t) + \delta H(\bar{J} - J_0) \; ; \; \text{if } S < 0 \end{cases} \tag{32}$$

SIMULATION RESULTS

Bridges Equipped With Rubber-Bearing Isolators

Simulation studies will be carried out for the bridge model considered in (Kawashima et al, 1992), see Fig. 1(a). Rubber bearings and variable dampers are installed between the girder and piers. The elastic stiffness of rubber bearings is designed such that the fundamental period of the entire bridge is one second. The bridge is modeled as a 9 degree-of-freedom system, as shown in Fig. 1(b). Due to the symmetry, it can be further reduced to a 4 degree-of-freedom system, as shown in Fig. 1(c). The mass of each nodal point is m_i=12.3, 0.408, 0.816 and 0.816 metric tons. The damping and stiffness matrices are given in (Kawashima et al, 1992). For the bridge without variable dampers, the damping ratio for the fundamental mode is 2%. A simulated earthquake ground acceleration shown in Fig. 2 is used as the input excitation. This input excitation was simulated such that the response spectra matched the target spectra specified in the Japanese design specifications for highway bridges (Kawashima et al, 1992). The maximum and minimum damping coefficients of variable dampers are, respectively, ξ_{imax}=532.35 tonf-s/m and ξ_{imin}=88.72 tonf-s/m. Within 50 seconds of the earthquake episode, the maximum response quantities for

relative deformations between nodal points x_1, x_2, x_3, and x_4 are shown in column 2 of Table 1, when variable dampers are not installed. Also shown in Table 1 as $\ddot{x}_{1a}$ and V_b are the maximum acceleration (absolute) of the bridge deck and the maximum base shear force of the pier, respectively.

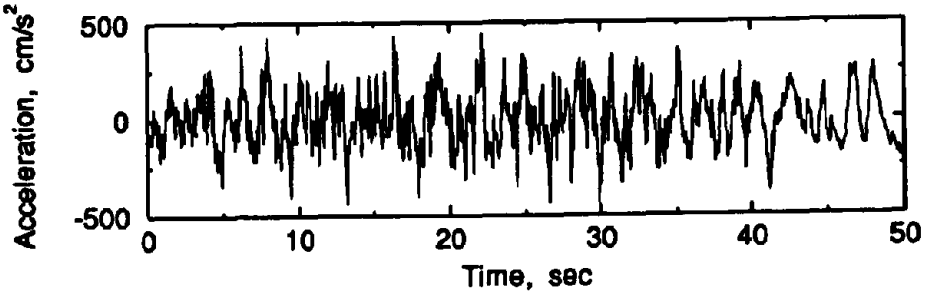

Fig.2 : Simulated Earthquake Ground Acceleration

Kawashima et al (1992) proposed a control law based on the response of rubber bearings, x_1, as follows. In the range of small displacement resulting from traffic loadings, the girder displacement should be reduced as much as possible. Hence ξ_i reduces linearly from $\xi_i=\xi_{imax}$ at $x_1=0$ to $\xi_i=\xi_{imin}$ at $x_1=1.06$cm. In the range of large response under strong earthquakes, a large damping coefficient is needed to prevent failures. Therefore, ξ_i increases linearly from $\xi_i=\xi_{imin}$ at $x_1=4.23$cm to $\xi_i=\xi_{imax}$ at $x_1=6.34$cm and $\xi_i=\xi_{imax}$ for $x_1 > 6.34$cm. In the response range of $1.06\text{cm} \le x_1 \le 4.23\text{cm}$, the energy dissipation is more beneficial and hence $\xi_i=\xi_{imin}$. The results for the maximum response quantities based on Kawashima's control law are shown in column (3) of Table 1. Using variable dampers and the direct output feedback, in which only the drift and velocity of rubber bearings, $x_1(t)$ and $\dot{x}_1(t)$, are measured, the sliding surface becomes

$$S = p_1 x_1 + \dot{x}_1 = 0 \tag{33}$$

Table 1 : Maximum Response Quantities of Bridge With Rubber-Bearing Isolators

Response (1)	RB (2)	Kawa-shima (3)	RB& OPD (4)	RB& TSD (5)	RB &VD (6)	RB &VD (7)	RB & ACT (FS) (8)	RB & ACT (OF) (9)	FB 40% (10)	FB & ACT (OF) (11)
x_1, cm	24.7	5.99	7.03	2.58	5.11	4.99	5.53	5.85	31.4	8.41
x_2, cm	3.96	1.68	1.44	1.99	1.59	1.47	1.46	1.93	1.62	0.21
x_3, cm	3.07	1.32	1.12	1.55	1.23	1.15	1.13	1.50	1.29	0.17
x_4, cm	1.25	0.55	0.46	0.63	0.50	0.47	0.46	0.62	0.54	0.07
$\ddot{x}_{1a}$, gal	1287	564	471	638	510	478	473	628	394	15
V_b, tonf	168	96	62	87	69	67	63	97	80	14
U, %w_1	-	-	-	-	-	-	40%	33%	-	53%

Instead of using the method of pole assignment, we can easily assign the p_1 value directly. For the sliding surface to be stable, p_1 should be greater than zero. With the two-state damper in Eq. (12) and $p_1=0.1$, the maximum response quantities are presented in column (5) of Table 1. A general trend observed is that the maximum response quantities are not sensitive to p_1. Using the controller given by Eqs. (13) and (14), referred to as the Type I controller, for the direct output feedback with the sliding surface given by Eq. (33), the corresponding maximum response quantities for $p_1=0.1$ and $\delta_1=250$ tonf-s/m are shown in column (6) of Table 1. We next consider the controller given by Eqs. (16) and (17), referred to as the Type II controller, for the direct output feedback with the sliding surface given by Eq. (33). The results for maximum response quantities are presented in column (7) of Table 1 for $p_1=0.1$, $\delta_1=250$ tonf-s/m, $\Delta_1=100$ tonf-s/m. It is observed from Table 1 that both Type I and Type II controllers perform very well. Further, the control designs presented above are robust with respect to system parametric uncertainties as evidenced by numerical simulation results. Due to space limitation, these results are not presented herein.

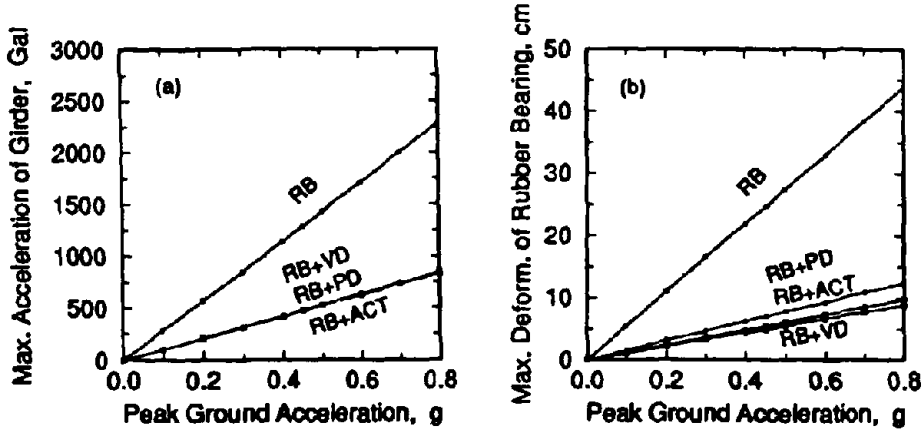

Fig.3 : Maximum Response Quantities of Bridge Equipped with Passive and Hybrid Systems; (a) Acceleration of Girder, (b) Deformation of Rubber Bearing, and (c) Base shear Force of Pier

Finally, let us consider the use of passive viscous dampers instead of variable dampers. The optimal damping coefficient for passive dampers is obtained by numerical simulations; with the result, $\xi=100$ tonf-s/m. With such optimal passive viscous dampers, the maximum response quantities of the bridge structure are shown in column (4) of Table 1. It is observed that the optimal passive dampers are quite effective in comparison with variable dampers except that the maximum drift of rubber bearings, x_1, is larger. However, the results shown in Table 1 are the indication of energy

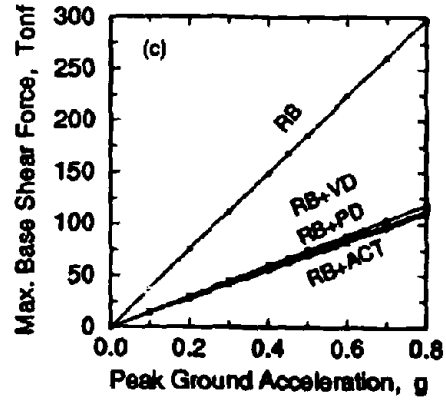

Fig. 3(c) : Max. Base Shear Force of Pier

Table 2 : Maximum Response Quantities of Bridge With Passive Sliding-Bearing Isolators

Response	Frictional Coefficient						
	10%	20%	30%	40%	60%	70%	100%
x_1, cm	75.7	30.8	34.6	31.4	16.8	19.0	12.4
x_2, cm	0.57	0.93	1.31	1.64	2.19	2.51	3.51
x_3, cm	0.46	0.74	1.04	1.29	1.71	1.96	2.75
x_4, cm	0.19	0.31	0.43	0.54	0.70	0.81	1.14
$\ddot{x}_{1a}$, gal	100	198	296	394	590	688	980
V_b , tonf	34.0	49.7	66.5	80.2	105	120	166

dissipation capacity only. These results do not reflect the flexibility that variable dampers possess. For instance, under traffic loadings (not earthquakes) passive dampers can not effectively reduce the motion of the bridge deck, because of small damping coefficient. It should be mentioned that the damping coefficient can be assigned to be ξ_{imax} for all variable dampers when $x_1 \leq 1.06$cm. In other words, the condition $\xi_i = \xi_{imax}$ for $x_1 \leq 1.06$cm can be incorporated in all the controllers presented previously to effectively reduce the motion of the bridge deck due to traffic loads.

Another hybrid system is to attach actuators to rubber-bearing isolators instead of variable dampers. In principle, actuators are capable of producing damping, stiffness and inertial forces. Hence, this type of hybrid system is investigated herein. The full-state-feedback controller given by Eq.(21) is used where the weighting matrix Q, Eq.(7), is considered a diagonal matrix with diagonal elements Q_{ii}=[30, 600, 600, 600, 1, 1, 1, 1] and $Q^*=0$, $\delta_1=0.01$ tonf. The maximum response quantities are presented in column (8) of Table 1, where the maximum required control force U is expressed in terms of the weight of bridge deck $w_1=m_1g$. We next use the controller given by Eqs. (21) and (22) and the direct output feedback with the sliding surface given by Eq.(33). For $\ddot{u}_{1max}=33\%\ w_1$, $\delta_1=0.2$ tonf and $p_1=10^5$, the maximum response quantities are presented in column (9) of Table 1. As observed from Table 1, the actuators are as effective as variable dampers.

To evaluate and compare the effectiveness of aseismic hybrid protective systems over a wide range of earthquake intensities, the design earthquake shown in Fig. 2 is scaled uniformly to different peak ground accelerations (PGA) to be used as the input excitations. The maximum response quantities for the deformation of rubber bearings, the acceleration of bridge deck (girder), and the base shear force of the pier are presented as functions of the input peak ground acceleration in Fig. 3. In Fig. 3, the curve denoted by "RB" represents the results using the passive rubber-bearing isolators alone. The curves indicated by "RB+PD", "RB+VD", and "RB+ACT", correspond to the results for hybrid systems using, respectively, optimal passive dampers, variable dampers and actuators. The control laws used for variable dampers and actuators are identical to the cases shown in columns (7) and (8), respectively, of Table 1. It is observed from Fig. 3 that

the performances of hybrid protective systems using optimal passive viscous dampers, variable dampers or actuators are almost the same. The disadvantage of using optimal passive dampers for traffic loads was described previously.

Bridges Equipped With Sliding-Bearing Isolators

Instead of rubber-bearing isolators, the frictional-type sliding-bearing isolators are considered for the same bridge structure. The frictional coefficient μ of the bearing is given by Eq. (26) in which μ_f=0.05 and a_μ=0.9 s/cm. With passive sliding isolators and the earthquake excitation given by Fig. 2, the maximum response quantities of the bridge are shown in Table 2 for different coefficients of friction, μ_m, at large velocity. As the frictional coefficient increases, the sliding displacement, x_1, reduces and the bridge response quantities increase as shown in Table 2. A comparison between Tables 1 and 2 indicates that the passive sliding-bearing isolators are more effective than the passive rubber-bearing isolators for the given excitation, Fig. 2.

The design earthquake in Fig. 2 is scaled to different levels of peak ground acceleration (PGA) and then used as the input excitations. The maximum acceleration of the girder and the maximum base shear force of the pier are presented in Fig. 4 as functions of the input peak ground acceleration (PGA) for different frictional coefficient μ_m. In Fig. 4, each curve is indicated by a frictional coefficient μ_m. As observed from Fig. 4(a), the maximum acceleration of the bridge girder is limited by a maximum value $\mu_m g$ regardless of the magnitude of the input PGA. This is due to the fact that the maximum force that can be transmitted from the pier to the girder is $m_1\mu_m g$. Hence the maximum girder acceleration is $\mu_m g$ regardless of the magnitude of the earthquake excitation. This upper bound limit for the girder acceleration is the most significant advantage of the sliding isolators over the rubber-bearing isolators, in particular, when the design earthquake is severe. A comparison between Fig. 4 and Fig. 3 indicates that the passive sliding-bearing isolators are more effective than the passive rubber-bearing isolators under strong earthquakes. The performance of the passive sliding-bearing isolators under strong earthquakes is quite remarkable

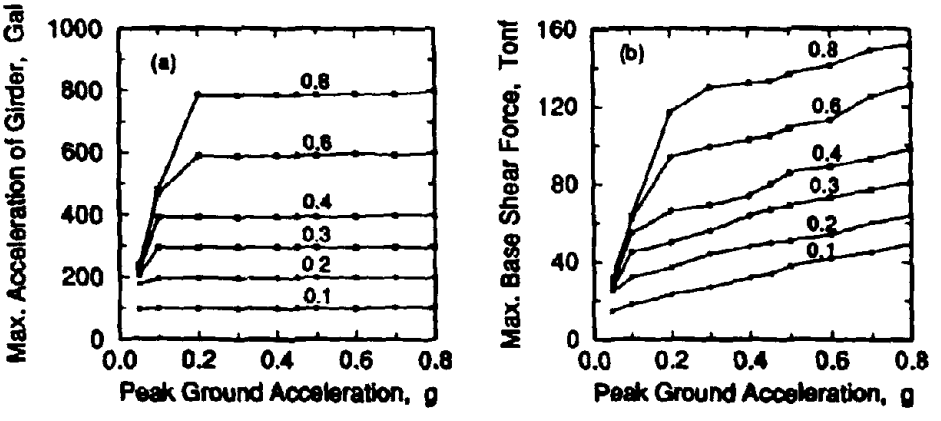

Fig.4 : Maximum Response Quantities of Bridge Equipped with Passive Sliding Bearings with Different Frictional Coefficients (Japanese Earthquake); (a) Acceleration of Girder, and (b) Base Shear Force of Pier

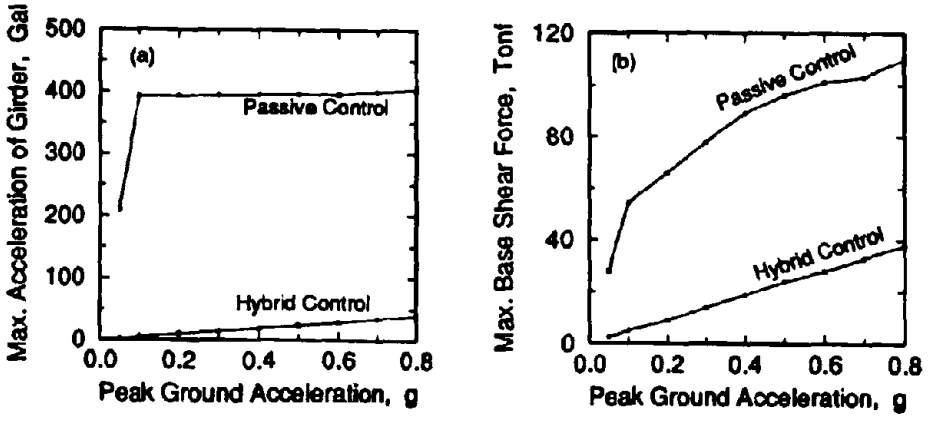

Fig.5 : Comparison for Maximum Response Quantities of Bridge Equipped with Passive Sliding Bearings with μ_m=40% and Hybrid Protective System;
(a) Acceleration of Girders, and (b) Base Shear Force of Pier

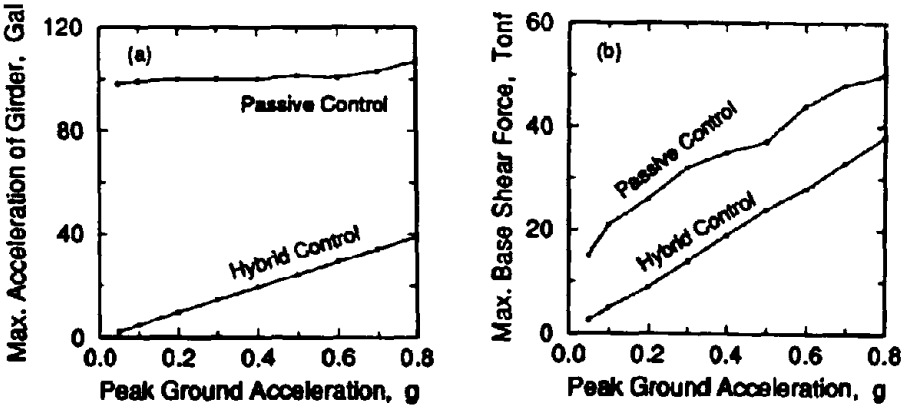

Fig.6 : Comparison for Maximum Response Quantities of Bridge Equipped with Passive Sliding Bearings with μ_m=10% and Hybrid Protective System;
(a) Acceleration of Girders, and (b) Base Shear Force of Pier

even for the coefficient of friction as high as 40%. Of course, for the PGA greater than 0.5g, the stiffness of rubber-bearing isolators should be redesigned to achieve a better performance. Likewise, variable dampers or actuators can be used to improve the effectiveness of the rubber-bearing isolators as shown in Fig. 3.

The effectiveness of the passive sliding isolators can further be improved by attaching actuators to them. For this type of hybrid protective system, a direct output feedback controller has been presented in Eq. (32). With the El Centro earthquake scaled to a PGA of 0.45g and the coefficient of friction μ_m=40% for the sliding bearings, the maximum response quantities of the bridge and the maximum required control force are presented in column (11) of Table 1. In this

case, $p_1 = 1.0$ and $\delta = 0.01$ tonf are used, Eq. (32). The corresponding maximum response quantities using only the passive sliding isolators are shown in column (10) of Table 1. A comparison between columns (10) and (11) of Table 1 indicates that the performance of the direct output feedback controller is remarkable. Next we scale the El Centro earthquake to different peak ground accelerations for the input excitations. The maximum girder acceleration and maximum base shear force of the pier for $\mu_m = 40\%$ are presented in Fig. 5. Figure 5 includes the results using the passive sliding isolators alone and using the hybrid protective systems (sliding bearings and actuators). The corresponding results for $\mu_m = 0.1$ are presented in Fig. 6. The results presented in Figs. 5 and 6 clearly demonstrate that the hybrid protective system is very effective.

CONCLUSION

Based on the theory of variable structure system (VSS) or sliding mode control (SMC), control methods are presented for applications to aseismic hybrid protective systems for bridge structures. Simulation results indicate that the performance of the control techniques presented is quite remarkable. The control methods are applicable to inelastic rubber-bearing isolators, although the results are not presented due to space limitations.

The effectiveness of hybrid protective systems and passive sliding isolators for reducing the seismic response of bridge structures has been evaluated by numerical simulations for a wide range of earthquake intensities. The following observations are obtained from numerical simulation results.

(a) The passive sliding-bearing isolators are more effective in reducing the bridge response than the passive rubber-bearing isolators for the peak ground acceleration exceeding 0.2g. This is because for sliding-bearing isolators, there is an upper bound limit , $\mu_m g$, for the acceleration of the bridge deck, where μ_m is the frictional coefficient of the bearings. Since the base shear force of the pier is mainly contributed by the acceleration of the bridge deck, the upper bound limit for the deck acceleration reduces significantly the bridge response under strong earthquakes.

(b) The effectiveness of the passive sliding isolation system for reducing the bridge response can be improved significantly by installing actuators. The performance of such a hybrid system is demonstrated to be excellent.

(c) Hybrid systems using rubber bearings and variable dampers or actuators are also demonstrated to be very effective in reducing the response of seismic-excited bridges.

ACKNOWLEDGMENT

This research is partially supported by the National Science Foundation Grant No. NSF-BCS-91-20128 and National Center for Earthquake Engineering Research NCEER-92-5001D

REFERENCES

1. Feng, Q., Fujii, S. and Shinozuka, M. (1990), "Use of a variable damper for hybrid control of bridge response under earthquake", Proc. U.S. National Workshop on Structural Control, USC, CA, 107-111.

2. Kawashima, K. et al (1991), "Current research efforts in Japan for passive and active control of highway bridges against earthquakes", 23rd Joint Meeting of U.S.-Japan Panel on Wind and Seismic Effects, U.J.N.R., Tsukuba, Japan.

3. Kawashima, K. et al (1992), "Effectiveness of the variable damper for reducing seismic response of highway bridges against earthquakes", Proc. 2nd US-Japan Workshop on Earthquake Protective System for Bridges, J-20, PWRI, Tsukuba, Japan.

4. Nagarajaiah, S., Riley, M.A. and Reinhorn, A.M. (1992a), "Control of sliding isolated bridges with absolute acceleration feedback", J. of Engr. Mech., ASCE, 119, (10).

5. Reinhorn, A.M., Nagarajaiah, S., Subramanian, R. and Riley, M. (1993), "Study of hybrid systems for structural and nonstructural systems", Proc. Int'l. Workshop on Structural Control and Intelligent Systems, Honolulu, HI (in press).

7. Soong, T.T. (1990), Active structural control: theory and application, New York: Longman Scientific and Technical, New York.

8. Utkin, V.I. (1992), Sliding modes in control optimization, Springer-Verlag, Berlin.

9. Yang, J.N., Li, Z. and Liu, S.C.(1992), "Stable controllers for instantaneous optimal control algorithm", Journal of Engineering Mechanics, ASCE, Vol.118, No. 8, pp. 1612-1630.

10. Yang, J.N., Li, Z. and Vongchavalitkul, S. (1993a), "Hybrid control of seismic-excited bridge structures using variable dampers", Structural Engineering in Natural Hazards Mitigation, 1, ASCE Structures Congress '93, 778-783.

11. Yang, J.N., Li, Z. and Wu, J.C. and Young (1993b), "A discontinuous control method for civil engineering structures", Proc. 9th VPI&SU Symposium on Dynamics and Control of Large Structures, edited by L. Meirovitch, Blacksburg, VA (in press).

12. Yang, J.N., Li, Z. and Wu, J.C. (1993c), "Discontinuous nonlinear control of base-isolated building", Proc. Int'l. Workshop on Structural Control, Honolulu, HI (in press).

13. Yang, J.N., Li, Z. and Wu, J.C. (1994), "Discontinuous control methods for linear and nonlinear structures", to appear as NCEER Technical Report.

14. Young, K.D.(editor) (1993), Variable structure control for robotics and aerospace applications, Elsevier, New York.

CLOSED-OPEN-LOOP CONTROL OF SEISMIC RESPONSE OF STRUCTURE WITH ACTIVE MASS DRIVER SYSTEM

Kenzo TOKI
School of Civil Engineering Kyoto University, Kyoto

Tadanobu SATO
Disaster Prevention Res. Inst., Kyoto University, Uji, Kyoto

Toshihiro MOCHIZUKI
Graduate Student, Kyoto University, Kyoto

and

Masaaki YOSHIKAWA
Tsukuba Research Institute, Okumura Corporation, Tsukuba

SUMMARY

In order to realize a practical control device of active mass driver (AMD) type for high-rise buildings, we developed a closed-open-loop optimal control algorithm that is derived by minimizing the sum of the quadratic time-dependent performance index and the seismic energy input to the structural system.

This new control law provides feasible control algorithms that can easily be implemented in AMD system and applied to earthquake-excited structures. This optimal algorithm is simple and reliable for on-line control operations because the control force does not depends on the rigidity of structural system.

We investigated the effects of two weighting matrices and a parameter expressing the amount of input seismic energy to structure in terms of the control efficiency. This new algorithm was applied to a model eight-story building to demonstrate the reduction of vibrations caused by medium earthquake ground motion.

INTRODUCTION

The problem of earthquake-induced vibration of tall buildings and long-span bridges is of prime concern to structural engineers. Control of such large and flexible structures by making use of active control forces is a recent area of research in civil engineering. All active control algorithms aim to find a feedback control law [1]. Classical active control algorithms of structures were applications of optimal regulator theories.

Every regulator problem is converted into a feedback algorithm optimized with respect to a quadratic performance index that includes product terms between the state and control values [2]. The feedback, therefore, does not include the non-homogeneous term that is a result of the earthquake excitation. Furthermore, the performance index is given by the integration of quadratic evaluation functions over the time interval from 0 to ∞. In this case, the duration de-

fined is longer than that of the earthquake and ,consequently, the entire history of the input excitation must be known in advance in order to calculate the state and control values.

Linear control laws are derived for open-loop and open-closed loop control schemes; but, the closed-loop control algorithms are widely used for earthquake-excited structures. This is the special case in which the control force is regulated by the response state vector and the Riccati matrix. It has been pointed out that because external excitation is ignored in the derivation of the Riccati equation, the closed-loop control law is not truly optimal. If the excitation term is included in the Riccati equation, its solution requires a priori knowledge of the loading history. This generally is not possible for excitations such as earthquakes. To overcome this difficulty several control algorithms have been proposed; the pole assignment method [3], the instantaneous optimal control [4], and the pulse control [5].

We proposed a new instantaneous closed-open-loop control which takes into account the input energy due to earthquake ground motion to the structure [6]. A time-dependent performance index similar to that defined in [4] was used to obtain the control vector. The instantaneous optimal control algorithms proposed in [4] were classified as open-loop, closed-loop and open-closed-loop controls; but, the control efficiencies were identical because the same performance index was minimized. This was referred to as Yang's optimal control algorithm. We defined a new objective function of which minimization results in different efficiencies for the three control algorithms [6].

We here examine the efficiency of proposed algorithm and give theoretical back ground for the feedforward term in the control algorithm. In our previous work [6], we assumed active tendon controllers which installed in every story unit. Because the realization of this type of control device is not feasible at present, in the present study, we here apply the developed closed-open-loop control algorithm to a model structure of 8-story frame with a control device of active mass driver type composed of AC servo motor and ball screw driver.

CONTROL ALGORITHM CONSIDERING INPUT ENERGY TO STRUCTURE

A structure that is idealized by an n-degree of freedom system is subjected to a one-dimensional earthquake ground acceleration $\ddot{X}_0$. The matrix equation of motion is expressed by

$$M\ddot{x}(t) + C\dot{x}(t) + Kx(t) = -m\ddot{X}_0(t) + Hu(t) \tag{1}$$

in which, M, C, and K are the mass, damping and stiffness matrices, u the r-dimensional control vector, and H a $(2n \times r)$ matrix specifying the location of active controllers.

The state space description of Eq.(1) is given by

$$\dot{z}(t) = Az(t) + Bu(t) + W_1\ddot{X}_0(t) \tag{2}$$

in which

$$z = \begin{Bmatrix} X \\ \dot{X} \end{Bmatrix} \quad A = \begin{bmatrix} 0 & I \\ -M^{-1}K & -M^{-1}C \end{bmatrix} \quad B = \begin{bmatrix} 0 \\ M^{-1}H \end{bmatrix} \quad W_1 = \begin{bmatrix} 0 \\ -M^{-1}m \end{bmatrix} \tag{3}$$

The solution of Eq.(2) is

$$z(t) = e^{A\Delta t}z(t-\Delta t) + e^{At}\int_{t-\Delta t}^{t}\left\{Bu(\tau) + W_1\ddot{X}_0(\tau)\right\}e^{-A\Delta\tau}\,d\tau \tag{4}$$

in which Δt is the time interval of integration. Using a trapezoidal approximation for the integral term, $z(t)$ is rewritten

$$z(t) = D(t-\Delta t) + \frac{\Delta t}{2}\left[Bu(t) + W_1\ddot{X}_0(t)\right] \tag{5}$$

in which

$$D(t-\Delta t) = e^{A\Delta t}\left\{z(t-\Delta t) + \frac{\Delta t}{2}\left[Bu(t-\Delta t) + W_1\ddot{X}_0(t-\Delta t)\right]\right\} \tag{6}$$

The time-dependent performance index $J_N(t)$ introducing the seismic energy input to structure is defined by

$$J_N(t) = \int_{t-\Delta t}^{t}\left[z^T(\tau)Qz(\tau) + u^T(\tau)Ru(\tau) + \alpha\left\{-\dot{x}^T(\tau)m\ddot{X}_0(\tau)\right\}\right]d\tau \tag{7}$$

As the result of trapezoidal integration of Eq.(7), we obtain

$$J_N(t) = z^T(t)Q'z(t) + u^T(t)R'u(t) - \alpha z^T(t)W_2\ddot{X}_0(t) + E'_2(t-\Delta t) \tag{8}$$

in which

$$E'_2(t-\Delta t) = z^T(t-\Delta t)Q'z(t-\Delta t) + u^T(t-\Delta t)R'u(t-\Delta t) - \alpha z^T(t-\Delta t)W_2\ddot{X}_0(t-\Delta t)$$

$$Q' = \frac{\Delta t}{2}Q \qquad R' = \frac{\Delta t}{2}R \tag{9}$$

Minimizing the performance index under the constraint of Eq.(5), the optimal control force is

$$u(t) = -\frac{\Delta t}{4}R^{-1}B^T(Q^T + Q)z(t) + \frac{\alpha}{2}R^{-1}B^TW_2\ddot{X}_0(t) \tag{10}$$

This control law has the closed-open-loop formula. The feedback term, however, is not affected by structural rigidity and the feedforward term is in the same phase with input seismic motion. Note that the Yang's optimal control algorithm [4] is obtained by putting α to be *0*.

APPLICATION OF MODAL ANALYSIS

The transformation into the generalized coordinate system using the eigen-function expansions

$$\{x\} = [\Phi]\{q\} \tag{11}$$

leads to differential equations as follows:

$$\{\ddot{q}\} + [\varsigma]\{\dot{q}\} + [\Omega]\{q\} = -[\Phi]^T\{m\}\ddot{X}_0 + [\Phi]^T\{H\}u(t) \tag{12}$$

in which $\{q\}$ is the vector of the modal amplitudes, $[\Phi]$ the matrix of normalized mode shapes, $[\varsigma]$ and $[\Omega]$ diagonal matrices with components $2h_i\omega_i$ and ω_i^2.

Assuming that only a certain number of modes are to be controlled, the modal amplitudes can be partitioned into controlled mode Φ_c and non-controlled mode Φ_r as follows:

$$[\Phi] = [\Phi_c \mid \Phi_r] \tag{13}$$

The equation of motion of controlled and non-controlled modes can be written as

$$\{\ddot{q}_c\} + [\varsigma_c]\{\dot{q}_c\} + [\Omega_c]\{q_c\} = -[\Phi_c]^T\{m\}\ddot{X}_0 + [\Phi_c]^T\{H\}u \tag{14}$$

$$\{\ddot{q}_r\} + [\varsigma_r]\{\dot{q}_r\} + [\Omega_r]\{q_r\} = -[\Phi_r]^T\{m\}\ddot{X}_0 + [\Phi_r]^T\{H\}u \tag{15}$$

The control force given by Eq.(10) could be rewritten in the following form:

$$u(t) = \{F_{BD}\}\{x\} + \{F_{BV}\}\{\dot{x}\} + F_f\ddot{X}_0 \tag{16}$$

in which $\{F_{BD}\}$ and $\{F_{BV}\}$ are feedback gains for relative displacement and velocity of structure, F_f the feedforward gain for input motion. Substituting Eq.(16) into Eqs.(14) and (15), we obtain the following equations for the controlled and non-controlled modes

$$\{\ddot{q}_c\}+\left([\varsigma_c]-[\Phi_c]^T\{H\}F_{BV}[\Phi_c]\right)\{\dot{q}_c\}+\left([\Omega_c]-[\Phi_c]^T\{H\}\{F_{BD}\}[\Phi_r]\right)\{q_c\}= -\left([\Phi_c]^T\{m\}+[\Phi_c]^T\{H\}F_f\right)\ddot{X}_0 \quad (17)$$

$$\{\ddot{q}_r\}+[\varsigma_r]\{\dot{q}_r\}+[\Omega_r]\{q_r\}= -\left([\Phi_r]^T\{m\}+[\Phi_r]^T\{H\}F_f\right)\ddot{X}_0+[\Phi_r]^T\{H\}\{F_{BD}\}[\Phi_c]\{q_c\}+[\Phi_r]^T\{H\}F_{BV}[\Phi_c]\{\dot{q}_c\} \quad (18)$$

The second and third terms of right hand side of Eq.(18) express the control spillover into non-controlled modes caused by the velocity and displacement feedback.

To make clear the effect of feedforward term, we examined the case that the control force is generated by such feedforward term as

$$u=F_f\ddot{X}_0 \quad (19)$$

Substituting Eq.(19) into Eq.(12), the equation of motion for the i th mode is given by

$$\ddot{q}_i+\varsigma_i\dot{q}_i+\Omega_i q_i=-\{\phi_i\}^T\{m\}\ddot{X}_0+\{\phi_i\}^T\{H\}F_f\ddot{X}_0 \quad (20)$$

It is obvious that the feedforward term in the control force can offset the excitation term of *i th* mode if F_f is chosen as the right hand side of Eq.(20) becomes zero

$$F_{f_i}=\frac{\{\phi_i^T\}\{m\}}{\phi_i^1} \quad (21)$$

in which ϕ_i^1 is the first component of vector $\{\phi_i\}$.

Although the excitation term becomes zero for the i th mode by using feedforward gain defined in Eq.(21), it affects the excitation term of other modes and the equation of motion of k th mode yields

$$\ddot{q}_k+\varsigma_k\dot{q}_k+\Omega_k q_k=-\left(\{\phi_k^T\}\{m\}-\frac{\phi_k^1}{\phi_i^1}\{\phi_i^T\}\{m\}\right)\ddot{X}_0,(k\neq i) \quad (22)$$

The participation factor of k th mode changes from $\{\phi_k^T\}\{m\}$ to

$$\{\phi_k^T\}\{m\}-\frac{\phi_k^1}{\phi_i^1}\{\phi_i^T\}\{m\} \quad (23)$$

This term is regarded as the leaking effect of control force to the other mode when i th mode is perfectly offset.

CONTROL SIGNAL USED IN THE MASS DRIVER SYSTEM

The control force generated by a mass driver system placed on the top floor of the structure is given by

$$u=-m_d\ddot{x}_d \quad (24)$$

in which m_d is the mass of the driver and x_d the relative displacement of driving mass to the top floor. The dynamic characteristics of AC servo motor is assumed to be expressed by the first order delay element as follows:

$$Y^* = T\ddot{x}_d + \dot{x}_d \tag{25}$$

in which Y^* is the control signal of AC servo motor and T time constant.

To define the control signal of AC servo motor as a function of structural response and the input motion, $\ddot{x}_d$ is eliminated from Eq.(25) by using Eqs.(24) and (16)

$$Y^* = -\frac{T}{m_d}\left(\{F_{BD}\}\{x\} + \{F_{BV}\}\{\dot{x}\} + F_f\ddot{X}_0 - \frac{m_d}{T}\dot{x}_d\right) \tag{26}$$

The following relationship is also obtained from Eqs.(24) and (16)

$$-m_d\ddot{x}_d = \{F_{BD}\}\{x\} + \{F_{BV}\}\{\dot{x}\} + F_f\ddot{X}_0 \tag{27}$$

Assumption of $\{F_{bd}\} = \{0\}$ and integration of Eq.(25) yield

$$\dot{x}_d = -\frac{\{F_{BV}\}}{m_d}\{x\} - \frac{F_f}{m_d}\dot{X}_0 \tag{28}$$

Eliminating $\dot{x}_d$ from Eq.(26) using Eq.(28), the control signal can be written in the following form

$$\begin{aligned} Y^* &= -\frac{T}{m_d}\left\{\{F_{BV}\}\left(\dot{x} + \frac{x}{T}\right) + F_f\left(\ddot{X}_0 + \frac{\dot{X}_0}{T}\right)\right\} \\ &= -\frac{T}{m_d}\left\{\{F_{BV}\}[\Phi]\left(\dot{q} + \frac{q}{T}\right) + F_f\left(\ddot{X}_0 + \frac{\dot{X}_0}{T}\right)\right\} \end{aligned} \tag{29}$$

To generate the control signal described above requires the modal displacements and modal velocities of control modes. Those modal states can be estimated from the output of sensors at different location of the building as follows:

$$\{q_c\} = [\Phi_c]^{-1}\{x_0\}, \qquad \{\dot{q}_c\} = [\Phi_c]^{-1}\{\dot{x}_0\} \tag{30}$$

in which $\{x_0\}$ and $\{\dot{x}_0\}$ are observed displacement and velocity vectors of the structure.

APPLICATION TO A SIMPLE STRUCTURE MODEL

To demonstrate the application of the algorithm, a eight-story model building as shown in Fig.1 was used for seismic response control experiment. Active mass driver controller was installed at top floor as shown in Fig.1. The dynamic characteristics of this model structure was estimated through several shaking table tests. The frequency response curve shown in Fig.2 was obtained by the harmonic excitation test with constant amplitude of 20 $cm/\sec^2$ and sweeping frequency 0 to 15Hz. The identified natural frequency and damping ratio of each mode is given in Table 1. Calculated frequency response and phase delay curves using identified dynamic characteristics are shown by full line in Fig.3.

The model building was reduced to a shearing beam model with 8 degree of freedom and was fixed at the base which was subjected to the seismic motion as shown Fig.4. The mass of each floor and equivalent stiffness of spring given to each story are listed in Table 2. The natural

frequencies of this model are also given in Table 2. In general, since the control effect depends on the characteristics of the external excitations under the same feedback and feedforward gains, we simulated the input ground motion by a white noise modified with an envelope function as shown in Fig.5. The peak amplitude of seismic motion were normalized to 10 cm/sec^2 for the numerical and experimental analyses.

To determine appropriate weighting matrices Q and R, Q is partitioned as follows:

$$Q=\begin{bmatrix} Q_{11} & Q_{12} \\ Q_{21} & Q_{22} \end{bmatrix} \tag{31}$$

in which the order of matrices Q_{ij} is (8×8). Note that the sub-matrices Q_{11} and Q_{12} do not contribute to the active forces because the matrix B which appears in Eq.(3) contains 0 matrix. Therefore, Q_{11} and Q_{12} are designated as zero even though Q must be positive definite symmetric matrix. For simplicity, Q_{21} and Q_{22} were considered to be equal and we assigned the unit matrix multiplied by r to R.

The appropriate assignment of the elements of Q_{21} and Q_{22} to achieve maximum control efficiency have not been investigated because it requires a two stage optimization technique that is beyond the scope of the present study. For the case of AMD system installed on the top floor of a structure, the matrix B becomes a vector in which only the eighth element is non-zero element with the value $1/(m_1+m_d)$; m_1 and m_d being the mass of the top floor and of the driving mass. Therefore the number of non-zero elements to be able to define independently is eight and the following formula for matrix Q_{21} is enough for controlling the AMD system.

$$Q_{21}=q\cdot\begin{bmatrix} q_1 & q_2 & \cdots & q_8 \\ q_2 & & & \\ \vdots & & [0] & \\ q_8 & & & \end{bmatrix} \tag{32}$$

To select appropriate value of q_i we examined the control characteristics of algorithm for the following four cases of q_i distribution and found that the case 4 gives the most stable control efficiency [7].

Case	q_1	q_2, q_3	q_4, q_5	$q_6 \sim q_8$
1	1000	1000	1000	1000
2	1000	1000	1000	500
3	1000	1000	500	500
4	500	500	250	250

The feedback and feedforward gains defined in Eq.(16) are expressed for this model structure as follows:

$$\{F_{BD}\}=-\frac{\Delta t}{4r}\left(\{m^{-1}\}\{H\}\right)^T\left[Q_{12}{}^T+Q_{21}\right]$$

$$\{F_{BV}\}=-\frac{\Delta t}{4r}\left(\{m^{-1}\}\{H\}\right)^T\left[Q_{22}{}^T+Q_{22}\right] \tag{33}$$

$$F_f=\frac{\Delta t}{8}\frac{\alpha}{r}$$

The optimal value of α/r to control i th mode vibration is defined by substituting Eq.(21) into third equation of Eq.(33)

$$(\alpha/r)_i = \frac{8}{\Delta t^2}\frac{\{\phi_i^T\}\{m\}}{\phi_i^1} \tag{34}$$

The value of α/r to offset the seismic excitation term of each vibration mode is given in Table 3. The leaking effect of external force from a control mode to other modes is shown in Fig.6. The participation factor of the k th mode which is defined in Eq.(23) and normalized by the original participation factor of k th mode ($\{\phi_i^T\}\{m\}$) is usually larger than 1.0. However, as shown in the vertical axsis of the figure, the normalised participation factor of the first mode of the first mode control and that of the second mode of the second mode control are eliminated.

Fig.7 shows the time histories of relative displacement at the top floor for both cases. By examining Figs.6 and 7, one observes that the response of top floor is larger in case of the second mode control than that of the first mode control even though the leaking effect being large for the case of the first mode control. Because, for this example, the response of the first mode is predominant, the leakage of the first mode in case of the second mode control causes the larger response of structure.

When the feedforward algorithm is applied only to control the structural response, the required maximum stroke and energy of AMD usually exceeds its capacity. Combined use of feedforward and feedback algorithm may overcome this problem. Three cases are investigated using the structural model taking into account only the first and second vibration modes. In the case 1, only the first mode response is controlled by both feedback and feedforward algorithms. In the case 2, the first mode is controlled by the feedback and the second mode is controlled by the feedforward algorithm. The third case reverses the order of control algorithm.

The relationship between the consumed AMD energy and AMD stroke as well as the response of top floor is shown in Fig.8 for three cases which are expressed by symbol, ◊. For the comparison, another two cases are also included in the figure. One is the case that both modes response are controlled by feedback algorithm (with symbol Δ and the other is the case that the first mode response is controlled by only feedforward algorithm (with symbol ×). The curve with symbol, ◊, starts at the point that optimal control is achieved by the feedforward algorithm. From the stand point to keep the AMD stroke within certain limit maintaining the same control efficiency achieved by feedback algorithm, the result shown in case 3 may be used to develop practical control device because AMD stroke dose not increase even if the consumed energy by AMD increases.

The effect of spillover to the second mode is shown in Fig.9 for the case that the first mode is controlled only by the feedback algorithm. Figure (a) is the frequency transfer function of the second mode and (b) is the control force of the first mode. Comparison between the case of the first mode control and that of full mode control is shown in Fig.10. The broken line is the former case and full line the latter case. As can be seen in this figure, the spillover effect to the second mode is very large for the structure model under investigation. The time historyies of the top floor response for both cases are shown in Fig.11.

Based on the above mentioned numerical studies, shaking table tests were conducted. The configuration of instrumentation in the model structure and the schematical representation of signal processing as well as the flow of control signal are shown in Fig.12. Fig.13 shows the dynamic characteristics of AC servo motor used to generate control force. To determine the

value of α/r for the experiments, the relationship between the maximum relative displacement at the top floor and the value of α/r was calculated based on the numerical simulation as shown in Fig.14. According to the figure, the optimal value of α/r is 57. This is almost same α/r value to offset the external excitation of the first mode even though the response of top floor is superposed the effect of all vibration modes. However the actual value of α/r used for experiments is 40 because the control system sometimes becomes unstable when the value of α/r reaches to about ten percent large of its optimal value.

Fig.15 shows the comparison of the control effects due to the differences in the control algorithms. In the figure, six cases are plotted. Open circle shows the root mean square relative velocity response of each floor for the case of uncontrolled structure. There are three cases for the feedback control algorithm obtained by solving Riccatti equation. One is the case of direct use of Eqs.(1) and (10) for controlling the structure with all floor response measurements (symbol MCK). The second is the case of full modal control algorithm (open triangle). The third (closed triangle) is the case of using algorithm controlling up to the second modes with three point response measurements (8, 6 and 3 floors).

The results obtained by the proposed control algorithm are shown by lines with the open and closed squares. The values of α/r are given in the figure. From this figure, the almost same control performance can be obtained not depending on the control algorithms used. The relationship between the relative displacement of driving mass to the top floor and the structural response is shown in Fig.16.

CONCLUDING REMARKS

We have developed a new closed-open-loop active control algorithm which takes into account the input seismic energy to the structural system. Experiments have been conducted to investigated the efficiency of the proposed control algorithm using a structural model equipped with an active mass driver. The principal results and conclusions of the present paper are summarized as follows.

(1) In order to derive a closed-open-loop control algorithm, the input seismic energy to the structure was considered for defining the time-dependent performance index. The control force obtained through performance index taking into account the seismic energy input to the structure was not affected by structural rigidity and, therefore, this algorithm is simple and applicable even to the structural system with non-linearity.

(2) The effect of control parameters on the system response are expressed by two independent variables; one controls the level of feedback, the other reflects the level of input excitation. For a given structural system, we found that there were appropriate control parameters to maximize control efficiencies. In the modal control algorithm, the optimal feedforward gain to offset the excitation term was derived. The spillover effect in the developed control algorithm was also investigated.

(3) In order to examine the applicability of developed optimal control algorithm to actual structures, we developed an active mass driver system driven by AC servo motor through a ball screw. The structural model we treated here is a eight story frame model which was subjected to series of shaking table tests. The experimental studies revealed that our proposed open-closed control algorithm performs better control efficiencies than the control algorithms based on the regulator theory.

REFERENCES

[1] Soong, T.T., Active Structural Control in Civil Engineering, National Center for Earthquake Engineering Research, Technical Report NCEER-87-0023, State University of New York at Buffalo, 1987.

[2] Leipholz, J.N. (1980), Structural Control, North-Holland Publishing Company, Amsterdam, The Netherlands.

[3] Bryson, A.E. Hr and Ho, Y.C., Applied Optimal Control, John Wiley and Sons, New York, U.S.A., 1975.

[4] Yang, J.N. Akbarpour, A. and Ghaemmaghami, P., New Optimal Control Algorithms for Structural Control, Journal of Engineering Mechanics, ASCE, Vol.113, No.9, 1987, pp.1369-1386.

[5] Udwadia, F.E. and Tabaie, S., Pulse Control of Structural and Mechanical Systems, Journal of Engineering Mechanics, ASCE, Vol.107, No.6, 1981, pp.1011-1028.

[6] Sato, T. and Toki K., Active Control of Seismic Response of Structures, Journal of Intelligent Material Systems and Structures, Vol.1, No.4, 1990, pp.447-475.

[7] Toki, K and Sato T., Optimal Control of Seismic Response of Structures using Mass Damper System, Proceedings of the Workshop on China-Japan Joint Research for Earthquake Disaster Prediction and Mitigation, 1992, pp.159-169.

Table 1 Dynamic characteristics of 8 story building model obtained by experiments.

	Mode	1	2	3	4	5	6	7	8
T	Natural Frequency (Hz)	1.25	3.72	6.19	8.55	10.47	12.24	13.42	14.30
I	Natural Frequency (Hz)	1.25	3.83	6.26	8.51	10.50	12.20	—	—
	Damping Ratio (%)	0.35	0.56	0.56	0.58	0.54	0.52	—	—

T : Test Result
I : Identification of Modal Constant from Resonance Curve

Table 2 Dynamic characteristics of structure analyzed.

No.	Mass (kgf)	Stiffness(kgf/cm)
1	123.1	150.6
2	123.1	245.0
3	123.1	245.0
4	123.1	245.0
5	123.1	245.0
6	123.1	245.0
7	123.1	245.0
8	123.1	245.0

Mode No.	Eigenvalue (Hz)
1	1.26
2	3.76
3	6.15
4	8.35
5	10.29
6	11.89
7	13.08
8	13.81

Damping facter of Structure(%)
0.268

Table 3 α/r value offset the excitation term of each mode.

Mode No.	1	2	3	4	5	6	7	8
α/R	56.6	-19.5	12.6	-10.0	8.6	-7.9	7.5	-7.3

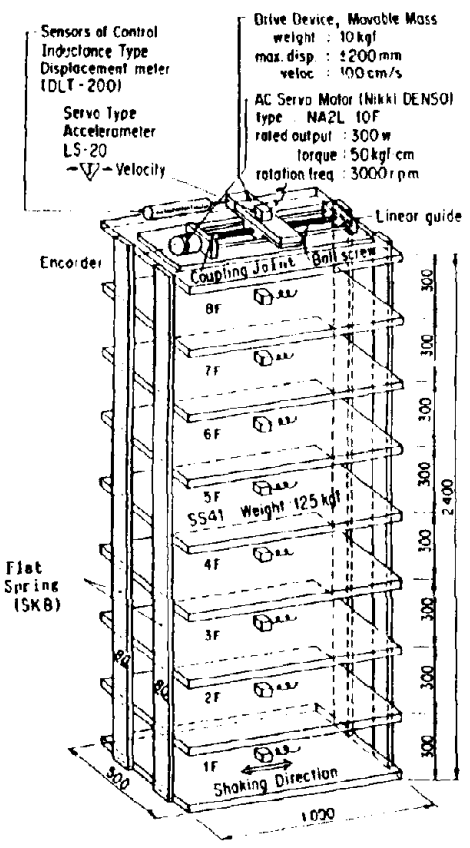

Fig. 1 Eight story building model with Active Mass Driving (AMD) system.

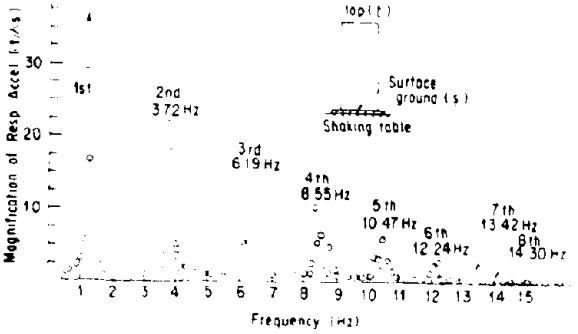

Fig. 2 Frequency response curve obtained by sweeping test with amplitude of 20 cm/sec^2.

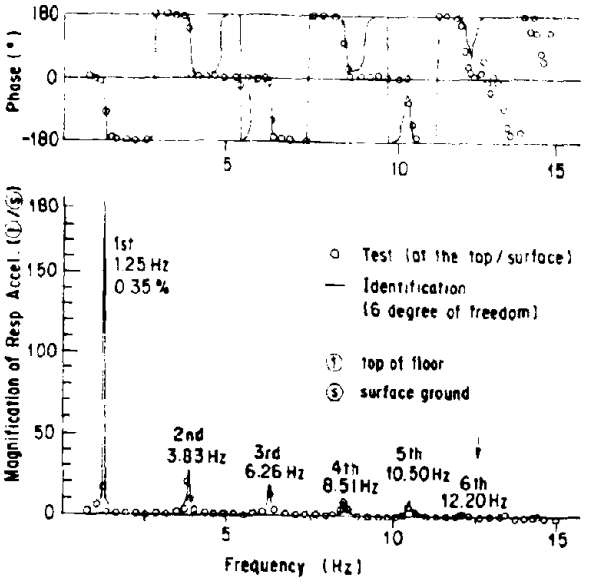

Fig. 3 Curve fitting identification.

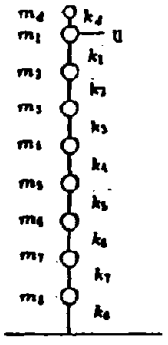

Fig. 4 Model of the structural system.

Fig. 5 Time History of simulated earthquake motion.

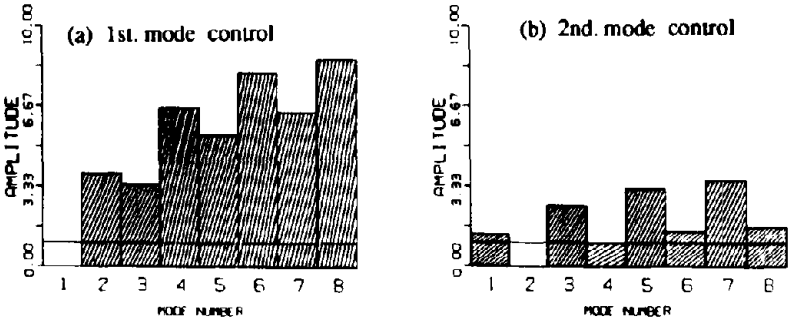

Fig. 6 Increase of participation factor of un-controlled modes.
(normalized by participation factor of each mode)

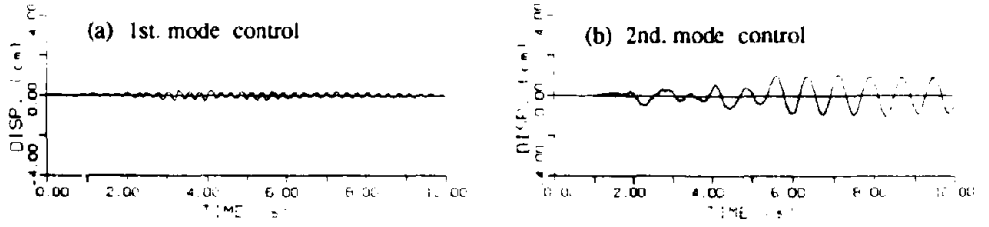

Fig. 7 Response of the top floor.

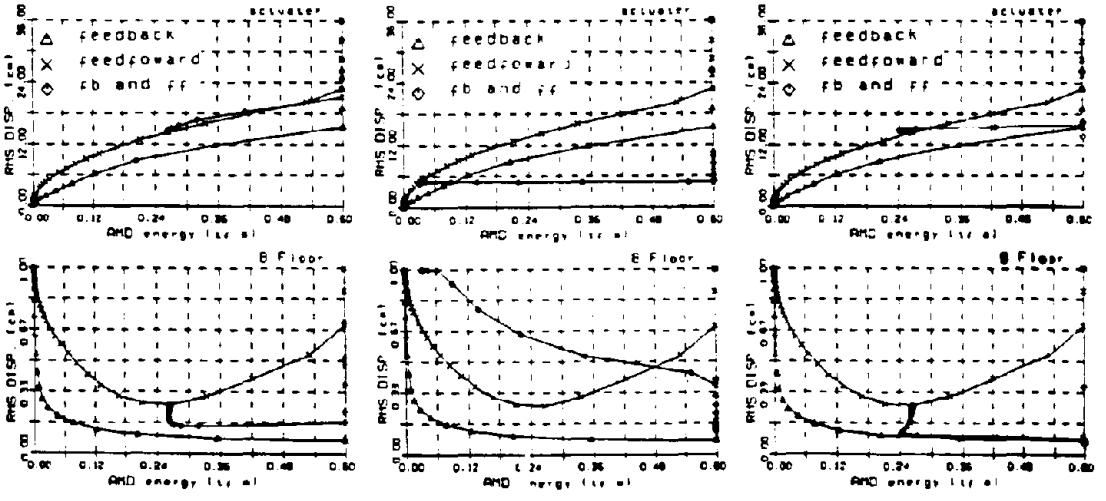

(a) CASE 1 (b) CASE 2 (c) CASE 3

Fig. 8 Relationship between energy dissipated by AMD and RMS of the relative displacement of the top floor (upper figures) and RMS of displacement of the actuator (lower figures).

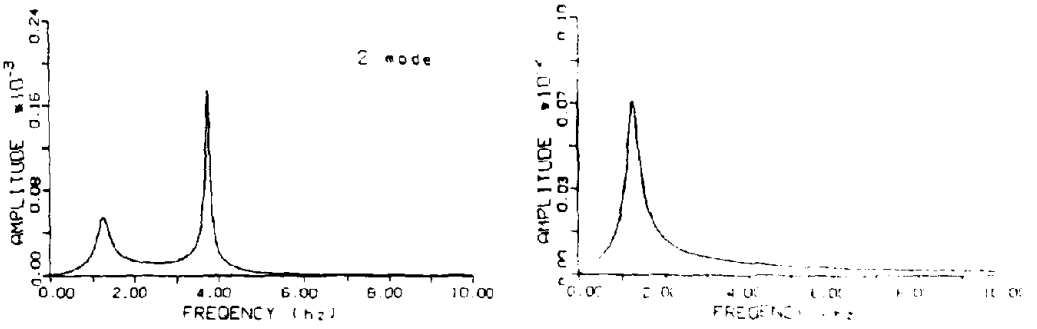

(a) spillover (b) control force

Fig. 9 Frequency response function of the 2nd mode and the control force of the case of the first mode control.

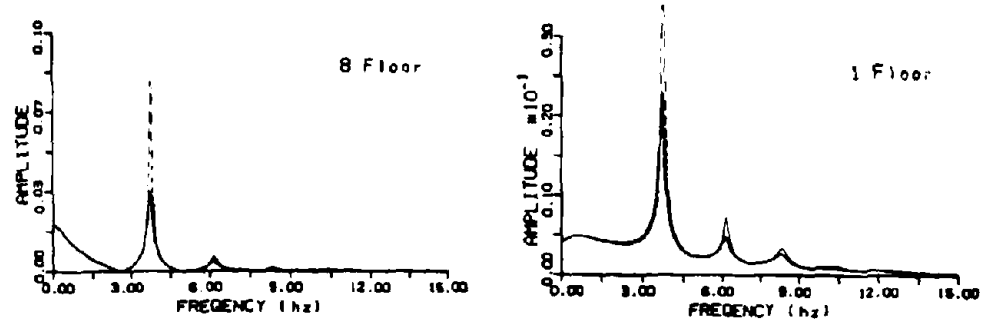

(a) Top floor (b) 1st. floor

Fig. 10 Frequency response function of the top floor and the first floor.
broken line : the case of the first mode control.
solid line : the case of the full mode control.

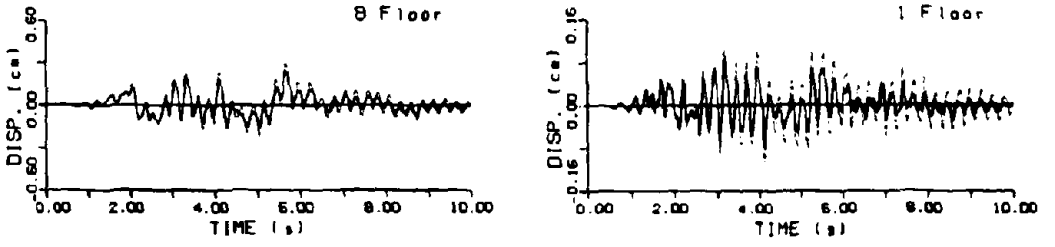

(a) Top floor (b) 1st. floor

Fig. 11 Time history of the top floor and the first floor.
broken line : the case of the first mode control.
solid line : the case of the full mode control.

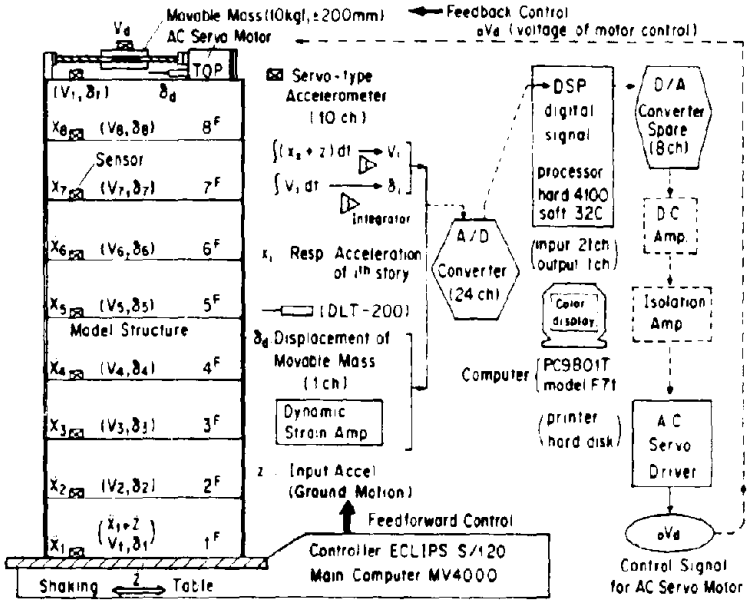

Fig. 12 Schematic diagram of the control system.

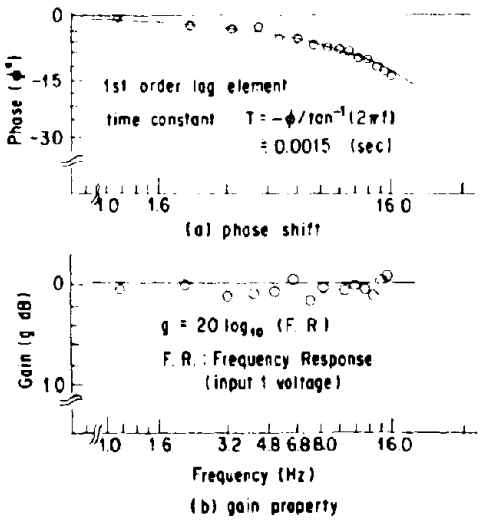

Fig. 13 Time constant of AC servo motor.

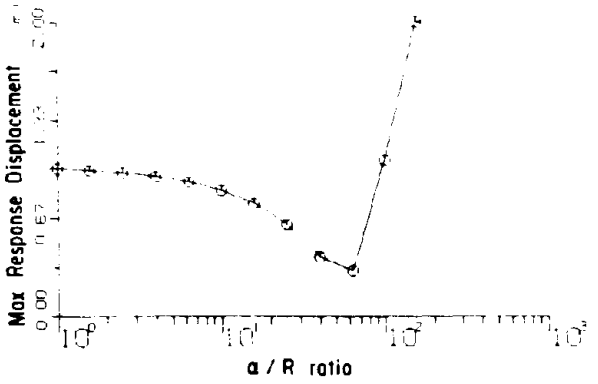

Fig. 14 Relationship between α/r and the maximum response of displacement.

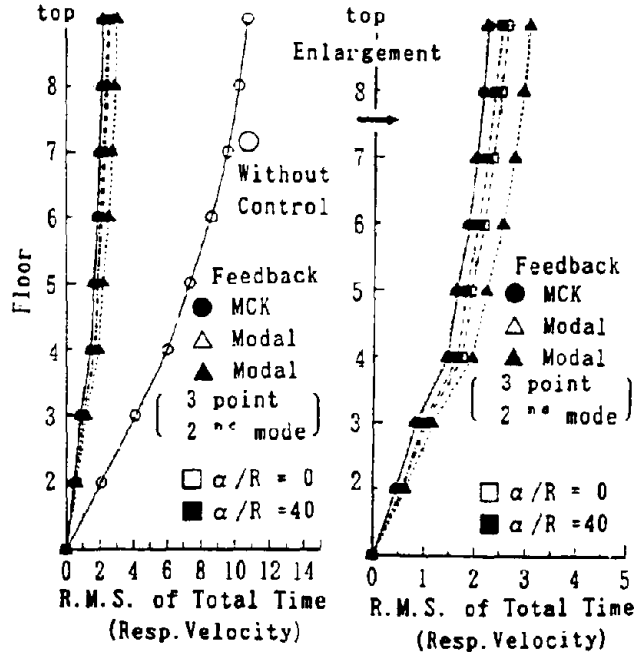

Fig. 15 Comparison of RMS of relative displacement obtained by several control algorithms.

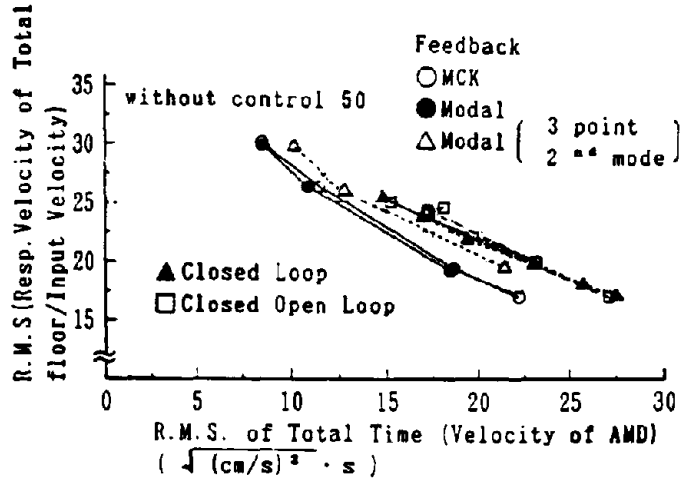

Fig. 16 Relationship between structural response and AMD movement.

Design Issues and Applications

Extension of Equivalent Energy Method for Menshin Bridges

Current CALTRANS Analysis Methods of Bridges Isolated with Bi-linear Hysteresis Bearings

Design of a Menshin Bridge on Soft Ground

Ultimate Restraint Considerations in Base-Isolated Bridges

Design Plan of Super Multi-Span Continuous Menshin Bridge with Deck Length of 725 M

Critical Loads of Elastomeric Isolators at High Shear Strain

A Comparison Study on the Support Systems of a Multi-Span Continuous Steel Bridge

Base Isolation of the University Bridge

Seismic Design of Continuous Steel-Box-Girder Bridge with Rubber Bearings for Trans-Tokyo Bay Highway Project

Earthquake Protective Systems for the Seismic Upgrade of the Golden Gate Bridge

Improvements in Earthquake Resistance of PC Cable-Stayed Bridges by Hysteresis Dampers

NIST

U.S. Department of Transportation
Federal Highway Administration

NATIONAL CENTER FOR EARTHQUAKE ENGINEERING RESEARCH

EXTENSION OF EQUIVALENT ENERGY METHOD FOR MENSHIN BRIDGES

[1)]Takashi Hirai and [2)]Michio Sugimoto

[1)]Takenaka Civil Engineering and Construction Co.,Ltd
[2)]Takenaka Corporation

SUMMARY

The objective of this paper is to present a simple method for estimating responses of the menshin bridge subjected to a strong earthquake. The basis for seismic design of ordinary highway bridges under a strong seismic moton is to estimate the capacity for the ductility of the column. The response of the system is typically obtained by using the equivalent energy method proposed by A.S.Veletsos and N.M.Newmark[1)] for nonlinear single-mass systems[2)]. A menshin bridge, however, should be regarded as a double-mass system. Therefore a new method, namely the "double mass energy method", is developed as an extension of Velestos and Newmark'sequivalent energy method for estimating the seismic response of the menshin bridge. Comparisons of ductility factors calculated using the new method and more precise analysis indicate that the maximum response of menshin bridges with RC columns is well approximated by the new method.

INTRODUCTION

In their proposed equivalent energy method A. S. Velestos and N. M. Newmark assume that the maximum strain energy of a single-mass nonlinear spring is equal to that of a linear spring with the initial stiffness of the nonlinear spring. Based on this assumption, the maximum response of the nonlinear system can be estimated by using the acceleration response spectrum. In the design of menshin bridges it is necessary to account not only for the nonlinearity of RC columns but, also, the nonlinearity arising from the the menshin bearings. The equivalent energy method which is applied to the design of an ordinary highway bridge is, however, inapplicable for the design of a menshin bridge for the following reasons:

(1) The applicability of the equivalent energy method has not been verified for values of ductility factor beyond 10 which is typically used in the design of menshin bearings.

(2) Menshin bridges can at best be idealized as double-mass systems and a single-mass models are inappropriate.

To resolve the first issue, a comparative study of the dynamic responses using the equivalent energy method and a more precise analytical method is carried out. These comparisons show that

while Velestos' and Newmark's method is inappropriate a revised procedure ,namely the "single mass energy method" ,can be devised to be still valid for ductility factors beyond 10.

To solve the second problem, the "double mass energy method", an extension of the "single mass energy method", is developed. This new method is based on the maximum strain energies which are distributed to the elements of a system in the principal vibration mode. The results of this method were verified by comparisons with results from more exact nonlinear analysis. These studies confirmed the accuracy of the new method for calculating the maximum relative displacements of the menshin bearing and the RC column which are critical in the design of a menshin bridge.

EQUIVALENT ENERGY METHOD

Basic Method The equivalent energy method as proposed by A.S.Velestos and N.M. Newmark considers a single-mass model as shown in Fig.1. It consists of a mass m and a weightless spring fixed at the base. Two types of resistance-deformation relationship, linear and nonlinear, are shown in Fig. 2 for the spring. The stiffness of the linear spring is equal to the initial stiffness of the nonlinear spring. Points B and E denote the maximum relative displacements of the linear and nonlinear springs, respectively. Velestos and Newmark assumed that the maximum strain energies described by polygons OAB and OCDE are equal. Based on this assumption, the following equation can be derived:

$$\frac{U_{emax}}{U_{nmax}} = \frac{\mu}{\sqrt{2\mu-1}} \tag{1}$$

where U_{emax} and U_{nmax} denote the maximum relative displacement of the linear and nonlinear springs, respectively. The ductility factor μ is expressed in the form,

$$\mu = \frac{U_{nmax}}{U_y} \tag{2}$$

where U_y is the yield displacemnent of the nonlinear spring. Using the equivalent energy method, the following equation can be evaluated.

$$\mu = \frac{1}{2}\left\{\left(\frac{mS_a}{Q}\right)^2+1\right\} \tag{3}$$

In the above equation m denotes mass and Q denotes maximum resistant force. S_a can be obtained from the acceralation response spectrum for natural period T of the single-mass linear spring. The equivalent energy method has been used for evaluating responses of systems with a bi-linear deformation-resistance relationship as shown in Fig.3. K_1 denotes the initial stiffness of the bi-linear spring and in the equivalent energy method it is, also, the stiffness of the linear spring. K_2 denotes the post-yield stiffness beyond the yield force Q_y. The maximum strain energy, E, of the linear spring can be expressed as

$$E = \frac{1}{2}\frac{(mS_a)^2}{K_1} \tag{4}$$

According to the equivalent energy method, the maximum strain energy of the bi-linear spring is equal to the maximum strain energy of the linear spring as expressed by Equation (4). Therefore, the following equation can be obtained for the maximum force, F_{max}, of the spring,

$$F_{max} = \left\{ 2E + \frac{K_1}{K_1 - K_2} Q_d^2 \right\}^{\frac{1}{2}} \quad (5)$$

In the equation Q_d denotes the characteristic shear strength as shown in Fig. 3. The maximum relative displacement of the bi-linear spring is given by

$$U_{max} = \frac{F_{max} - Q_d}{K_2} \quad (6)$$

and the ductility factor, μ, by

$$\mu = \left(\frac{F_{max}}{Q_d} - 1 \right) \left(\frac{K_1}{K_2} - 1 \right) \quad (7)$$

Limit of Application In the study of A. S. Velestos and N. M. Newmark, Equation (1) was validated for ductility factors of 10 or less. Menshin bearings in menshin bridges subjected to strong earthquakes are typically designed for ductility factors of 10 or more. Therefore, it is necessary to validate Velestos and Newmark's method for ductility factors in the range of 10 and higher.

In the verification, a single-mass system as shown in Fig.1 is used. Springs with two bilinear resistance-deformation relationships as depicted in Fig.4 and an idealized hysteresis loop shown in Fig.5 are used. The weight of the mass is 1032tf. The damping of the system is associated with the hysterisis loop. Fig. 6 shows the three types of standard ground motions used in highway bridge design. The acceleration response spectra of the three standard waves are shown in Fig.7. The amplitude of each wave is magnified accordingly to arrive at the desired range of the ductility factor.

The maximum responses from a nonlinear time-history analysis are presented in Table 1 and Table 2 for bilinear type 1 and 2, respectively. In all cases, the maximum ductility factors were estimated by the equivalent energy method. The maximum strain energy used to estimate the maximum deformation of the nonlinear spring is calculated per Equation (4). The maximum acceleration S_a in this equation is evaluated by multiplying the acceleration from the acceleration response spectrumn corresponding to the natural period of the system by the ampification factor. The natural period T is calculated from the following equation

$$T = 2\pi \sqrt{\frac{m}{K}} \quad (8)$$

where K is the initial stiffness of the bi-linear springs shown in Fig. 4. The maximum force acting on the spring is evaluated from Equation (5) and the maximum relative displacement of the spring is calculated from Equation (6). Equation (7) is then used to evaluate the ductility μ. The estimated ductilities are shown in Figs. 8 and 9 for bilinear springs 1 and 2, respectively, comparing with the corresponding values calculated using a nonlinear time-history method.

It is seen from these figures that the ductilities estimated by the equivalent energy method become lower than the "true" value for ductilities in the range of 10 and higher. For the case of the wave 1 in Fig.5, the difference between the ductility factors estimated by the equivalent energy method and by the nonlinear time-history method is greater than 40 %. Therefore, the equivalent energy method can not be considered to be applicable for ductilities in the range 10 or higher.

EXTENSION OF EQUIVALENT ENERGY METHOD

Single Mass Energy Method The equivalent energy method is seen to be inapplicable for ductility values of 10 or higher. The reason why the estimated ductilities are smaller than those calculated by the more precise nonlinear time-history analysis is most likely the result of underestimating the maximum strain energy using the equivalent energy method compared to the value calculated from the more precise analysis.

A new, more accurate method, the "single mass energy method," is presented to estimate the maximum response of a single mass model with a nonlinear spring. In this new method, the stiffness of the linear model which is used to estimate the maximum strain energy of the nonlinear model is not the initial stiffness but the equivalent stiffness for the maximum deformation of the nonlinear spring. The equivalent stiffness K_{eq} is expressed as

$$K_{eq} = \frac{F_{max}}{U_{max}} \tag{9}$$

where F_{max} is the maximum force acting on the nonlinear spring and U_{max} is the maximum relative displacement of the nonlinear spring. K_{eq} can be evaluated using an iterative procedure shown by the flow-chart of Fig. 10. The initial value of K_{eq} in the flowchart can be set as the equivalent stiffness evaluated from Equation (9) using U_{max} and F_{max} estimated by the equivalent energy method. The natural period T_{eq} is calculated per Equation (8) for K_{eq} at any step in the flowchart of Fig.10. The equivalent maximum strain energy of the nonlinear system at any step is evaluated from Equation (4) by using S_a calculated from the acceleration response spectrum at the natural period T_{eq} calculated using K_{eq} instead of K_1. The maximum force F_{max} acting on the spring and the maximum relative displacement U_{max} are calculated from Equations (5) and (6), respectively. The ductility factor μ is evaluated per Equation (7) at any step in the flowchart. F_{max}, U_{max} and μ are estimated at the final step when the difference between the K_{eq}'s at the current and immediately prior steps become less than a very small pre-set value.

Verification of Single Mass Energy Method To verify the accuracy of "single mass energy method", the ductility factors estimated by this method are compared with the respective values calculated from the nonlinear time-history analysis using cases similar to those listed in Table 1 and Table 2 for the verification of the equivalent energy method. The ductility factors calculated from the nonlinear time-history analysis and those estimated by the "single mass energy method" are shown in Figs.11 and 12 for bilnear springs 1 and 2 shown in Fig. 4, respectively.

Comparing the results shown in Figs. 11 and 12 with those in Figs. 8 and 9 it is clear that the ductility factors evaluated by the new method at ductilities 10 or higher are much closer than those calculated using the equivalent energy method to the values from the more precise nonlinear time-history analysis. As an example, using the new method for case wave 1 shown in Fig.12, the diference in the ductilities is 3.4 at a ductility of 12.2 calculated from the time-history analysis while it is 5.8 for the equivalent energy method as shown in Figure 9.

EXTENSION FOR MENSHIN BRIDGES

In the design of Menshin bridges it is necessary to consider the nonlinearity of both the RC columns and the bearings, in order to accurately estimate the ductility of the system. Also, in the dynamic analysis of Menshin bridges they should be idealized as a double-mass spring as it is necessary to model the system of girders connected to the Menshin bearings in addition to the system of columns fixed on the ground. Therefore, the "single mass energy method" presented in the preceding section for a single-mass system is not applicable. To estimate the maximum response of a Menshin bridge an extension of the "single mass energy method" ,the "double mass energy method" ,is presented in this section.

Double Mass Energy Method This method has been developed to estimate the maximum response of double mass systems as shown in Fig.13. The model has two masses , m1 and m2 , and two nonlinear springs, spring1 and spring2, whose deformation-force relationships are shown in Fig. 14. In this figure, P_{y1} and P_{y2} denote the yield force of spring1 and spring2, respectively. K_{11} and K_{21} denote the initial stiffnesses and K_{12} and K_{22} denote the post-yield stiffnesses of spring1 and spring2, respectively. The maximum strain energy of each spring is expressed by Equations (10) and (11).

$$\text{Spring1:}\quad E_1 = \frac{1}{2}\left\{\left(\frac{1}{K_{11}} - \frac{1}{K_{12}}\right)P_{y1}^2 + \frac{1}{K_{12}}F_{max1}^2\right\} \tag{10}$$

$$\text{Spring2:}\quad E_2 = \frac{1}{2}\left\{\left(\frac{1}{K_{21}} - \frac{1}{K_{22}}\right)P_{y2}^2 + \frac{1}{K_{22}}F_{max2}^2\right\} \tag{11}$$

where F_{max1} and F_{max2} denote the maximum forces in spring1 and spring2, respectively. In this new method, the first mode is assumed to be the primary mode of vibration during a seismic excitation. Therefore, the distribution of the displacement of the two masses at the time when the displacement of the upper mass becomes maximum can be approximated by the static deformation under the body forces producted by a constant acceleration. Thus, the relationship between F_{max1} and F_{max2} is expressed in the following equation

$$F_{max2} = \beta F_{max1} \tag{12}$$

where β is expressed as

$$\beta = \left(1 + \frac{m_2}{m_1}\right) \tag{13}$$

The above assumption implies that the deformation of each spring reaches a maximum at the same time. Therefore, the total maximum strain energy of the system, E_T, is expressed in the following equation.

$$E_T = E_1 + E_2 \tag{14}$$

The maximum response of the system is estimated using the iterative procedure shown in the flowchart of Fig.15. The maximum force acting on spring1 is evaluated from the following equation

$$F_{max1} = \left(\frac{K_{12}K_{22}}{K_{22} + \beta^2 K_{12}}\right)^{\frac{1}{2}}\left\{\left(\frac{1}{K_{11}} - \frac{1}{K_{12}}\right)P_{y1}^2 + \left(\frac{1}{K_{21}} - \frac{1}{K_{22}}\right)P_{y2}^2 - 2E_T\right\}^{\frac{1}{2}} \tag{15}$$

In this equation F_{max1} at the present step can be evaluated using E_T from the previous step. Then, F_{max2} is calculated from Equation (12). The maximum relative displacement of each spring can be evaluated as follows:

$$\text{Spring1:}\quad U_{max1} = U_{y1} + \frac{F_{max1} - P_{y1}}{K_{12}} \tag{16}$$

$$\text{Spring2:}\quad U_{max2} = U_{y2} + \frac{F_{max2} - P_{y2}}{K_{22}} \tag{17}$$

The maximum strain energy E_T at each step of the iteration other than the initial step is evaluated by Equation (4) in which the maximum acceleration S_a is calculated at the equivalent natural period of the springs. The equivalent natural period T_{eq} of the springs are evaluated from the equivalent stiffness which in turn are approximated by

$$\text{Spring1:}\quad K_{eq1} = \frac{F_{max1}}{U_{max1}} \tag{18}$$

$$\text{Spring2:}\quad K_{eq2} = \frac{F_{max2}}{U_{max2}} \tag{19}$$

To calculate the maximum strain energy of the nonlinear double-mass system, an equivalent single-mass system with mass m_{eq} and spring stiffness K_{eq} is assumed. The mass m_{eq} and spring stiffness K_{eq} of the equivalent single-mass system are given as follows:

$$m_{eq} = m_1 + \alpha m_2 \tag{20}$$

$$K_{eq} = \frac{K_{eq1}\, K_{eq2}}{K_{eq2} + \beta K_{eq1}} \tag{21}$$

where α is a coefficient in the range of $0 < \alpha < 1$ and β is a parameter related to the balance between the two masses and is evaluated as per Equation (13). The equivalent natural period T_{eq} is evaluated using the values of m_{eq} and K_{eq} in equation (8). $S_a(T_{eq})$ and m_{eq} are then used in Equation (4) to calculate the total strain energy E_T at the current step. The maximum force and deformation of each spring is estimated at the final step when the difference in E_T at the final and the immediately previous step becomes smaller than a pre-set value.

Application for Menshin Bridge To verify the applicability of the "double mass energy method" for a Menshin bridge subjected to a strong earthquake, the maximum responses calculated by a nonlinear time-history analysis are compared with the corresponding values estimated using the new method. The menshin bridge presented here consists of a 210 meter,6 span continuous PC girder and RC columns. The double-mass model which is an idealization of a part of the menshin bridge shown in Fig.16 is used in the verification. This part consists of a single RC column and two bearings connected to the girder. The weight of the upper mass representing the girder is 1032 tf and that of the lower mass representing the column is 244 tf. The deformation-resistance relationships of the the Menshin bearing and the RC column are shown in Fig.17. The hysteresis loop of the bearing is assumed to be bi-linear as shown in Fig. 5. On the other hand the hysteresis of the RC column is assumed to be tri-linear as shown in Fig.18. Only hysteretic damping is considered in the dynamic response analysis. The input seismic motions are the same standard waves shown in Fig. 6 and their amplitudes are appropriately factored to make both springs nonlinear. The maximum responses of the analysis are tabulated in Table 3 and the spectrums of acceleration responses at each mass are shown in Fig.19 for three types of the input seismic

motions. The values used in the comparison are the ductilities of both springs defined as follows:

$$\text{Bearing:} \quad \nu = \frac{U_{bmax}}{U_{by}} \tag{22}$$

$$\text{Column:} \quad \mu = \frac{U_{cmax}}{U_{cy}} \tag{23}$$

where

U_{by} : the yield relative displacement of the bearing
U_{bmax} : the maximum relative displacement of the bearing
U_{cy} : the yield relative displacement of the column
U_{cmax} : the maximum relative displacement of the column.

In the case of the nonlinear time-history analysis these values are calculated from the maximum relative displacements of both springs which are listed in Table 3. On the other hand for the "double mass energy method" the maximum relative displacements obtained from Equations (16) and (17) are used in Equations (22) and (23). In this estimation α was set to 0 and β to 1.2 . The ductility factors obtained from the nonlinear time-history analysis and the "double mass energy method" are shown in Fig.20.

From the result of the precise response analysis as shown in Fig.19,it appears that first mode is the primary mode at the girder. Therefore the assumption in the "double mass energy method" is considered to be appropreate for the menshin bridge. The maximum difference between the ductility factors estimated by the "double mass energy method" and the more precise analysis is 1.3 at the analytical ductility of 5.4 for the RC column. As seen in Fig. 20(a) the estimated ductility values are tightly distributed in the neighborhood of the perfect fit line. Therefore, it appears that the ductility of the column during a strong earthquake are well estimated by the "double mass energy method". On the other hand the maximum difference of the ductility factors of the bearing estimated using the proposed simple method and the more precise analysis is 4.4 at the analytical ductility value of 20.8. In addition, the estimated values are consistently lower as is evident in Fig. 20(b). Therefore, the new method can be considered to be inapplicable for estimating the maximum response of the bearing but to be possible to apply the estimated value multiplied by any coefficient for the design of the menshin bridge.

CONCLUSION

(1) The equivalent energy method proposed by A. S. Veletsos and N. M. Newmark can be successfully used to estimate the maximum response of a single-mass system with a nonlinear spring during a seismic excitation in the range where the ductility factor is less than 10. However, the error in the estimation dramatically increases for ductilities beyond 10. The maximum strain energy of the nonlinear system using the equivalent energy method is consistently smaller than the real maximum energy in the higher range of the ductility factor. It appears that in the higher range, the maximum strain energy should be estimated by using a linear system not with a hard spring having the initial stiffness of the nonlinear spring but with a softer spring.

(2) "Single mass energy method" is developed to estimate the maximum response of a

nonlinear single-mass system in the higher range of the ductility factor. Comparisons with the results of a nonlinear time-history analysis indicate that the maximum response of the nonlinear single-mass system is well estimated by the new method in the range of the ductility factor beyond 10.

(3)" Double mass energy method" is developped to estimate the maximum response of both masses of a nonlinear double-mass system during a seismic motion. In this method an assumtion is made that the first mode is the primary mode of vibration during the seismic excitation. To verify the applicability of this method for a Menshin bridge, the maximum responses of a Menshin bridge subjected to a strong earthquake are evaluated by this method and compared to the maximum responses obtained using a nonlinear time-history analysis. The comparison indicate that the maximum responses of the nonlinear RC column are well approximated by the new method.

ACKNOWLEDGEMENT

This investigation was conducted as an extension of the joint research program for "Development of Menshin System of Highway Bridges" between PWRI and 28 private firms in Japan. The authors would like to thank Dr. K. Kawashima and Mr. S. Unjo for their advice and suggestion.

REFERENCES

1)Veletsos, A.: Effect of Inelastic Behavior on The Response of Simple System to Earthquake Motions,Proc. of 2nd WCEE,1960.

2)Japan Road Association: Design Specifications for Highway Bridges -Part V Seismic Design -,1990

3)PWRI and 28 private firms: Development of Menshin Systems for Highway Bridges,Report No.3,1992.

4)Penzien, J : Elasto-plastic Response of Idealized Multi-sto Structures Subjected to A Strong Motion Earthquake,Proc. of 2nd WCEE,1960.

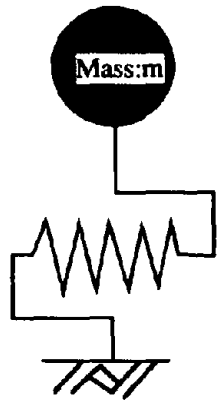

Fig.1 Single Mass Model

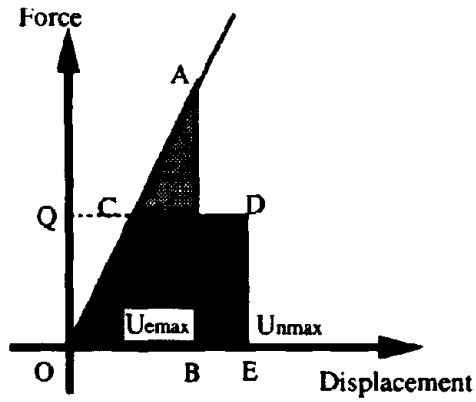

Fig.2 Deformation-Resistance Relationship

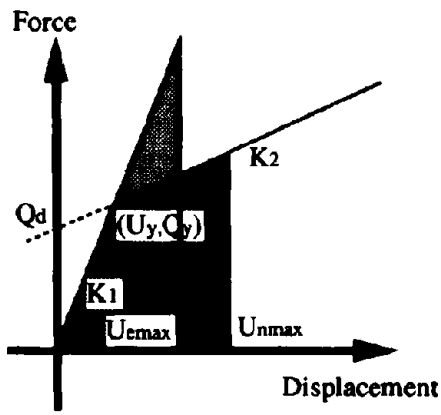

Fig.3 Bi-linear Relationship

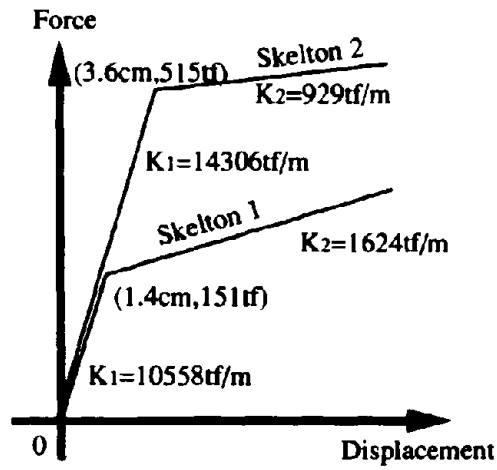

Fig.4 Two Types of Skeltons for Verification

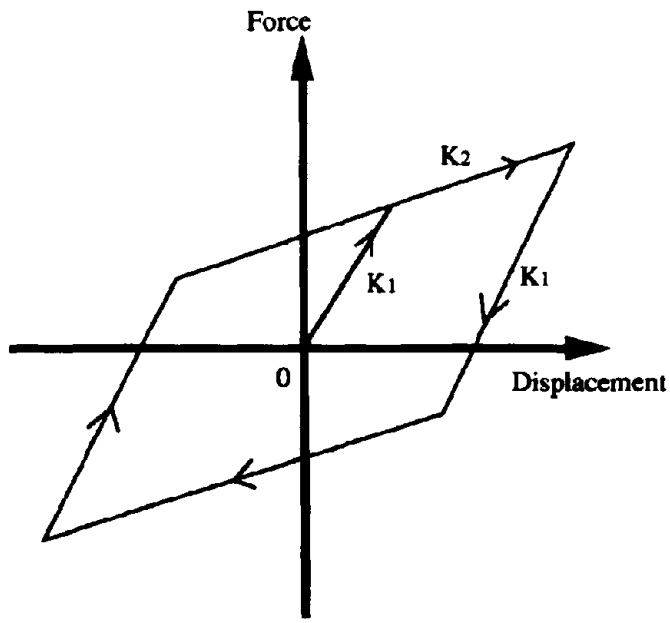

Fig.5 Idealized Hysteresis Loop for Bi-linear Type

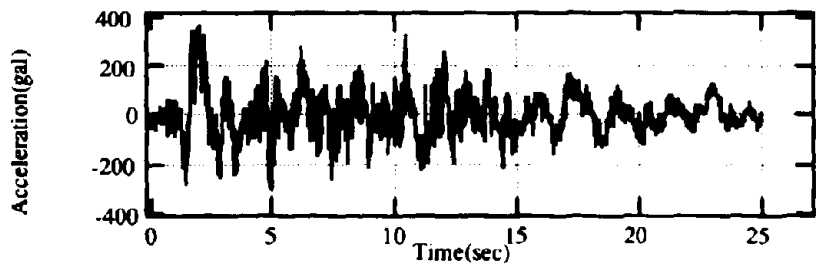

(a) wave 1 (Soil Type I)

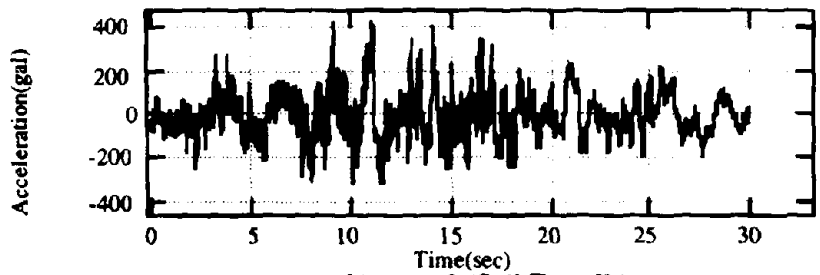

(b) wave 2 (Soil Type II)

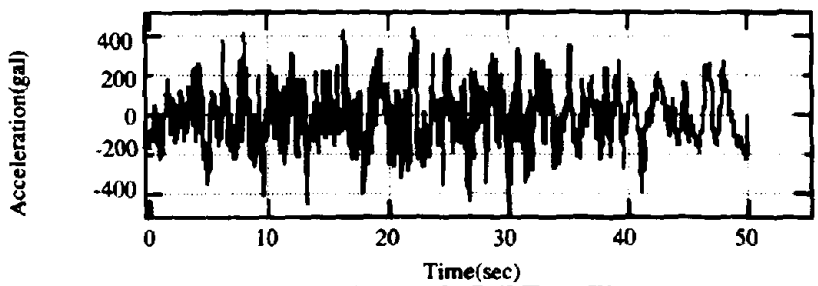

(c) wave 3 (Soil Type III)

Fig.6 Standard Waves for Highway Bridge Design

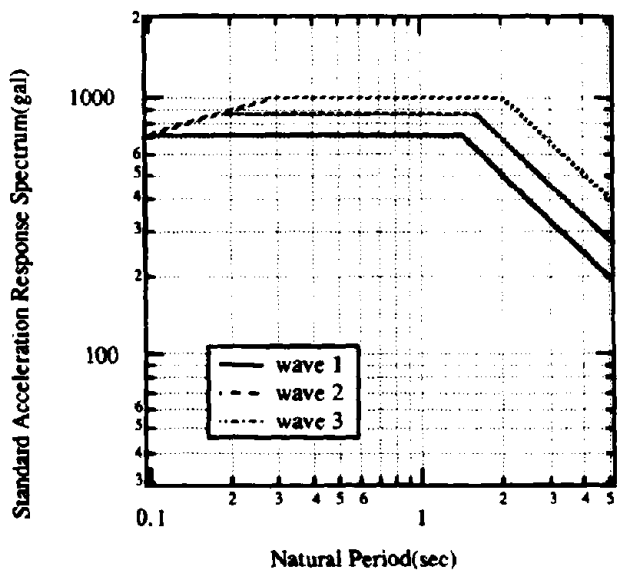

Fig.7 Standard Acceleration Response Spectrum of Standard Waves in Fig.6

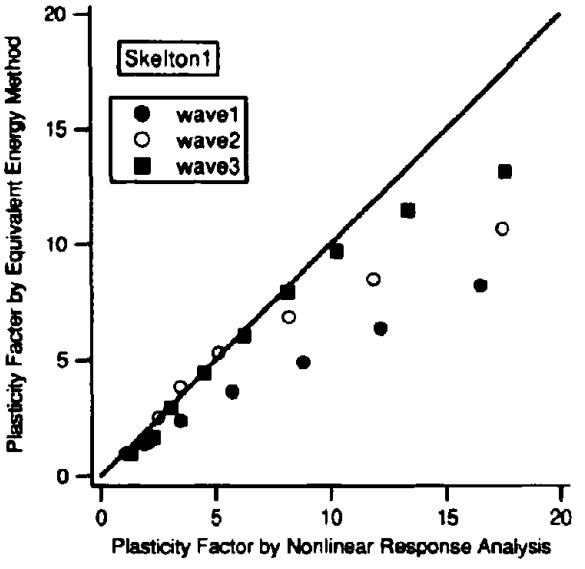

Fig.8 Verification of Equivalent Energy Method for Skelton 1

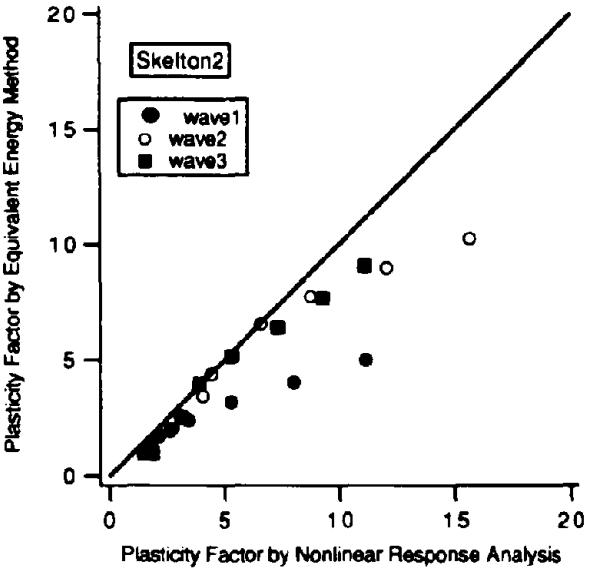

Fig.9 Verification of Equivalent Energy Method for Skelton 2

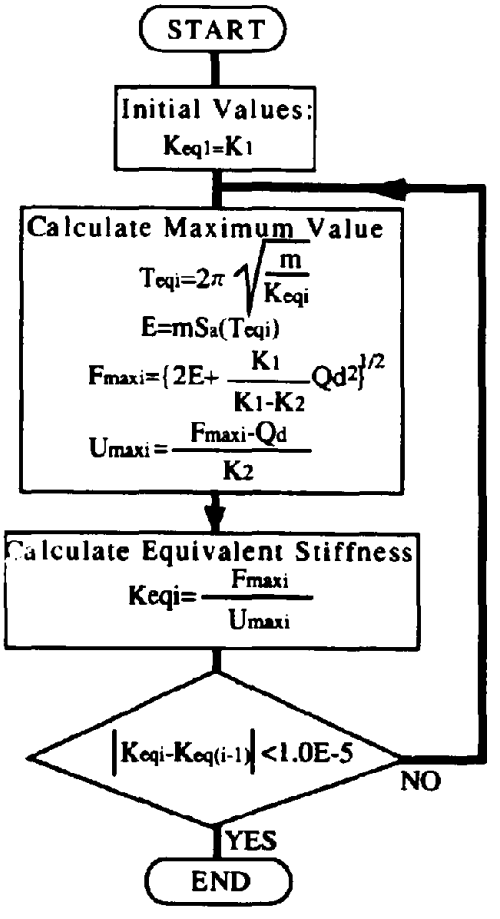

Fig.10 Flow of Single Mass Energy Method

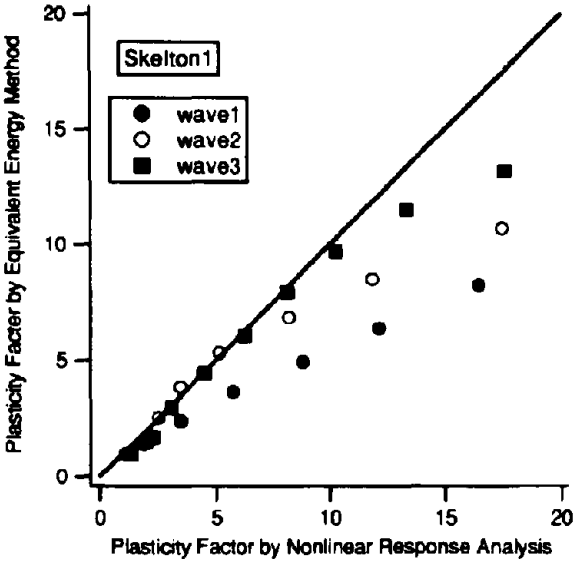

Fig.8 Verification of Equivalent Energy Method for Skelton 1

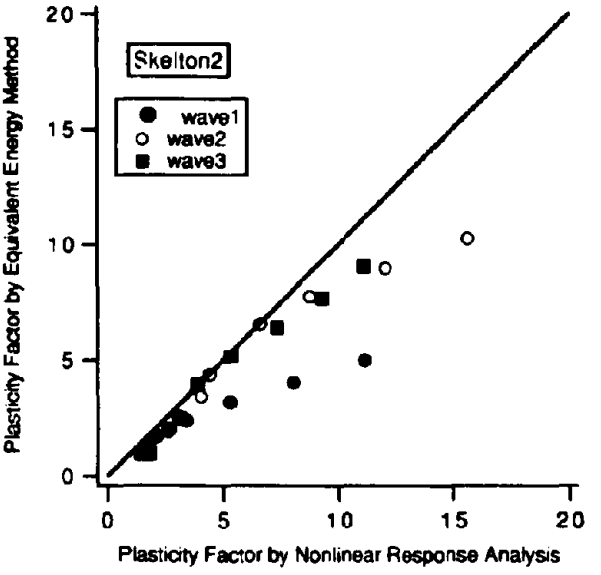

Fig.9 Verification of Equivalent Energy Method for Skelton 2

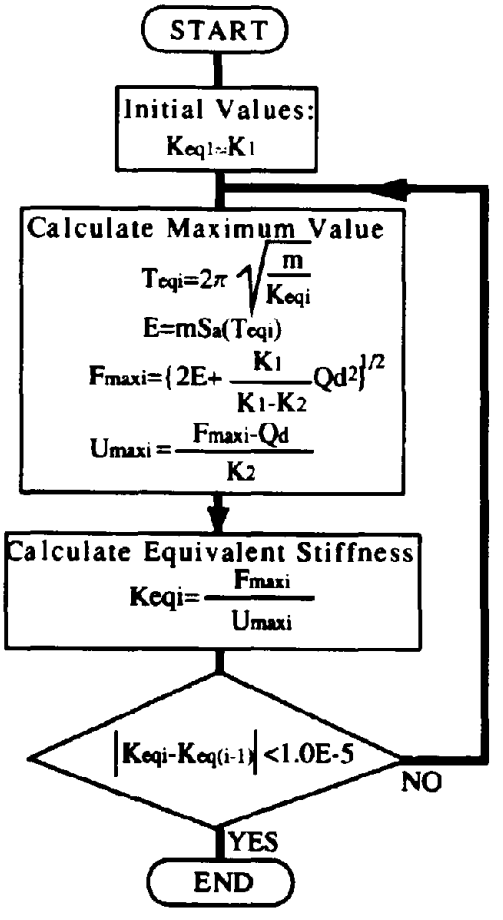

Fig.10 Flow of Single Mass Energy Method

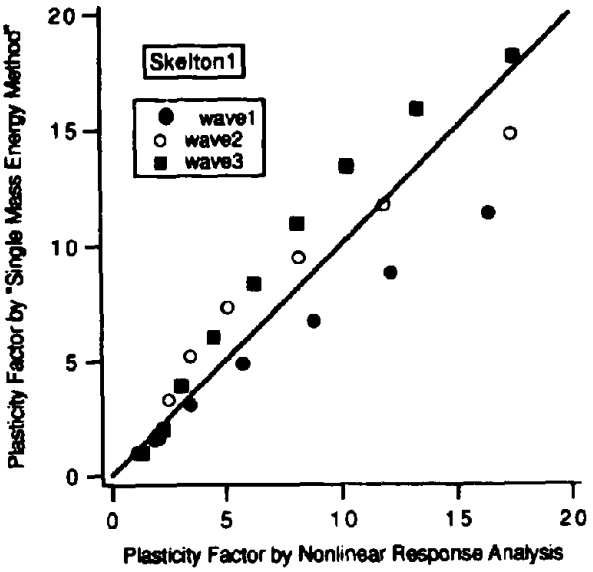

Fig.11 Verification of Single Mass Energy Method for Skelton 1

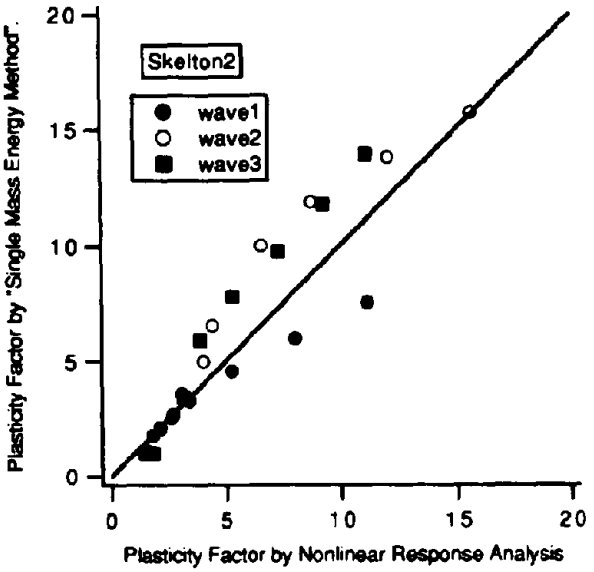

Fig.12 Verification of Single Mass Energy Method for Skelton 2

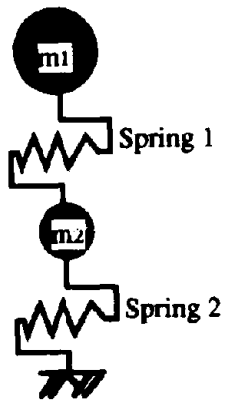

Fig.13 Double Mass Model

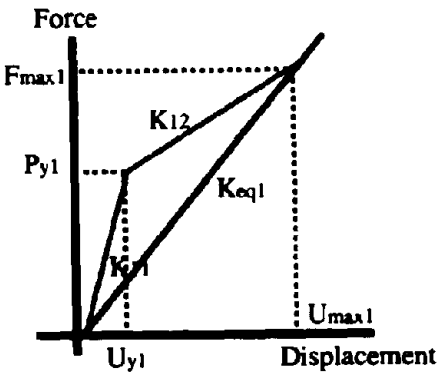

(a) Spring 1

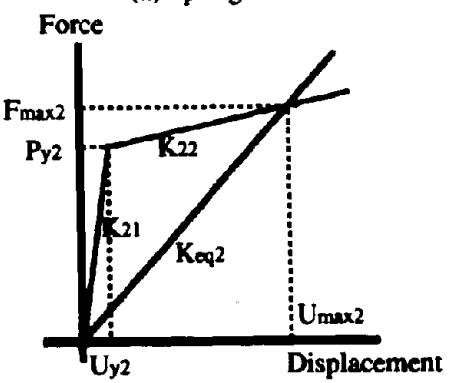

(b)Spring 2

Fig. 14 Nonlinear Skelton of Spring

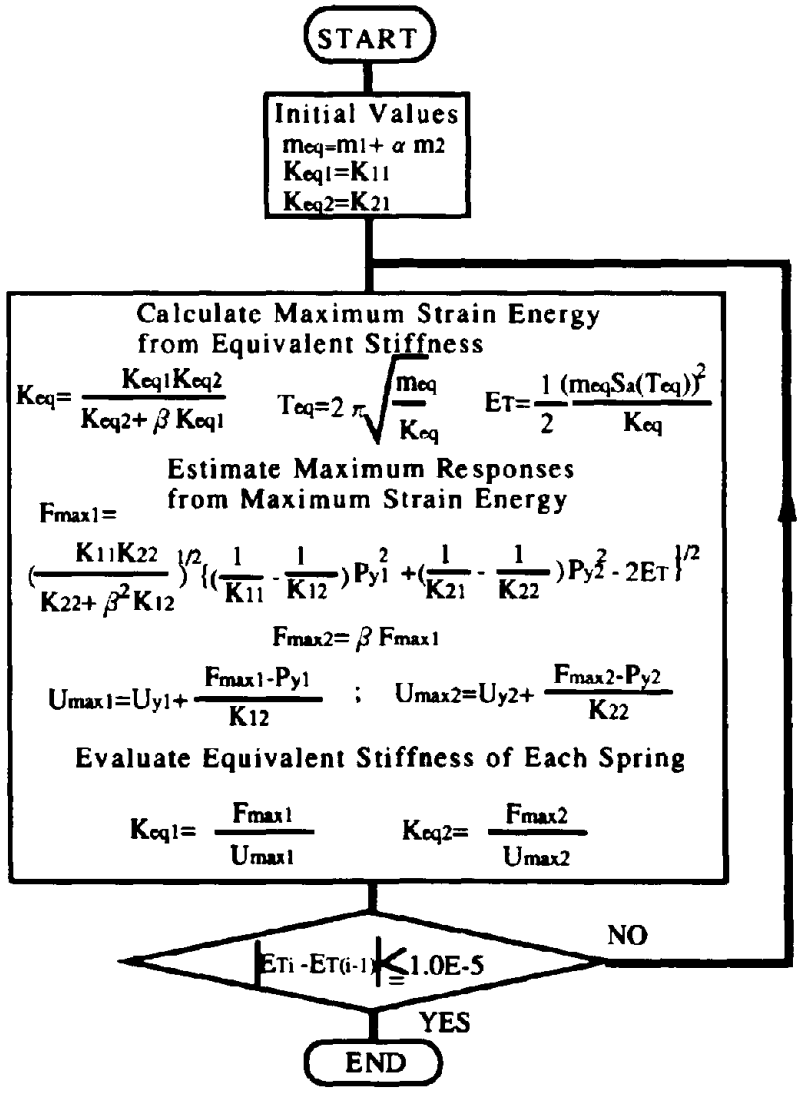

Fig.15 Flow of Double Mass Energy Method

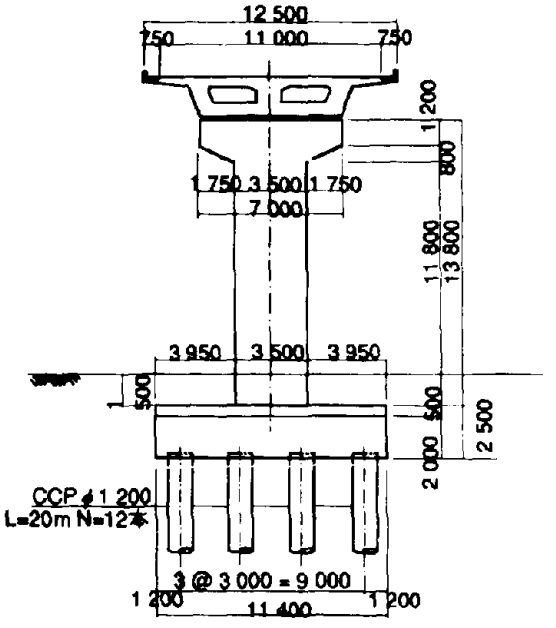

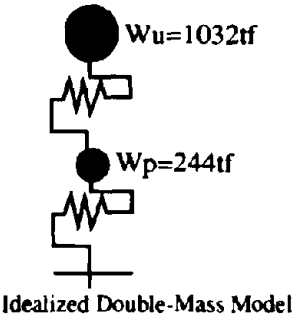

Fig.16 RC Column of Menshin Bridge

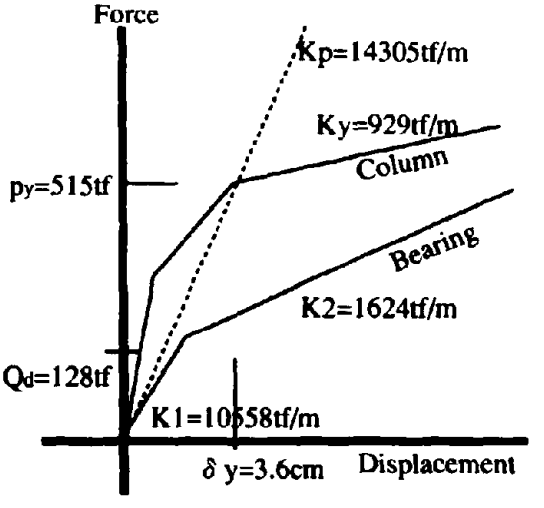

Fig.17 Skelton of Column and Bearing

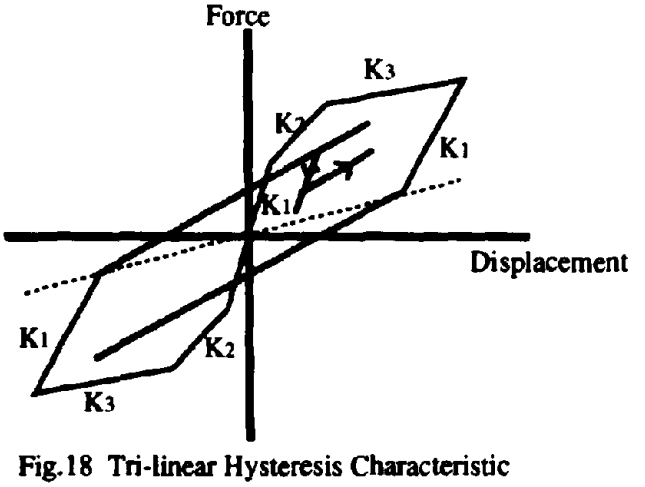

Fig.18 Tri-linear Hysteresis Characteristic

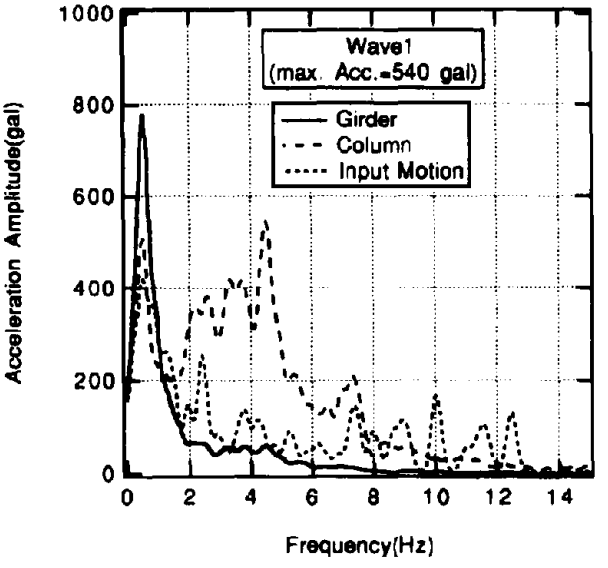

(a)Wave1 (Max. Acc.=540 gal)

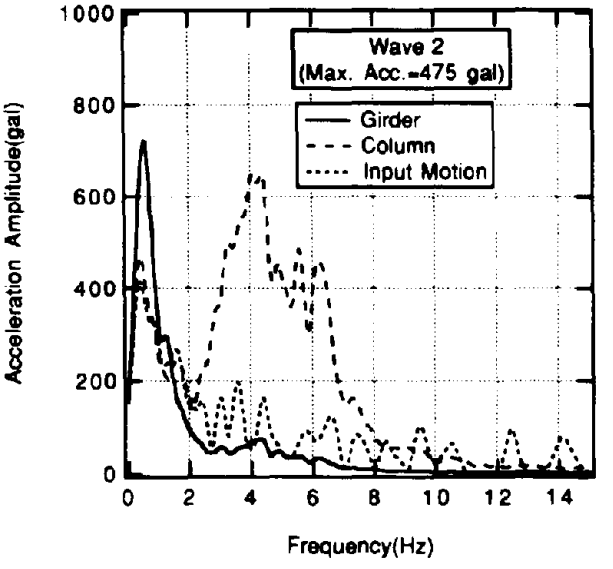

(b)Wave2 (Max. Acc.=475 gal)

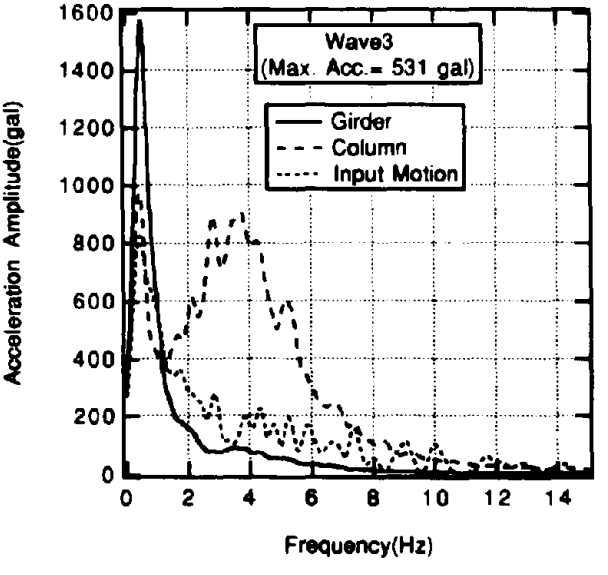

(c)Wave 3 (Max. Acc.= 531 gal)

Fig.19 Fourier Spectrum of Acceleration Responses

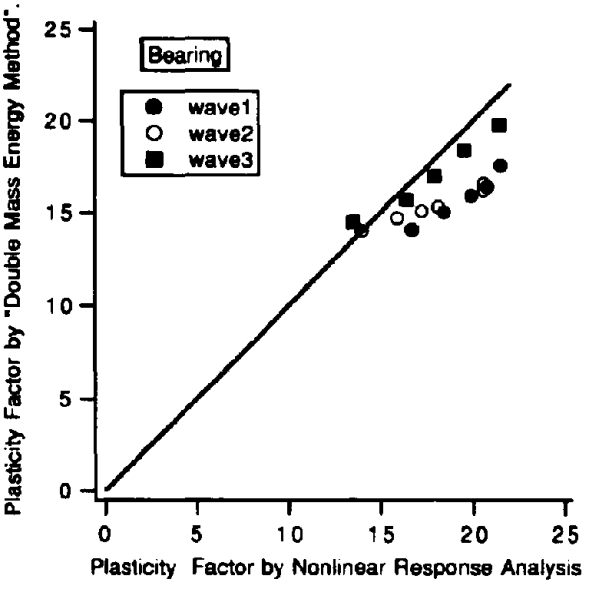

(a) Menshin Bearing (Spring 1)

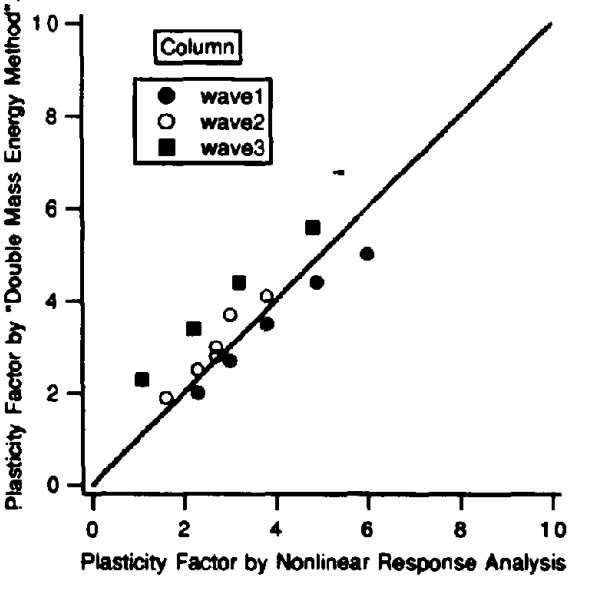

(b) RC Column (Spring 2)

Fig.20 Verification of Double Mass Energy Method for Menshin Bridge

Table 1 Maximum Responses of Nonlinear Response Analysis for Skelton 1

Input Motion	Maximum Acceleration of Input Motion (gal)	Maximum Acceleration Response (gal)	Maximum Deformation Response (cm)	Maximum Force of Spring (tf)	Plasticity Factor
Wave 1	360	487	23.7	512.5	16.5
	300	392	17.5	412.4	12.2
	250	317	12.7	334.0	8.8
	200	249	8.3	262.5	5.8
	150	199	5.0	210.0	3.5
	100	163	2.7	171.5	1.9
	70	147	1.6	154.6	1.1
Wave 2	417	509	25.1	535.7	17.4
	350	385	17.1	405.3	11.9
	300	304	11.8	320.3	8.2
	250	235	7.4	247.9	5.1
	200	199	5.0	209.8	3.5
	150	177	3.6	186.2	2.5
	100	168	3.0	177.4	2.1
	50	151	1.9	159.1	1.3
Wave 3	443	511	25.3	538.5	17.6
	400	418	19.2	440.7	13.3
	350	350	14.8	368.5	10.3
	300	302	11.7	317.9	8.1
	250	260	9.0	274.1	6.3
	200	222	6.5	233.3	4.5
	150	189	4.4	199.3	3.1
	100	172	3.3	181.1	2.3
	50	151	1.9	159.0	1.3

Table 2 Maximum Responses of Nonlinear Response Analysis for Skelton 2

Input Motion	Maximum Acceleration of Input Motion (gal)	Maximum Acceleration Response (gal)	Maximum Deformation Response (cm)	Maximum Force of Spring (tf)	Plasticity Factor
Wave 1	360	514	6.4	541.1	1.8
	400	524	7.6	552.3	2.1
	450	542	9.6	571.2	2.7
	500	565	12.2	595.2	3.4
	600	624	19.0	657.7	5.3
	700	712	28.9	749.6	8.0
	800	811	40.1	854.4	11.1
Wave 2	417	540	9.4	568.6	2.6
	250	507	5.7	534.2	1.6
	500	554	11.0	583.4	3.1
	600	585	14.5	616.0	4.0
	700	598	15.9	629.7	4.4
	900	666	23.7	701.4	6.6
	1000	735	31.5	773.8	8.8
	1100	840	43.4	884.4	12.1
	1200	954	56.3	1004.7	15.6
Wave 3	443	556	11.2	585.4	3.1
	150	503	5.2	530.0	1.4
	200	514	6.5	541.9	1.8
	600	581	14.0	611.5	3.9
	700	625	19.1	658.8	5.3
	800	689	26.3	725.6	7.3
	900	752	33.4	792.1	9.3
	1000	810	40.0	853.6	11.1

Table 3 Maximum Responses of Nonlinear Response Analysis by Idealized Using Double-Mass Mode of Menshin Bridge

Input Condition		Result of Analysis					
Input Seismc Motion	Max. Acc.of Input Motion (gal)	Maximum Accelelation of Girder (gal)	Maximum Acceleration of Column (gal)	Maximum Relative Disp. of Bearing (cm)	Plasticity Factor of Bearing: ν	Maximum Relative Disp. of Column (cm)	Plasticity Factor of Bearing: μ
Wave 1	360	458	843	21.8	15.1	5.5	1.5
	396	493	953	24.1	16.7	8.1	2.3
	432	529	842	26.5	18.4	10.8	3.0
	468	562	970	28.7	19.9	13.8	3.8
	504	581	1008	29.9	20.8	17.7	4.9
	540	597	1031	31.0	21.5	21.7	6.0
Wave 2	417	503	1398	24.8	17.2	9.6	2.7
	350	392	1154	17.5	12.2	4.3	1.2
	375	433	1151	20.2	14.0	5.8	1.6
	400	473	1235	22.9	15.9	8.1	2.3
	425	527	1322	26.1	18.1	9.7	2.7
	450	579	1066	29.7	20.6	10.7	3.0
	475	578	1098	29.7	20.8	13.8	3.8
Wave 3	443	520	1169	25.8	17.9	11.4	3.2
	354	420	1071	19.4	13.5	3.9	1.1
	399	486	1185	23.6	16.4	7.8	2.2
	487	554	1194	28.1	19.5	17.1	4.8
	531	596	1144	30.8	21.4	19.3	5.4

CURRENT CALTRANS ANALYSIS METHODS OF BRIDGES ISOLATED WITH BI-LINEAR HYSTERESIS BEARINGS

L.H. Sheng[1], J.S. Hwang[2] and J. H. Gates[3]

ABSTRACT

Two methods were recently proposed by the California Department of Transportation (CALTRANS) for the analysis of bridges isolated with bearings whose hysteresis behavior can be appropriately represented by a bi-linear model. In the first CALTRANS proposed method, the hysteresis behavior of a base-isolated regular bridge was idealized by a bi-linear model in the direction of consideration. Based on the hysteresis loop of the entire base-isolated bridge, an empirical model was used to determine the effective period and equivalent viscous damping ratio of the bridge. In the second CALTRANS proposed method, the empirical model was employed to determine the effective stiffness and equivalent damping ratio of isolation bearings rather than the base-isolated bridge, and a modal strain energy method combined with the concept of component energy ratio was utilized to formulate the "composite damping ratio" of the entire base-isolated bridge. A five-span regular bridge subjected to three design earthquakes and ten recorded ground motions is employed to investigate the accuracy of prediction using CALTRANS proposed methods. The analysis results are compared with those from the analyses using AASHTO isolation guide specifications, JPWRI menshin design manual and the inelastic analysis program DRAIN-2D.

INTRODUCTION

The bridge engineering society has recently adopted equivalent elastic seismic analysis methods for practical analysis of base-isolated bridges. Various equivalent elastic models have been provided among others by the American Association of State Highway and Transportation Officials (AASHTO) (Guide Specifications 1991; Mayes, et al. 1992), the Japanese Public Works Research Institute (JPWRI) (Manual 1992), and the New Zealand Ministry of Works and Development (NZMWD) (Design 1983). All of these equivalent elastic models have been developed primarily based on: (1) the formulation of the equivalent (or effective) viscous

---

1. Senior Bridge Engineer, Division of Structures, California Department of Transportation, 1801 30th Street, West Building, Division of Structures, Sacramento, CA 95816
2. Civil Engineer, Division of Structures, California Department of Transportation, Sacramento,
3. Supervising Bridge Engineer, Division of Structures, California Department of Transportation.

damping ratio and effective stiffness (or period) of isolation bearings and isolated bridges; and (2) the establishment of an iteration procedure for the design displacements of isolation bearings corresponding to specified design earthquakes.

The major differences between these equivalent elastic analysis methods are the determinations of equivalent viscous damping ratios and effective stiffness of isolation bearings and base-isolated bridges. All of the methods were developed to approximate the maximum inelastic seismic responses of base-isolated bridges so that the base-isolated bridges can be analyzed and designed by bridge engineers without complex inelastic modeling. Based on the same purpose, two CALTRANS analysis methods are formulated in this study with emphasis on the bridges isolated by bi-linear hystersis bearings such as lead-rubber bearings and elastomeric bearings combined with yielding devices. The analysis results are compared with various equivalent elastic models and an inelastic analysis.

CALTRANS PROPOSED METHOD 1

An empirical model was obtained (Hwang and Sheng 1993) from a modification of the model proposed by Iwan (1980) which was employed to approximate the inelastic displacement response spectra of a single degree of freedom (SDOF) system using an elastic analysis method. The modified model is used in this proposd method to determine the equivalent damping ratio and effective period (or stiffness) of base-isolated regular bridges defined by AASHTO (Standard 1991). The base-isolated regular bridge is idealized as a SDOF system in the direction of consideration. The effective period shift and equivalent damping ratio of the base-isolated regular bridge are determined by

$$\frac{T_{eff}}{T_0} - 1 = \ln\left[1 + 0.13(\mu - 1)^{1.137}\right] \tag{1}$$

and

$$\xi_e = \xi_0 + 0.1352\left(\frac{T_{eff}}{T_0} - 1\right)^{0.3952} \tag{2}$$

where μ is denoted as the "shear displacement ductility ratio" of the base-isolated bridge, which is defined as the design displacement d_i divided by the yielding displacement d_y. It is noted that d_i and d_y are measured at the bridge deck in this proposed method; ξ_0 = viscous damping ratio for which a nominal value of 5% is usually assumed; and T_0, T_{eff} = the fundamental period and effective period, respectively, of the base-isolated regular bridge in the direction of consideration. The formulation of a base-isolated regular bridge shown in Figure 1 is summarized as follows.

The superstructure of the base-isolated bridge is presumed to be relatively rigid in the longitudinal and transverse directions in comparison with the stiffness of isolation units and bridge piers (or column bents). The bridge deck is assumed to be continuous over the piers or

bents, i.e., there are no intermediate hinges within isolated spans. Because the hysteresis behavior of isolation bearings is represented by a bi-linear model, the hysteresis loop of the isolated bridge will generally be a multi-linear curve as shown in Figure 2. The yielding events during a loading process represent the subsequent yielding at different isolation units. However, this multi-linear hysteresis curve is approximated in this proposed method by a bi-linear curve as shown in Figure 2. The corresponding yielding displacement and yielding force are calculated using

$$d_y = \frac{(F_y)_l - K_d(d_y)_l}{K_u - K_d} \tag{3}$$

and

$$F_y = K_u d_y \tag{4}$$

where K_u = the total elastic stiffness of the isolated bridge which is equal to the sum of the elastic stiffness of each combined system shown in Figure 1; K_d = the total inelastic stiffness of the isolated bridge which is calculated by summing the inelastic stiffness of each combined system. The inelastic stiffness of each combined system is determined assuming the abutment or pier remains elastic during earthquakes; $(d_y)_s$ = the smallest yielding displacement among all combined systems; and $(F_y)_l$ = the yielding force corresponding to the largest yielding displacement $(d_y)_l$ of all combined systems, and is expressed in the form of

$$(F_y)_l = \sum_i (F_{yc})_i + \sum_i (K_{dc})_i \left[(d_y)_l - (d_{yc})_i\right] \tag{5}$$

where $(F_{yc})_i$, $(d_{yc})_i$ = respectively the yielding force and yielding displacement of combined system i ; and $(K_{dc})_i$ = the inelastic stiffness of combined system i .

Using Equations (1), (2), (3) and an iteration procedure, the maximum seismic inelastic displacement or design displacement at the bridge deck is calculated corresponding to a design earthquake. The seismic coefficient is then obtained as

$$C_s = \frac{F_y}{W}\left[1 + \alpha(\mu - 1)\right] \tag{6}$$

where W = the total bridge weight supported by isolation units and α = the hardening ratio equal to K_d / K_u. The maximum seismic deformations and forces of structural components of the base-isolated bridge can then be computed.

In the formulations, the base-isolated regular bridge is idealized as a SDOF system in the direction of consideration. As a result, the proposition is only appropriate for the single mode analysis. Furthermore, the equivalent damping ratio determined from Equation (2) is applied directly to the analysis rather than employing a damping coefficient (Guide Specifications 1991)

or a damping modification factor (Manual 1992) to scale the 5% damped design spectra. The design response spectrum corresponding to the calculated equivalent damping ratio for each step of iteration should be determined. Thus, the generation of a ground motion time history compatible with a desired design spectrum is necessary before the establishment of an appropriate damping coefficient or damping modification factor corresponding to this analysis method.

CALTRANS PROPOSED METHOD 2

In the second CALTRANS proposed method, the empirical model is used to determine the effective stiffness and equivalent damping ratio of each isolation unit. Based on Equations (1) and (2), the effective stiffness and equivalent damping ratio of isolation unit i are given by

$$(K_{eff})_i = \frac{(K_u)_i}{\{1 + \ln[1 + 0.13(\mu_i - 1)^{1.137}]\}^2} \tag{7}$$

and

$$(\xi_e)_i = 0.1352 \left[\sqrt{\frac{(K_u)_i}{(K_{eff})_i}} - 1\right]^{0.3952} \tag{8}$$

where μ_i is the "ductility ratio" and is calculated by $(d_i)_i / (d_y)_i$ which are, respectively, the maximum and yielding displacements of isolation unit i ; $(K_u)_i$ and $(K_{eff})_i$ are the elastic and effective stiffness of isolation unit i , respectively. With the effective stiffness and equivalent damping ratio of each isolation unit determined, the remaining task is to determine the effective stiffness and equivalent damping ratio of the base-isolated bridge. For the combination of the effective stiffness of isolation units and the elastic stiffness of other structural components, the procedure is simple and straightforward. Regarding the combination of damping ratios, Turkington et al (1989) calculated the system damping of the entire base-isolated bridge by summing the equivalent damping ratio of isolators together with the nominal 5% damping assigned for other bridge components. However, the isolation bearings are connected in series with other bridge components, the direct summation of the viscous damping ratio and equivalent damping ratio may not be reasonable. In this study, some rational methods proposed by Raggett (1975) and Johnson and Kienholz (1982) are adopted to formulate the "composite damping ratio" of the entire base-isolated bridge. According to Raggett's study (1975), the damping ratios of structural components can be represented by component energy ratios. The overall system damping ratio is determined by combining the component energy ratios weighted by the respective ratio of the potential energy of each component to the total potential energy of the complete system. Similar to Raggett's concept, a modal strain energy method was later formulated by Johnson and Kienholz (1982) for modeling a constrained viscoelastic layer. This modal strain energy method was recently applied by Soong and Lai (1991) and Chang et al (1992) for the analysis of viscoelastically damped building structures. However, only the

damping contributed by viscoelastic dampers is considered in the formulation.

In this study the modal strain energy method is employed to determine the equivalent viscous damping ratio of a base-isolated bridge. Employing Raggett's concept, the damping contributed by the isolation units and other structural components are all taken into account. The equivalent viscous damping ratio or the "composite damping ratio" of the j th vibration mode of a base-isolated bridge is then obtained as

$$(\xi_e)_j = \frac{\sum_i \xi_i \, \phi_j^T \, K_i \, \phi_j}{\phi_j^T \, K_B \, \phi_j} \tag{9}$$

where ϕ_j = the j th mode shape vector; ξ_i = the equivalent damping ratio of isolation unit i given in Equation (8) or the viscous damping ratios of other bridge components; K_i = the structural stiffness matrix attributed to isolation unit or bridge component i ; and K_B = the stiffness matrix of the entire base-isolated bridge. Based on Equations (7), (8) and (9), an iteration process is used to determine the maximum inelastic displacement or design displacement d_i of isolation unit i corresponding a design earthquake. Similar to Equation (6), the seismic coefficient is calculated as

$$C_s = \sum_i \frac{(F_y)_i}{W} \left[1 + \alpha_i \left(\mu_i - 1 \right) \right] \tag{10}$$

where α_i = the hardening ratio of isolation unit i which is equal to $(K_d)_i / (K_u)_i$. The application of this method will require the generation of design response spectra corresponding to different equivalent modal damping ratios for the iteration process. This may be better achieved using an artificial ground motion time history compatible with the desired design spectrum.

If the superstructure of a regular bridge is assumed to be relatively rigid compared to the stiffness of isolators and piers in the direction of consideration and if the torsionally coupled responses are not considered, single mode analysis may be appropriate. Assuming a fixed-base condition for piers and abutments, the equivalent viscous damping ratio of the base-isolated bridge shown in Figure 1 can easily be determined by substituting the following equations of each combined system i

$$(\phi_j)_i = \begin{bmatrix} \left[1 + \dfrac{(K_{eff})_i}{(K_p)_i} \right] d_i \\ \dfrac{(K_{eff})_i}{(K_p)_i} \, d_i \end{bmatrix} \tag{11}$$

and

$$K_i = \begin{bmatrix} (K_{eff})_i & 0 \\ 0 & (K_p)_i \end{bmatrix} \tag{12}$$

$$(K_B)_i = \begin{bmatrix} (K_{eff})_i & -(K_{eff})_i \\ -(K_{eff})_i & (K_{eff})_i + (K_p)_i \end{bmatrix} \tag{13}$$

into Equation (9). $(\phi_j)_i$, K_i and $(K_B)_i$ are the mode shape vector, component stiffness matrix and system stiffness of combined system i , respectively. The equivalent viscous damping ratio of the base-isolated bridge for single mode analysis is then derived as

$$\xi_e = \frac{\Sigma\, (K_{eff})_i\, d_i^2\, [(\xi_e)_i + (\xi_p)_i \dfrac{(K_{eff})_i}{(K_p)_i}]}{\Sigma\, (K_{eff})_i\, d_i^2\, [1 + \dfrac{(K_{eff})_i}{(K_p)_i}]} \tag{14}$$

where $(K_p)_i$, $(\xi_p)_i$ = the lateral stiffness and viscous damping ratio of pier or abutment i , respectively.

ANALYSIS OF AN EXAMPLE BRIDGE

In order to compare two CALTRANS methods with AASHTO (Guide Specifications 1991) and JPWRI (Manual 1992) equivalent elastic methods, a five-span example bridge is assumed in Figure 3. Three types of isolation bearings with different mechanical characteristics are used on the abutments and piers. The mechanical characteristics of each isolation unit are summarized in Figure 3.

As listed in Table 1, ten recorded earthquake ground motions and three design earthquakes are employed to excite the bridge in the longitudinal direction. These three design response spectra are: (1) the AASHTO isolation design spectrum with A = 0.4 and soil type = S1 (Guide Specifications 1991); (2) the CALTRANS design ARS curves S.6GA51 (Gates 1979); and (3) the JPWRI design spectrum S_{20} with soil type I (Manual 1992). Artificial ground acceleration time histories compatible with the AASHTO and CALTRANS design spectra are generated (Xu et al 1990). The standard acceleration time history compatible with the S_{20} spectrum for soil type I provided in the JPWRI manual (Manual 1992) is used. The design spectra and JPWRI standard S_{20} ground acceleration time history are shown in Figures 4 and 5 respectively.

In the analysis the bridge deck is assumed to be much stiffer than the base isolators and other bridge components in the longitudinal direction. A nominal 5% damping ratio is presumed for various components other than the isolation units. The foundation is assumed to be fixed.

The analysis results show that the convergence of the iteration procedure is satisfied for the analyses using these 13 earthquake ground motions in spite of different initial trials for the maximum displacements. A typical example is given in Figure 6 where the equivalent elastic analysis converges to the same displacement response despite of different initial trials of the design displacements.

The maximum seismic responses of the bridge subjected to the 13 earthquake ground motions in the longitudinal direction are summarized in Table 1 where the maximum displacements at the bridge deck and the corresponding total shear forces are calculated using two Caltrans methods, AASHTO equivalent elastic method and JPWRI bearing capacity method (Kawashima 1992). In addition, the inelastic solutions obtained using the computer program DRAIN-2D (Kanaan and Powell 1973) are used as exact solutions for comparison purposes. From Table 1 it is observed that the accuracy of prediction using various equivalent elastic models are acceptable for the purpose of practical design. The largest difference occurs when the bridge is subjected to the 1966 Parkfield earthquake which was characterized as an earthquake with larger dispersion (Wu and Hanson 1991). From Table 1 it is also realized that the accuracy of prediction using equivalent elastic methods also depends on earthquake ground motions.

CONCLUSIONS

Two methods proposed by CALTRANS are summarized in this paper. The analysis results from Caltrans proposed methods are compared with those from AASHTO and JPWRI equivalent elastic analysis methods and the inelastic solutions of DRAIN-2D. For the 5-span example bridge subjected to 3 design earthquakes and 10 recorded ground motions, all of the equivalent elastic models implemented with an iteration process predict the maximum inelastic seismic responses with acceptable accuracy. From a practical engineering standpoint, these equivalent elastic analysis methods may be appropriate for the seismic analysis and design of base-isolated regular bridges. However, it is realized from Table 1 that the accuracy of prediction is also earthquake dependent. The development of more sophisticated equivalent elastic analysis models with the consideration of certain important characteristics of earthquake ground motions may be helpful in improving the accuracy of prediction.

REFERENCES

Chang, K.C., Soong, T.T., Oh, S.T. and Lai, M.L. (1992). "Effect of Ambient Temperature on Viscoelastically Damped Structure." Journal of Structural Engineering, ASCE, Vol. 118, No. 7, pp. 1955-1973.

Design of Lead-Rubber Bridge Bearings. (1983). Civil Division Publication 818/A, New Zealand Ministry of Works and Development, Wellington, New Zealand.

Gates, J.H. (1979). "Factors Considered in the Developmentof the California Seismic Design Criteria for Bridges." Workshop on the Earthquake Resistance of Highway Bridges, Applied Technology Council, California.

Guide Specifications for Seismic Isolation Design. (1991). American Association of State Highway and Transportation Officials,Washington, D.C.

Hwang, J.S. and Sheng, L.H. (1993)."Effective Stiffness and Equivalent Damping of Isolated Bridges." Journal of Structural Engineering, ASCE, Vol. 119, No. 10, pp. 3094-3101.

Iwan, W.D. (1980). "Estimating Inelastic Response Spectra from Elastic Spectra." Earthquake Engineering and Structural Dynamics, Vol. 8, 375-388.

Johnson, C.D., and Kienholz, D.A. (1982). "Finite Element Prediction of Damping in Structures with Constrained Viscoelastic Layers." AIAA Journal, Vol 20, No. 9, pp. 1284-1290.

Kanaan, A.E. and Powell, G.H. (1973). "DRAIN-2D, A General Purpose Computer Program for Dynamic Analysis of Inelastic Plane Structures." Report No. UCB/EERC-73/6 and 73/22, Earthquake Engineering Research Center, University of California, Berkeley.

Kawashima, K. (1992). "Manual for Menshin Design of Highway Bridges." The Second U.S.-Japan Workshop on Earthquake Protective Systems for Bridges, Publica Works Research Institute, Tsukuba City, Japan.

Manual for Menshin Design of Highway Bridges. (1992). Public Work Research Institute, Tsukuba City, Japan (in Japanese).

Mayes, R.L., Buckle, I.G., Kelly, T.E. and Jones, L.R. (1992). "AASHTO Seismic Isolation Design Requirements for Highway Bridges." Journal of Structural Engineering, ASCE, Vol. 118, No. 1, pp. 284-304.

Raggett, J.D. (1975). "Estimating Damping of Real Structures." Journal of Structural Division, ASCE, Vol. 101, No. ST9, pp. 1823-1835.

Soong, T.T. and Lai, M.L. (1991). "Correlation of Experimental Results with Predictions of Viscoelastic Damping for a Model Structure." Proceeding Damping 1991, Air Force Systems Command, Wright-Patterson Air Force Base, Ohio, FCB1-7.

Standard Specifications for Seismic Design of Highway Bridges. (1991). American Association of State Highway and Transportation Officials, Washington, D.C.

Turkington, D.H., Carr, A.J., Cooke, N. and Moss, P.J. (1989). "Seismic Design of Bridges on Lead-Rubber Bearings." Journal of Structural Engineering, ASCE, Vol. 115, No. 12, pp. 3000-3016.

Wu, J. and Hanson, R.D. (1989). "Study of Inelastic Spectra with High Damping." Journal of Structural Engineering, ASCE, Vol 115, No. 6. pp. 1412-1431.

Xu, J., Philippacopoulas, A.J., Miller, C.A. and Costantino, C.J. (1990). "CARES -- Computer Analysis for Rapid Evaluation of Structures." NUREG/CR-5588, U.S. Nuclear Regulatory Commission, Washington, D.C.

Earthquake Ground Motions	DRAIN-2D		AASHTO		CALTRANS 1		CALTRANS 2		JPWRI	
	D (cm)	F (KN)	D (cm)	F (KN)	D (cm)	F (KN)	D (cm)	F (KN)	D (cm)	F (KN)
AASHTO Design Earthquake A=0.4, Soil=S1	9.1	3131.9	9.8	3300.7	8.5	3000.7	8.7	3059.6	9.5	3677.4
CALTRANS ARS Design Curve S.6GA51	22.4	6966.3	30.4	8711.0	27.4	7175.3	24.8	6601.2	28.4	7862.0
JPWRI Design Earthquake S_{20}, Soil=1	31.4	8028.0	36.9	9252.3	40.7	10102.8	38.4	9594.2	35.7	9479.4
1940 Imperial Valley El Centro (N-S)	6.2	2492.5	5.1	2252.4	7.3	2740.3	7.5	2791.8	5.8	2845.0
1989 Loma Prieta (00) Capitola -- Fire Station	10.9	3537.3	14.0	4217.4	12.8	3961.8	13.5	4108.3	16.1	5156.2
1989 Loma Prieta (00) Corralitos - Eureka Canyon Road	9.2	3132.1	6.3	2521.8	7.7	2839.3	8.0	2892.2	7.4	3223.8
1989 Loma Prieta (200) Oakland - 2-Story Building	9.5	3225.1	12.1	3801.8	10.5	3443.6	11.0	3559.3	14.0	4697.1
1989 Loma Prieta (290) Oakland -- 2-Story Building	26.0	6829.8	27.2	7129.9	26.6	6987.7	26.6	6982.2	29.9	8201.4
1949 Olympia (N86E) Washington Highway Test Lab	3.9	1998.9	4.3	2083.3	3.6	1926.1	3.8	1975.8	3.5	2321.2
1966 Parkfield (N65E) Cholame Shandon	19.0	5317.8	26.3	6935.4	27.6	7219.7	26.2	6894.1	25.9	7322.5
1992 Petrolia (E-W) Panter Street Overpass	10.6	3472.9	11.2	3595.9	9.4	3215.0	10.9	3547.5	10.0	3789.8
1992 Petrolia (N-S) Panter Street Overpass	7.3	2492.5	7.3	2739.4	9.0	3123.5	9.4	3201.4	8.3	3417.0
1971 San Fernando Pacoima Dam (S74W)	32.9	8346.0	37.3	9349.3	33.6	8524.3	32.1	8195.6	38.0	9985.3

TABLE 1 Comparison Between Inelastic and Equivalent Elastic Analysis Results

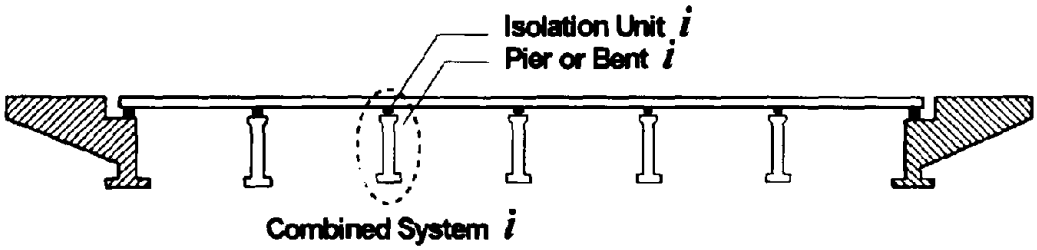

Figure 1 A Base-Isolated Regular Bridge

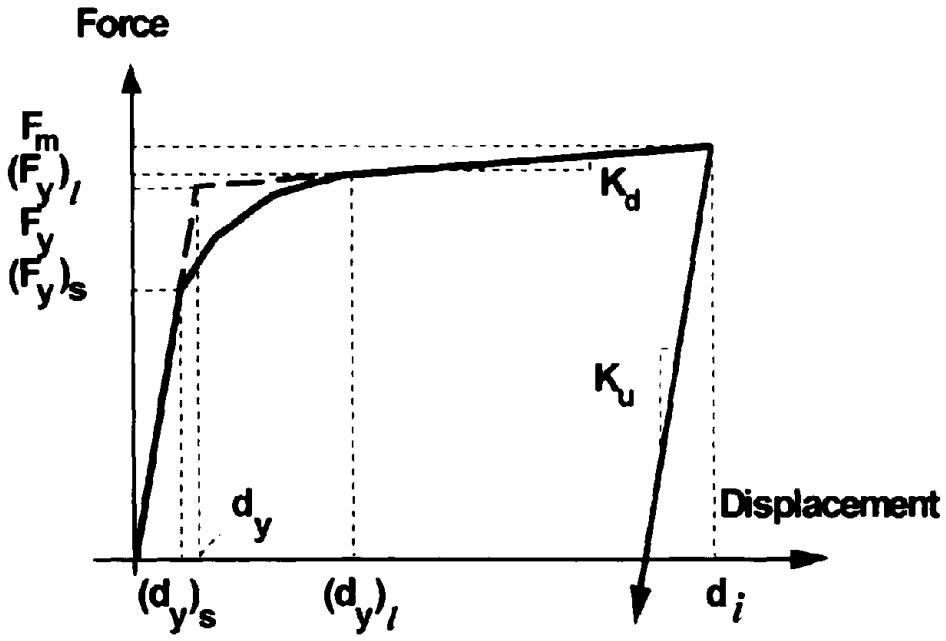

Figure 2 Idealization of A Multi-linear Model by A Bi-linear Model

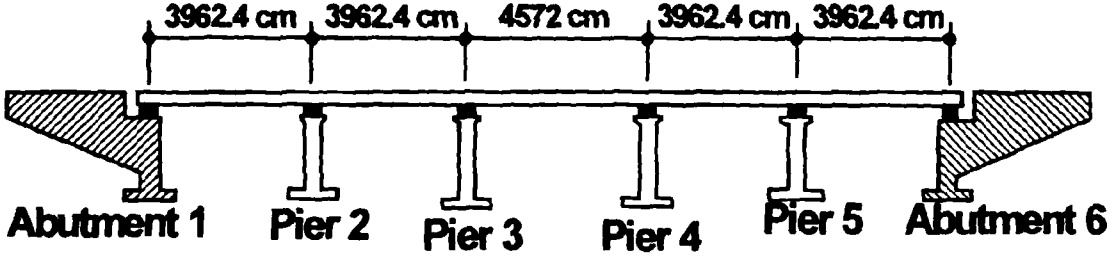

Abutments 1 & 6 :

$(K_p)_{1,6} = 402791.8$ kN/m

$(K_u)_{1,6} = 12686.2$ kN/m

$(K_d)_{1,6} = 1954.4$ kN/m

$(F_y)_{1,6} = 145.9$ kN

Piers 2 & 5 :

$(K_p)_{2,5} = 52538.1$ kN/m

$(K_u)_{2,5} = 32510.5$ kN/m

$(K_d)_{2,5} = 5001.6$ kN/m

$(F_y)_{2,5} = 291.8$ kN

Piers 3 & 4 :

$(K_p)_{3,4} = 43781.7$ kN/m

$(K_u)_{3,4} = 32510.5$ kN/m

$(K_d)_{3,4} = 5001.6$ kN/m

$(F_y)_{3,4} = 291.8$ kN

Total Weight of Superstructure :

$W = 22018.7$ kN

Figure 3 An Example Bridge and Mechanical Characteristics of Isolation Units

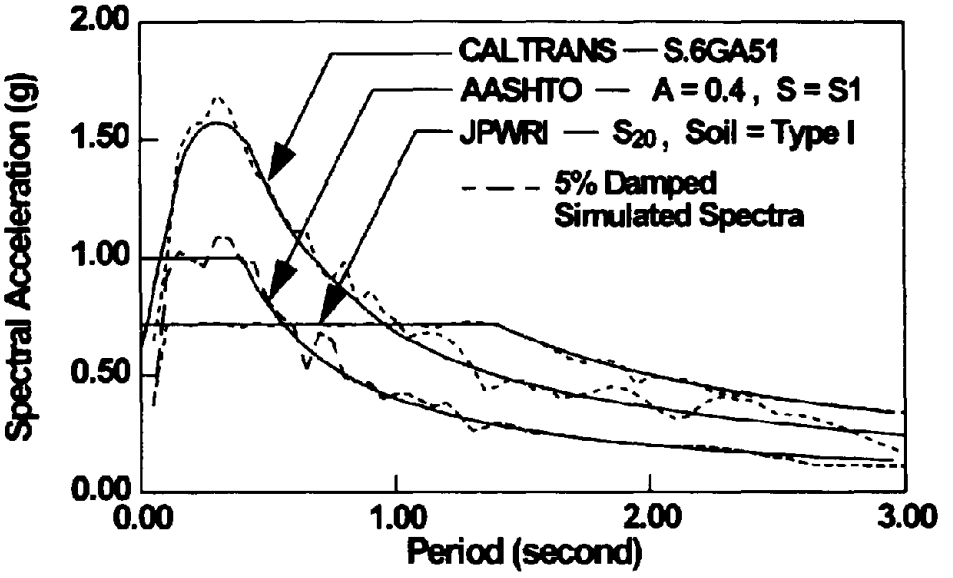

Figure 4 AASHTO, CALTRANS and JPWRI 5% Damped Design Spectra

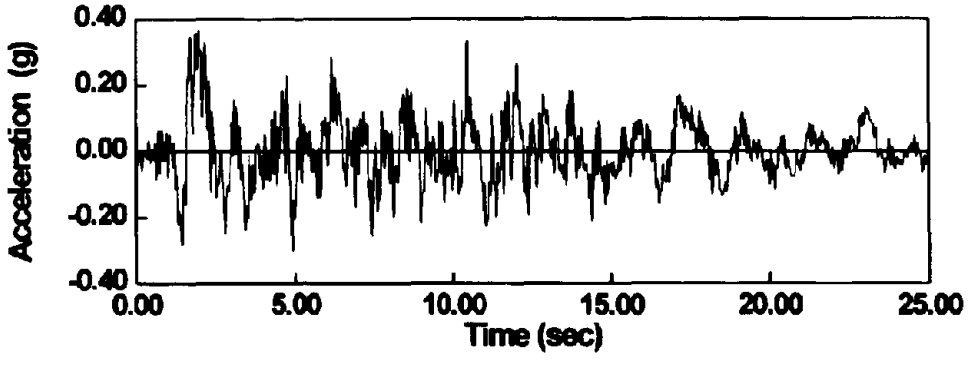

Figure 5 Standard Acceleration Time History Compatible with JPWRI S_{20} Design Spectrum

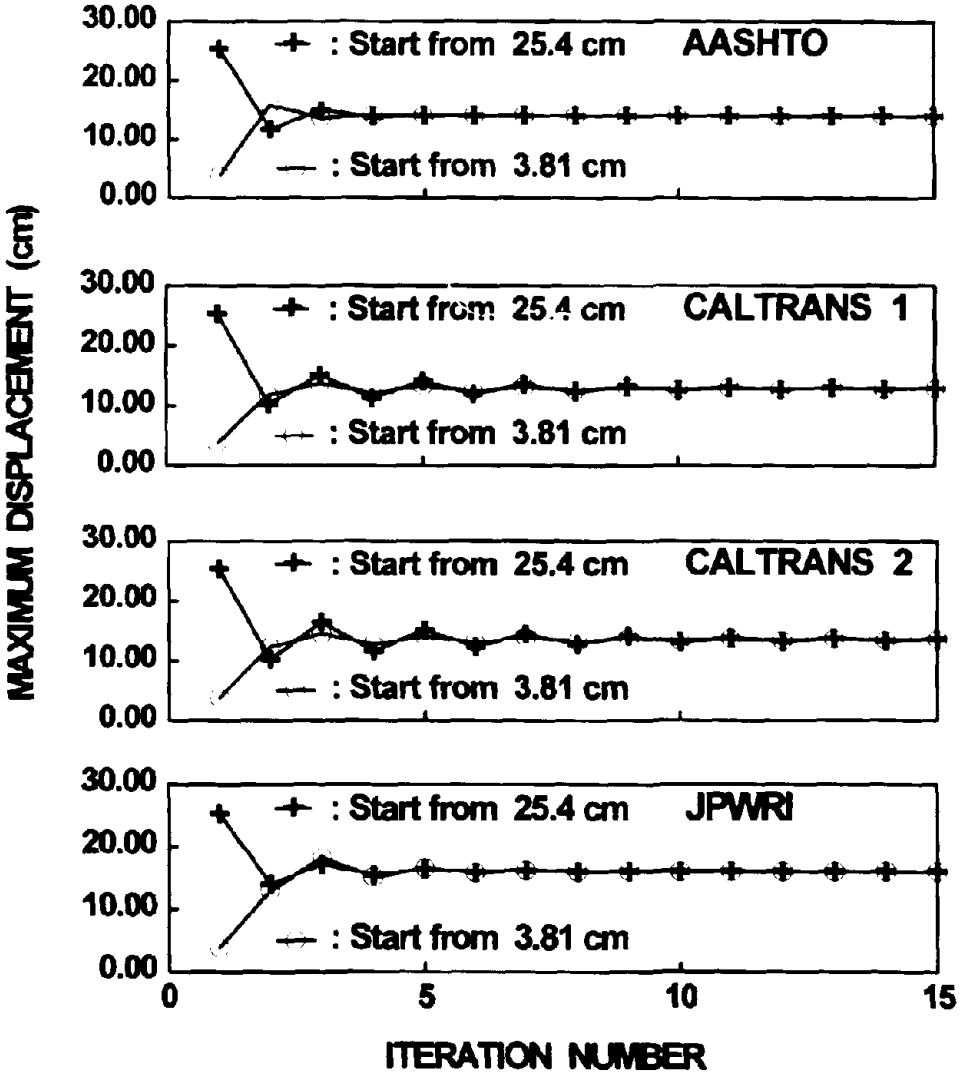

Figure 6 Convergence of Iteration Procedure – 5-Span Example Bridge Subjected to 1989 Loma Prieta Earthquake Measured at Capitola

DESIGN OF A MENSHIN BRIDGE ON SOFT GROUND

by Akio Hayashi
Research Department, Pacific Consultants Co., Ltd., Tokyo, Japan

A B S T R A C T

As the seismic motion in soft ground contains relatively long period components, their effects are not easily discernable. Therefore, in a soft ground area the application of the Menshin (seismic isolation) design method is not recommended.

To satisfy the severe seismic resisting conditions that are required on soft ground, it is believed that inertial force reduction by applying Menshin is a beneficial means for the design of bridge structures on soft ground.

In Japan, many bridge construction sites are located on soft ground classified as Type III Ground. Thus, it is important to determine whether or not Menshin should be applied in soft ground areas.

In this paper the author made an examination to determine whether or not the Menshin design is applicable on soft ground by using the design seismic wave that is to be used on Type III Ground.

In the examination, the following three items were major subjects:
- How to determine Menshin characteristics that can attain a sufficiently long period of motion and energy dissipation.
- If it is possible to make bridge piers slimmer by the selected Menshin devices' inertial force reduction effect.
- Is the Menshin bridge safe even when the pier members become plastic condition during an extra large earthquake?

Regarding the first item, the author felt that it would be convenient to use charts when examining the appropriateness of the seismic isolation characteristics for selection. In this paper the author proposes the method for preparing the charts.

As for the second item, a model bridge was used for the study and the bridge's practical characteristics were selected by using the charts and the range of how much the pier columns could be made slimmer was then confirmed.

Regarding the third item, the level of safety against the plastic condition was evaluated by using the equivalent linear analysis method, the equivalent energy analysis method, and the nonlinear time-history response analysis method.

INTRODUCTION

As for the design criteria of an earthquake resistant design, two stages of design earthquakes are to be given by taking into consideration the relationship between the bridge's service life and the earthquake's return period. One stage is the seismic coefficient method in which stresses caused by seismic motions in each member of the structure must be less than the allowable stress. In the case

where a bridge has Menshin devices, each beam must not hit other beams nor the abutment parapet.

The other stage is the ultimate lateral strength method during earthquakes. In this method, the plastic condition created in part of a structure is unavoidable. But, a sufficient allowance for the final strain must be provided.

As the seismic restoring force characteristics of Menshin devices change according to the amount of displacement, an optimum bridge designed using one of the above mentioned criteria may not be optimum for the other criteria.

Therefore, it is necessary to establish the characteristics of the Menshin devices by equally evaluating the seismic response of the structures to the two types of seismic motions. For this reason, the author thought that it would be more appropriate to evaluate the characteristics by using charts rather than by mathematically analyzing the optimum values.

The design seismic spectrum in Type III Ground is shown in Fig. 1

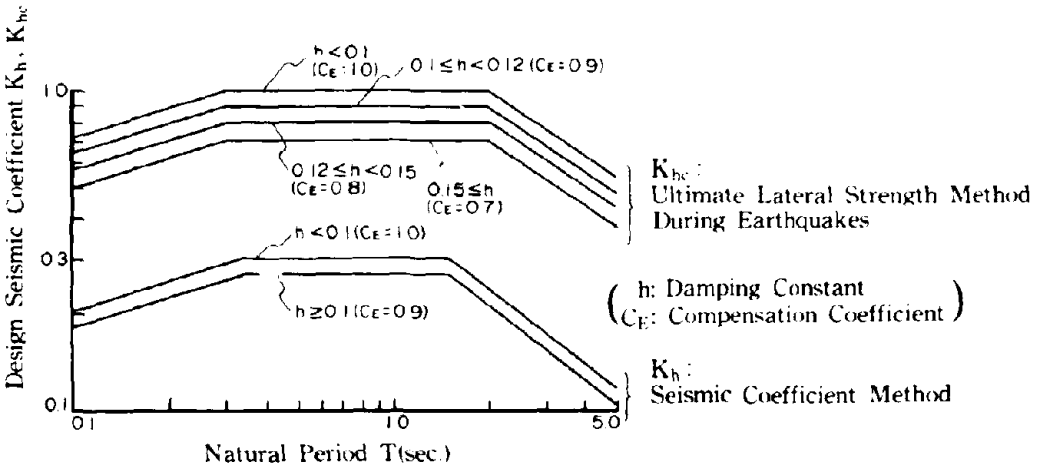

Fig.1 Relationship between the Design Seismic Coefficient, and the Natural Period T and the Damping Constant h

A CHART FOR ESTABLISHING SEISMIC ISOLATION CHARACTERISTIC VALUES

In the design of an ordinary bridge, inertial force due to the mass of the superstructure is predominant and the mass of the substructure may be neglected. In the parameter study, the bridge model can be simplified and, as shown in Fig.

2, a model of single mass and single degree of freedom consisting of the mass of the superstructure, the restoring force characteristics of the Menshin devices, and the resturing force characteristics of the substructure is adopted.

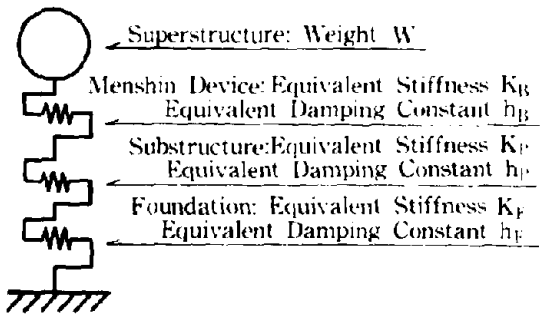

Fig. 2 Bridge Model for Parameter Study

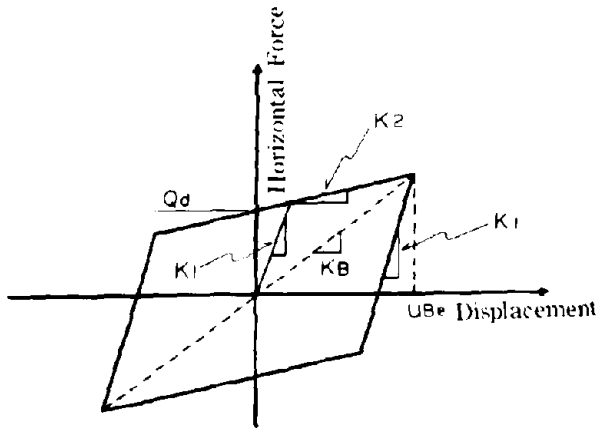

Fig. 3 Relationship Between Menshin Devices' Horizontal Force and Displacement

The restoring force characteristics of the Menshin devices were simplified in the bilinear type model shown in Fig.3, and the secant grade stiffness K_B of equation (1) was set as the equivalent stiffness and the damping constant h_B of equation (2) was set as the equivalent damping constant.

$$K_B = \frac{Q_d}{u_{Be}} + K_2 \qquad (1)$$

$$h_B = \frac{\Delta W}{4\pi W} = \frac{2Q_d(u_{Be} + Q_d/(K_2 - K_1))}{\pi \cdot u_{Be}(Q_d + u_{Be} \cdot K_2)} \qquad (2)$$

where, Q_d is an apparent yield load that is the value on the vertical axis in Fig. 3 in which the Menshin devices are assumed to have bilinear type restoring force characteristics. K_1 is the first grade stiffness, K_2 the second grade stiffness, ΔW the area enveloped by the hysteresis loop of the Menshin devices, W the area of the triangle OAB. u_{Be} is the effective displacement of the Menshin

devices that is to be 70% of actual displacement u_b. But, u_b is unknown at the outset of the analysis; thus, the u_b value is assumed at the initial stage.

Natural period T of the entire bridge can be obtained from equation (3) and the damping constant h of the entire bridge can be obtained from equation (5).

$$T=2\pi\sqrt{\frac{W}{g\cdot K}} \qquad (3)$$

$$K=\frac{1}{\frac{1}{K_B}+\frac{1}{K_P}+\frac{1}{K_F}} \qquad (4)$$

$$h=\frac{h_B+\frac{h_P\cdot K_B}{K_P}+\frac{h_F\cdot K_B}{K_F}}{1+\frac{K_B}{K_P}+\frac{K_B}{K_F}} \qquad (5)$$

where, g is the acceleration of gravity, K the stiffness of the entire bridge shown by equation (4), K_P the equivalent stiffness of the substructure, K_F the equivalent stiffness of the foundation, h_P the equivalent damping constant of the substructure, h_F the equivalent damping constant of the foundation. As the values of the natural period T in equation (3) are different for the seismic coefficient method and for the ultimate lateral strength method during earthquakes, the value for the former method is indicated as T_s and the value for the latter method is indicated as T_c in this paper. In the parameter study it was assumed that the entire pier section is effective for the stiffness of the pier column. The softening effect that may occur in the plastic condition during a severe earthquake was neglected.

The initially unknown displacement u_B of the Menshin devices can be obtained by equation (6). If the calculated value deviates from the initially assumed value, use the calculated value as u_B and repeat the above calculation. After processing several iterations, a sufficiently accurate u_B value can be obtained.

$$u_B=\frac{W\cdot K_h}{K_B} \qquad (6)$$

where K_h is the design seismic coefficient shown in Fig. 1. In the ultimate lateral strength method, K_{hc} vice K_h should be used.

The Menshin devices are rubber bearings having lead plugs. The rubber bearings' restoring force characteristics can be obtained by equations (7) through (12).

$$Q_d = A_P \cdot q_0 \qquad (7)$$

$$K_1 = 6.5 K_2 \qquad (8)$$

$$K_2 = \frac{F - Q_d}{u_B} \qquad (9)$$

$$F = A_R \cdot G \cdot \gamma + A_P \cdot q \qquad (10)$$

$$\gamma = \frac{U_{Be}}{\Sigma te} \qquad (11)$$

$$q = -283.6\gamma^2 + 183.8\gamma + 85.0 \quad (0 \le \gamma \le 0.5)$$
$$q = 28.3\gamma^2 - 128.1\gamma + 163.0 \quad (0.5 < \gamma \le 2.0) \qquad (12)$$
$$q = 20 \quad (2.0 < \gamma \le 2.5)$$

where, A_p is the cross sectional area of the lead plug, q_0 the shear stress of the lead plugs under yield load (85.0 kgf/cm²), A_R the cross sectional area of the rubber bearings, G shearing modulus of rubber (10 kgf/cm²), γ effective strain of rubber, q the shear stress of the lead plugs (kgf/cm²), and Σte the total thickness of the rubber bearing.

Grades K_1 and K_2 in the restoring force characteristics of Menshin devices are not specific values for the devices. They vary according to the displacement of Menshin devices (rubber's strain). Specific values for given Menshin devices are A_R, Σte, and A_p. By determining these three values, Menshin devices restoring force characteristics can be decided upon.

The parameter study can be carried out according to the following procedures: In equation (3), the bridge's natural period T has two values because the stiffness K is different for the seismic coefficient method and for the ultimate lateral strength method. To distinguish the two different natural periods, suffixes are added as T_1 for the seismic coefficient method and T_2 for the ultimate lateral strength method. Once the natural period T_2 for the ultimate lateral strength method is determined, the stiffness K can be obtained by equation (3) because the superstructure's weight W is known. The pier's

stiffness K_1 and the foundation's stiffness K_f are known. Thus, the Menshin devices' equivalent stiffness K_e can be obtained by equation (4). The Menshin devices' second grade stiffness K_2 can be calculated by equation (13) that was derived from equation (1). The Menshin devices' displacement u_s is the value obtained by equation (6).

$$K_2 = K_B - \frac{Q_d}{U_{te}} \qquad (13)$$

Once Q_d and Σte are decided upon, then, given Menshin devices' specific values A_R, Σte, and A_1 can be determined by equations (7) through (12). The rubber layers' total thickness Σte is to be obtained by equation (14). γ_c in equation (14) is the rubber layers' strain that is empirically recommended to be 70% of the allowable strain of rubber material.

$$\Sigma te = \frac{u_{se}}{\gamma_c} \qquad (14)$$

Seismic response of the bridge by the seismic coefficient method can be obtained by equations (3) through (5) and (7) through (12) using the Menshin devices' A_R, Σte, and Q_d values. At the beginning of the series of these calculations, the Menshin devices' displacement u_s is unknown. Thus, an assumed u_s value should be used at the first stage and the calculations should be repeated until the value agrees with the one obtained by equation (6).

To figure out the parameter study result in order to reference the characteristic values, each parameter should be expressed as a general index without regarding the weight of the superstructure as follows: The yield load ratio should be set up by dividing the Menshin devices yield load Q_d by the superstructure's weight W as Q_d/W, and the parameter of the stiffness of the Menshin devices should be indicated by using the natural period of the entire bridge that can be calculated by equation (3).

The characteristics in equations (3) through (5) that are not specific values are the substructure's stiffnesses K_p and K_f and the damping constants h_p and h_f. If the substructure's structure type and height do no substantially deviate, the ratios of K_p and K_f to the superstructure's weight W are almost constant. As the damping constants h_p and h_f can be made non-dimensional values, the chart drawn by those characteristic values can be thought to provide general indexes for practical use. Thus, the clarified result by investigation using variable parameters can provide useful indexes for selecting the Menshin devices' characteristic values at the early design stage.

SELECTION OF MENSHIN CHARACTERISTIC VALUES

Fig. 4 shows a model bridge for parametric study as an example. The superstructures are 50m long steel box girders that weigh 750 tons each. The 15 m high substructures are made of reinforced concrete. The foundations are the cast-in-place reinforced concrete pile type having 1.0 m diameter piles. The

Menshin devices' yield load ratio Q_y/W was changed within a range of between 1% to 17% while the rubber stiffness was gradually changed from absolute stiff towards a less stiff value.

Soft ground, known in Japan as Type III Ground in the seismic design code, was selected for the example. The relationships between the bridge's design seismic coefficients and the damping constant, and the generalized parameters Q_y/W and T_s are shown in Figs. 5 through 8.

Natural periods shown as T_s on the horizontal axes in Figs. 5 and 6 were calculated from equations (3) and (4) by using the equivalent stiffness of the Menshin devices under the design seismic coefficients for the ultimate lateral strength method.

Figs. 7 and 8 show the results obtained by using the seismic coefficient method; but, the natural period is shown as T_s vice T_s on the horizontal axes and is the same as those shown in Figs. 5 and 6. Thus, the same values of T_s correspond to the same Menshin devices.

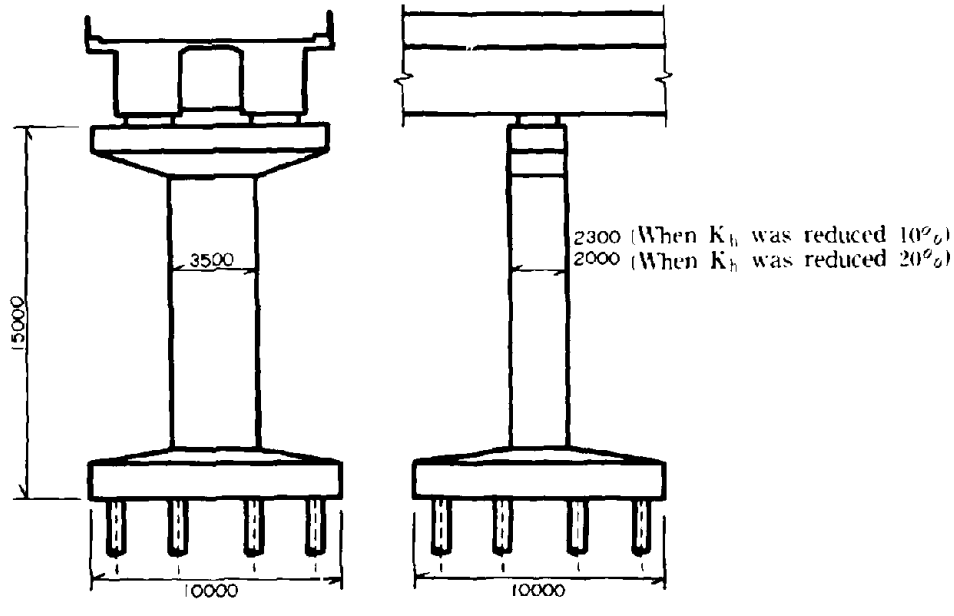

Fig. 4. General Features of a Model Bridge

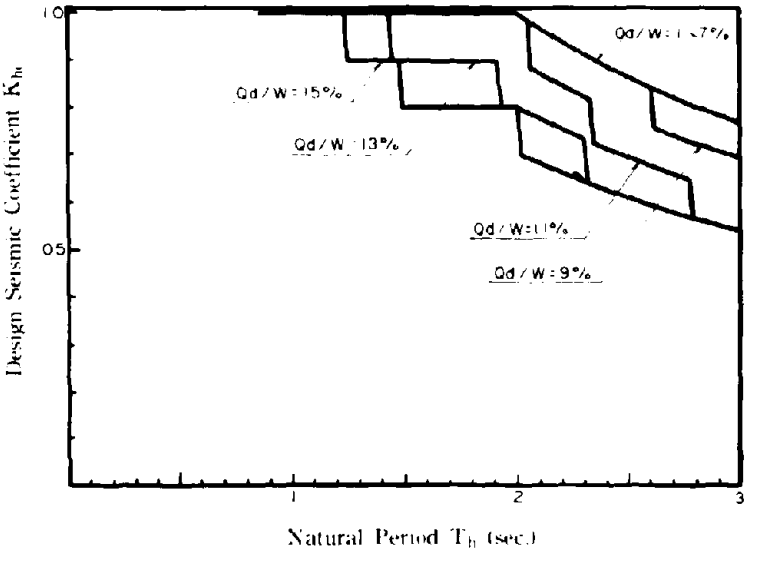

Fig. 5 Relationship between the Natural Period T_1 and the Menshin Devices' Yield Load Ratio Q_d/W, and the Design Seismic Coefficient (Ultimate Lateral 22Strength Method)

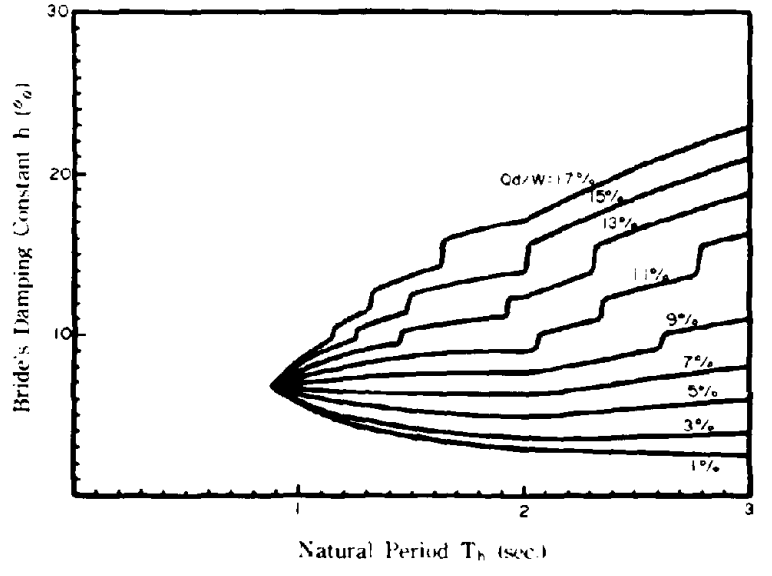

Fig. 6 Relationship between the Natural Period T_1 and the Menshin Devices' Yield Load Ratio Q_d/W, and the Bridge's Damping Constant h (Ultimate Lateral Strength Method)

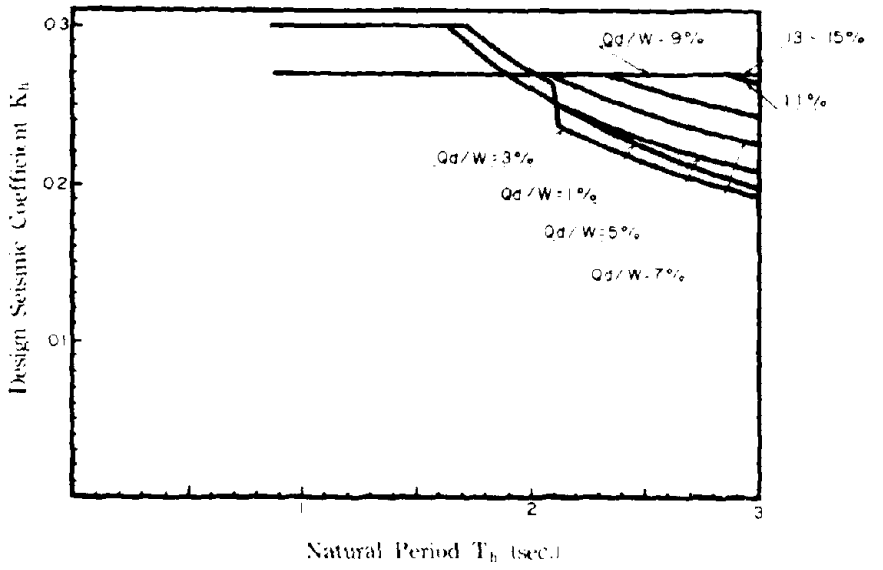

Fig. 7 Relationship between the Natural Period T_h and the Menshin Devices' Yield Load Ratio Q_d/W, and the Design Seismic Coefficient (Seismic Coefficient Method)

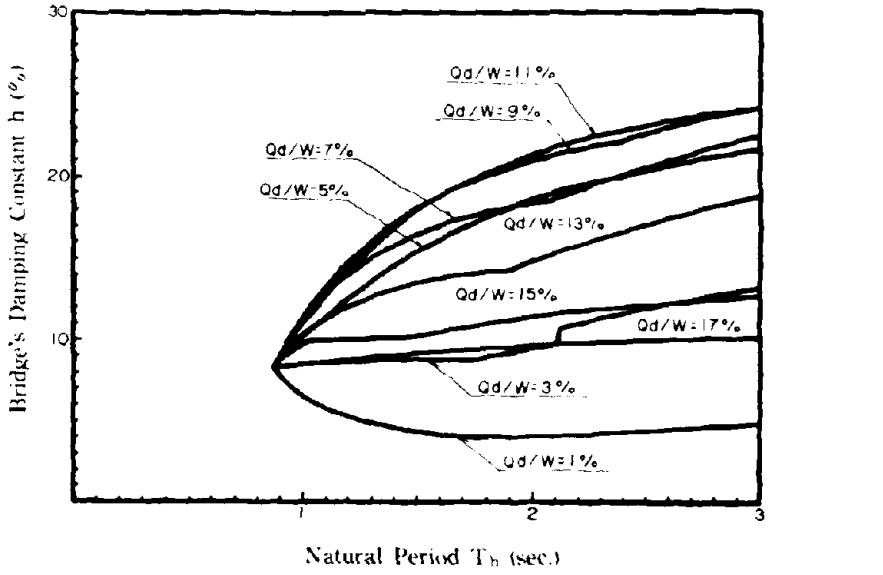

Fig. 8 Relationship between the Natural Period T_h and the Menshin Devices' Yield Load Ratio Q_d/W, and the Bridge's Damping Constant h (Seismic Coefficient Method)

From Fig. 6, it can be seen that the bridge's damping constant in the ultimate lateral strength method increases according to the increase of the yield load ratio Q_d/W of the Menshin devices in the range of 1 to 17% of Q_d/W. On the other hand, from Fig. 8, it can be seen that the bridge's damping constant in the seismic coefficient method becomes maximum at about Q_d/W=11% then decreases when Q_d/W exceeds 11%.

In the seismic coefficient method, the compensating coefficient rate c, that is based on the damping constant h becomes 0.9 when the bridge's damping constant exceeds 10% and the design seismic coefficient decreases due to the energy dissipating effect. As a result, the substructure's material amount can be reduced.

In Fig. 8, the area where the bridge's damping constant in the seismic coefficient method exceeds 10% is in a range where the yield load ratio Q_y/W is greater than 3% but less than 15%. This area is thought to be the boundary of Q_d/W in which it is possible to reduce the substructure's material amount. Thus, from Figs. 5 through 8, three cases of the combinations of the characteristic values that may possibly be used for practical design were selected and adopted for the design of this example.

In Case 1, the maximum value of Q_d/W was set as 15% and the natural period T_2 was set as 1.6 seconds to limit the amount of the displacement of the Menshin devices. If T_2 is less than 1.6 seconds, the thickness of the Menshin devices becomes too thin and the lead plugs' width to length ratio becomes less than 1.25 [6] which is recommended to be the empirical limit value.

This case was intentionally selected to accomplish the Menshin devices' energy dissipating effect without much period shift effect.

In Case 2, Q_d/W and T_2 were so assorted that the design seismic coefficients K_2 and $K_{2'}$ could be the minimum, then Q_d/W=8.6% and T_2=2.9 seconds were selected.

In Case 3, Q_d/W was set as the lower limit 3%, and T_2 was set relatively long as 2.2 seconds. This case was intended mainly for the period shift effect but not for counting much energy dissipating effect of the Menshin devices.

The obtained structural responses are shown in Table 1. The dimensions and material characteristics of the Menshin devices are shown in Table 2.

Table 1 Structural Response When Menshin Devices Were Used

	Case 1	Case 2	Case 3
Seismic Isolation Devices' Specific Yield Load Ratio Q_y/W(%)	15.0	8.6	3.0
Ultimate Lateral Strength Method:			
Bridge's Natural Period T_r(s)	1.6	2.9	2.2
Seismic Isolation Devices' Damping Constant h_g(%)	15.92	10.71	2.88
Bridge's Damping Constant h(%)	12.96	10.15	3.54
Design Seismic Coefficient K_r	0.8	0.7	0.94
Substructure's Bearable Seismic Coefficient	0.945	0.723	0.945
Seismic Isolation Devices' Displacement u_g(cm)	35.75	129.9	95.21
Seismic Coefficient Method:			
Bridge's Natural Period T_r(s)	0.769	1.895	1.852
Seismic Isolation Devices' Damping Constant h_g(%)	15.19	26.87	11.14
Bridge's Damping Constant h(%)	10.40	23.77	10.94
Design Seismic Coefficient K_r	0.27	0.23	0.23
Substructure's Bearable Seismic Coefficient	0.27	0.24	0.27
Seismic Isolation Devices' Displacement u_g(cm)	1.30	17.60	18.16

Table 2 Details of Seismic Isolation Devices

		Case 1	Case 2	Case 3
Lead Plug	Number	4	1	1
	Diameter D_p(cm)	14.5	22.0	13.0
Rubber Layer	Shearing Modulus (kgf/cm²)	10	8	10
	Size (cm)	115 x 115	145 x 145	120 x 120
	Total Thickness Σte (cm)	17.0	94.3	39.2
	Layer Thickness te (cm) x Number	3.4cm x 5	2.3cm x 41	2.8cm x 14

When rearranging the dimensions of the pier whose cross sectional area was reduced by the effect of the Menshin design, the obtained results are as follows: The pier column width in the beam direction was 2.6m without Menshin devices. But, with Menshin devices, it became 2.3m in Cases 1 and 3 and 2.0m in Case 2. The design seismic coefficient K_r could be reduced by 10% in Cases 1 and 3 and 20% in Case 2 comparing with the coefficient without Menshin devices.

EFFECT OF PLASTIC CONDITION IN SUBSTRUCTURE

In the investigation at the early design stage, the stiffness of the pier column

was regarded as the stiffness of the yield point. It is believed that the effect of the substructure's plastic condition can be neglected to reduce repetitive calculations when the preliminary investigation is to be conducted. Thus, the value k_{hc} that was obtained in the calculation was a provisional one. The value $k_{hc} \cdot W$ was compared with the column's allowable strength P_a obtained by equation (17) to examine the stability of the pier column. The value k_{he} obtained by equation (15) is based on the equivalent energy method.

$$k_{he} = \frac{k_{hc}}{\sqrt{2\mu_a - 1}} \tag{15}$$

$$\mu_a = 1 + \frac{\delta_u - \delta_y}{\alpha \cdot \delta_y} \tag{16}$$

$$P_a = P_y + \frac{P_u - P_y}{\alpha} \tag{17}$$

where, δ_u and δ_y are the substructure's displacements at its ultimate and yielded stages. The safety factor of α is 1.5. P_u and P_y are the horizontal forces on the pier column at the ultimate and yield stages. μ_a is the allowable ductility ratio.

EVALUATION OF THE PLASTIC CONDITION AT THE PIER BOTTOM WITH OTHER METHOD

In this section the author examined further the plastic condition of the pier bottom by using a different method. In the procedure, the calculations were made by equally linearizing not only the Menshin devices' characteristics but also the pier's restoring force characteristics. Then, the ductility ratio μ created by the substructure's deflection displacement δ was obtained. The ductility ratio μ obtained by equation (18) is to be compared with the allowable ductility ratio μ_a of the pier column when the stability of the pier column is being examined. The allowable ductility ratio μ_a of the pier column can be obtained by equation (16).

$$\mu = \frac{\delta}{\delta_y} \tag{18}$$

In this procedure, the hysteresis loop was prepared by setting up the relationship between the substructure's horizontal force and the displacement as shown in Fig. 9 by referencing the continually degrading model that was proposed as the reinforced concrete member's time-history restoring force characteristic model.[3] The author thought that the substructure's restoring force characteristic would be expressed by the bilinear type hysteresis loop as shown in Fig. 10, and obtained the equivalent stiffness K_e by equation (19) and the equivalent damping constant h_e by equation (20).

$$K_p = \frac{P_q}{\delta_{pe}} + K_u \qquad (19)$$

$$h_p = \frac{\Delta W}{4\pi W} = \frac{1}{\pi}\left(1 - \frac{P_y + K_u \cdot \delta_{pe}}{K_y \cdot \delta_{pe}}\right) \qquad (20)$$

where, P_y is the value on the vertical axis when the substructure has the bilinear type restoring force characteristic as shown in Fig. 10. K_y is the secant grade stiffness at the yielding time, and K_u is the tangent grade stiffness after yielding. δ_{pe} is the substructure's effective displacement and is 70% of the displacement δ_y.

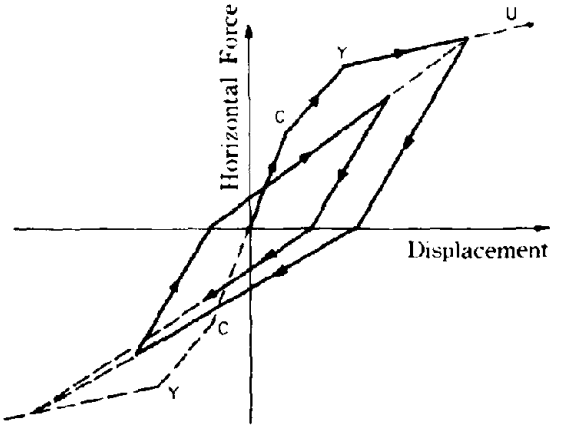

Fig. 9 Relationship between the Horizontal Force on the Substructure and the Displacement's Elasto-plasticity.

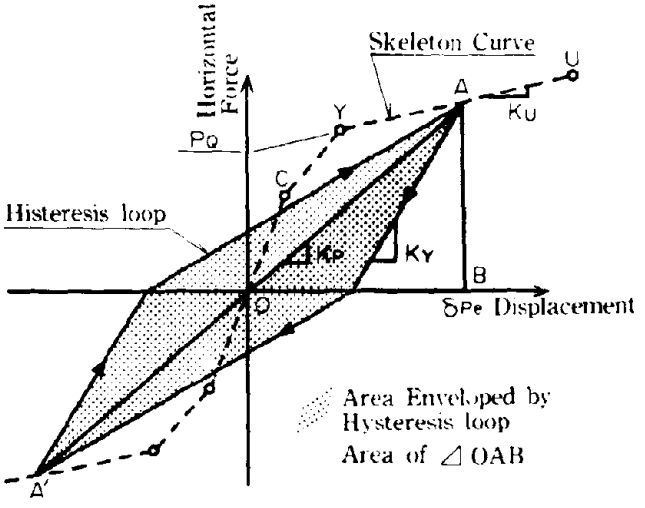

Fig. 10 Equivalent Linearization of the Substructure's Restoring Force Characteristics

The design earthquake used in this section was the standard acceleration response spectrum S_i given by equations (21) and (22). These were proposed by reference 1) as the input seismic motion for evaluating the ultimate lateral strength method.

$$S_i = C_Z \cdot C_I \cdot C_D \cdot S_{i0} \tag{21}$$

$$C_D = \frac{1.5}{40h+1} + 0.5 \tag{22}$$

where, C_I and C_I are compensation coefficients for region and importance respectively. C_D is a compensation coefficient for each damping constant. S_{i0} is given by the standard acceleration response spectrum shown in Fig. 11.

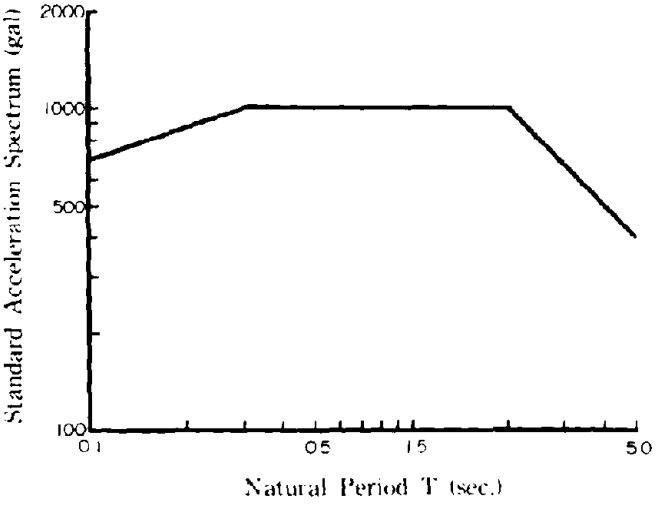

Fig. 11 Standard Acceleration Response Spectrum

The structure model used for the example was the same as the one shown in Fig. 2.

Structure responses obtained by applying the equivalent linear analysis method to the three cases in Table 1 that were used for the ordinary design method are shown in Table 3.

Table 3 Structure Responses Obtained by Applying the Method Described in This Section

	Case 1	Case 2	Case 3
Seismic Isolation Devices' Displacement u_B(cm)	28.88	88.14	67.91
Pier Column's Deflection Displacement δ(cm)	30.12	16.55	29.69
Pier Column's Yield Displacement δ_y(cm)	6.381	7.204	6.381
Pier Column's Ductility Ratio μ	4.720	2.297	4.652
Pier Column's Allowable Plasticity Rate μ_a	2.867	2.429	2.867

NONLINEAR RESPONSE ANALYSIS

The nonlinear time-history response analysis method was applied to the three cases in Table 2. The obtained results were compared with those obtained by the above-mentioned methods. In this analysis, a model having the four masses and seven degrees of freedom shown in Fig. 13 were used.

The time-history characteristic having the bilinear type envelope shape was given

for the Menshin devices' restoring force. The time-history characteristic having the tri-linear type continually degrading model shown in Fig. 9 was given for the pier column's restoring force.

The incident seismic wave used in the example was the standard acceleration wave pattern shown in Fig. 12. The seismic wave was made so that the response spectrum would fit well to the standard acceleration spectrum in Fig. 11.

The results of the analysis are shown in Table 4 and Fig. 14.

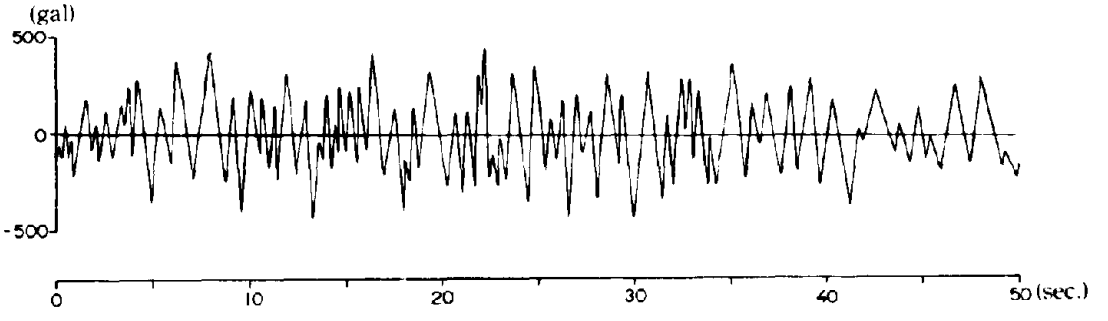

Fig. 12 Incident Seismic Wave

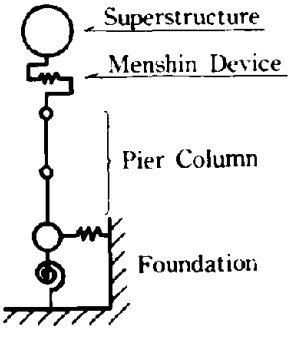

Fig. 13 Structure Model for the Nonlinear Time-history Response Analysis Method

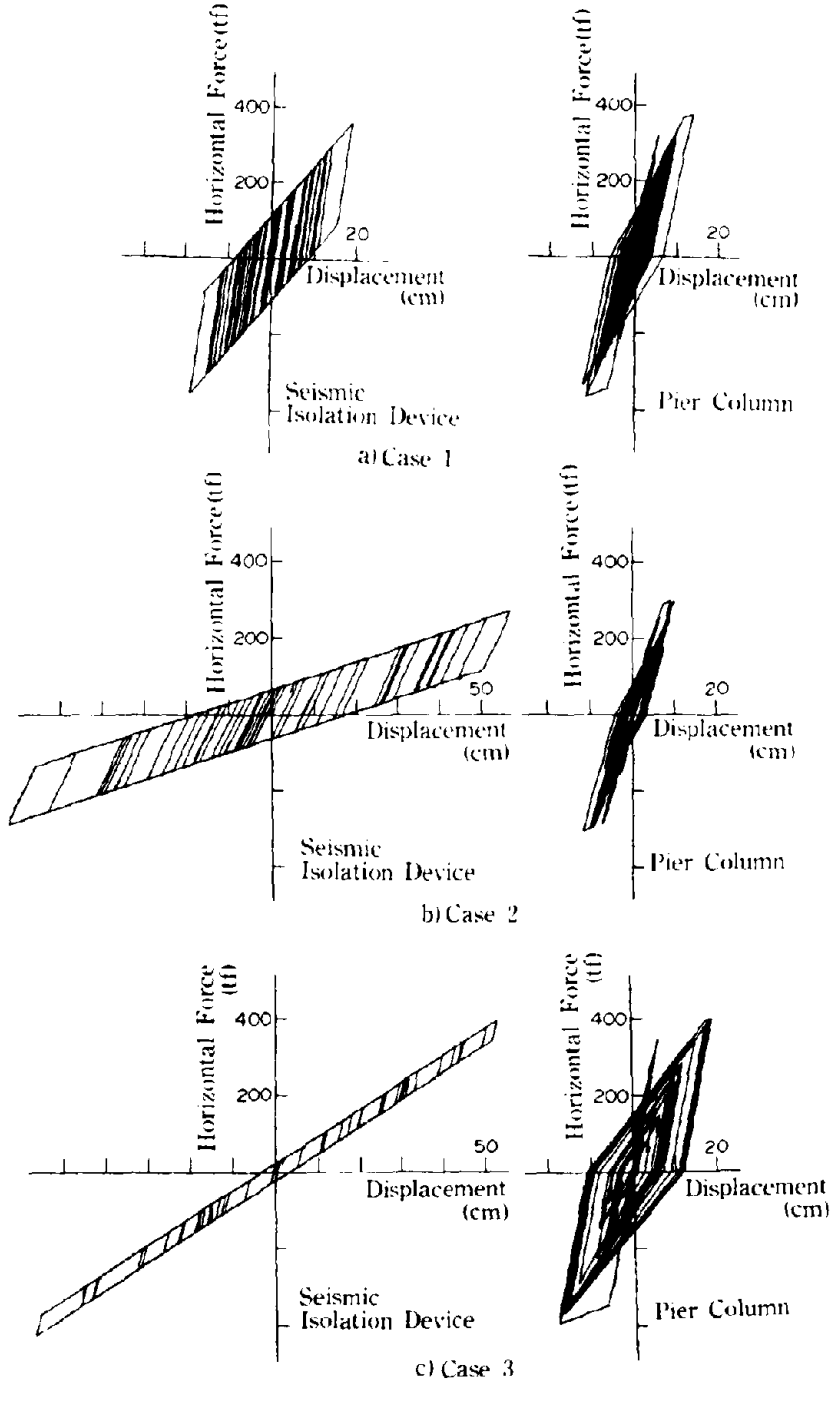

Fig. 14 Time-history of Horizontal Forces Acting on the Menshin Devices and Pier Column and Their Reactions

Table 4 Results of the Nonlinear Time-History Response Analysis

	Case 1	Case 2	Case 3
Seismic Isolation Devices' Displacement u_B(cm)	18.65	62.58	56.72
Pier Column's Deflection Displacement δ_2	13.77	11.79	19.44
Pier Column's Yield Displacement δ_y(cm)	6.381	7.204	6.381
Pier Column's Ductility Ratio μ	2.157	1.637	3.046
Pier Column's Allowable Plasticity Rate μ_a	2.867	2.429	2.867

As seen in Table 4, the ductility ratio μ obtained from the substructure's deflection displacement δ_2 were smaller than the allowable ductility ratio μ_a in Cases 1 and 2.

On the other hand, in Case 3 in which the yield load ratio Q_y/W was set small as 3%, the ductility ratio μ was slightly larger than μ_a and the substructure was evaluated as being uncertain in its plasticity. The Menshin devices' displacement u_B is considerably smaller than the one in Table 1 which was obtained by the ordinary design method. The Menshin devices's displacement value in Table 3 which was obtained by the equivalent linear analysis method is much closer to the value in Table 4 than it is to the one in Table 1. Thus, it can be evaluated that the value in Table 3 indicates a realistic displacement value of the Menshin devices.

As seen in Fig. 14, the Menshin devices demonstrated a constant energy dissipating effect. But, the substructure reached the maximum displacement in the plastic condition within one cycle seismic motion. It is believed that the structure response was controlled by energy dissipation occurring when the displacement exceeded the yield displacement.

CONCLUSION

The following aspects became clear through the examination described in this paper:

1) It is possible to apply the Menshin design method to bridge structures even on soft ground (known in Japan as Type III Ground), and it is possible to make pier columns slimmer even if the amount of the displacement of the Menshin devices' displacement is limited to a certain range.
2) Of the three cases selected at the early design stage, the Menshin devices' displacement of Case 1 was the smallest value, 36 cm. With this level of displacement, it is possible to design a bridge having Menshin devices whose stress would be sufficiently smaller than the allowable amount.
3) In case 2, the Menshin devices' displacement exceeded 120cm. It is thought that the large displacement was calculated because the decrease of the pier column's stiffness due to the plastic condition was not taken into account in the calculation. When the decrease of the pier column's stiffness due to the plastic condition was taken into account, the displacement was calculated as being 88cm. It was also calculated as being 63cm by the

nonlinear response analysis method. Of the three cases, Case 2 showed the largest inertial force reduction effect.

4) In Case 3, the Menshin devices having relatively poor Q_s were selected by mainly expecting the period shift effect but not counting much on the Menshin devices' energy dissipating effect. At the early design stage, this case seemed to be applicable for practical use. But, it was found that the pier would be subjected to an excessive plastic deformation when the bridge is hit by a seismic motion that is equivalent to the one used for the ultimate lateral strength method.

ACKNOWLEDGEMENT

This study was conducted as extended work of the joint research program for the "Development of Menshin System of Highway Bridges" that was supported by the Public Works Research Institute of the Ministry of Construction and by twenty-eight private firms in Japan. The author expresses his appreciation to the Public Works Research Institute and the twenty-eight firms for allowing him to utilize the results of the joint research.

REFERENCES

1) The Public Works Research Institute of the Ministry of Construction and 28 private firms in Japan, Joint Research Program Report on the "Development of Menshin System of Highway Bridges," October 1992.

2) Japan Road Association, Highway Bridge Design Manual and Its Interpretation, "Chapter V, Earthquake-resistant Design," February 1991.

3) Jennings, Paul C., "Equivalent Viscous Damping for Yielding Structures," Proceedings of the American Society of Civil Engineers, pp., 103-116, February 1968.

4) Veletos, A.S., Newmark, N.M, and Chelapati, C.V., "Deformation Spectra for Elastic and Elasto-plastic System Subjected to Ground Shock and Earthquake Motions," Proceedings of 3rd WCEE, pp., II663-680, 1965.

5) Takeda, T., Sozen, M.A., and Nielsen, N.N., "Reinforced Concrete Response to Simulated Earthquakes," Proceedings of 3rd Japan Earthquake Engineering Symposium, pp., 357-364, November 1970.

6) Japan Institute of Construction Engineering, "Seismic Isolation Design Guidelines for Road Bridges (Draft)", March 1991.

ULTIMATE RESTRAINT CONSIDERATIONS IN BASE-ISOLATED BRIDGES

Bryan A. Allred and Robin Shepherd
Department of Civil and Environmental Engineering
University of California, Irvine

Ludi J. Billings
Fluor Daniel Inc.
Irvine, California

ABSTRACT

Whether specifically carried on seismic isolation bearings or, as is more usual, supported on normal bridge bearings, bridge decks require displacement control to prevent the deck falling off the supporting structure in strong seismic shaking.

Transverse restraint is frequently provided by some form of slack "key" whereas longitudinal movement is often controlled by using the abutments as buffers. Such restraints have to be designed to allow normal differential movements such as are prompted by thermal changes, traffic vibration and braking, or small earthquake shaking, but they must be capable of surviving strong earthquake motion generated displacements. It is a matter of concern lest the protection conferred by the flexible bearings on piers, columns or abutments may be depleted significantly by the effects of shock throughout the bridge as the displacement control is activated.

This paper describes progress with an ongoing project involving the mathematical modeling of a simple bridge structure supported on bearings such that the longitudinal natural period is substantially lengthened from the non-isolated condition. Provision is made for the superstructure to be subjected to longitudinal displacement control as the deck impacts the abutments, or stops provided at the tops of the pier walls or columns, under the action of strong ground motion.

BACKGROUND

Californian efforts in seismic isolation of bridge structures have been directed primarily at retrofitting by installing isolation bearings at the top of columns to reduce the loads experienced by the support structure in strong seismic shaking [1]. Few modified structures have yet experienced significant ground motion.

The Sierra Point Overhead, carrying route 101 over a railroad line close to San Francisco international airport, was constructed in 1956 with welded steel girders supported on concrete columns to provide a ten span, eight lane bridge. As a result of analyses which indicated that the structure was seriously earthquake resistance deficient and in recognition of the difficulty in completing a superstructure strengthening program without seriously disrupting the operation of the railroad, prior to the 1989 Loma Prieta earthquake thirty six existing steel bearings were replaced by lead filled rubber units in anticipation that the demand on the columns would be greatly reduced in future earthquakes. During the Loma Prieta event instruments recorded accelerations of the order of 0.3g at the column tops but the shaking was insufficient to activate the isolation bearings and no appreciable difference was detected above and below the isolators. Some spalling of one abutment structure was observed but the force levels generated were not sufficient to fracture the backwall haunch and thereby to allow significant displacements to occur [2].

The Eel River Bridge, originally of three 300 foot steel truss configuration, suffered a span collapse in a flood and was rebuilt with lead filled rubber isolators incorporated at the truss supports to protect the otherwise seismically inadequate piers. In the first meaningful strong motion test of a base isolation bearing retrofitted bridge, this structure behaved well in the April 1992 Petrolia earthquake [3]. The isolated truss spans moved approximately eight inches longitudinally and four inches transversely, subsequently recentering themselves when the shaking ceased. Although the Eel River Bridge was not instrumented, records made on the nearby Painter Street Overcrossing in Rio Dell included 0.55g and 0.39g in the longitudinal and transverse directions respectively. It can be concluded that this structure behaved as it was intended to do when subjected to strong ground shaking.

Japanese advances in the area of Menshin design [4] are impressive and the basic characteristic of devices such as expansion joints, stoppers and knock-off abutments are well understood. The outstanding experimental test facilities available to Japanese development engineers undoubtedly encourage a prototype testing approach to innovation in bridge engineering.

Mutual benefit is likely to be obtained from the combined resources of Japanese and U.S. researchers if the strengths of each of the participating groups are exploited. Since the hardware and software facilities available in the U.S. are at least comparable with those available in Japan, it is more than probable that a worthwhile U.S. contribution can be provided by the establishment of analytical tools which will allow mathematical modelling to be carried out and the direction of further experimental investigations to be influenced by results of such theoretical studies. This ambition prompts the ongoing project which forms the basis of this paper.

ANALYSIS TOOLS

Several computer based mathematical modeling codes are available to facilitate analysis of base isolated systems. Success [5] in using the MARC k.5 nonlinear, general purpose, finite element code [6] in an investigation of the mechanics of elastomeric seismic isolation bearings influenced its use in the current project. The MARC code is specifically designed for non-linear application and includes provision for three dimensional contact and incompressible materials such as elastomers. Additionally the MARC code has provision for large displacement and can cope with the significant deformations suffered by seismically isolated systems. The code includes a CONTACT option which enables detection to be made of deformable body to deformable body or of rigid body to deformable body contact and also a gap element. This provides for gap and frictional connections between any two nodes of the structure. Essentially the element is based on imposition of a gap closure constant and friction stick or slip via Lagrange multipliers. The element is implemented as a four node link. The first and fourth nodes have Cartesian displacements to couple to the rest of the structure. The second node is the gap node; it has one degree of freedom, the force being carried across the link. The third node is the friction node with degrees of freedom corresponding to the frictional force being carried across the link and the net frictional slip.

ISOLATION CONSIDERATIONS SPECIFIC TO BRIDGES

Whereas the objective in seismic base isolating a building is usually to reduce the earthquake loads sustained by the superstructure, or to protect the contents, the aim of seismically isolating bridges is different. Since the earthquake vulnerable portions of bridges are normally not the superstructure but rather the abutments, columns and pier walls, and their foundations, it is for the benefit of these components that seismic isolation is likely to be adopted.

In rare cases such as a bridge with very high piers some form of isolation may be incorporated at the base of the piers [7] but the great majority of applications involve the isolation of the deck structure from the substructure, typically by installing isolators at the top of the columns, pier walls or abutments. The objective is both to reduce the seismic loads and to distribute them in a manner appropriate to the relative strengths of the various support elements. Current AASHTO requirements [8] call for adequate clearance to be provided for the displacements in either of the two orthogonal directions however displacements in the longitudinal direction of a bridge usually have to be limited to minimize the problem of carrying traffic across the seismic gap, although innovative solutions to this restriction have been developed [4]. AASHTO recognizes such possibilities by allowing a design alternative in the longitudinal direction, namely the provision of a knock-off abutment detail but does not indicate specifically how any adverse results of the impact should be addressed.

Since the pier walls, columns and abutments are not isolated from ground motions, they behave as separate structures, albeit with some top restraint which, particularly in the situation when

displacement control devices are present, will be distinctly non-linear.

The concern in the case of seismically base isolated buildings subject to displacement control is whether the superstructure will suffer from shock loads that would manifest themselves as sharp spikes on the floor response spectra. In the case of bridges the possible detrimental effect of superstructure base isolation is more likely to be the introduction of shock loads to the columns, pier walls and abutments. It is to this concern that the current investigation is addressed.

COMBINATION OF ISOLATOR AND SUPPORT PROPERTIES

When a seismic base isolator is installed at the top of a bridge column, beneath the deck structure, the parameters of the column combine with those of the isolator to provide composite dynamic characteristics of the support. The characteristics of the overall superstructure isolation system then reflect the combination of the individual composite dynamic parameters [7].

For most practical situations, the superstructure mass is much greater than that of the column and hence the first mode of vibration is dominated by the superstructure whereas the second mode involves lateral motion of the top of the column with little movement of the superstructure (Figure 1). The effect of having a lateral flexible column beneath a given isolator is to reduce the stiffness of the support compared with the situation in which the same isolator sits on a rigid base. If all the superstructure moves together in essentially rigid body lateral motion the individual support stiffnesses can be combined to determine the total stiffness and the overall damping is a weighted sum of the individual values.

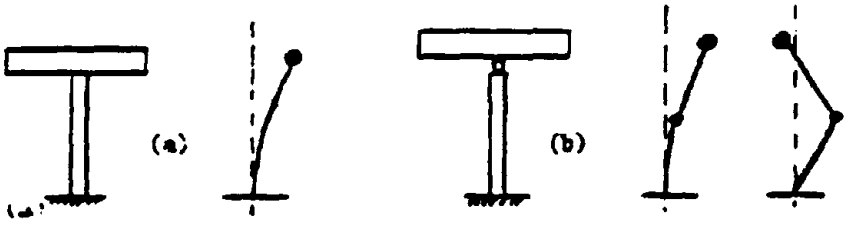

Figure 1. Lateral direction mode shapes, bridge deck supported on single column (a) non-isolated and (b) isolated

The initial analysis undertaken in this project was that of a bridge pier wall support, being part of an idealized two full and two half bay road bridge (Figure 2). Subsequent work will involve extension to the complete structure.

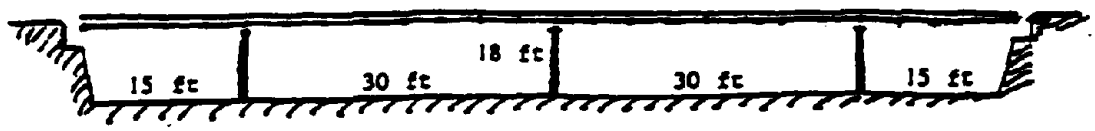

Figure 2. Idealized bridge

IDEALIZED BRIDGE

For the purpose of analysis the idealized reinforced concrete structure shown in Figure 2 is assumed to be of 20 ft. width and to have a uniform slab deck 18 inches thick which is free to slide at the abutments. All the mass is assumed carried on the three pier walls, each being 18 ft. high and of 20 ft. x 1.5 ft. cross section. The longitudinal fundamental frequency, assuming each pier wall to be fixed at its base and pinned at its top, is approximately 2.8 hz.

FINITE ELEMENT ANALYSES

A typical pier wall was modeled using thirty six, six inch long, two dimensional beam elements. The first node, corresponding to ground level, is restrained in all directions to simulate a fixed base condition. Excitation was applied though the first node as horizontal acceleration representative of the 1940 N/S El Centro motion.

To verify the model, modal analyses were conducted on the fixed base (Figures 3 and 4) and isolated systems (Figures 5 and 6). Good agreement was obtained between hand calculations and the frequency from the F.E. analyses.

Two models were examined. One had the deck fastened to the top of the pier by way of a pin and the second had the deck isolated form the top of pier wall by being connected by a linear spring of stiffness 21.43 kips per foot, the period of the deck on the support then being 2.8 seconds. This spring represented the isolator. Restraint was provided to the deck in the y direction, only x translation being permitted.

Dynamic analyses were undertaken to determine the displacement response of both the top of the pier and of the deck (Figure 7 and 8). The beneficial effects of isolation are illustrated in the acceleration plots shown in figures 9 and 10.

Displacement control of the deck with respect to the top of the pier was simulated by providing a + 9 inches gap or rattle space between the top of the pier and the displacement limit provided

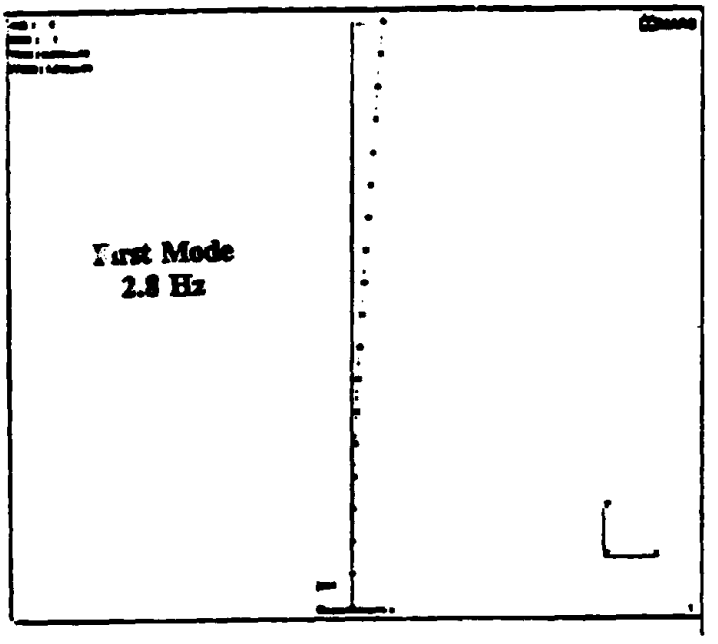

Figure 3. First Mode Shape - Non Isolated System

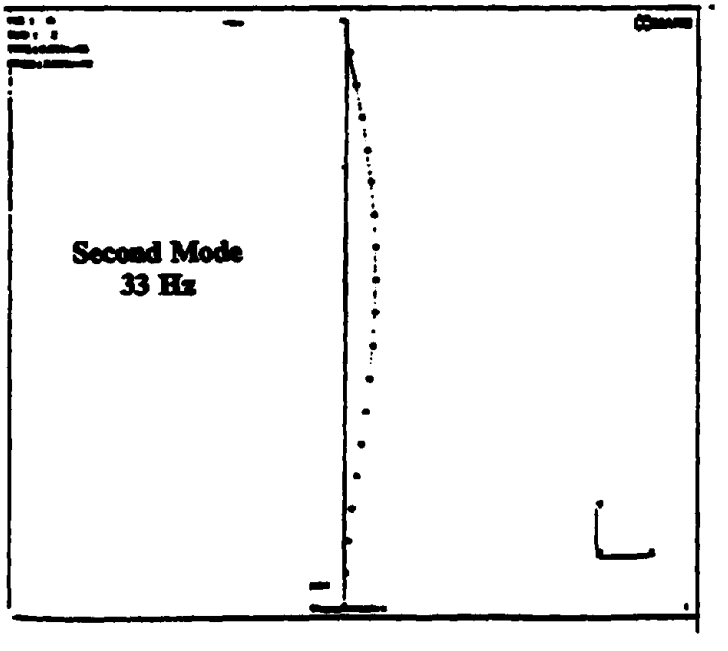

Figure 4. Second Mode Shape - Non Isolated System

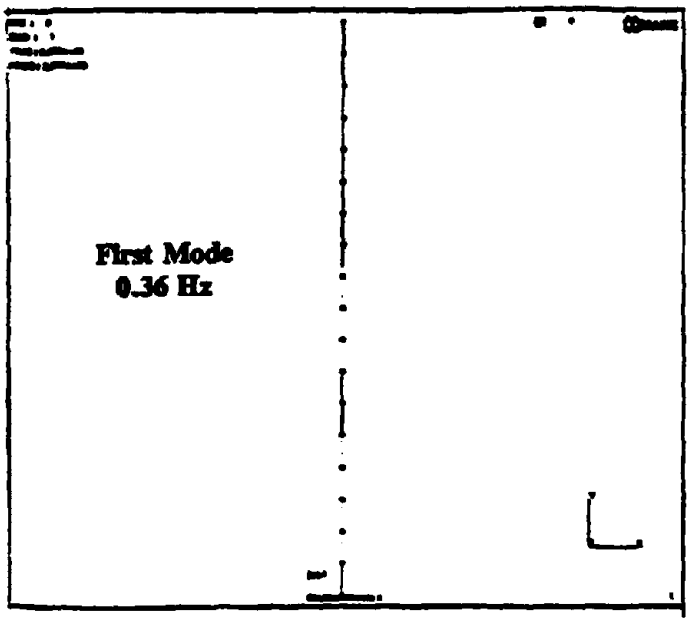

Figure 5. First Mode Shape - Isolated System

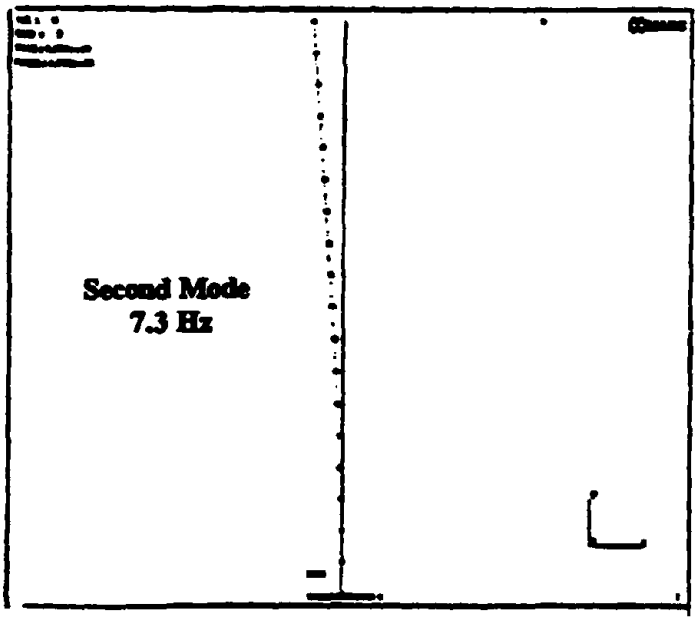

Figure 6. Second Mode Shape - Isolated System

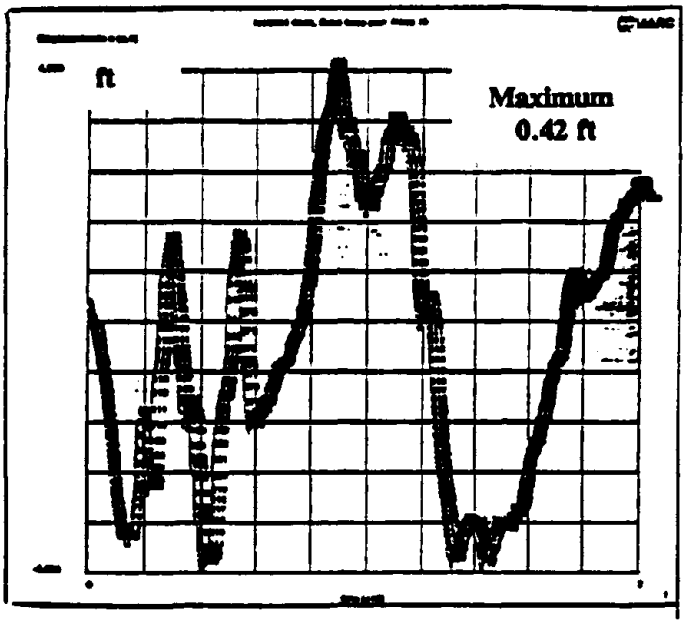

Figure 7. Displacement Pier Top - Isolated System

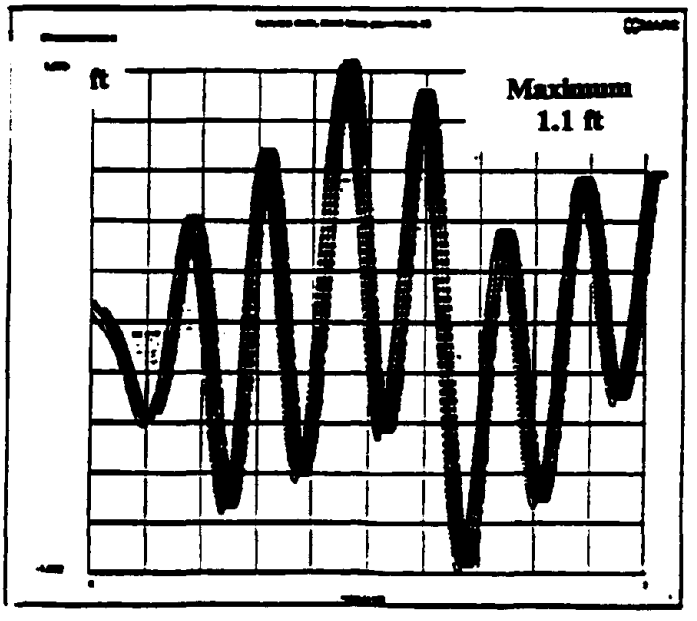

Figure 8. Displacement of Deck - Isolated System

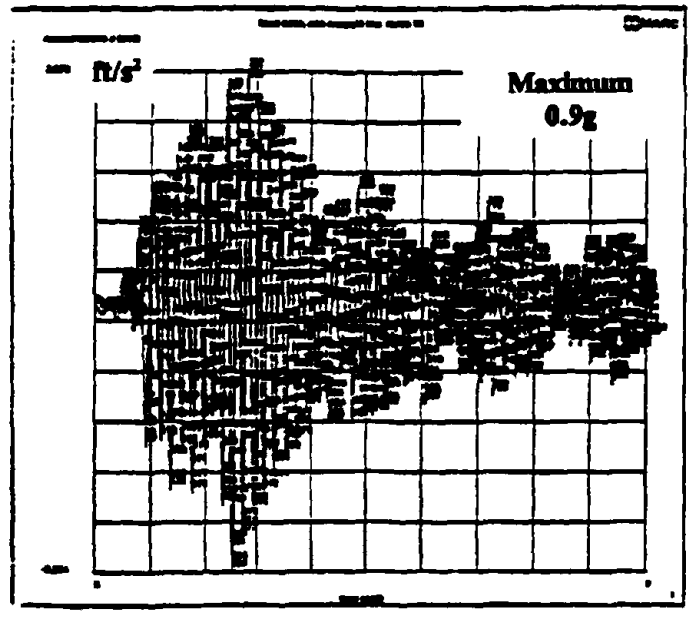

Figure 9. Acceleration of Deck - Non Isolated System

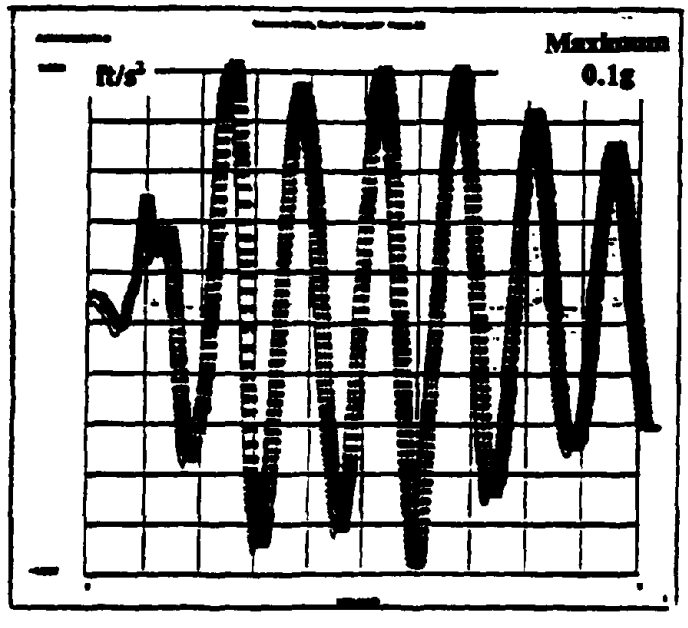

Figure 10. Acceleration of Deck - Isolated System

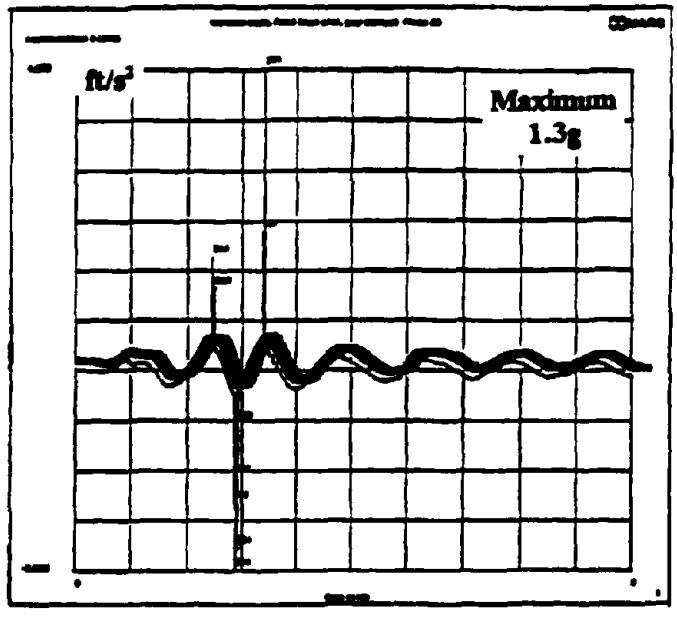

Figure 11. Acceleration of Deck - Isolated and Impact

by the deck. The adverse effect of isolation with impact is evident from the acceleration spikes in figure 11. It is noted that the dynamic transient analyses were performed with 0.02 second time step and Rayleigh damping coefficients 0.233 and 0.0013 for the mass and stiffness respectively.

CONCLUSIONS

The analyses undertaken to date indicate that the MARC coding provides a viable method of determining the effects of displacement control of bridge structures. The next stage is to extend the analyses to investigate the effects of impact on the pier. Subsequently sensitivityanalyses involving different choices of input and gap size will be undertaken.

ACKNOWLEDGEMENTS

The continuing interest and support of Dr. Thomas L. Anderson, Engineering Manager, Fluor Daniel Inc., and Dr. Ian G. Buckle, Deputy Director, National Center for Earthquake Engineering Research, is recorded with gratitude. This research is supported by a grant from the National Center for Earthquake Engineering Research and by the University of California, Irvine, through an allocation of computer resources.

The cooperation of Dr. Yozo Goto, Technical Research Institute, Obayashi Corporation, in arranging for the authors to visit many seismic base isolated facilities in Japan, and the forbearance of numerous Japanese engineers who gave up their time to conduct tours of their sites, are much appreciated.

REFERENCES

1. Buckle I.G and Mayes R.L., "History and Application of Seismic Isolation to Highway Bridges in the United States", Proceedings, First U.S.-Japan Workshop on Earthquake Protective Systems for Bridges, Buffalo, N.Y., 1992, pp 27-40.

2. Thorkildsen E., "CALTRANS Seismic Isolation Design and Future Concepts", Internal Memorandum, CALTRANS 1992.

3. Roberts J.E., "Sharing California's Seismic Lessons", Modern Steel Construction, AISC, July 1992.

4. Goto Y., Kikuchi T., Kimishima T., Matsumoto F., Ozaki D. and Tsukamoto A., "Development of Expansion Joint, Stopper and Knock-off Abutment for Menshin Bridges." Proceedings, Second U.S.-Japan Workshop on Earthquake Protective Systems for Bridges, Tsukuba, Japan, 1992, pp 255-273.

5. ----- MARC Users Information Manual, MARC Analysis Research Corporation, Palo Alto, California 1990

6. Billings, L.J., "Finite Element Modeling of Elastomeric Seismic Isolation Bearings." Thesis presented in partial satisfaction of the Ph.D. degree, University of California, Irvine, 1992.

7. Skinner R.I., Robinson W.H. and McVerry G.H., "An Introduction to Seismic Isolation." John Wiley, 1993

8. ----- AASHTO, "Standard Specifications for Highway Bridges". American Association for State Highway and Transportation Officials, 15th. Edition, 1989 and Interim Specifications, 1990,1991.

DESIGN PLAN OF SUPER MULTI-SPAN CONTINUOUS MENSHIN BRIDGE WITH DECK LENGTH OF 725 M

Hideji Masumoto*, Koji Hara, and Mikio Yamashita*****

***Director, Road Construction Division, Public Works Department, Shizuoko Prefectural Government**

****Assistant Chief, Construction Section 2, Numazu Public Works Office, Shizuoka Prefectural Government**

*****Director, Technical Department, KAIHATSU Consultant Co., Ltd. Higashiueno 2-9-4, Taitoku, Tokyo**

INTRODUCTION

The basic framework of the national highway system on Izu Peninsula in Shizuoka Prefecture is formed by Highway 135, which winds along the east coast of the Izu Peninsula, and Highways 136 and 414, which originate at Shimoda City and extend along the west coast of the peninsula to Mishima City. These highways contribute to development and tourism in Izu. Measures must be taken to deal with the traffic congestion that occurs on all parts of the peninsula as a result of the fact that most of the 80 million tourists and other travellers visit Izu Peninsula each year by car. As one measure to alleviate this problem, a 13.8 km stretch of highway is being built to smooth the flow of traffic in central Izu. One 5.2 km section on the Trans Izu Highway is a high-standard trunk road connecting Kannami-chou Tsukamoto to Shuzenji, where traffic congestion is particularly severe. The other section is an 8.6 km bypass on National Highway 136.

The Ohito Viaduct, with length of 1,929 m will be constructed in the Ohito-chou district of Tagata-gun in Shizuoka Prefecture as part of the high-standard trunk road (Trans Izu Highway) section of the above project (See Figure 1 and Photo 1).

This paper presents planning of this viaduct and describes the design plan of a super multi-span continuous Menshin bridge.

Photo 1. Location of the Ohito Viaduct Project

SUMMARY OF THE OHITO VIADUCT

The Ohito Viaduct, which will be constructed along the bank of the Kano River, will link the Kanogawa Interchange to the Ohito Interchange on the planned highway. This viaduct will consist of a series of five bridges. Table 1 Shows the bridge type adopted for each bridge.

From the beginning of the project, multi-span continuous bridges were planned to improve the maintainability and the road service standards. Bridge 2 is planned to be a 29-span continuous PC hollow-slab bridge with bridge length of 725 m, which will be the longest concrete bridge in Japan. Furthermore Menshin design is adopted for this bridge. A number of Menshin bridges have been constructed since 1991 when the Miyagawa Bridge which is the first Menshin bridge in Japan in Shizuoka Prefecture have been opened to traffic. Then the Menshin design is being widely applied for jointless measures for existing simply supported bridges. Furthermore, basic research on super multi-span continuous Menshin bridges, such as the Ohito Viaduct bridges, has been conducted as part of the "Joint Research Program on the Development of Menshin Systems for Highway Bridges", which is a joint government--private sector research project. As a result of this research, the super multi-span continuous Menshin bridge has been proposed as a highly feasible type of bridge, and studies are under way for its practical application. Before it can be applied to real bridges, solutions must be found to many unsolved problems. To prepare for the design work on these bridges, the basic design policies were established through the deliberation and guidance by the "Ohito Viaduct (Super multi-span Continuous Menshin Bridge) Committee of Inquiry" (Chairman: Dr. M. Fujiwara, Director of the Bridge and Structure Department, Public Works Research Institute, Ministry of Construction).

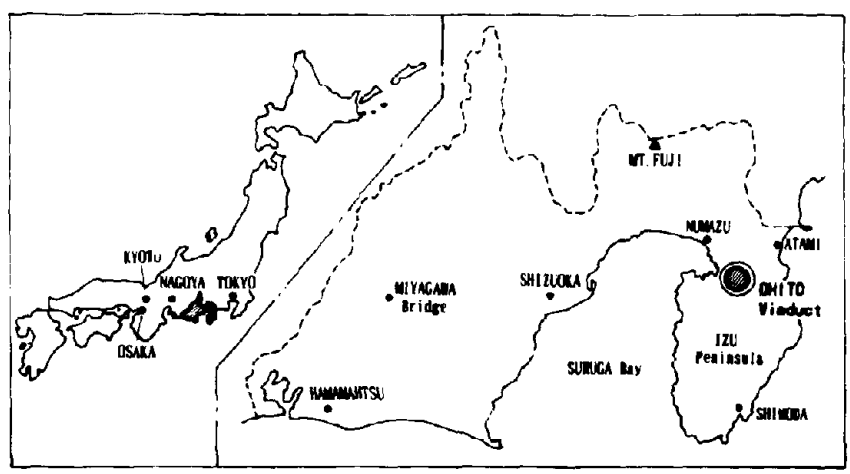

Figure 1. Location of the Ohito Viaduct

Table 1. Bridge Categories

Bridge 1	7-span continuous PC hollow slab bridge	L = 175.0m
Bridge 2	29-span continuous PC hollow slab bridge	L = 725.0m
Bridge 3	15-span continuous PC hollow slab bridge	L = 375.0m
Bridge 4	3-span continuous steel Box Girder bridge	L = 337.5m
Bridge 5	12-span continuous PC hollow slab bridge	L = 290.4m

STRUCTURAL DESIGN OF THE SUPER MULTI-SPAN CONTINUOUS MENSHIN BRIDGE

The following is a description of the structural design for bridge 2, which is the longest bridge in this viaduct project (See Figure 3).

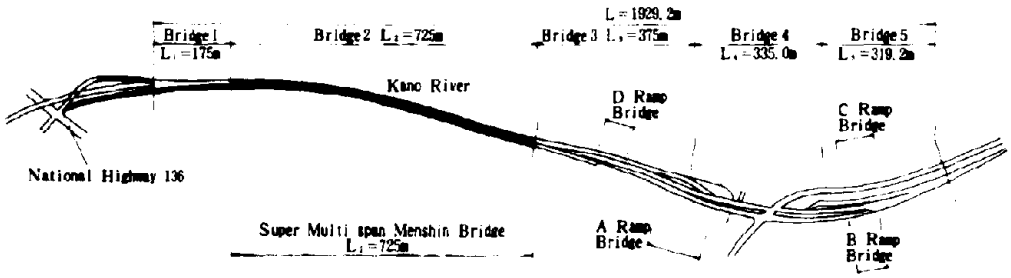

Figure 2. Plane View of the Ohito Viaduct

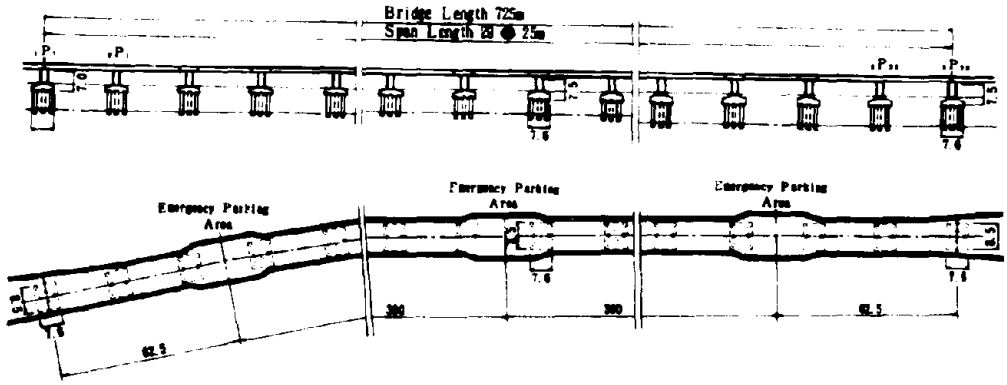

Figure 3. View of Bridge 2

1) Bridge Design conditions

*	Highway Standard	: 1 - 3
*	Design Vehicle Speed	: V = 80km/h
*	Width Configuration	: Total width W = 11.70 m (See Figure 4)
*	Effective Width	: We = 10.50 m (1.75m+3.50m+1.75m)
*	Cross section gradient:	: Standard 2.0%
*	Bridge Class	: First class bridge
*	Live Load	: TL-20, TT-43
*	Surface Material	: Asphalt paving V = 80 mm (design load thickness = 100 mm)
*	Handrail	: Concrete barrier curb (parapet) thickness = 300 mm
*	Noise barrier load	: W = 154.0 kgf/m
*	Ground condition	: Class 2

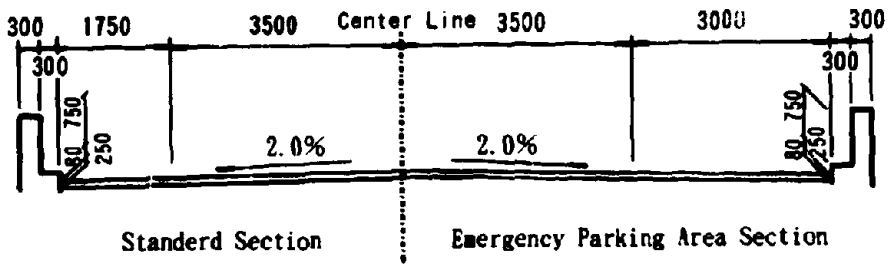

Figure 4. Cross Section of Roadway

2) Outline of the Ground

Figure 5 shows the structure of the strata in the cross longitudinal direction of the bridge based upon geological survey in the project area. A tertiary tuff stratum is found at approximately GL-40 m.The diluvium stratum above it consists of between 30 to 35 m of alternating strata of gravel, sand or clay layers. An alluvial gravel stratum Ag with N-value close to 50 is found near the surface. Initially this layer could be used as the supporting strata. However, the results of an on-site loading test conducted as part of a supplementary detailed geological survey showed that it would be difficult to rely on this as the supporting stratum. Accordingly, the underlying diluvial gravel strata Dql is planned to be the supporting stratum.

Table 2 shows the ground condition for the Menshin design, which is a key aspect of the bridge design. It is estimated as Class II through both the N-value and the shear wave velocity of the grounds.

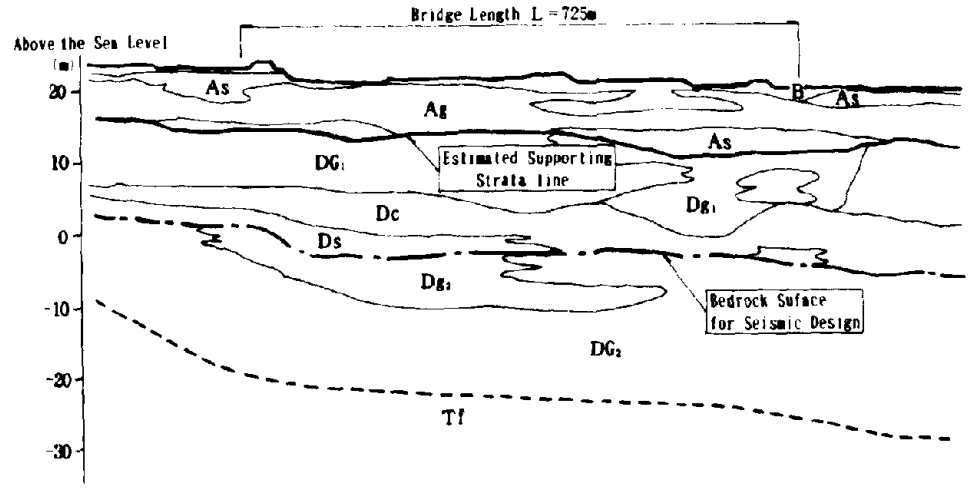

Figure 5. Longitudinal Diagram of the strata

Table 2. Ground Characteristic Value

Boring No.		Estimates Based on N-values		Computations Based on shear wave velocity	
		Ground Characteristic Value TG (sec)	Ground Class	Ground Characteristic Value TG (sec)	Ground Class
Prior Survey	H1-7	0.2≤0.328<0.6	Type II	———	———
	H2-6	0.2≤0.296<0.6	Type II	———	———
	H1-6	0.2≤0.588<0.6	Type II	———	———
New Survey	P4	0.2≤0.324<0.6	Type II	0.2≤0.245<0.6	Type II
	P19	0.2≤0.300<0.6	Type II	———	———
	P25	0.2≤0.316<0.6	Type II	0.2≤0.332<0.6	Type II
	P29	0.2≤0.352<0.6	Type II	———	———

3) Superstructure Design

(a) Structure Selection

The Type of superstructure is selected from among a range of structures determined by the restriction conditions described above. The span is determined by the crossing conditions, and the form of the superstructure was also restricted by the structural height. Consequently, a span length of 25 m was chosen. A PC hollow-slab bridge as the concrete girder type, and a multi-beam non-composite plate girder bridge as the steel girder type is selected for the comparison of bridge types. The conventional factors such as economic efficiency, structural properties, maintainability, harmony with adjoining sections, constructability, and environmental adaptability are considered, for the comparison, and their suitability for Menshin design and the thermal expansion and contraction properties of long girder were also considered.

Eventually PC continuous hollowslab bridges are selected .This bridge type is superior in terms of economic efficiency, continuity of the structure with that of the emergency parking areas, the integrated form of its superstructure and substructure, the stability of the Menshin bearing, and the expansion and contraction of the girder.

(b) Materials

* Concrete Strength : $\sigma_{ck} = 350 kgf/cm^2$
  $\sigma_{ck} = 210 kgf/cm^2$
* Reinforcing Bar : SD 295
* Prestressing Steel : SWPR 7 A 12T12.4
  SBPR 930/1180, Ø32mm

(c) Construction Method

Because this viaduct will be a 29-span continuous bridge, another prerequisite condition is that it must be constructed in separate sections. A study focused on the suitability for the site conditions, cost efficiency and the residual deformation during and after construction was conducted to determine specific type of construction method.

The use of a movable falsework is generally selected in the construction of a multi-span bridge in order to reduce labor requirements. However, a comparative study on partial construction using the support method showed that the support method was more cost efficient. Therefore, the support method was adopted as the basic construction method. Figure 6 shows residual deformation (drying shrinkage, creep deformation) according to the construction methods.

(d) Deformation of the Bearings and the Construction Method

In the case of this bridge, the residual deformation caused by the creep and drying shrinkage of PC girder will be as much as approximately 114.7 mm at the ends of the girder, even when a standard construction method is employed. Furthermore, the expansion and contraction of the girder under the effect of temperature change deformation will be ±75.2 mm. Figure 7 shows the deformation of the girder caused by creep, drying shrinkage and temperature change. On the one hand, if the bearings are simply designed to absorb these deformations, the thickness of the rubber of the bearings will increase, and the shearing stiffness of the bearings will decrease, resulted in the lengthening of the natural period. The displacement of the superstructure during an earthquake will also increase, and the design of ancillary structures will be influenced. For this reason, it is absolutely essential that one of two measures be adopted to deal with the residual deformation occurring in the superstructure. Either a reverse displacement is to be added when the bearings are manufactured in the factory, or else the deformation is to be corrected at site after the bearings are installed. Basic policies regarding these problems with the design of the bridge were laid out and all necessary studies were performed in the planning stage. Figure 8 shows the hypothetical range of bearing deformation. Because the method to add a reverse deformation to the bearings in the factory had already been used in a number of locations, the study was directed at deformation correction methods to be employed at site. Figure 9 shows a summary of the construction method proposed on the basis of this study.

Specific design detail and methods to be employed in the adoption of this method are now being studied, and plans call for additional experiments to be conducted and final decisions will be made by the time when the superstructure is constructed.

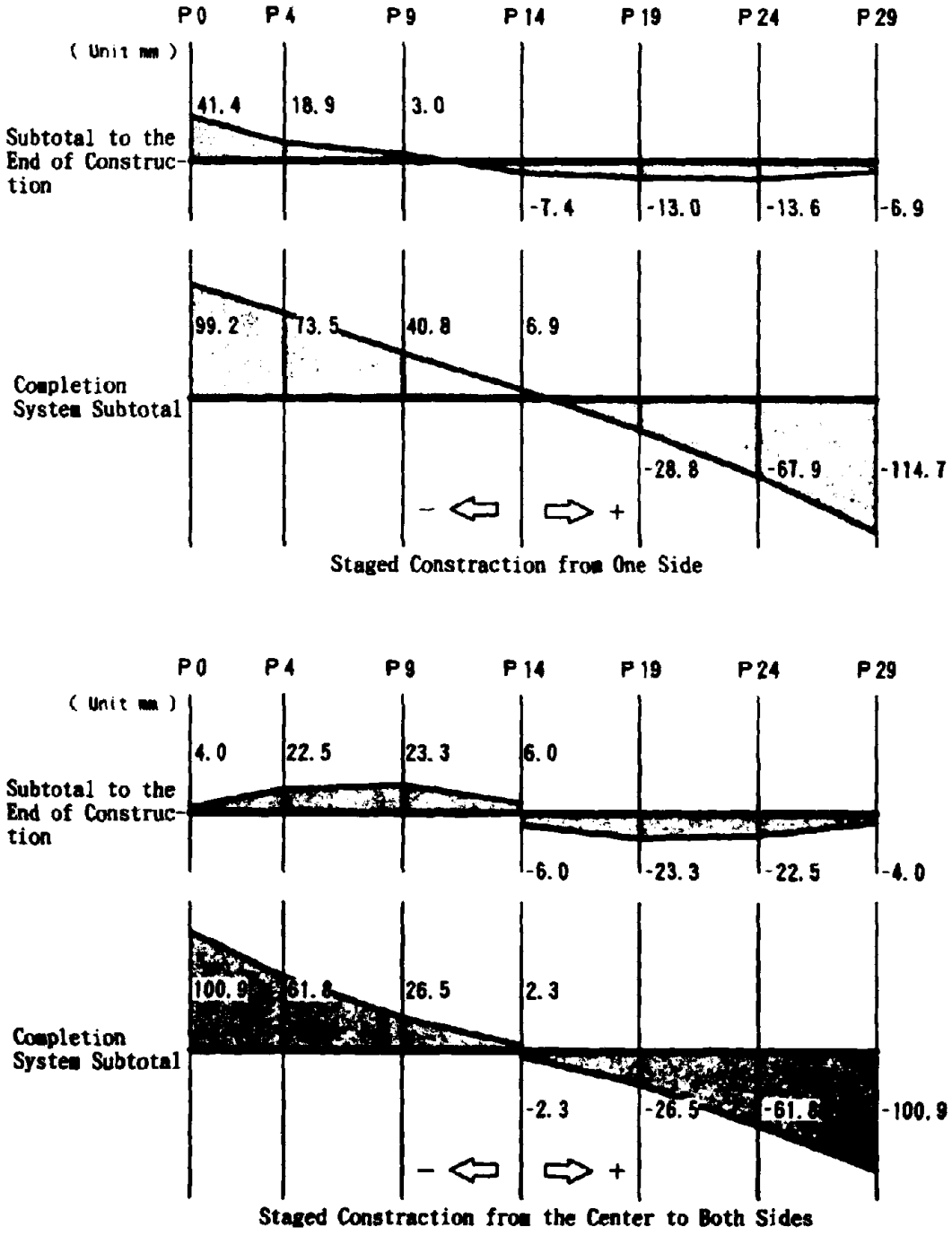

Figure 6. Residual Deformation Caused by Creep and Drying Shrinkage

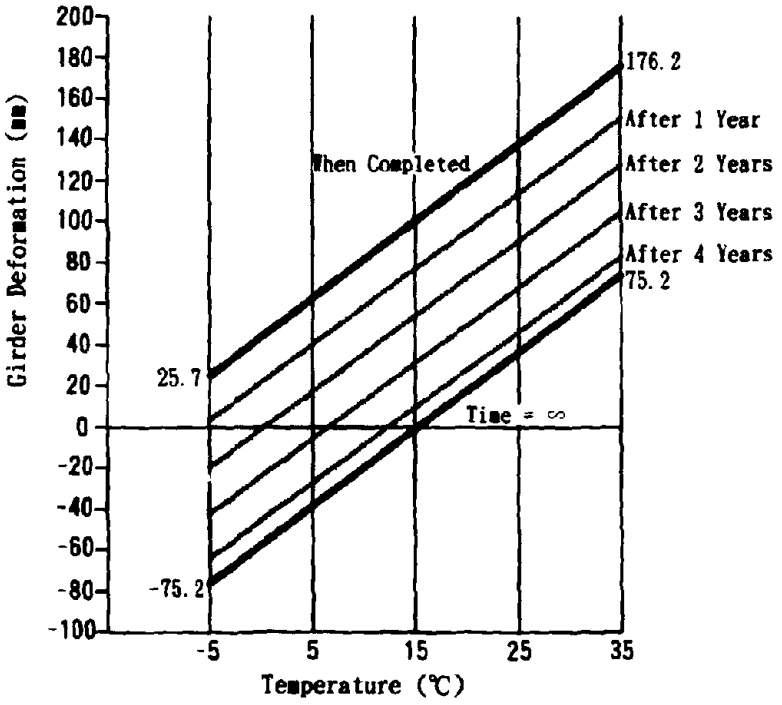

Figure 7. Deformation of Girder Caused by Creep, Drying Shrinkage, and Temperature Change

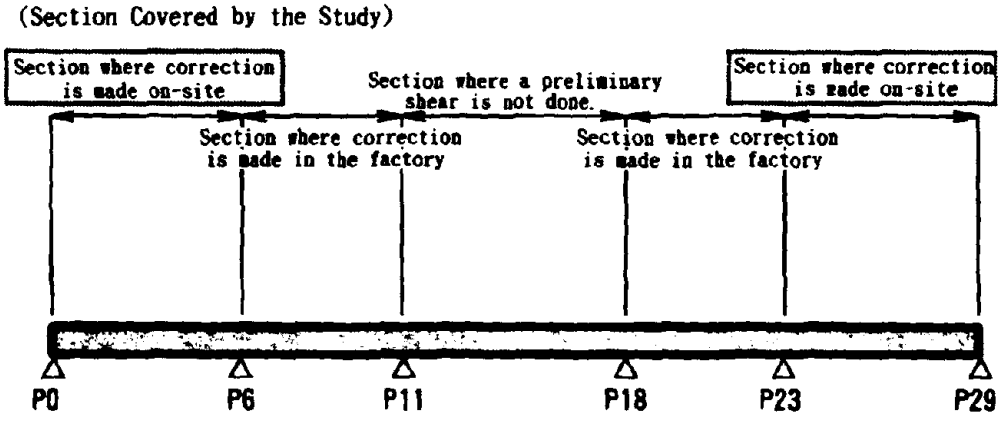

This scale, however, assumes the use of a conventional constraction method, and the range must be examined according to the condition.

Figure 8. Hypothetical Diagram of the Bearing Deformation Correction Range

① Ancher Bolt Installation

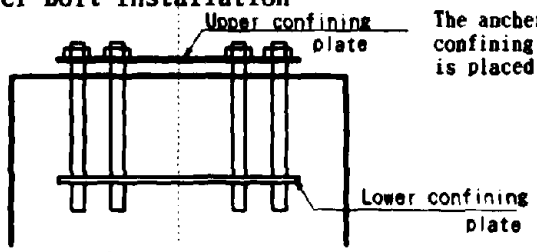

The ancher bolts fixed by the upper and lower confining plates, and the bridge pier concrete is placed

② Base Plate Installation

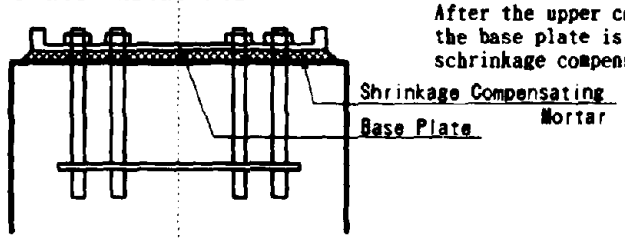

After the upper confining plate is removed, the base plate is set prescribed position, and schrinkage compensating mortar is placed.

③ Bearing(LRB) Installation and Placing Concrete for the Main Beam

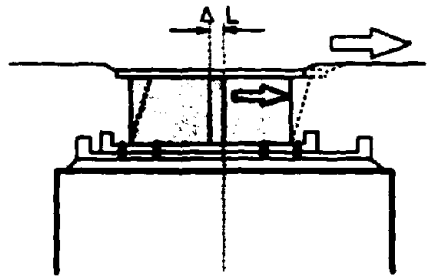

Only the deformation ΔL of the main beam is shifted, the bearing is set in place, and the main beam concrete is placed.

★The bottom plate and base plate are temporarily fixed in place with bolts at the temporarily installation location.

④ Post-strain Adjustment

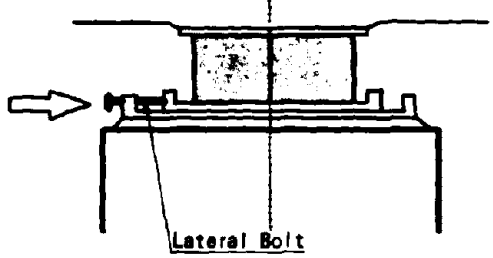

After the main beam is completed, post-strain adjustment is made with a horizontal bolts.

★It is necessary to perform staged post-strain adjustment at the ends.

★The use of a vertical jack to reduce the reaction force is being considered.

★Depending on the circum-stances, it is moved with a center-hole jack and fixed with a boltt.

⑤ Fixing the Lowar Plate and Base Plate

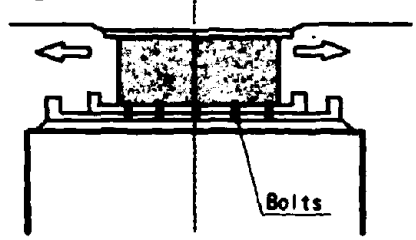

After post-strain adjustment has been co-mpleted, the bottom plate and base plate are fixed withe bolts.

★In a case when the movement and the error are large, the bottom plate and the base plate are fixed by welding

Figure 9. Proposed Bearing Deformation Correction Method

(e) Prestressing Steel Based on Statically Indeterminate force

As a result of residual deformation of the girder and temperature change deformation, additional axial force and moment act on the girder. These statically indeterminate forces is influenced by the stiffness of the Menshin bearings and by the stiffness of the bridge piers including the foundation. The deformation that occurs in the superstructure during construction and the residual deformation are dealt with separately. But the force generated by the expansion and contraction of the girder as a result of continuous temperature change deformation is a major factor because there are many supports and because of the long length of the girder. Figure 10 shows the thermal lateral force generated by Menshin bearings designed on the basis of one hypothesis and the results of computations of the axial force generated on the girder.

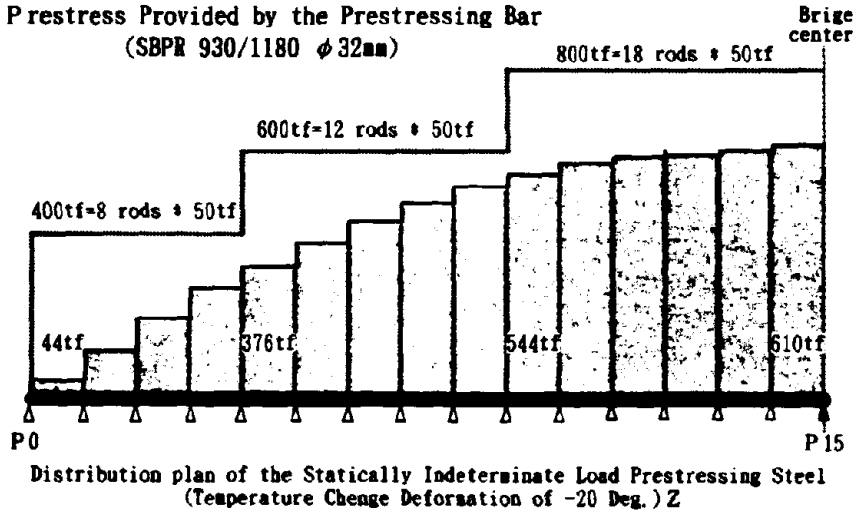

Figure 10. Axial Force Produced in the Girder by Temperature Change Deformation

Measures to deal with these statically indeterminate forces is examined. The best approach would be to handle the problem by installing prestressing bar (SBPR 930/1180) for statically indeterminate forces, which is in principle installed in the axial line of girder, in addition to prestressing cable (SWPR 7A-12T12.4) that handles the normal principle loads. Figure 11 shows the standard cross sections for the distribution of prestressing cable for principle loads and that for prestressing bar against statically indeterminate forces.

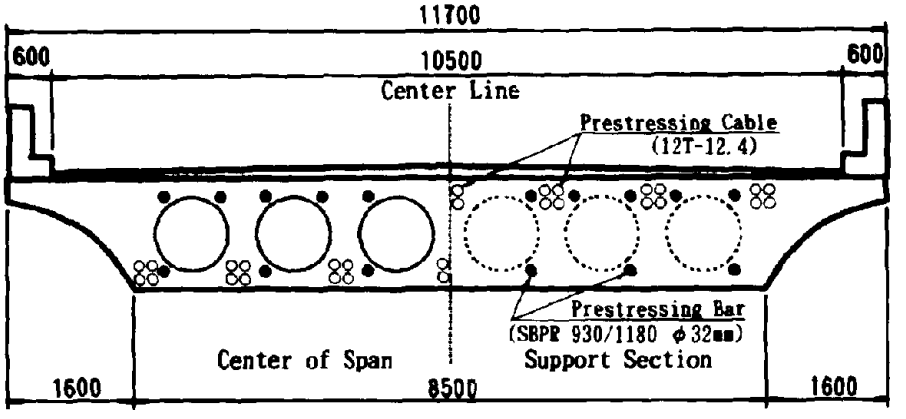

Figure 11. Distribution of Prestressing Steel in a Standard Cross Section

4) Design of the Substructure

(a) Design of the Shape

The bridge piers will be low, ranging from 7.0 m to 7.5 m high, since the longitudinal gradient is gentle, the ground at the site is flat, and pile foundation is employed. Ordinary walltype bridge piers will be selected, and their shape as shown in Figure 12 is employed in order to provide continuity with the cross section of the superstructure and to convey stability. To determine the shape of the substructure, three shapes compatible with the cantilever processing of the superstructure were compared and the one found to be visually superior was selected. Concerning the visual aspects in particular, the plan for the substructure of the entire viaduct varies from the basic single wall approach, to the substructure consist of two-column, or of a three-column rigid-frame type. Continuity among all sections was considered.

The wall thickness of intermediate piers other than end piers was found by simulating the volume of installed reinforcing bar, and carrying out a comprehensive comparison and assessment of thermal change deformation lateral forces, the lateral force of an L1 earthquake, the ultimate lateral strength during an L2 earthquake, based on the bridge pier stiffness in each case. The standard wall thickness was set at 2.0 m. Figure 13 shows the cross section of the bridge piers and the distribution of reinforcing bar.

(b) Materials

* Concrete : $\sigma_{ck} = 210 kgf/cm^2$
* Reinforcing Bar : SD 295 $\sigma_{sy} = 2{,}700 kgf/cm^2$

(c) Foundation

In the original plans, the direct foundation was placed on the gravel strata with N value between 40 and 50 found near the surface. However, the results of a later survey (including a plate bearing test) showed that this would be difficult, so the supporting layer was changed to the diluvial gravel found beneath it (Dg1).

Consequently, a pile foundation with length between 6 and 8 m was selected. Following a comparison of various types of piles, cast in place concrete piles (1,200 mm) are selected in consideration with bearing capacity efficiency, constructability, and cost efficiency.

(d) Substructure Stiffness

Table 3 shows an example of the computation of substructure stiffness, and Figure 14 shows the P-δ curve for the pier. Because the lateral reaction force caused by temperature change deformation is an important element in this design, when the spring constant of the pile foundation during a temperature change deformation is computed, it is assessed by the static normal spring of ground. The dynamic ground spring indicated in the Seismic Design of the highway bridge specifications is used as the ground spring constant during L1 and L2 earthquakes.

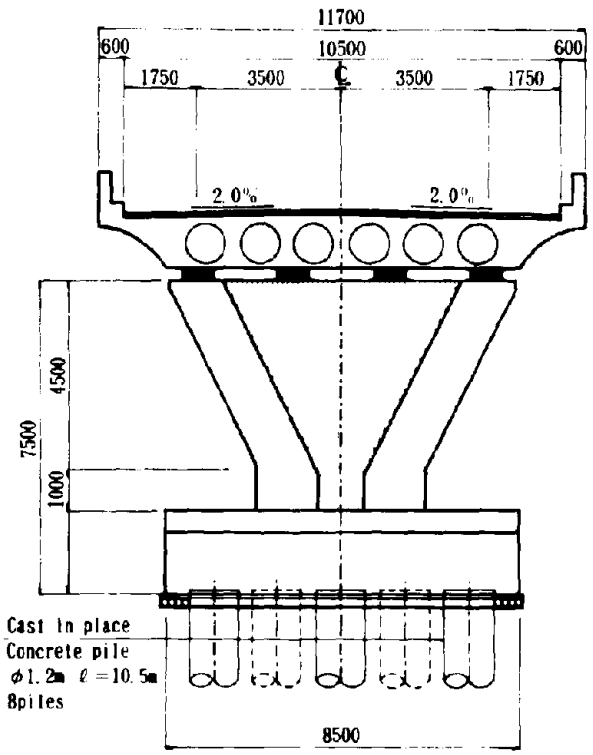

Figure 12. View of the standard Bridge Pier Configuration

Table 3. Substructure Stiffness Table

Bridge Pier Number	P_0	P_1~P_5	P_6~P_{10}	P_{11}~P_{14}	P_{15}~P_{18}	P_{19}~P_{23}	P_{24}~P_{28}	P_{29}
Elastic Stiffness of the Substructure Kca(tf/m)	17,700	16,500	24,100	16,000	14,000	17,700	19,100	20,000
Yield Stiffness of the Substructure Kyn(tf/m)	17,500	15,600	23,000	15,600	12,700	15,600	16,400	19,700

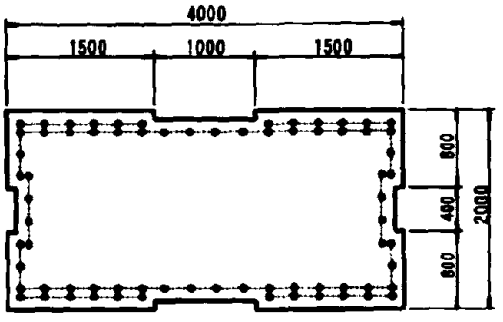

Principal Reinforcing Bar in the Bridge Axis Direction D25
Principal Reinforcing Bar in the Transverse Direction D16

Figure 13. Cross Section and Reinforcing Bar Arrangement in the Bridge Pier

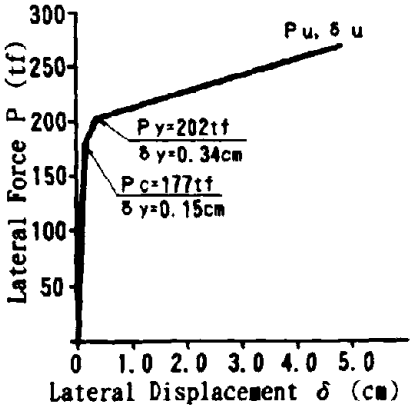

Figure 14. P-δ Curve of the Wall

MENSHIN DESIGN

The final design requirements for the Menshin design of this bridge have not yet been finalized, because the basic items dealt with during the planning and design of this bridge will be determined in accordance with the deliberations and guidance of a supervisory committee. This committee is now considering the many items described above. This section presents details on all the studies of Menshin design conducted up until this time, but is still incomplete.

1) Basic Design Policies

The basic design policies will conform to the provisions of the "highway bridge specifications", items that are peculiar to Menshin design and those that are not prescribed by the highway bridge specifications will conform to the "Manual for the Menshin Design of Highway Bridges (draft)" from the Public Works Research Center, and such design will be conducted in accordance with policies approved by the supervisory committee.

2) Menshin Design

The balance between the thermal change deformation lateral forces and the seismic lateral forces is one of the major items. A trial computation of the stiffness of the Menshin devices is carried out in order to avoid a situation in which the shape of the substructure would be determined by the forces applied during a temperature change deformation. For example, thermal lateral force and other lateral forces during an earthquake shown on Figure 15(A) and (B) shows the relation between the natural period of vibration and the thermal lateral force and seismic lateral force. Figure (A) shows the relationship with thermal lateral force generated in a typical pier, and Figure (B) shows the relationship with the bearing's relative displacement during an L1 and L2 earthquake. These trial computations clarify that if Menshin devices are not to be determined by temperature change deformation, the natural period during an L2 level earthquake would have to be between 1.3 and 1.4 seconds. Various other studies are now in progress. As a reference, Table 4 presents the results of Menshin design trial computations in a case where the natural period is 1.4 seconds.

Table 4. Menshin Design Trial Calculation Results Table (T = 1.4 sec.)

(Lateral Force and Stiffness are all Values Per Single Bridge Pier)

Bridge Pier Number				P_1	$P_2 \sim P_6$	$P_7 \sim P_{11}$	$P_{12} \sim P_{22}$	$P_{23} \sim P_{24}$	$P_{25} \sim P_{26}$	P_{27}	P_{28}
Number of Piers				1	4	5	11	2	2	2	1
Bearing Shape		Lateral Rubber Laminated	A × B (cm)	55×55	75×80	75×80	75×80	75×80	75×80	75×80	55×55
			Σ te (cm)	14.0	12.8	12.8	12.8	12.8	12.8	12.8	14.0
Normal Conditions	Lateral Displacement of Bearing		Uo (cm)	8.2	7.2	5.1	3.4	2.0	4.9	6.9	8.2
	Lateral Shear Force of Bearing (slow-rate)		Fs (tf)	62.7	121.7	86.2	57.5	33.8	82.8	116.7	62.7
	Effective Cross Section Area of the Rubber		A_{RC} (cm^2)	2242	4849	5013	5145	5304	5028	4872	2037
	Check of Bearing Stress	σmax(kgf/cm^2)[<80]		61.1	57.1	50.5	49.2	47.7	55.1	56.9	67.3
Seismic Coefficient Method Level	Design Displacement of Menshin Devices		Us (cm)	4.61	4.18	4.20	4.23	3.84	3.96	3.96	4.50
	Effective Design Displacement of Menshin Devices		Use (cm)	3.23	2.93	2.94	2.96	2.76	2.78	2.78	3.15
	Equivalent Stiffness of Menshin Devices		Ke (tf/m)	521.8	1201.2	1197.2	1192.4	1247.7	1243.5	1243.5	529.8
	Equivalent Stiffness of synthesizing the Menshin Device and Substructure		Kr (tf/m)	1923	4017	4024	4033	3935	3942	3942	1907
	Equivalent Damping Ratio of Menshin Devices		hs	0.251	0.254	0.254	0.254	0.257	0.257	0.257	0.252
	Allotment Rate of Horizontal Foce		η	0.0694	0.1449	0.1452	0.1455	0.1419	0.1422	0.1422	0.0688
	Natural period of the Bridge		T (sec)	0.898							
	Equivalent Damping Ratio of the Bridge		h	0.220							
	Lateral Seismic Coefficient		Kh	0.25							
	Design Lateral seismic Force		F (tf)	96	201	201	202	197	197	197	95
	Extent of Superstructure Displacement		Ur (tf)	5.002							
Ultimate Lateral Strength Level During an Earthquake	Design Displacement of Menshin Devices		Us (cm)	32.79	30.86	31.19	31.58	29.42	30.57	30.57	32.64
	Effective Design Displacement of Menshin Devices		Use (cm)	22.95	21.60	21.84	22.10	20.59	21.40	21.40	22.85
	Equivalent Stiffness of Menshin Devices		Ke (tf/m)	199.3	441.1	440.9	440.7	442.0	441.2	441.2	199.3
	Effective Equivalent Stiffness of Menshin Devices		Kse (tf/m)	208.0	458.7	457.6	456.3	464.3	458.8	459.8	208.2
	Equivalent Stiffness of synthesizing the Menshin Device and Substructure		Kre (tf/m)	787	1631	1646	1662	1569	1619	1618	784
	Equivalent Damping Ratio of Menshin Devices		hse	0.142	0.146	0.145	0.143	0.151	0.147	0.147	0.142
	Allotment Rate of Horizontal Foce		η	0.0693	0.1444	0.1458	0.1478	0.1379	0.1430	0.1430	0.0690
	Natural period of the Bridge		T (sec)	1.405							
	Equivalent Damping Ratio of the Bridge		he	0.135							
	Lateral Seismic Coefficient		khc	0.68							
	Design Lateral seismic Force		F (tf)	261	545	550	557	520	540	540	260
	Extent of Superstructure Displacement		Ur (cm)	34.568							

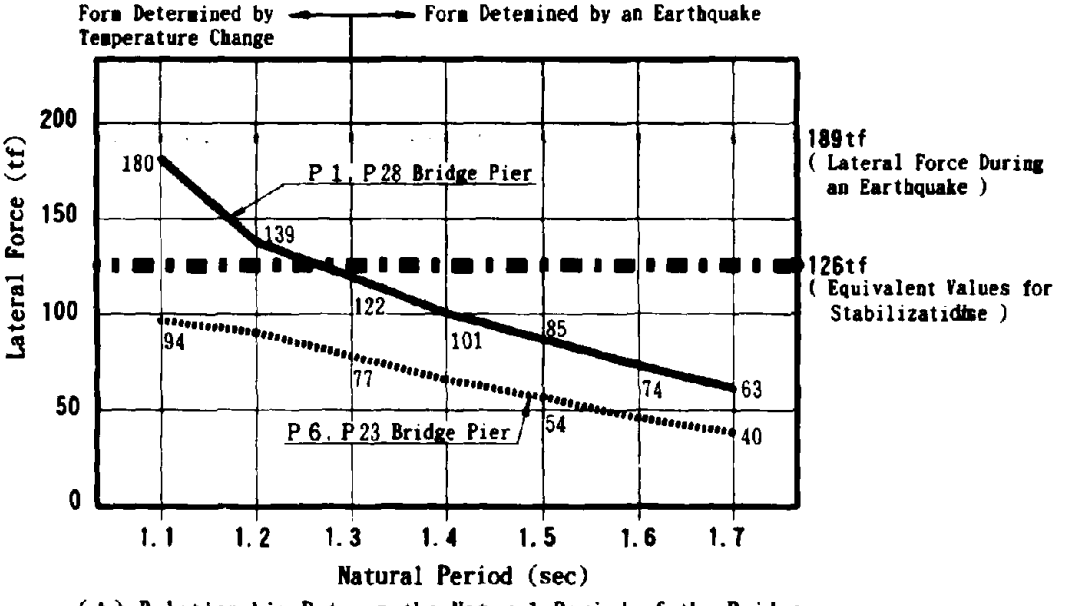

(A) Relationship Between the Natural Period of the Bridge and Thermal Lateral Force

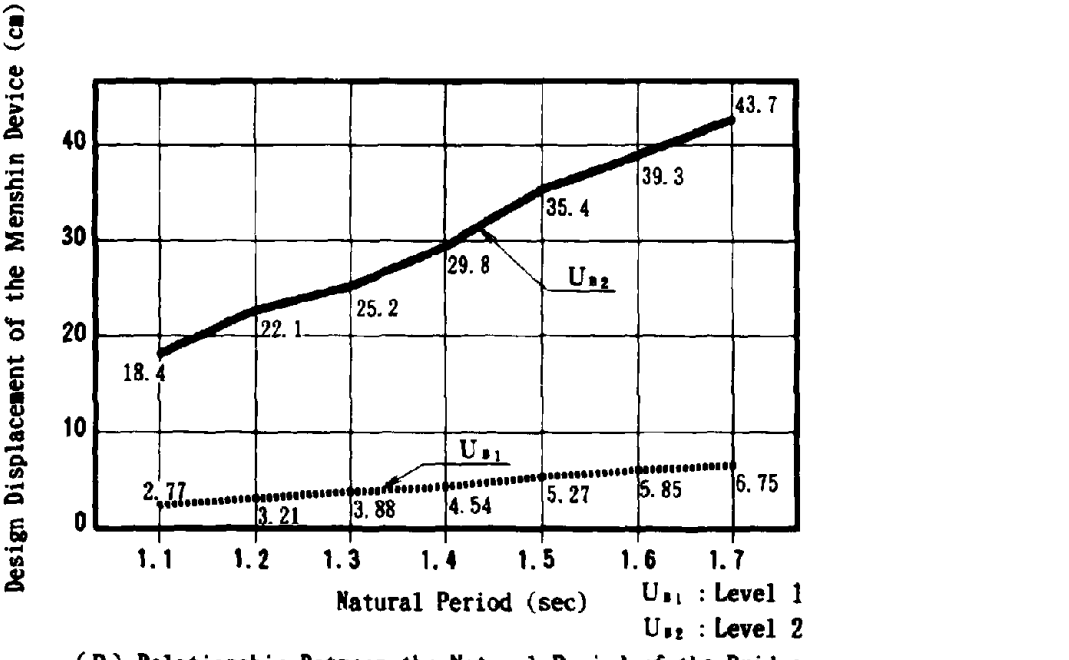

(B) Relationship Between the Natural Period of the Bridge and the Design Bearing Displacement

Figure 15.

CONCLUSION

At this time, the planning and design of this project has reached the stage where a variety of studies are in progress in accordance with basic policies. Because the examples introduced in this paper represent only part of the overall research effort, reports on details of these studies, the results of final design work, and the actual construction will be made available at every opportunity.

We would like to express our deep appreciation to members of the supervisory committee and to other related organizations for their generous cooperation and guidance with this project.

REFERENCES

1) Public Works Research Institute: Manual for Menshin Design of Highway Bridges (Drafts), Technical Note of Public Works Research Institute, Vol. 60, December, 1992.
2) Japan Road Association: Specifications for Highway Bridge , Part I to V, February, 1990.
3) Civil Engineering Journal, Vol. 35, No. 1, January, 1993.

CRITICAL LOADS OF ELASTOMERIC ISOLATORS AT HIGH SHEAR STRAIN

Ian G. Buckle and He Liu
Department of Civil Engineering
State University of New York at Buffalo
Buffalo, New York 14261

ABSTRACT

Most isolation systems in use today are based on elastomeric bearings. The combination of rubber layers and reinforcing steel gives an isolator which is stiff axially but soft laterally. Large period shifts may be achieved with these bearings simply by increasing the number and thickness of the rubber layers.

However, the shear flexibility of these short columns can lead to relatively low buckling loads which may be further reduced when high shear strains are simultaneously imposed. Various approximate methods have been proposed to account for the reduction in buckling load due to shear. The most common method is the area reduction formula which implies that the critical load is zero when the shear displacement is equal to the width of the bearing. This result is presumed to be conservative but the degree of conservatism is unknown.

This paper describes both analytical and experimental studies to determine the effect of high shear strain on the critical loads of a set of 5 inch and 10 inch square elastomeric bearings with shape factors ranging from 1.7 to 10.0. The results from ADINA finite element solutions are described and compared against experimental tests. Demonstration of significant axial load capacity at high shear strain is presented, and the effect of end (boundary) conditions is illustrated.

It is proposed that three regions be defined on the critical load-shear displacement plot which identify stable, unstable and transition conditions respectively.

INTRODUCTION

Recent surveys of seismic isolation systems around the world indicate that the majority of these systems use elastomeric bearings as the element of flexibility. These bearings may be of natural or synthetic rubber and maybe specially compounded to enhance their hysteretic damping. Alternatively the bearings may be structurally modified to include a damping element, such as the inclusion of a lead or granular core on the vertical axis of the bearing.

In a typical building, isolators are located under each column, usually in a sub-basement. In a bridge they may be placed under each girder at the abutment seats and between the column capbeam and the superstructure. There may be from 40 to 400 bearings in such a structure depending on its size and weight. The individual bearings

which make up the isolation system are frequently interconnected by a diaphragm which is rigid in its own plane and which enforces displacement compatibility amongst the various isolators.

Of particular interest to the design engineer is the failure mode or limit state of the system. This is currently done by examining three separate limit states for each individual bearing. These are the maximum shear strain in the elastomer, the displacement at which rollover commences and the load at which buckling may occur. The shear strain in the elastomer is used as a measure of load capacity since it compares the total strain from all sources (compression, shear and rotation) against the elongation-at-break for the elastomer. The other two limit states are measures of bearing stability. System stability is currently estimated by examining the bearing with the lightest axial load, in the case of rollover, and the greatest axial load, in the case of buckling.

This paper is concerned with the buckling loads of single elastomeric bearings under the combined actions of compression and shear forces (Figure 1). Although it is recognized [1,2] that system stability is a function of the spatial distribution of axial load and bearing (shear) stiffness (and is not solely governed by the condition of the most heavily loaded isolator), the properties of individual bearings must be well understood in order to make meaningful calculations of system response.

BUCKLING LIMIT STATE

Elastomeric bearings exhibit buckling phenomena in much the same way that structural columns are susceptible to compressive loads. Despite their short length, these "columns" may have low critical loads due to their extreme flexibility in shear. The buckling theory for these bearings at zero shear displacement, has been developed by Haringx [3] and Gent [4]. It is also summarized in Reference 5. It will be found in these references that the critical buckling load for an elastomeric bearing is given by:

$$P_c = \frac{R}{2}\left[\sqrt{1 + 4P_E/R} - 1\right] \qquad (1)$$

where:

P_E	=	$\pi^2 T/H^2$	
T	=	tilting (bending) stiffness for bearing of unit total height	
	=	$(E_b I)\,(H/T_r)$	
R	=	shear stiffness for bearing of unit total height	
	=	$K_r H$	
K_r	=	shear stiffness ignoring axial load effects	
	=	GA/T_r	
G	=	shear modulus of rubber	
A	=	bonded area of rubber	
T_r	=	total thickness of rubber (excludes shims)	
H	=	effective height of bearing (includes shims)	
E_b	=	bending modulus	
	=	$E_o\,(1 + f_b S^2)$	

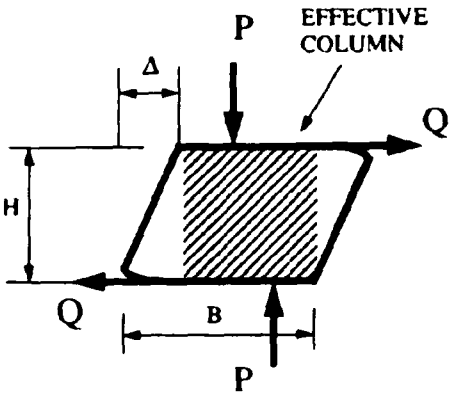

Fig.1 ELASTOMERIC BEARING UNDER COMBINED COMPRESSION AND SHEAR

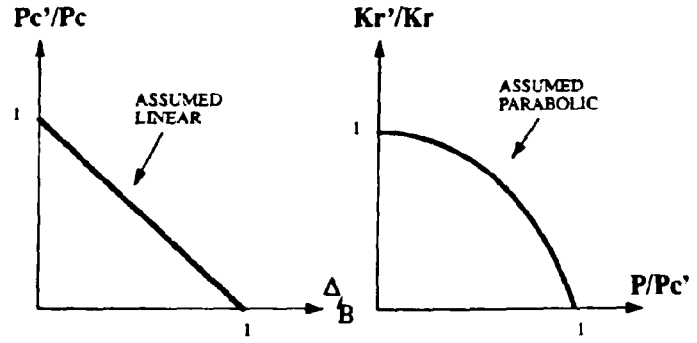

(a) BUCKLING LOAD-DISPLACEMENT CURVE

(b) SHEAR STIFFNESS-AXIAL LOAD CURVE

Fig.2 APPROXIMATE EFFECT OF SHEAR DISPLACEMENT ON CRITICAL LOAD AND SHEAR STIFFNESS

E_o = elastic modulus of rubber
f_b = bending constant
S = layer shape factor
I = moment of inertia of bearing about axis of bending

However this expression neglects the effect of large shear deformation on the properties of the elastomeric "column". In some design codes for bridges, where elastomeric bearings are used to accommodate thermal expansion, the effect of shear deformation is empirically included by reducing the critical load at zero displacement, Equation 1, by a factor based on the area of the effective column (Figure 1). The result, for rectangular bearings, is then as follows:

$$P_c' = P_c\left(1 - \frac{\Delta}{B}\right) \tag{2}$$

where: P_c' = modified buckling load
P_c = classical buckling load given by Equation (1)
Δ = shear displacement
B = bearing width

This relationship is illustrated in Figure 2a. One consequence of this expression is that as Δ approaches B, the effective buckling load becomes vanishingly small, a result which is not seen in practice.

Associated with the buckling phenomenon is the corresponding dependence of shear stiffness (Kr) on axial load (a decrease in stiffness may be used to indicate the onset of buckling). The relationship between axial load and shear stiffness at small shear deformations has also been established [4] and approximate formulations developed which are slightly easier to use. For example the following approximation is sometimes used [5]:

$$Kr' = Kr\left(1 - \left(\frac{P}{Pc'}\right)^2\right) \tag{3}$$

where Kr' = modified shear stiffness

This relationship is illustrated in Figure 2b. It will be seen that when the axial load is small compared to the buckling load ($P<0.3Pc'$), there is less than a 10% reduction in stiffness and in these cases this effect can be neglected. Since most elastomeric bearings have squat aspect ratios, their buckling loads are inherently high at small shear displacements. But, at higher displacements and for bearings with more slender geometries, this reduction in stiffness will be significant. Kr' becomes vanishingly small if P should approach Pc' which may easily happen if Equation (2) is correct and Δ is of

the same order as B. Such a reduction in stiffness has important consequences for the lateral stability of the bearing and the system of bearings of which it is a part. In view of the apparent profound effect that shear displacements may have on load capacity and shear stiffness, it is important that the validity of Equation (2) be established. A series of analytical studies was therefore undertaken to determine this effect, followed by a set of experimental tests to check the analytical results. These studies are described in subsequent sections of this paper.

FINITE ELEMENT ANALYTICAL STUDY

The approach used for the analytical study was to study a series of single elastomeric bearings of varying shape factors while deformed to increasing shear strains, using a nonlinear finite element model. Critical loads at each imposed shear strain were determined using three different procedures and these loads were then plotted against the Δ/B ratio.

The procedures used included a Southwell Plot Method, a Constant Shear Force Method and Constant Displacement Method.

Finite Element Solution

The ADINA [6] computer program was used for this analysis. ADINA permits the geometrical and material nonlinear analysis of both compressible and almost incompressible solids. Incremental analysis, using contact boundary elements as necessary, is performed using a displacement - pressure finite element formulation. The Mooney-Rivlin material model was used to characterize the elastomer at high strains and large deformations. A hydrostatic work term was added to the energy function to permit the inclusion of compressibility in the elastomer (although very small).

In order to reduce the computational effort, a plane strain restriction was imposed so that 2-dimensional analyses could be performed. This assumption is valid for strip bearings, but care should be taken when applying these results to square or rectangular bearings. For this reason the *ratio* of the critical loads at different Δ is considered to be more useful than the absolute value of the critical load.

Bearings Analyzed

Table 1 summarizes the six bearings analyzed. They are seen to comprise three, 5 inch wide bearings with internal layers of 1/4, 1/2 and 3/4 inch and 3, 10 inch wide bearings with the same range of layer thicknesses. The shape factors range from 3.3 to 20. The number of layers also varies so that the total height remains virtually constant (which was considered to be important in a comparative study of buckling loads).

The finite element mesh for a 2 dimensional slice through a 5 inch wide bearing with 4 layers comprised 651 nodes, 150 elements and 1240 displacement degrees of freedom.

TABLE 1

BEARING DETAILS AND CRITICAL LOADS AT SMALL SHEAR DISPLACEMENTS

Bearing Series No.	Bearing Size	No. of Layers	Thickness of Rubber (in)	Shape Factor	Critical Loads at Small Shear Displacement			
					Gent [4] Pcr (Δ=0) (kip)	ADINA Pmax (kip)	ADINA Southwell (kip)	ADINA $P_{Q=0}$
100	5x4.375	3	0.75	3.33	4.47	5.31	5.43	5.60
200	5x4.375	4	0.50	5.0	6.96	8.91	9.02	9.15
300	5x4.385	8	0.25	10.0	13.30	12.97	13.11	13.38
400	10x4.375	3	0.75	6.67	32.78	29.69	30.27	31.88
500	10x4.375	4	0.50	10.0	54.01	50.08	50.40	55.0
600	10x4.385	8	0.25	20.0	106.77	80.63	77.86	86.50

Analysis Procedure

As noted previously, ADINA was used to estimate the buckling loads by different techniques. These included the Southwell Plot Method, a Constant Shear Force and a Constant Displacement Method. Each is briefly described below.

Southwell Plot Method

Each bearing was first deformed in shear to a predetermined lateral displacement (Δ) and then additional lateral displacement (δ) were monitored as the axial load (P) was montonically increased. The ratio P/δ was plotted against P, as in the Southwell procedure, and a straight line fitted to the calculated responses. The intercept of this line with the horizontal axis is an indicator of the critical load at the initial displacement Δ. Δ was then increased, and the procedure repeated to find a new critical load corresponding to this new displacement. Figure 3 shows the Southwell plot for a 10 inch bearing, that has 8, 1/4 inch rubber layers, a shape factor of 20, and an initial shear displacement (Δ) of 2.9 inches. The apparent critical load is 51 kips. This value is compared to the value at zero shear displacement (which was 102.5 kip) and the ratio (0.5) may then be plotted against Δ/B (0.29) to develop a relationship between load and displacement for comparison with that in Figure 2a.

Constant Shear Force Method

As in the Southwell Plot Method, each bearing was first deformed in shear to a predetermined lateral displacement, Δ, and then while the shear force was held constant, the axial load was montonically increased. However, in contrast to the Southwell Method, the load was increased until a maximum or limiting value was reached. This

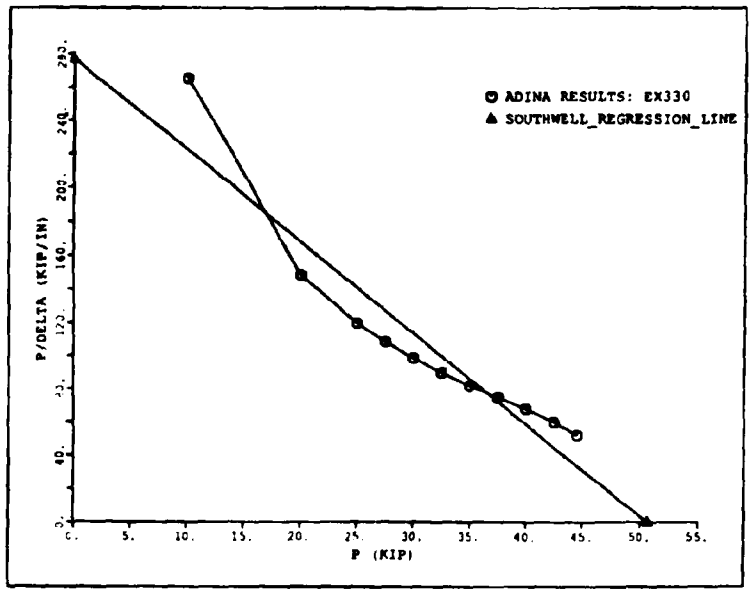

Fig. 3 SOUTHWELL PLOT FOR A 10 INCH ELASTOMERIC BEARING AT 2.9 INCH INITIAL SHEAR DISPLACEMENT

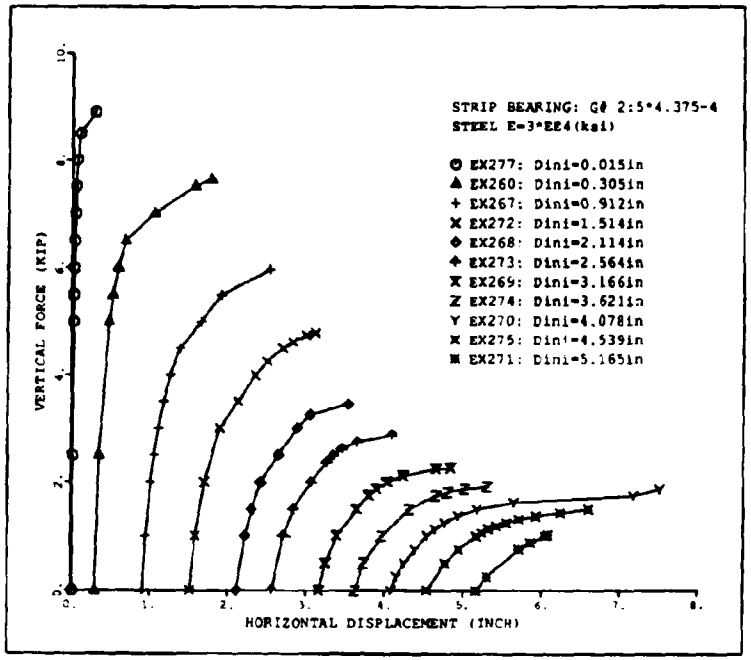

Fig. 4 MAXIMUM VERTICAL LOAD (P_{max}) FOR 5 INCH BEARING AT VARIOUS INITIAL DISPLACEMENTS (ADINA SOLUTIONS)

value was determined by plotting the axial load against the horizontal displacement and identifying the load at which softening occurs (rapid increases in displacement for small increases in load). One such plot is shown in Figure 4. This is for a 5 inch bearing with four, 1/2 inch thick rubber layers and for initial displacements ranging from 0.015 in up to 5.165 ins.

Constant Displacement Method

In both the Southwell and Constant Shear Force methods, the lateral displacement increases beyond the initial displacement as the axial load increases. The displacement which corresponds to the calculated critical load is therefore uncertain. In the Constant Displacement Method, the initial displacement was held constant while the axial load was increased. The shear force, Q, necessary to hold the bearing at this displacement was monitored and the critical load condition was assumed to occur when this force became zero; i.e., when Q = 0. The advantage of this method is the clear definition of the critical load and the corresponding shear displacement.

Figure 5 shows a plot of P against Q for the same bearing as in Figure 4 (5 inch width, four 1/2 inch rubber layers). The shear force Q is seen to decrease from the initial value (which corresponds to the imposed shear displacement) as the axial load is increased. Critical axial loads are given by the intercept on the Q = 0 axis. It will be seen the critical loads in Figure 5 are higher than they are in Figure 4 for the same initial shear displacement. One reason for this is that the imposed boundary conditions are different for the two cases. The implication of restraining the shear displacement to a constant value (Figure 5) is a more stable "column" with higher buckling loads. It should also be noted that the critical loads given in Figure 4 and 5 are for a one-inch slice of an infinitely long strip. Approximate estimates of the critical load for a 5 inch square bearing may be found by multiplying these values by 5. The number so obtained will be an upper bound on the true buckling load.

Analytical Results and Discussion

Buckling loads from the various methods described above have been plotted against the shear displacement in Figure 6. Both the loads and displacements are expressed by non-dimensional ratios critical loads (Pc') are given as a fraction of the critical load at zero displacement (Pc). Shear displacements (Δ) are given as a fraction of the bearing width (B).

Also shown in Figure 6 is the relationship given by Equation 2. Whereas it is clear that Pc' does reduce with increasing Δ it does not do so at the rate indicated by Equation 2. The ADINA solutions in Figure 6 indicate substantial residual capacity at Δ = B whereas Equation 2 implies that Pc' should be zero at this point.

It is also clear that the boundary conditions have a significant effect on Pc' at any given value for Δ/B. In Figure 6, two Southwell curves are given - one based on the initial displacement and the other based on the "final" displacement (the displacement calculated for the last load step in the Southwell procedure). Also plotted is the result from the constant displacement procedure. It is seen that for a given value of Δ/B, the

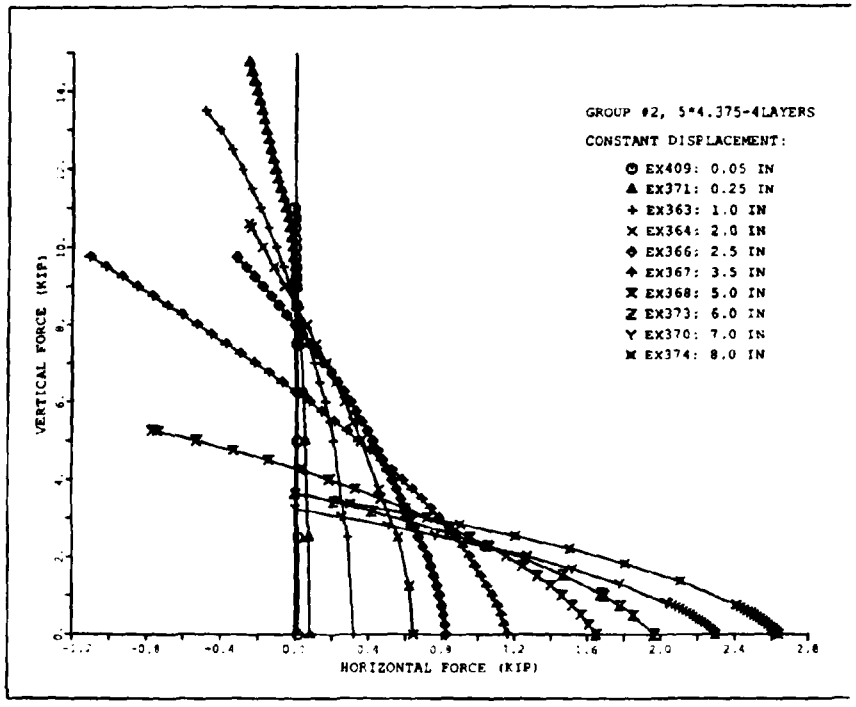

Fig.5 HORIZONTAL SHEAR (Q) vs VERTICAL LOAD P
FOR CONSTANT DISPLACEMENT METHOD
(ADINA SOLUTIONS)

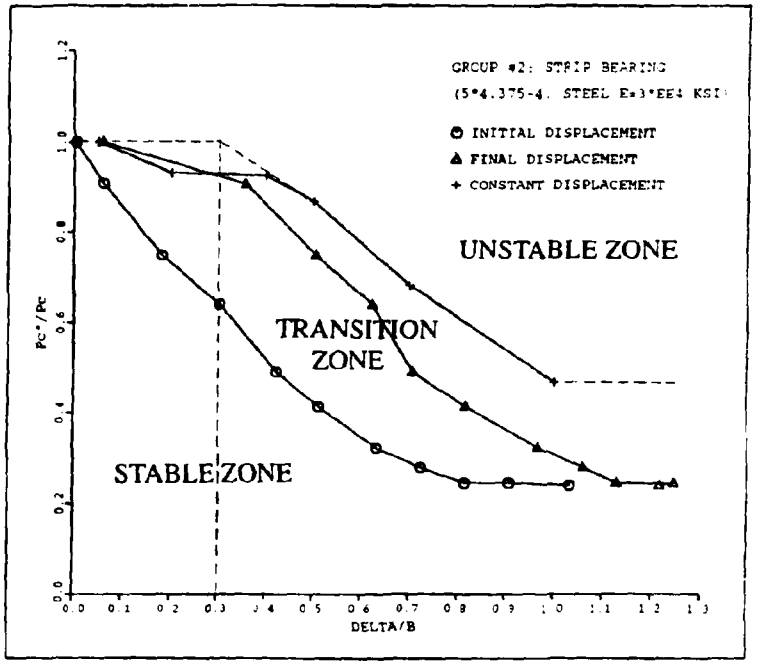

Fig. 6 CRITICAL LOAD RATIO vs Δ / B
FROM SOUTHWELL METHOD AND
CONSTANT DISPLACEMENT METHOD
(ADINA SOLUTIONS)

calculated buckling load depends on whether the bearing is unrestrained and free to displace from its initial value or whether the bearing is restrained against further shear displacement. It can be argued that boundary conditions in the field fall somewhere between these two extremes.

Based on these results, it appears feasible to define stable and unstable regions with a transition zone that is dependent on the characteristics of the isolation system i.e., the degree of restraint provided by other, non-critical, bearings adjacent to the subject bearing. Such a set of regions is illustrated in Figure 6.

EXPERIMENTAL STUDIES

An experimental test program was undertaken to verify the ADINA solutions. These tests were performed at the Earthquake Engineering Research Center (EERC) of the University of California at Berkeley.

Bearings Tested

Eighteen bearings of the same size and construction as those given in Table 1 were fabricated from natural rubber with a nominal shear modulus, at 50% strain, of 100 psi. These 18 bearings comprised three specimens of each of the six types listed in Table 1. The bearings are identified as follows:

5 inch square:	3x3/4 inch layers:	Nos 101, 102, 103
	4x1/2 inch layers:	Nos 201, 202, 203
	8x1/4 inch layers:	Nos 301, 302, 303
10 inch square:	3x3/4 inch layers:	Nos 401, 402, 403
	4x1/2 inch layers:	Nos 501, 502, 503
	8x1/4 inch layers:	Nos 601, 602, 603

Test Procedure

The single bearing test machine at the EERC, Richmond Field Station, was used for these tests (Figure 7). The Constant Displacement Method (used for the ADINA solutions) was chosen for these tests because it enabled excellent control over the experiment and assured the safety of the actuators and personnel. By contrast, under the Southwell and Constant Shear Force Methods, the testing machine is less "stable" because of the unrestrained shear displacements.

The test sequence for each of the eighteen bearings was as follows:

(a) select a shear displacement (Δ)
(b) perform 5 cycles of reversed shear to $\pm\Delta$ to scrag the bearing to this displacement
(c) perform 5 cycles of revised shear to $\pm\Delta$ to obtain the shear stiffness of the scragged bearing
(d) perform the stability test by first imposing Δ and then increasing the axial load until the shear force, required to maintain Δ, becomes zero

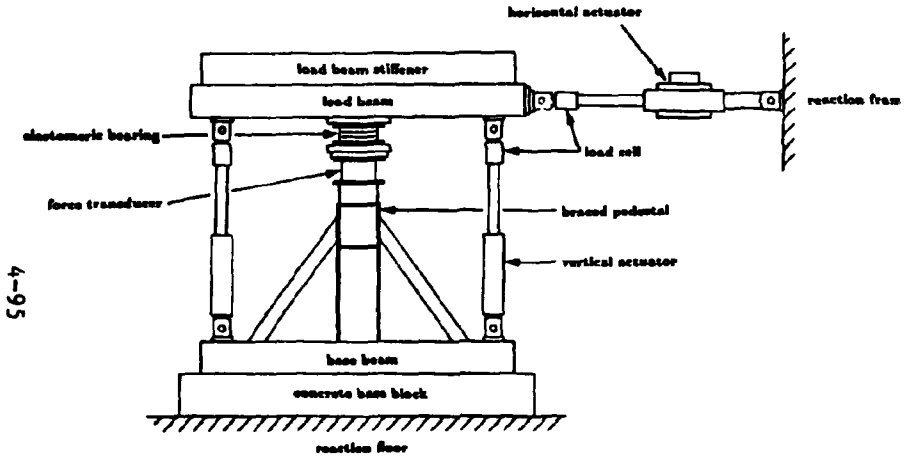

Fig. 7 SINGLE BEARING MACHINE FOR COMBINED COMPRESSION AND SHEAR TESTS (FROM [7])

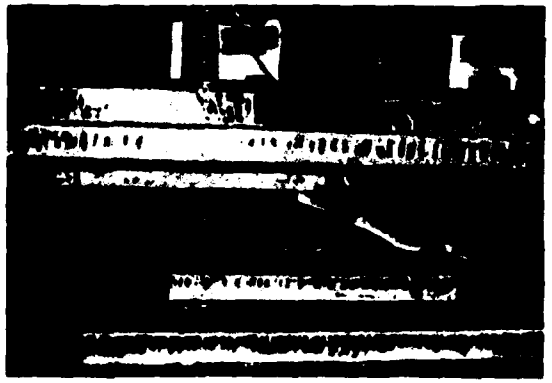

Fig. 8 10 INCH BEARING (No. 501) AT SHEAR DISPLACEMENT = 0.6B

(e) perform 5 cycles of reversed shear to $\pm\Delta$ to obtain a new value of shear stiffness to compare with the previous value

(f) increase the shear displacement and repeat from (b) above

Values for Δ ranged from 0.2B to 1.2B in increments of 0.2B. Corresponding shear strains in the elastomer ranged from 0.5 to 3.0 for the 5 inch bearings and from 1.0 to 6.0 for the 10 inch bearings. Figure 8 shows a 10 inch bearing at Δ = 0.6B (shear strain = 3.0) sustaining a load close to its critical load.

Due to the severe strain demand in the 10 inch bearings, at the high end of the range for Δ, rupturing was common during step (f) and sensible buckling tests could not be completed for values of Δ exceeding 0.8B (shear strain = 4.0). Also, the vertical load capacity of the test machine was limited to about 250 kips which meant that the 10 inch bearings could not be loaded to their critical state while at small shear displacement. Therefore, to obtain these critical loads extrapolation from the test data is necessary.

Test Results

Figure 9 shows the P-Q curves for bearing number 202 (5 inch square, four 1/2 inch layers). This figure is the experimental equivalent of the ADINA solution given in Figure 5. Results for imposed displacements of 0.2B, 0.4B, 0.6B, 0.8B, 1.0B and 1.2B are shown. Whereas a direct comparison with Figure 5 is not possible (Figure 5 is for a one-inch slice of an infinite strip), it is clear that the trends are the same.

To enable direct comparisons to be made between experiment and theory, both sets of results are first normalized with respect to the critical load at zero displacement. Also the shear displacements are expressed as a fraction of the bearing width. When this is done for the set of 5 inch bearings, the results shown in Figures 10, 11 and 12 are obtained. Good agreement is demonstrated for all three bearings across the entire range of displacement (Δ/B).

CONCLUSIONS

It may be concluded, based on the results presented here, that the reduction in critical load due to the effect of high shear strain is conservatively estimated by the area reduction formula. It appears from a limited set of ADINA finite element analyses and a corresponding set of experimental tests that substantial reserve of vertical load capacity exists even when the shear displacement is equal to the width of the bearing.

It is also clear that the end conditions are very significant and that if the bearing is unrestrained (in shear) the critical loads may be substantially less. Since there is some degree of restraint in most multiple bearing isolation systems (provided by the "non-critical" bearings) the unrestrained results may be unduly conservative. A transition zone is therefore identified in this paper between stable and unstable regions. If more rigorous results are required, an analysis of the stability of the complete isolation system is recommended.

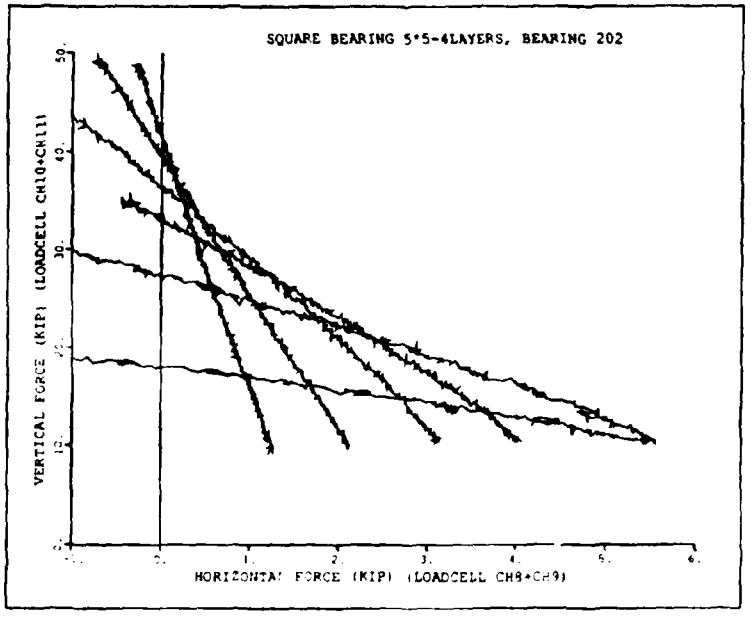

Fig. 9 P-Q CURVES FOR BEARING 202
EXPERIMENTAL RESULTS

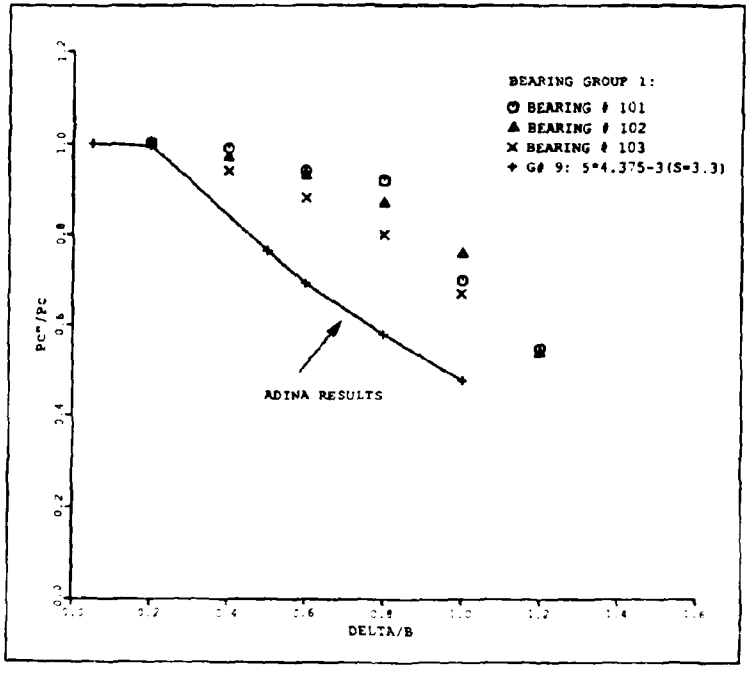

Fig. 10 COMPARISON BETWEEN ADINA AND EXPERIMENTS
FOR CRITICAL LOAD RATIOS vs Δ / B
(BEARING GROUP 1)

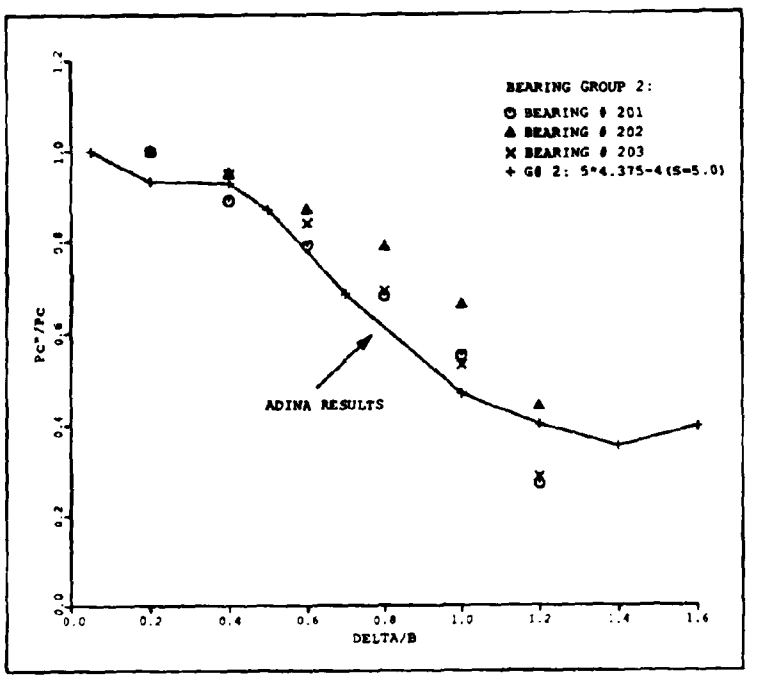

Fig. 11 COMPARISON BETWEEN ADINA AND EXPERIMENTS FOR CRITICAL LOAD RATIOS vs Δ / B (BEARING GROUP 2)

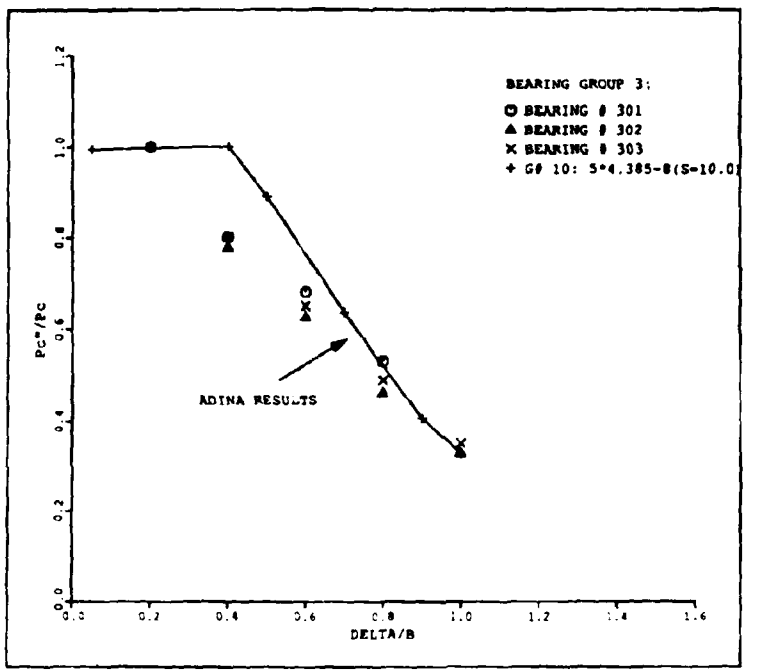

Fig. 12 COMPARISON BETWEEN ADINA AND EXPERIMENTS FOR CRITICAL LOAD RATIOS vs Δ / B (BEARING GROUP 3)

ACKNOWLEDGEMENTS

The work described in this paper was funded by the National Science Foundation through the National Center for Earthquake Engineering Research. It is part of a larger coordinated study on the mechanics of elastomeric isolation bearings at high shear strain which involves researchers at the State University of New York at Buffalo, the University of California at Irvine and the University of Washington. The contributions of these researchers to this study is hereby acknowledged.

The experimental work reported herein was conducted with the cooperation of Professor J. M. Kelly of the Earthquake Engineering Research Center of the University of California at Berkeley. The assistance of Dr. Kelly, Dr. Aiken, Peter Clark and the technical staff at EERC is gratefully acknowledged.

REFERENCES

1. Buckle, I.G. and Liu, He, "Stability of elastomeric base isolators," Proc. Second US-Japan Workshop on Earthquake Protective Systems for Bridges, Public Works Research Institute, Tsukuba, Japan, 1992, pp. 241-253.

2. Buckle, I.G. and Liu, He, "Stability of elastomeric seismic isolation systems," Proc. Sem. Seismic Isolation, Passive Energy Dissipation and Active Control, Applied Technology Council Report ATC 17-1, 1993, pp. 293-305.

3. Haringx, J.A., "On highly compressible helical springs and rubber rods and their application for vibration-free mountings, II," Philips Research Report, Vol 4, No. 49, 1949.

4. Gent, A.N., "Elastic stability of rubber compression springs," Jl, Mechanical Engineering Science, Vol. 6, No. 4, 1964, pp. 318-326.

5. Buckle, I.G. and Kelly, J.M., "Properties of slender elastomeric isolation bearings during shake table studies of a large scale model bridge deck," Proc. Second World Congress on Joints and Bearings, San Antonio, 1986, also in Special Publication on Joint Sealing and Bearing Systems for Concrete Structures. American Concrete Institute, SP-94, Detroit, 1986, pp. 247-269.

6. Bathe, K.J., "Nonlinear finite element analysis and ADINA," Proc. Sixth ADINA Conference, Massachusetts Institute of Technology, Cambridge, 1987.

7. Kelly, J.M., and Quiroz, E., "Mechanical characteristics of neoprene isolation bearings" University of California, Berkeley, Report UCB/EERC 92/11, 1992, 54 pp.

A COMPARISON STUDY ON THE SUPPORT SYSTEMS OF A MULTI-SPAN CONTINUOUS STEEL BRIDGE

Jun NANJOH, Motohiko NISHIBAYASHI and Yukio ADACHI

Hanshin Expressway Public Corporation
4-1-3 Kyutaro-cho chuoh-ku Osaka 541 JAPAN

SUMMARY

A comparison study on support systems is performed for a multi-span continuous steel bridge approximately 1.25km long. Two support systems, conventional rubber bearings and menshin bearings, are considered in this study. In the case of this long bridge, the longitudinal movement due to temperature fluctuation is 22.5cm. If the conventional rubber bearings are employed, the longitudinal displacement caused by the Japanese level-1 earthquake is greater than that by the temperature fluctuation. On the other hand, if the menshin bearings are employed, the longitudinal displacement can be less than that by the temperature change. But the seismic coefficient of the bridge with the menshin bearings is slightly greater than that of the bridge with the conventional rubber bearings. However, because of a large L/B ratio, the bending stiffness of the girder is very weak in the transverse direction so that the transverse movement in the middle of the bridge for both bearings is almost as much as or greater than the longitudinal movement, while the transverse movement at the end is so slight that the end supports can be pin-fixed in the transverse direction.

INTRODUCTION

Minimizing the number of expansion joints in highway bridges is one of the main approaches of reducing noise and vibration problems, reducing maintenance works and improving driving condition. In order to minimize the number of expansion joints, Hanshin Expressway has employed conventional rubber bearings for the support systems of many highway bridges.

From the view point of seismic design, the roles of these conventional rubber bearings are:

1) To distribute the horizontal inertia force of girders to each column pier
2) To reduce the seismic force by making a long-period structure.

The conventional rubber bearings have been employed for many multi-span continuous bridges with span lengths of 200m~300m. This design method does not rely on the damping effect of the bearings because it is so slight.

On the other hand, menshin bearings have such great damping effects that the menshin bearings have an additional role:

3) To reduce the seismic force and the displacement by the damping effects.

Therefore, the use of the menshin bearings might make more multi-span and longer continuous bridges.

From this point of view, this study tries to determine the possibility of more multi-span and longer continuous bridges using an actual road alignment condition, and also tries to determine the advantages and the disadvantages of the conventional rubber bearings and the menshin bearings.

BRIDGE SITE AND BRIDGE CONFIGURATION

BRIDGE SITE

The road alignment for a multi-span continuous bridge is considered better if it satisfies the following conditions:

1) The plane alignment is almost straight.
2) The vertical alignment is almost flat.
3) Each span is almost the same.
4) Each foundation type is the same.

From this point of view, the "Kobe-Port Island" section of the Bay Route in the Hanshin Expressway network is selected as a highly feasible place for the bridge. Fig.1 shows the bridge site.

BRIDGE CONFIGURATIONS

Fig.2 shows the rough drawings of the bridge. The superstructure is a 20-span continuous steel box-girder bridge with a concrete deck; the span length and the width are 50m+2x55m+14x66.5m+2x55m+50m=1252.5m and 27.5m respectively. Concrete framed column piers are considered for the substructure in this case. The height of the substructure is 22m~27m. The foundation is cast-in-place concrete piles.

GROUND CONDITION

The Kobe-Port Island is a man-made island reclaimed almost 40 years ago. Fig.3 shows typical boring log data. The dynamic characteristic value (T_G) of this site is 1.0~1.5sec, which is considered somewhat long, so that this site is classified as Group-3 (Soft ground) by the Japanese Design Specifications for Highway Bridges. Nevertheless, alluvium clay strata several meters deep under the old sea bed have already been consolidated and have 3~5 N-value; furthermore, any dynamic soil parameter of the reclaimed layer is not required to be reduced to zero by the Japanese code even if the reclaimed layer has some possibility of liquidation. Therefore, this site is not so bad for constructing such a long-period bridge as this.

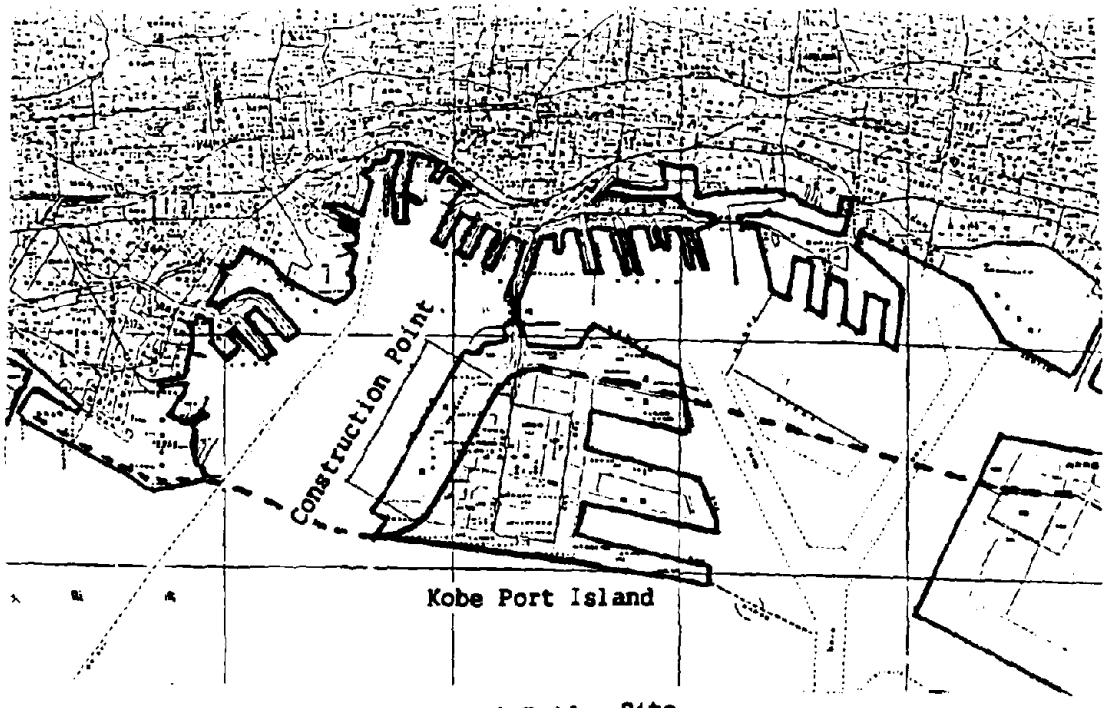

Fig.1 Bridge Site

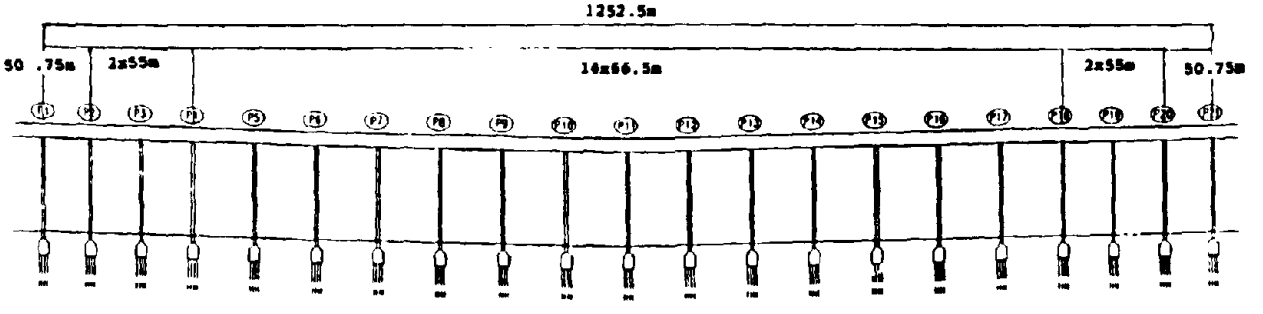

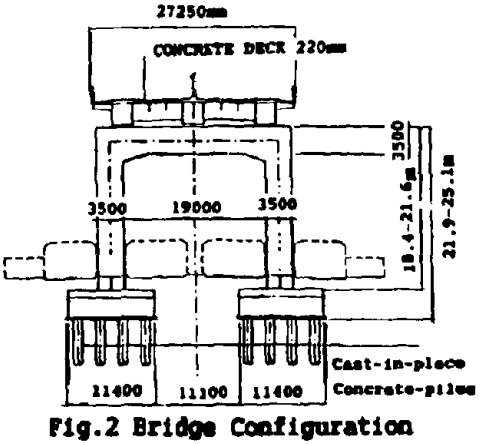

Fig.2 Bridge Configuration

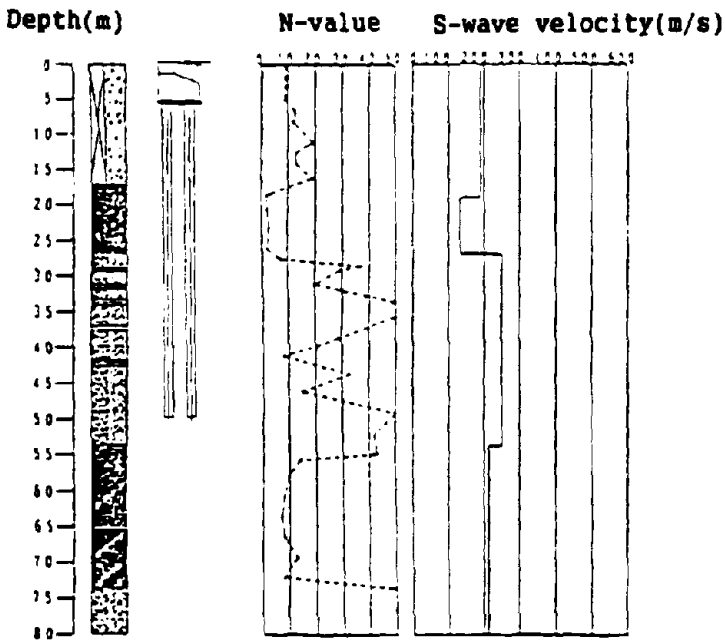

Fig.3(a) Typical Boring Data(a)

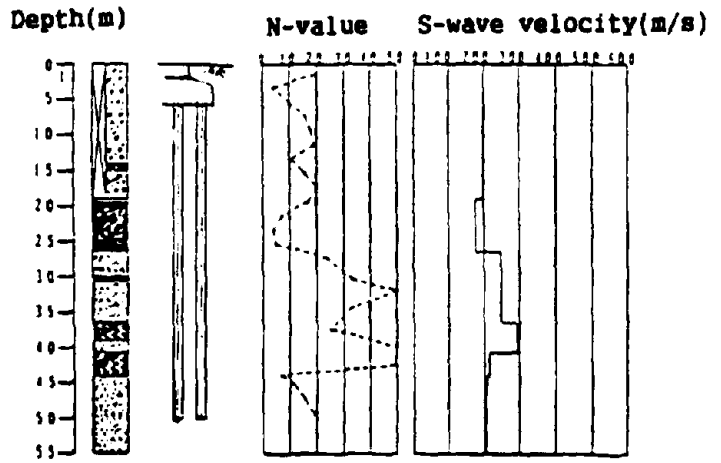

Fig.3(b) Typical Boring Data(b)

SUPPORT SYSTEMS

Two support systems are considered for the support system of the multi-span continuous steel bridge. These are conventional rubber bearings (CRB) and menshin bearings.

This study mainly discusses the difference between these two bearings.

END SUPPORT SYSTEM

END SUPPORT IN THE TRANSVERSE DIRECTION

If conventional rubber bearings and menshin bearings are used, they can reduce seismic force not only in the longitudinal direction but also in the transverse direction, because of their long natural periods. Continuous bridges of ordinary length are relatively wide compared to the length so that the bending stiffness (EI_z/L) in the transverse direction is relatively stiff. Therefore, the superstructure of continuous bridges of ordinary length can be considered as a rigid body in the transverse direction. On the contrary, in the case of the multi-span continuous bridge approximately 1.25km long, the superstructure may not move as a rigid body because the bending stiffness in the transverse direction is relatively weak compared to that of the continuous bridge of ordinary length.

In order to ensure the transverse movement of the long bridge with soft supports, the vibration modes are investigated. In this study, the framed column piers are treated as single column piers that have the same dynamic properties in the elastic region and all bearings are treated as elastic bearings with the average bearing stiffness calculated from the rubber properties and the dimension required by the service load condition. The vibration modes are calculated for the following two conditions;

1) Both end bearings are pin-fixed and other supports are conventional rubber bearings or menshin bearings in the transverse direction.
2) All supports are conventional rubber bearings or menshin bearings in the transverse direction.

Fig.4 shows the eigenvalues and the mode shapes of the bridge. For both cases, the eigenvalues and mode shapes of the first mode are almost the same. In other words, there is no difference in the first mode whether the end bearings are pin-fixed or elasticly supported. Furthermore, in the second case, the transverse movement at the end of the third mode is not large while the end supports are not pin-fixed. The effective masses of the first and the third modes are almost 90% (The effective masses of the first mode are 75%~77%). Therefore, in the case of a long bridge like this, there is little difference to the vibration modes whether both ends are supported elasticly or pin-fixed in the transverse direction.

END SUPPORT IN THE LONGITUDINAL DIRECTION

According to the Japanese code, the temperature range is -10°C~50°C. The longitudinal movement due to temperature change is 22.5cm at the end support as shown in Fig.5. Therefore, the dimension of the end support is very big compared to the other bearings. However, the vertical force at the end support

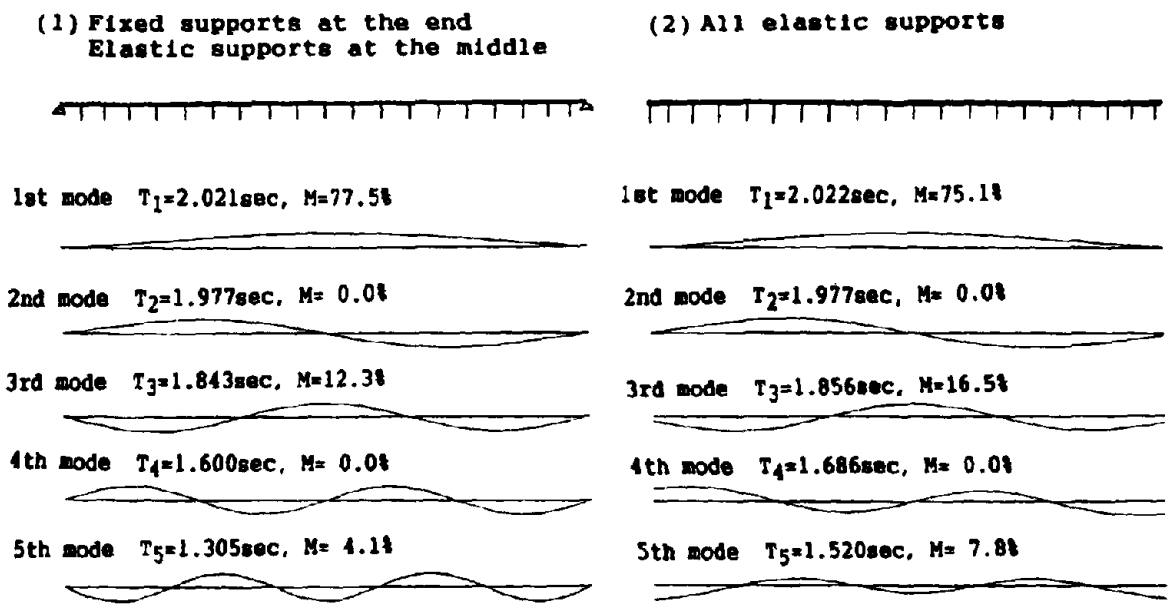

Fig. 4 Transverse Vibration Modes

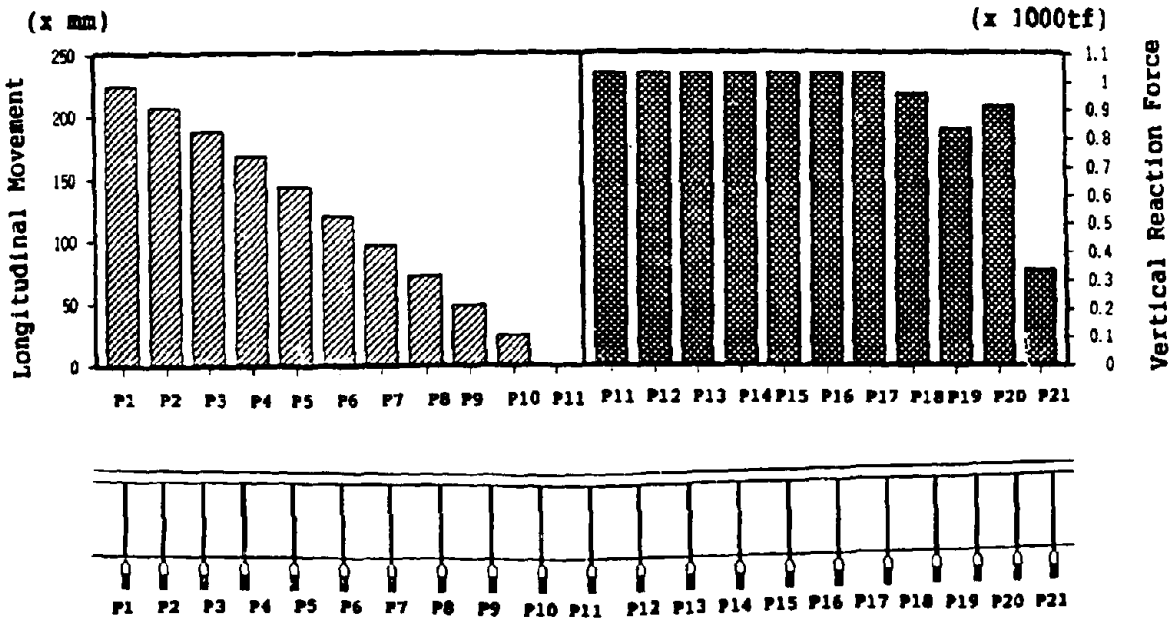

Fig. 5 Longitudinal Displacement by temperature change and Vertical Reaction Force of the bearings

is very small, as also shown in Fig.5. Therefore, the end bearings are very hard to design.

END SUPPORT CONDITION

According to the two reasons mentioned above, there is no positive reason to employ elastic bearings to the end supports. It might be appropriate to pin-fix the end bearings in the transverse direction while allowing it to be free in the longitudinal direction.

Therefore, in this study, the end bearings are free in the longitudinal direction and pin-fixed in the transverse direction.

COMPARISON BETWEEN SEISMIC ISOLATION BY CONVENTIONAL RUBBER BEARING AND MENSHIN BEARING

COMPARISON STUDY ON SUPPORT SYSTEMS

This study investigates the difference between multi-span continuous bridges with conventional rubber bearings and with menshin bearings (CRB design and menshin design) from the viewpoint of temperature changes and earthquakes. Lead rubber bearings are used to represent the menshin bearings in this study.

In design of a long-span bridge, there is a number of possibilities to design bearings. The following three conditions are considered for designing bearings in this study. The first 2 cases are designed according to the service load and the Japanese level-1 earthquake load. The last case is designed according to the service load condition and the Japanese level-2 earthquake load. The menshin bearings must be satisfied with the level-2 earthquake so that the menshin bearings of the first 2 cases violate the menshin code.

CASE(1) Minimum sized bearings for the service load condition

The displacement due to temperature fluctuation is very big in this case. If the bearings are designed according to the service load conditions, the Japanese level-1 earthquake conditions are automatically satisfied.

CASE(2) Bearings designed by the CRB design method

The fundamental seismic coefficient(k_h) of the Japanese level-1 earthquake for Group-3 (Soft soil) is 0.24g. The seismic coefficient in the range of 0.17~2.1sec is greater than 0.24g and the seismic coefficient of T=2.1sec is 0.24g. Usually, the bridge with conventional rubber bearings targets this period. If the damping effect of menshin bearings is ignored, the menshin bearings can be treated as conventional rubber bearings. From this viewpoint, both bearings are designed following to the CRB design method.

CASE(3) Bearings designed by the menshin code

The conventional rubber bearings are not required to resist against the Japanese level-2 earthquake load because stoppers are mounted for avoiding the excessive movement beyond the movement calculated by the level-1 earthquake. However, according to the menshin code, the menshin

bearings must be designed against the Japanese level-2 earthquake and the stoppers are not usually mounted. Therefore, only menshin bearings are investigated.

Fig.6 shows the Japanese level-1 and level-2 earthquake spectra.

All results are represented by those of P-7 because the height of P-7 is the average and the seismic force of P-7 in the transverse direction is almost the largest.

All results are obtained from the static analysis. In this calculation, the equivalent stiffness of each menshin bearing depends on the displacement so that iterated calculations are performed.

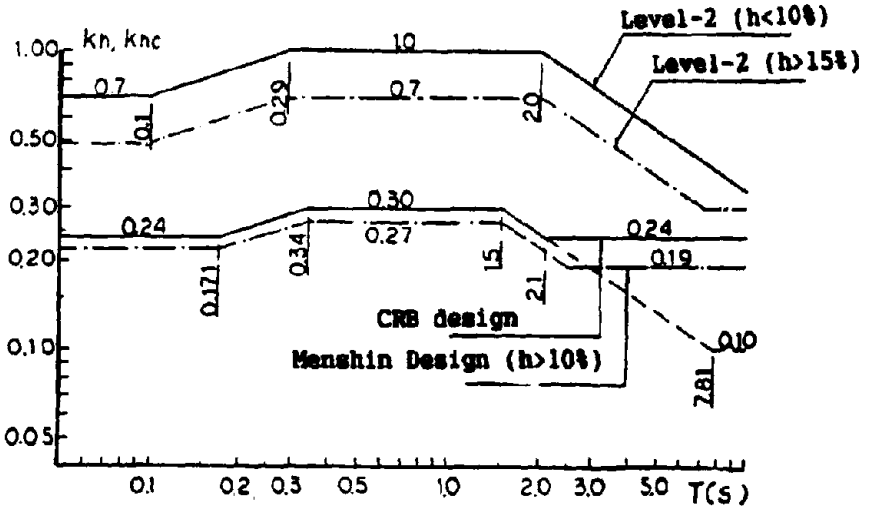

Fig.6 Design Earthquake Spectra

CASE(1) MINIMUM SEIZED BEARINGS FOR THE SERVICE LOAD CONDITIONS

Table 1 shows the dimension of the bearings. Fig.7 and Fig.8 show the results of displacement and horizontal design force.

In case of the conventional rubber bearings, the longitudinal displacement caused by the Japanese level-1 earthquake is greater than the movement due to temperature fluctuation so that the design displacement is determined by the earthquake load. However, in the case of the menshin bearings, the displacement is less than the movement due to the temperature change so that the design displacement of this case is determined by the temperature change.

The design horizontal force due to the level-1 earthquake for both directions are greater than the force due to temperature change so that the design horizontal force is determined by the earthquake load. The seismic force of the conventional rubber bearings is greater than that of the menshin bearings.

The interesting point is that the design horizontal force in the transverse direction is greater than that in the longitudinal direction while the seismic movement in the transverse direction is almost the same as the longitudinal one.

CASE(2) BEARINGS DESIGNED BY THE CRB DESIGN METHOD

Table 2 shows the dimension of the bearings. The results are shown in Fig.9 and Fig.10.

In the case of the CRB design, the displacement resulting from the level-1 earthquake is still greater than that by temperature change while it is slightly less than that of the first case. The displacement of the menshin design is almost the same as that by the temperature change.

The seismic force of the menshin design is less than that of the CRB design. The transverse seismic forces are somewhat greater than the longitudinal ones.

CASE(3) BEARINGS DESIGNED BY THE MENSHIN CODE

The dimensions of the bearings are determined by the Japanese level-2 earthquake condition.

All results are shown in Fig.11 and Fig.12. Table 3 shows the dimension of the bearings.

In this case, the menshin bearings are designed in order that the natural period of the bridge equals T=1.2sec (Twice of the natural period (0.6sec) of the bridge without the menshin bearings). In this case, the displacement due to the level-1 earthquake is less than the displacement due to the temperature fluctuation. However, the seismic coefficient of the menshin design for the level-1 earthquake is slightly greater than that of the second case of the CRB design.

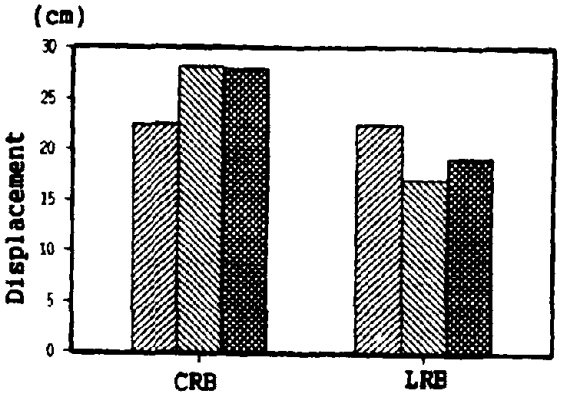

▨ Temperature ▧ Longitudinal ▩ Transverse

Fig.7 Comparison between the Movement by Temperature and Earthquake (Case 1)

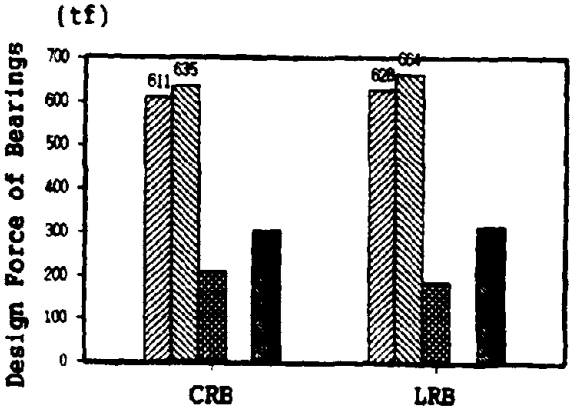

▨ F_{EQ}(Long.) ▧ F_{EQ}(Trans.) ▩ $F_{Temp.}$(@P7) ▩ $F_{Temp.}$(@P2)

Fig.8 Comparison between the Force by Temperature and Earthquake (Case 1)

Table 1 Bearing Dimensions and Natural Period and Seismic Coefficient of the Bridge(Case 1)

Substructure	Bearing	Dimension	Period	Seismic Coeff.
Concrete Column Pier	CRB	125x125x19.2~28.8	2.23sec(Long.) 2.22sec(Trans.)	0.23g(Long.) 0.23g(Trans.)
	LRB	130x130x24.0~30.0 Lead 4xφ15	1.63sec(Long.) 1.79sec(Trans.)	0.26g(Long.) 0.24g(Trans.)

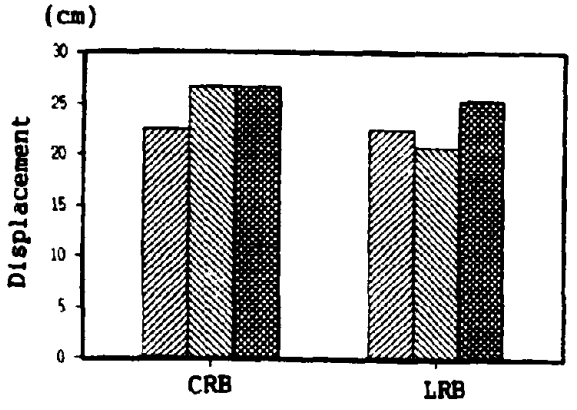

Fig.9 Comparison between the Movement by Temperature and Earthquake (Case 2)

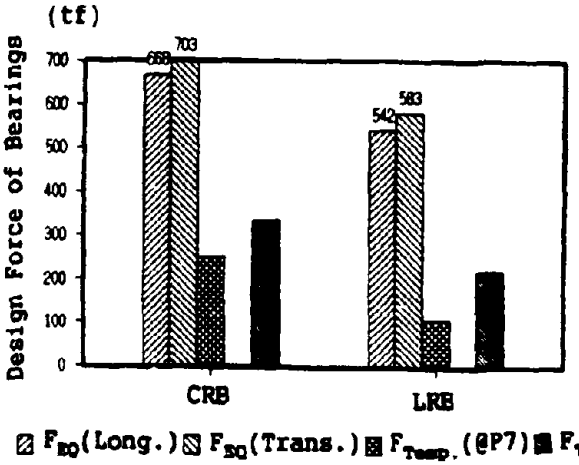

Fig.10 Comparison between the Force by Temperature and Earthquake (Case 2)

Table 2 Bearing Dimensions and Natural Period and Seismic Coefficient of the Bridge(Case 2)

Substructure	Bearing	Dimension	Period	Seismic Coeff.
Concrete Column Pier	CRB	125x125x21.0~35.0	2.04sec(Long.) 1.96sec(Trans.)	0.24g(Long.) 0.25g(Trans.)
	LRB	130x130x36.0 Lead 4xϕ15	1.90sec(Long.) 2.21sec(Trans.)	0.23g(Long.) 0.21g(Trans.)

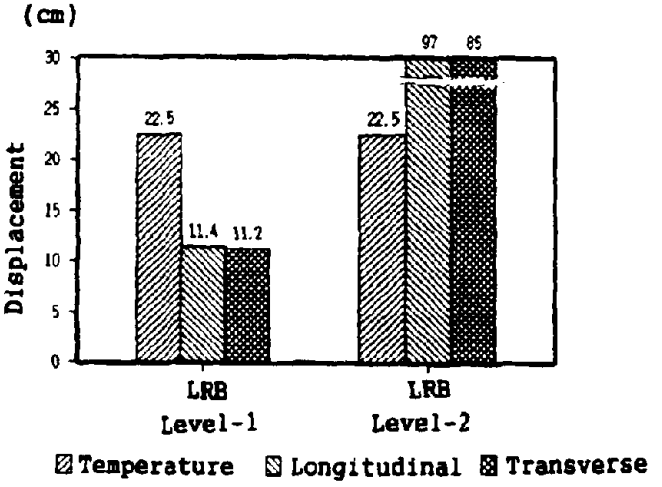

Fig.11 Comparison between the Movement by Temperature and Earthquake (Case 3)

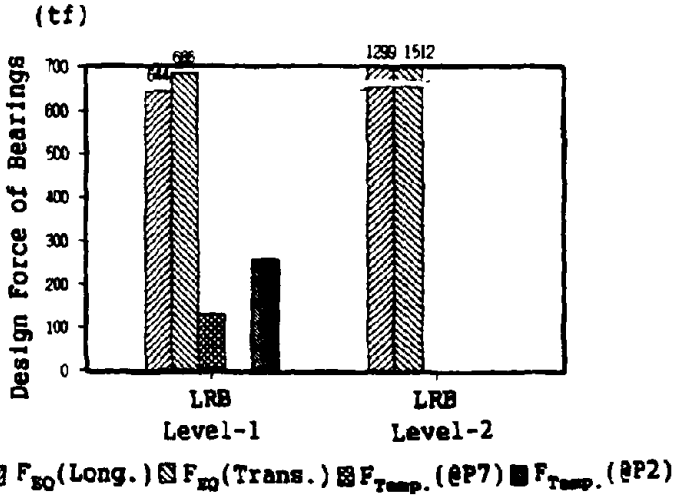

Fig.12 Comparison between the Force by Temperature and Earthquake (Case 3)

Table 3 Bearing Dimensions and Natural Period and Seismic Coefficient of the Bridge(Case 3)

Substructure	Bearing	Dimension	Period	Seismic Coeff.
Concrete Column Pier	LRB	145x145x48.0 Lead 4xϕ20	Level-1 1.21sec(Long.) 1.16sec(Trans.)	Level-1 0.27g(Long.) 0.27g(Trans.)
			Level-2 2.55sec(Long.) 2.59sec(Trans.)	Level-2 0.59g(Long.) 0.59g(Trans.)

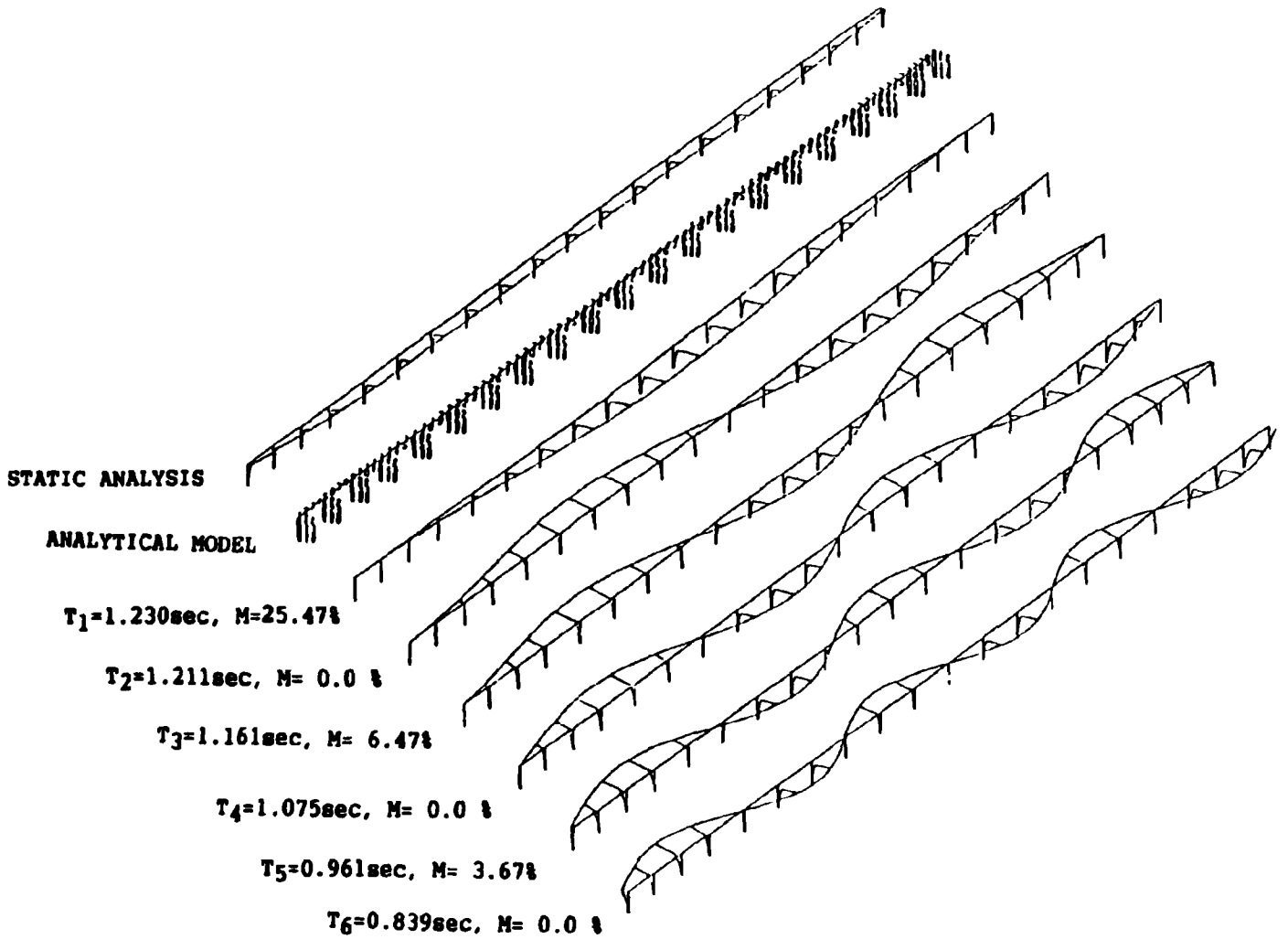

Fig.13 Comparison between Static Deformation Mode and Vibration Modes (Case 3)
(the Japanese level-1 earthquake, Concrete Column Pier)

First two designs are based on the Japanese level-1 earthquake design. From these results, it is obvious that the menshin design is superior to the CRB design because the seismic force can be controlled to the same level as that of the CRB design while the seismic displacement can be limited to the temperature movement.

However, the menshin bearings must be satisfied with the level-2 earthquake conditions so that the third case is investigated. From the third result, if the seismic displacement is better to be limited to the movement of temperature change, the seismic coefficient of the menshin design caused by the Japanese level-1 earthquake is slightly greater than that of the CRB design.

CONCLUSION

This study investigates feasibility of constructing a multi-span continuous bridge 1.25km long at a soft ground site.

From these results, this long bridge can be designed by using both conventional rubber bearings and menshin bearings. If conventional rubber bearings are employed, the longitudinal displacement due to the Japanese level-1 earthquake is greater than that due to temperature change. If menshin bearings are employed, the seismic displacement caused by the Japanese level-1 earthquake can be limited to the movement caused by temperature change. But the seismic coefficient of the menshin design due to the Japanese level-1 earthquake is slightly greater than that of the CRB design.

The lateral stiffness of the girder is very weak in the transverse direction so that the seismic movement and the seismic force in the middle of the girder are almost the same as or greater than those in the longitudinal direction, while the end bearings can be pin-fixed in the transverse direction. Furthermore, Fig.13 shows that the calculated deformation mode by the static analysis is different from the first vibration mode by the dynamic analysis. Therefore, the dynamic analysis in the transverse direction seems necessary for such a long bridge.

ACKOWLEDGEMENT

This paper summarizes the result of the research by "The committee on a multi-span continuous bridge". The authors are grateful to the members of this committee for their advice and support.

Base Isolation of the University Bridge

Dimitrios P. Koutsoukos * and John H. Clark †

Abstract

The design of the base isolation system for the seismic retrofit of the University Bridge Approaches in Seattle is described. The design allows traffic to continue uninterrupted during construction and avoids costly footing retrofit work at the bridge piers in the water. The limited space that is available for the installation of the isolation system presented unique difficulties that required innovative design solutions. The end product is a structure that can safely survive the design earthquake with minimal damage and, therefore, a low post-earthquake repair and maintenance cost.

Introduction

Although the need to retrofit existing highway bridges for seismic loading has been evident for many years, the seismic risk to bridges was brought to the public's attention during the recent years, especially since the October 1989 Loma Prieta earthquake shook the greater San Francisco area. The dramatic collapse of the double-deck Cypress Viaduct in Oakland during that earthquake gave public agencies the required impetus to undertake a widespread evaluation of virtually all bridges built in earthquake-prone areas.

The Seattle Engineering Department initiated an extended evaluation of the seismic risk to the bridges built in the City of Seattle. Among them is the University Bridge, a vital transportation artery in service since the 1930's. A preliminary seismic vulnerability study [7, 8] concluded that serious retrofit work needs to be performed for the structure to remain functional after a major earthquake.

This paper describes the base isolation system that will be installed in the South and North Approaches of the University Bridge. Seismic isolation was selected over more

*Bridge Engineer, Andersen Bjornstad Kane Jacobs, Inc., Seattle, Washington 98119-4108

†Vice President and Chief Bridge Engineer, Andersen Bjornstad Kane Jacobs, Inc., Seattle, Washington 98119-4108

traditional retrofit solutions, i.e., strengthening and stiffening of the bridge, primarily because it will relieve the substructure from excessive seismic forces that would require costly retrofit work.

Bridge Description

The University Bridge was designed and constructed in the early 1930's over Lake Union Ship Canal in Seattle. The bridge carries four lanes of traffic and two sidewalk/bicycle lanes on the north-south route of Eastlake Avenue. The structure is divided into the South Approach, the Bascule Bridge and the North Approach (Fig. 1).

The South Approach is a 200-foot long 3-span truss bridge. The superstructure is a cast-in-place reinforced concrete deck slab on two 10-foot deep trusses. The substructure consists of two-column bents, 45 feet wide, with tapered concrete columns and a lightly reinforced haunched crossbeam (Fig. 2). The south end of the approach is supported by the South Abutment, which consists of a hollow concrete box, with two pedestals that support the truss bearings. The north end is supported by the South Bascule Pier. The foundation of Pier 2 consists of two rectangular footings with 54 timber piles each. Pier 3 is in the water and its foundation consists of two square footings with 64 timber piles each. The truss is supported by steel rocker bearings on the South Abutment and South Bascule Pier. These bearings allow both translation (expansion) and rotation in the longitudinal bridge direction. At Piers 2 and 3 the trusses are supported on fixed steel bearings that act as pins in the longitudinal direction.

The North Approach is a 17-span bridge with two 7.25-foot cantilevers and a total length of 975 feet. From the North Bascule Pier to Pier 10, the superstructure consists of a reinforced concrete deck slab on two 12.5-foot deep steel deck trusses. From Pier 10 to the North Abutment, the superstructure is a reinforced concrete deck slab on four reinforced concrete haunched girders that are monolithic and have integral crossbeams at the pier tops. From the North Bascule Pier to Pier 10 the bridge substructure consists of 45-foot wide two-column bents, with tapered concrete columns connected by a haunched crossbeam. From Pier 11 to the North Abutment the bridge superstructure is supported by four-column bents with square columns that are transversely spaced at 17 to 20 feet. The columns are connected at midheight with one or two concrete crossbeams depending on the height. Piers 4 to 10 have square reinforced concrete spread footings on top of concrete seals. Pier 16 has two spread footings on piles and the rest of the piers are supported on reinforced concrete pedestal footings. A combination of fixed and expansion bearings connect the trusses to the substructure from the North Bascule Pier to Pier 10.

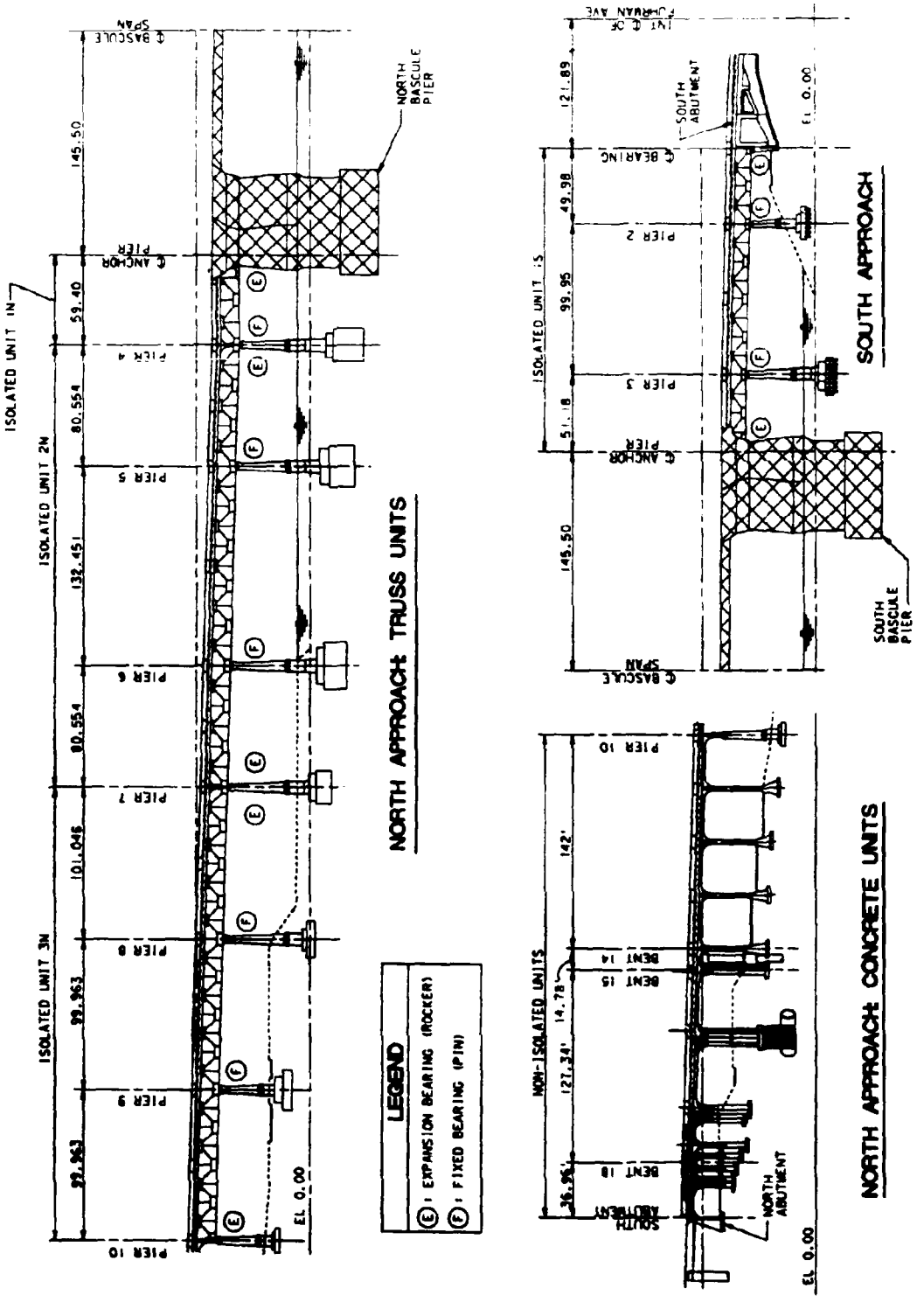

Figure 1: General Layout of the University Bridge

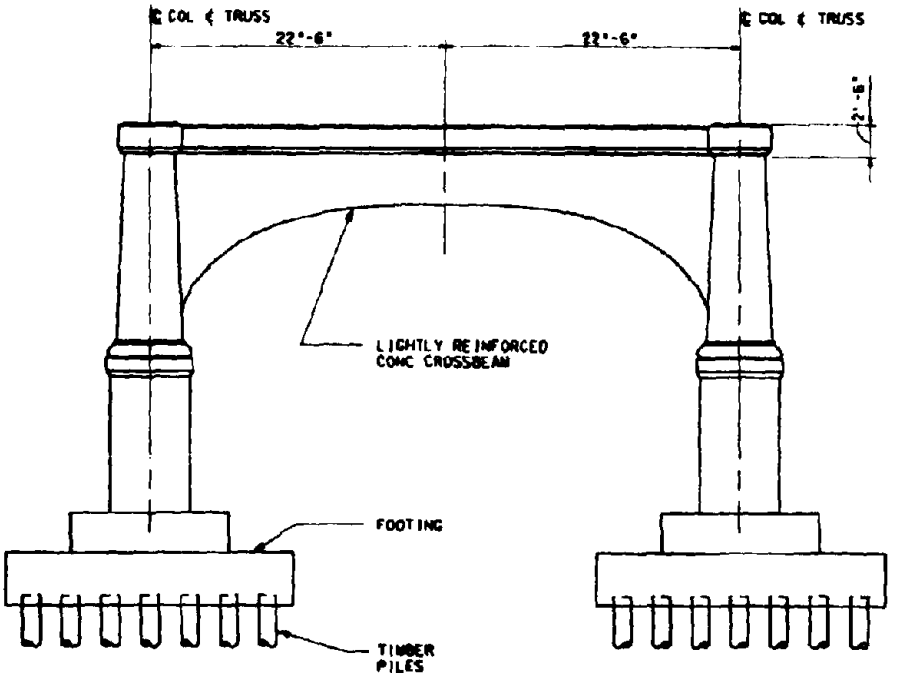

Figure 2: University Bridge Pier Elevation (Typical)

The concrete girders at Pier 10 are supported by rocker bearings. From Bent 11 to Bent 16, the superstructure crossbeam is cast monolithically with the substructure. Steel rocker bearings connect the superstructure to the substructure at Bents 17 and 18.

Background Information

The specifications used for the design of the South and North Approaches of the University Bridge are unknown. The approaches were originally constructed in 1930 (South Approach) and 1932 (North Approach). The Importance Classification of the University Bridge is "I," with a Seismic Performance Category "D," i.e., it is an essential bridge carrying an emergency route that has to remain functional immediately after the design seismic event. The geotechnical recommendations suggest that the AASHTO spectrum [1] with $a_{max} = 0.30g$ and Soil Profile Type "II" adequately describes the expected seismic motions.

The overall bridge condition is good. Some concrete spalls can be observed under the sidewalks and around the railings and most are being repaired by the Seattle Engineering Department. Some cracks emanating from the anchor bolts can also be observed at the top of the piers that support truss rocker bearings. In addition, some rocker bearings appear tilted. Both the concrete cracking and the tilting of the rocker bearings are indications of "frozen" bearings, i.e., the bearings appear to be "locked-up." "Frozen" bearings do not allow translation and could introduce large forces in the structure with often adverse effects on the bridge substructure.

The preliminary seismic vulnerability assessment of the University Bridge [7, 8] iden-

tified significant structural deficiencies and concluded that seismic retrofit of the bridge is required if the structure is to carry traffic immediately after the design earthquake. Specifically, it was found that the seat widths of the existing bearings are inadequate and that the shear capacities of the bearing anchor bolts are smaller than the imposed demands. Thus, the superstructure could break away from and topple off its supports during a major earthquake. Moreover, plastic hinging is expected at a number of piers, creating additional problems in the bar anchorage and splicing of the piers' longitudinal reinforcement. This behavior is amplified by the spacing of the existing horizontal confinement reinforcement (18″) which far exceeds the current AASHTO code [1] requirement of 4″.

The preliminary study [7, 8] proposed strengthening and stiffening of the bridge as a remedy against the structure's seismic deficiencies. Specifically, the study called for an improved linkage between the superstructure and the substructure and for an increase in the strength and ductility of the piers. The addition of stiff structural elements (superbents) were also included at the North Approach retrofit, in an attempt to limit the structural displacements and, thus, reduce the seismic demand/capacity (D/C) ratios at the existing piers and bents.

Retrofit Options for the University Bridge

Three major strategies are available for seismic retrofit of bridge structures [2, 6]: (a) improve the linkage between the bridge components by using restrainers, (b) improve the strength and/or ductility of the bridge piers, and (c) improve the seismic response of the structure by installing special devices mechanical systems. Several systems are currently available for the implementation of the third seismic retrofit strategy. These systems, known as isolation systems, have been already used in both new and retrofitted bridges to improve their seismic response by protecting mainly the structural parts that are below the plane of the isolation system. In general, seismic isolation aims at an improvement of the bridge seismic behavior by incorporating devices that: (a) reduce the inertia forces acting on the structure by sufficiently lengthening the fundamental periods of structural vibration, i.e., by creating a "softer" structure, and, (b) limit the structural deflections by increasing the damping and/or energy absorption characteristics of the structure. The result of the seismic isolation retrofit approach is that lower inertia forces are applied on the bridge, so that the structure is, in effect, "isolated" from the damaging forces of earthquakes.

The above three retrofit strategies were investigated during an extensive analytical

study undertaken by Andersen Bjornstad Kane Jacobs, Inc. (ABKJ). Among other tasks, the analyses involved the construction of three-dimensional frame models representing the existing conditions as well as the retrofitted conditions. The models were then used in association with the software package GT-STRUDL to analyze the structure's response under the design earthquake. According to the results of the analyses, the installation of an appropriate seismic isolation system at the University Bridge Approaches would be very beneficial for the survival of the structure. Specifically, the study dictated the following for the effective bridge rehabilitation:

1). The adoption of the "softening" approach, implemented with the installation of seismic isolators, as the defense mechanism of the University Bridge against strong ground motions.

2). The seismic isolators will be installed only under the truss units, where they can be inserted between the superstructure (trusses) and the substructure (piers). Thus, the entire South Approach (200 feet) and most of the North Approach (655 feet of a total of 975 feet) will be seismically isolated (Fig. 1).

3). To simplify the isolation installation, the existing bearing shoes will be retained everywhere and the isolators will be installed under the sole plates of the existing bearing shoes.

4). The retrofit work will be performed mostly underneath the existing roadway so that vehicular traffic can continue uninterrupted. This includes the jacking of the existing truss bearings to relieve the bridge dead and live loads.

5). Replacement of the existing expansion joints will be performed in such a way that only partial closures of the bridge traffic lanes will occur.

The seismic isolation of the University Bridge Approaches possesses the following distinct benefits over other, more traditional retrofit strategies that are based on an increase of the structure's stiffness and strength:

a). The seismic isolation system protects efficiently the bridge substructure by minimizing the seismic forces that are transmitted from the superstructure. A major design limitation was the lack of reserve strength of the Bascule Piers to carry the increased forces resulting from a stiffened structure. Thus, extensive retrofit work would have to be performed at the Bascule Piers. This work is eliminated as a result of the seismic isolation design. Similar arguments also hold for the rest of the substructural elements (South Abutment, Piers 2 to 10 and their footings) that are now protected from the damaging effects of major earthquakes. With seismic isolation, the substructure elements will remain "elastic" during the design earthquake, with static capacities exceeding the seismic demands. Expensive footing retrofit work, that would have to be performed under water at several locations (Piers 3, 4, 5, and 6), is eliminated in the proposed seismic retrofit.

Such work would possibly include footing extensions and footing tie-downs, necessary to carry the increased seismic demands. Other retrofit work that is eliminated in the current retrofit design involves friction slabs or abutment tie-backs at the South Abutment, prestressing of the pier crossbeams and stiffening/strengthening of the existing trusses.

b) Installation of the seismic isolators requires relieving the load (dead load, live load and impact) from the existing bearings so that the anchor bolts, rocker nests and masonry plates can be removed making space for the isolation system. This is an expensive procedure posing significant difficulties in the seismic isolation installation process. However, most of the existing rocker nests already show signs of distress. Furthermore, the number of existing anchor bolts is inadequate for holding the superstructure in place during the design earthquake. As a result, replacement of the existing anchor bolts with new of a higher strength and/or additional anchor bolts is warranted. Thus, most of the expense associated with the installation of the seismic isolators is unavoidable, making the base isolation concept more feasible from an economic point of view.

c) An efficient seismic isolated bridge constitutes a reliable structure that can survive strong earthquakes with minimal damage. Such system reliability gains an increased significance if one considers the unpredictable nature of earthquakes. Occurrence of a seismic event with damage potential and characteristics (duration, magnitude, frequencies, input energy) greater than those of the design event used in the retrofit design is possible. By minimizing the inertia forces to the structure, the margin of safety of efficient defense of the structure against stronger-than-design events is substantially increased in seismic isolated structures versus structures that have been retrofitted according to traditional concepts.

Several seismic isolation systems were examined as candidates for installation in the University Bridge. However, the extremely limited vertical space available for installation (5″ minimum) proved to be the governing factor in the system selection. The tightest clearance exists at the North Approach, underneath the fixed bearings at Piers 5, 6, 8 and 9. Isolation systems taller than the units selected for this project would require major retrofit of the pier caps and crossbeams for installation. Consequently, a low profile isolation system that minimizes modifications of the pier caps and crossbeams is the best selection for this particular application. A custom fabricated low profile elastomeric bearing with a lead core fulfilled all the criteria and requirements and was selected as the most appropriate. However, the design specifications describe the performance characteristics of a suitable isolation system and allow the Contractor to consider several other alternative systems.

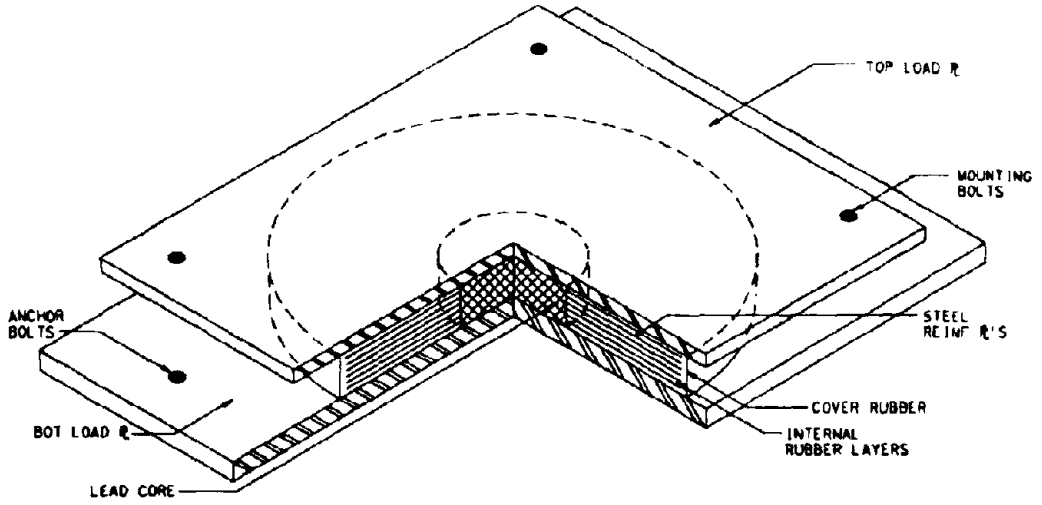

Figure 3: Seismic Isolation System

Description of the Seismic Isolation System

The selected isolation system consists of installing a total of twenty six lead-filled elastomeric bearings each fabricated of alternate layers of rubber and steel plates that are vulcanized together (Fig. 3). A preformed hole at the center of each unit is filled tight with a lead plug. The lead core and the alternate layers of rubber and steel form the isolator unit which is circular. A rectangular steel plate, the top load plate, is bonded to the circular isolator unit and it is used for attaching the isolator unit to the existing bearing shoe. A second rectangular steel plate, the bottom load plate, is bonded to the lower part of the isolator unit and is used as the masonry plate for the connection of the isolator unit to the pier cap.

Welding, as a means of connecting the top load plate to the existing bearing shoe, is minimized so that damage of the elastomer is avoided. In cases where welding is necessary, it is performed so that the temperature at any point of the isolator unit does not exceed 200°F. A325 bolts, $1\frac{1}{2}$ inch in diameter, are used for attaching the isolator unit to the existing bearing shoe. The isolator unit is secured to the column cap with an appropriate number of anchor bolts. Typically, the position of the anchor bolts falls outside the existing longitudinal column reinforcement and hoop cage. Therefore, a new concrete shell and 4-#7 reinforcing hoops with mechanical splice couplers are built around the existing column cap to confine the new anchor bolts (Figs. 5 and 6).

Table 1 designates the type of existing bearings at each pier. The South Abutment, South and North Bascule, and Pier 10 have rocker bearings. At these locations the isolation bearings are installed under the existing bearing shoes after the removal of the rocker nest and existing masonry plates. Typically, ample space is available for the installation of the new low profile bearings and therefore, only limited chipping of the concrete cap, as required for the removal of the existing masonry plates, is performed.

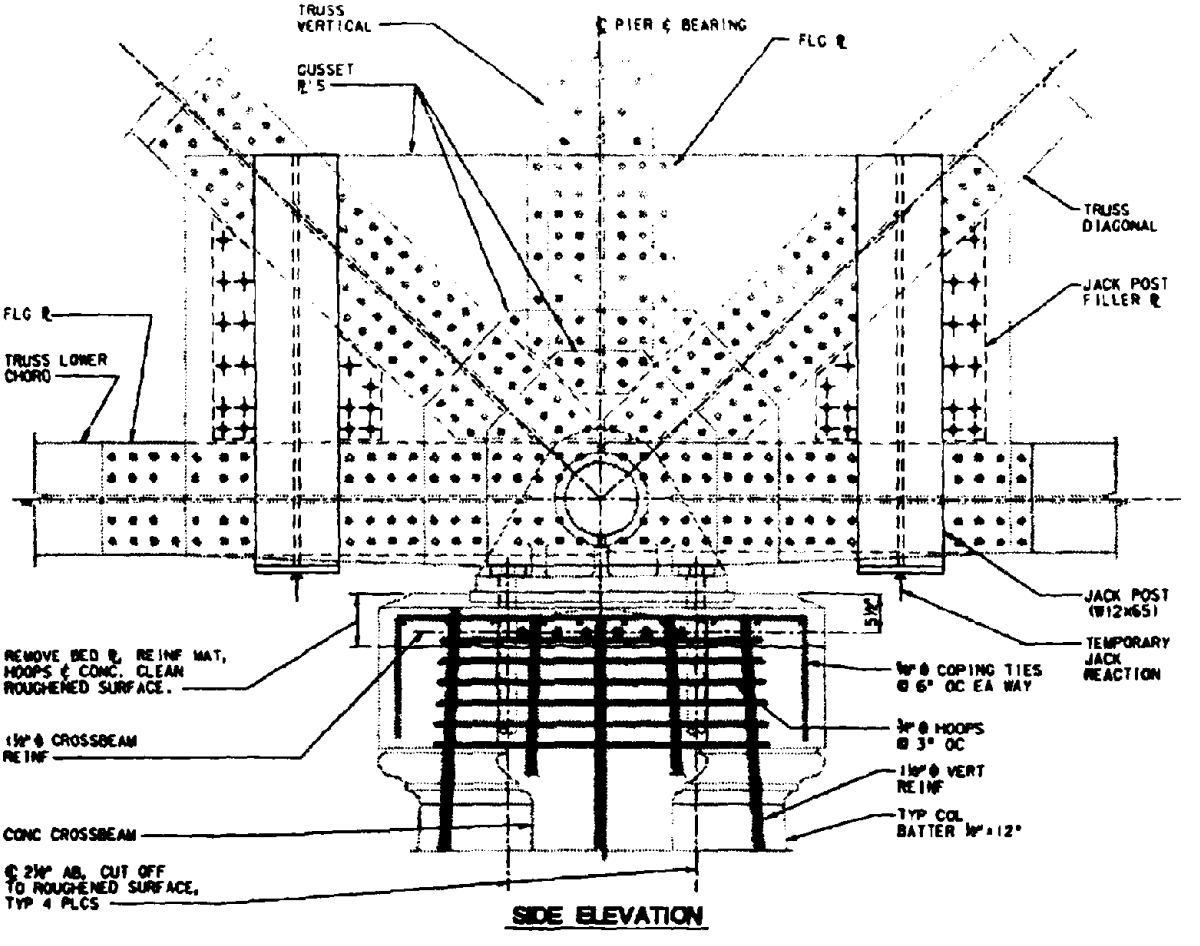

Figure 4: Existing Pin Bearing and Jack Post (Typical)

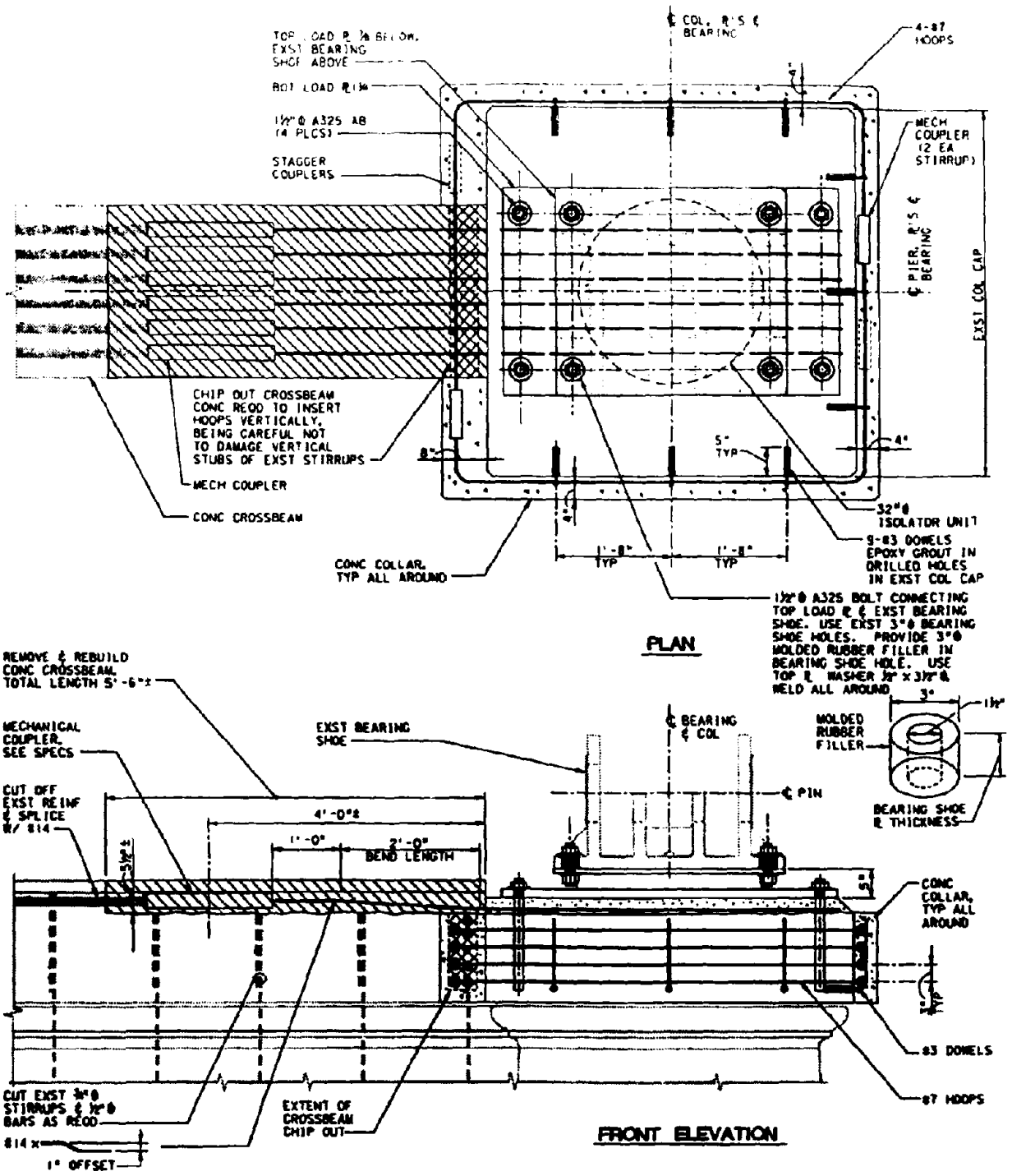

Figure 5: Isolation System for Pin Bearings (Typical)

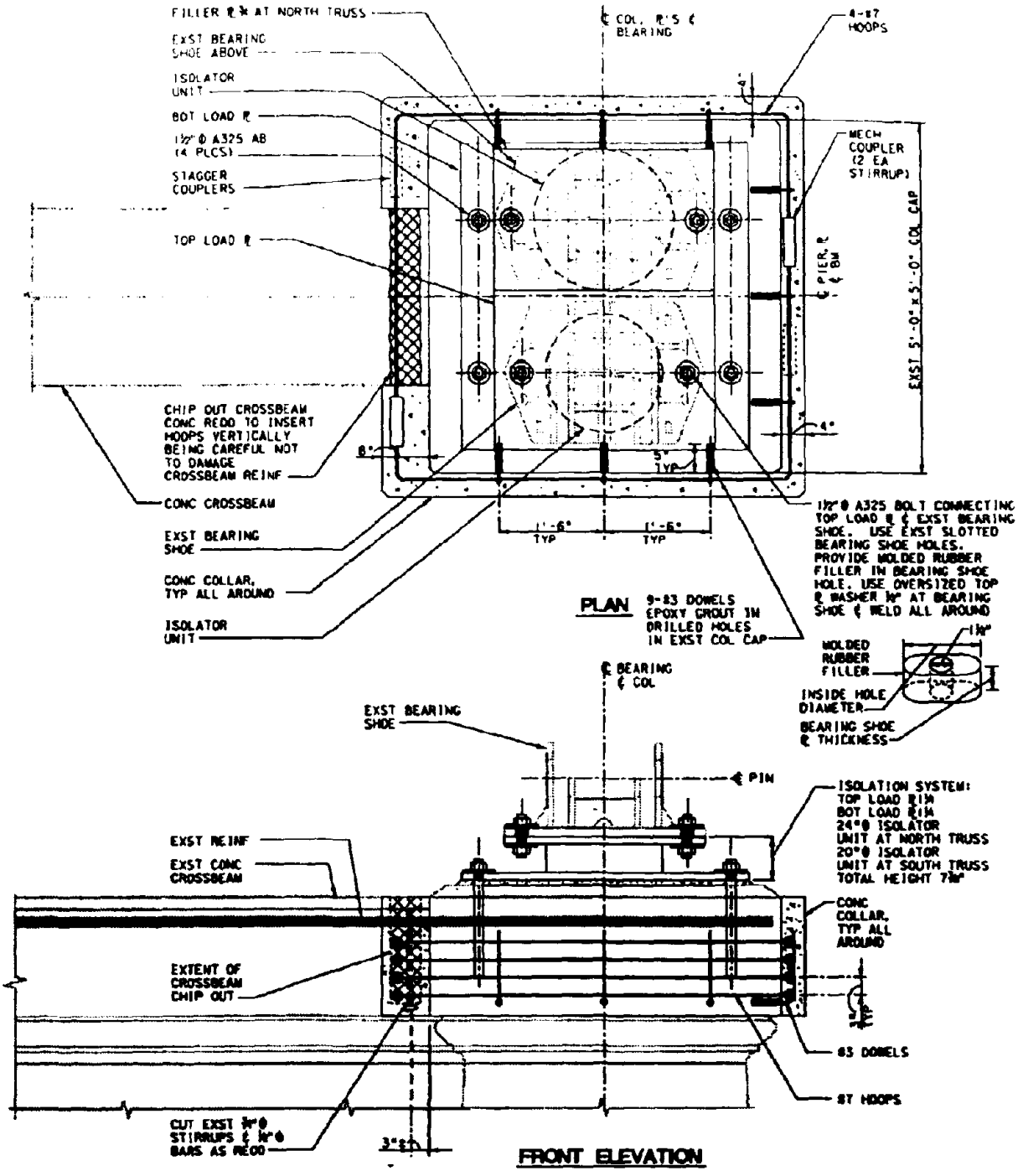

Figure 6: Isolation System for Rocker Bearings (Typical)

Location	Type of Existing Bearing	External Hoops	Rebar Cutting	Isolators (per Pier)	DL [Kips]	LL [Kips]
S.Abutment	Rocker	-	-	2	90	42
Pier 2	Fixed	•	-	2	735	160
Pier 3	Fixed	-	-	2	735	160
S.Bascule	Rocker	-	-	2	90	42
N.Bascule	Rocker	-	-	2	233	155
Pier 4	Rocker + Fixed	-	-	2	431	324
Pier 5	Fixed	•	•	2	1005	285
Pier 6	Fixed	•	•	2	1005	285
Pier 7	Rocker + Rocker	•	-	4	528	339
Pier 8	Fixed	•	•	2	908	275
Pier 9	Fixed	•	•	2	908	275
Pier 10	Rocker	•	-	2	330	170

Table 1: Existing Bearings and Major Retrofit Work (DL and LL are per Column)

At Piers 2, 3, 5, 6, 8 and 9 the total available space for the installation of the isolation bearings is limited by the top longitudinal reinforcing of the crossbeam (Fig. 4). Typically, the crossbeam reinforcing passes a scant 5 $\frac{1}{2}''$ below the existing bearing shoes. The crossbeam reinforcing is placed slightly deeper at Piers 2 and 3 of the South Approach. In general, the selection of the low profile bearings requires limited concrete removal and no cutting of the longitudinal crossbeam rebars. However, at Piers 5, 6, 8 and 9 where space is extremely tight, cutting of the crossbeam reinforcement is necessary for the installation of the isolators. At these locations, the soffit of the top crossbeam concrete is chipped for a length of 5' - 6", and mechanical couplers are used to connect the existing (cut) rebars with new offset bent bars that provide the necessary vertical clearance for the isolators (Fig. 5).

Expansion joints exist at Piers 4 and 7 which support two different trusses from opposite directions. At Pier 4, Unit 1N is supported by a fixed bearing and Unit 2N by a rocker bearing (Fig. 1). To avoid cutting the crossbeam rebar under the fixed bearing, an isolator bearing replaces the rocker bearing and a thin PTFE bearing is placed under the fixed bearing. The two trusses are connected together at the gusset plates, above the existing bearings, and at the roadway. As a result, Units 1N and 2N will move together during the

Pier	Longitudinal Direction			Transverse Direction		
	Existing	Isolated	Diff. (%)	Existing	Isolated	Diff. (%)
2	2.86	0.73	-75	1.38	0.46	-67
3	1.69	0.81	-52	0.57	0.67	+18
4	1.94	0.82	-58	1.05	0.87	-17
5	1.49	0.49	-67	1.09	0.49	-55
6	1.71	0.57	-67	1.65	0.58	-65
7	1.11	0.88	-21	2.68	0.55	-80
8	1.00	0.45	-55	1.10	0.42	-62
9	1.33	0.31	-77	0.79	0.19	-76
Average	-	-	-59	-	-	-50

Table 2: Column Moment Demand/Capacity Ratios

design earthquake, with Unit 1N sliding on the PTFE pad and Unit 2N displacing on the seismic isolator. The truss units 2N and 3N are supported by Pier 7 on rocker bearings (Fig. 6). Here, two isolator bearings replace the existing rocker nests and the two truss units are connected to displace as one. It is expected that the isolation system will cause the three truss units of the North Approach to "float" as one body during an earthquake. In addition to the other benefits of the isolation system, the danger of structural pounding as a result of out-of-phase motion of adjacent truss units is eliminated.

Multimodal elastic spectra analyses of the isolated structure were performed according to the provisions of AASHTO [1]. Table 2 compares the column flexural demand/capacity ratios (D/C) for the existing and seismic isolated conditions at Piers 2 to 9. Pier 10 is not included in the table, because the seismic loading from the concrete units dominates its seismic response. According to the values of Table 2, the bridge substructure (piers) will remain "elastic" during the design earthquake with D/C ratios consistently below 1. In the longitudinal bridge direction, an average improvement of 59% in the moment D/C ratios is noted as a result of the seismic isolation, i.e., the isolated moment D/C ratios are 59% smaller from the existing moment D/C ratios. Similar behavior is also observed at the South Abutment, and at the South and North Bascule.

A substantial decrease in the level of shear demands is also observed at all locations at the bridge substructure, as a result of the seismic isolation. For example, the transverse shear demand at the South Bascule and North Bascule Piers has dropped from 811 and

538 kips to 60 and 71 kips, respectively. Decreases in the shear demands on the order of 60% are expected. On the other hand, with the new bearings in place, larger displacements of the superstructure are expected during a major earthquake. The estimated longitudinal and transverse displacements during the design event are on the order of 4 $\frac{1}{2}''$. To accommodate these deflections, the existing expansion joints, which currently allow only about 1″ longitudinal displacement, will be modified. Sacrificial expansion joints are designed at all locations where the isolated truss units border the bascule piers and the traditionally retrofitted concrete units. The new joints allow small thermal movements (about 2″) and break-away to free the structure to displace freely at larger deflections.

Summary and Conclusions

Base isolation was selected for the retrofit of the truss units of the University Bridge Approaches instead of more conventional methods of structural rehabilitation. Base isolation provides a reliable system that reduces the lateral forces to "elastic" levels under the design earthquake. Furthermore, base isolation eliminates major retrofit work at the bridge superstructure and substructure. Post-earthquake repairs to the bridge should be limited to expansion joint details and the bridge is expected to remain functional.

Limited vertical clearance under the existing bearings shoes available for the installation of the isolation bearings resulted in the selection of specially-made low-profile lead-rubber bearings. Constructions issues relevant to the installation of the isolation system included expansion joint modification and crossbeam reinforcing details.

A comparative study of the responses to the design earthquake of the existing and retrofitted bridge revealed a significant improvement in the demand/capacity ratios of the isolated versus existing structures. The forces transmitted from the superstructure to the substructure are substantially decreased and thus, the substructure is protected from major damage.

A preliminary estimate of construction costs for the seismic isolation of the University Bridge Approaches, in 1994 dollars, is $ 2.0 Million. This estimate includes mark-up costs such as mobilization, contingency and profit.

Acknowledgments

The support of Mr. Frank S. Yanagimachi, Project Manager for the City of Seattle Engineering Department, is greatly appreciated. The authors wish to thank Mr. Thomas

A. Kane, Chairman of the Board at ABKJ, and Ms. Joyce M. Lem, Project Manager at ABKJ, for their impeccable editing of the draft versions. The help of the following individuals is also gratefully acknowledged: Mr. Eysteinn Einarsson for his valuable comments, Ms. Betty J. Birk for preparing the figures of this paper, Mr. Paul W. Grant, Vice President at Shannon & Wilson, Inc., for providing the geotechnical review, and Mr. Robert S. Currie for the preliminary estimates of construction costs. Furthermore, the authors wish to thank Dr. Deepak Choudhury, Senior Project Engineer at Dynamic Isolation Systems, for his valuable suggestions in overcoming several design problems. Finally, the support of this work by ABKJ is gratefully acknowledged.

References

[1] AASHTO (American Association of State Highway and Transportation Officials) (1989). *Standard Specifications for Highway Bridges.* 14th Edition. Washington, DC.

[2] Chapman, H. E. (1991). "Seismic Retrofitting of Highway Bridges." *Bulletin of New Zealand National Society for Earthquake Engineering.* Vol. 24, No. 2., pp. 177-185.

[3] Dynamic Isolation Systems, Inc. (1993). *AASHTO Design Procedures for Seismically Isolated Bridges.* Berkeley, CA.

[4] Popov, E.P., Yang, T.-S., and Grigorian, C.E. (1993). "New Directions in Structural Seismic Designs." *Earthquake Spectra.* Vol. 9, No. 4, pp. 845-875.

[5] Priestley, M.J.N., Seible, F. and Chai, Y.H. (1992). "Design Guidelines for Assessment Retrofit and Repair of Bridges for Seismic Performance." *Structural Systems Research Project, Report SSRP-92/01.* University of California, San Diego, CA.

[6] Priestley, M.J.N. and Seible, F. (1991). "Seismic Assessment and Retrofit of Bridges." *Structural Systems Research Project, Report SSRP-91/03.* University of California, San Diego, CA.

[7] Sverdrup Corporation (1992). "Final Report : University Bridge - South Approach." *Bridge Seismic Retrofit Study for the Seattle Engineering Department.* Seattle, WA.

[8] Sverdrup Corporation (1992). "Final Report : University Bridge - North Approach." *Bridge Seismic Retrofit Study for the Seattle Engineering Department.* Seattle, WA.

SEISMIC DESIGN OF CONTINUOUS STEEL-BOX-GIRDER BRIDGE WITH RUBBER BEARINGS FOR TRANS-TOKYO BAY HIGHWAY PROJECT

Yukitake Shioi, Yoshitaka Yoshida, Kazushige Takahashi
Design and Engineering Dept., Trans-Tokyo Bay Highway Corporation

Abstract

The superstructure of the Trans-Tokyo Bay Highway Bridge, which is a steel-deck continuous box-girder bridge, was designed as a multi-span continuous structure with a minimum number of expansion joints in order to achieve high earthquake resistance, smooth road surface, and ease of maintenance. A series of experiments on large rubber bearings were conducted to confirm their dynamic and static performance, such as deformation capacity, and a superstructure incorporating those rubber bearings was designed.

Introduction

Crossing the middle of Tokyo Bay when completed, the Trans-Tokyo Bay Highway will be a 15.1 km long motorway linking Kawasaki, Kanagawa Prefecture, and Kisarazu, Chiba Prefecture, and consisting of a tunnel, a bridge and two man-made islands (Figs. 1 and 2). As shown in Fig. 3, a 4.4 km long bridge section will link Kisarazu Man-Made

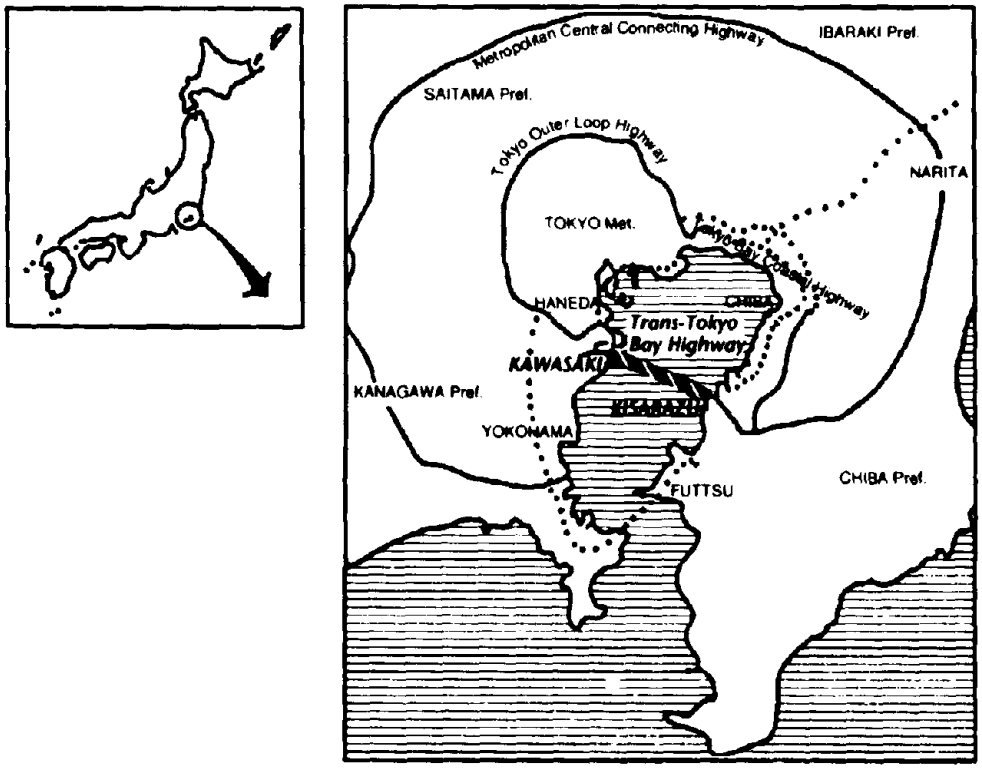

Fig. 1 Location Map

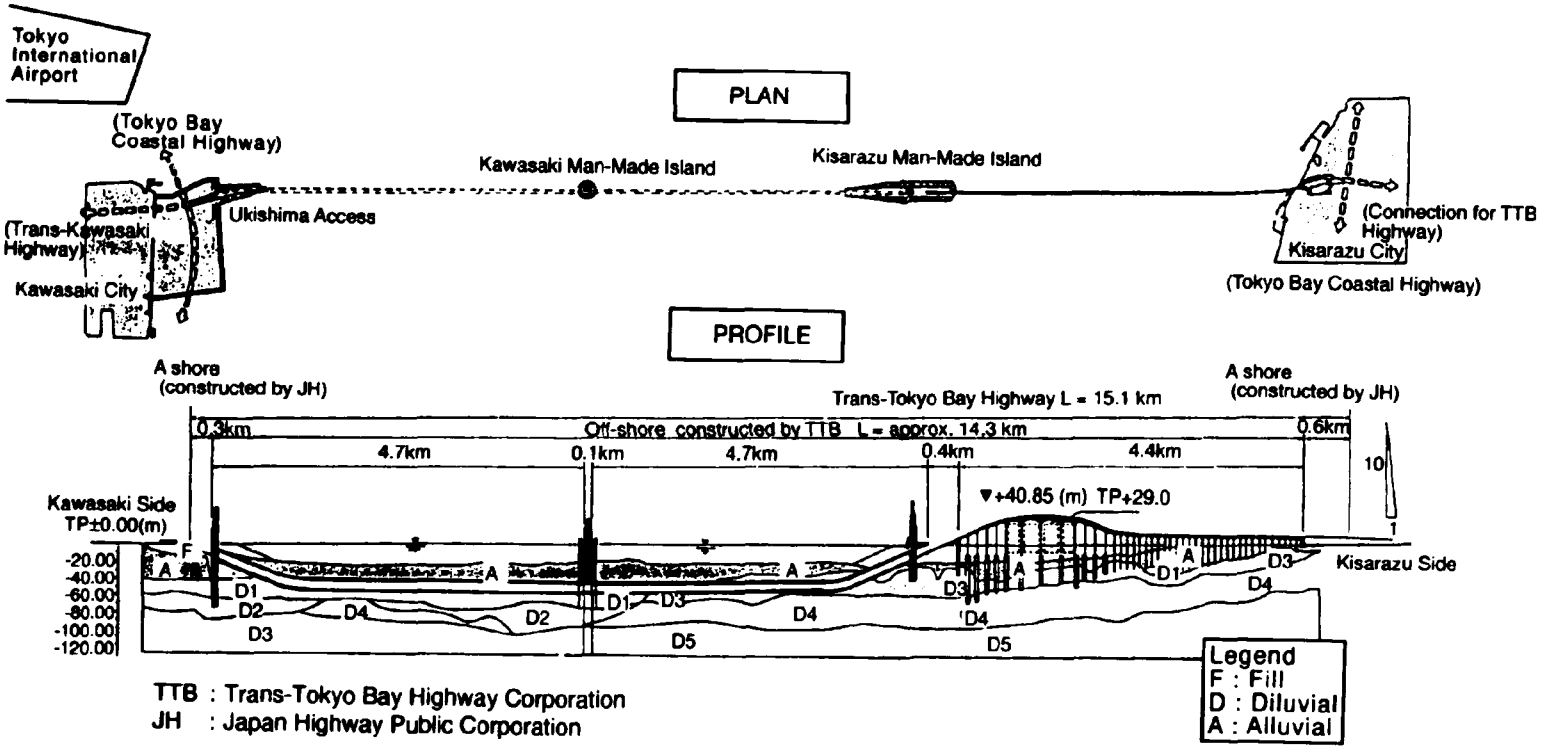

Fig. 2 General View of Trans-Tokyo Bay Highway

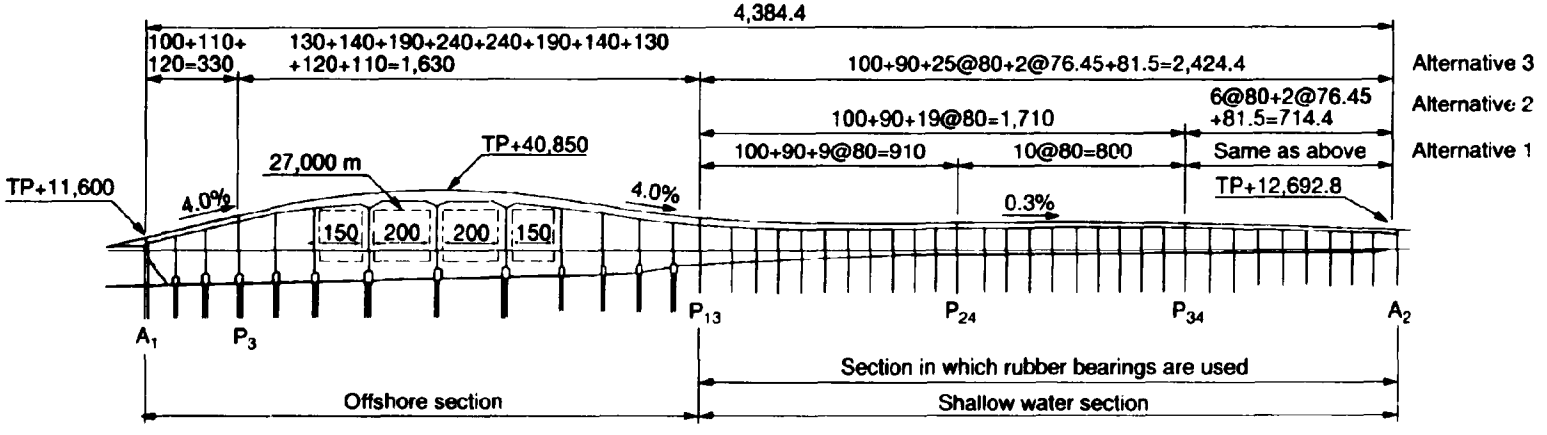

Fig. 3 General View of Bridge Section

Island with the landing position of the highway on the Kisarazu side. The bridge can largely be divided into an offshore section (A1, P1–P13) at water depths of 23–10 m and a shallow water section (P13–P42) at depths of 8–0 m.

Table 1 shows the design data for the bridge. The offshore section will have steel piers built on steel sheet pile foundations, and the shallow water section will have concrete piers built on steel pipe sheet pile foundations.

This paper outlines the design of a multi-span continuous bridge section with rubber bearings used in the shallow water section and reports on performance tests on rubber bearings.

Multi-Span Continuous Structure

Method of Constructing Multi-Span Continuous Bridge

There are several methods of constructing a multi-span continuous bridge, as shown in Fig. 4. In the horizontal force centralization method, inertia forces during an earthquake can be concentrated on certain piers; since this necessitates the use of large piers, there is a limit to the application of this method to multi-span bridges. The horizontal force decentralization method is suitable for a flexible structure with tall steel piers, such as the offshore section. This method, therefore, has been adopted for the offshore section, which has been designed as a 1,630 m long 10-span continuous bridge.

The shallow water section has short reinforced-concrete piers. If the horizontal force decentralization method were used, therefore, piers would have to be uneconomically large. In the damper method, additional dampers other than those to bear vertical forces would be necessary. Thus, the rubber bearing method was employed to construct the multi-span structure in the shallow water section.

Table 1 Design Data

Route Name		National Highway No. 409
Design Speed		80 km/h
Roadway		Four 3.5 m lanes (to be expanded into six lanes)
Structure	Superstructure	Steel-deck continuous box-girder structure (1-box, 3-cell)
	Substructure (offshore section)	Steel piers, steel pipe pile foundation
	Substructure (shallow water section)	Reinforced concrete piers, steel pipe sheet pile foundation
Estimated Traffic		33,000 vehicles/day in the 1st year 64,000 vehicles/day after 20 years

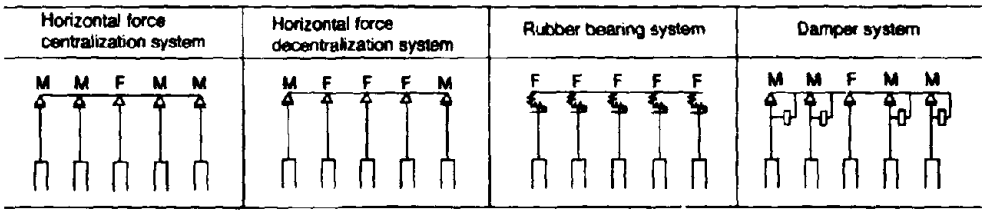

Fig. 4 Types of Multi-Span Continuous Structure

Rubber Bearings

Rubber bearings absorb deformations (displacement, rotation) of the superstructure by their elastic deformation. The rubber bearings used in the bridge are laminated structures of rubber and steel plates and have high load-bearing capacity. Fig. 5 shows the rubber bearings that have been adopted. The ring bearing shown here has already been used extensively as a large bearing for bridges, and this bearing is characterized by a ring-shaped opening in the steel plates. The High Damping Rubber Bearing (HDR) and the Lead Rubber Bearing (LRB), both of which have damping effect, have been widely used to seismically isolate buildings and, recently, bridges, too. The HDR uses special energy-absorbing rubber. The LRB is a rubber bearing with lead bars inserted in it and absorbs energy by plastic deformations of lead. In the bridge in the shallow water section, these three types of rubber bearings are used; however, they were chosen from the viewpoint of the functionality of rubber bearings alone because they had never been used to seismically isolate highway bridges, and the energy absorption capacity of the HDR or LRB was not evaluated in design.

Determination of the Number of Continuous Spans

Three alternatives regarding the number of continuous spans, as shown in Fig. 3, were considered.

Alternative 1: To divide 30 spans into 3 sections (11 + 10 + 9 spans)

Alternative 2: To divide 30 spans into 2 sections (21 + 9 spans)

Alternative 3: To construct 30 spans as a continuous structure

The analytical model used in the design of rubber bearings was constructed with springs representing rubber bearings, and springs representing the substructure that had been obtained on the assumption that the bottoms of the piers were fixed. It was also assumed that during an earthquake the continuous superstructure behaved as a single body. Design calculations indicated that the required dimensions of bearings were similar irrespective of the type of structure. As a typical example, Table 2 shows the results of

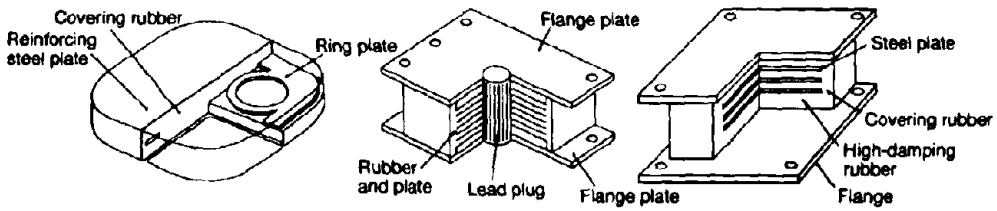

Fig. 5 Types of Rubber Bearing

Table 2 Design Calculations for Rubber Bearing (Ring Bearing)

			Alternative I		
Number of Continuous Spans			11	10	9
Dimensions: Width x Length x Rubber Thickness	Largest bearing	mm	1,550 x 1,550 x 234	1,450 x 1,450 x 200	1,450 x 1,450 x 200
	Smallest bearing	mm	1,350 x 1,350 x 149	1,350 x 1,350 x 176	1,350 x 1,350 x 180
Horizontal Displacement of Superstructure (Max.)	Normal conditions (at section end)	mm	196	168	151
	Under earthquake	mm	255	250	250
Natural Period of Bridge		sec	2.03	2.01	2.01

design calculations for the case where ring bearings are used. Since the natural period of ground is 1–1.2 seconds, the target natural period of the bridge was set at 2 seconds so as not to cause resonance. The vertical reaction of the shoe is 1,500–1,700 tf.

In Alternative 1, the width of the bearing in the 11-span section, for example, was around 1,600 mm; displacement along the bridge axis at the girder end was within about 200 mm at changing temperatures (±35°C), and within 250 mm even during an earthquake. In Alternative 2, the width of the bearing in the 21-span section was larger than in the 11-span section in Alternative 1 by only 100 mm or so, but the height of the bearing was about 1.8 times greater. The reason for this is as follows: Although there is not any substantial difference in horizontal dimensions because compressive stress in the bearing is the governing factor, the height is governed by shear strain in the bearing (= shear deformation / total rubber thickness < 70% at ordinary times, 150% during earthquake). Hence, as horizontal displacement due to temperature changes increases to 360 mm, the required thickness of rubber increases, too. In Alternative 3, this tendency becomes more pronounced, making the rubber bearing thickness of 631 mm and the bearing width of 1,900 mm necessary. Since these values cannot be achieved with the present level of manufacturing technology, it was decided that Alternative 3 was impractical. Although Alternative 2 was technically possible, it required further research to develop bearings and expansion mechanisms that could absorb large deformations. Therefore, Alternative 1, which was feasible with the available technology, was adopted.

The bearings adopted are as follows: the HDR for the 11-span 900 m section on the offshore side, the LRB for the 10-span 800 m section in the middle, and the ring bearing for the 9-span 714.4 m section on the land side.

Seismic Design

Overview of Design

The seismic design of the bridge, which conforms to the Design Standard for the Trans-Tokyo Bay Highway Bridge (draft) and the Standard Specifications for Highway Bridges with Commentary (hereafter referred to as "SSHB"), was basically static design based on the seismic coefficient method, and the validity of the design was evaluated through dynamic response analysis. The design of the 11-span 910 m long section (P13–P23) is outlined below.

(a) Static Design

The values of the seismic coefficient used in the static design were calculated in accordance with the SSHB. Table 3 shows the calculated values.

$$k_h = C_Z \cdot C_G \cdot C_I \cdot C_T \cdot k_{h0} \quad (1)$$

where

C_Z : regional correction coefficient (Area A) = 1.0
C_G : ground type correction coefficient (T_G = 1.2 seconds) = 1.2
C_I : importance correction coefficient (Grade 1) = 1.0
C_T : natural period correction coefficient
k_{h0} : standard design horizontal seismic coefficient = 0.2

Table 3 Design Horizontal Seismic Coefficient (P13–P24)

Direction	Natural Period (sec)	Correction Coefficient C_Z	Horizontal Seismic Coefficient K_h
Bridge-axis direction	1.75	1.13	0.27
Perpendicular-to-bridge-axis direction	0.94	1.25	0.30

Although the natural period in the bridge-axis direction was 2.0 seconds as in the design of the rubber bearing, variations in the quality of rubber bearings were reasonably expected. Therefore, the spring constant for the bearing was multiplied by 1.3 and thus the natural period of 1.75 seconds was used to calculate the values of the correction coefficients so that up to twice the tolerance (±15%) of the spring constant was permitted.

(b) Evaluation through Dynamic Analysis

In dynamic analysis, safety was checked against two target levels of earthquake resistance. Table 4 shows the earthquake resistance criteria used and the evaluation procedures. For each of these two levels of earthquake resistance, input earthquake motions to be applied, in dynamic analysis, to structures constituting the Trans-Tokyo Bay Highway were formed: Expected values of response spectrum were determined according to earthquake motions observed in and around the Tokyo Bay area, and the input earthquake motions were determined by adjusting the amplitude of historical earthquake motions so that they agreed with the expected response spectra in terms of spectrum characteristics.

Dynamic Analysis

(a) Method of Dynamic Analysis

The analysis model used was a lumped mass system model; it was an 11-span whole system analysis model. Fig. 6 and Table 5 show the analysis model and method used, respectively. Before the analysis of the whole system, a multiple reflection analysis was conducted. In this analysis, Layer D5 in Fig. 2 was assumed to be basement and the response of the ground system was analyzed taking account of the nonlinearity of strain and ground properties (shear stiffness, damping factor). It is the results obtained from this analysis that were used in the evaluation of ground stiffness and used as earthquake

Table 4 Evaluation Criteria Used in Seismic Design

Level	Description
L-1	The structure should not suffer damage likely to impair primary function when subject to earthquake motion likely to occur during its life span. In addition, the structure should be easily repairable following the earthquake so that the full function before the earthquake can be quickly recovered.
L-2	When subject to a major earthquake likely to occur only rarely at the site, whilst it is acceptable that structural members suffer heavy damage, structural failure likely to endanger human life should be prevented. In addition, following the earthquake, it must be possible by repair, strengthening, or partial replacement, to restore the function of the structure.

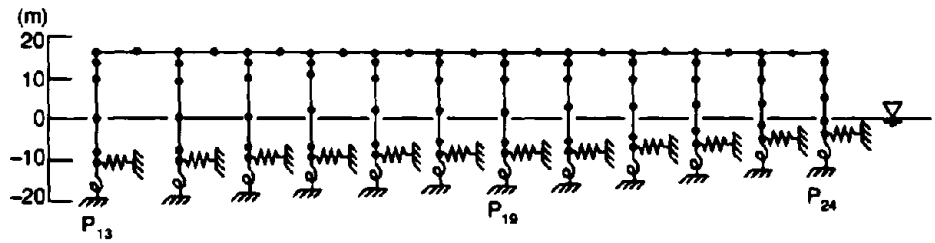

Fig. 6 Whole System Dynamic Analysis Model

Table 5 Method of Whole System Analysis

Method	Time-series response analysis using modal method
Direction	Bridge-axis and perpendicular-to-bridge-axis directions
Input Earthquake Motion	L-1 and L-2 are used as base waves, and response waves from the footing are obtained from ground response analysis.
Damping Factor	Modal damping is based on assumed proportionality to strain energy; damping factor for each element is in accordance with SSHB.
Analysis Model	
Superstructure	Beam–mass model
Substructure	Beam–mass model; P–δ curves are used at level L-2 to take account of decrease in stiffness.
Ground–pile	Ground stiffness determined from multiple reflection analysis is used to calculate spring constants in accordance with SSHB.

motions inputted into the whole system. As shown in Fig. 7, the piers in the shallow water section are to be built on steel pipe sheet pile foundations. In constructing the model, an analysis using a symmetrical FEM model was performed to properly evaluate dynamic interaction between the ground and the caisson foundation. Then, the damping factor for the ground–foundation system was determined accordingly.

(b) Results

Fig. 8 shows the first- and second-mode diagrams for the bridge-axis and perpendicular-to-bridge-axis directions. In the first mode in the bridge-axis direction, deformations of the rubber bearings predominated; the superstructure behaved as a unit, and there was little deformation of the substructure.

Table 6 shows section forces acting at the bases of the piers in the bridge-axis direction. As shown, dynamic response section forces at level L-1 except at P13 were lower than the static design values. P13 was reinforced with additional steel. At level L-2, the requirements of the SSHB were satisfied, and the shear strength and ultimate horizontal strength were not smaller than the force obtained by multiplying the lateral seismic coefficient used in strength evaluation by the equivalent weight ("equivalent lateral force" in the table). It was decided, therefore, that the required level of safety was achieved.

Table 7 shows the response of the bearings in the bridge-axis direction. The required level of safety is achieved since the dynamic response displacements at level L-1 were lower than the static design values. At level L-2, the dynamic response displacements were greater than the static design values; however, it was decided that this did not pose a problem because the bearings had sufficient deformation capacity and displacements of the end bearing were within the distance between the girder end and the edge of the substructure ($S\varepsilon$ = 2,450 mm).

Rubber Performance Tests

The feasibility of the multi-span continuous structure of this bridge is dependent on the large deformation capacity of the rubber bearings and the use of the largest rubber bearings available today. A series of tests were conducted, therefore, to confirm the performance (basic characteristics, large deformation capacity, and dynamic performance) of the rubber bearings.

The performance tests can largely be divided into dynamic performance tests and static performance tests. As specimens, 1/4-scale models were used in the former, and full-scale models were used in the latter. The test results reported below mainly concern HDRs.

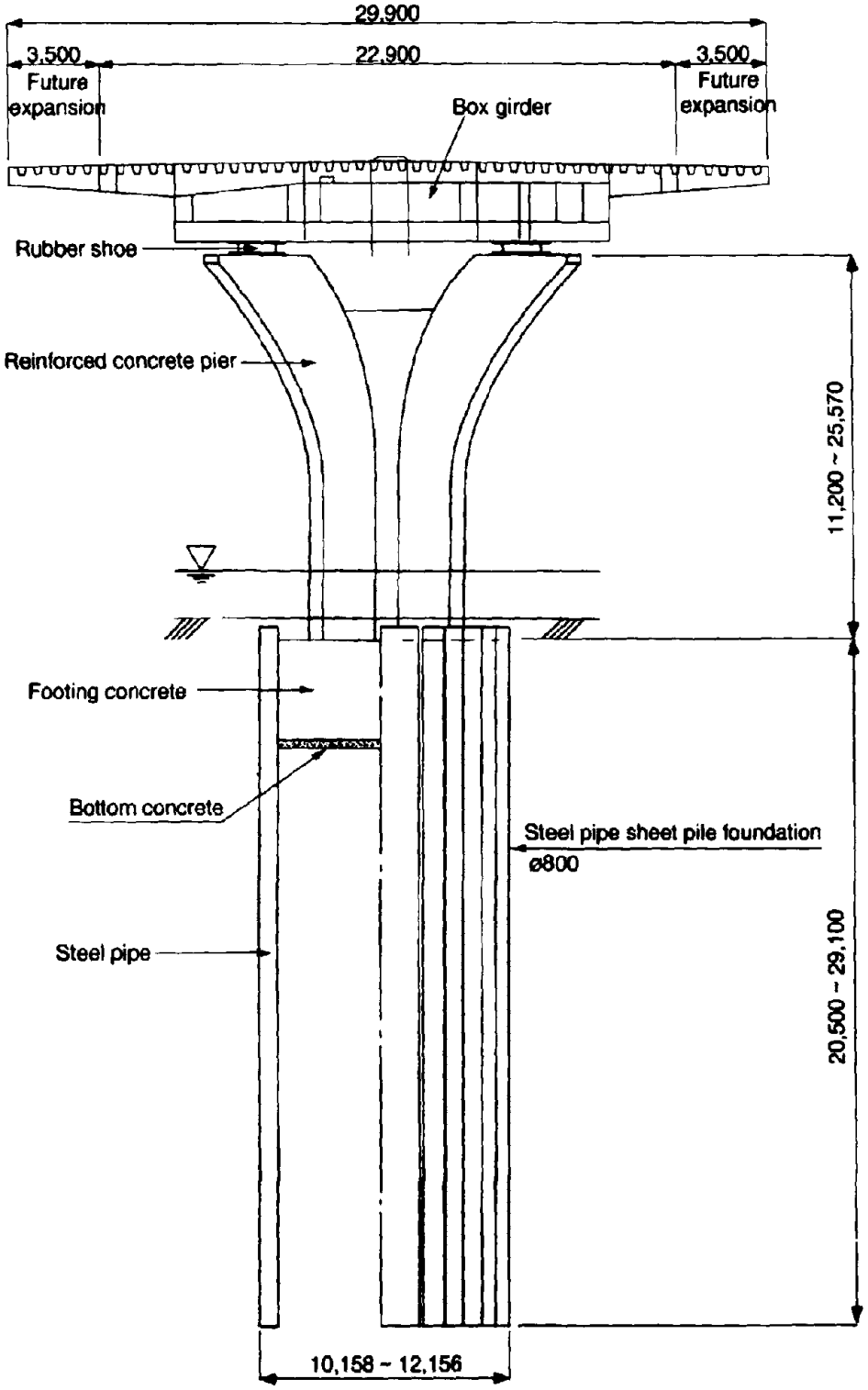

Fig. 7 Superstructure and Substructure (Shallow Water Section)

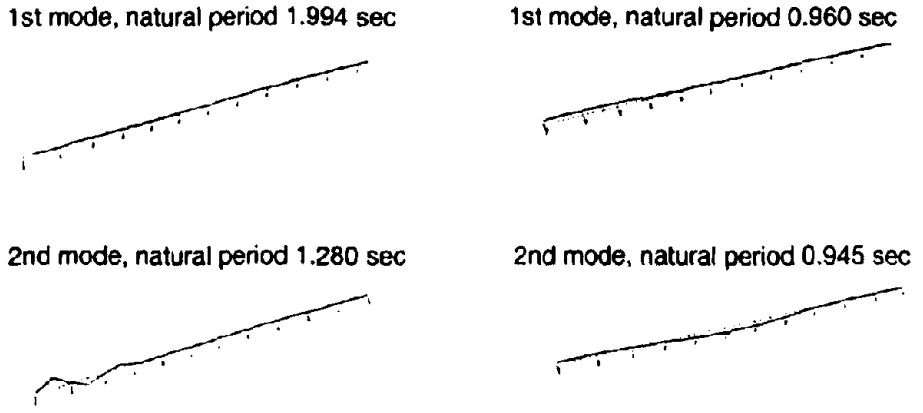

(a) Bridge-Axis Direction **(b) Perpendicular-to-Bridge-Axis Direction**

Fig. 8 Mode Diagrams for Whole System

Table 6 Response Section Forces (Bridge-Axis Direction)

	P_{13}	P_{14}	P_{22}	P_{23}
Bending Moment (tf-m)				
Static response	13013	24108	14258	12825
Dynamic response (L-1)	19503	12722	8189	7587
Shear Force (tf)				
Static response	891	1296	910	878
Dynamic response (L-1)	1092	700	516	522
Evaluation Concerning Bending Failure				
Ultimate horizontal resistance (tf)	1173	1631	1228	1322
Equivalent horizontal force (tf)	1038	809	704	711
Evaluation Concerning Shear Failure				
Shear strength (tf)	5767	4751	3801	3801
Equivalent horizontal force (tf)	1671	950	718	730

Dynamic Performance Tests

In order to simulate the state of the rubber bearing during an earthquake, the specimen was subjected to reversed cycles of horizontal loading while being under a load equal to deal load reaction. In the tests, the following performance was examined:

(1) Values of spring constant and damping factor of rubber bearing used in design
(2) Stability under dynamic cyclic loading
(3) Stability depending on loading history
(4) Stability depending on the rate of deformation

The load–displacement test for the shear deformation of the HDR of 100% and the vibration frequency of 0.5 Hz indicated that the stiffness was relatively high during the first loading cycle, but, as the overlapped curves for the second and later loading cycles indicate, the performance of the rubber bearing was stabilized during and after the second cycle. Fig. 9 shows the relationships between the vibration frequency, equivalent spring constant, and equivalent damping factor. The equivalent spring constant tended to increase with vibration frequency, and the equivalent damping factor tended to decrease

Table 7 Response at Bearing (P13–P23, Bridge-Axis Direction)

Item			Symbol	Unit	P_{13}	P_{14}	P_{15}	P_{16}	P_{22}	P_{23}
Specifications of Rubber Bearing	Dimensions		$a_0 \times b_0$	mm		1700 x 1700	1450 x 1450		1450 x 1450	1550 x 1550
	Rubber thickness		t_e	mm		253	182		182	209
Horizontal Shear Spring				t/cm		23.26	23.36		23.36	23.36
Displacement of Girder	Normal	Temperature	Δl	mm	197	155	177	84	117	151
	Earthquake	Static	Δl_e	mm	283					
		Dynamic L1	Δl_{e1}	mm	154	153	152	151	150	151
		Dynamic L2	Δl_{e2}	mm	368	367	364	363	360	361
Displacement of Bearing	Normal	Temperature	δ	mm		127	96	68	96	123
	Earthquake	Static	δ_e	mm		231	231		231	231
		Dynamic L1	δ_{e1}	mm	153	153	152	151	150	151
		Dynamic L2	δ_{e2}	mm	368	366	364	363	361	362
Shear Strain	Normal	Temperature	γ			0.50	0.53	0.38	0.53	0.59
	Earthquake	Static	γ_e			0.91	1.27	1.27	1.27	1.11
		Dynamic L1	γ_{e1}			0.56	0.72	0.75	0.74	0.65
		Dynamic L2	γ_{e2}			1.21	1.54	1.67	1.62	1.45
Horizontal Force	Normal	Temperature	H	tf		148	112	80	112	145
	Earthquake	Static	H_e	tf		331	270			270
		Dynamic L1	H_{e1}	tf		164	159	159	157	159
		Dynamic L2	H_{e2}	tf		357	355	356	344	355

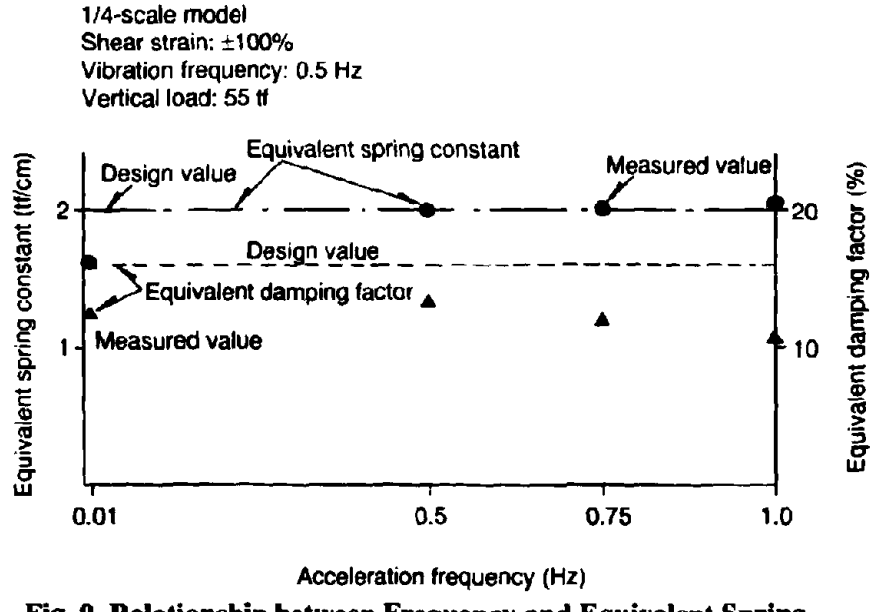

Fig. 9 Relationship between Frequency and Equivalent Spring Constant/Equivalent Damping Factor

with vibration frequency. The variations were small, however, as compared with the values of the spring constant and damping factor calculated from the design formulas, and these results indicate that the equivalent spring constant and the equivalent damping are hardly dependent on vibration frequency.

Static Performance Tests

(a) Compression Deformation Test

This test was conducted with a view to confirming the compression deformation capacity. In the test, the specimen was subjected to vertical loads of 0 tf to 1,350 tf (dead load + live load + impact), and then the load was decreased to 850 tf (dead load only). The spring constant in the vertical direction was about 4,500 tf/cm, which is nearly 460 times as large as the spring constant in the horizontal direction (design value 9.62 tf/cm). This indicates that the stiffness was very high and the maximum displacement was as small as about 5 mm. The design spring constant of 4,979 tf showed fair agreement with measured values.

(b) Cyclic Shear Deformation Test

This test was conducted for the purpose of confirming the durability of the rubber bearing under horizontal cyclic displacements due to temperature changes. While being under the maximum vertical load of 1,350 tf (dead load + live load + impact), the specimen was subjected to 100 continuous loading cycles so that deformations of ±70% (tolerance at changing temperatures) occurred. After the test, the rubber bearing did not show any sign of abnormality. Fig. 10 shows the relationships between the values of the equivalent spring constant and equivalent damping factor and the number of loading cycles. The fact that both the equivalent spring constant and equivalent damping factor tended to decrease only slightly with the increase in the number of loading cycles indicates that the performance of the rubber bearing remained stable.

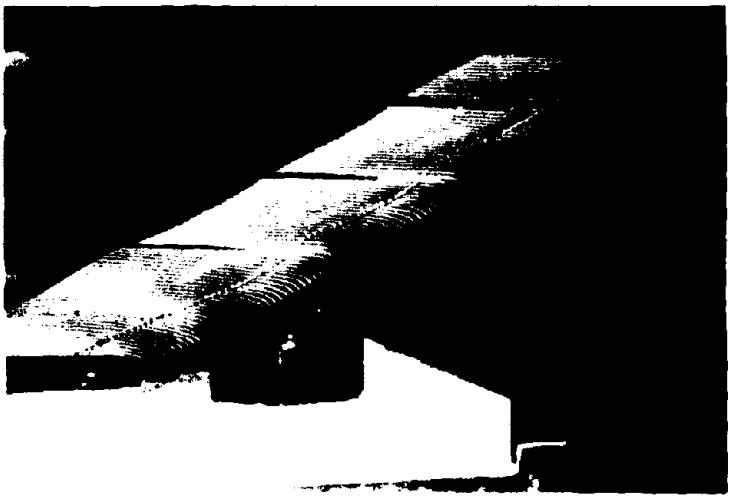

Photo 1 Large Deformation Test (γ=220%)

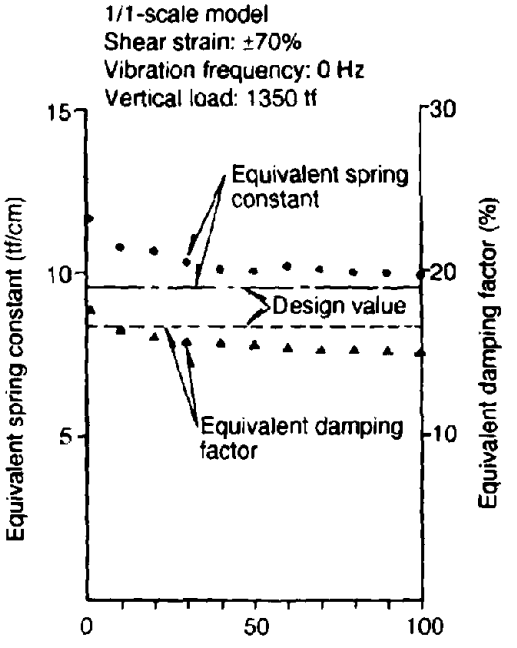

Fig. 10 Cyclic Shear Deformation Test

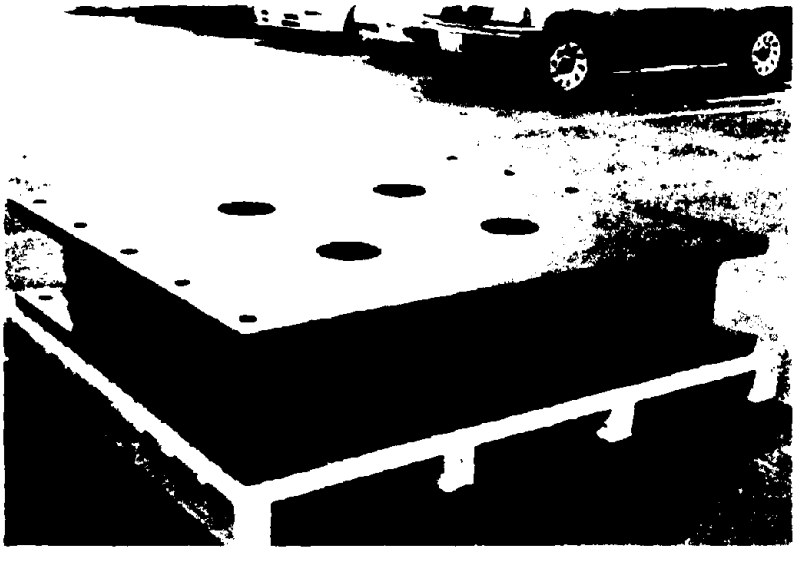

Photo 2 Lead Rubber Bearing in Process of Manufacture (1500 × 1500 × 553 mm)

(c) Large Deformation Capacity Test

This test was conducted to examine the extra deformation capacity of the rubber bearing subjected to very rare cases of loading. The assumed large deformation was 220%, which was the sum of the allowable shear strain due to earthquake loading (150%) and the allowable shear strain due to thermal loading (70%). This is about 1.5 times as large as the allowable deformation due to earthquake loading. The vertical load applied was 850 tf, which was equal to the deal load.

Fig. 11 shows the load–displacement curves for the three types of rubber bearing adopted. As shown, the load–displacement relationship for the ring bearing is linear, while the larger areas of the loops for HDR and LRB indicate that they do have damping effect.

Fig. 12 shows the load–displacement curves for HDR loaded for shear strains of ±220%. Hardening of rubber was observed when the shear strain exceeded 150%, but the curves show overall stability.

The horizontal displacement–vertical displacement test for shear strains of 220% indicated that as shear deformation increased, the effective area of bearing surface decreased and vertical displacement increased. The vertical displacement, however, was 3 mm or so at maximum (about 1.5% of rubber thickness) and it did not pose any practical problem. The fact that no substantial damage to the rubber bearing was observed after the test indicates that the bearing had sufficient deformation capacity.

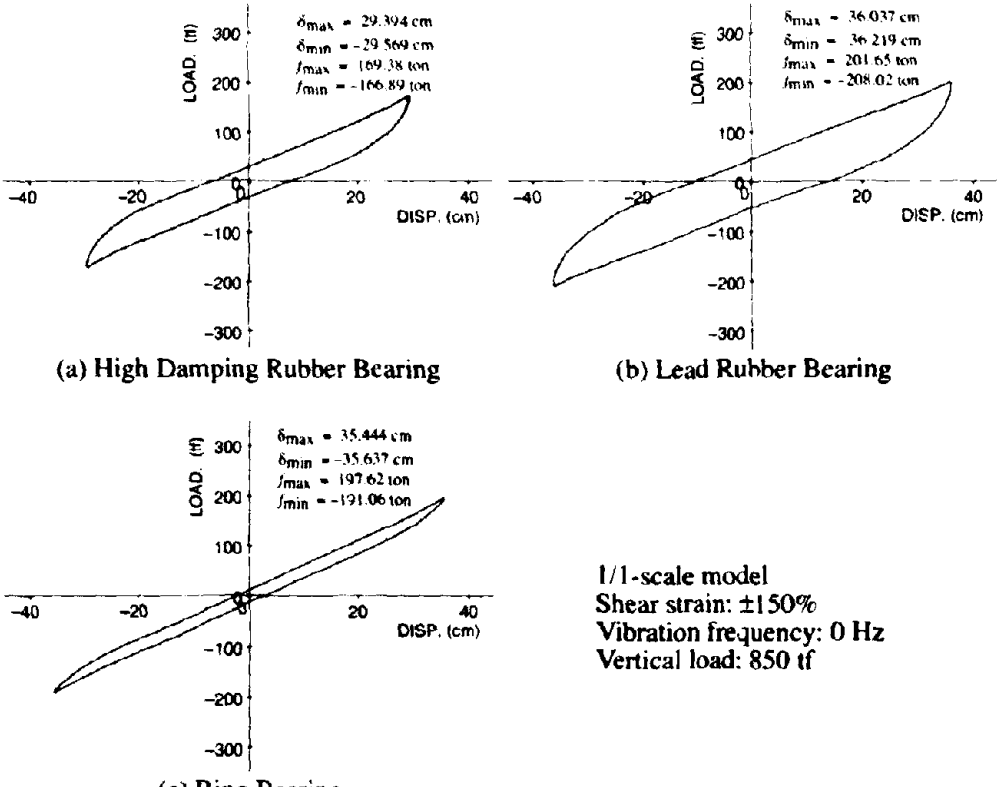

(a) High Damping Rubber Bearing

(b) Lead Rubber Bearing

(c) Ring Bearing

1/1-scale model
Shear strain: ±150%
Vibration frequency: 0 Hz
Vertical load: 850 tf

Fig. 11 Static Shear Deformation Test (1/1-Scale Model; Number of Repetition 3–10)

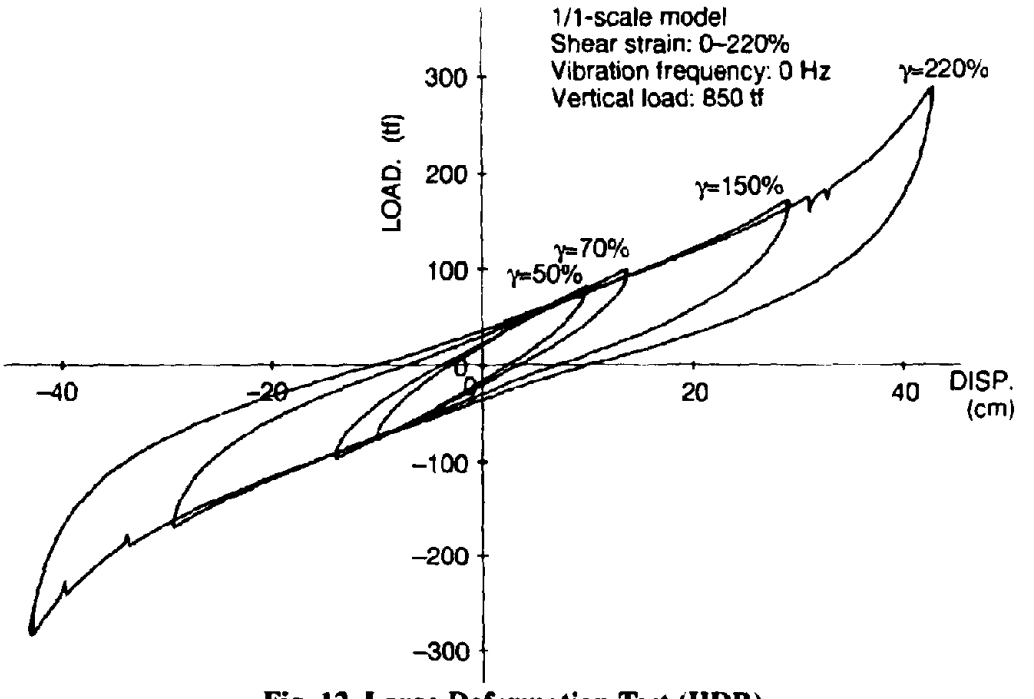

Fig. 12 Large Deformation Test (HDR)

Conclusion

The design of a multi-span continuous bridge with rubber bearings planned in the shallow water section of the Trans-Tokyo Bay Highway, as well as performance tests on rubber bearings, has been outlined. Rubber bearings were introduced to make multi-span continuous structure possible by reducing and distributing inertia forces due to earthquake loading and reducing indeterminate forces due to such factors as temperature changes. By improving the performance of rubber bearings and accumulating experience in using those bearings, multi-span continuous bridges can be more cost-effective.

The piers of the bridge are now almost complete, and in September 1992 the first superstructure was completed (Photo 3). Consisting of only four multi-span sections, the 4.4 km long bridge will have an exceptionally smooth road surface.

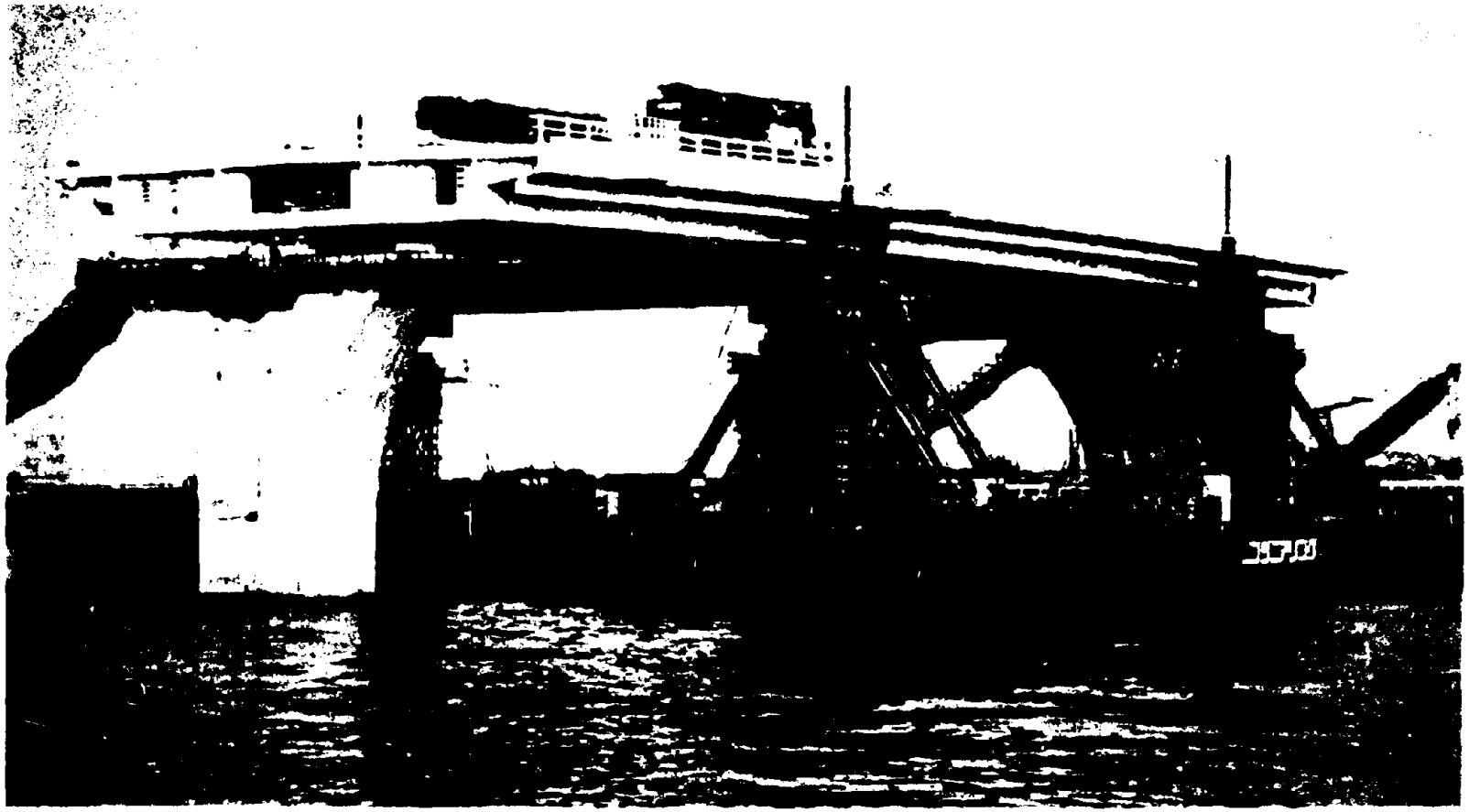

Photo 3 Erection of Girder Using Barge

Earthquake Protective Systems for the Seismic Upgrade of the Golden Gate Bridge

Santiago Rodriguez, P.E.[1], Charles Seim, P.E. F. ASCE[2], and Tim Ingham, Ph.D., S.E.[3]

ABSTRACT

The Golden Gate Bridge has endured since its opening in 1937 as a symbol of the City of San Francisco, and is one of the most famous bridges in the world. The bridge functions as an important transportation link for Bay Area commerce and commuters. It is owned, operated and maintained by the Golden Gate Bridge, Highway and Transportation District.

Immediately after the Loma Prieta earthquake in October of 1989, the District engaged T.Y. Lin International (TYLI) to perform seismic evaluation and retrofit studies of the bridge. The First Phase evaluation studies concluded that a major earthquake occurring on the San Andreas Fault and centered near the bridge may cause severe damage to the bridge and a prolonged interruption of service to the communities it serves. The Second Phase retrofit studies included development of measures and cost estimates to retrofit the bridge against such an occurrence.

Several consultants, in addition to T.Y. Lin International, are now working on the Third Phase that consists of final retrofit designs and preparation of construction plans, specifications and cost estimates. Construction is expected to start immediately thereafter and be completed by the end of 1998.

This paper describes the seismic analysis and behavior of the suspension bridge and offers an interim report on several retrofit ideas based on modifying its seismic response. The seismic retrofit alternatives considered for the final design require both tuning and strengthening the structures. The tuning concepts investigated for the suspension spans include allowing rocking to limit the seismic forces and installing structural fuses and dampers to change the dynamic response and dissipate energy.

[1] Project Engineer, T.Y. Lin International, 825 Battery Street, San Francisco, CA 94111

[2] Senior Principal, T.Y. Lin International, 825 Battery Street, San Francisco, CA 94111

[3] Senior Project Engineer, T.Y. Lin International, 825 Battery Street, San Francisco, CA 94111

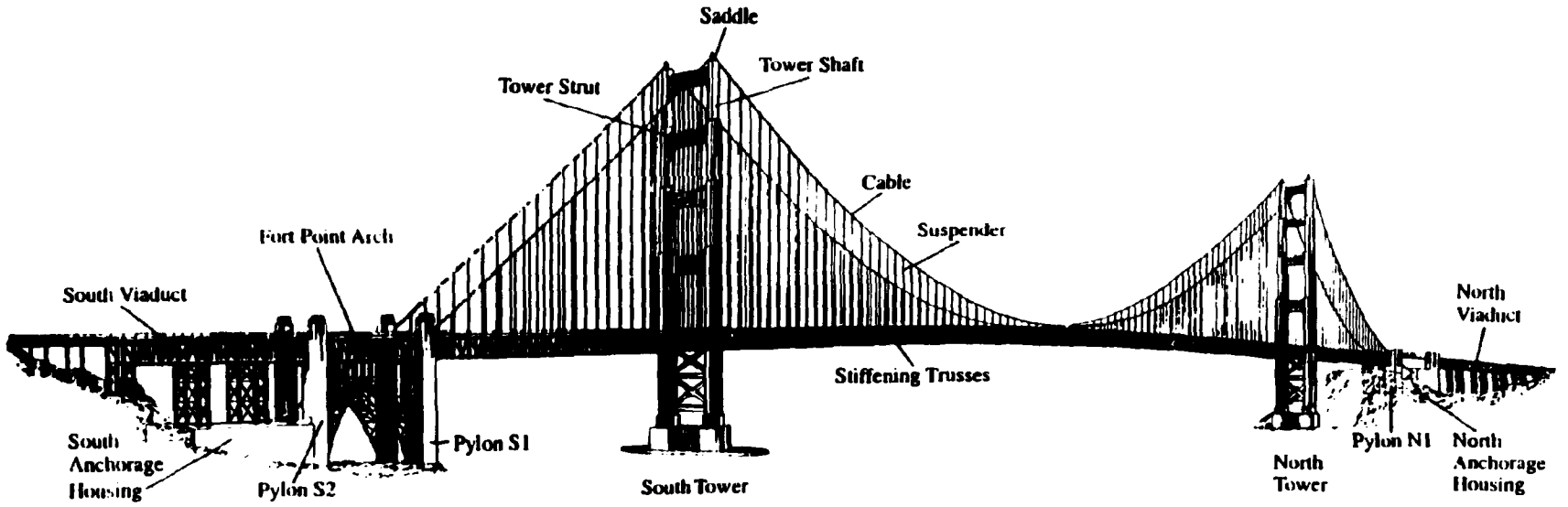

Figure 1. Golden Gate Bridge Structures

INTRODUCTION

One of the most renowned bridges in the world, the Golden Gate Bridge opened to traffic on May 28, 1937. The design and construction of the Bridge are well documented in the Chief Engineer's final report [5]. The Bridge is operated by the Golden Gate Bridge, Highway and Transportation District (District).

The 2790m overall length of the Golden Gate Bridge consists of a number of different structure types as shown in Figure 1. The bridge's major components are the steel truss approach viaducts, the Fort Point steel arch, the steel cable's concrete anchorage's and concrete anchorage housings, the steel suspension bridge, and the art deco concrete pylons. All of the foundations for these structures except the northern viaduct are supported directly on rock. The northern viaduct piers are founded on spread footing bearing on competent soil.

This paper focuses on the 1280m span suspension bridge. The major components of the suspension bridge are steel towers, main cables and suspenders, stiffening truss, concrete anchorage blocks and pylons. The towers consist of multicellular steel shafts braced with struts. The towers are supported on reinforced concrete piers.

The suspended structure consists of 7.6m deep parallel-chord stiffening trusses spaced 27.4m apart in the plane of the cables. The trusses are connected to each other by way of a top lateral bracing system that was part of the original construction, and a bottom lateral bracing system added to the stiffening truss as part of a wind retrofit in 1954. The stiffening trusses consist of laced members with riveted connections.

The vertical suspenders were replaced in the mid 1970s. The original concrete deck was replaced in 1985 with a lightweight orthotropic steel deck that reduced the total weight about 11,000 tons.

The Loma Prieta earthquake on October 17, 1989, was rated at a magnitude of 7.1. The Golden Gate Bridge was not instrumented, but appeared to be in an area where the bed rock acceleration was about 0.08 of gravity. Immediately following the earthquake, the District engaged T.Y. Lin International (TYLI) to perform a seismic evaluation, and about a year later, concept retrofit studies and approximate construction costs. The results of the seismic evaluation were presented in The Golden Gate Bridge Seismic Evaluation [1] by T.Y. Lin International in November 1990. The evaluation revealed that a major earthquake on a nearby segment of the San Andreas or Hayward Faults would likely cause severe damage to the bridge and could cause interruption of traffic and require significant repairs. The Golden Gate Bridge Seismic Retrofit Studies [2] in July 1991 included development and evaluation of concept retrofit measures as well as estimation of their construction costs and schedules.

SITE SPECIFIC SEISMIC RISK, RESPONSE SPECTRUM AND GROUND MOTIONS

The determination of site specific seismic risk, response spectrum and ground motions was based on evaluations of the geology, the relative location of nearby faults and the reoccurrence interval of the seismic event, seismic risk analyses, and computer simulations of ruptures on nearby faults. The results of these studies are presented in 'Geological, Geotechnical and Ground motion

studies for seismic retrofit of the Golden Gate Bridge" in July, 1992 [3] by Geospectra, Inc., Richmond, CA.

Seismic risk was evaluated by applying a probabilistic assessment of ground motion using the maximum expected design earthquake values of about 1,000 years return period for the two main nearby faults, the San Andreas and the Hayward, with a magnitude of 8.25 and 7.3 respectively. The peak ground acceleration estimated for an event comparable to the 1906 San Francisco earthquake on the San Andreas is 0.65g. Site-specific longitudinal, transverse and vertical response spectra were developed on the basis of these seismic risk analyses.

Three different seismic events (San Andreas fault rupture scenario) were developed by Geospectra Inc. to define three independent ground motions. One set of ground motions was developed for the Hayward fault, but the evaluation studies showed that it did not control.

For the suspension spans, for each of the three events, six multiple ground motions containing proper estimates of the phase delay and incoherency were used as inputs to the two main towers, the two flanking concrete pylons, and the two cable anchorage's.

SEISMIC PERFORMANCE CRITERIA

The seismic performance criteria for a retrofitted suspension bridge presents a compromise between available retrofit measures, constructibility constraints, user and owner's expectations, and cost. The retrofit measures for the Golden Gate Bridge must preserve life and allow the bridge to be used immediately after the largest expected event, first for emergency vehicles and then for the toll paying general public. To guide the designers, design criteria for the retrofit project was developed by T.Y. Lin International based on the Design Criteria from the new AASHTO Load and Resistance Factor Design.

The Evaluation Studies and the Seismic Retrofit Studies used only dead load and seismic loads were considered. For the final design phase, the Design Criteria requires also using 50% of live load in addition to dead and seismic loads.

SUSPENSION BRIDGE CHARACTERISTICS

The characteristics of the suspension bridge that most significantly influence its seismic response and the analysis requirements related to those characteristics are summarized below.

Large Displacement Effects and Multiple Support Excitation

The stiffness of the structure, which is provided mainly by the shape of the cable adjusted to the applied loads, is very sensitive to its geometry. The distortion of its geometry under applied loads causes its stiffness to change as the loads change. A geometrically nonlinear analysis that considers large displacement effects is required to capture the full behavior under dynamic excitation.

The multiple support excitation imposes relative displacements between the towers and the anchorage blocks that induce both static and dynamic stresses and displacements. The out-of-phase motions were found to give only a minor increase, or in many cases a decrease, in the stresses in the structure, as might be expected considering the flexibility of the bridge. The demands on the expansion joints, however, are generally larger with the multiple support excitation.

Dynamic Characteristics

Due to their dimensions and flexibility, suspension bridges have a long fundamental period of vibration. The seismic response for long period structures is characterized by large displacements and lower seismic forces than for shorter period structures. Although often ignored, higher vibration modes with a shorter period make an important contribution to the seismic forces in a suspension bridge. In a response spectrum analysis based on a mode-superposition procedure, it is necessary to consider a very high number of vibrational modes in order to include the modes with a natural period in the range of the maximum spectral acceleration. The higher modes have a small mass participation when compared with the fundamental modes but may actually have a very large participation in the response of local elements, such as the towers.

For example, in the seismic analysis of the Golden Gate Bridge, it was found that a longitudinal mode for the towers, coupled with the side span, with a period of 1.8 seconds, contributed greatly to the towers' seismic forces. However, this mode is the 47th mode for the bridge as a whole and it would be overlooked in an analysis considering less than 47 mode shapes.

A time history analysis performed by direct integration of the coupled equations of motion avoids the problems associated with the mode superposition method.

Material Nonlinearity

The main cables and suspenders of the Golden Gate Bridge respond to the maximum credible earthquake in the elastic range. Yielding of structural elements is confined to local areas such as parts of the towers, pylons and some elements in the stiffening truss. The stiffening truss elements and the steel plates at the towers do not comply with current seismic codes, and may buckle locally thus losing load carrying capacity in compression.

Displacement Compatibility

Due to the long natural period suspension bridges have, the seismic displacements are large, on the order of several feet across the expansion joints. In addition to this, different parts of the structure are subjected to different ground motions, thus creating large relative displacements at the expansion joints. When the displacement across an expansion joint reaches the maximum capacity, the expansion joint closes and transmits impact forces. A joint closure changes the dynamic properties and the response of the bridge. These effects are considered in the analyses by means of nonlinear gap elements.

Support Conditions

It is also important to consider changes in the support conditions due to seismic forces. In the case of the Golden Gate Bridge, the towers are weakly anchored to the underlying reinforced concrete piers. For service loads, the towers can be considered to be fixed to the piers because the dead load produces compressive stresses that are not exceeded by the bending stresses due to wind loads. However, rocking of the towers can be expected in strong earthquakes. This rocking can significantly change the towers' response characteristics. The rocking motion of the towers actually reduces the seismic stresses at the towers but increases the deflections. The nonlinear rocking behavior is considered in the seismic analysis of the suspension bridge.

ANALYSIS METHODOLOGY

The analysis of the seismic response of the Golden Gate Bridge requires the following three steps of increasing complexity: definition of the dead load state, modal analysis and response spectrum analysis assuming linear behavior, and nonlinear time history analysis, considering multiple-support ground motion.

Definition of the dead load state

The dead load state was defined starting with the geometry and dead load corresponding to the time the construction was completed. The dead load and the construction procedure determined the initial stresses. A static nonlinear analysis considering large displacement theory was performed to check equilibrium and to fine-tune the original geometry. The result of this analysis yielded the dead load state at the completion of construction.

The Newton-Raphson method, based on tangent stiffness iteration, was used for this static load analysis to account for the large displacement effects. For the Design Phase, 50% of live load is added to the dead stress for combining with the dynamic analysis.

Modal and Response Spectrum Analysis

Once the dead load state was determined, a modal analysis was performed to compute the vibrational properties. The modal analysis assumes linear behavior for small deformations from the dead load state. The natural frequencies and mode shapes computed from the analysis were compared with the ones obtained from ambient vibration tests. This comparison provided a way to verify the computer models.

Following the modal analysis, a response spectrum analysis was performed for the maximum credible earthquake. The response spectrum analysis did not include the effects of the nonlinear behavior or the multiple support excitation. However, it gave an initial insight into the magnitude of the seismic forces, thus redirecting the modeling and analysis efforts towards the problem areas.

Nonlinear Time History Analysis

The analyses of the global response of the bridge to multiple-support ground motion excitations are performed using a dynamic nonlinear finite element computer program, in which large displacement effects are considered by establishing the static or dynamic equilibrium of the structure in its deformed configuration. The effect of a limited displacement capacity at the expansion joints and the nonlinear rocking behavior of the tower's bases is examined by using "gap" elements.

The nonlinear dynamic analyses are performed by integrating the coupled equations of motion in the time domain. The ground motion excitation was applied as a time-varying displacement boundary condition at each of the supports. In each time step, the nonlinear system of equations relating the effective dynamic loads and the nodal accelerations are solved by using the Newton-Raphson method, based on tangent stiffness iteration. Rayleigh damping is assumed, in which the damping matrix is proportional to a linear combination of the mass and stiffness matrices. The proportionality factors were computed to yield a damping ratio of 5% at periods of 0.5 seconds and 20 seconds. The damping ratios for periods between those two values are smaller, with a minimum of 1.5% at a period of 3 seconds. These values are consistent with ambient vibration measurements.

SEISMIC RESPONSE AND VULNERABILITIES OF THE SUSPENSION BRIDGE

The expected seismic response is calculated by the dynamic analysis of structural models subjected to artificially generated ground motions. The seismic response is very complex in nature due to the high participation of secondary vibration modes, coupling between longitudinal and vertical motion, large displacement effects and the multiple support excitation. The first step when designing earthquake protective systems for a complex structure such as the Golden Gate Bridge is to understand which modes of behavior contribute to potential seismic vulnerabilities.

The tuning measures presented in this paper were designed to modify or eliminate those modes of behavior so that demands on structural members and strengthening requirements are reduced to a minimum. Three main approaches that can be used for the modification of the seismic response are energy dissipation, structural fuses and changes in the vibrational characteristics. These tuning measures were developed from an intuitive description of the seismic response, but they were ultimately tested with three-dimensional nonlinear models of the structure. We are still evaluating these retrofit measures and they are presented here as an interim report of our retrofit development.

Vertical Response

Suspension bridges like the Golden Gate Bridge carry vertical loads through tension on the main cables which mimic the funicular curve of the total dead load. In general, the vertical response by itself does not create demands exceeding the capacity because of the existing factor of safety for dead load. However, the seismic vertical response differs from the dead load in that it does not always produce uniformly distributed seismic forces due to the participation of secondary modes.

a) Vertical Mode. Mode Number 19. Period = 3.5 seconds

b) Longitudinal Mode. Mode Number 5. Period = 7.1 seconds

c) Longitudinal Mode. Mode Number 47. Period = 1.8 seconds

d) Transverse Mode. Mode Number 17. Period = 3.5 seconds

Figure 2. Golden Gate Bridge Mode Shapes

Figure 2a shows mode shape number 19 with a period of 3.5 seconds. A mode like this produces moments and shear in the stiffening truss that uniform loads would not create. Vertical vibrations are also frequently coupled with longitudinal vibrations.

Longitudinal Response

The main span stiffening truss is longitudinally free with expansion joints at both ends. The only longitudinal restraint is provided by the suspenders. Figure 2b shows mode shape number 5, with a period of 7.1 seconds, in which the main span moves as a pendulum hanging from the suspenders. The expansion joints are the interface between two systems with different natural periods. The main span longitudinal mode has a period of 7.1 seconds; whereas the tower longitudinal mode has a period of 1.8 seconds. The main span would have a displacement relative to the tower of 47 inches if left unrestrained. This displacement exceeds the 18 inch capacity of the existing expansion joints and wind locks. The result is impact forces that could damage the wind locks. Longitudinal dampers at the main span expansion joints can eliminate this problem by dissipating seismic energy.

In addition to providing support for vertical loads, the main cables provide longitudinal restraint at the tops of the towers by way of the saddles. Longitudinally, the towers behave as guyed columns, simply supported at the top and fixed at the bottom. When the moment at the base exceeds the moment capacity of the existing connection, the towers rock, rotate and become simply supported at both top and bottom.

The side span stiffening trusses are longitudinally pinned to the towers and have longitudinal expansion joints at the reinforced concrete pylons. The connection between the side span and the tower delivers longitudinal forces on the order of 10,000 k that contribute to the longitudinal deflection of the towers. Figure 2c shows mode shape number 47 with a period of 1.8 seconds. This mode is responsible for the coupled response between the side span and the tower. The coupled response of the towers and side spans causes high demands in the towers due to bending moments about a transverse axis, both at the bottom and in the area above the roadway. The South and North pylons behave as a column fixed at the foundation and free at the top, with longitudinal shear and moments exceeding their capacity.

The longitudinal vibration of the side spans, towers, and pylons can be controlled by installing structural fuses and longitudinal dampers at the side span expansion joints, and by allowing rocking at the tower base.

Transverse Response

The structural system for transverse forces is straight forward. The side spans are simply supported at the pylon and the tower. The main span is simply supported at the towers. The main cables and suspenders provide some transverse stiffness at the main span but this contribution is small for the side spans. The pylons and towers behave as cantilevered columns, with transverse loads coming from the cables and stiffening trusses, in addition to their own inertial forces.

The side span transverse response is mainly in the first transverse mode, with a period of 3.8 seconds (see Figure 2d). The south side span presents a secondary mode with a period of 0.5 seconds coupled with the South pylon that greatly contributes to the seismic demand. The side

span transverse deformation produces high demands in the stiffening truss chords and in the lateral braces. The ductility demand calculated assuming elastic material behavior reaches 1.7 for the chords and 2.8 for the lateral braces. The ductility demand obtained when considering inelastic yielding and buckling is even greater. The chord axial forces come from the global bending of the stiffening truss. The lateral brace axial forces come from global shear. Secondary modes also produce important shear in the middle of the side spans thus affecting the laterals in that area.

The main span responds transversally mainly in secondary modes. The first transverse mode with a period of 20 seconds has a very small participation. The global bending moments do not produce high demands in the chords but the secondary modes produce shear in the central part of the span. Unfortunately, the lateral bracing system of the stiffening truss was designed for wind loads and is not prepared to carry high global shears in the middle of the span.

The demands on the side span stiffening trusses can be reduced by using wind-lock dampers, lateral bracing dampers or stiffening truss hinges. These retrofit schemes are described below.

LONGITUDINAL DAMPERS AT THE STIFFENING TRUSS EXPANSION JOINTS

The impact between the main span stiffening trusses and the towers occurs because the seismic displacements exceed the existing displacement capacity. The side spans present a similar problem at the pylon expansion joints where seismic displacements exceed the existing displacement capacity. In addition to this, the longitudinal connection between the side span and the tower causes coupled vibration of these two elements. This longitudinal connection can be replaced with a structural fuse that would be able to carry services loads, but would break during strong earthquakes. Longitudinal dampers at the expansion joints between the side span and the pylons and between the side spans and the towers can provide energy dissipation and displacement control. The dampers significantly reduce the impact forces between the stiffening trusses and the towers, and tower shaft and stiffening truss chord stresses.

For both the main and the side span dampers, the properties of the dampers have been optimized to achieve an appropriate reduction of the relative displacements and stresses, keeping the damper force within reasonable limits. Viscous devices are the best option because slow temperature displacements must be accommodated without forces at the dampers. Hydraulic devices have a restoring force (F) which is a function of the relative velocity (V). The constitutive law is:

$$F = C \cdot V^n$$

Different values for the exponent n have been evaluated. Powers $n = 0$, ½, 1, and 2 were considered. A power $n = 2$ represents the classical behavior of a fluid moving through a Bernoullian orifice, where pressure is proportional to velocity squared. A power $n = 1$ corresponds to classical linear damping. A power $n = ½$ is near the minimum power available from hydraulic devices. A power $n = 0$ simulates a perfectly plastic device, producing a force independent of the device velocity.

Figure 3 shows the energy dissipated by the side span dampers (summed over the south side span/pylon and south side span/tower dampers) as a function of the peak damper. Points C

(constant force) correspond to $n = 0$ dampers, points L (linear) correspond to $n = 1$ dampers, points S (square root) correspond to $n = ½$ dampers, and points P (parabolic) correspond to $n = 2$ dampers. The trend is quite clear; small power n dampers are preferable, dissipating more energy for the same peak force than large power dampers. Considering these results, a power $n = ¼$ was selected for optimization of the damper coefficient C. The power $n = ¼$ is a compromise between the theoretically optimum power and the known capabilities of damper manufacturers.

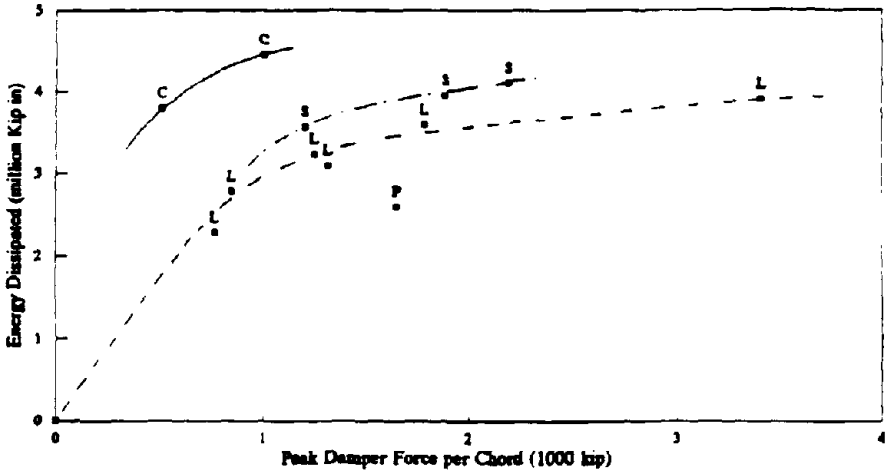

Figure 3. Energy Dissipated by the Side Span Dampers

The dampers were next optimized with respect to the coefficient C, considering energy dissipated, peak damper forces, stiffening truss chord stresses and expansion joint displacements. A coefficient C = 100 kip·sec^{¼}/in^{¼} per chord was selected as being a good compromise between peak damper forces and expansion joint displacements. The chord stress does not decrease much for coefficients larger than the selected value. The peak damper force per chord corresponding to these dampers is 2500 Kip.

Besides seismic excitation, the dampers installed between the main span and the towers will be subjected to thermal movements, wind excitation and small amplitude, high frequency vibrations caused by traffic on the bridge. The final damper design must be able to perform under all these environments.

TOWER BASE ROCKING

Rocking at the tower base occurs when the moment demand exceeds the capacity of the existing connection. The rocking motion of the tower improves the global seismic performance and it will

not be prevented with the retrofit. The effect of rocking is to limit the longitudinal bending moment at the base of the tower. The tower becomes pinned at the bottom and the longitudinal period of vibration increases. The rocking of the towers also increases their longitudinal displacements which can be controlled by longitudinal dampers. The longitudinal stability of the towers is assured by the longitudinal restraint provided by the main cables.

WIND LOCK DAMPERS

The installation of longitudinal dampers for the side spans is equivalent to seismically isolating the side spans in longitudinal direction. The side spans could also be isolated transversely. The side span stiffening trusses are transversely connected to the pylon and tower by means of sliding blocks able to transfer transverse shear without longitudinal forces.

In this scheme, shown in Figure 4a, the sliding blocks would be replaced with blocks designed to fail under seismic excitation. Lateral loads would then be transferred by "wind-lock" dampers placed between the stiffening trusses and the towers and pylons. Frictional, LED or viscous dampers would be suitable.

As the damper capacity is reduced, the stiffening truss becomes "isolated" from transverse excitation. At the limit of zero damper capacity, transverse excitation would be applied to the stiffening truss only through the cable system, which is very flexible. In the limit, the stiffening truss would act as a pendulum, with a period of 21 seconds. The acceleration response of the stiffening truss would then be very low. The retrofit would ideally reduce the shearing and bending of the stiffening truss, without excessive transverse movement.

This scheme requires redesigning of several elements to accommodate transverse relative displacement. The expansion joints between the stiffening trusses and the towers and pylons cannot tolerate transverse movement. To avoid severe damage, these would have to be replaced with "swivel-type" (or similar) modular joints able to accommodate transverse movement. The rocker links supporting the end panels of the stiffening trusses cannot tolerate transverse movement either, and would have to be re-articulated.

The transverse movement of the stiffening trusses would also affect any longitudinal dampers installed between the stiffening trusses and the towers and pylons. The transverse movement would only be a fraction of the length of the dampers (≈15%), however, so that the angle change of the dampers would be small (≈10°).

Several alternatives were developed, with dampers having a capacity equal to the factored wind loads multiplied by a factor that varied from 0.7 to 1.2. The wind loads were calculated from a 100-year return period yielding a mean hourly wind speed of 76 mph. This was increased to 97 mph over 30 seconds, to calculate the static wind pressure on the stiffening truss. The wind force on the stiffening truss was calculated using a drag coefficient of 0.35. Three different locations for the dampers were also considered: dampers located at both ends, dampers at the pylon only and dampers at the tower only. The dampers were modeled as rigid-plastic devices. Viscous or other dampers would give similar results.

For the alternative in which dampers are installed at both ends with a capacity equal to the factored wind load the peak demand-capacity ratios on the lateral bracing are less than 0.9. The demand-capacity ratios on the chords are less than 0.75. The peak transverse displacement of the side span relative to the pylon or the tower is 2 feet. This scheme is successful in reducing the demand on the side spans, but has the drawback of having to accommodate important transverse displacements.

LATERAL BRACING DAMPERS

In this scheme ductile deformation of the lateral bracing system would limit the bending demands on the chords. The deformation would be concentrated into "lateral bracing" dampers integrated into the lateral bracing system. Figure 4b shows one way to install dampers between the lateral bracing and the floorbeams. The dampers would act through the relative deformation between the bracing members on opposite sides of the floorbeam. Elastic-plastic (ideally rigid-plastic) devices would be used to resist wind and other lateral loads. Frictional, LED or steel yielding dampers would be suitable.

If the capacity of the dampers is small (but sufficient to carry wind loads, etc.) the distortion of the stiffening truss will be high, and the demands on the chords low. The distortion of the stiffening truss might induce moments in the lateral bracing, chords and floorbeams, that were not considered in the original design. If the capacity of the dampers is large, on the other hand, the distortion of the stiffening truss will be low, and the demands on the chords high.

Ideally, the retrofit would reduce the bending of the stiffening truss, without too much distortion. The lateral bracing connections might or might not need strengthening depending on the capacity of the dampers.

Several alternatives were developed with dampers having a total shear capacity, transversely to the bridge centerline, varying from 215 to 1000 kips for the dampers in the top laterals and from 135 to 260 kips for the dampers in the bottom laterals. In some of the alternatives the dampers, modeled as rigid-plastic devices, are located only near the ends whereas in others they occupy the whole length of the side span. The damper capacity exceeds the factored wind load at each panel.

For the alternative in which the dampers are located at the end of the side span stiffening truss and have a small capacity (just the minimum required for wind loads) the peak demand-capacity ratios on the chords and lateral bracing are less than 1.0, except near the pylon where the laterals have a demand-capacity ratio of 1.5. The peak damper relative displacements are nearly 12 inches.

The relative displacements at the dampers can be reduced by increasing the capacity of the devices and extending them along the side span. However, the relative displacements at the dampers diminish very slowly as the capacity of the dampers is increased. For an alternative with devices with capacities up to 1000 kip the peak damper relative displacement is about 8 inches. The demand-capacity ratios reach 1.5 in about half of the side span and can not be reduced below 1.0 if the dampers have a capacity larger than the factored wind loads. Therefore, this alternative does not seem to be successful in the seismic upgrade of the side span.

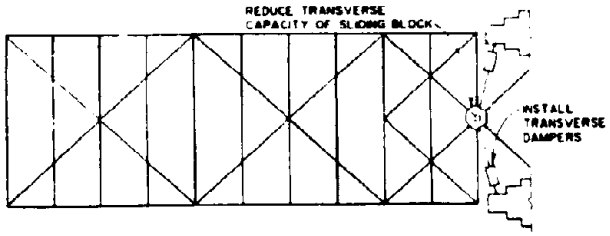

Figure 4. Transverse Wind Lock Dampers

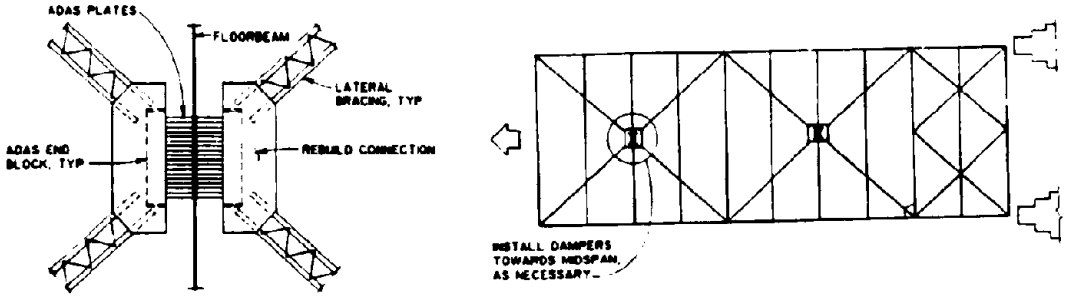

Figure 5. Lateral Bracing Dampers

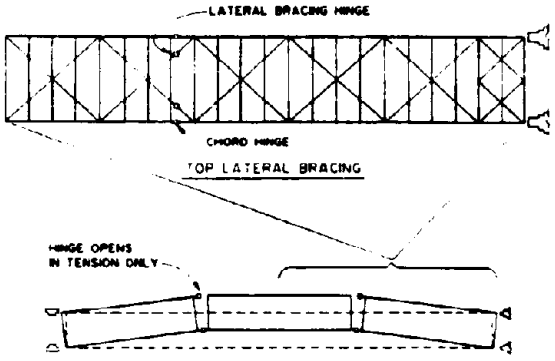

Figure 6. Stiffening Truss Hinges

STIFFENING TRUSS HINGES

The two previous schemes attempted to reduce the seismic demands in the side spans by limiting the shear that can be transmitted either by the wind locks or by the lateral bracing system. As a final scheme for protecting the side span, the bending moment developed in the stiffening truss can be limited by inserting "hinges" into the stiffening truss chords and lateral bracing members near the third-points of the side spans. This is turn would limit the development of shear, since shear cannot develop in the absence of moment. This scheme is not a practical retrofit alternative but is included here to show all the possible ways of limiting the seismic demands in the stiffening truss.

As Figure 4c shows, the stiffening truss would be able to deform as a segmented rigid body, rather than in flexure or shear. The hinges would be bolted closed to resist live and wind loads. The restraining bolts would be designed to fail in tension before the chords on the opposite side of the stiffening truss could fail in compression. Dampers would be placed across the hinges to dissipate energy as the hinges opened and closed.

Although mathematically elegant, this scheme dramatically changes the stiffening truss, and possibly degrades its performance with respect to live and wind loads. Also, construction of the hinges would be difficult.

The hinges were modeled with gap elements, able to resist compression only. The restraining bolts were modeled with rigid links, able to resist tension only; the links were modeled to have brittle failure when their capacity was exceeded. The capacity of the bolts was set equal to

$$T = \frac{1.3 \times \text{Live Load} + 0.3 \times \text{Wind Load}}{0.8} + 3000 \text{ kips},$$

where the live load included future transit vehicles, and 0.8 is a bolt "resistance factor." The capacity of the chord is about 5000 kips. Viscous dampers with $C = 25$ kip·sec$^{3/4}$/in$^{3/4}$, $n = 3/4$, were placed across each hinge.

The nonlinear dynamic analysis of this scheme shows how demand-capacity ratios on the chords are less than 1.0, but not on the lateral bracing. The demand-capacity ratios on the bottom lateral bracing are particularly large in the vicinity of the hinge near the pylon. The peak displacement across one of the hinges is 28 inches.

This scheme cannot be called a success. The demands on the lateral bracing and the relative displacements at the hinges are still excessive.

CONCLUSIONS

This paper has shown how the most important vulnerabilities of the Golden Gate Bridge are related to three modes of behavior; coupled longitudinal vibration of the side spans and towers, longitudinal vibration of the main span and transverse vibration of the stiffening trusses.

The vulnerabilities associated with longitudinal vibration can be mitigated by installing longitudinal dampers at the stiffening truss expansion joints and allowing rocking at the tower base.

Three schemes for protecting the side span stiffening trusses against transverse excitation were also evaluated. The installation of dampers in order to isolate the side span transversely is the most efficient scheme in reducing the demands, but it requires redesigning the wind locks, rocker links and expansion joints to accommodate transverse displacements. The second scheme is based on installing dampers between the lateral bracing. A third and not very practical scheme is based on creating hinges in the stiffening truss. The last two schemes are less successful in reducing seismic demands and also require large relative displacements at the location of the dampers.

Our design team is currently evaluating combinations of the first two schemes as well as alternatives that require limited strengthening before recommending a final solution.

ACKNOWLEDGMENTS

All of the Golden Gate Bridge studies summarized in this paper were made under the direction of the Golden Gate Bridge Highway and Transportation District. The authors wish to thank General Manager Carney Campion, District Engineer Daniel Mohn, Deputy District Engineer Mervin Giacomini and Senior Civil Engineers Jerry Kao and Noel Stampfli for their support.

REFERENCES

1. Golden Gate Bridge Seismic Evaluation, T.Y. Lin International, Golden Gate Bridge, Highway and Transportation District, San Francisco, CA, November 1990.

2. Golden Gate Bridge Seismic Retrofit Studies, T.Y. Lin International, Golden Gate Bridge, Highway and Transportation District, San Francisco, CA, July 1991.

3. Geological, Geotechnical and Ground Motion Studies for Seismic Retrofit of the Golden Gate Bridge, Geospectra, Inc., Golden Gate Bridge, Highway and Transportation District, San Francisco, CA, July 1992.

4. Housner, G.W., et. al., Competing Against Time, Report to Governor George Deukmejian from the Governor's Board of Inquiry on the 1989 Loma Prieta Earthquake, State of California, Office of Planning and Research, May 31, 1990.

5. Strauss, J., The Golden Gate Bridge: Report of the Chief Engineer to the Board of Directors of the Golden Gate Bridge and Highway District, California, 1937, San Francisco, California, Golden Gate Bridge and Highway District, 1938.

IMPROVEMENTS IN EARTHQUAKE RESISTANCE OF PC CABLE-STAYED BRIDGES BY HYSTERESIS DAMPERS

Yuji NIIHARA, Tetsuo TAKEDA, Toshimichi ICHINOMIYA
and Rie SUZUKI

Civil Engineering Department I
KAJIMA Technical Research Institute
Chofu-shi, Tokyo 182, Japan

SUMMARY

Investigation into the improvement of seismic resistance of long span PC cable stayed bridges with hysteresis damper supports was conducted using time history response analysis. Reductions in the displacement of the deck and the bending moments in the towers and piers are discussed from the point of view of the stay cable arrangement and the span length. The results show that a semi-harp shape configuration is more effective than a harp shape configuration for long span PC cable stayed bridges with hysteresis damper supports. Hysteresis dampers increase the seismic resistance of PC cable stayed bridges regardless of the span length. The damper is also effective when structural menbers are plasticized during large earthquakes.

INTRODUCTION

In recent years examples of middle and long span prestressed concrete (PC) cable stayed bridges have been increasing. In general, when compared with steel cable stayed bridges, PC cable stayed bridges are heavier so their wind resistance stability is superior, but the inertial force during earthquakes is larger so their earthquake resistance is relatively lower. Long span PC cable stayed bridges constructed in seismically active regions are often designed as a floating type in which the deck is not restrained along the bridge axis in order to increase their earthquake resistance. However, for the floating type, the deck displacement will become excessive at the ends and the inertial force of the deck will act directly on the towers through the stay cables, so the bending moment at the bottom of the towers can become excessive.

Concerning the actual floating type PC cable stayed bridge with a 250m center span, the authors carried out analytical investigations into the increase in seismic resistance

with hysteresis dampers in the supports[1]. These results shows that, with hysteresis dampers, (1) the displacement of the deck along the bridge axis can be reduced to about 60% compared with the floating type, (2) the bending moments in the towers and main piers can be reduced compared with either the fixed or floating type, (3) the optimum stiffness and yielding displacement of the hysteresis dampers can be determined.

In this paper, time history response analyses are carried out on the effectiveness of hysteresis dampers for, in particular, longer span PC cable stayed bridges. There focused on the displacement of the deck, which becomes large during earthquakes, and the bending moments at the bottom of the towers and piers, where the cross-sectional forces are often critical during earthquakes.

To begin with, based on an actual $195m$ two-span continuous cable stayed bridge which was designed following the *Specifications for Highway Bridges*, analysis models of a three-span continuous cable stayed bridge with center span of $400m$ are made. Then the effects of two different arrangements of stay cables (semi-harp shape and harp shape) on the seismic resistance of PC cable stayed bridges are investigated. Regarding the effects of hysteresis dampers, parametric studies of damper stiffness are also conducted for the different span length models($400m$, $250m$, $150m$). Finally, the effects of the dampers, when the structural members are plasticized during large earthquakes, are examined[2].

ANALYSIS OUTLINE

Analysis Model

In order to understand the seismic response along the bridge axis, $2D$ lumped mass finite element system frame models are chosen as the analysis model for the PC cable stayed bridge. The bridge is symmetrical at the center of the main span, so only the half of the bridge is modeled. Three types of support condition for the deck along the bridge axis (floating, fixed, and with dampers) are investigated. The support conditions at the main pier and the end pier for each type are shown in Table 1. The stiffness of the end pier is set at half the stiffness of the main pier.

Table 1 Condition of Deck Connection

	Main Pier	End Pier
Floating Type	Free	Roller
Fixed Type	Pin	Roller
Damper Type	Bilinear Damper	Bilinear Damper

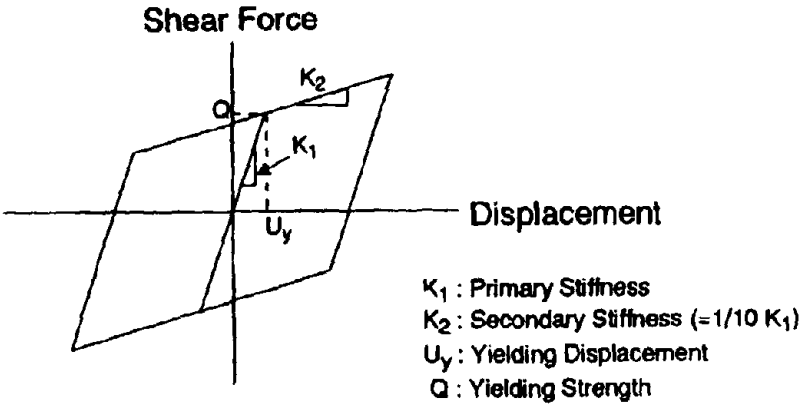

Fig. 1 Force-Displacement Characteristics of Hysteresis Damper

Hysteresis Damper Modeling

The hysteresis dampers are expressed as a bilinear spring (as shown in Fig.1). The yielding displacement is set at $1cm$, and the secondary stiffness of the damper after yielding is set at the 1/10 of the primary stiffness. Dampers are placed on the top of both the main pier and the end pier. The stiffness of the damper on the end pier is set at half the stiffness of the damper on the main pier.

Analysis Method

Time history response analyses using the direct integral method are carried out to investigate the effect of the hysteresis dampers. The damping of the structure is given as a Rayleigh damping which modal damping factors of 1^{st} and 2^{nd} modes are 5%. Before carrying out the time history response analysis, it is necessary to obtain the natural periods of the 1^{st} and 2^{nd} modes by eigenvalue analyses. In the eigenvalue analyses, the bilinear springs expressing the hysteresis dampers are treated as linear springs with their primary stiffness values.

Input Wave and Its Acceleration Response Spectrum

The acceleration response spectrum of the input acceleration wave used in the analyses is the same as that in the *Specifications for Highway Bridges, Part V Seismic Design* (for class I ground). However, this standard acceleration response spectrum is stipulated only that the natural period is in the range from $0.1sec.$ to $5sec.$. For the $400m$ semi-harp shape cable stayed bridge used in this analysis, the natural period of the 1^{st} mode is about $9sec.$, so it is not possible to use the standard acceleration response spectrum as it is. Therefore, for the range where the natural period is longer than $5sec.$, the acceleration response spectrum is reduced linearly on the logrithmic plane. The input acceleration wave is formed based on the observed seismic wave at *KAIHOKU BRIDGE* in 1978. The input acceleration wave and its acceleration response spectrum are shown in Fig.2.

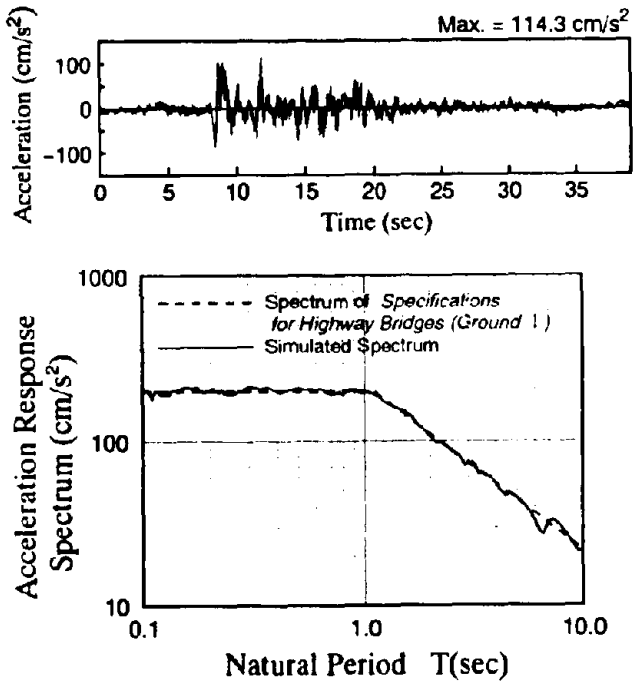

Fig. 2 Input Acceleration Wave and Response Acceleration Spectrum

RESPONSE CHARACTERISTICS FOR DIFFERENT ARRANGEMENTS OF STAY CABLES

Analysis Model

Analysis models for the 400*m* cable stayed bridge (semi-harp shape and harp shape) are shown in Fig.3. The cross-sectional data of the structural members are the same for both types, as shown in Table 2. The primary stiffness of the damper is 200*tf/cm*, the secondary stiffness is 20*tf/cm* and the yielding displacement is 1*cm*. The 1st and 2nd natural modes of the floating types are shown in Fig.4. The 1st natural period of the floating type is extremely long, 8.99*sec*. for the semi-harp shape, and 4.66*sec*. for the harp shape.

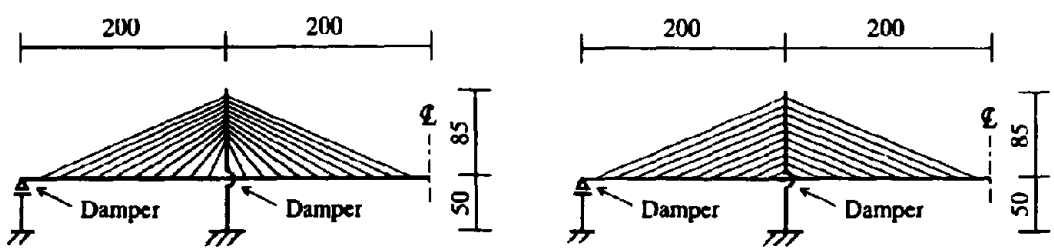

(a) Semi-Harp Shape **(b) Harp Shape**

Fig. 3 Analysis Models for 400*m* Cable Stayed Bridge (unit:*m*)

Table 2 Structural Data of $400m$ Cable Stayed Bridge

	$E(tf/m^2)$	$A(m^2)$	$I(m^4)$	$W(tf/m^3)$
Deck	3.1×10^6	13.3	14.0	2.9
Tower	3.1×10^6	28.2	70.9	2.5
Main Pier	3.1×10^6	210.3	1054.4	2.5
End Pier	3.1×10^6	105.2	527.2	2.5
Cable	1.95×10^7	0.0316	–	10.0

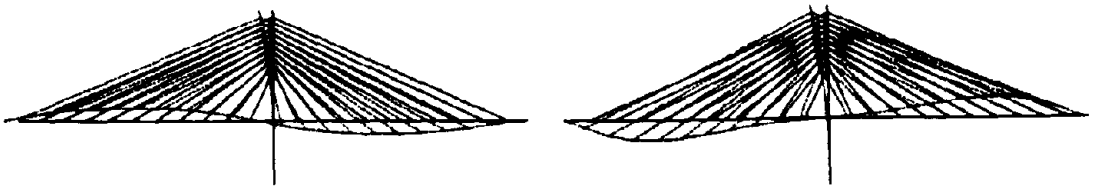

1^{st} Mode ($T_1 = 8.99\,sec.$) 2^{nd} Mode ($T_2 = 3.31\,sec.$)

(a) Semi-Harp Shape Arrangement

1^{st} Mode ($T_1 = 4.66\,sec.$) 2^{nd} Mode ($T_2 = 2.37\,sec.$)

(b) Harp Shape Arrangement

Fig. 4 1^{st} and 2^{nd} Natural Modes of the Floating Types

Response Characteristics of Semi-Harp Shape

The results of the time history response analyses of the floating, fixed, and damper type are shown in Table 3. The displacement of the deck for the floating type is $38.2cm$, while that for the damper type is reduced to $12.3cm$, about one third of the displacement for the floating type. The moment at the bottom of the tower for the damper type is almost the same as that for fixed type, approximately half of that for the floating type. The moment in the bottom of the main pier for the damper type is almost the same as that for the floating type, and about one third of that for the fixed type.

The displacement responses of the deck along the bridge axis are shown in Fig.5(a)-(c). For the floating type, even after the main earthquake shock calmed down, the large amplitude response of the deck, with period of about $9sec.$, continues. For the damper type, the response decreases rapidly and no large amplitude vibration can be seen after the main earthquake shock. However, after the main earthquake shock finishes the displacement of the deck does not return to zero, as there is a residual deformation in hysteresis dampers.

Table 3 Maximum Response Displacement and Moment (Semi-Harp Shape)

	Displacement of Deck (cm)	Moment at the Bottom of Tower (tfm)	Moment at the Bottom of Main Pier (tfm)
Floating Type	38.2	31990	80130
Fixed Type	6.8	16490	263600
Damper Type	12.3	17900	86900

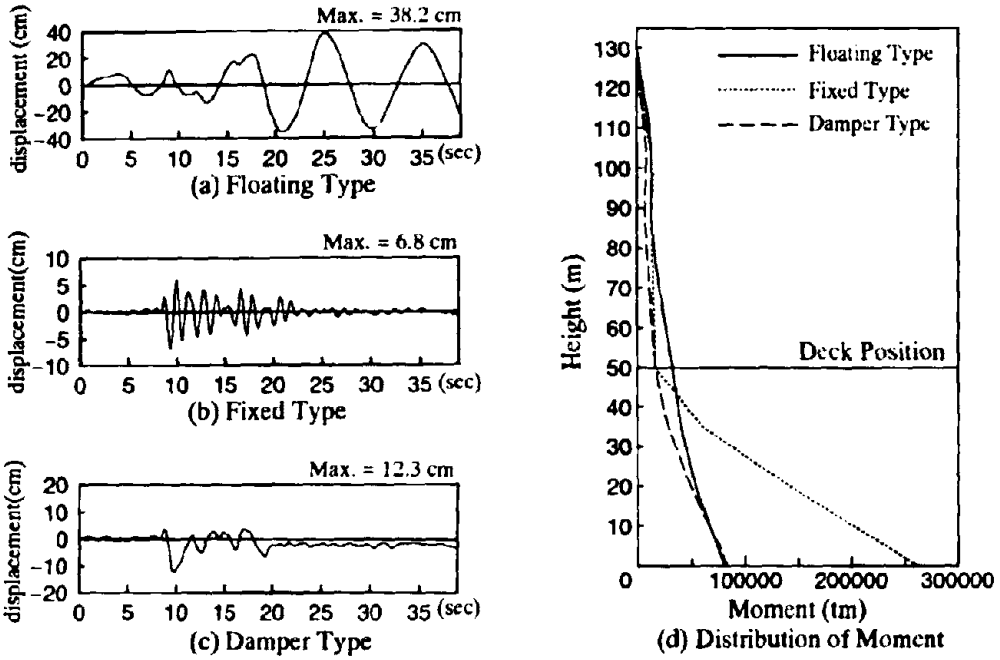

Fig. 5 Response Displacement of Deck and Moment in Tower and Pier (Semi-Harp Shape Arrangement)

Distribution of the bending moments in the tower and the pier are shown in Fig.5(d). The moment at the bottom of the pier for the damper type is slightly larger than that for the floating type, but as a whole, the damper type has the lowest bending moment among the three support systems.

Response Characteristics of Harp Shape

The results of the time history response analyses for the three support types with a harp shape configuration, are shown in Table 4. For the harp shape floating type, with the restraint effects of the lower cables, the displacement of the deck is relatively small(11.8cm), compared with that of the semi-harp shape. For the damper type, the deck displacement is 9.4cm, 80% of that of the floating type. The displacement responses of the deck are shown in Fig.6(a)-(c). For the harp shape too, damping of the response for the damper type is rapid and after the main earthquake shock calms down there are no large vibrations.

Table 4 Maximum Response Displacement and Moment (Harp Shape)

	Displacement of Deck (cm)	Moment at the Bottom of Tower (tfm)	Moment at the Bottom of Main Pier (tfm)
Floating Type	11.8	27030	170500
Fixed Type	6.8	31370	272300
Damper Type	9.4	18210	160800

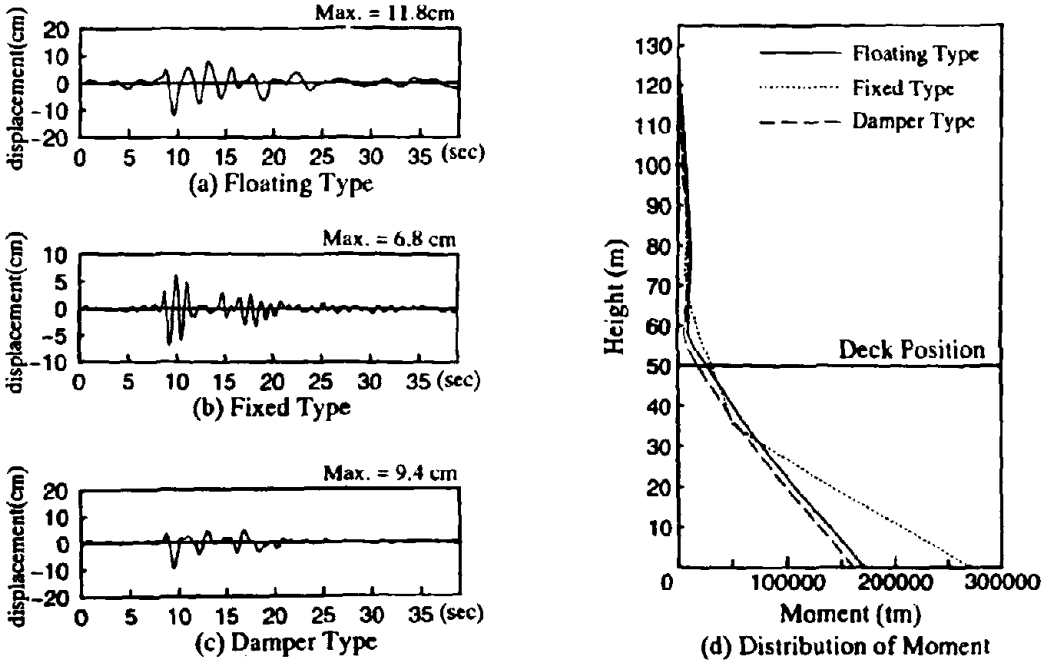

Fig. 6 Response Displacement of Deck and Moment in Tower and Pier (Harp Shape Arrangement)

The bending moment distributions in the tower and the pier is shown in Fig.6(d). The moment distributions in the tower are almost the same for the three types. However, the moment in the pier for the damper type is much smaller than that for the fixed type and slightly less than that for the floating type.

Effects of the Different Stay Cable Arrangements

Concerning the damper type, deck displacements with the semi-harp shape and the harp shape are almost the same. However for the floating type, the deck displacement with the semi-harp shape is much larger than that with the harp shape, so from the point of view of the reduction due to the hysteresis dampers, the semi-harp shape is more effective.

Regarding the bending moment in the towers, with the harp shape, the inertial force of the deck transmitted to the tower through the cables is distributed through the whole of the tower, so the effects of hysteresis dampers are small even if one is installed at the

bottom of the tower. However, with the semi-harp shape the inertial force of the deck acts high up in the tower, so dampers can reduce the bending moments along the whole of the tower and pier by acting on a part of inertial force at the bottom of the tower.

That is to say the effects of installing hysteresis dampers are larger with the semi-harp shape than with the harp shape.

DAMPING EFFECTS OF HYSTERESIS DAMPERS WITH DIFFERENT SPAN LENGTHS

Analysis Model

In this section the effects of hysteresis dampers are examined for different bridge spans. Three different of center span lenghts, 400m, 250m and 150m, are used in the analyses. Time history response analyses are carried out, changing the primary stiffness of the hysteresis dampers parametrically. The bending stiffness of the tower and the shear stiffness of the damper have a large influence on the effect of hysteresis dampers, so deciding upon the tower stiffness of the analytical models is important. Therefore for the 250m and 150m analysis models, using structural data from actual PC cable stayed bridges, the width of the deck is changed to 19m which is the same as the deck width for the 400m analysis model. The bending stiffness of the towers are changed in the same proportions. Each model has the semi-harp shape stay cable arrangement. The gaps between the stay cables of the 250m and 150m models are the same as in the 400m model, the number of cables alone being reduced. The 250m and 150m analysis models are shown in Fig.7 and the 1st and 2nd modes are shown in Fig.8.

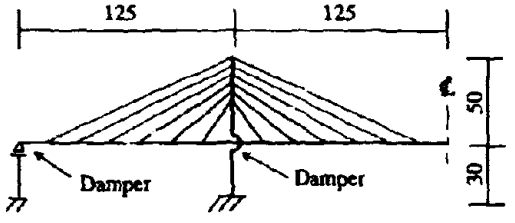

	$E(tf/m^2)$	$A(m^2)$	$I(m^4)$	$W(tf/m^3)$
Deck	3.1×10^6	13.3	14.0	2.9
Tower	3.1×10^6	18.0	34.8	2.5
Main Pier	3.1×10^6	121.5	609.0	2.5
End Pier	3.1×10^6	60.8	304.5	2.5
Cable	1.95×10^7	0.0316	–	10.0

(a) 250m Model

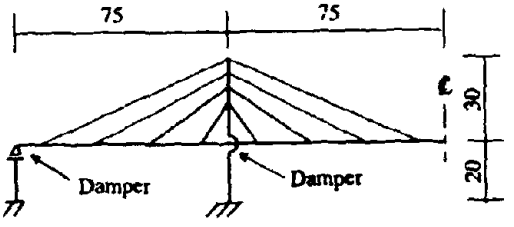

	$E(tf/m^2)$	$A(m^2)$	$I(m^4)$	$W(tf/m^3)$
Deck	3.1×10^6	13.3	14.0	2.9
Tower	3.1×10^6	15.0	16.0	2.5
Main Pier	3.1×10^6	110.0	230.0	2.5
End Pier	3.1×10^6	55.0	115.0	2.5
Cable	1.95×10^7	0.0316	–	10.0

(b) 150m Model

Fig. 7 Analysis Models for 250m and 150m Cable Stayed Bridges (unit:m)

1^{st} mode ($T_1 = 4.33\,sec.$) 2^{nd} mode ($T_2 = 1.70\,sec.$)

(a) 250m Analysis Model

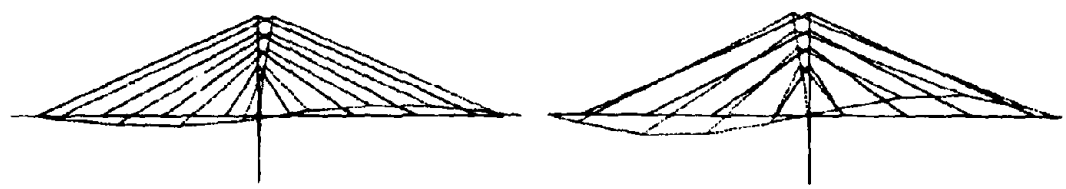

1^{st} mode ($T_1 = 1.99\,sec.$) 2^{nd} mode ($T_2 = 0.85\,sec.$)

(b) 150m Analysis Model

Fig. 8 1^{st} and 2^{nd} Natural Modes of the Floating Types (250m and 150m)

Effects of Center Span Length

The bending moment distributions in the tower and the pier, with changing primary stiffness of dampers, are shown in Fig.9. As the damper stiffness increases, the moment at the bottom of the tower becomes smaller, while that of the main pier becomes larger. It may be seen that there is an optimum damper stiffness which reduce the bending moment along the whole tower and pier, when compared with the floating type.

Fig.10 shows the relationship between the primary stiffness of the dampers, K_1, and the reduction ratio for the maximum response in the damper type compared with that in the floating type. Regarding the reduction in the response of the 400m cable stayed bridge, both the deck displacement and the bending moment in the tower and the pier are much lower up to K_1=100tf/cm . However the displacement of the deck and the moment in the tower do not become much lower even as the stiffness of the dampers increases, while the moment in the main pier sharply rises. The same tendency can be seen for the 250m and 150m models, but the damper stiffness which minimizes the moment of the main pier is rather larger than that for the 400m model.

For this reason, the following is considered. The height of the tower in the 150m model is lower than that in 250m and 400m models, so the bending stiffness of the tower in the 150m model is relatively large compared with that in the 250m and 400m models. Thus in the 150m bridge, the tower bears a proportionally greater part of the inertial force of the deck, and even if the stiffness of the dampers increase, the effects of the dampers are not easily seen.

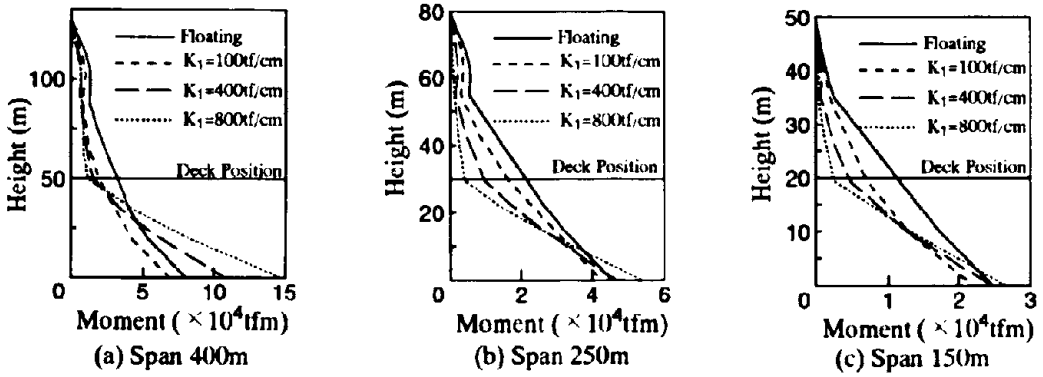

Fig. 9 K_1 of Damper v.s. Bending Moment of Tower and Pier

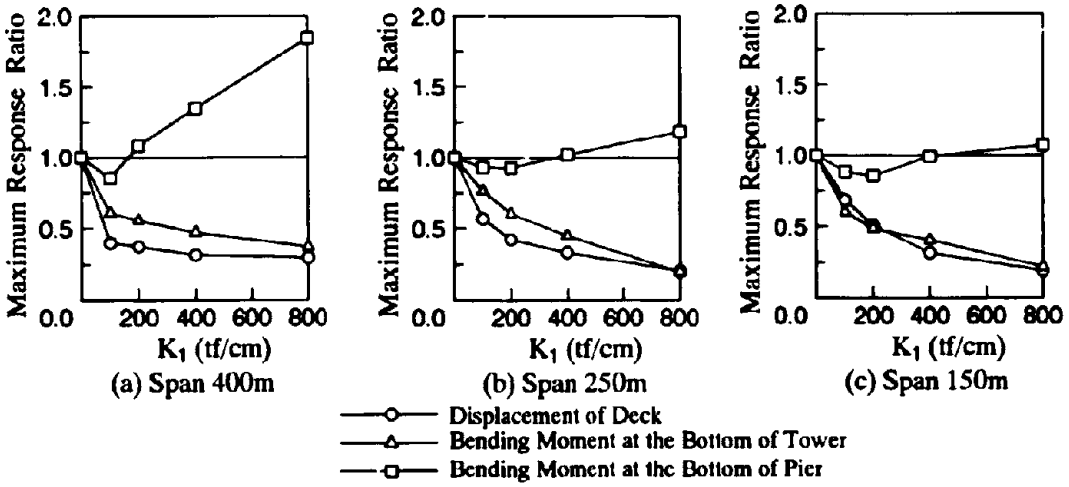

Fig. 10 K_1 of Damper v.s. Maximum Response Ratio

The stiffness of the dampers and the bending stiffness of the tower has a large influence on the effects of the dampers. The following non-dimensional parameter can be defined.

$$\frac{K_{eq}}{(EI/h^3)_{Tower}} \tag{1}$$

K_{eq} is the equivalent stiffness of the dampers when the deck displacement is maximum, and $(EI/h^3)_{Tower}$ expresses the bending stiffness of the tower as a cantilever beam. The reduction in the responses with regard to the above non-dimensional parameter are shown in Fig.11.

The characteristics of the deck displacement and the moment at the tower bottom are almost identical in spite of the different span lengths. With the ratio of the equivalent stiffness of the dampers and the stiffness of the tower as a cantilever beam, the reduction in the displacement of the deck and the moment in the towers may be evaluated.

For the moment at the bottom of the pier, the length of the main pier is involved as a parameter, so the tendency seems to be different from the others.

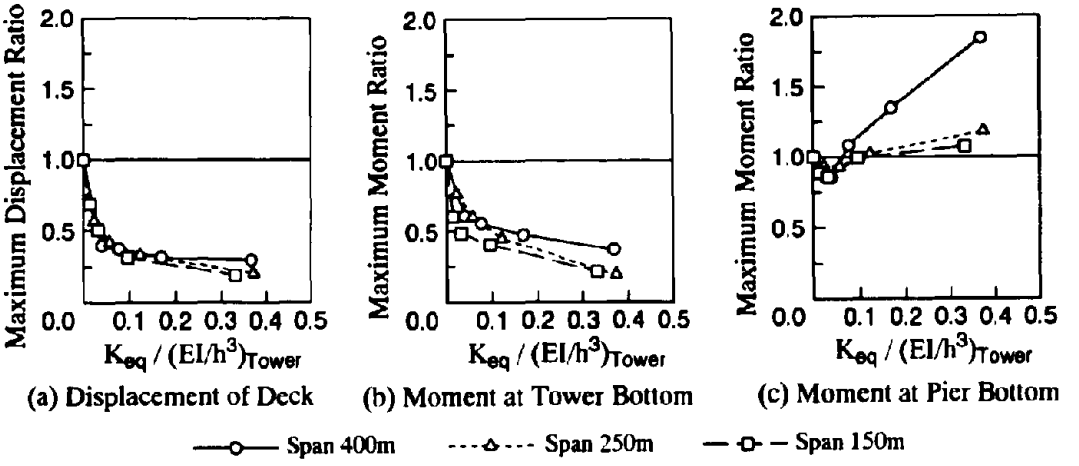

Fig. 11 $K_{eq}/(EI/h^3)_{Tower}$ **v.s. Maximum Response Ratio**

ELASTO-PLASTIC RESPONSE ANALYSIS

Analysis Model and Input Acceleration Wave

The effects of the hysteresis dampers when the structural members are plasticized during large earthquakes are examined. The analytical model is a lumped mass frame model of a semi-harp shape PC cable stayed bridge with 400m span (as shown in Fig.12). The length of the beam elements in the tower and the pier are short compared with those used in the elastic response analysis. The hysteresis characteristics of the beam elements in the tower and the main pier are expressed as a trilinear model with the cracking moment, yielding moment, and ultimate moment as shown in Table 5, while those of the deck are elastic. The moment-curvature characteristics of the restoring force used in the analysis is shown in Fig.13. The characteristics of the damper on the main pier is K_1=200tf/cm, K_2=20tf/cm and U_y=1cm. And the damper on the end pier has the half of the stiffness of that on the main pier.

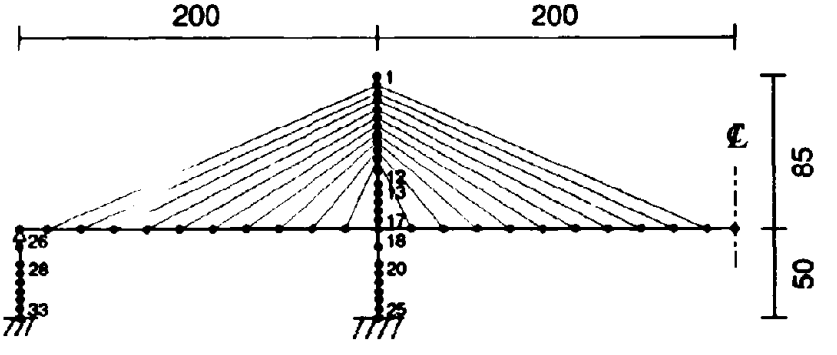

Fig. 12 Elasto-Plastic Analysis Model (unit:m)

Table 5 Moment-Curvature Relationship

element No.*	M_c (tfm)	M_y (tfm)	M_u (tfm)	ϕ_c $(1/m)$	ϕ_y $(1/m)$	ϕ_u $(1/m)$
$1 \sim 12$	16750	27080	39690	7.400×10^{-5}	3.710×10^{-4}	2.510×10^{-2}
$13 \sim 17$	27750	44430	69470	5.100×10^{-5}	2.560×10^{-4}	1.170×10^{-2}
18, 19	46170	142800	155200	1.400×10^{-5}	2.660×10^{-4}	2.480×10^{-2}
$20 \sim 25$	116500	348400	410000	2.400×10^{-5}	2.720×10^{-4}	2.425×10^{-2}
26, 27	23090	71400	77600	0.700×10^{-5}	1.330×10^{-4}	1.240×10^{-2}
$28 \sim 33$	58250	174200	205000	1.200×10^{-5}	1.360×10^{-4}	1.213×10^{-2}

* Element No. are referred to Fig.12

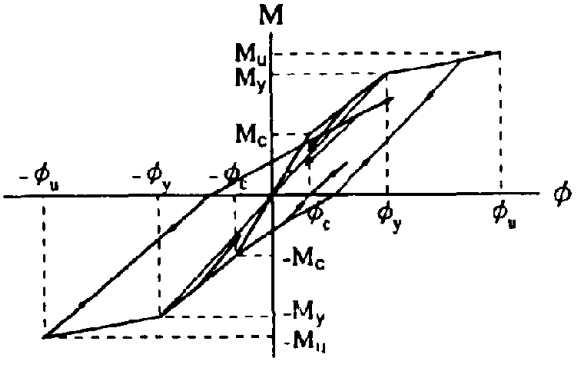

Fig. 13 $M - \phi$ Relationship
(Muto Model)

The acceleration response spectrum of the input acceleration wave is the same as in that of the *Specifications for Highway Bridges, Part V Seismic Design* with regard to checking the ductility of reinforced concrete piers. And because of the same reasons described in the sections on elastic analyses, the acceleration response spectrum where the natural period is longer than $5sec.$ is reduced linearly on the logrithmic plane. The input acceleration wave and its acceleration response spectrum are shown in Fig.14 .

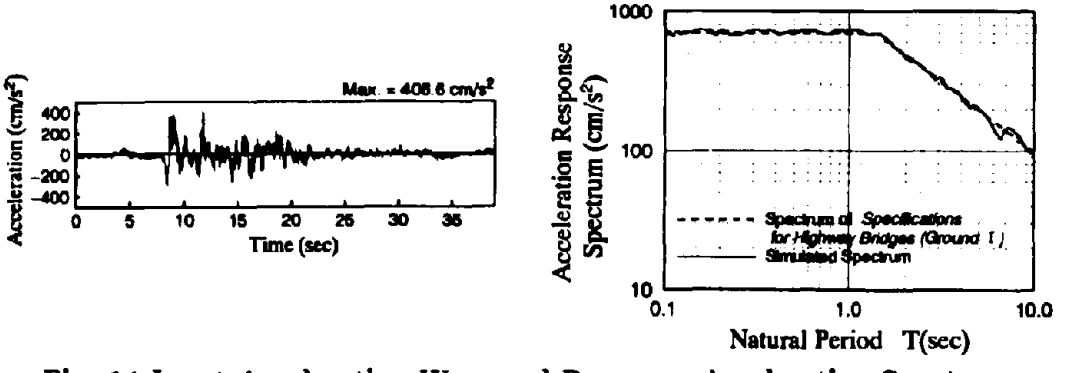

Fig. 14 Input Acceleration Wave and Response Acceleration Spectrum
(Elasto-Plastic Response Analysis)

Results of the Elasto-Plastic Response Analysis

The maximum response of the longitudinal displacement of the deck and the maximum bending moment in the tower and the pier obtained by elasto-plastic analyses are shown in Table 6. The maximum displacement of the deck for the floating type is 136cm and that for the damper type is 69.8cm, which is approximately 50% of the floating type. The bending moment at the bottom of the tower for the damper type is the smallest among the three support systems. The bending moment at the bottom of the pier for the damper type is about 60% of that for the fixed type.

Fig. 15 shows the time history displacement responses of the deck for the three types. For the floating type, as being similar to the results of the elastic response analysis, the large amplitude vibrations of the deck continue after the main earthquake shock. For the damper type, the deck vibration decreases rapidly and there are no large vibrations after the main earthquake shock.

Table 6 Maximum Response Displacement and Moment
(Elasto-Plastic Response Analysis)

	Displacement of Deck (cm)	Moment at the Bottom of Tower (tfm)	Moment at the Bottom of Main Pier (tfm)
Floating Type	136	54600	203000
Fixed Type	45.5	48700	409000
Damper Type	69.8	46400	247000

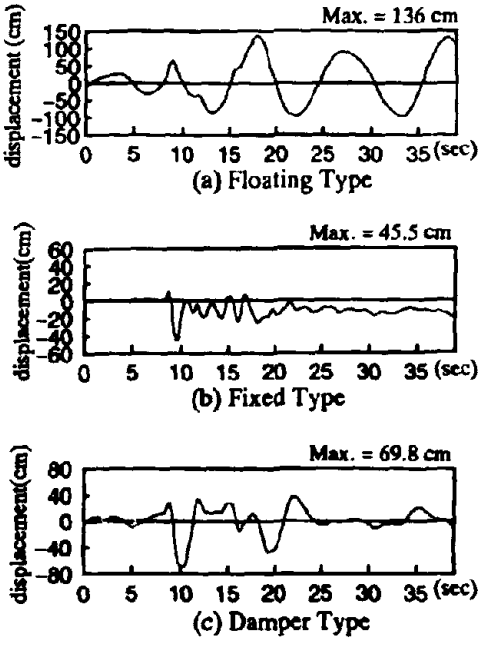

Fig. 15 Response Displacement of Deck (Elasto-Plastic Response Analysis)

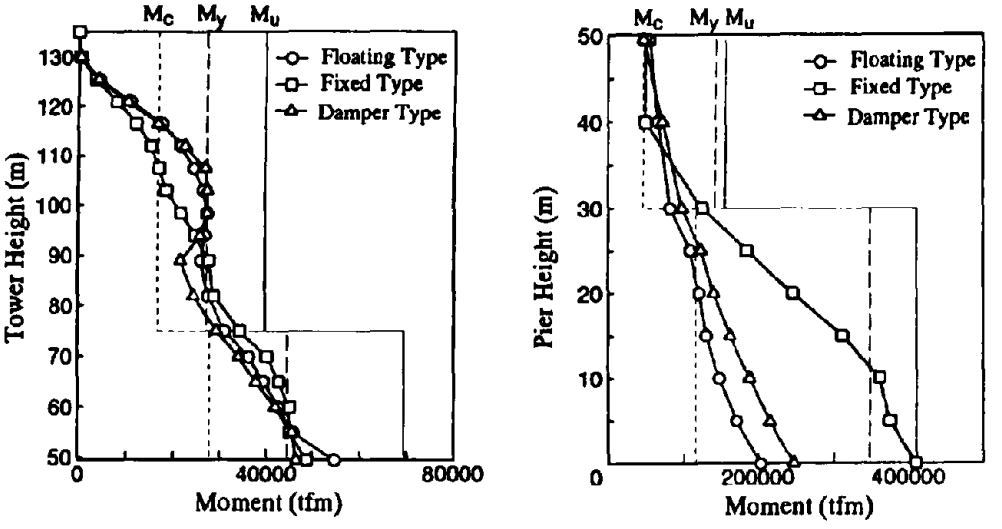

(a) Bending Moment in Tower (b) Bending Moment in Pier

Fig. 16 Bending Moment Distribution in Tower and Pier (Elasto-Plastic Response Analysis)

The bending moment distributions in the tower and the pier are shown in Fig.16. Below the cable anchorages in the tower the bending moment for the damper type is the smallest and all types reach the yielding moment at the bottom of the tower(Fig.16(a)). The ductility factors at the bottom of the tower are 19.2 for the floating type, 8.6 for the fixed type, 4.5 for the damper type. Concerning the bending moment at the bottom of the pier, the fixed type reaches the yielding moment but the floating type and the damper type do not reach the yielding moment. The maximum bending moment in the pier for the damper type is 60% of that for the fixed type.

Therefore, hysteresis dampers are also effective when the structural menbers are plasticized during large earthquakes.

DISCUSSION ON APPLICATION OF HYSTERESIS DAMPERS TO ACTUAL BRIDGES

From the point of view of reducing the response of the floating type PC cable stayed bridges using hysteresis dampers, it seems reasonable to say that the semi-harp shape cable arrangement is more effective than the harp shape. For the dead load and usual live load, the semi-harp shape is superior to the harp shape because the cables are lengthened vertically. Therefore, for long span PC cable stayed bridges, hysteresis dampers can improve the earthquake resistance with a semi-harp shape arrangement more effectively than with harp shape arrangement.

In recent years, construction of base isolated girder bridges is increasing rapidly. The

base isolation system consists of two devices; an isolator which supports the weight of the superstructure softly in the horizontal direction but rigidly in vertical direction, and a damper which absorbs the energy and restrains excessive displacements. Cable stayed bridges can support the deck with the stay cables, so isolators to support the weight of the deck are not necessary. Therefore, in order to increase the earthquake resistance in cable stayed bridges, dampers alone are considered sufficient and it is not necessary to have an aseismic base isolation system, such as those used in girder bridges.

In order to decide upon the most appropriate damper stiffness and yielding displacement during the design stage, one method is chosen. By considering the influence of the usual temperature and earthquake load on the expansion joint structures at the end of the deck and on the cross-sectional reinforcement in the towers and the main piers, this will minimize the whole cost of the bridge. With the installation of dampers, the displacement of the deck and the moment in the towers and piers will be reduced, and the optimum system may be chosen by evaluating the relationship between costs and effects.

Concerning the application of hysteresis dampers to actual PC cable stayed bridges, residual displacements may be left in the dampers after earthquakes. In general, the deck of PC cable stayed bridges is a box girder cross-section, so the dampers can be easily installed and removed by using the inside of the box girder structure. It is also easy to treat displacements due to drying shrinkage and creep in the same way.

CONCLUSIONS

For long span PC cable stayed bridges, the increase in earthquake resistance with the use of hysteresis dampers is examined. The results are as follows.

- From the elastic response analyses of a $400m$ PC cable stayed bridge, the semi-harp shape arrangement is better than the harp shape, for the increase in the earthquake resistance due to hysteresis dampers.
- According to the analyses of $400m$, $250m$ and $150m$ cable stayed bridges, earthquake resistance when dampers are installed is shown to be improved regardless of the span length. In addition, there is an optimum damper stiffness which reduces the moment in the whole tower and pier compared with the floating type.
- The reduction in the responses can be evaluated using the ratio of the equivalent stiffness of the dampers and the bending stiffness of the towers expressed with non-dimensional parameters, even if the span lengths are different.
- Hysteresis dampers are also effective in $400m$ PC cable stayed bridge, when the structural members are plasticized during large earthquakes.

ACKNOWLEDGEMENT

The authers would like to thank Mr. Shinichi Yamanobe of KAJIMA Technical Research Institute, Mr. Yoshihide Okimi of KAJIMA Imformation Processing Center and Mr. Katsuhisa Kanda of Kobori Research Complex for their contribution to this research.

REFERENCES

1. Ichinomiya, T., Takeda, T., and Kanda, K., "Improvement of Earthquake Resistance of Prestressed Concrete Cable-Stayed Bridges by Hysteresis Dampers", *Proceedings of the 2nd U.S.-Japan Workshop on Earthquake Protective Systems For Bridges*, Public Works Research Institute, Japan, Dec., 1992.
2. Ministry of Construction, *Manual for Menshin Design of Highway Bridges*, in Japanese, Japan, 1992.

EXPERIMENTAL AND FIELD OBSERVATIONS

Vibration Test of a Menshin Designed Multi-Span Continuous Prestressed Concrete Bridge

Field Testing of Bridges Before and After Retrofitting with Seismic Isolation Bearings

Design of a Long Prestressed Concrete Continuous Girder Bridge Using Base Isolators

Field Testing of the Seismically Isolated Walnut Creek Viaduct

Response of On-Netoh Bridge During Kushiro-Oki Earthquake of January 1993

CALTRANS/FHWA Program for Performance Testing of Seismic Isolation and Energy Dissipation Systems

Seismic Response Characteristics of the Hokumei-Bridge Using Rubber Bearings

Guidelines for Pre-Qualification, Prototype, and Quality Control Testing of Seismic Isolation Systems

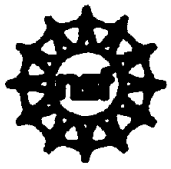

NIST

VIBRATION TEST OF A MENSHIN DESIGNED MULTI-SPAN CONTINUOUS PRESTRESSED CONCRETE BRIDGE

Takashi Kakinuma[*1], Kazuhiko Kawakami[*2]
Kazuomi Kumakura[*3], Hideo Tani[*4]
Noboru Abe[*5]

1. Director, Road Construction Division, Department of Public Works
Tochigi Prefectural Government, Utsunomiya-shi, Tochigi, Japan

2. Section Chief, Ditto

3. Senior Officer, Ditto

4. Technical Staff, Ditto

5. Deputy Manager, CTI Engineering Co., LTD., Chuo-ku, Tokyo, Japan

SUMMARY

Yamaage Bridge is the longest prestressed concrete bridge in Japan, where the Menshin Design was adapted. The bridge has a 6-span continuous girder with total length of 246.3m and deck width from 10.5m (standard section) to 13.5m (wide section). It was originally designed by the conventional Seismic Lateral Force Coefficient Method and the earthquake resistance was enhanced by the Menshin Design. In order to investigate the dynamic characteristics of the Menshin-designed bridge, Yamaage Bridge was tested through free vibration test method. This paper presents an analysis of vibration test conducted at Yamaage Bridge.

INTRODUCTION

Yamaage Bridge is located on National Highway No.294 in Tochigi Prefecture. It was designed in accordance with the regulations of the Design Specifications for Highway Bridges[1]. The Menshin Design was referred to Guidelines for Base Isolation of Highway Bridges (Draft)[2] and Manual for Menshin Design of Highway Bridges (Draft)[3]. The vibration test was conducted in September 1992. And completion of the bridge was in May 1993.

YAMAAGE BRIDGE AND ITS MENSHIN DESIGN

Outline of Bridge Yamaage Bridge is located on National highway No.294 in Tochigi Prefecture. The type of superstructure is a 6-span continuous prestressed concrete two-cell box-girder. The abutment is an inverted T-type, while the pier is rectangular wall shaped. The view of the bridge is shown in Photo 1.

Geotechnical Feature The soil profile of the site consists of sand-gravel layers and slate formation. According to standard penetration test results, the N-values of the sand-gravel layers are 30 to 50, and that of the slate formation is above 50.

Menshin Design

(1) Design Policy

The design and the characteristics of the bridge structure were reported in the previous paper[6], therefore outline of the Menshin Design is summarized in this paper. Design policy to adapt the Menshin Design to Yamaage Bridge, are as follows.

(a) The Menshin Design is applied only in the longitudinal direction of the bridge. Transverse direction of the bridge is restrained by stopper.

(b) The design displacement of superstructure is assumed as the sum of drying shrinkage, creep, elastic deformation, and the temperature deformation.

(c) The seismic lateral force coefficient applied to check of bearing capacity for lateral force was computed by using the whole structural model analysis including spring stiffness of the foundation and the bearings.

(2) Bearing

The High Damping laminated Rubber (HDR) is employed for the bridge. It was designed considering the Bearing Capacity Method. The dimension and characteristic of bearing are shown in Table 1, and Figure 1.

(3) Stopper for transverse direction

In order to restrain displacement of the girder in the transverse direction of the bridge, stoppers were installed to each abutment and pier. The girder and the stopper are free to slide in the longitudinal direction of the bridge.

(4) Menshin Design

Figure 2 shows the theoretical model used for the design. The bridge is modeled as elastic beams and the bearing's and foundation's are also modeled as linear spring elements. The Menshin Design for Ymaage Bridge was made in accordance with the Guidelines for Base Isolation of Highway Bridges[2] and Manual for Menshin Design of Highway Bridges[3]. The bridge was designed by both the Seismic Lateral Force Coefficient Method and the Bearing Capacity Method. In the seismic lateral force design, the seismic lateral force is applied to the bridge and the safety of the bridge is checked based on the Allowable Stress Design Method. In the Bearing Capacity Method, ductility of the pier is considered.

When the Menshin Design is employed, the seismic lateral force can be reduced by damping effects of Menshin bearings. However, it was not decreased because the construction of the bridge is one of pilot projects to investigate effectiveness of Menshin Design.

For the Dynamic Analysis, the damping ratio of the first vibration mode of bridge was 14.3%. Natural period of the bridge in longitudinal direction was 1.56 second in the Seismic Lateral Force Coefficient Method and 1.77 second in the Bearing Capacity Method.
Table 2 shows the comparison of design forces for the substructures between Menshin Design and conventional design. The design forces by Menshin Design are successfully decreased.

OBJECTIVES AND METHODS OF VIBRATION TEST

After installation of the HDR bearings and completion of concrete girder, the bridge was tested in September, 1992. It took us 10 days to finish spot tests, and we had an open test one of the days. About 500 people came to the test site, and it was selected the place of study tour, the 2nd U.S-Japan Workshop in Japan.

Objectives of Test The main objective of the vibration test was to study the vibration characteristics of the Menshin-designed bridge on site. The follows were examined.

(1)Equivalent stiffness of HDR bearings.

(2)Effect of distribution of lateral force by HDR bearings.

(3)Natural period of the bridge.

(4)Damping ratio of the bridge.

Test Methods

(1)Static Loading Test using Jack (Test No.1)

In order to investigate the equivalent stiffness of HDR bearings and the effect of distribution of lateral force by HDR bearings. the girder was statically displaced in the longitudinal direction by the jacks. Relative displacement of HDR bearings. in other; relative displacement between superstructure and substructures. was assumed as 7 cm which corresponds to the design displacement in Seismic Lateral Force Coefficient Method (= 7.78 cm).

(2)Forced Excitation Test using Exciter (Test No.2)

The bridge was using by the exciter generating sine-waves within a range of 0.5 ~ 3.5 Hz. The exciter is EX-6300H-VF type for horizontal excitation with maximum force of 20 tf and owned by the Public Works Research Institute of Ministry of Construction. It was installed on the girder as shown in Figure 3. The purpose of this test was to investigate the resonant frequency and the vibration mode.

(3)Free Excitation Test using Exciter (Test No.3)

After the bridge is excited at the resonant frequency, the excitation was stopped. The free vibration was measured and the damping ratio of the bridge was computed from free vibration.

(4)Excitation Test using Hydraulic Jack (Test No.4)

Twelve sets of hydraulic jack were mounted at the crest of A_1 abutment and all piers two sets each. Six sets of jack are owned by the laboratory of the Japan HighWay Public Corporation and the rest are owned by Kawada Construction Co.,LTD, Tokyo, Japan. Those jacks have the loading capacity of 180 tf with rapid-release valves. The deck was displaced in the longitudinal direction by jacks. the pressures were rapidly released and resulting in free vibration. The state jacks and meters like a acceleration-meter set on the bridge. is shown in Figure 3. The purpose of this test was to investigate the natural period and the damping ratio under free vibration of the bridge. Photo 2 shows the setting of jacks.

TEST RESULTS

Equivalent Stiffness of HDR Bearing Because stiffness of bearing varies according to different dimension. the dimension of bearing was sussed out by a computer application, which is shown in Table 1.

In the test. the maximum displacement of bearing was assumed as 7 cm. Figure 4 shows the load-displacement relation obtained through the test at the bearings on P_1 pier. The characteristic of HDR bearing was represented by a hysteresis curve so clearly.

Table 3 shows the comparison of equivalent stiffness of bearings between designed and testing values. The design values were re-computed assuming the displacement value as 7 cm, and testing values were computed from the reaction forces of each jacks.

Due to the loading direction from A_1 to A_2, and the earth pressure behind the A_2 abutment, the theoretical model in Figure 5 was applied to computation of test results. The theoretical model replaces the bridge with elastic beams including the jacks. Further, at the analysis, spring of foundation ground was not applied the value against Level 1 seismic force. Because the superstructure was loaded statically, we considered that the ground condition was practically statical rather than the condition of Level 1.

Results of the test and analysis, we could obtained the good data about the equivalent stiffness of bearings on actual bridge.

Effect of Distribution of Lateral Force by HDR Bearings In the design of the Yamaage Bridge, the distribution of seismic lateral force was assumed as shown in Table 4. And Figure 6 shows the variation of distribution ratio, that were caused by changing the bearing's displacement from 10 to 70 mm. The displacement was larger, the distribution ratio was almost the same as the design value. We considered the reason of this result was an influence of the fill behind the A_2 abutment and initial stiffness of bearings. Therefore, we confirmed that the lateral force was distributed as design values.

Natural Period of Bridge The natural period of the Yamaage Bridge was obtained by the excitation test by hydraulic jack. Tests were carried out assuming smaller initial displacement. (The relative displacement between superstructure and substructure by Test No.4 were 30 and 50 mm.) Therefore, the displacement value of design (7.77 cm, at Level 1 seismic force) was changed 30 and 50 mm, and we computed the natural period of the bridge again. The wave forms obtained by the Test No.4 are shown in Figure 7 and 8.

Table 5 shows the re-computation value of the natural period, in case the relative displacement, bearing stiffness, and state of geotechnical foundation were changed as parameters. We did not compute the equivalent stiffness, in case the displacement were 30 and 50 mm. Because the 1st response amplitude of bearings , when the jack were abruptly released on the tests, was within the limits of amplitude on the initial stiffness.

The natural period of 0.951 and 1.026 second were obtained for the relative displacements of 30 and 50 mm. The computed natural period of the 50 mm displacement is similar to re-computation

data No.7, and of the 30 mm is in the middle of data No.10 and No.11.

We considered that the springs of bearing were within the range of initial stiffness, because of the effect of damping of bearings, and further, in case of the 30 mm displacement, spring of foundation ground was not work, because the displacement was so small.

Damping Ratio of the Bridge Table 6 shows the damping ratio of structural model used for the design. And, as the damping ratio of the bearing changes the value which depends on the variation of displacement, that was obtained by loading test. Result of design, the damping ratio of 1st vibration mode was 14.3 %.

Table 7 shows the damping ratio obtained through the tests. The resonance curve and 1st vibration mode curve that the most predominate to the vibration of the bridge are shown in Figures 9 to 10. In the excitation test using exciter, the damping ratio was obtained by the Half Power Method as shown in Figure 11.
And at the excitation test using hydraulic jack, the damping ratio was computed by formula as

$$h_i = 1/2\pi \times \log_e (x_i / x_{i+1})$$

$$x_i = 1/2 \times (1/2 \times (x_i + x_{i+1}))$$

where

h_i : damping ratio of i-th response amplitude when the jack was rapidly released

x_i : i-th response amplitude

The damping ratio obtained by the excitation test using hydraulic jacks was almost the same as that assumed in the design. However, the damping ratio obtained by the excitation test using exciter was the nearly value to that of the superstructure and substructure. This is , because of the displacement by exciter was so small, the effect of bearing's damping was not appeared.

CONCLUSION

Although this series of vibration test left a fear of an insufficient simulation of strong earthquakes because of smaller scale of vibration of small amplitude, it was enough to give the fundamental characteristics of a bridge of the Monshin Design.

The strong motion seismograph was installed on the bridge. When earthquakes occur and are

recorded, we would like to report the response analysis of the Yamaage Bridge using data of actual earthquakes in the future.

REFERENCES

1. Japan Road Association : Design Specifications for High Way Bridges, part V, February 1990 (in Japanese)

2. Technology Research Center for National Land Development : Guidelines for Base Isolation of High Way Bridges (Draft), March 1989 (in Japanese)

3. Public Works Research Institute : Manual for Menshin Design of Highway Bridges (Draft), October 1992, Technical Note of Public Works Research Institute, Vol.60 (in Japanese)

4. Ikeda, T. Ozeki, K. Kumakura, K. and Abe, N. : Design of the Karasuyama No.1 Bridge (Base Isolated Bridge), Bridge and Foundation Engineers, Vol.25, No.6, June 1991 (in Japanese)

5. Ikeda, T. Kumakura, K. Tani, H. and Abe, N. : Plan and Design of the Karasuyama No.1 Bridge, Bridge Engineering, Vol.26, No.6, June 1991 (in Japanese)

6. Uzuka, K. KAWAKAMI, K. KUMAKURA, K. TANI, H. : Menshin Design and Construction of Multi-Span Continuous Prestressed Concrete Bridge, Proceedings the 2nd U.S-Japan Workshop on Earthquake Protective Systems for Bridges, Technical Memorandum of PWRI, NO.3196, December 1992

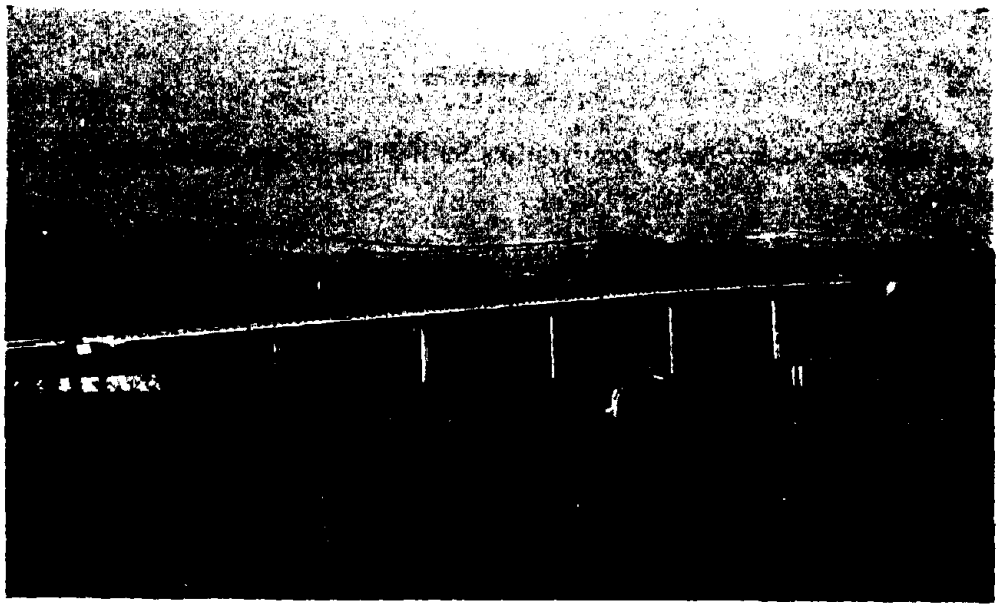

Photo 1 The Yamaage Bridge

Photo 2 The Hydraulic Jack

Table 1 Dimension of Bearings (Unit:mm)

Item	A_1	P_1	P_2	P_3	P_4	P_5	A_2
Plane Dimensions	700 ϕ855	950 ϕ1500	1030 ϕ1580	950 ϕ1500	950 ϕ1500	950 ϕ1500	700 ϕ855
Number of Rubber Layers	14	6	3	5	6	8	19
Thickness of Rubbers	205.8	126.0	102.0	120.0	144.0	149.6	262.2
Thickness of Insert Plates	54.6	21.0	8.4	16.8	21.0	29.4	75.6
Height of Bearings	260.4	147.0	110.4	136.8	165.0	179.0	337.8

Table 2 Comparison of Menshin Design with Conventional Design

(1)Bending Moment at Pier Bottom (Unit:tf·m)

	P_1	P_2	P_3	P_4	P_5
Menshin Design	4704.7	3677.2	2824.4	2345.0	2017.0
Conventional Design	4793.2	5062.8	4760.8	4601.5	4578.2

(2)Shear Force at Pier Bottom (Unit: tf)

	P_1	P_2	P_3	P_4	P_5
Menshin Design	336.6	287.2	241.8	220.1	221.0
Conventional Design	359.3	388.4	392.4	414.8	479.0

Table 3 Comparison of Equivalent Stiffness

(Unit: tf/m)

Substructure	Tested (a)	Designed (b)	(a)/(b)
A_1	873	865	1.009
P_1	2.578	2.603	0.990
P_2	3.227	3.262	0.989
P_3	2.719	2.657	1.023
P_4	2.372	2.460	0.964
P_5	2.206	2.420	0.912

Table 4 Design Lateral Force for Substructures

Substructure	Lateral Force H (tf)	Distribution Ratio (%)
A_1	84.1	9.0
P_1	194.5	20.8
P_2	175.1	18.7
P_3	161.7	17.3
P_4	154.6	16.6
P_5	164.1	17.6
Total	934.1	100.0

Note) Lateral Force is computed by

$$H_i = R_{di} * k_h$$

Where

H_i : Seismic Lateral Force for i-th Substructure (tf)

R_{di} : Dead Load for i-th Substructure

k_h : Design Seismic Coefficient.

Table 5 Re-computation of the Natural Period

Parameters			Natural Period	Data NO.
Displacement	Stiffness of Bearings	Stiffness of Pier and Soil Foundation		
U = 7.784 cm (Design Value)	Equivalent Stiffness (k_e)	Total Structure	1.556 sec	1
		Fixed Condition of Foundation	1.393	2
		Ridded Condition of Pier and Soil Foundation	1.303	3
	Initial Stiffness (k_i)	Total Structure	1.095	4
		Fixed Condition of Foundation	0.930	5
		Ridded Condition of Pier and Soil Foundation	0.783	6
U = 5.0 cm	Initial Stiffness (k_i)	Total Structure	1.052	7
		Fixed Condition of Foundation	0.882	8
		Ridded Condition of Pier and Soil Foundation	0.724	9
U = 3.0 cm	Initial Stiffness (k_i)	Total Structure	1.015	10
		Fixed Condition of Foundation	0.841	11
		Ridded Condition of Pier and Soil Foundation	0.677	12

Table 6 Design Damping Ratio of Structural Members

Structural Member	Damping ratio (%)
Superstructure	3.0
Substructure	5.0
Soil foundation	10.0
HDR Bearings	16.8

Table 7 Damping Ratio obtained trough the Vibration

Testing Cases	Damping Ratio (%)
Excitation Test by Jack (Displacement:50mm)	15.4
Excitation Test by Jack (Displacement:30mm)	12.0
Excitation Test by Exciter	5.7

Design Value	14.3

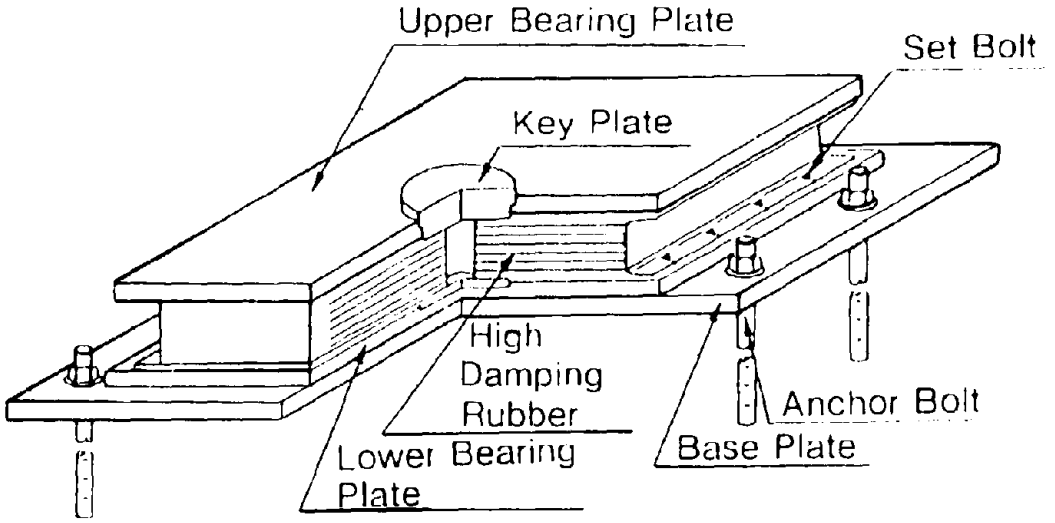

Figure 1 Structure of HDR Bearing

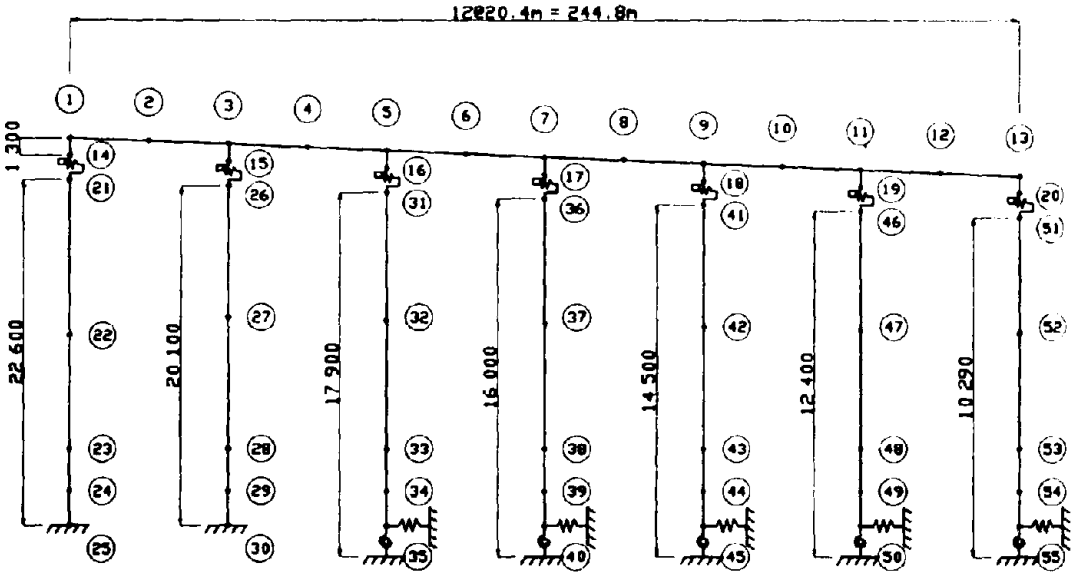

Figure 2 Theoretical Model Applied the Design

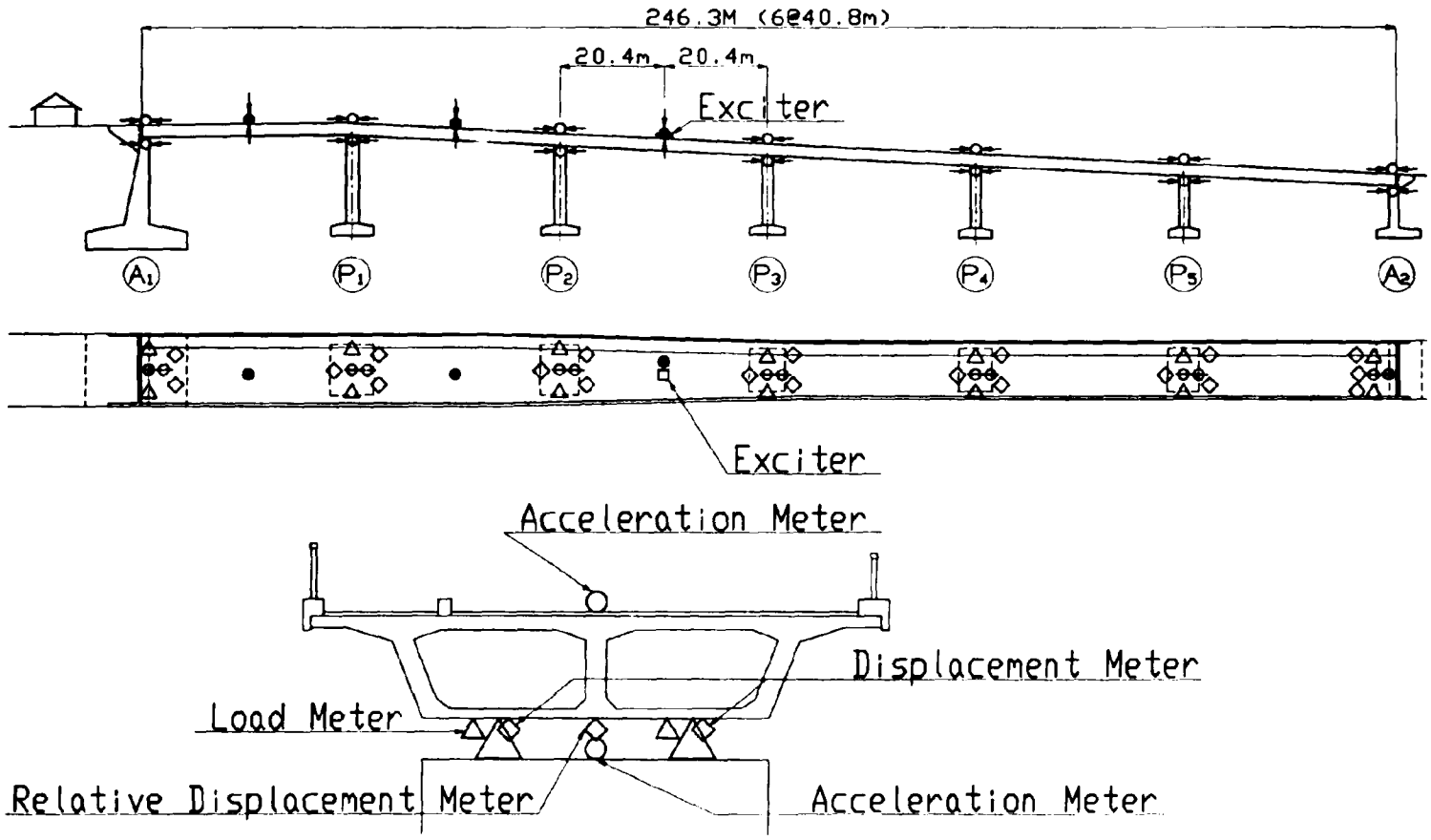

Figure 3 The State Installed the Exciter, Jacks and other Meters

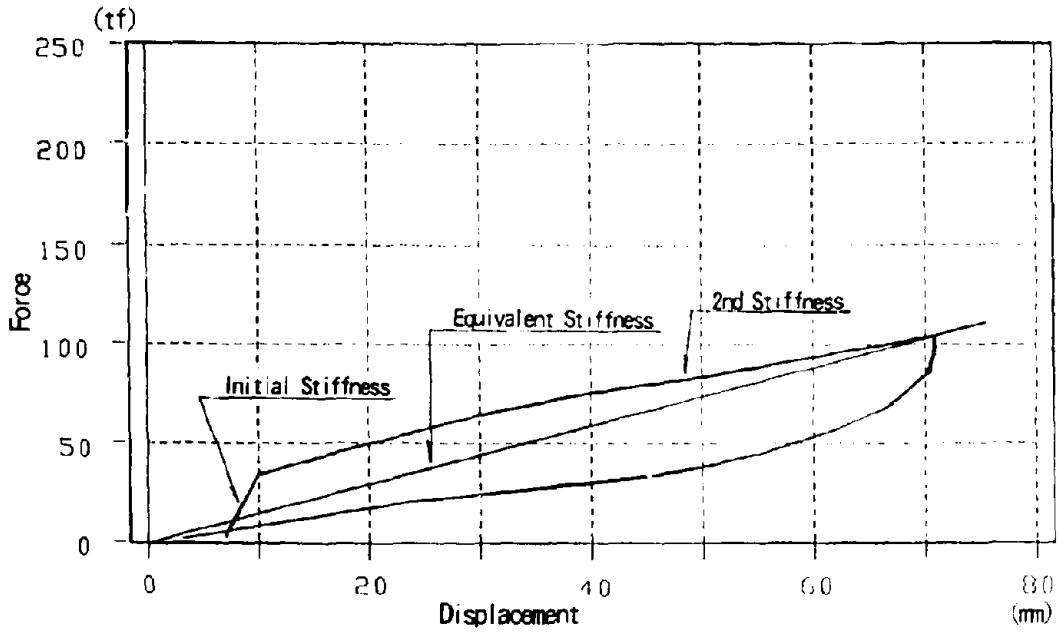

Figure 4 Hysteresis Loop

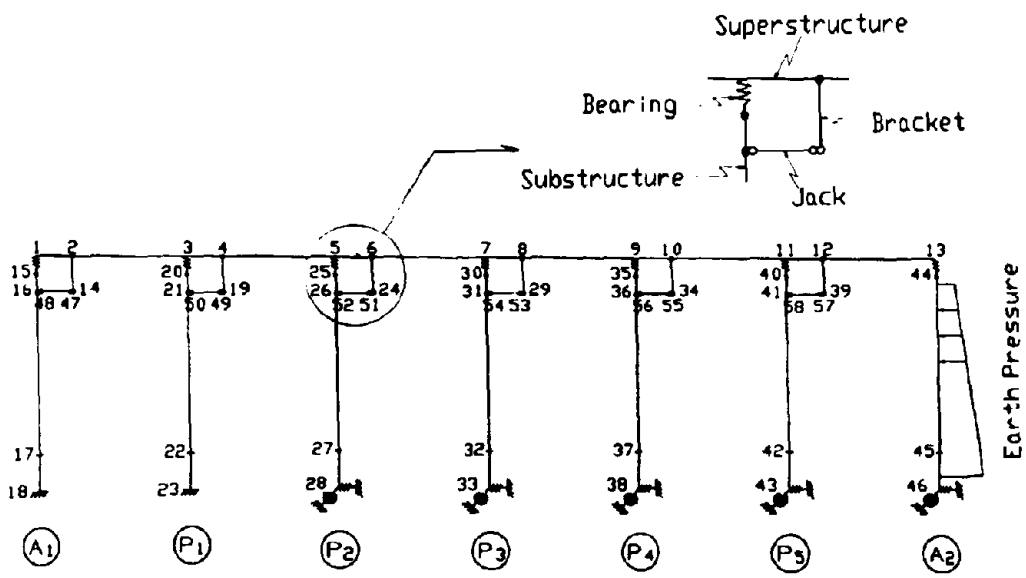

Figure 5 Theoretical Model to Obtain the Equivalent Stiffness

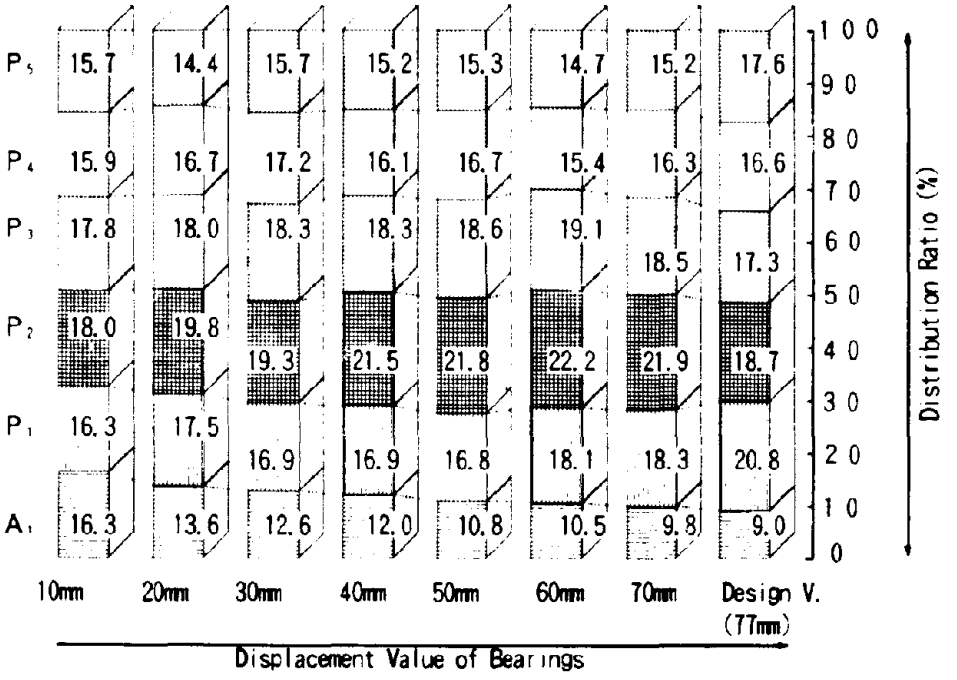

Figure 6 Effect of Distribution of Lateral Force

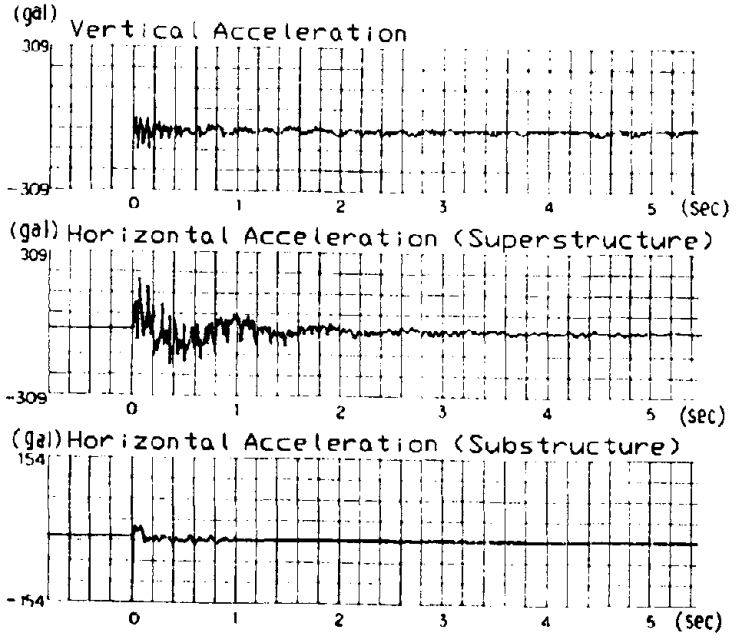

Figure 7 Vibration Wave Forms

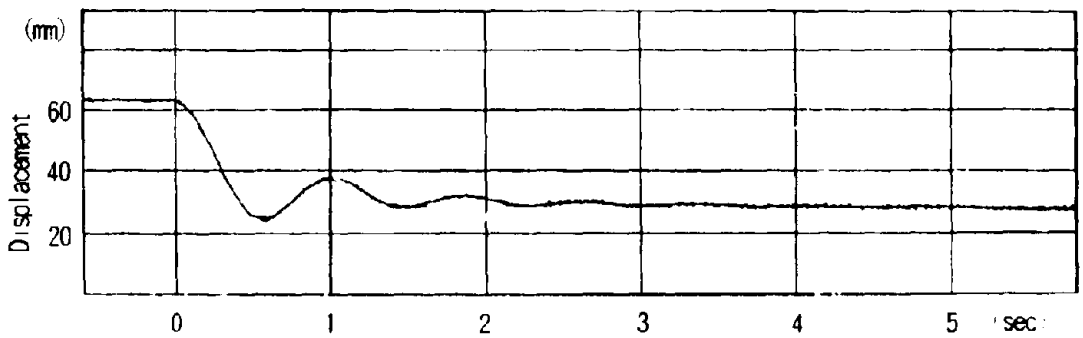

Figure 8 Relative Displacement of Bearing

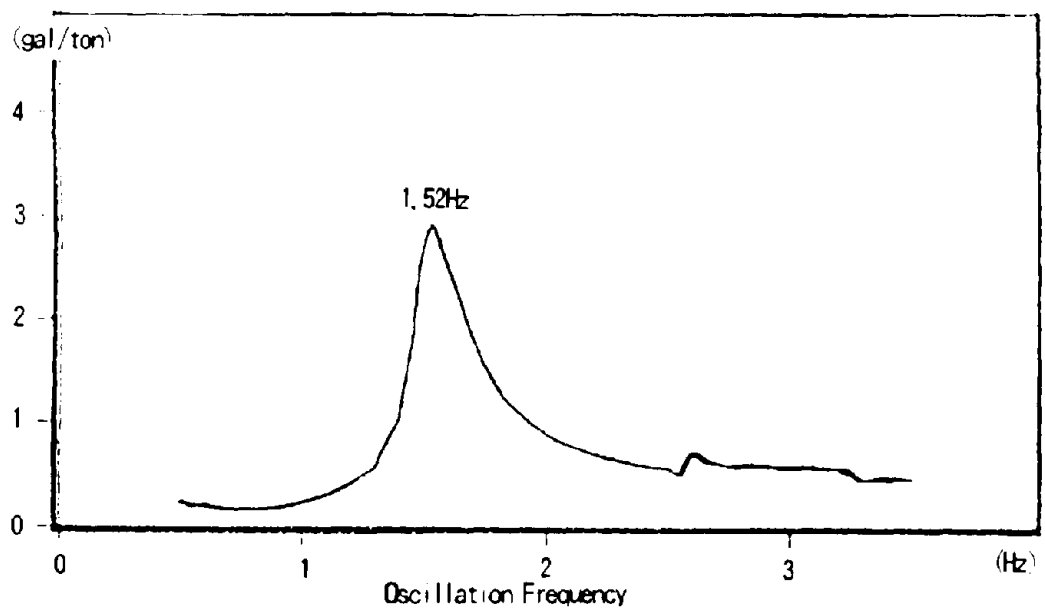

Figure 9 Resonance Curve

Oscillation Frequency : 1.52 Hz

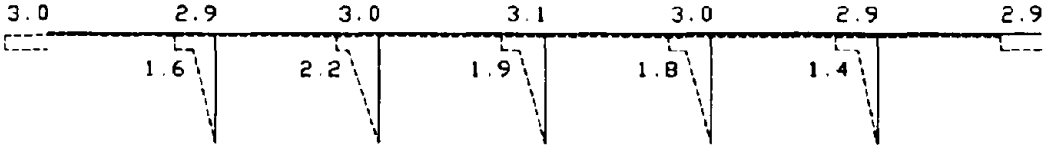

Figure 10 1st Vibration Mode

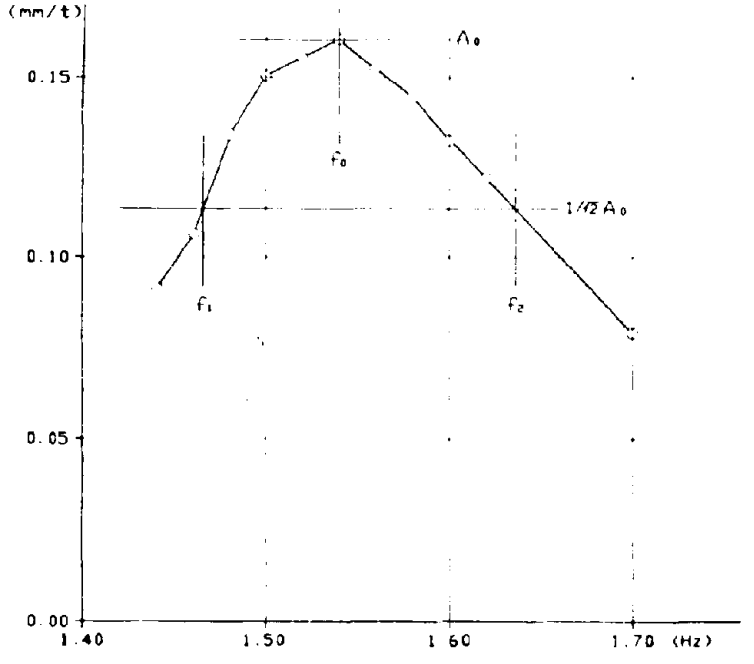

A_0 = 0.161 ●●/t
f_0 = 1.520 Hz
f_1 = 1.445 Hz
f_2 = 1.619 Hz
h = 5.7×10^{-2}

Figure 11 Half Power Method

FIELD TESTING OF BRIDGES BEFORE AND AFTER RETROFITTING WITH SEISMIC ISOLATION BEARINGS

by
S.S. Chen and J.B. Mander
Department of Civil Engineering,
State University of New York at Buffalo, USA

ABSTRACT

This paper reports on full-scale large-amplitude field experimental studies being conducted in conjunction with bearing component tests, results to date and their comparison with theoretical modeling predictions, for a pair of 3-span continuous slab-on-girder bridges whose existing steel bearings are being retrofitted with laminated elastomeric bearings and lead-rubber bearings. The results of this study will assist a bridge engineer to make more informed decisions among the fundamental options for analytical modeling and for seismic retrofitting of such bridges.

INTRODUCTION

The fundamental options confronting a bridge engineer charged with determining a suitable bridge seismic retrofit strategy are the following (excluding foundation rehabilitation):

a) do nothing
b) bearing retrofit
   i) using standard elastomeric bearings, or
   ii) seismic isolation bearings, and
c) substructure (column) strengthening.

In the central and eastern United States, it is becoming commonplace to retrofit slab-on-girder bridge structures with some form of laminated elastomeric bearings. With the availability of the AASHTO Guide Specifications on Seismic Isolation Design [1], lead-cores are now on some occasions being added to these bearings to provide additional seismic protection. The relative paucity of information available on the in-situ efficacy of such bridge bearing retrofits motivates the use of full-scale large-amplitude field vibration tests. Other such tests are described in [2] and [3]. This paper describes the ongoing, large-scale field verification studies of two 3-span continuous slab-on-girder bridges near Buffalo, New York being retrofitted with standard laminated elastomeric bearings and lead-core elastomeric bearings. Companion studies of old bearings being retrieved from the bridges and of new bearings being installed in the same bridges are also briefly described herein.

The current field testing is believed to be the first quick release field test on a seismically isolated bridge in the United States and thus will provide much-needed insight into the in-situ behavior of such bearings and the bridges they are being used to retrofit.

BRIDGE DESCRIPTION

Figure 1 shows a side elevation view of the bridges carrying Rte. 400 over the Cazenovia Creek some 50 km southeast of Buffalo, NY. The abutments and two-column reinforced concrete pier bents are supported by a concrete pile cap and battered steel H-piles extending 50 ft to 70

ft into the soil. Both bridges were constructed in 1967 supported on high-type steel fixed and rocker bearings over the piers and low-type steel-bronze sliding expansion bearings over the abutments.

Seismic retrofits using rubber bearings were prescribed by the New York State Dept. of Transportation to be installed following rehabilitation work on the reinforced concrete decks. The northbound bridge was retrofitted during October - December 1993 with circular laminated elastomeric bearings, while the southbound bridge is currently (January 1994) being retrofitted with square laminated elastomeric lead-core seismic isolation bearings on each abutment and with standard square laminated elastomeric bearings on each pier. The old steel bearings are shown in Fig. 2, while descriptions of the new bearings are provided in Table 1.

PROJECT OVERVIEW AND STATUS

The principal project objectives are the following:

1. Measurement and assessment of in-situ dynamic behavior and performance of a typical slab-on-girder bridge subjected to transverse quick-release loading and supported on the 3 different types of bearings, and
2. Quantification of the in-situ dynamic performance change attributable to:
   a. bearing retrofit using standard laminated elastomeric bearings, and
   b. bearing retrofit using seismic isolation bearings.

A snap-back (quick-release) technique has been employed in the field on both pre-retrofit bridges and is being employed on both post-retrofit bridges, complemented by ambient vibration tests. Ambient and post- snap recordings resulting from the free vibration response are examined to infer in situ frequencies, mode shapes, damping ratios, and higher mode effects Static (pre-snap) data also provides insight into in-situ pier and diaphragm flexibility, which are of use in calibrating analytical models.

The field quick-release experimentation is complemented by laboratory tests performed on actual bearings from the bridges (both old steel bearings salvaged from the pre-retrofit bridges and new bearings used in the aseismic retrofits) along with finite element analysis, informed by these bearing test results, at several levels of modeling detail. These global and component-based experimental studies combined with the analytical studies will enable an assessment of suitable analytical modeling approaches as well as quantification of the in-situ dynamic performance change attributable to the aseismic bearing retrofits of the two subject bridges.

Figure 3 shows the various aspects of the project and their interrelationships and status. Quick-release tests have been conducted on both bridges supported on their original steel bearings. The planned winter-weather tests are expected to provide valuable data on the in-situ cold-temperature performance of the seismic isolation and standard laminated elastomeric bearings as reflected in the quick-release experiments.

FIELD EXPERIMENTAL PLAN AND SETUP

Due to the distance between the bridges (60 ft clear), it was decided to construct a tension-based loading scheme using high-strength 1-1/4" dia. DYWIDAG™ prestressing threadbars. The technique uses a tension loading scheme different from the one utilized by the authors in previous

quick-release tests of other bridges [4] in that it pulls from the adjacent bridge. Figure 4 shows the quick-release loading scheme employed for testing the southbound bridge. The tension bars straddle the near column of the anchor pier and pass through holes cored into both curbs of the tested bridge, being anchored on the far side of the tested bridge.

Figure 5 depicts one of the instrumentation layouts employed in the quick-release tests conducted of the southbound bridge. The top part of the figure shows the accelerometer layout, while the bottom shows the corresponding displacement transducer layout.

The instruments used consisted of 33 ENDEVCO type 2262-25 accelerometers with a response of $\pm 25g$ @ 0 - 100 Hz and 20 linear motion potentiometers. All the accelerometers were connected to a model 2310 Micro Measurements signal conditioner. Based on analytical behavior predictions and ambient vibration tests, the signal was filtered by the conditioners with a low pass band of 25 Hz. Two 486 computers with ADAC 12- and 16-bit A/D boards handling up to 32 channels each, were used for the data acquisition. A 140 Hz dynamic sampling rate was used to record 20 sec post-snap data sets. The loading bars themselves were instrumented with strain gauges to determine the applied load before and after release.

ANALYTICAL MODELING

Analytical models at several distinct levels of detail are being investigated in tandem with the experimental portions of this study. Model 1, a 3-D model implemented using the SAP90 software, is shown in Fig. 6. This model, based on the original construction drawings, incorporates each member of the structure and accounts for their finite depth, the 9° bridge skew, and the structure's superelevation. Pier columns are modeled using three equal-length frame elements, each using the average geometric properties of its segment. The pier cap beam is modeled by employing frame elements along its varying neutral axis, with rigid links connecting it to the top of the bearing support pedestal. The bearings are modeled as frame elements whose stiffnesses are based on an experimental study [5][6] which measured the elastic stiffness of steel bearings similar to those of the subject bridge but which were retrieved from a different bridge. When these frame elements are used to model the new bearings, they are based on properties of:

a) the actual bearings used in the northbound bridge, based on tests performed at SUNY at Buffalo on these bearings prior to their shipment to the field, and
b) bearings identical to those used in the southbound bridge, which are to be tested in early 1994 (see Fig. 3).

The superstructure in Model 1 uses frame elements to represent the curbs, girder flanges, the diaphragms and the stiffeners to which they are connected. Shell elements are used for the concrete deck and girder webs. For dynamic purposes the masses were lumped at the nodes. In order to attain a close match with static pre-snap displacements recorded in the field, adjustments were needed in bearing stiffnesses, diaphragm stiffnesses via rigid offsets, and soil/foundation stiffness, the latter being initially accomodated by artificially lengthening pier columns with $EI_{cracked}$ set at 60% of EI_{gross}.

Model 2, a considerably simplified model for transverse analysis implemented using the DRAIN-2D software [7], is shown in Fig. 7. Aggregate deck and girder properties are transformed into frame elements connected by diaphragm springs as shown in the figure. To enable comparisons, the diaphragm stiffness was adjusted so that the first transverse frequency

could match the first transverse frequency obtained from Model 1.

PARTIAL RESULTS TO DATE

The Fourier analysis technique was applied in this study to determine the natural frequencies of the structure and the associated mode shapes [8][9]. To reduce leakage effects three different windows were evaluated (Hanning, Hamming, and Kaiser) [10][11]. The time histories were smoothed using a Hanning window, which produced the best results.

For the purpose of determining the natural frequencies and mode shapes, the Fourier amplitude spectra and the phase spectra were computed for each digital record. Natural frequencies were estimated from the Fourier spectra, whose magnitude was used to construct a normalized vector dividing the values of each accelerometer station for a given frequency by the largest value. The phase spectra were used to identify the arithmetic sign of the modes. For this work the construction of the vertical modes was done using the normalized modes obtained using the quick-release test data augmented by modal information obtained from ambient vibration tests, which oriented deck-level accelerometers in the vertical direction.

The modes, obtained using discrete points, were fitted using a Kriging procedure. Experimental mode shapes are compared in Fig. 8 with the results obtained from Model 1 for the southbound bridge on the original steel bearings. The damping of the structure was obtained using the half-power method [12]. For a given frequency, the damping was extracted from the Fourier spectra for each station and averaged to obtain the values shown in Fig. 8.

For a single-pier fuse snap, the recorded loading bar time-history is shown in Fig. 9. Using this loading as input, reasonable agreement is obtained between the transverse deck-level accelerations in the field and those of Model 1 (shown in Fig. 10) and Model 2 (shown in Fig. 11).

LABORATORY EXPERIMENTS ON OLD AND NEW BEARINGS

As mentioned earlier, analytical modeling efforts incorporate or will incorporate bearing stiffnesses obtained from tests on actual or identical bearings, both old and new, employed in the subject bridges. For the new bearings, example hysteresis data obtained from a northbound bridge bearing prior to its installation in the bridge is shown in Fig. 12a. Until data is obtained from the lead-core bearings, the idealization shown in Fig. 12b is being used.

PREDICTIONS OF RETROFITTED BRIDGE BEHAVIOR

Model 2 is employed with bearing stiffness data from Fig. 12 to predict the retrofitted behavior of both bridges, using the idealized release scenario shown in Fig. 13. Comparisons between anticipated quick-release behavior of the two bridges are shown in Fig. 14 for the the one-pier snap and Fig. 15 for the two-pier snap. Both displacement and acceleration response are anticipated to be significantly reduced by the presence of the lead-core bearings, which are used on the southbound bridge abutments. Fig. 16 shows the lead-core bearing hysteretic response corresponding to the one-pier and two-pier snaps, respectively.

DISCUSSION AND SUMMARY

A comprehensive project investigating the use of quick-release field experiments to determine the in-situ efficacy of seismic retrofits using different types of rubber bearings is described in this paper. It is anticipated that the results will provide valuable insight into appropriate modeling approaches as well as in-situ bearing performance for existing steel bearings, laminated elastomeric bearings and lead-core bearings in slab-on-girder bridges. Improvements are currently being made to the modeling of soil-structure interaction and the construction of a more controllable quick-release mechanism.

ACKNOWLEDGMENTS

Funding support for this study is being provided by the National Center for Earthquake Engineering Research through the Federal Highway Administration project on Seismic Vulnerability of Existing Highway Construction (Contract DTFH61-92-C-00106). The New York State Dept. of Transportation has provided for site access and field coordination with the reconstruction work along with steel bearing salvage, the latter in conjunction with Union Concrete and Construction Corp. Dynamic Isolation Systems provided elastomeric and lead-core bearings for the laboratory studies. The work of graduate research assistants D. A. Wendichansky, P. G. Dreyer, and D.-K. Kim with preparation of various portions of this paper is gratefully acknowledged, as is the help of Prof. B. M. Douglas, who provided the loading jacks used in the study to date.

REFERENCES

[1] _____, Guide Specifications for Seismic Isolation Design, American Association of State Highway and Transportation Officials, June 1991.

[2] Lam, V., "The System Identification of a Nonlinearly Responding Base-Isolated Bridge", Ph.D. Dissertation, Dept. of Civil Engineering, University of Auckland, NZ, Feb. 1990.

[3] Kawashima, K., Nagashima, H., Masumoto, S., and Hara, K., "Response Analysis of Miyagawa Bridge Based on a Measured Acceleration Record", in Proceedings of the Second U.S.-Japan Workshop on Earthquake Protective Systems for Bridges, Technical Memorandum of PWRI No. 3196, Public Works Research Institute of Japan, December 7-8, 1992, pp. 467-476.

[4] Chen, S. S., Mander, J. B., MacEwan, D. S., and Mahmoodzadegan, B., "Quick-Release Behavior of Two Eastern US Highway Bridges", Proceedings of the 10th International Bridge Conference, Pittsburgh, PA, Paper No. 93-34, June 1993.

[5] Premus, G. J., "The Experimental Behavior of Steel Bridge Bearings under Reversed Cyclic Loading", MS Thesis in Civil Engineering, SUNY at Buffalo, 1993.

[6] Mander, J. B., Kim, J. H., and Chen, S. S., "The Experimental Performance and Modeling Study of a 30 Year Old Bridge with Steel Bearings", Transportation Research Record No. 1393, August 1993, pp. 65-74.

[7] Powell, G. H., et al., "DRAIN-2DX Version 1.03 User's Guide," Report No. UCB/SEMM-92/29, Dept. of Civil Engineering, University of California at Berkeley, 1992.

[8] Trifunac, M. D., "Ambient Vibration Tests of a 39-Story Steel Frame Building", Technical Report No. EERL-70-02, Pasadena CA, July 1970.

[9] Douglas, B. M., "Quick Release Pullback Testing and Analytical Seismic Analysis of a Six-Span Composite Girder Bridge", Technical Report No. FHWA-RD-76-173, 1976.

[10] Harris, F. J., "On the Use of Windows for Harmonic Analysis with the Discrete Fourier Transform", Proceedings of the IEEE, Vol. 66, No. 1, Jan. 1978, pp. 51-83.

[11] Richardson, J. A., "Dynamic Response Analysis of the Dominion Road Bridge Test Data", Ph.D. Dissertation, Department of Civil Engineering, University of Nevada at Reno, 1988.

[12] Clough, R. W., and Penzien, J., Dynamics of Structures, 2nd ed., McGraw-Hill, 1993.

	BEARING TYPE		
	PRE-RETROFIT	POST-RETROFIT	
	S. BOUND & N. BOUND	S. BOUND	N. BOUND
N. ABUT.	LOW STL. EXP.	LEAD CORE ELAST.	STD. ELAST.
PIER #1	HIGH STL. FIXED	STD. ELAST.	STD. ELAST.
PIER #2	HIGH. STL. EXP.	STD. ELAST.	STD. ELAST.
S. ABUT.	LOW STL. EXP.	LEAD CORE ELAST.	STD. ELAST.

NOTE: * - UNIQUE TO NORTH BOUND BRIDGE

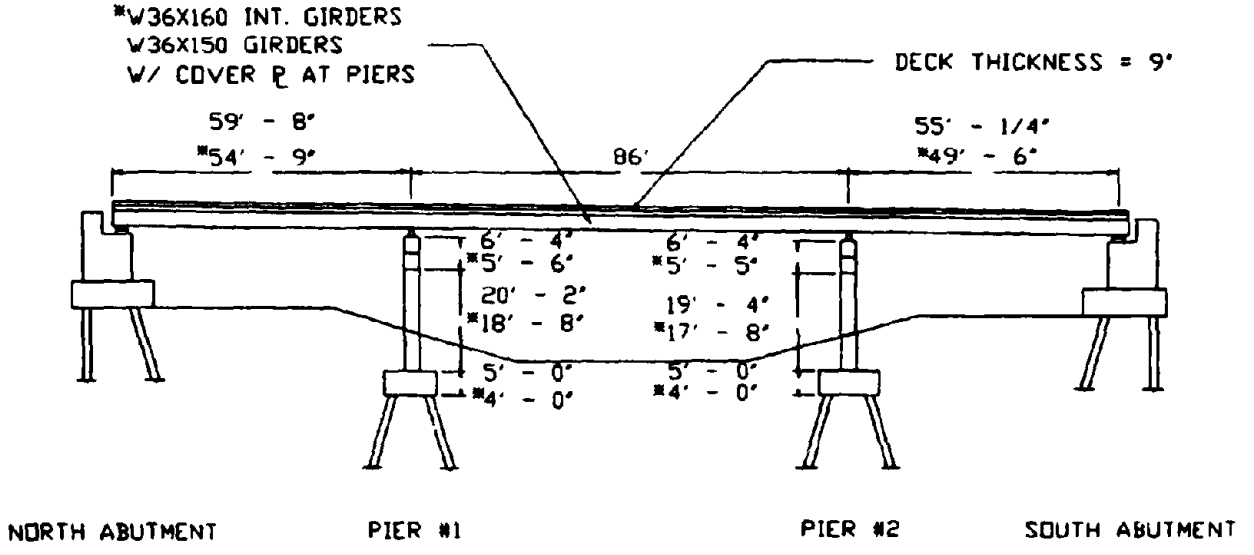

Fig. 1 Elevation View of Bridges and Bearing Schedule

LOCATION	SHAPE FACTOR	DIAMETER (inch)	TOTAL RUBBER THICKNESS (inch)	HEIGHT (inch)
N. ABUT.	8.00	12	1.1250	1.3750
PIER 1	10.70	16	1.1250	1.3750
PIER 2	9.14	16	2.1875	2.6875
S. ABUT.	7.00	14	1.0000	1.6250

Table 1a New Bearings (Northbound Bridge)

LOCATION	SHAPE FACTOR	AREA (in*in)	TOTAL RUBBER THICKNESS (inch)	HEIGHT (inch)	LEAD DIAMETER (inch)
ABUTMENTS (LEAD RUBBER)	6.67	11*11	3.75	6.875	2.5
PIERS (ELASTOMERIC)	8.00	13*13	5.25	8.875	-

Table 1b New Bearings (Southbound Bridge)

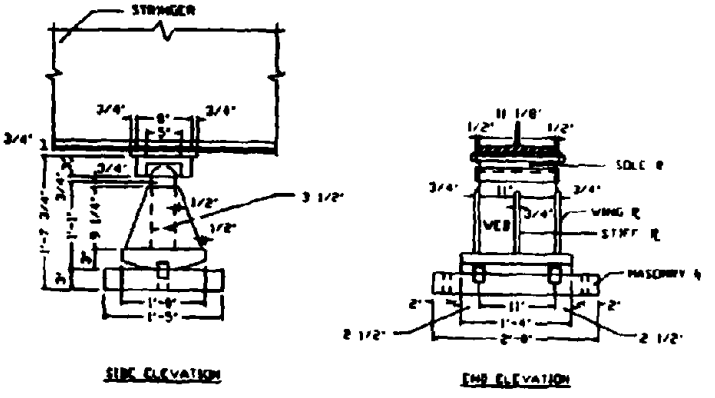

EXPANSION BEARINGS AT PIER

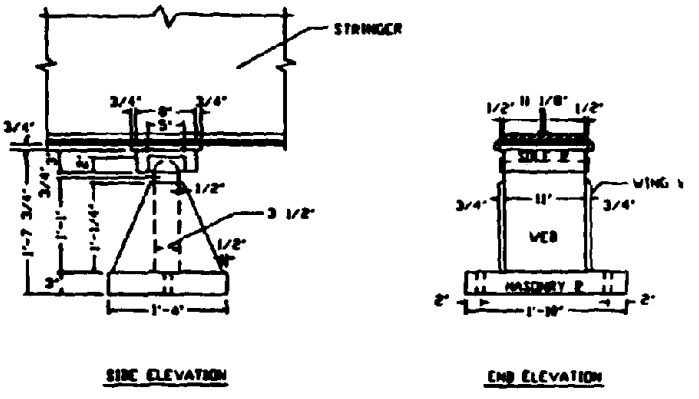

FIXED BEARINGS AT PIER

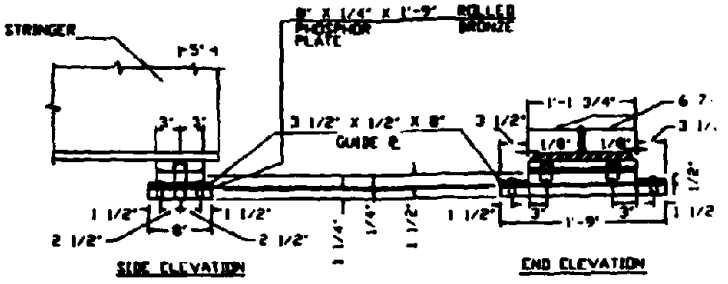

EXPANSION BEARINGS AT ABUTMENTS

Fig. 2 Old Steel Bearings

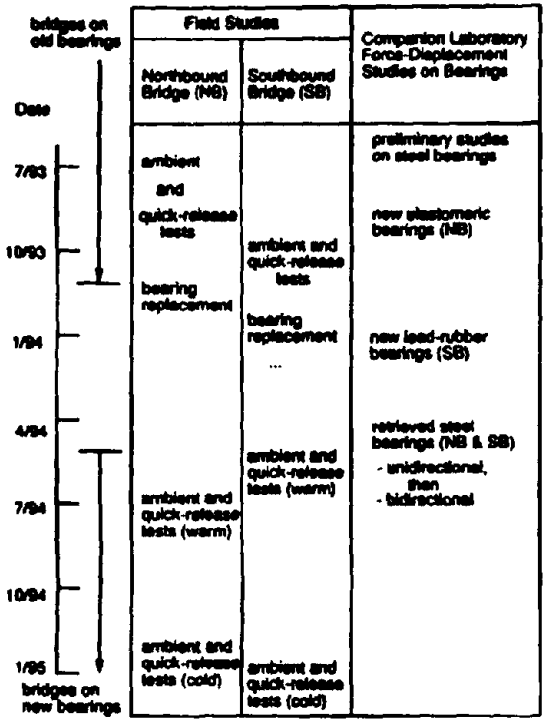

Fig. 3 Project Overview

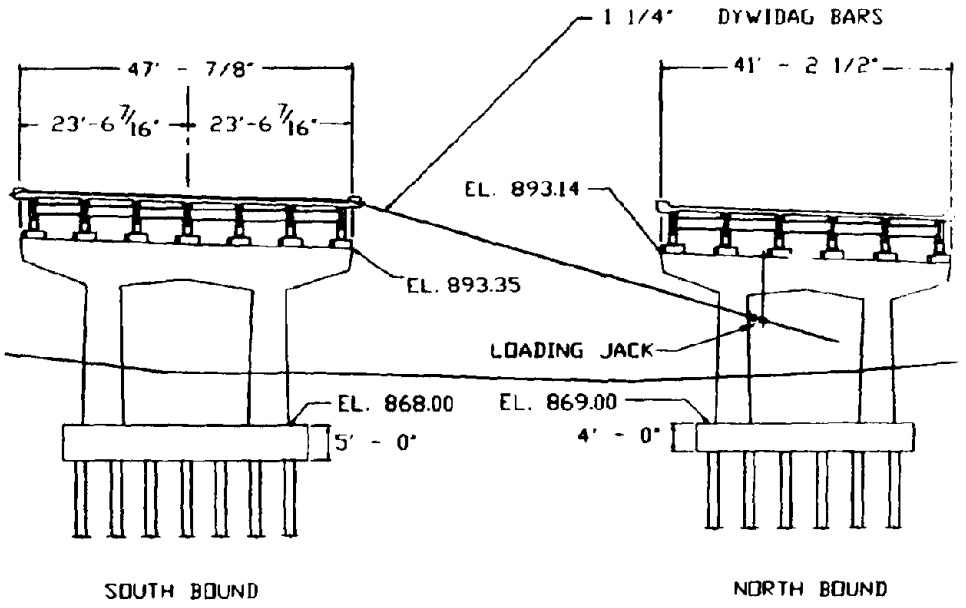

Fig. 4 Quick-Release Loading Scheme Employed for Southbound Bridge Test

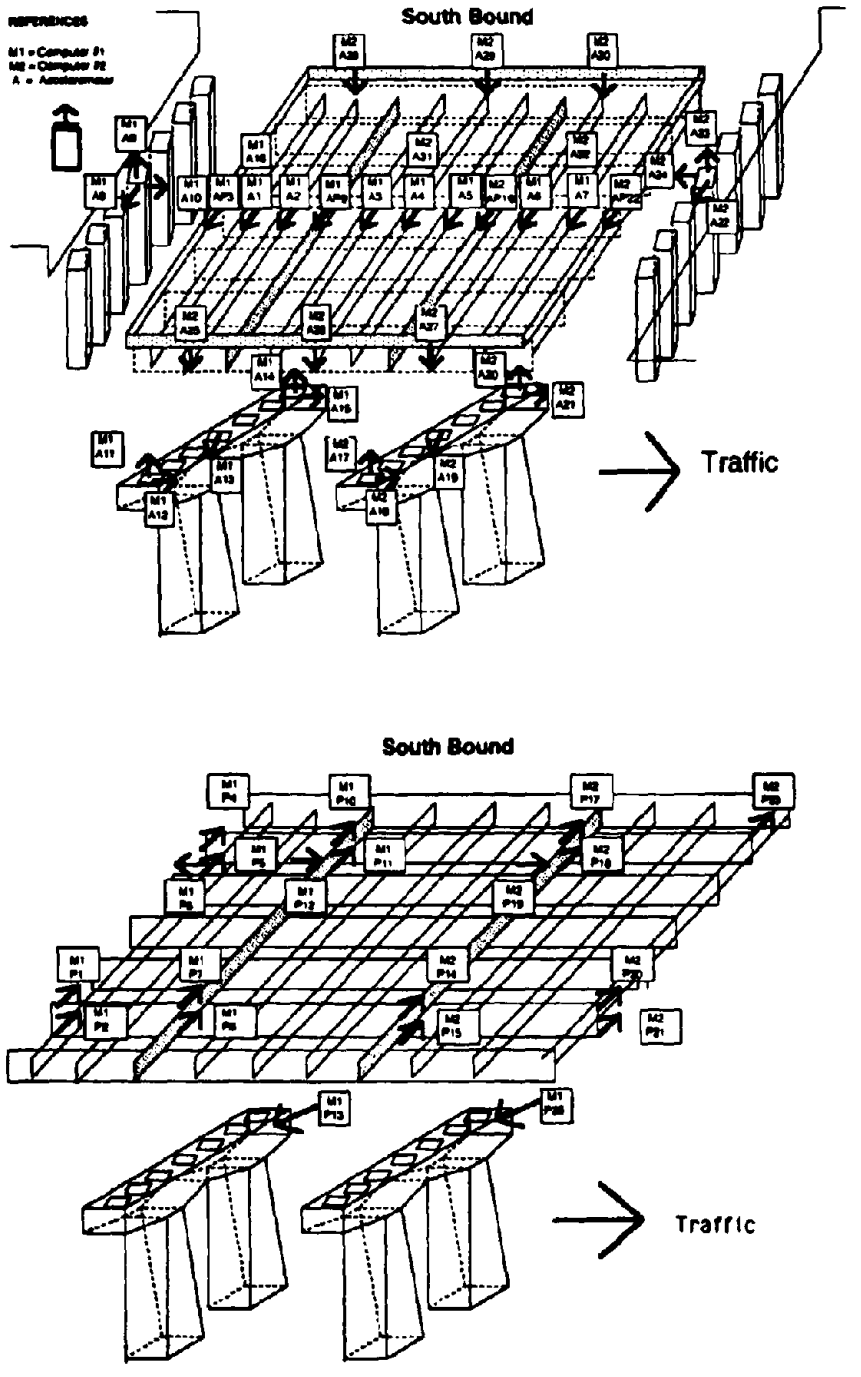

Fig. 5 Instrumentation Layout

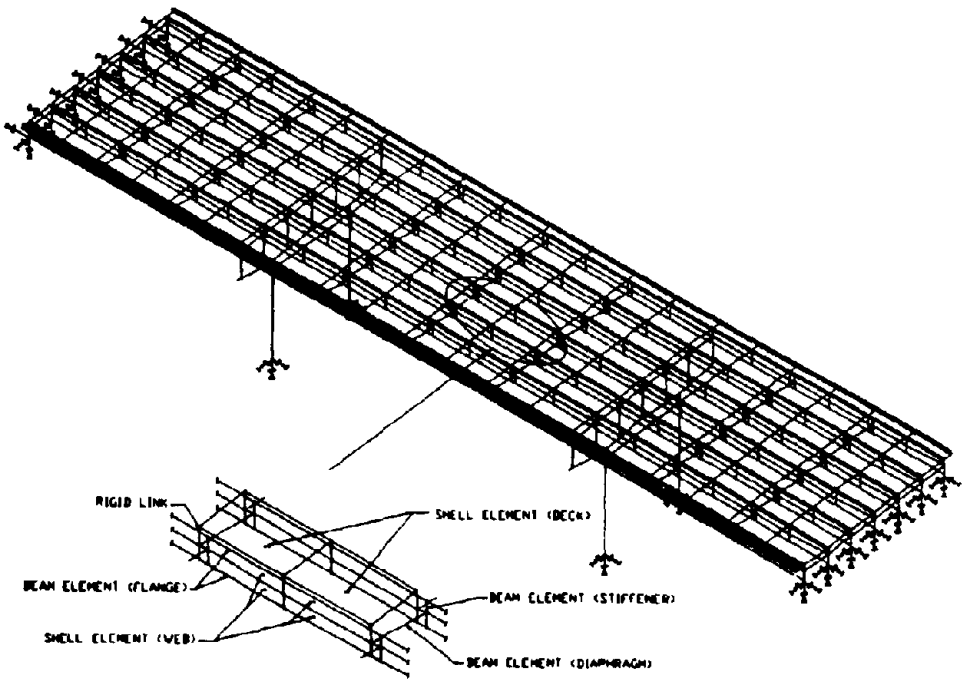

Fig. 6 Finite Element Model 1

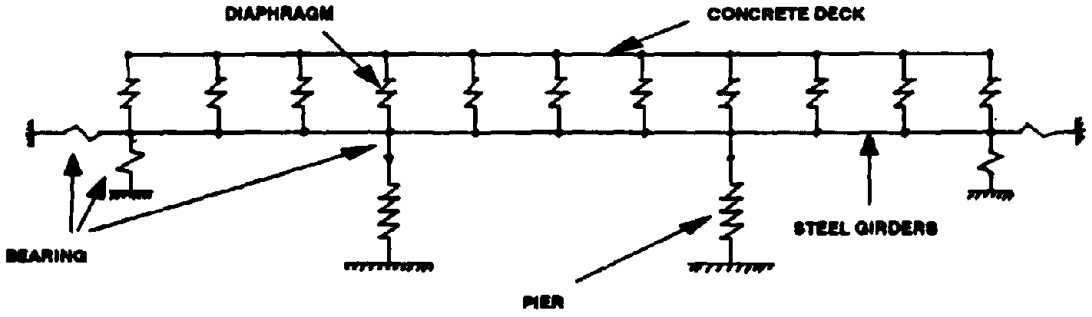

Fig. 7 Finite Element Model 2

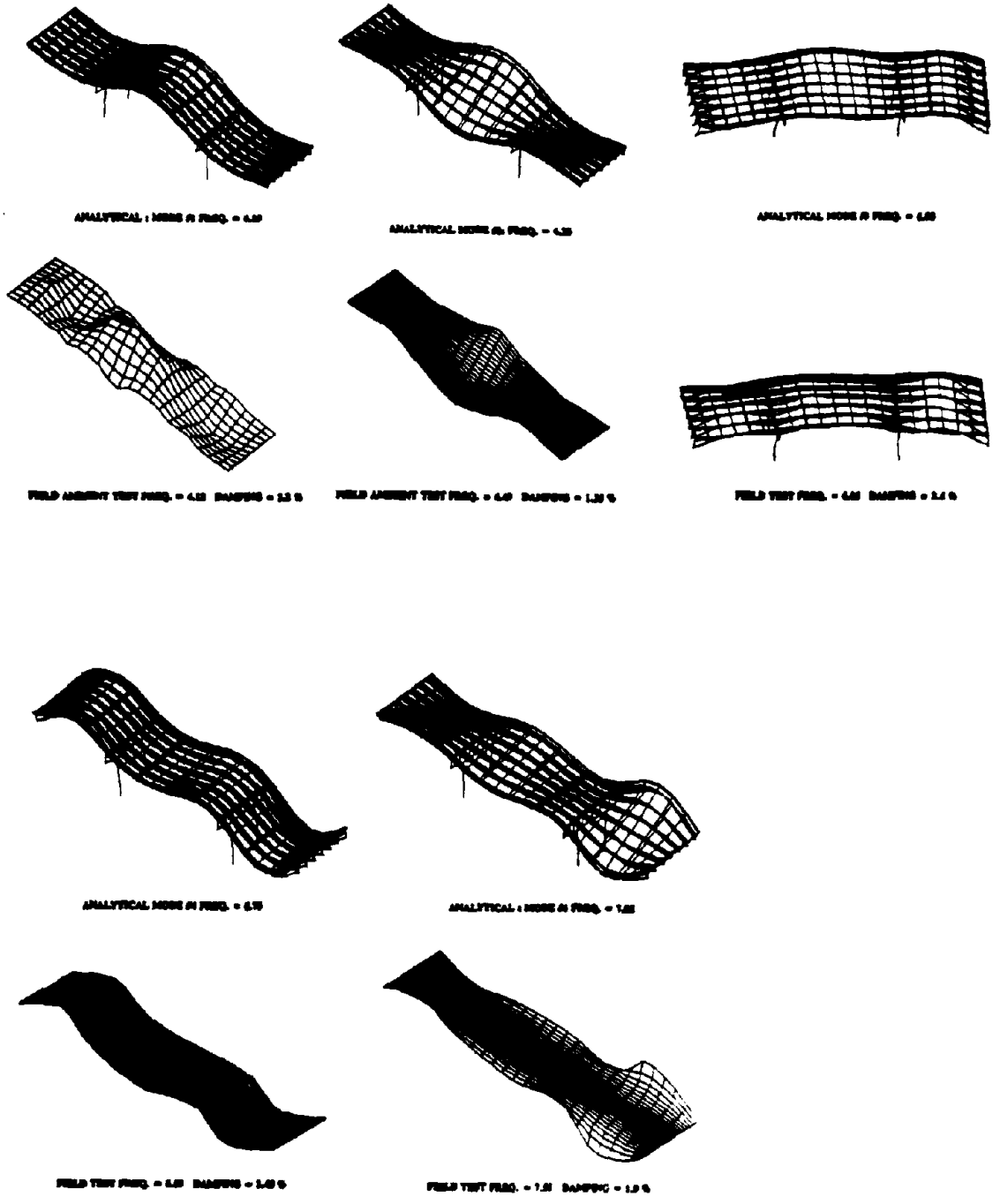

Fig. 8 Mode Shapes (Model 1 vs. Experiment)

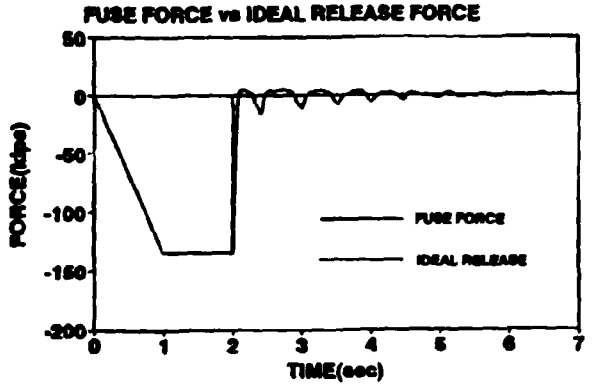

Fig. 9 Loading Bar Force Release

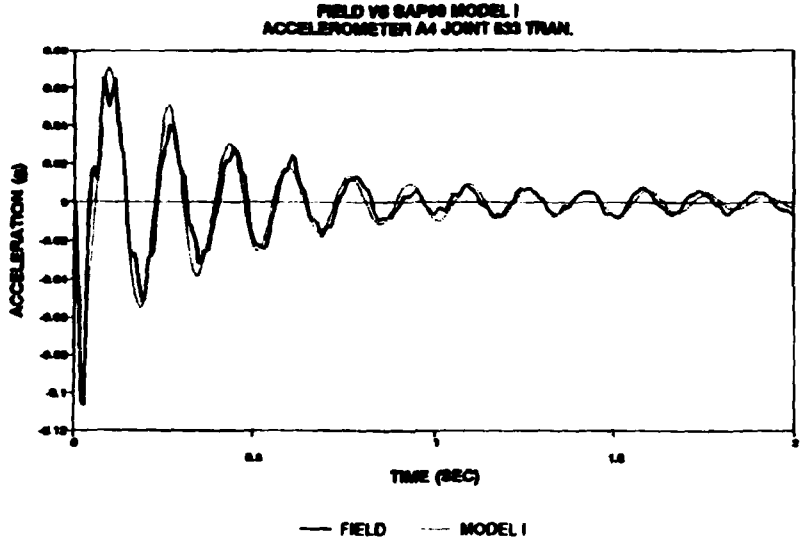

Fig. 10 Transverse Deck-Level Acceleration Time-History (Model 1 vs. Experiment)

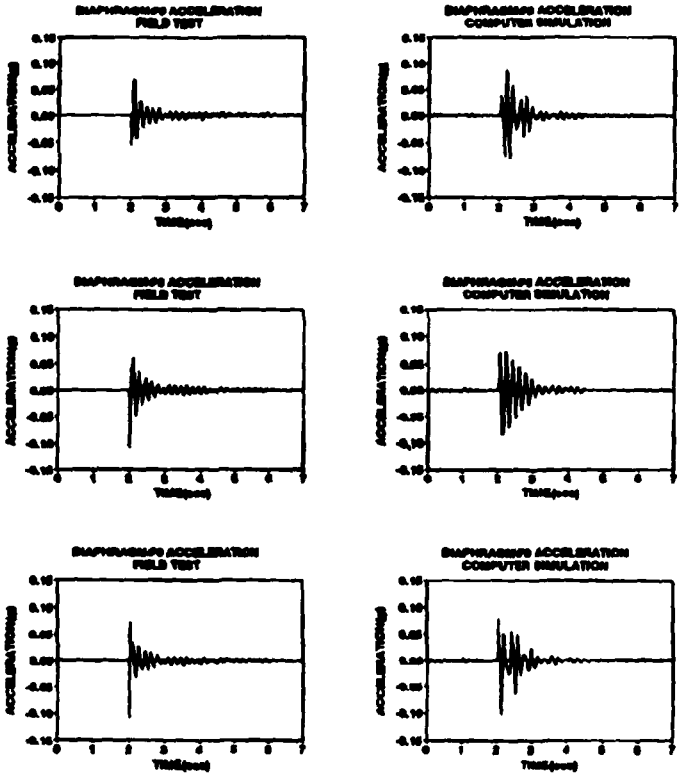

Fig. 11 Transverse Deck-Level Acceleration Time-Histories (Model 2 vs. Experiment)

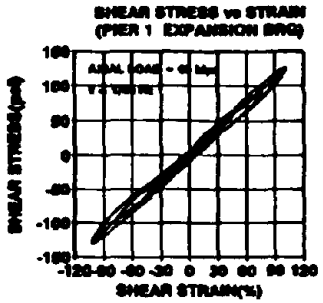

Fig. 12a Northbound Sample Bearing Hysteresis

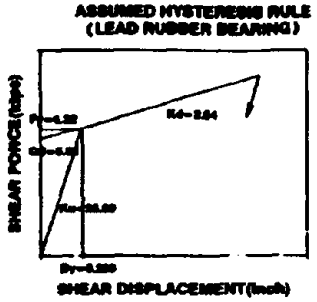

Fig. 12b Southbound Assumed Lead-Core Bearing Stiffness

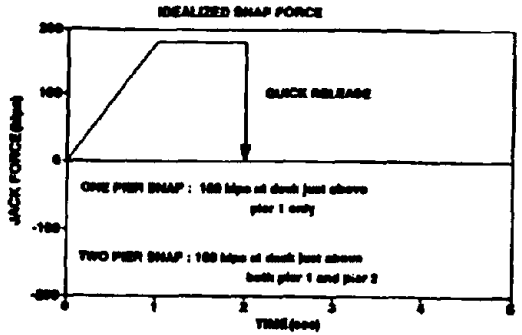

Fig. 13 Assumed Loading Bar Force Release for Retrofitted Bridge Study

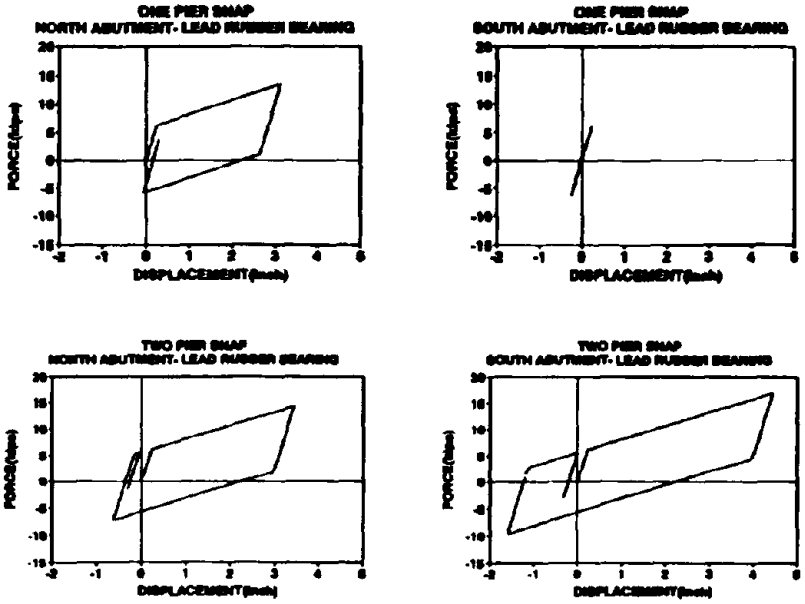

Fig. 16 Predicted Lead-Core Bearing Hysteresis

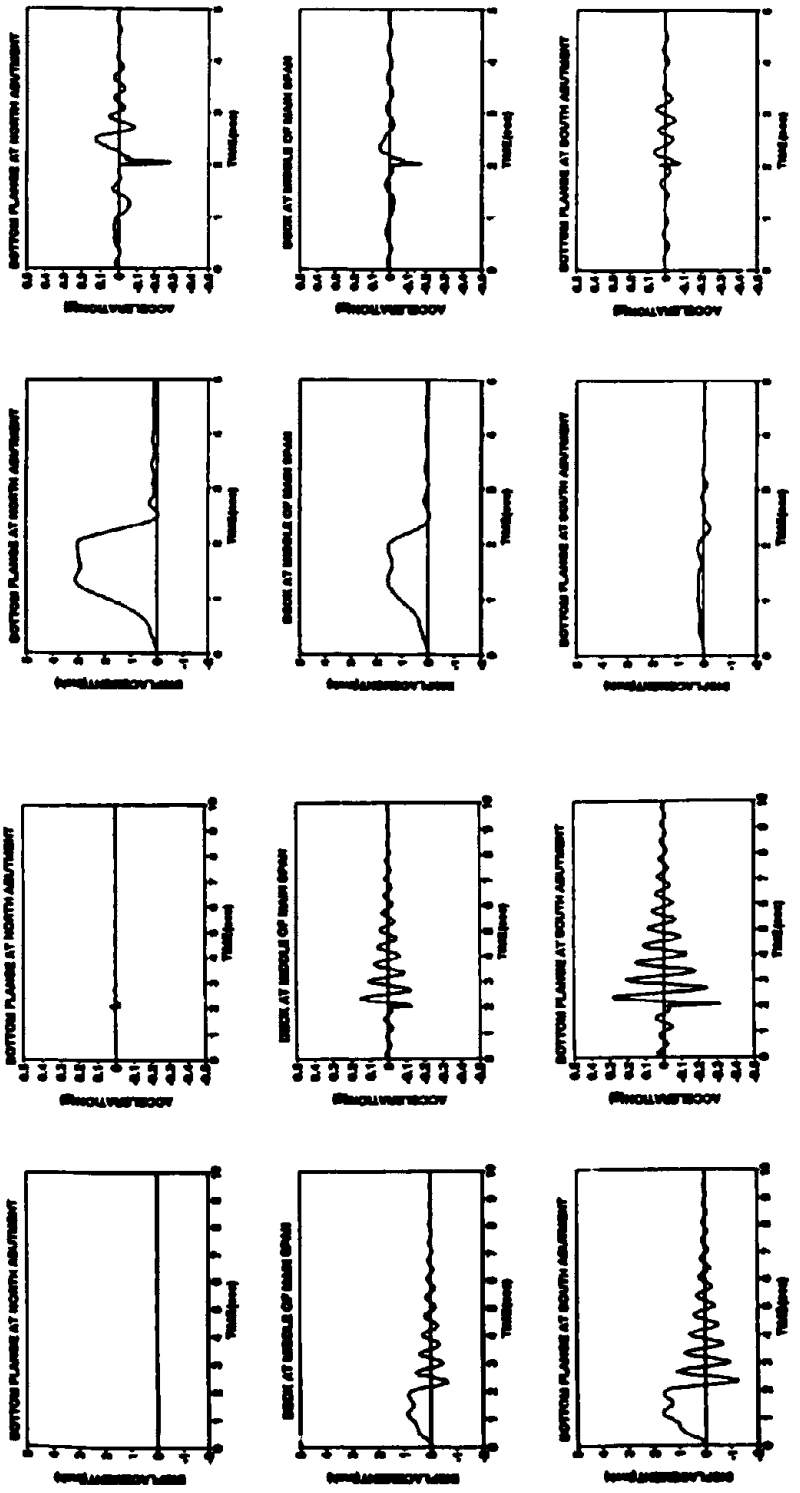

Fig. 14 Predicted Retrofitted Quick-Release Behavior, One Pier Snap

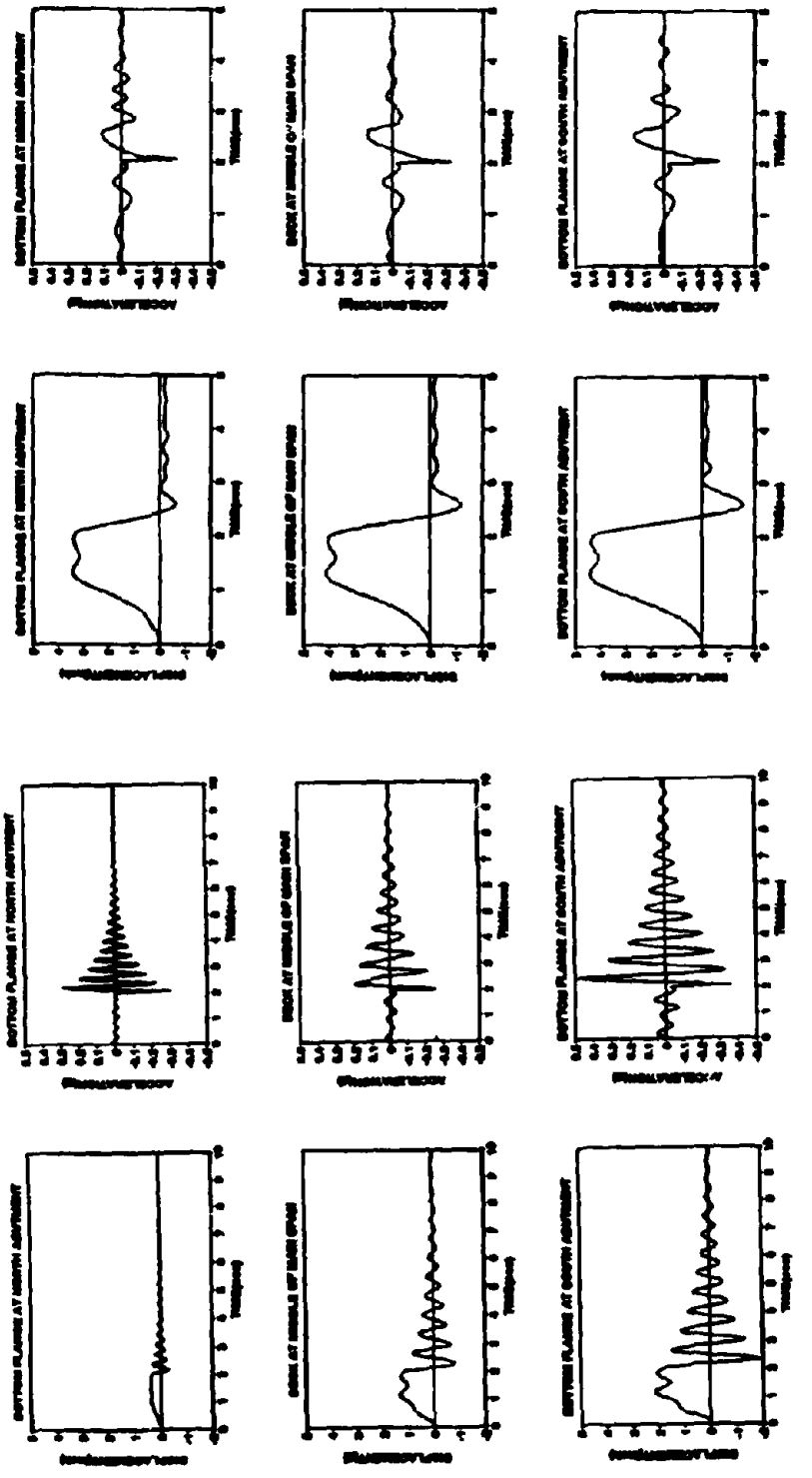

Fig. 15 Predicted Retrofitted Quick-Release Behavior, Two Pier Snap

Design of A Long Prestressed Concrete Continuous Girder Bridge Using Base Isolators

Kazuo Hasegawa[1], Shigemi Shikauchi[1], Hiroshi Osaki[1], and Yasuhisa Fujiwara[2]

1) Bay-shore Route Construction Bureau, Metropolitan Expressway Pub. Co.
2) Dept. of Civil Engineering, Sumitomo construction Co.Ltd.

ABSTRACT

The Higashi-Ohgishima viaduct of Metropolitan Expressway, Bay-shore Route (4th phase), is a 9-span continuous prestressed concrete box-girder bridge using base isolator. In order to improve seismic resistance, a reaction distribution method using rubber bearing supports was adopted for the bridge. In addition, seismic design using menshin technology was carried out so that the piers, bearing supports and main girders would withstand an earthquake of the magnitude of the Great Earthquake of 1923. For the bearing, the LRB bearing having energy dissipating capability was adopted, and its dynamic characteristics were verified by approving test for dynamic load and elasto-plastic dynamic analysis. Vibration test were also performed on the bridge itself during construction to confirm the propriety of the design.

INTRODUCTION

The Higashi-Ohgishima viaduct of the Expressway Bay-shore Route, which forms part of the Tokyo Bay Ring Road, is situated in the Higashi-Ohgishima district of Kawasaki City, Kanagawa Prefecture. The viaduct crosses a local road of Kawasaki City, and has a total length of 417.6m.

Since the Metropolitan Expressway Bay-shore Route is a arterial road for the Tokyo region, it was felt necessary, in addition to adopting a reaction distribution method using rubber bearings, to incorporate seismic isolation in the design, in accordance with the "Manual of Menshin Design for Highway Bridges" (PWRI, et al). Laminated rubber bearings with lead plugs (LRB) were used as base isolators. This bridge is one of the largest prestressed concrete bridge using Menshin design in the world, and therefore bearing support approving tests, vibration tests on the bridge itself, and observations of seismic shocks are carried out.

OUTLINE OF THE VIADUCT

The viaduct is a 9-span continuous prestressed concrete box-girder bridge with a standard span length of 45m. Span A1 to P8 of the superstructure were constructed using stagings. while construction of span P8 to A2, which crosses Kawasaki City road were constructed using a cantilevering method. out of considerations of safety and maintaining an uninterrupted flow of traffic.

The specifications of the viaduct are as follows:

- Road category: Class 1 (design load: TL-20, TT-43)
- Bridge length: 417.6m (8 @45.0+55.0)
- Effective width: 2 ×13.25m (one-side three lanes)
- Temperature change: ±20℃
- Superstructure: 9-span continuous prestressed concrete box-girder
- Substructure: abutment (2), pier (8)
- Foundation type: Steel pipe pile (φ800)
- Ground classification: TypeⅢ (classification for seismic design)

A general view is shown in Fig.-1.

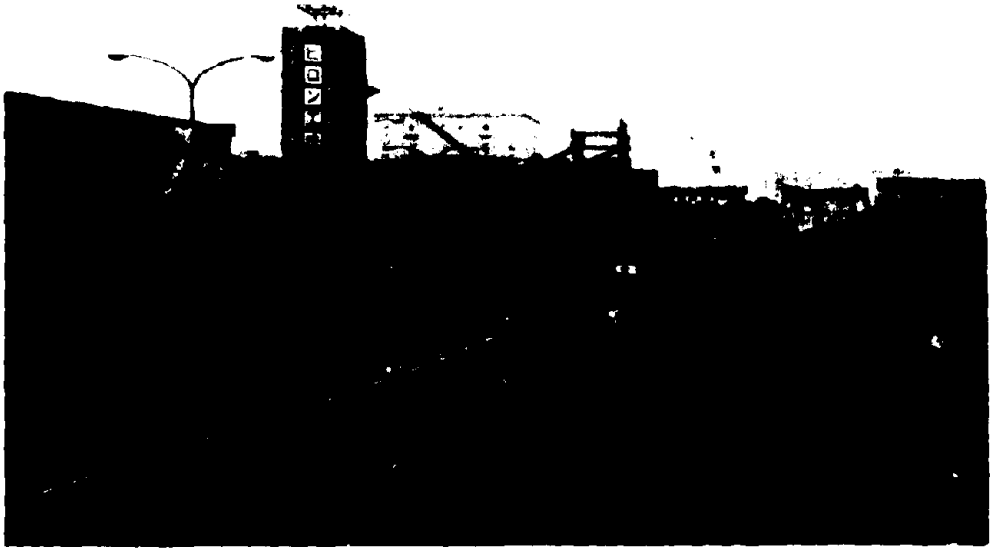

Photo 1 Cantileveling Construction

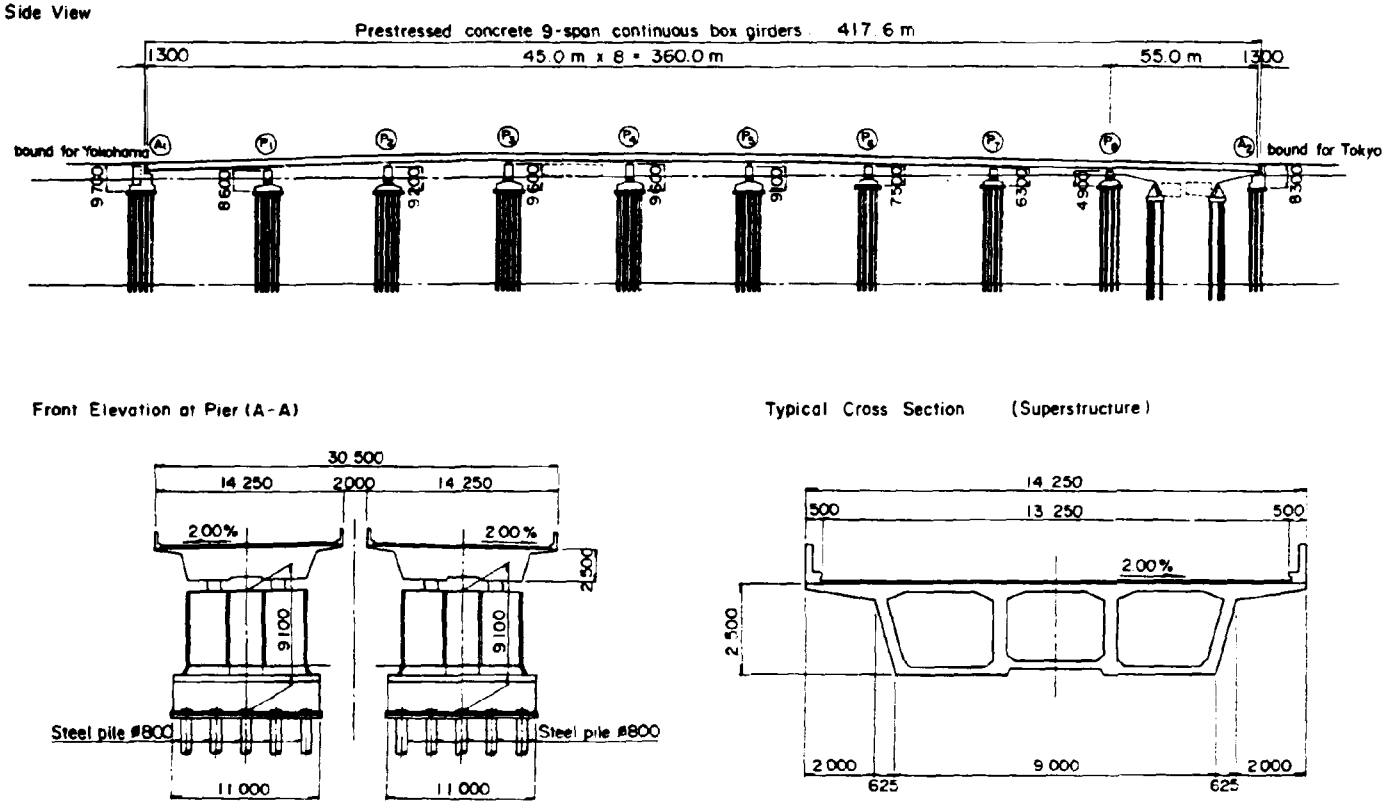

Fig. 1 General View

MENSHIN DESIGN

Design of Menshin Device

Menshin design is a form of aseismic design which aims to reduce inertia force by elongating the natural period of a bridge while also increasing energy dissipating capability. In this case, since the ground at the location of the bridge is weak, including layers of land-fill (known as type Ⅲ ground), a major elongation of the natural period would have been necessary to reduce the inertia force. In this case, the displacement of the superstructure would have increased, and the size of the bearings implied in this design would have been uneconomical. The decision was therefore taken not to attempt to elongate the natural period of the bridge more than was economical, but rather to reduce the inertia force by increasing energy dissipating capability.

Laminated rubber bearings with lead plugs were adopted as an isolation mechanism. Bearings are isolated in the longitudinal direction for earthquakes of normal magnitude, and fixed in the transverse direction using steel side-blocks. Seismic isolation in both directions was introduced with respect to ultimate level earthquakes(level of checking bearing capacity for lateral force). This was achieved by fitting steel side-blocks which would break during ultimate-level earthquakes along and athwart the bridge axis. The bearing supports are shown in Fig.2, and the design results in Tables 1 and 2.

Given the length of the bridge , significant levels of main girder creep and drying shrinkage suggests a need for large bearings. A mechanism was therefore developed to allow shear deformation in the bearings after completion of the bridge, in order to eliminate the effects of girder creep and drying shrinkage. Fig.3 shows an outline of the post-strain adjustment method.

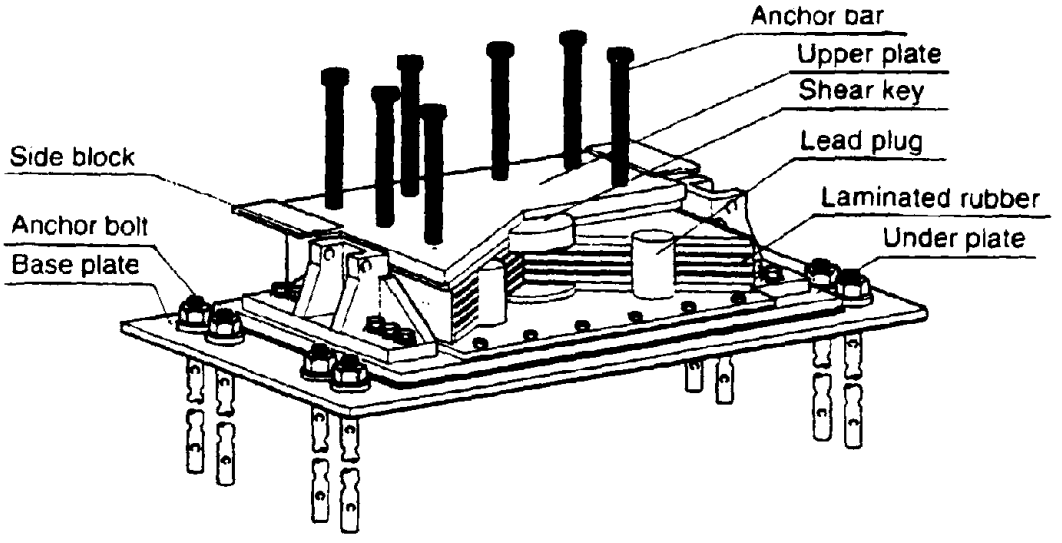

Fig. 2 Structure of LRB

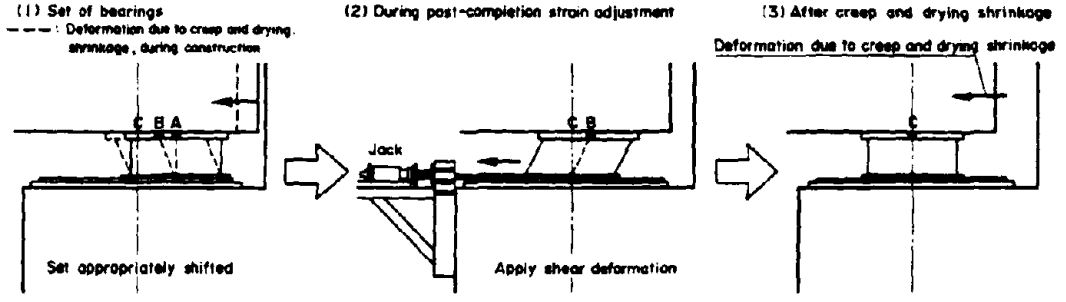

Fig. 3 Method of applying post-completion strain adjustment

Table 1 Design Criteria and Result for LRB

Item		Abutments (A_1, A_2)	Piers (P_2)
Dead Load Reaction (tf)		418	953
Live Load Reaction (tf)		167	299
Disp. (mm)	Creep, Shrinkage	111	71
	temperature(±20℃)	±41	±30
Size of LRB (cm²)		123×180 = 22140	
Thickness of Rubber (cm)		3.6× 5 = 18.0	
Area of Lead Plug (cm²)		φ20× 4 = 1257	

Table 2 Dynamic Properties of LRB and Bridge

Item \ Earthquake Level		Normal Level	Ultimate Level
Dynamic Properties of LRB (one pier)	Post-yield Stiffness (tf)	3699	1953
	Characteristic Shear Strength Load (tf)	213	213
	Effective Stiffness (tf/m)	7525	2436
Properties of Bridge	Natural period (sec)	0.941	1.570
	Damping ratio of Bridge (%)	23.5	15.4
	Design Lateral Force Coefficient	0.30	0.77
	Displacement of Superstructure (mm)	65	471

Girder Clearance

The clearance between the main girders and the abutments is set at 300mm in consideration of movement of the main girders due to temperature change and creep, and drying shrinkage, as well as an earthquake of normal magnitude. It is possible, therefore, that the main girder may collide with the abutment during ultimate level earthquakes. The effect of collision of this type between major structural members on the aseismicity of the bridge as a whole was studied using dynamic analysis.

Effect of Menshin design on Substructures

Design of the substructure was carried out as prescribed in the Highway Specifications[2], which do not envisage any seismic damping effect from the bearings, as such structures have not yet been subjected to major eathquakes. Fig. 4 shows the relationship between lateral force and displacement in pier P4. The figure shows the ductility ratio of piers with and without menshin design, when subjected to an ultimate level earthquake. The figure shows that with seismic isolation, the ductility ratio $\mu =$ 1.96, and only minor damage is sustained even during large earthquakes.

Approving Test of Confirming Requirements for Dynamic Load

The relationship between the shear force of LRB and its deformation is almost bilinear, and as shown in Fig.-5, can be modeled as an idealised hysteresis loop. In Menshin design, design is carried out by changing this into effective lateral stiffness and effective damping ratio.
In order to prove the appropriateness of those models on this bridge, performance test were carried out on full-size models of the bearings. Fig.-5 shows one example of results of lateral stiffness test on a bearing.

Also, the permitted discrepancy between measured and calculated values was set at $\pm 20\%$, and it was confirmed that even a discrepancy of this magnitude would cause no problems in the bearings, substructure or superstructure.

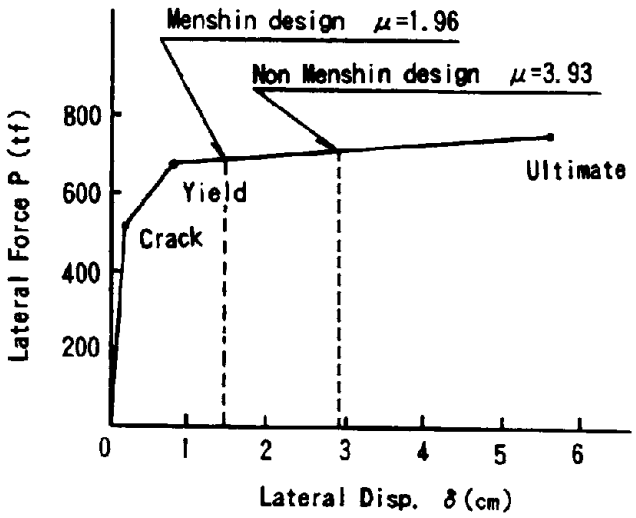

Fig. 4 Relationship between Lateral Force and Displacement of pier

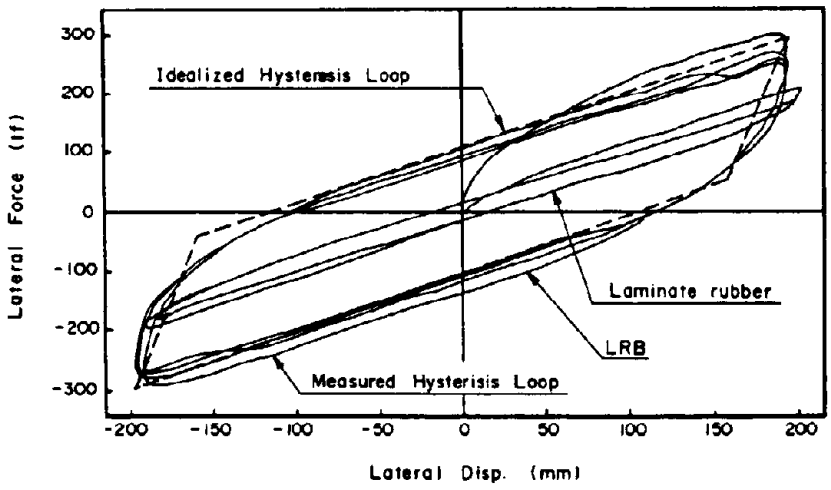

Fig. 5 Actual hysteresisloop

DYNAMIC ANALYSIS

Analysis Method

An elasto-plastic dynamic analysis was carried out with aim of obtaining the vibration properties of the bridge during ultimate level earthquakes, and of confirming seismic safety. The method used for dynamic analysis is elasto-plastic time history response analysis, taking into account the non-linearity of the bearings and the piers, using a overall skeleton model as the analysis model.(refer to Fig.-6.) The seismic wave data input is shown in Fig.-7. The basis for this data is the revised seismic wave for the earthquake of Tsugaru, issued by the PWRI, multiplied by modification factor for importance of 1.1, to account for the type Ⅲ ground.

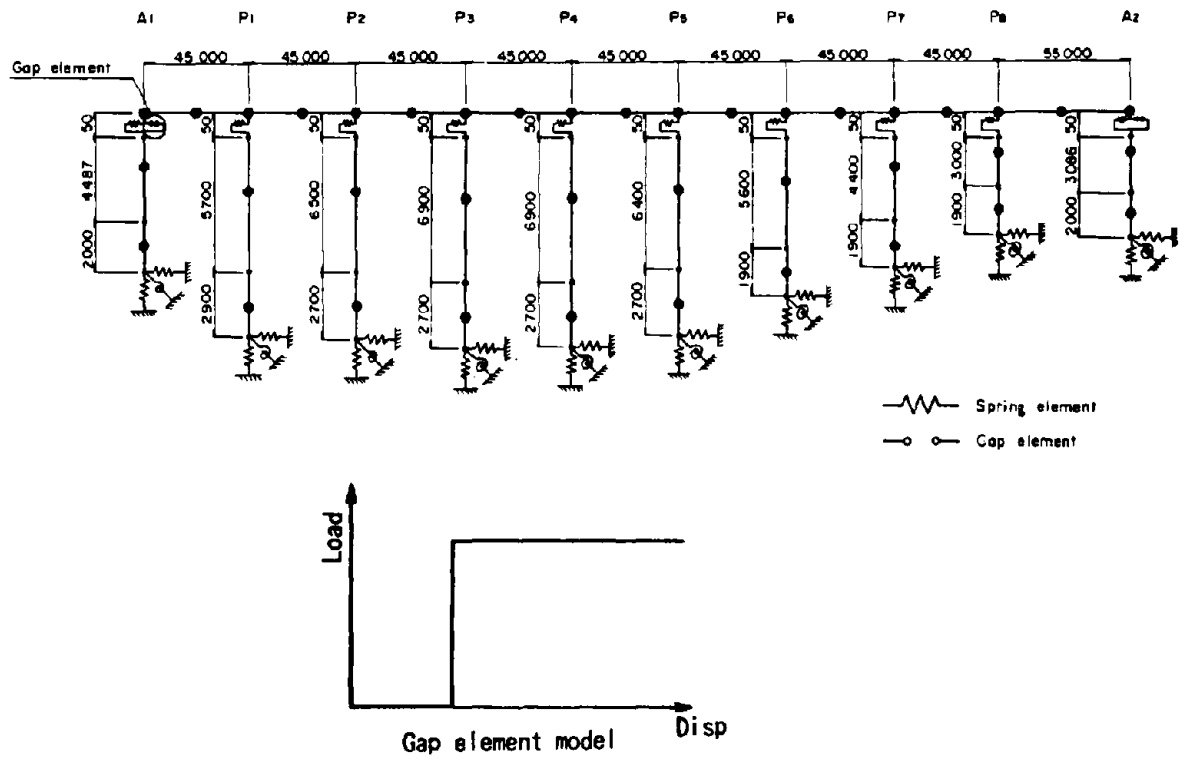

Fig. 6 Analysis model

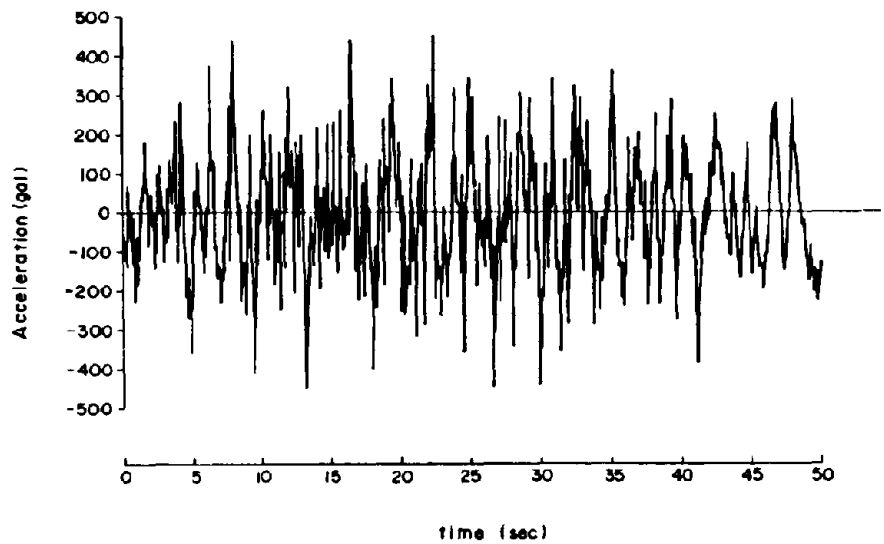

Fig. 7 Input Acceleration

Analysis Results

In the analysis model in the longitudinal direction, gap elements are included in abutments A1 and A2, to allow for collisions between the main girders and the abutments. The gap element is an element which has no effect up to a certain level of displacement, but takes effect suddenly when that level is passed. The results obtained from dynamic analysis are roughly 80% of those of obtained from static analysis, thus confirming the safety of the static design. (refer to table 3) Fig.-8 shows the relationship between the clearance and the lateral forces working on the abutments. The diagram shows that with narrower clearances, the lateral forces increase, and when the clearance is less than 160mm, these forces become larger than the lateral resistance of the abutments. However, according to this analysis, when creep and drying shrinkage are completed, the clearance will be at least 260mm, eliminating the possibility of collision between the girder and the abutment, leaving the bridge functioning as a whole following an ultimate level earthquake.

Table 3 Comparison of Dynamic Analysis Values and Static Analysis Values

Item		Static Analysis Values	Dynamic Analysis Values
Displacement Superstructure		471mm	235mm
Bending Moment on the Bottom of Pier	A_1	4846tf	3738tf
	P_1	6156tf	4658tf
	P_4	7452tf	5668tf
	P_8	3240tf	2471tf
	A_2	3333tf	2553tf

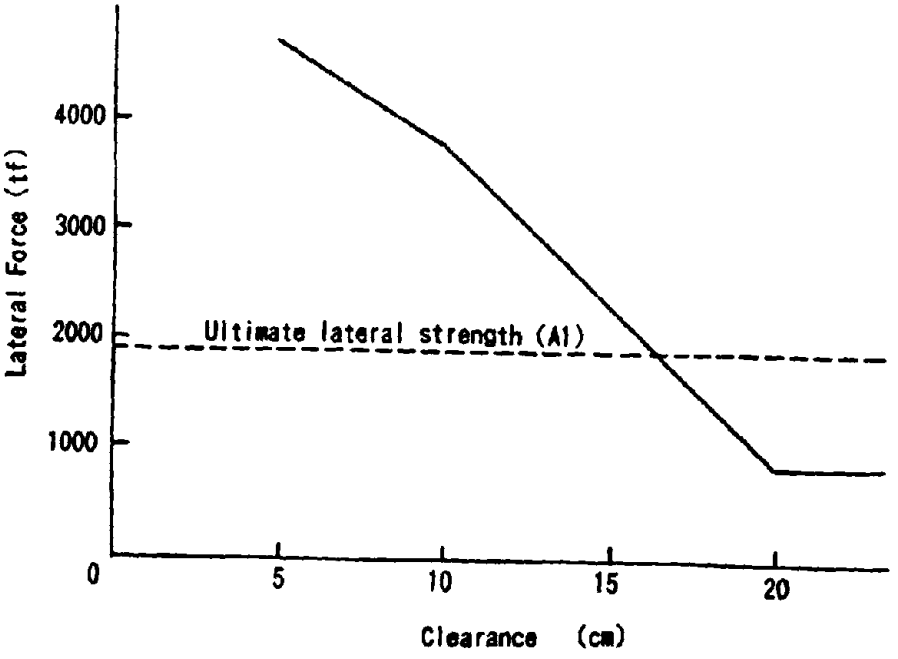

Fig. 8 Relationship Between Lateral Force and Clearance

VIBRATION TEST ON THE BRIDGE

Test Model

The weight of the superstructure at the completion of the viaduct is 14,400tf. In order to give a larger displacement amplitude using the existing actuator, the two-span structural system under construction shown in Fig.-9 was selected as the test model. The weight of the concrete main girders is about 3,200tf, and the vertical reaction of P_4, P_5 and P_6 are 895tf, 1,395tf and 910tf respectively. Two identically shaped LRB are installed on each pier.

Test Method

The test consisted of artificially inducing displacement of the main girders and piers(bearing supports) along the longitudinal direction, using hydraulic jacks, then inducing a free damped vibration by releasing the jacking pressure instantly (rapid release test). A total of six hydraulic jacks with rapid-release valves (capacity 180tf., stroke 150mm) was installed, two on each pier.

The acceleration of the main girders and piers, the relative displacement of the bearing supports, the stress of the pier concrete, and the jack oil pressure were measured by sixteen servo type accelerometers, six displacement sensor and thirty strain gauges shown in Fig.-9.

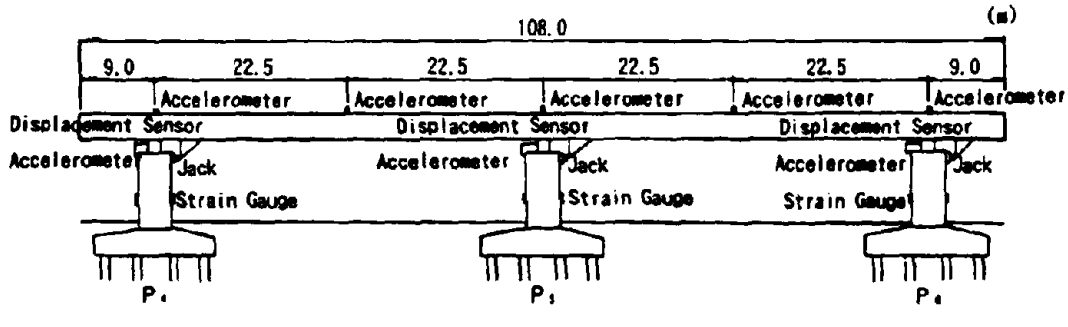

Fig. 9 Configuration of the Test Bridge and Arrangement of the Test Devices

The forced displacement of the bearing supprts in the rapid-release test was established to the following two types.
(1) 3cm displacement test:
Bearing support displacement of about half the normal earthquake level, induced by a force of about 100tf per jack.
(2) 6cm displacement test:
Bearing support displacement equivalent to the normal earthquake level, induced by a force of about 150tf per jack.

Test results and discussion

Fig.-10,-11 shows the free damped wave pattern of displacement and acceleration obtained from the rapid release test. In both the 3cm and 6cm displacement tests, vibration stopped after about two seconds, and both tests resulted in residual displacement. Conceptual graphs of a strain control bearing support performance test conducted previously were drawn up(Fig.12)based on the results of dynamic analysis, in order to assist in understanding this vibration property. After releasing the load of the hydraulic jacks, the displacement returns to a level balancing the restoring force(first vibration zone), after which vibration continues around this level(second vibration zone), and then ceases (residual displacement). The residual displacement decreases to about 65% after 19 hours.

A summary of the test is shouwn in Table-4. The natural frequency of 1.2 to 1.8Hz almost coincides with the design value. The measured value for the damping ratio is 20 to 30% in the first vibration zone, and 15 to 16% in the second vibration zone. The values for pier stress remained within 10 % of each other as shown in Table-4, and the identical phasing of the wave patterns confirms the good dispersibility of the structure.

CONCLUSION

(1) The adoption of Menshin design reduces to a minimum the damage sustained by piers, even during a major earthquake.
(2) The propriety of the bearing support structure, girder clearance etc. were verified by dynamic analysis.
(3) Performance confirmation testing of the bearing supports, and vibration tests on the actual bridge, confirmed the dynamic characteristics of the bridge and the propriety of Menshin design.

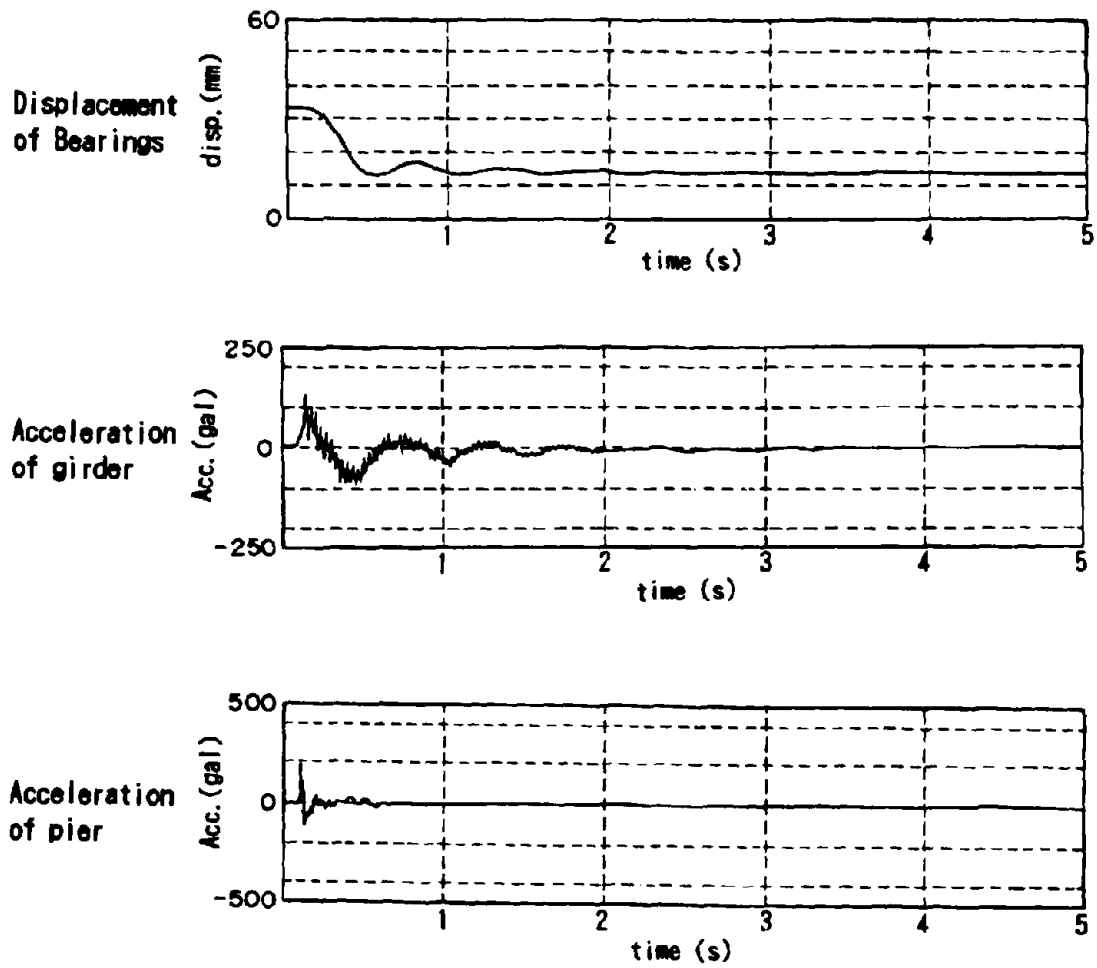

Fig. 10 Test Results (1)
(3cm)

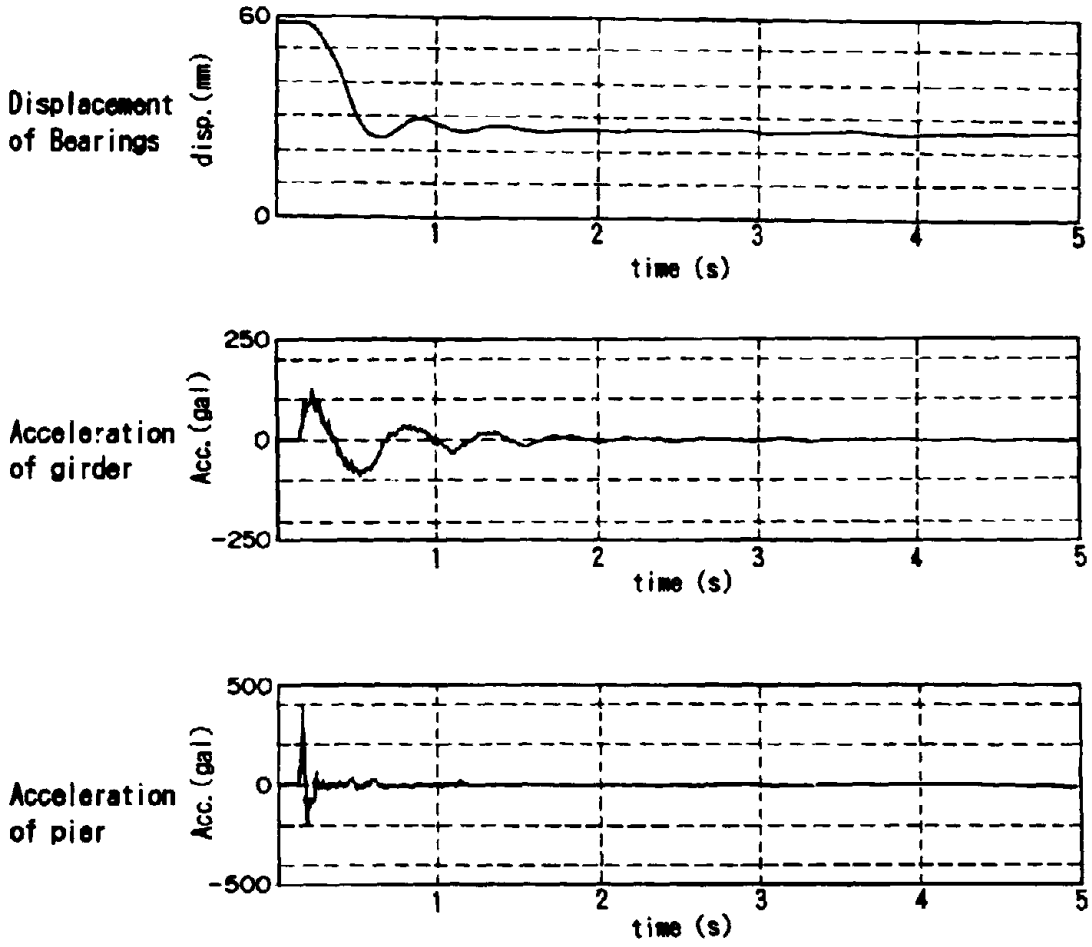

Fig. 11 Test Results (2)
(6cm)

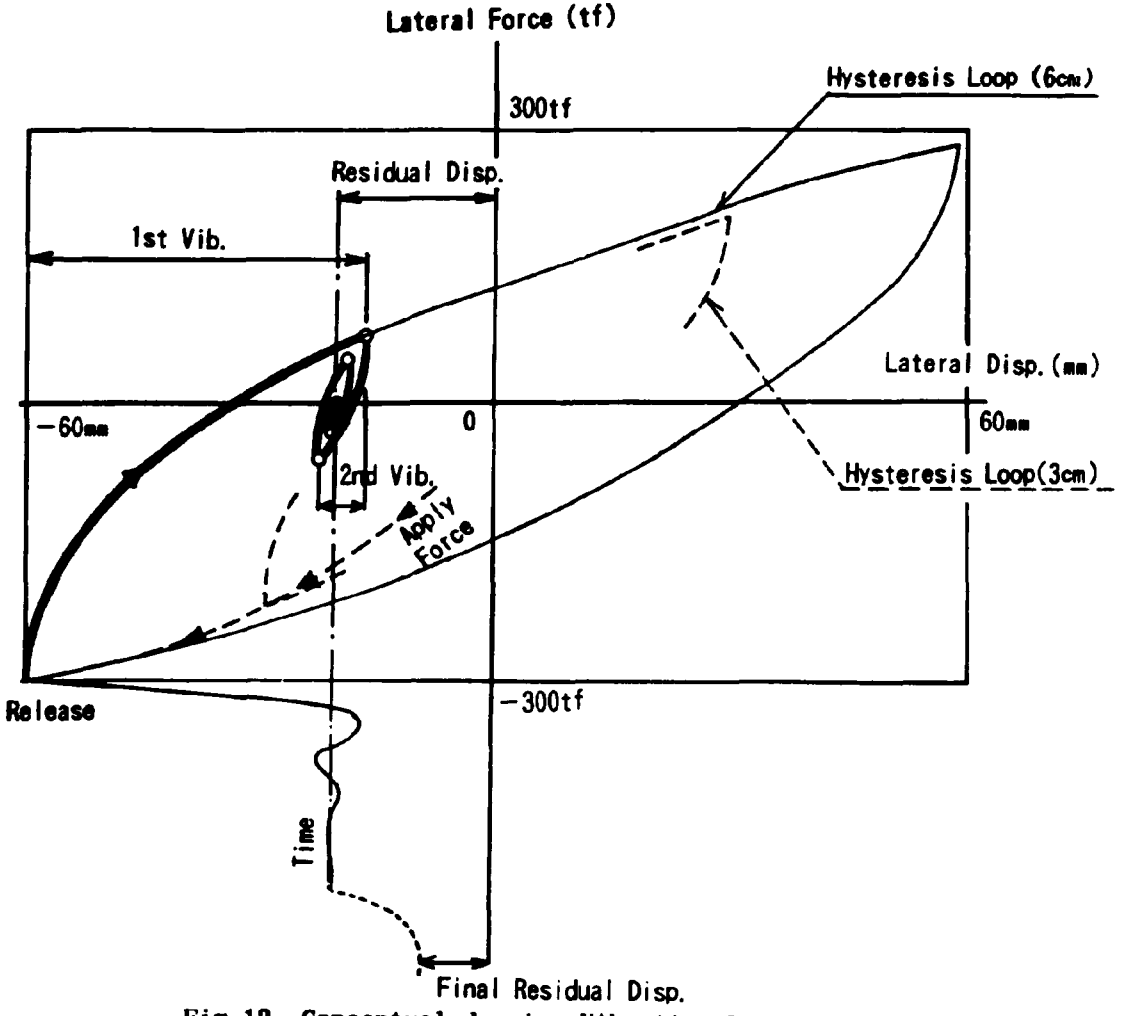

Fig. 12 Conceptual drawing Vibration Test

Table 4 Summary of Test Results

Vibration Mode			
Item		3 cm	6 cm
Frequency (Hz)	1st Vib.	1.30	1.25
	2nd Vib.	1.80	1.80
Damping Ratio (%)	1st Vib.	20 ~ 30	
	2nd Vib.	15 ~ 16	
Maximum [P5] acceleration (Gal)	Girder	126	161
	Pier Top	196	291
Piers Stress (kgf/cm²)	P 4	3.0	4.5
	P 5	3.2	4.7
	P 6	3.6	5.2

REFERENCES

1. PWRI: Manual of Menshin Design for Highway Bridge. December 1992.
2. Japan Road Association: Design Specification for Highway Bridge. Part V , Earthquake-resistant design. February 1990.
3. Kubota, Shikauchi, Osaki, Mitake, Arai: Design of 9-span Continuous Prestressed Concrete Girder Bridge with Base Isolators. The second U.S. Japan Workshop on Earthquake Protective System for Bridges. 1992.
4. Mitake, Shikauchi, Fujiwara, Nagai: Menshin Design of Higashi-Ohgishima Viaduct. Proceeding of the 48th Annual Conference of Japan Society of Civil Engineering.
5. Fujiwara, Mitake, Osaki, Fujita: Actual Viaduct Vibration Test of Higashi-Ohgishima. Proceeding of the 48th Annual conference of Japan Society of civil Engineering.

FIELD TESTING OF THE SEISMICALLY ISOLATED WALNUT CREEK VIADUCT

Stephen Mahin, Ian Aiken and Amir Gilani
Earthquake Engineering Research Center
University of California at Berkeley

ABSTRACT

A field test program is underway in Walnut Creek, California, to assess the reliably of analytical models and typical design assumptions for seismically isolated bridge structures. The bridge being tested is part of a temporary viaduct being constructed by the California Department of Transportation (Caltrans) at the I680/24 interchange. Seismic isolation is provided by 15 lead rubber bearings. The deck consists of steel girders and composite reinforced concrete slabs. The substructure consists of reinforced concrete single column bents. Testing consists of quick release and ambient tests on the piers prior to installation of the deck, and forced vibration and quick release tests of the completed structure. Post-test analytical studies will be undertaken to assess the adequacy of analytical modeling procedures and design assumptions. This paper describes the test program and preliminary results.

INTRODUCTION

The analysis and design of bridge structures requires adoption of numerous assumptions. In many cases, these have been validated on the basis of satisfactory performance of structures under service conditions, laboratory testing of components and assemblages, refined analytical models, and observed behavior during earthquakes. In the case of new types of structures, only limited laboratory testing can generally be done prior to field application. Similarly, component and assemblage tests and analyses may not provide sufficient information to predict with certainty the overall response of a structure. Thus, field testing of full scale structures has been used successfully by Caltrans and others to assess complications arising from the interaction of components, foundation and abutment conditions, and uncertainties in mechanical and dynamic characteristics. Reconciliation of measured response values with analytical predictions obtained using standard techniques provides verification of current design methods. Where correlation of predicted and measured responses is inadequate, the measured data provides the motivation and basis for developing improved methods.

An example of successful prior Caltrans-sponsored field investigations includes testing of a segment of the I-880 Cypress Viaduct in Oakland, CA following the Loma Prieta earthquake [1]. These tests included ambient and forced vibration tests of the as-built structure and destructive lateral load tests of the as-built and retrofit structure. These tests indicated that simple elastic models were able to predict the mode of failure observed, and provided important quantitative information on the efficacy of various retrofits. They also indicated the importance of foundation modeling on assessing the periods, mode shapes and damping of the structure.

Many new concepts, like seismic isolation, are being suggested for the design of bridges in California, and numerous modeling uncertainties remain in the analysis of bridges in general. These uncertainties with regards to analysis and performance may result in hesitation on the part of designers to utilize these new concepts. Real world field tests and related analyses can be effectively utilized to reduce these uncertainties, address issues related to the integrity of new types of structures, and improve design and analysis methods.

OBJECTIVES

A number of field tests and related analyses are currently underway with Caltrans sponsorship which take advantage of unique opportunities made possible by the construction, retrofit and demolition programs at the I 680/24 interchange in Walnut Creek, California. The overall goal of this work is to evaluate and, where necessary, improve design methods and analysis assumptions. In addition to field testing and analysis of the new temporary seismically isolated viaduct, tests and analyses will also be performed on an existing elevated single column viaduct at the site scheduled for demolition in early April 1994. This paper only addresses issues related to testing of the seismically isolated viaduct.

DESCRIPTION OF THE VIADUCT

The new temporary viaduct in Walnut Creek, California, is currently under constructed. It will carry southbound I-680 traffic through the new I680/24 interchange . The southern end of the temporary viaduct incorporates a seismically-isolated, four-span, 700-ft long, composite steel girder bridge structure. This segment of the viaduct is the first new bridge in the state of California to be seismically-isolated.

Assumptions and criteria used in the design of the viaduct, methods employed to specify required bearing characteristics for the contract bidding process, and the typical details utilized in the construction are described by Thorkildsen in a paper presented at the first U.S.-Japan Workshop on Protective Systems for Bridges [2]. It is significant to note that the viaduct has been designed as if it were a permanent structure and complies with all Caltrans design requirements in effect at the time of its design.

A peak ground acceleration of 60% g was assumed for the design of the viaduct. The design spectrum is based on 10 to 80 feet of soil underlying the viaduct. The periods of the un-isolated portions of the viaduct range from 0.5 to 0.8 seconds. The effective period considered in the design of the isolators was about 1.8 seconds.

The viaduct is intended to serve temporarily during construction of permanent interchange connectors that will pass underneath the temporary viaduct. Approximately 40,000 vehicles per day are expected to use initially the viaduct. The temporary viaduct will be demolished in about 1998. The steel deck girders used in the seismically isolated portion of the viaduct will be moved a short distance at the same site and used as part of a new off-ramp connector. In its new location, the connector will again be seismically isolated.

Non-isolated portions of the viaduct to the north of the test structure consist of post-tensioned concrete box girder frames supported monolithically on reinforced concrete columns. Drop in steel simply supported steel girders are utilized between the reinforced concrete frames in order to facilitate demolition of the sections of the viaduct passing over the new roadways in the interchange.

RESEARCH PROGRAM

A unique opportunity exists to obtain field test data on the mechanical and dynamic properties of this bridge that can be used to assess the reliability of modeling and analysis assumptions used in design. The dynamic properties of the bridge will be experimentally measured at different stages of construction, and this data will be used, along with existing information on the mechanical properties of the individual isolators and of the soil at the site, in dynamic response analyses to validate modeling and analysis assumptions. Three different phases

of vibration testing are planned. These will allow precise determination of a number of dynamic properties that to date have not been the subject of careful determination in other studies of seismically-isolated bridges.

Because of construction delays, only the first phase of testing has been completed at this time. Preparations for the remaining phases of testing are currently underway.

Phase 1 - Column Tests

Pull over and quick release tests have been conducted on four of the individual bents supporting the seismically isolated portion of the viaduct prior to placement of the deck structure. These tests were used to determine the flexibility and damping characteristics of the CIDH column/pile assemblages used. This information will greatly assist in developing a reliable analytical dynamic model of the entire structure, and help in assessing the contribution of various structural components to overall system damping.

These tests consisted of lateral loading of each bent. A hydraulic jack was used to load wire cables connecting two adjacent bents (Figs. 1 and 2) Several levels of loading up to approximately 20% of the design load were applied in this manner. Quick release was effectively achieved by means of an explosive bolt installed between segments of the cabling (Fig. 3).

The quick release tests allowed determination of periods and damping characteristics for each of the supporting columns. Instrumentation consisted of two force balance accelerometers at the top of the bent cap and one at ground level. Ranger seismographs were utilized for ambient acceleration measurement and ground level measurements as well. Portable data acquisition system including a spectrum analyzer was used to capture response data.

Results were very clean, having little transient interference. A typical result is shown in Fig. 4. Peak accelerations of 0.25g or more were typically induced at the tops of the column bents during the tests. One of the lines shown in Fig. 4 is the measured acceleration, while the other corresponds to the analytical solution for a viscously damped single degree of freedom oscillator. For the three taller (about 7 m) bents measured periods ranged between approximately 0.15 and 0.2 seconds and damping ratios ranged from 5 to 6 percent of critical. It is interesting to note that the horizontal accelerations at the ground level ranged for 25 to 40 percent of those measured at the top. For the shorter bent (about 2 meters tall) the period was about 0.11 seconds and damping increased to about 15 percent of critical.

The explosive bolts were found to be a practical and reliable means of carrying out the quick release tests. As a result they are to also to be utilized in the subsequent tests of the entire structure.

Phase 2 - Forced Vibration Tests of the Entire Four Span Frame

The second phase of testing involves the forced vibration of the completed bridge. Two rotating-mass shakers will be utilized, as done in the forced vibration tests of the Cypress viaduct. These shakers can be precisely controlled over a wide frequency and phase ranges to allow determination of periods, mode shapes and damping ratios. Dynamic loading will be applied in the longitudinal, transverse and torsional (about a vertical axis) directions. The vibration generators will be located near the quarter points along the length of the frame, nearly 350 feet apart.

Accelerometers will be strategically located along the top of the bridge deck, immediately above the isolators, below the isolators at the top of the bents and at the ground surface level to help identify modal characteristics. Accelerometers will be oriented in the longitudinal and

transverse directions of the bent. In addition, displacement transducers will be positioned to measure transverse and longitudinal relative displacement of the isolators. Nearly 60 channels of data will be recorded during the tests.

These tests will involve relatively low levels of response. However, they will provide results that can be used to validate elastic analytical models consistent with these levels of response, and they will provide information on the response in the transverse and torsional directions (Fig. 1) that will not be obtained in the Phase 3 quick release tests.

Phase 3 - Snap-back Free Vibration Tests of the Entire Four-Span Frame

The third phase of testing involves loading the bridge deck along its longitudinal axis using hydraulic jacks, and quickly releasing the imposed displacement using a special restraint device activated by explosive bolts so that the free vibration response of the bridge can be measured. The deformations imposed on the bridge deck will be about 6 inches (15 cm) roughly 2/3 of the design amplitude for the isolation bearings. Thus, information obtained in this portion of the test will capture some of the nonlinear inelastic response characteristics of the bridge expected during an earthquake similar to the design level event; something not possible in the Phase 2 tests.

Loading will be accomplished with four 200-ton capacity hydraulic jacks. It was believed to be important to obtain good free vibration response measurements of the bridge during the crucial first large amplitude cycle of nonlinear response. Initially, consideration was given to using specially modified jacks capable of retracting quickly (as done for the testing of the Yamaage Bridge [3] in Karasuyama, Japan). The success with explosive bolts during the phase I tests and concerns regarding the ability of the hydraulic jacks to retract faster than the initial response of the bridge deck led to use of a special quick release, displacement restraint device.

In this case the device used was borrowed from ISMES in Italy. The device is shown schematically in Fig. 5 and a photo is presented in Fig. 6. The device is loaded in compression. Equilibrium is maintained by the tension bolt passing across the diagonal. Explosive charges are loaded into each bolt to effect the quick release. Twin charges are utilized to insure fail-safe release of load. Three of these restraint devices will be employed.

Thus, the planned test sequence consists of displacing the bridge longitudinally by means of hydraulic jacks. Restraining the bridge in the deformed configuration by means of the displacement restraint device and shims. The hydraulic jacks will then be retracted and the displacement will be released by setting off the charges in the explosive bolts.

Instrumentation consists of that used in Phase 2 plus additional transducers to measure applied force and the absolute displacement of the bridge deck at several locations.

Because the abutment at the end of the viaduct is designed only to carry the reaction for the three isolators it supports, it is not possible to load the viaduct from the abutment. Instead, loading reaction will be provided by the reinforced concrete frame to the north of the seismically isolated frame. This frame was conventionally design and has a strength and stiffness considerably higher than that of the isolated frame.

Closure strips and expansion joints will not be in place at the time of testing. This will allow the isolated bridge to vibrate unimpeded by these mechanical attachments.

Phase 4 - Data Interpretation and Analysis

Analysis and interpretation of the collected data will be undertaken upon completion of testing. Data analysis will include identification of system frequencies, mode shapes and damping characteristics. Any unusual features of the response and dependence of the dynamic characteristics on amplitude of motion will be noted.

The above results will be compared with values obtained in the design analyses. In addition, an analytical model will be formulated to develop an accurate representation of the complete structural system that accounts for foundation, bent, isolation bearing and superstructure dynamic properties. Both linear elastic and inelastic models will be developed to represent the experimental results. Experimental and analytical results will be compared. Improvements in modeling and analysis assumptions will be recommended, if necessary to obtain better agreement between predicted and observed responses.

SUMMARY

Field tests are underway on a new seismically isolated bridge in Walnut Creek, California. The tests will measure the dynamic properties of the bridge at various stages of construction. Testing will consist of low level quick release and forced vibration tests. In addition, quick release of displacements approaching the design level will be carried out. Good results have been obtained utilizing specially designed explosive bolt devices to implement the quick release tests. Testing is scheduled for completion by during the beginning of February 1994.

ACKNOWLEDGMENTS

The work described in this paper is funded by Caltrans. This support is gratefully acknowledged as is the guidance and motivation provided by the Caltrans project monitor, Eric Thorkildsen. The assistance by Fadal Allamadine, George Amaro, John Hicks, Pete Siegenthaler, Michael Trafallis, and others at Caltrans is greatly appreciated.

Numerous students and members of the staff at U.C. Berkeley have contributed to this project. In particular, the assistance of Professor Greg Fenves, the principal investigator for testing of the non-isolated existing viaduct and the site is appreciated. In addition, the assistance of Drs. M. Blondet and C. Yin has been invaluable.

REFERENCES

1. Bollo, M., Mahin, S., Moehle, J. and Stephen, R., "Observations and Implications of Tests on the Cypress Street Viaduct Test Structure," ***Report No. UCB/EERC-90/21***, Earthquake Engineering Research Center, University of California, Berkeley, CA, Dec. 1990.

2. Thorkildsen, E., "Caltrans Seismic Design and Future Concepts," ***Proceeding***, First U.S.-Japan Workshop on Eathquake Protective Systems for Bridges, Technical Report NCEER-92-0004, National Center for Earthquake Engineering Research, State University of New York at Buffalo, Feb. 1992.

3. Kakinuma, T., Kawakami, K., Kumakura, K. Tani, H., and Abe, N., Vibration Test of a Menshin Designed Multi-span Continuous Prestressed Concrete Bridge, ***Preprints***, Third U.S.-Japan Workshop on Earthquake Protective Systems for Bridges, National Center for Earthquake Engineering Research, State University of New York at Buffalo, Jan. 1994.

Fig. 1 Typical Column Bent Showing Cabling used for Phase 1 Quick Release Test

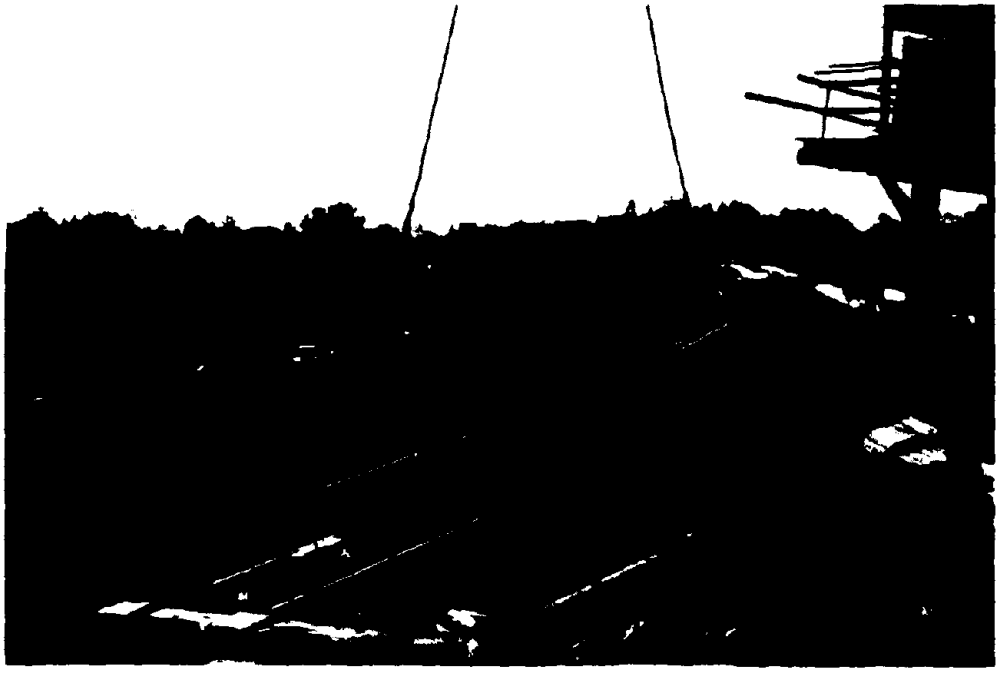

Fig. 2 Haudraulic Jack Used In-line for Phase 1 Quick Release Test

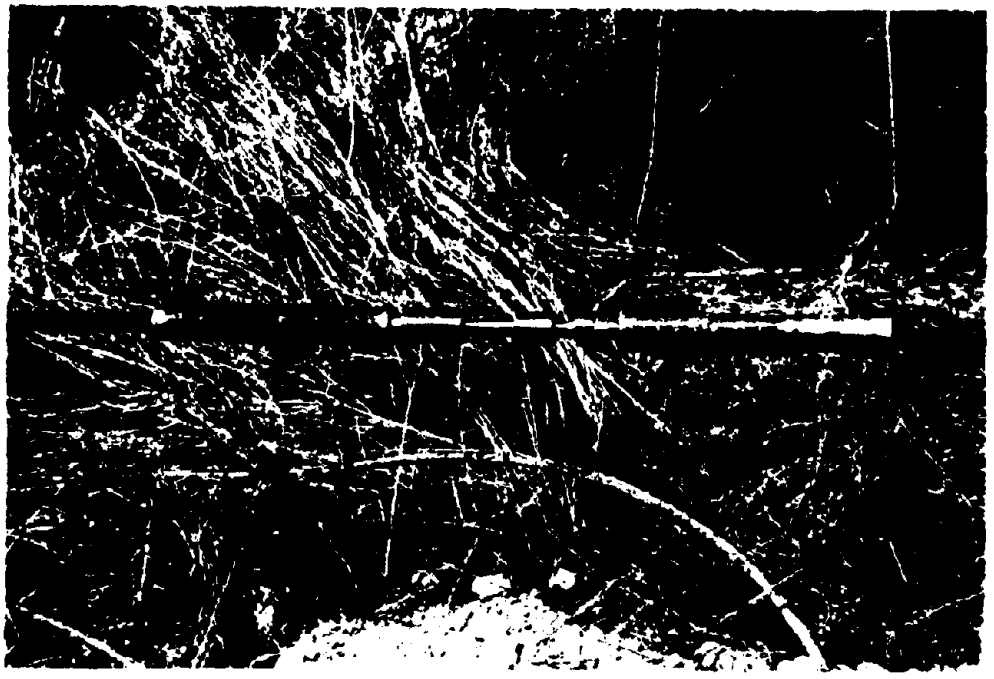

Fig. 3 Explosive Bolt Assembly for Phase 1 Quick Release Tests

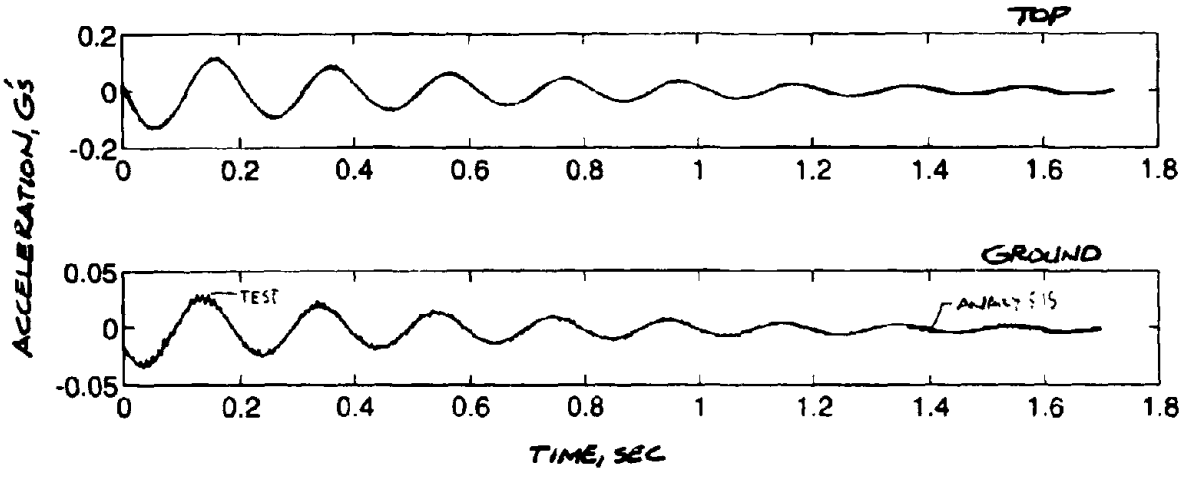

Fig. 4 Typical Phase 1 Quick Release Results for Column Bent 3

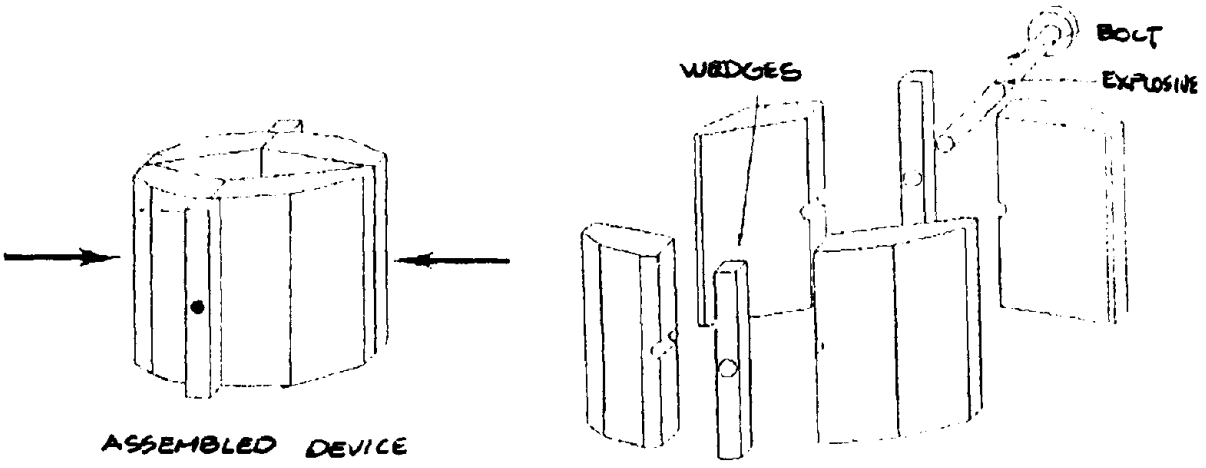

Fig. 5 Schematic Diagram of Phase 3 Quick Release Displacement Restraint Device

Fig. 6 Photo of Phase 3 Quick Release Device (ISMES)

RESPONSE OF ON-NETOH BRIDGE DURING KUSHIRO-OKI EARTHQUAKE OF JANUARY 1993

Masashi SATO[1], Hiroaki NISHI[2], Kazuhiko KAWASHIMA[3] and Shigeki UNJOH[4]

1) Head, Structure Division, Structure Department, Civil Engineering Research Institute, Hokkaido Development Bureau, Hiragishi 1-3, Toyohira-ku, Sapporo, Japan
2) Research Engineer, ditto
3) Head, Earthquake Engineering Division, Public Works Research Institute, Ministry of Construction, Tsukuba Science City, Japan
4) Senior Research Engineer, ditto

ABSTRACT

On-netoh bridge is being constructed in the East of Hokkaido for the replacement of the existing bridge. Menshin design using lead rubber bearings is employed for the On-netoh bridge. In January, 1993, the Kushiro-oki Earthquake with magnitude of 7.8 occurred and it was the first time that a Menshin designed bridge experienced a major earthquake. This paper presents earthquake response characteristics of a Menshin designed bridge during the Kushiro-oki Earthquake. The analysis of acceleration records measured close to the On-netoh bridge and the simulation analysis using the measured record are made.

INTRODUCTION

The On-netoh bridge is now under construction on the national highway No.44 at Nemuro City in Hokkaido[1]. The Menshin design was adopted for the side-span of the On-netoh bridge. Since Hokkaido is located in the North of Japan and is in a cold district, one of the authors have been studied the temperature dependency of the horizontal stiffness of laminated rubber bearings through loading tests of full-size models. It was found that the stiffness of the isolation bearings have the relatively strong temperature dependency[2].

In January, 1993, the Kushiro-oki Earthquake with magnitude of 7.8 on the Richiter scale occurred approximately 100km from the On-netoh bridge as shown in Fig. 1. It was the first time that a major earthquake occurred near the Menshin designed bridge and also that it was at a low temperature condition. Although the strong motion observation was not

made for the On−netoh bridge, it was obtained at the existing bridge which is located less than 200m from the On−netoh bridge. Earthquake response characteristics of the On−netoh bridge is studied through the analysis of measured acceleration records and the simulation analysis of the On−netoh bridge.

ON−NETOH BRIDGE

The existing bridge was constructed in 1961 on National Highway No.44 at On−netoh in Nemuro, Hokkaido. **Fig. 2** shows the side view of the existing bridge. The bridge length is 96.95m long which consists of a steel Warren−type truss bridge with span length of 60m and a steel composite girder bridge with that of 35m. Width of the deck is 7.5m. Since the existing bridge becomes too old for use and the On−netoh bridge is now being constructed for the replacement of the existing bridge. **Fig. 3** shows the locations of two bridges.

Fig. 4 shows the On−netoh bridge which is constructed by the Hokkaido Development Bureau. Bridge length is 456m long and the bridge consists of 3 four−span continuous plate girder bridges with bridge length of 102.2m, 104.8m and 104.8m and Nielsen−type Lohse girder bridge with span length of 140m. The construction will be completed in 1995. The Menshin design using lead rubber bearings is employed for the side bridge at the Kushiro side. **Photo 1** shows the general view of the bridge. The site is in a cold region where the mean of the lowest temperature for the last 30 years at the site is −9.1℃. Therefore, it is a distinctive characteristics of the bridge that the Menshin design is adopted for a bridge in a cold district.

Rubber bearings are used for the both ends of the girder of the On−netoh bridge, i.e., at A1 abutment and P4 pier. Lead rubber bearings are used at Piers P1, P2 and P3. The stiffness of the bearings are designed so that the distribution ratio of the inertia force of a superstructure in the longitudinal direction be 5% for A1 and P4, and 30% for P1, P2 and P3. On the other hand, the stoppers to prevent displacement in the transverse direction are installed at all of the bearings. **Fig. 5** shows the bearings used for the bridge.

Fig. 6 shows a cross section of the strata of the construction site of the On−netoh bridge. It consists of sand (AS1), silt (AC), sand (AS2) and loam (Nm) layers. The loam layer which is selected as the supporting layer of the foundations is inclined with angle of about 10% from the Kushiro side to the central span. The supporting layer is located at 10m for A1 to 19m for P1 under the sea level.

The On−netoh bridge is designed according to the Design Specifications of Highway Bridges issued in 1980[3]. The seismic lateral force was not decreased considering the damping effects of the Menshin bearings. **Table 1** shows the natural periods of substructures and the corresponding seismic lateral force coefficients. **Table 2** shows the design conditions for the Menshin bearings. Menshin design was made according to Guidelines for base Isolation of Highway Bridges[4] and Manual for Menshin Design of

Highway Bridges[5].

Table 1 Natural Period and Lateral Force Coefficient

	Ground Condition	Natural Period (sec)	Lateral Force Coefficient (Kh)
A1	Type I	0.964	0.23
P1	Type II	0.970	0.25
P2	Type II	1.044	0.28
P3	Type II	1.062	0.28

Table 2 Design Conditions of Bearings

		RB	LRB
Maximum Vertical Reaction Force	R (tf)	50.0	135.0
Dead-Load Reaction Force	W (tf)	23.0	92.0
Live-Load Reaction Force	W (tf)	27.0	43.0
Design Displacement (Bearing Capacity Method, Type H Ground)	U_B (cm)		15.0
Equivalent Stiffness	K_B (kgf/cm)	615	2280
Equivalent Damping Ratio	h_{eq}		0.21

Note) RB and LRB represent rubber bearing and lead rubber bearing, respectively

EARTHQUAKE RESPONSE OF ON-NETOH BRIDGE DURING KUSHIRO-OKI EARTHQUAKE OF 1993

The Kushiro-oki Earthquake occurred at 8:06 PM, January 15, 1993. The earthquake was located in the center of eastern Hokkaido and affected over a wide area including Tohoku and Kanto regions. The earthquake registered magnitude of 7.8 on the Richiter scale and the epicenter was reported as approximately 30km off the south coast of Kushiro city at lat. 42° 51' N, long. 144° 23' E. Depth was 107km. A number of aftershocks with epicenters of over 90km deep occurred within one day after the main shock and a few occurred after two days.

Three SMAC-Q type strong motion seismographs are installed at the pier crest, abutment crest and ground surface near the abutment of the existing bridge. Strong motions were successively measured at three seismographs. Fig. 7 shows the measured acceleration records. Duration time is over 240 seconds. Table 3 shows the peak

acceleration measured at the ground surface and the abutment. Peak accelerations of the ground surface are 341.5cm/sec^2 in the longitudinal direction and 363.1cm/sec^2 in the transverse direction. The peak acceleration of UD component is 114.4cm/sec^2 which corresponds to about 33% of horizontal peak accelerations. Peak accelerations of the abutment in the longitudinal and transverse directions are about 425cm/sec^2 and 300cm/sec^2, respectively. **Fig. 8** shows acceleration response spectrum of the measured strong motion at the ground surface. The analysis was made for the main shaking of 40 seconds from the time of 90 second to 130 second. The predominant period of the response spectrum of horizontal components was found to be in the range of 0.5 to 4.0 second, which contains relatively long period components and the peak is around 0.8 second. The predominant period of UD component is less than 1 sec.

Table 3 Measured Peak Acceleration (cm/sec^2)

	LG	TR	UD
Ground	342	363	114
Abutment	425	300	–

Photo 2 shows the situation of the bearings of the On−netoh bridge after the earthquake. The rubbing between the sole plate of the bearing and the side stopper occurred and the coming off of the painting was found. According to the marks, peak relative displacement of the bearings is estimated as about 4 to 5cm. Larger displacement was found at Pier P4 than the other piers and abutment. No damage or mark were found at expansion joints or hand rails at A1 abutment side.

RESPONSE ANALYSIS OF THE ON−NETOH BRIDGE

Nonlinear time history response analysis for the On−netoh bridge was made. Direct integration method using Newmark β algorithm was used for the analysis. Reyleigh−type damping was assumed to represent the damping characteristics of the bridge. **Fig. 9** shows the analytical idealization of the On−netoh bridge. It was assumed that the piers be in the elastic range and that nonlinear effect of Menshin bearings be expressed as a bi−linear model.

The foundations of A1, P1～P3, which are the pile foundation, are modelled as a linear spring model. On the other hand, that of P4, which is a direct foundation, is assumed as fixed. The characteristics of the bearings used for the analysis are shown in **Table 4**. Although the mean and lowest temperature in the Nemuro region at the time of the earthquake were reported as −4.8℃ and −7.9℃, respectively, the stiffness of Menshin bearings at the temperature of 20℃ and −20℃ was assumed in this analysis. Stiffness of

the Menshin bearings at those temperature condition were computed based on the loading tests of bearings. Analysis was made for the longitudinal direction which corresponded to the direction of Menshin design. The strong motion data with duration time of 120 seconds between the time of 50 second to 170 second was used as an input ground motion.

Table 4 Characteristics of Bearings for Analysis

Bearings	Characteristics		20°	−20°
RB	Stiffness	K_{RB} (tf/m)	363.0	472.0
LRB	First Stiffness	K_1 (tf/m)	5188.0	8953.2
	Second Stiffness	K_2 (tf/m)	471.1	645.0
	Ratio of Stiffness	K_2/K_1	0.07212	0.07204
	Yield Displacement	δ (m)	0.01832	0.01244

Note) RB and LRB represent rubber bearing and lead rubber bearing, respectively

Fig. 10 shows the time histories of acceleration and displacement of deck and relative displacement of bearing at pier P2 when the temperature is assumed as −20℃. The responses of the deck were not elongated comparing with the ground motion because the stiffness of the bearings become relatively large in the cold district. Peak deck acceleration is computed as 505cm/sec^2. Amplification of the ground motion is estimated as 1.48. However, the response acceleration of the deck seems to be decreased during the time of 45 to 60 second when the excitation of the strong ground motion. The response of deck displacement and relative displacement of bearings are almost the same and the peak response occurred around the peak of the input ground motion. The residual displacement with about 2mm is found at the bearings.

Table 5 shows the computed peak bending moment at the bottom of piers. Although the peak bending moment at the bottom of pier P1 to P3 is in the range of 1,200 to 1,500tf·m when the temperature is assumed as 20℃, on the other hand, they become twice when the temperature is assumed as −20℃. However, those for Abutment A1 and Pier P4 do not change drastically depending on the temperature, because the variation of the stiffness of rubber bearings with temperature is relatively small. Comparing the bending moment of the piers between computed through the nonlinear analysis and designed, the computed bending moment is about twice the designed bending moment.

Relative displacement of bearings are also shown in Table 5. As mentioned before, the peak relative displacement was estimated as 4 to 5cm from the observation of the bridge after the Earthquake, however, that computed with assumption of temperature of −20℃ is about 8 to 9cm. Therefore, relative displacement of expansion joints is also estimated as 8 to 9cm. Design displacement according to seismic lateral force coefficient

method is 5.5 to 6.6cm. Based on the analysis, it is estimated that the inertia force beyond the design seismic lateral force acted to the piers. However, the actual bridge response is much smaller than the computed one.

Table 5 Computed Peak Response

	Peak Bending Moment at the Base of Pier (tfm)			Peak Relative Displacement of Bearing (cm)
	20°	−20°	design value	−20
A1	485.7	475.8		
P1	1175.6	2227.5	806.0	9.0
P2	1295.2	2464.8	1053.0	8.6
P3	1528.1	2733.9	1203.0	8.0
P4	58488	60157	19129	

CONCLUSIONS

The On−netoh bridge, which employs the Menshin design in the cold and snowy district at Nemuro, Hokkaido, experienced the Kushiro−oki Earthquake of 1993. The peak acceleration measured on the ground surface is over 350cm/sec^2. The analytical simulation using the measured ground motion shows that the bending moment at the bottom of pier is estimated to be over the designed one. The effect of the earthquake may be small and the seismic isolation may be successively functioned.

REFERENCES

1) Ikeda, H., Matsumoto, N. and Fukuda, K. : Design Plan of On−netoh Bridge − Design of the Bridge with Menshin Devices −, Bridges and Foundations, Vol. 90−5, 1990
2) Nakano, O., Taniguchi, H. and Nishi, H. : Effect of Temperature on the Dynamic Behavior of Base−Isolated Bearings, Proceedings of the 24th Joint Meeting, Wind and Seismic Effects, UJNR, Gaithersburg, May, 1991
3) Japan Road Association : Part V, Seismic Design of Design Specifications of Highway bridges, 1990
4) Technology Research Center for National Land Development : Guidelines for Base Isolation of Highway Bridges, 1989
5) Public Works Research Institute : Development of Menshin Design of Highway Bridges, October 1992, Technical Note of Public Works Research Institute, Vol. 60

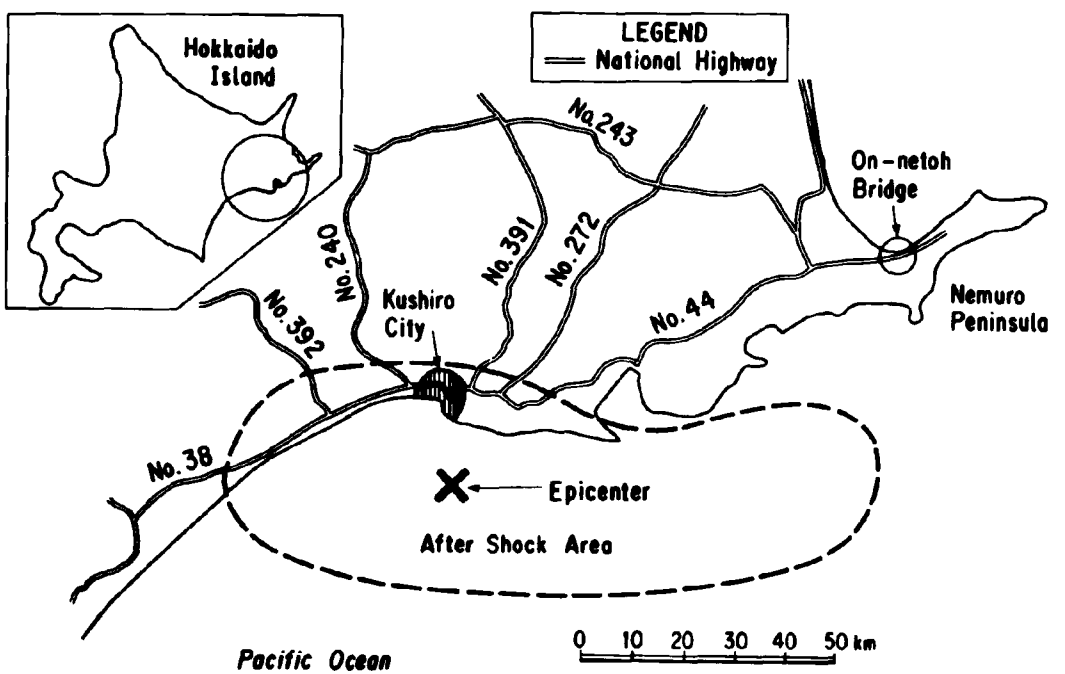

Fig. 1 Locations of the On-netoh Bridge and the Earthquake Epicenter

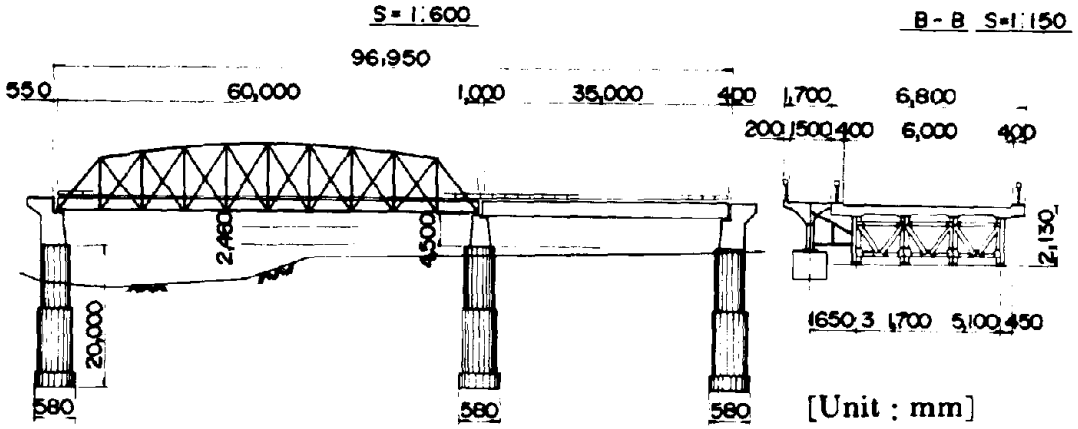

Fig. 2 Side View of the Existing Bridge

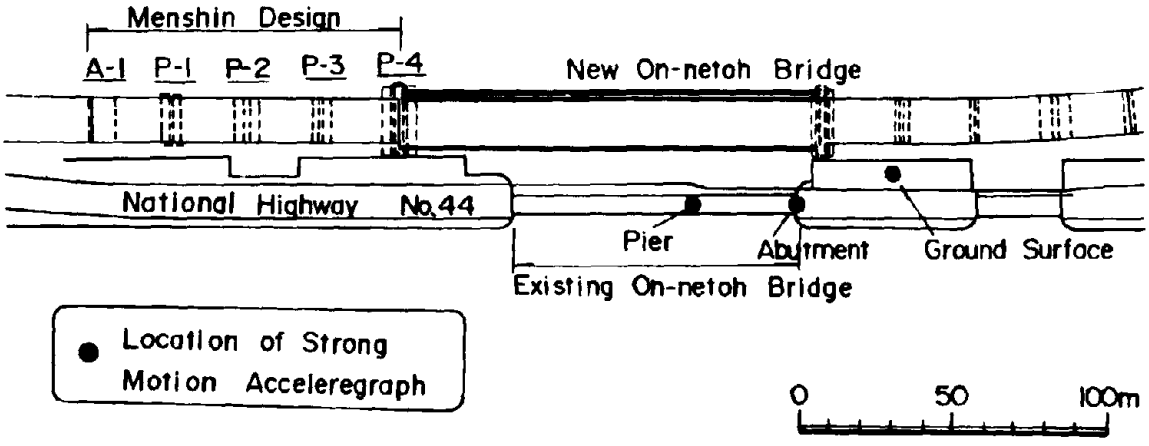

Fig. 3 Locations of two Bridges

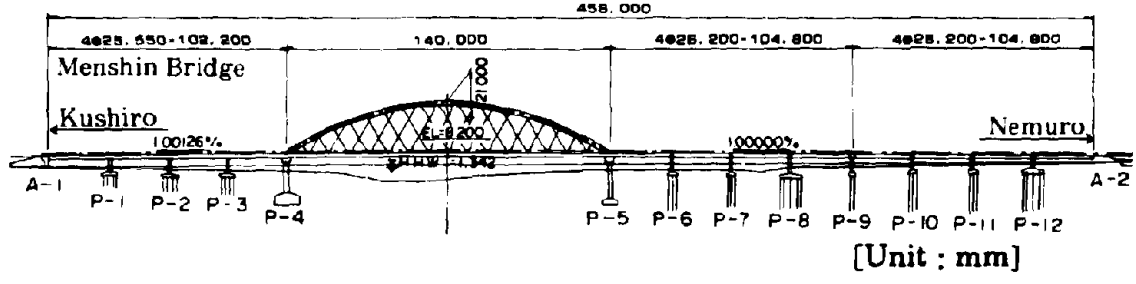

Fig. 4 Side View of the On−netoh Bridge

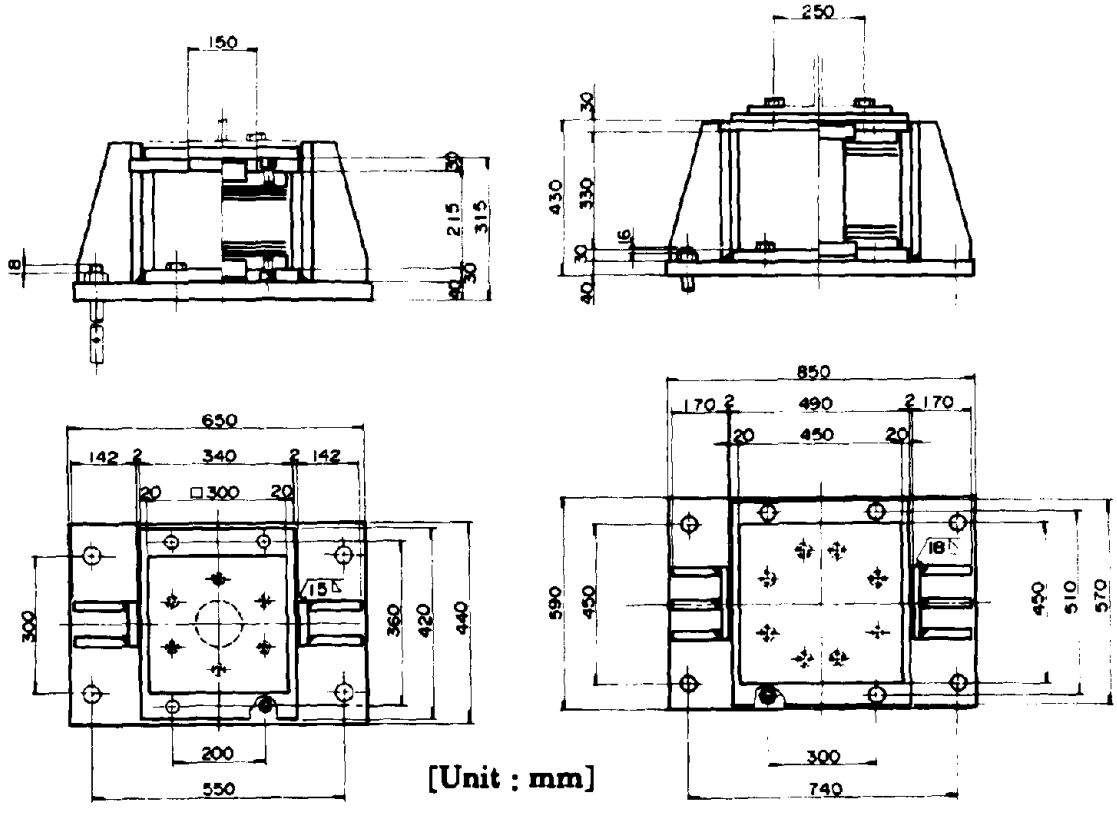

Fig. 5 Bearings used for the On−netoh Bridge

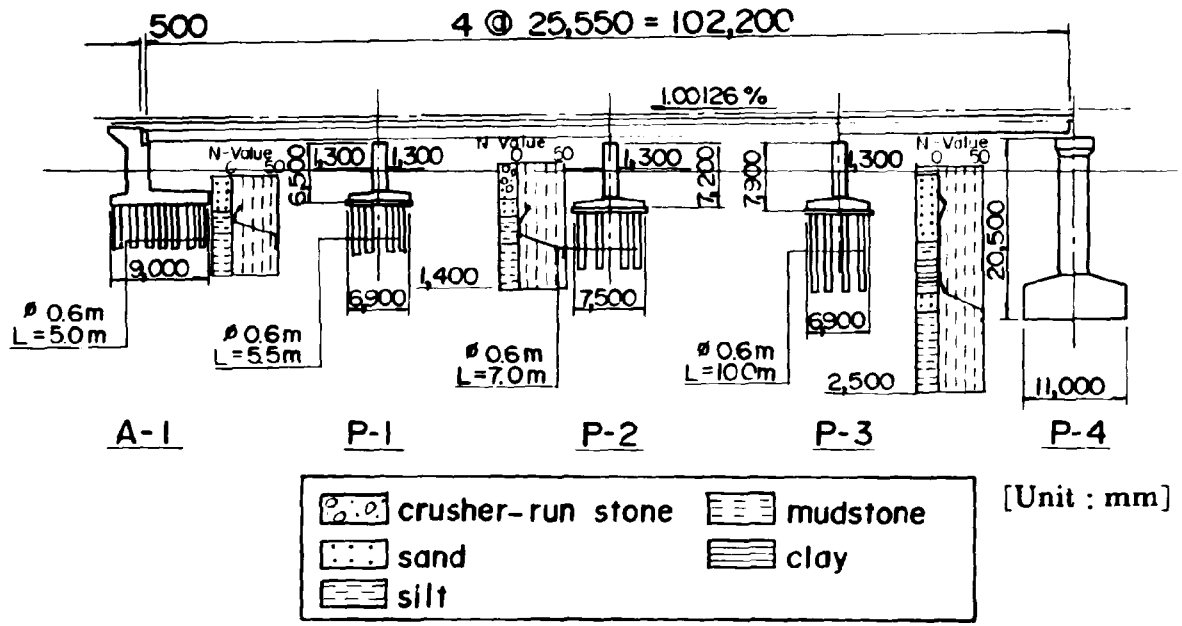

Fig. 6 Ground Condition of the On-netoh Bridge

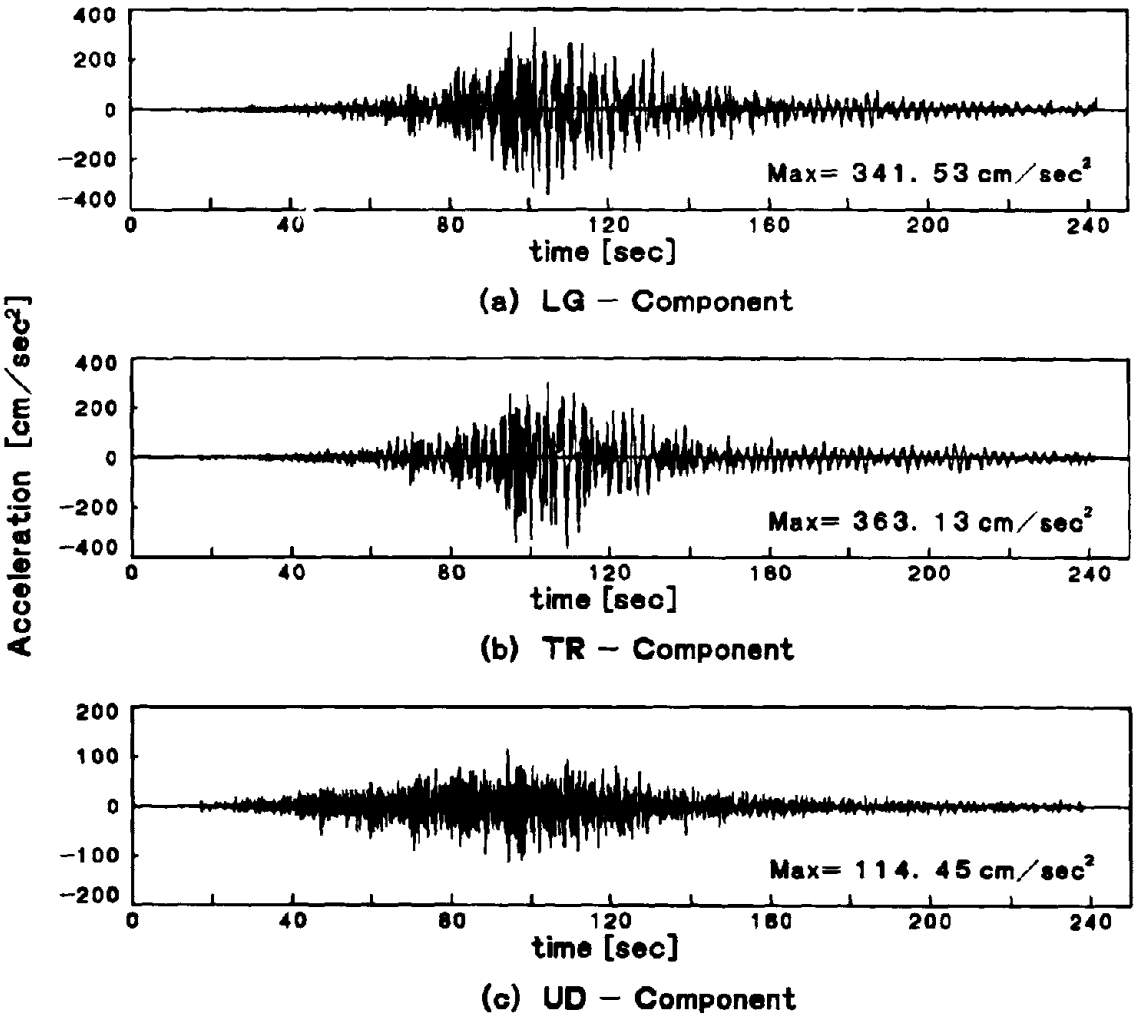

Fig. 7 Strong Motion Record on the Ground Surface

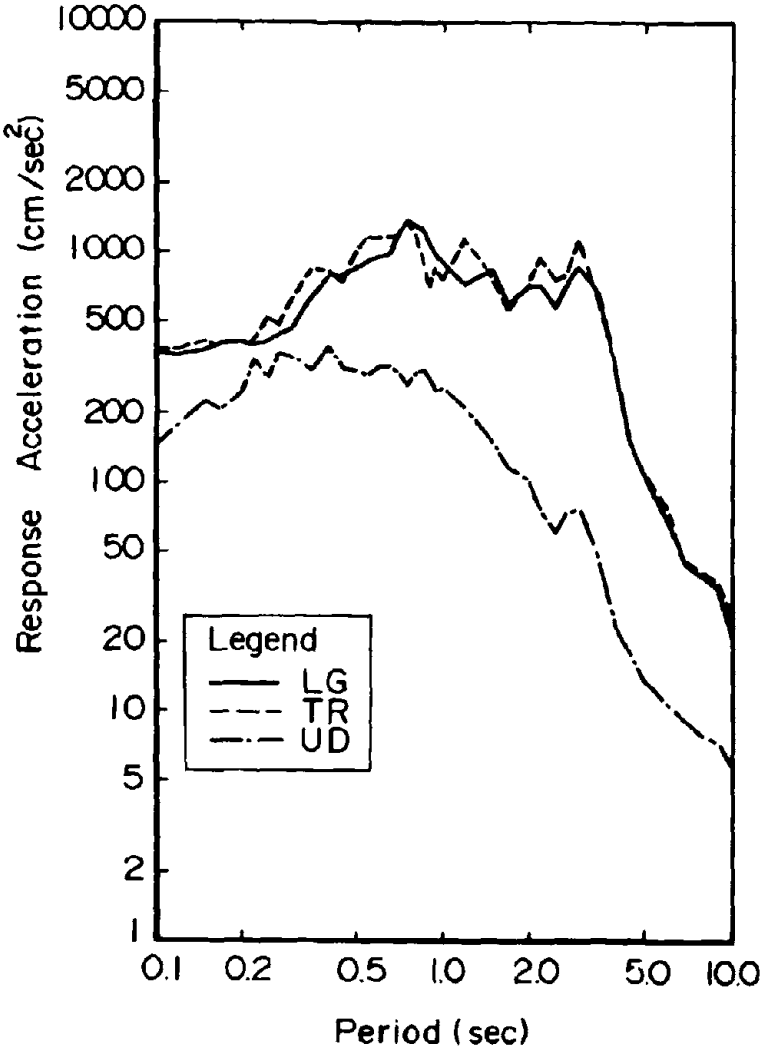

Fig. 8 Acceleration Response Spectrum

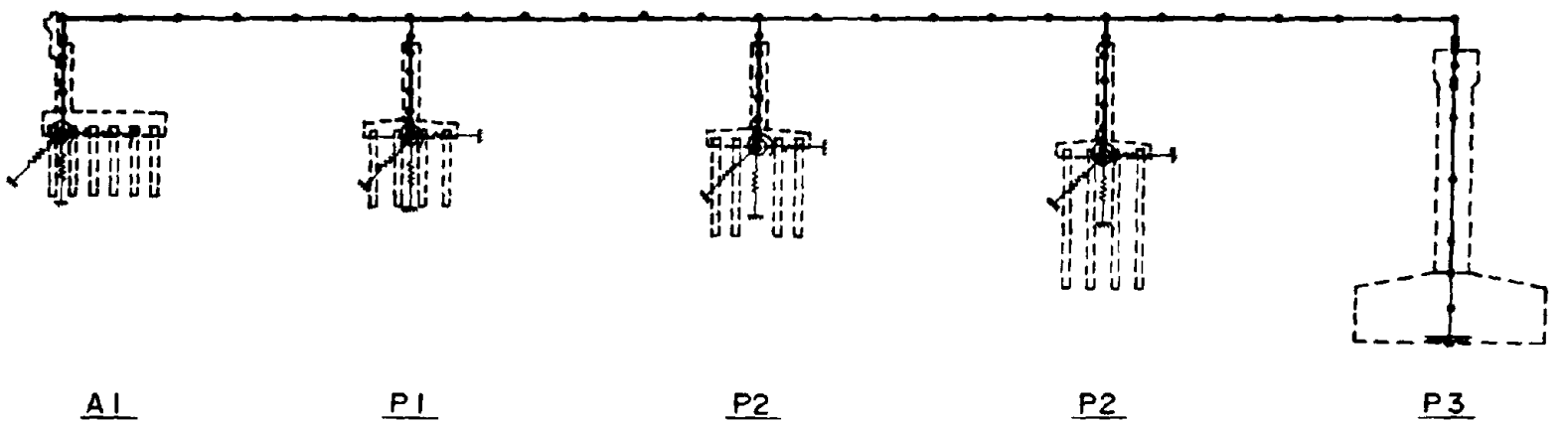

Fig. 9 Analytical Idealization

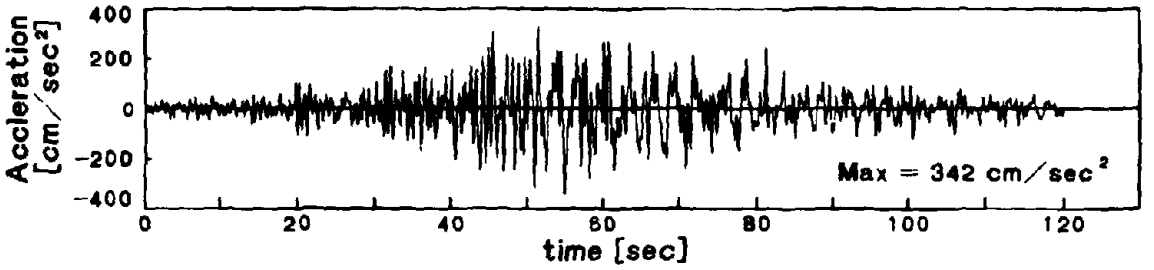

(a) Input Ground Motion

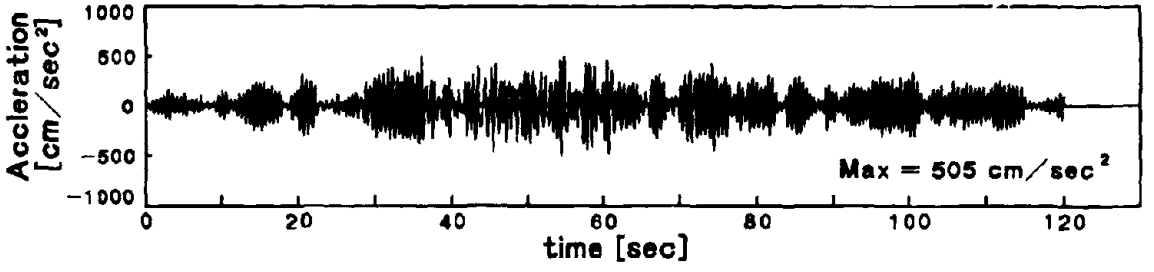

(b) Response Acceleration of Deck

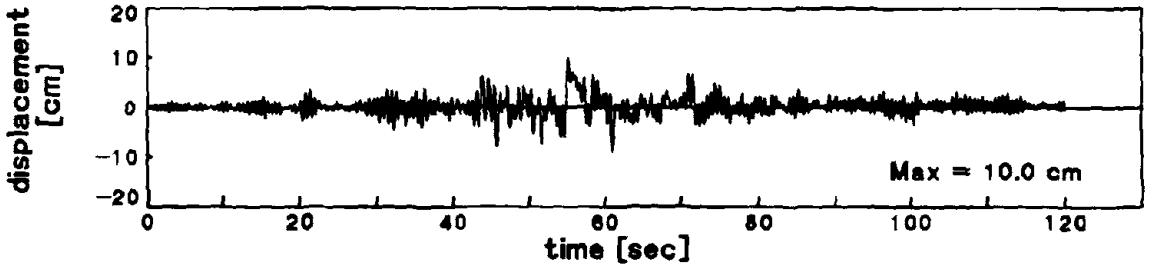

(c) Displacement of Deck

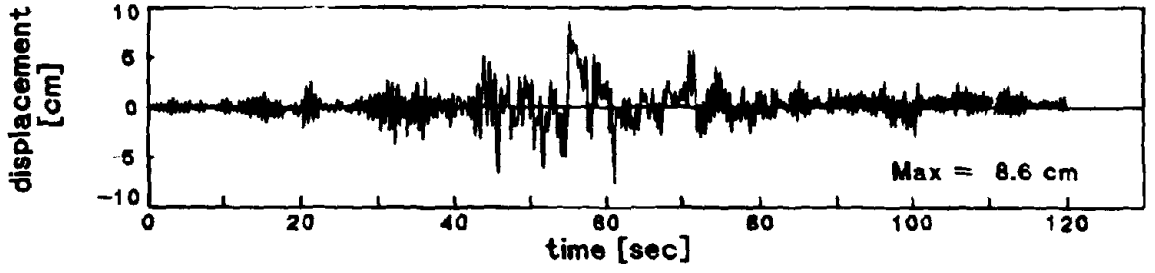

(d) Relative Displacement of Lead Rubber Bearing

Fig. 16 Time Histories computed by Simulation Analysis

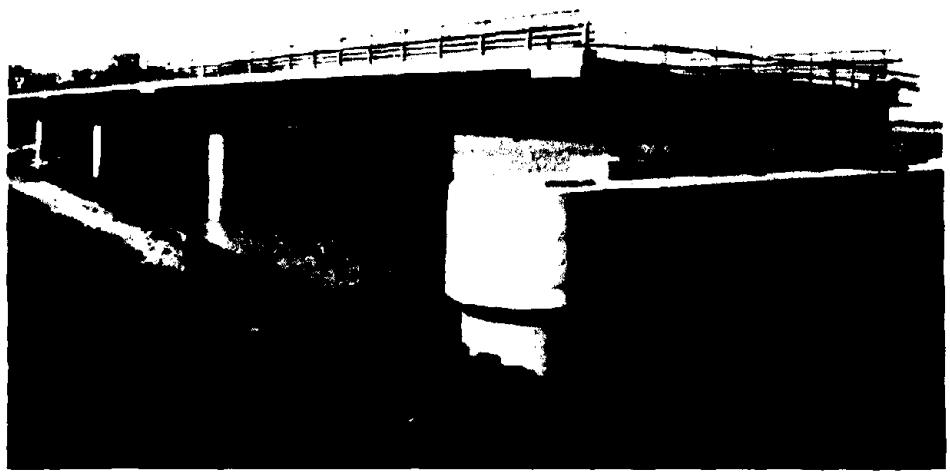

Photo 1 On–netoh Bridge

(a) A1 (RB)

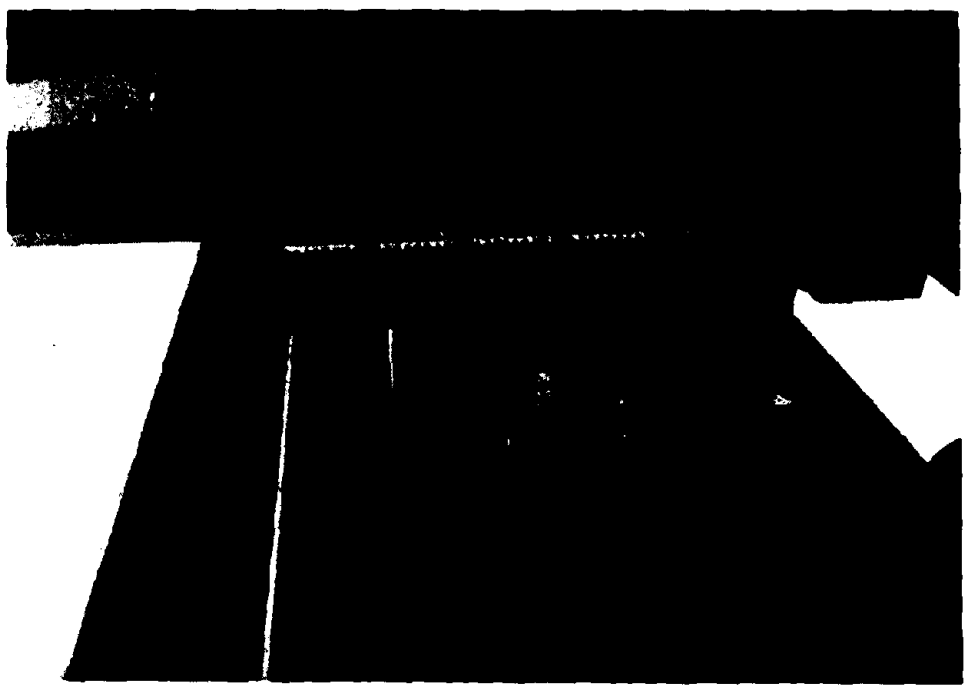

(b) P2 (LRB)

Photo 2 Bearings after the Earthquake

Caltrans/FHWA Program for Performance Testing of Seismic Isolation and Energy Dissipation Systems

By

MOHSEN SULTAN and LI-HONG SHENG

CALIFORNIA DEPARTMENT OF TRANSPORTATION
Division of Structures
Office of Earthquake Engineering

Introduction

The California Department of Transportation (Caltrans) was the first U.S. Transportation agency to use seismic isolation on a bridge at the Sierra Point O.C. in 1985. Since then, two other bridges were retrofitted using isolation devices. In addition, the current construction of a new 680/24 Interchange project includes a temporary bridge (Br. #28-312K) which has been isolated. All four bridges used the lead core rubber bearing.

Caltrans is interested in opening the market to different manufacturers that offer a variety of systems, including elasto-plastic devices, elastomeric, visco-elastic and sliding systems among others. There are certain advantages to each system, however, the performance of any device depends greatly on the quality control used by the manufacturers and proper design of all components. Due to the lack of an industry that brings those suppliers together, there has been no uniformity of design standards, performance criteria or even an agreement on prototype testing. Caltrans experience has shown that generic specification is not an appropriate tool in this particular case. Rather, a listing of pre-approved systems may save a lot of unnecessary complications at the quality assurance stages. Such specification system has been used by public agencies on machinery, equipment and earth retaining systems.

National Cooperative Program

In cooperation with the Federal Highway Administration (FHWA), Caltrans is launching a full-scale dynamic shake table testing program. This work will be a cooperative effort with several states, industry and academia. All promising systems' manufacturers

will be given the opportunity to participate. Seismic evaluation will be conducted at different earthquake levels to establish behavior and performance characteristics applicable to different seismic regions. Experience learned under this program can be used on future applications using isolation and/or energy dissipation devices, both in California and nationwide.

Testing Plan

Several systems have undergone static and dynamic testing. Often, however, the testing consisted of static actuator tests or reduced scale shake table tests. Certain characteristics can be correlated from static to dynamic behavior. Nevertheless, a full-scale dynamic shake table test is the only test of the true behavior of a system under an earthquake.

The problem in the past has been that, in order to operate a full-scale shake table test, one would require a major source of energy, which is not available to most laboratories in the U.S.A. Other countries, such as Italy and Japan, have such capabilities and thus were able to develop a higher confidence level, which resulted in many more applications than in the U.S.A.

Caltrans is considering several possible testing facilities to perform all, or part, of the testing program. We have identified the laboratories of the Energy Technology Engineering Center (ETEC), as having the necessary capabilities to perform the proposed testing. The facilities at ETEC do provide us with the option to test systems full-scale, at dynamic speeds. ETEC is owned by the Department of Energy and operated by the Rocketdyne Division, a subsidiary of Rockwell International. Another facility we are considering is the Colorado Shake Facility, of the Rail Dynamics Laboratory. This facility is affiliated with AAR. Also under consideration, are laboratories operated by academic institutions across the nation.

The program calls for inviting the manufacturers of different systems (isolators and energy dissipaters) to participate in a testing program designed and supervised by Caltrans. The purpose is to evaluate the various systems and their dynamic performance, which accounts for the quality of workmanship, not just theoretical dynamic behavior, and to re-write the specifications that would list pre-approved systems and testing requirements unique to each system. Evaluation will be conducted at different earthquake levels

to establish behavior and performance characteristics applicable to different seismic regions. In addition, experience learned by Caltrans under this program can be used on future applications using isolation and/or energy dissipation devices, both in California and nationwide.

Attached is a preliminary testing plan, that will be used as a guide for the evaluation process.

Evaluation Process

In accordance with guidelines for the implementation of the Applied Research and Technology (ART) program, a federal grant program under section 6005 of ISTEA, the proposed program will utilize the "HITEC" process. HITEC stands for "Highway Innovative Technology Evaluation Center". It is a non-profit organization established under an agreement between the FHWA and the Civil Engineering Research Foundation (CERF), a subsidiary of ASCE. The mission of HITEC is to evaluate new products, materials, and equipment, for which industry standards or specifications do not exist, and to work towards overcoming barriers to innovation. In fulfilling its mission, HITEC will facilitate the conduct of national, consensus based, evaluations utilizing public highway agencies and other organizations. HITEC came into existence in 1989, but will officially function beginning January 1994.

The evaluation process, HITEC established, includes several steps, which will be used in our program. The following description summarizes some of the key steps. The process starts with inviting applications from companies that meet "Eligibility Criteria", reviewing those applications, assembling review teams, developing and executing an action plan. The review team or panel will have approximately 10 members, guided by a chairperson appointed by HITEC. The panel will consist of multi-disciplinary volunteer experts, which generally include several state DOT representatives, a university researcher, a county employee, FHWA, HITEC, and private business representatives. All panel members must be independent, unbiased and objective in their evaluation. Technical consultants, as well as administrative support, will be provided to the panel through contracting means.

Program Financing

In general, product manufacturers would be responsible for the payment of testing charges incurred by the testing facility. Federal financial assistance may be available under the ART program. Additional funding for the project is necessary to fund expenses incurred by Caltrans personnel supervising the work and for needed equipment to monitor testing as well as future systems' performance. Expenses would cover engineering time, related overhead, some preliminary testing and travel expense. Such funding will be jointly financed by Caltrans and the FHWA.

Duration of Program

Once contractual arrangements are finalized, we expect that testing would take approximately 6-9 months. Additional time may be needed if participation from industry is high.

Program Impacts

This testing program is expected to have a major impact on the use of isolation systems nationwide. Several states are just beginning to retrofit structures against seismic forces and isolation devices may very well be seriously considered. Usually states, which do not have the earthquake engineering experience, rely heavily on Caltrans' experience. Also, the NIST is in the process of developing "Guidelines for prototype testing of seismic isolation systems" and related "Performance Criteria". We feel that the proposed Caltrans program would provide an invaluable hands-on resource and useful data that would help the NIST committee develop guidelines based on true experience with all different systems: elastomeric, sliding and hybrid.

FHWA/HITEC Participation and National Benefits

Caltrans welcomes the support of the FHWA and their encouragement to carry out this program in partnership with others under the auspices of "HITEC". We believe that many benefits will be realized through such cooperative effort, including:

1 - Industry will have greater participation role and will be able to justify their share of the cost, since testing will have national application. In other words, they will save

money, not only on testing, but also on the expensive, and sometimes prohibitive, marketing effort.

2 - Review and specifications writing time, by public agencies, will be drastically reduced and will save the nation millions of dollars in engineering review time.

3 - Better understanding of the various systems' performance and limitations will be identified. Therefore, larger applications should result, on both retrofit and new construction projects, once confidence levels in the systems are established.

4 - It is a healthy partnering effort which satisfies provisions of ISTEA.

Acknowledgment

The authors wish to aknowledge Mr. Roland Nimis, regional structural engineer and acting Director of Engineering (Region 9), Mr. James Cooper, Chief of Structures Division (HNR-10) and Ms. Nancy McMullin Bobb, Division Bridge Engineer, all from the FHWA, for their contributions to the subject program and for their continued encouragement and support of the Caltrans effort. We also wish to aknowledge Mr. Peter Kissinger, Director of HITEC, for his efforts organizing the many administrative and logistical aspects of the evaluation process. The Caltrans plan could not have resulted into a national program without the support of those recognized herein and many others that worked tirelessly towards a common goal.

Appendix

Caltrans' Base Isolator Pre-Qualification Test Plan

Revised: January 19, 1994

Definition of Base Isolator

Any bearing device which isolate superstructure from the sub-structure and lengthen fundamental structural vibration period. This device can have an internal or external component to improve its damping factor, which means it can be a rubber or neoprene, or rubber or neoprene with lead core, or rubber or neoprene with other high damping material in its core, or rubber or neoprene with external damping device, or friction type device, or friction type device with internal or external damping device, or other approved bearing device with internal or external damping device. In general, they can be classified into four different group:

1. Displacement dependent
2. Velocity dependent
3. Friction dependent
4. Hybrid

Performance test

An isolation bearing will be tested for its performance if the material or bearing type matched described purposes.

1. Material tests:
These tests are used to ensure the quality control of said device used in a bridge project. The effect of the following factors will be tested, as required:

1.1 Temperature
1.2 UV resistance
1.3 Moisture
1.4 Fatigue
1.5 Corrosion resistance
1.6 Friction deterioration
1.7 Ozone resistance

2. Static or Pseudo-Dynamic test
To ensure the performance of isolator's characteristic and reliability.

2.1 Equivalent stiffness and damping test under service load:

Purpose:
To ensure the equivalent stiffness and damping factor used during the design process.

Procedure: Ten fully reversed cycles of maximum live load displacement. Test should be performed in three stages. Test the first 10 cycles under the design dead load. The next 10 cycles should be tested under DL+ half of maximum LL reaction. The last ten cycles should be tested under DL+LL. All tests should use the structure fundamental period under LL. The performance of the last 7 cycles of every stage will be used to determine the equivalent stiffness, damping, and friction coefficient. No parts of the tested device should suffer permanent deformation. For non-circular device, test will be performed at 0, 22.5, 45, 67.5, 90 degrees.

2.2 Equivalent stiffness and damping test under maximum design displacement:

Purpose: To ensure the equivalent stiffness and damping factor used during the design process.

Procedure: Ten fully reversed cycles of maximum design displacement. Test should be performed in three stages. Test the first 10 cycles under the design dead load. The next 10 cycles should be tested under DL+ half of maximum LL reaction. The last ten cycles should be tested under DL+LL. All tests should use the structure fundamental period under design earthquake load. The performance of the last 7 cycles of every stage will be used to determine the equivalent stiffness, damping, and friction coefficient. For non-circular device, test will be performed at 0, 22.5, 45, 67.5, 90 degrees. Sacrificial parts are allowed to be replaced between testing stages.

2.3 Survival serviceability test:

Purpose: To ensure the isolation device can servive a number of strong motion cycles.

Procedure: 50 fully reversed cycles of maximum design displacement at design vibration period. No loss of service form this device is allowed.

2.4 Residual displacement test:

Purpose: To identify the restoring capability of isolator.

Procedure: Force bearing to displace at design LL movement rating under DL+ LL and hold in position for a minimum of 5 seconds. Promptly release and measure the displacement after 5 seconds. Repeat this test with full design displacement.

2.5 Displacement stability test:

Purpose: To satisfy the static stability of rubber or neoprene based device or other device which might loss support and cause stability problem.

Procedure: 10 fully reversed cycles of 150% design displacement at 0.5 Hz.

or

Purpose: To satisfy the displacement uncertainty from MCE.

Procedure: 5 fully reversed cycles of 200% design displacement at 0.5 Hz.

2.6 Velocity dependent test.

Purpose: To ensure isolator performance based on velocity variation.

Procedure: 10 fully reversed cycles of 100% design displacement at 0.2 Hz, 0.5 Hz, 1 Hz, and 2 Hz.

2.7 Temperature dependent test:

Purpose: To ensure isolator performance based on temperature variation.

Procedure: 10 fully reversed cycles of 100% design displacement at 40, 75, 105 degrees F. of 0.5 Hz.

3. Dynamic Test:

All dynamic tests will be subject to 8 different time histories. Six of these time histories are recorded strong ground motion, whereas, the other two are simulated time histories. They are:

a. 1940 El Centro
b. 1952 Taft
c. 1985 Mexico City (Mexico City)
d. 1989 Loma Prieta (Oakland Wharf)
e. 1971 San Fernando (Pacoma Dam)
f. 1964 Alaska
g. Seed 8+
h. To be determined

This will be a shaking table test. A simple bridge span will be supported by 4 isolators on two bridge piers. Because the difference in these two pier stiffnesses, the isolators must be designed for the structure layout to satisfy a performance requirement defined in advance. The design approach will be the one used by the manufacturer. All manufacturers must submit the anticipated performance before experiments begin. Test will begin at .2g for each time history with .2g increment until system response reach design displacement or 1.0g are reached.

3.1 Longitudinal test

Purpose: To verify isolator dynamic performance for uniform motion.

3.2 Transverse test:

Purpose: To verify isolator dynamic performance for non-uniform motion caused by different from the sub-structure.

3.3 Arbitrary attack angle test:

Purpose: To verify isolator dynamic performance for non-uniform motion such as torsion of the deck and different bearing stiffness for biaxial motion.

Procedure: Dynamic load will be introduced from 22.5, 45, and 67.5 degrees.

3.4 Longitudinal harmonic test:

Purpose: To verify isolator dynamic performance under a harmonic motion. Consequently compare with pseudo-dynamic result.

Procedure: Structure will be tested with design LL.

3.5 Arbitrary skew test:

Purpose: To verify isolator dynamic performance for skewed structure for potential biaxial motion.

Procedure: Skew angle will be introduced at both ends from 0, 22.5, and 45 degrees. Configuration of skew ends will be determined later.

3.6 Survivability test (Shake down test)

Purpose: To test isolators if they can survive after a design earthquake with two aftershocks.

Procedure: Test structure with design earthquake with two aftershocks which are 80% and 60% intensitives to the main shock. Setup configuration and earthquake will be determined later.

SEISMIC RESPONSE CHARACTERISTICS OF THE HOKUMEI-BRIDGE USING RUBBER BEARINGS

Sachio Kawamura
Sapporo Construction Bureau, Japan Highway Public Corporation,
Japan

Yuji Tarumi
Research and Engineering Dept., Japan Highway Public Corporation,
Japan

Akihide Kubo
Research and Engineering Dept., P.S. Corporation,
Japan

ABSTRACT

This paper describes the seismic response characteristics of the Hokumei Bridge using laminated rubber bearings. The bridge is a prestressed concrete bridge with 11 continuous spans, and it has the most spans in Japan. The expected effects of laminated rubber bearings are (1) suitable distribution of seismic response shear force to piers, and (2) reducing seismic response accompanied by long natural periods. Vibration tests on the bridge were carried out in July, 1992.
The Hokumei Bridge suffered some damage during the Kushiro Earthquake in January, 1993, it had been completed and was waiting for the completion of connective roads. The natural period of the bridge is prolonged between 1.359 to 1.628 sec by using rubber bearings. The girder of the bridge had a joint-clearance of 70mm from an abutment, and was in the process of concrete dry-shrinkage. The girder pushed up the finger-joint, and the parapet of the abutment cracked at its neck during the earthquake. The magnitude of the earthquake was greater than the seismic design load. This paper reports the damage to the bridge during the earthquake, and describes some results from computer simulation of the damage to the bridge too. The location of the bridge is shown in the Hokkaido Map as Fig.1. The view of the Hokumei Bridge from the A2 abutment is shown in Photo.1.

INTRODUCTION

Recently, rubber bearings are often used for large scale bridge structures for the following reasons:

1) Rubber bearings are economical, and the cost is about half the price of Steel bearings.
2) The shock-absorbing capacity of rubber bearings against to a seismic load is better than steel bearings.

However, enough studies on seismic response characteristics of a bridge using rubber bearings have not been done. Therefore, Japan Highway Public Corporation started to do

vibration tests on the Hokumei Bridge.

The Hokumei Bridge is 304m long with 11 continuous spans, and it has the most spans in Japan. The mean span is 27.5 m long. The pier height is 24.0 to 27.0 m. The girder weight is 6,000 tons and it is almost a straight bridge. The laminated rubber bearings used in the bridge are the ordinary rectangular type. Vibration tests on the bridge were carried out in July, 1992. In the vibration test, a free vibration was made in the longitudinal direction and observed.

A vibration test on the Ishikari River Bridge was carried out in May, 1989. The results of the vibration test were compared. The Ishikari River Bridge is 544m long with 8 continuous spans, and it is the largest structure of these prestressed concrete bridges in Japan. The girder weight is 12,000 tons. The bearings are round type laminated rubber bearings reinforced by steel-rings. And the vibration tests were performed using an abutment and piers as a reaction-object in the longitudinal and transverse directions. Then, pier vibration tests were performed on each of the seven piers, using the girder as a reaction-object. Pier vibration tests on three piers had also been performed independently during the construction.

These bridges were designed to be economical comparing with a total construction cost. The expected effects of the laminated rubber bearing were (1) suitable distribution of earthquake response shear force to piers, and (2) reducing seismic response with prolonged natural periods. The results of the vibration test on the Hokumei bridge are discussed, below.

Design Condition

Road Name	Hokkaido Odan Highway (A highway crossing Hokkaido)
Grade	Highway,Rank 2-B according to the Japan Road Standard
Length	302.4 m
Width	10.0 m
Girder Type	Prestressed concrete girder with 11 continuous spans, hollow slab type
Class of Loading	TL-20,TT-43
Seismic Load	Kh=0.23
Foundations	Pier :Spread foundation Abutment :Pile foundation built at execution site

Design of the rubber bearings

The slide-rubber combination bearings were used on A1 and A2 abutments to prevent seismic horizontal force being distributed to the abutments. The bearings used on piers are the ordinary laminated rubber bearings of a rectangular type with rubber layers and steel-plates. Four rubber bearings are used on one pier. The size of a rectangular type rubber bearing is "700mm × 700mm", the thickness of a rubber bearing is about 180mm, and the total thickness of rubber layers is about 100mm to 150mm. The rubber type is CR. Before setting laminated rubber bearings on each pier, static lateral shear tests were carried out under an axial loading.

In the determination of the thickness of rubber bearings, the suitable distribution of seismic

response shear force to each pier was considered. The bearings need to be deformed according to the girder deformation by temperature or wheel loads. The bearings also need to be deformed according to the dry-shrinkage of the prestressed concrete girder. During the construction of the Hokumei Bridge, the deformation of rubber bearings grown by the concrete dry-shrinkage of the girder was sometimes released by jacking the girder up over the pier. When the Kushiro earthquake damaged the bridge, the dry-shrinkage of the prestressed concrete girder was still progressing. The thickness of rubber bearings were decided upon mainly by considering the dry-shrinkage of the girder predicted to be grown after the last releasing. The rubber bearings were not connected into the girder or piers by any bolts. All shear force loaded between the girder and piers should be transmitted by the friction between the rubber bearing surface and the girder or pier. The coefficient of friction was assumed to be 0.3. The safety factor of the friction was adapted of 1.0. The size of the rubber bearings used for the bridge are shown in Table.1. The rubber bearing is shown in Fig.2. The characteristics of the rubber bearings are as follows;

Maximum allowable compression stress : σ max=80.0 kgf/cm^2
Minimum allowable compression stress : σ min=15.0 kgf/cm^2
Static elastic shear modulus : G0 =8.0 kgf/cm^2
Ratio of allowable elastic shear deformation :
Under ordinary loads 70%
Under an earthquake 150%

Deformation releasing on the rubber bearings

A prestressed concrete girder will be shortened due to concrete dry-shrinkage, this may be a problem for a long prestressed concrete bridge like the Hokumei Bridge. The bearings used for the bridge need to be deformed according with the dry-shrinkage of the girder. During the construction of the bridge, the deformation on the rubber bearing grown by the dry-shrinkage was sometimes released by jacking the girder up over the pier. For the jacking-up, the rubber bearing does not have any bolts to connect into the girder or pier. All shear force loading between the girder and a pier should be transmitted by friction through the bearings. In jacking up, every rubber bearing was always raised over the pier together with the girder. In the jacking up, four jacks were used and the total jacking force was observed about 550tf on one pier. The vertical dead load was about 150 tf on one bearing. Then, the jacking force of inner side two jacks were observed as 70% less than of outside two jacks. On the observation, the vertical load of a bearing may be different dependent on it's position.

VIBRATION TEST

Testing methods

The jacking force for a vibration test was loaded using two jacks. The jack has a capacity of 180 tf and instantaneous release mechanism for oil pressure. Testing procedure was as follows; The girder was first pushed in the longitudinal direction, then jacking force was released and a free vibration followed. During the pushing, deformations were measured at 100tf, 200tf and 300tf. In a vibration, the relative displacements between the girder and piers

or abutments were observed by deformation-meters, and the accelerations on the girder and piers were observed by accelerometers. The arrangement of measuring machines during the vibration tests is shown in Fig.3.

Results

Damping ratio

Damping ratio was analyzed by the following equation using a deformation record observed in the vibration test. In the equation below (1), the a1 or the a2 is an amplitude as a cross line within envelope curves covering a deformation record. The a1 and the a2 are separated with the 1.18 seconds as it is natural period from each another.

(1) $h = (1/2\pi)\log(a2/a1)$

The analyzed damping ratio on the Hokumei Bridge was about 0.06 to 0.07. The deformation records observed in the first try in the vibration tests are as shown in Fig.4. The damping ratio analyzed using the deformation records observed at the A1 abutment is as shown in Fig.5, and, the damping ratio of Ishikari River Bridge was about 0.05 to 0.06.

Nonlinear characteristics of rubber bearings

The frequency analyzed using initial 2048 acceleration data was 0.879 Hz, meanwhile, the one analyzed using last 2048 data was 1.074 Hz, and different from the former in every acceleration record. The spectrum interval was 0.09766Hz. This phenomenon is considered with an effect by a nonlinear characteristic of the rubber bearings within a small amplitude area. The frequency was analyzed by the FFT method.

As an additional matter, slide-rubber bearings on the A1 and the A2 abutments had faults on their slide mechanism during the vibration tests. Therefore, the bearings at the A1 and the A2 abutments were regarded as rubber bearings in the analysis. After the vibration tests, those bearings had recovered their slide-rubber mechanism. The power spectrums analyzed using 2048 acceleration data observed on the girder at P5 is shown in Fig.6. The Power Spectrums may show a transformation of the dominant frequency according to the amplitude.

Dynamic shear springs of rubber bearings

The dynamic shear springs of the bearings were analyzed by the following procedure.

1) The lateral shear springs of the rubber bearings were first assumed from the results of static shear tests. And the stiffness of the piers were assumed from the design specification. The ground foundations were rigid enough and so the ground conditions in the simulation model are assumed to be rigid.

2) The dynamic shear springs of bearings and the rigidity of the piers as assumed in above 1) were modified according to the results of the static loading tests in the execution site. In the static loading tests, deformations were measured at jacking forces of 100tf, 200tf and 300tf.

3) The dynamic shear springs of the rubber bearings and the rigidity of the piers assumed in 2) were input into the equation of the Hokumei Bridge model. The natural periods of the

bridge were calculated using the modal analysis. If calculated natural periods agree with those observed in the vibration test, the input shear springs and the input rigidity are considered to be actual dynamic shear springs and stiffness. The load-deformation relation of a rubber bearing under axial loading is shown in Fig.7

The dynamic shear springs of the rubber bearings in the small amplitude area were analyzed in the above manner. Those analyzed dynamic shear springs corresponded to the design springs multiplied by 1.7 to 1.8. The value as 1.7 to 1.8 was a mean magnification of all bearings too, because initial deformations in each bearings were different. Also, the maximum deformation measured in the vibration tests was 23mm, and then the shear strain of the rubber bearing was about 15%.

RESPONSE ANALYSIS ON A BRIDGE USING RUBBER BEARINGS

The static analysis under an equivalent seismic load is a straight forward method. The dynamic response analysis using a hysteresis rule may be able to simulate the performances of a bridge using rubber bearings. Also the response spectrum method is often used. The response of five cases were simulated using above three methods. The Hokumei Bridge simulation model for these analyses is shown in Fig.8. The parameters used in this model are shown in Table.2. The 5% was used as a damping factor. The oscillated hysteresis calculated by the above ④ method is shown in Fig.9. Response displacements on the girder and the piers, and response shear forces of the rubber bearings are shown in Table.3. And five cases are as follows;

① Static analysis under equivalent earthquake load (HOKUS4)
② Response spectrum method by the design shear springs (HOKUA4)
③ Response spectrum method by the shear springs in the small amplitude area(HOKUA41)
④ Dynamic response analysis using a hysteresis rule (HOKUN42)
⑤ Dynamic response analysis using design shear springs (HOKUN5)

Dynamic Response Analysis using a hysteresis rule

The laminated rubber bearings had nonlinear characteristics within the small amplitude area. The shear spring within the small amplitude area corresponded to the static design shear spring multiplied by 1.7 to 1.8. So, the dynamic response analysis using a hysteresis rule, i.e. the backbone curve with two rigidities and the response point always moves on the backbone curve, was carried out. The hysteresis rule to be used in these analyses was based on the load-deformation relation observed in the static shear tests. The rubber bearings in this model did not have any hysteresis damping. A damping matrix (C) was assumed to be proportional to the instantaneous stiffness matrix, and to be equal to the instantaneous stiffness matrix multiplied by β. While, the instantaneous stiffness matrix(Kt) is equal to the initial stiffness matrix(K0) constant within the small amplitude area, i.e. Kt =K0. However, in the region over the small amplitude area, the instantaneous stiffness matrix varies with the amplitude. So, in these analyses, the instantaneous stiffness matrix(Kt) is assumed to be a constant equivalent stiffness matrix(K), and to be equal to the initial stiffness matrix(K0) multiplied by γ. The deformation where the rigidity changed variable was assumed as 10mm. The equation of the above relation is as below;

(2) $C=\beta \cdot K=\beta \cdot \gamma \cdot K0$

On the Hokunei Bridge simulation model, dynamic response analyses were carried out. The earthquake record of Type I Ground in the Japan Road Standard was used in these analyses. The 5% was used as the damping factor. The γ was assumed to be 72.4% by another calculation as below. The β was calculated to be 0.0184. The result is shown in HOKUN42. The response acceleration calculated by the above β method was 163gal on the girder. In the hysteresis rule, the natural period for the initial rigidity is 1.359 seconds, and the one for the second rigidity is 1.628 seconds, as below:

For the initial rigidity : T1= 1.359 sec. → K=2.181 tf/m
For the second rigidity : T1= 1.628 sec. → K=2.520 tf/m

The γ to multiply the initial stiffness matrix for making the equivalent stiffness matrix was calculated using two single mass models as followed: The one is a model of the hysteresis rule with two different rigidities. Then, the natural period for the initial rigidity was 1.359 seconds, and the natural period for the second rigidity was 1.628 seconds. Another model was a constant rigidity model. The dynamic response analysis using the former model was done, and the dynamic response analysis using the latter model was done many times. If the response acceleration on the analysis using the latter model corresponded with the one(143 cm/sec^2) calculated on the analysis using the former model, the rigidity of the latter model was regarded as an equivalent rigidity. The equivalent stiffness matrix was calculated to be equal to the initial stiffness matrix multiplied by 0.724(1.580/2.181) in the analysis. The parameters used in this analysis are as below:

The hysteresis rule : $K0=2.181$, $\gamma=0.724$, $K=\gamma \times K0=0.724 \times 2.181=1.58$, $\omega=3.935$
$\beta=2h\gamma/\omega=2\times0.05\times0.724/3.935=0.0184$
The linear rule : $K=1.580$, $\omega=(9.8\times1.58)^{0.5}=3.935$
$\beta=2h/\omega=2\times0.05/3.935=0.0254$

By the way, the check for the hysteresis rule with two different rigidities was done. Two single mass models were used in this analysis check. The one was a model of the hysteresis rule with two different rigidities. In the model, the region of the initial rigidity was made very small and the response deformation went to the second rigidity region soon. The second rigidity(2.04tf/m) was corresponding to the initial rigidity(5.1tf/m) multiplied by 0.4. Another model is a constant rigidity model, and it's rigidity is equal to the second rigidity(2.04tf/m) of the former model. Then, the response acceleration(159 cm/sec^2) and the response deformation(7.8cm) calculated in the analysis check were corresponding to each other. The parameters used in the analysis check are as below:

The hysteresis rule : $K0=5.1$, $\gamma=0.4$, $K=\gamma \times K0=0.4\times5.1=2.04$, $\omega=4.471$
$\beta=2h\gamma/\omega=2\times0.05\times0.4/4.471=0.009$
The linear rule : $K=2.04$, $\omega=(9.8\times2.04)^{0.5}=4.471$
$\beta=2h/\omega=2\times0.05/4.471=0.022$

DAMAGE DURING THE KUSHIRO EARTHQUAKE

Damage

The Kushiro Earthquake occurred at a Kushiro offshore point in January, 1993. Some

structures located on Kushiro and Obihiro Regions suffered damage during the earthquake. The Hokumei Bridge, located in the Obihiro Region, was also damaged during the earthquake. The grade of the earthquake was graded as five degrees intensity in Obihiro Region by Meteorological Agency. An earthquake with the same magnitude usually causes an acceleration of as much as 100 to 200 gal on the base ground. The Obihiro Gas Corp. accelerometer graded the earthquake of 250gal more. Seismic design on the Hokumei Bridge had been done based on the Earthquake Resistance Volume of the Japan Road Standard. For the Hokumei Bridge, the 0.23 was used as a horizontal seismic design load according to J.R.S. Some days after the Kushiro Earthquake, the Hokumei Bridge was surveyed for damage caused by the earthquake. The damage was as below;

① The girder was vibrated during the Kushiro Earthquake. It's response displacement was too large, so the girder pushed the finger-joint broken at the A2 abutment, and the parapet of the abutment cracked at its neck.

The A1 abutment got a small crack at the neck of the parapet.
The A2 abutment got a severe crack at the neck of the parapet.(Photo.2)
A finger-joint between the girder and the A2 abutment was broken by movement of the girder.(Photo.3)

When the Kushiro Earthquake occurred in January, 1993, the Hokumei Bridge had been completed and was waiting for the completion of the other construction work. The natural period of the Hokumei Bridge was prolonged between 1.359 to 1.628 sec by using rubber bearings, which were expected to reduce the response forces on the piers. The girder had the 70mm joint-clearance at the abutment, the 210mm clearance between the girder and an abutment, and the girder was proceeding in concrete dry-shrinkage. The magnitude of the Kushiro Earthquake was greater than that used in the design on the Hokumei Bridge. The response displacement of the girder was larger than the temporary joint-clearance. While, the girder had returned to the correct position after the earthquake. This matter shows the rubber bearings might work as springs even under severe earthquake condition, seismic loads might be distributed evenly between each pier. So, the seismic loads might be reduced by the effect of prolonged natural periods. Also, the damage on joint-units under seismic loads may be allowable based on the Standard of J.H.P.C.

② The small slide-moves between some rubber bearings and piers were found by the survey after the earthquake. The slide-moves were confirmed by a comparison with the positions of the rubber bearings marked while the jacking-up took place.

During the construction of the Hokumei Bridge, the deformation grown on the rubber bearing by the dry-shrinkage was sometimes released by jacking the girder up over the piers. For the jacking-up, the rubber bearing does not have any bolts to connect into the girder or pier. All shear force loading between the girder and a pier should be transmitted by friction through the bearings. In jacking up, every rubber bearing was always raised over the pier together with the girder. On the measuring in the jacking up, the vertical reaction force of a bearing may be different depending on it's position.

③ The girder got a small crack on the side-surface of a part on the P1 pier, as the rear of the girder, where the anchor-caps capped anchor bolt stoppers.(Photo.4)

There were three stoppers buried which consisted of four anchor bolts(ϕ55) on a pier. The anchor-caps buried in the girder have enough clearance in longitudinal direction, but very small clearance in transverse direction to the anchor bolts. This may be an explanation for the crack in that the anchor bolts guided the running-girder into the longitudinal direction, while the guiding force, possibly an impact force on the P1 pier, caused a crack on the side-surface of the rear of the girder.

Demanded clearance

Maximum allowable clearance was designed as 170mm under a seismic load, as 38mm under temperature change(+-25℃), and the summation was 208mm between the girder and the abutment. In the joint-clearance, the temperature load was considered but the seismic load was not according to the Standard of J.H.P.C. The joint-clearance had been calculated 38mm for the temperature change, the 13mm was for a supplement, and the summation 51mm was set-up during it's construction. When the Kushiro Earthquake occurred in January, 1993, the Hokumei Bridge had been completed. However, the concrete dry shrinkage of the girder was still proceeding. The joint-clearance was measured 70mm between the girder and the A1 abutment, and 80mm between the girder and the A2 abutment after the earthquake. The 80mm between the girder and the A2 abutment might be explained in that the clearance was widened by 10mm by the girder pushing.

The acceleration record of the Kushiro Earthquake

The acceleration record for Type I Ground in the Japan Road Standard, the acceleration records of the Kushiro Earthquake from East-West direction and from North-South direction are shown as oscillatory drawings and Fourier-Spectrums in Fig.10. The response spectrum of them are shown in Fig.11. The acceleration records of the Kushiro Earthquake were observed by Meteorological Agency.

Simulations on the behavior of the Hokumei Bridge during the Kushiro Earthquake

Dynamic Response Analysis using a hysteresis rule

The dynamic response analysis using the hysteresis rule was carried out to simulate the performances of the Hokumei Bridge during the Kushiro Earthquake. The rubber bearing in this model does not have hysteresis damping. The 5% was used as the damping factor in this simulation. The damping matrix assumed to be proportional to the instantaneous stiffness matrix(Kt) multiplied by β. The equivalent stiffness matrix was assumed as the initial stiffness matrix multiplied by γ. The deformation where the rigidities changed variable was assumed as 10mm. The Kushiro Earthquake recorded East-West was in the same direction as the Hokumei Bridge and was used in this simulation. The rigidities of piers were assumed to be elastic even under the seismic load. The γ was assumed as 0.724 as for the Kushiro Earthquake load, and the β was assumed as 0.0184. The response acceleration was 300gal on the girder. The response displacement was 12.8cm on the girder. The response deformation was 15.97cm on the rubber bearing at the P2 pier. Then the shear strain was

about 130% considering that the total thickness of rubber layers in a rubber bearing was equal to 12.5cm. If the spring of the rubber bearing was replaced by the spring multiplied by 1000, the response displacement of the girder was 11.1cm, the one of a pier was 11.1cm and the response shear force was about 500tf. If the spring of the rubber bearing was replaced by the spring multiplied by 1/4, the response displacement of the girder was 7.6cm, one of the piers was 18 to 19cm and the response shear force was about 500tf.

When the Kushiro Earthquake records from North-South were used, the response values were as follows; The response acceleration was 470gal and the response displacement was 30.0cm on the girder. The response deformation was 26.83cm on the rubber bearing at P5 pier. The response spectrum analyzed using the record of Type I Ground in J.R.S were as follows; Keeping the natural period to be 1.628sec, the response acceleration spectrum was 133gal and the response displacement spectrum was 8.9cm. The response table calculated using the hysteresis rule model is shown in Table.4. The response oscillatory drawings calculated on the hysteresis rule model using the Kushiro Earthquake records from East-West and North-South are shown in Fig.12.

Dynamic Response Analysis using a bilinear model

The model used in the former simulation is a model using the rubber bearings with no hysteresis damping. In this simulation, the model which rubber bearings were replaced by high damping rubber bearings with a bilinear-type hysteresis damping was used. The 5% was used as the damping factor in this simulation, and the effect of the hysteresis damping should be laid over the system damping of the 5%. The Kushiro Earthquake records from East-West were used in this simulation.

For this bilinear-type hysteresis model, the initial rigidity was assumed equal to the initial rigidity of the former simulation. The second rigidity was assumed to be 25% of the initial rigidity. The equivalent rigidity was assumed 35% of the initial rigidity. The natural period for the equivalent rigidity is 1.964 seconds. The hysteresis rule of these high damping rubber bearings was assumed comparing with the one used in the Miyagawa Bridge, which was a "Menshin bridge". The damping matrix assumed to be proportional to the instantaneous stiffness matrix multiplied by β. The equivalent stiffness matrix was assumed as the initial stiffness matrix multiplied by γ. The deformation where the rigidity changed was assumed as 20mm. The spring of piers were assumed to be elastic even under the seismic load. The γ was assumed as 35%, and the β was assumed as 0.0313. The parameters used in this analysis are as follows;

$$T1=1.964\text{sec}\ ,\omega=2\pi/1.964=3.200\ ,\gamma=0.35\ ,\ \beta=2h/\omega=2\times0.05/3.200=0.0313$$

The response acceleration was 190gal on the girder. The response displacement was 8.8cm on the girder. The response deformation was 11.09cm on the rubber bearings at P5 pier. Then the shear strain was about 90%. By using above high damping rubber bearings, the response displacement of the girder was reduced about by 30%. The response oscillatory drawings calculated on the hysteresis rule model and the bilinear model using the Kushiro Earthquake records from East-West are shown in Fig.13. The response relative oscillatory drawings calculated on the model with the hysteresis rule and the bilinear model using the Kushiro Earthquake records from East-West are shown in Fig.14.

CONCLUSIONS

The vibration tests and analytical studies were carried out for the Hokumei bridge using laminated rubber bearings. From the results, following conclusions may be drawn:

1) The laminated rubber bearing has nonlinear characteristic within small amplitude area. The dynamic shear spring within small amplitude area corresponded to the static design spring multiplied by 1.7 to 1.8.

2) Seismic response shear force is distributed evenly in each pier due to rubber bearings.

3) Seismic response shear force is reduced by a prolonged natural period due to rubber bearings.

4) The damping ratio of a prestressed concrete continuous bridge using laminated rubber bearings may be about 0•05 to 0•06.

ACKNOWLEDGMENT

These experimental studies were carried out in the execution site of the Hokumei Bridge, and of the Ishikari River Bridge some years ago too. The many precious suggestions contributed by Public Research Institute have been greatly appreciated.

REFERENCES

1) Dr. K. Kawashima, K. Hasegawa, T. Koyama and T. Yoshida; "Experiments on Cyclic Shear Characteristics of Rubber Pads for Bridge Bearing Support",by P.W.R.I., 1986.

2) Y. Hiyama,Y. Suzuki, A. Kubo and T. Ikeda; "Design and Construction of Ishikari River Bridge",Bridge and Foundation Engineering, Vol.25 No.11, 1 991.

3) Y. Hiyama, and A. Kubo; "Vibration Tests in Ishikari River Bridge",The 1 st. SINO-JAPAN Workshop on Cable Stayed Bridges in October, 1992.

4) Y.Hiyama, S.Matsubara, A.Kubo and K.Ozaki; "Vibration Tests in Ishikari River Bridge and Hokumei Bridge", FIP Symposium on prestressed concrete technique,1993.

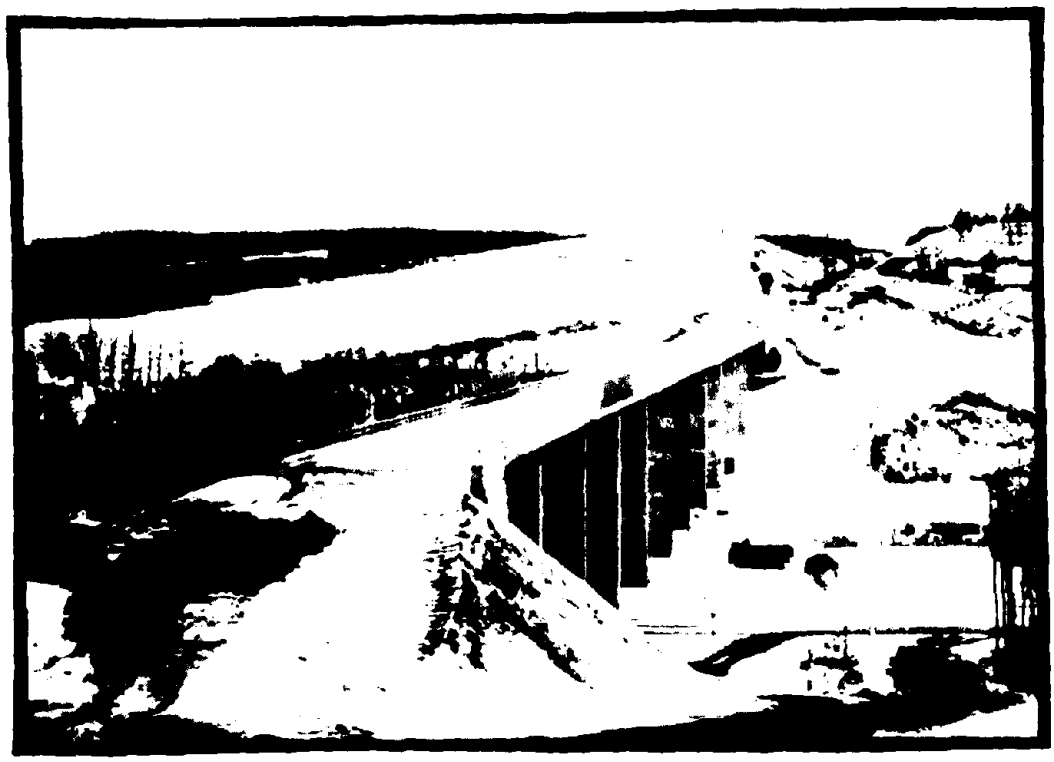

Photo.1 The view of the Hokumei Bridge from the A2 abutment.

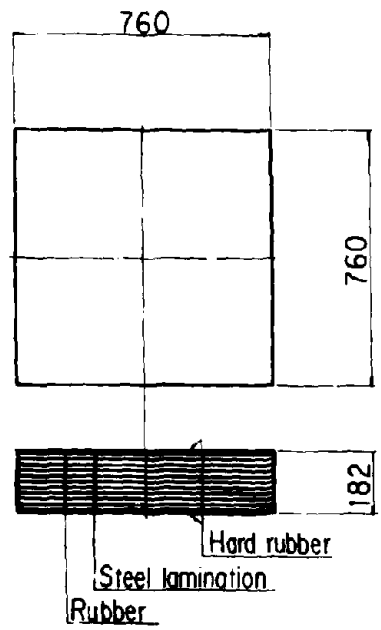

Fig.2 The laminated rubber bearing used in the Hokumei Bridge

	Size (mm)	Area (cm²)	Thickness of a layer (mm)	Number of layers	Total thickness Σte (mm)
A1	250x650	1 625	10	3	30
P1	760x760	5 776	15	10	150
P2	700x720	5 040	15	9	135
P3	650x650	4 225	15	8	120
P4	660x700	4 620	15	7	105
P5	650x650	4 225	15	8	120
P6	610x650	3 965	15	8	120
P7	660x670	4 422	15	7	105
P8	690x700	4 830	15	8	120
P9	700x700	4 900	15	9	135
P10	750x750	5 625	15	10	150
A2	250x650	1 625	10	3	30

Table.1 The size of the laminated rubber bearings used in the Hokumei Bridge

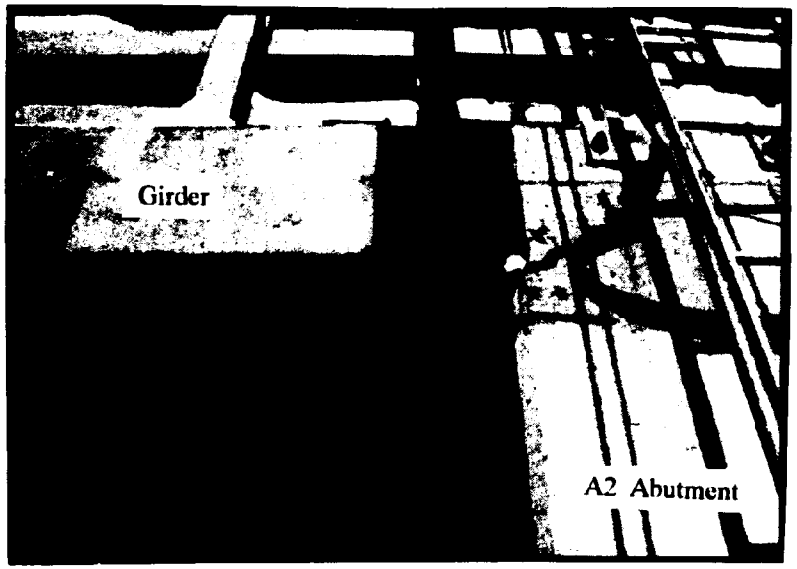

Photo.2 The A2 abutment getting a crack at the neck of the parapet.

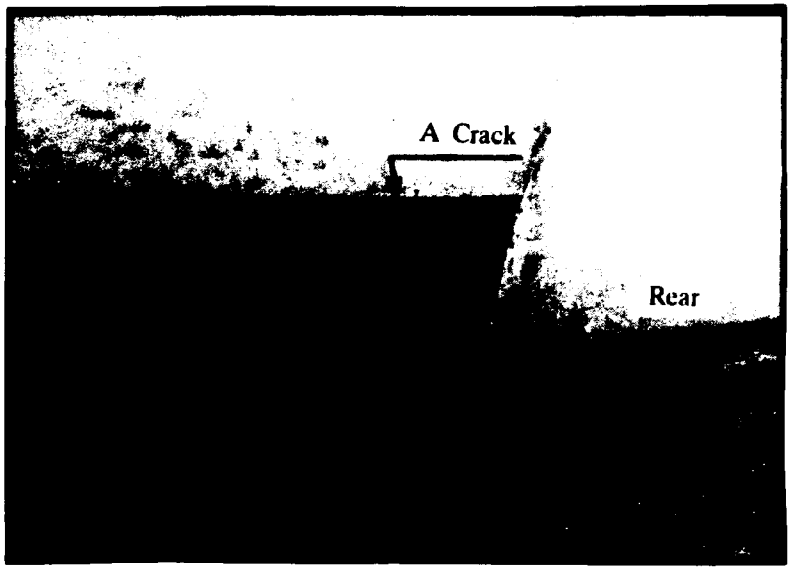

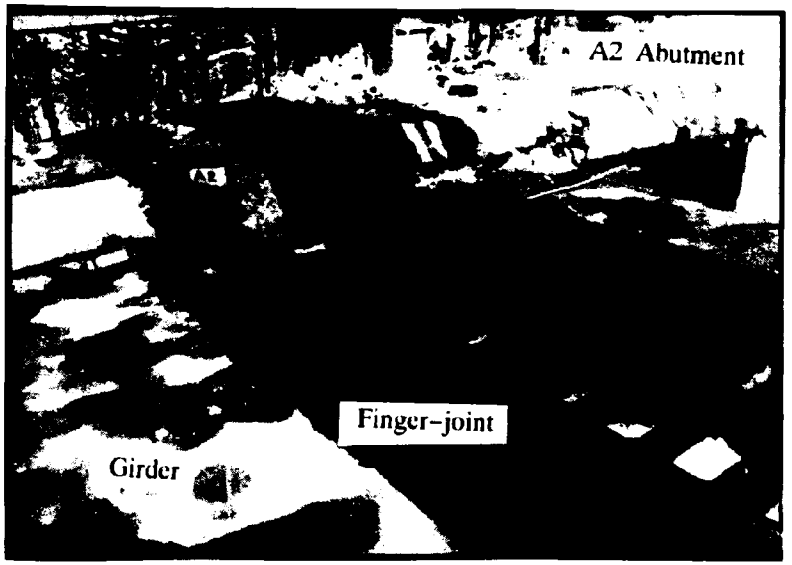

Photo.3 The finger-joint at the A2 abutment broken by the girder movement

Photo.4 A crack on the side-surface of the rear of the girder, which covers an anchor bolts stopper at the P1 pier.

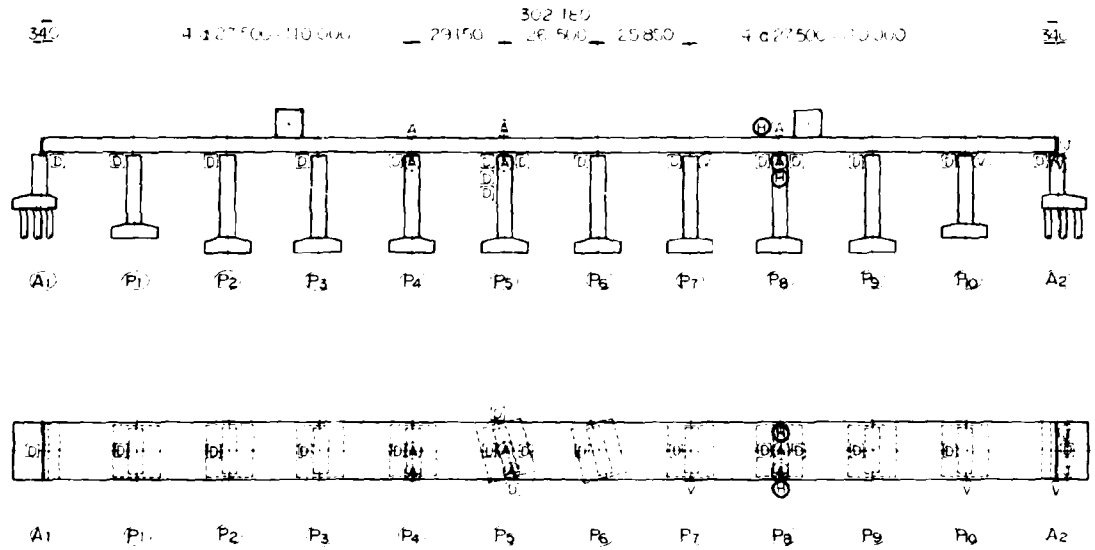

Fig.3 The arrangement of measuring-machines during the vibration tests.

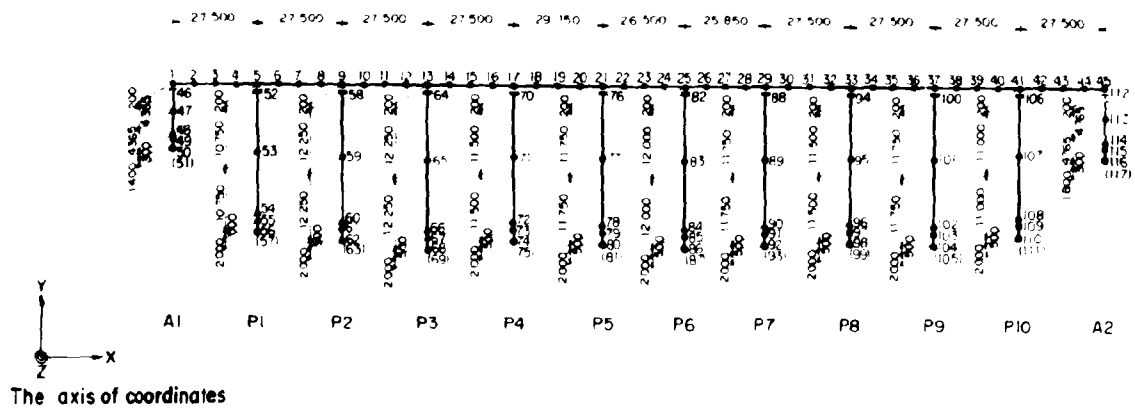

The axis of coordinates

Fig.8 The Hokumei Bridge model used in these simulations

Node

No.	X (m)	Y (m)	Z (m)	M
1	0.0000	0.0000	0.0000	1
2	6.8754	-0.1030	-0.1482	0
3	13.7509	-0.2013	-0.2940	6
4	20.6268	-0.2948	-0.4372	0
5	27.5031	-0.3836	-0.5773	2
6	34.3796	-0.4677	-0.7140	0
7	41.2565	-0.5471	-0.8471	6
8	48.1338	-0.6217	-0.9763	5
9	55.0114	-0.692	-1.1011	4
10	61.8894	-0.7568	-1.2212	0
11	68.7677	-0.8173	-1.3364	6
12	75.6464	-0.873	-1.4463	0
13	82.5255	-0.924	-1.5506	2
14	89.4049	-0.9703	-1.6489	0
15	96.2846	-1.0118	-1.741	6
16	103.1647	-1.0487	-1.8265	5
17	110.0452	-1.0808	-1.905	4
18	116.926	-1.1081	-1.9763	0
19	123.8072	-1.1308	-2.0401	6
20	130.6887	-1.1487	-2.0958	0
21	139.2347	-1.1644	-2.1538	3
22	144.2025	-1.1701	-2.1813	0
23	150.8347	-1.1748	-2.2109	6
24	157.4671	-1.1734	-2.2319	0
25	165.7321	-1.1666	-2.2458	3
26	170.9832	-1.1588	-2.2472	0
27	177.8668	-1.1443	-2.2401	6
28	184.7507	-1.1251	-2.2226	0
29	191.6348	-1.1011	-2.1943	4
30	198.5191	-1.0725	-2.1548	5
31	205.4036	-1.0391	-2.1040	6
32	212.2882	-1.0010	-2.0413	0
33	219.1731	-0.9581	-1.9666	2
34	226.058	-0.9106	-1.8794	0
35	232.9431	-0.8583	-1.7786	6
36	239.8282	-0.8013	-1.6668	0
37	246.7133	-0.7395	-1.5402	4
38	253.5985	-0.6730	-1.4002	5
39	260.4836	-0.6018	-1.2461	6
40	267.3687	-0.5259	-1.0776	0
41	274.2537	-0.4453	-0.8944	2
42	281.1385	-0.3599	-0.6962	0
43	288.0231	-0.2698	-0.4826	6
44	294.9074	-0.1750	-0.2534	0
45	301.7923	-0.0754	-0.0083	1
46	0.0000	-0.2363	0.0000	0
47	0.0000	-4.6013	0.0000	0
48	0.0000	-8.9663	0.0000	0
49	0.0000	-9.2663	0.0000	0
50	0.0000	-10.6663	0.0000	0
51	0.0000	-10.6663	0.0000	0
52	27.5031	-0.8063	-0.5773	0
53	27.5031	-11.5563	-0.5773	0
54	27.5031	-22.3063	-0.5773	0
55	27.5031	-22.8063	-0.5773	0
56	27.5031	-24.8063	-0.5773	0
57	27.5031	-24.8063	-0.5773	0
58	55.0114	-1.0463	-1.1011	0
59	55.0114	-12.5863	-1.1011	0
60	55.0114	-24.0463	-1.1011	0
61	55.0114	-24.5863	-1.1011	0
62	55.0114	-26.5863	-1.1011	0
63	55.0114	-26.5863	-1.1011	0
64	82.5255	-1.2863	-1.5506	0
65	82.5255	-13.5363	-1.5506	0
66	82.5255	-25.7863	-1.5506	0
67	82.5255	-26.2863	-1.5506	0
68	82.5255	-28.2863	-1.5506	0
69	82.5255	-28.2863	-1.5506	0
70	110.0452	-1.4513	-1.9050	0
71	110.0452	-12.9513	-1.9050	0
72	110.0452	-24.4513	-1.9050	0
73	110.0452	-24.9513	-1.9050	0
74	110.0452	-26.9513	-1.9050	0
75	110.0452	-26.9513	-1.9050	0
76	139.2347	-1.5273	-2.1538	0
77	139.2347	-13.2773	-2.1538	0
78	139.2347	-25.0273	-2.1538	0
79	139.2347	-25.5273	-2.1538	0
80	139.2347	-27.5273	-2.1538	0
81	139.2347	-27.5273	-2.1538	0
82	165.7321	-1.5263	-2.2458	0
83	165.7321	-13.5263	-2.2458	0
84	165.7321	-25.5263	-2.2458	0
85	165.7321	-26.0263	-2.2458	0
86	165.7321	-28.0263	-2.2458	0
87	165.7321	-28.0263	-2.2458	0
88	191.6348	-1.4623	-2.1943	0
89	191.6348	-13.2123	-2.1943	0
90	191.6348	-24.9623	-2.1943	0
91	191.6348	-25.4623	-2.1943	0
92	191.6348	-27.4623	-2.1943	0
93	191.6349	-27.4623	-2.1943	0
94	219.1731	-1.3243	-1.9666	0
95	219.1731	-12.8243	-1.9666	0
96	219.1731	-24.3243	-1.9666	0
97	219.1731	-24.8243	-1.9666	0
98	219.1731	-26.8243	-1.9666	0
99	219.1731	-26.8243	-1.9666	0
100	246.7133	-1.1343	-1.5402	0
101	246.7133	-12.8843	-1.5402	0
102	246.7133	-24.6343	-1.5402	0
103	246.7133	-25.1343	-1.5402	0
104	246.7133	-27.1343	-1.5402	0
105	246.7133	-27.1343	-1.5402	0
106	274.2537	-0.8683	-0.8944	0
107	274.2537	-11.8683	-0.8944	0
108	274.2537	-22.8683	-0.8944	0
109	274.2537	-23.3683	-0.8944	0
110	274.2537	-25.3683	-0.8944	0
111	274.2537	-25.3683	-0.8944	0
112	301.7923	-0.3123	-0.0083	0
113	301.7923	-5.0773	-0.0083	0
114	301.7923	-9.8423	-0.0083	0
115	301.7923	-10.1423	-0.0083	0
116	301.7923	-11.9423	-0.0083	0
117	301.7923	-11.9423	-0.0083	0
118	1.0000	0.0000	0.0000	0
119	28.5031	-0.3836	-0.5773	0
120	56.0114	-0.692	-1.1011	0
121	83.5255	-0.924	-1.5506	0
122	111.0452	-1.0808	-1.905	0
123	140.2347	-1.1644	-2.1538	0
124	166.7321	-1.1666	-2.2458	0
125	192.6348	-1.1011	-2.1943	0
126	220.1731	-0.8581	-1.9666	0
127	247.7133	-0.7395	-1.5402	0
128	275.2537	-0.4453	-0.8944	0
129	302.7923	-0.0754	-0.0083	0
130	1.0000	-10.6663	0.0000	0
131	28.5031	-24.8063	-0.5773	0
132	56.0114	-26.5863	-1.1011	0
133	83.5255	-28.2863	-1.5506	0
134	111.0452	-26.9513	-1.9050	0
135	140.2347	-27.5273	-2.1538	0
136	166.7321	-28.0263	-2.2458	0
137	192.6348	-27.4623	-2.1943	0
138	220.1731	-26.8243	-1.9666	0
139	247.7133	-27.1343	-1.5402	0
140	275.2537	-25.3683	-0.8944	0
141	302.7923	-11.9423	-0.0083	0

Concentrated masses (ton)

No.	M_x	M_y	M_z
1	29.6	29.6	29.6
2	28.9	28.9	28.9
3	33.5	33.5	33.5
4	50.6	50.6	50.6
5	36.5	36.5	36.5
6	3.4	3.4	3.4

Beam elements

B No.	E (tf/m²)	G (tf/m²)	A (m²)	I_x (m⁴)	I_y (m⁴)	I_z (m⁴)	w (tf/m)
1	2.95 E6	1.28 E6	6.830	0.197	60.500	1.251	17.500
2	2.50 E8	1.09 E8	1.0 E4	1.0 E5	1.05 E5	1.0 E5	44.690
3	2.49 E6	1.08 E6	17.100	19.439	104.170	5.700	41.900
4	2.26 E8	1.08 E8	17.100	19.439	104.170	5.700	41.900
5	2.58 E6	1.08 E6	17.100	19.439	104.170	5.700	41.900
6	4.00 E6	1.08 E8	17.100	19.439	104.170	5.700	41.900
7	4.00 E6	1.08 E6	18.000	20.639	112.760	6.000	44.100
8	2.23 E6	1.08 E8	18.000	20.639	112.760	6.000	44.100
9	2.60 E6	1.08 E8	17.100	19.439	104.170	5.700	41.900
10	4.30 E6	1.08 E8	17.100	19.439	104.170	5.700	41.900
11	3.27 E6	1.08 E8	17.100	19.439	104.170	5.700	41.900
12	2.29 E8	1.08 E8	17.100	19.439	104.170	5.700	41.900
13	2.50 E8	1.08 E8	137.500	2637.800	1386.500	1790.370	198.080
14	2.50 E8	1.08 E8	137.500	2637.800	1386.500	1790.370	336.880
15	2.50 E8	1.08 E8	132.000	2440.900	1331.000	1584.900	191.350
16	2.50 E8	1.08 E8	132.000	2440.900	1331.000	1584.000	323.400
17	2.50 E8	1.08 E8	96.900	1266.900	1049.400	583.419	143.840
18	2.50 E8	1.08 E8	96.900	1266.900	1049.400	583.419	237.410

Spring elements

S No.	K_x (tf/m)	K_y (tf/m)	K_z (tf/m)	K_{xx} (tf·m/m)	K_{yy} (tf·m/m)	K_{zz} (tf·m/m)
1	0.1	105838.	1.0 E8	640925.	0.1	1104.
2	1232.	16705.	1.0 E8	101068.	7455.	1608.
3	1195.	17168.	1.0 E8	103867.	7228.	1402.
4	1127.	16975.	1.0 E8	102696.	6816.	1195.
5	1408.	28468.	1.0 E8	172229.	8518.	2067.
6	1127.	16875.	1.0 E8	111270.	7385.	1195.
7	1057.	15133.	1.0 E8	99197.	6931.	938.
8	1348.	26271.	1.0 E8	158940.	8153.	1907.
9	1288.	21630.	1.0 E8	130860.	7792.	1716.
10	1161.	16327.	1.0 E8	98778.	7027.	1333.
11	1200.	15838.	1.0 E8	96422.	7260.	1494.
12	0.1	105838.	1.0 E8	640925.	0.1	1104.
13	1.0 E8	1.0 E8	1.0 E8	1.0 E8	1.0 E8	1.0 E8

Table.2 The parameters table in the Nobunel Bridge model

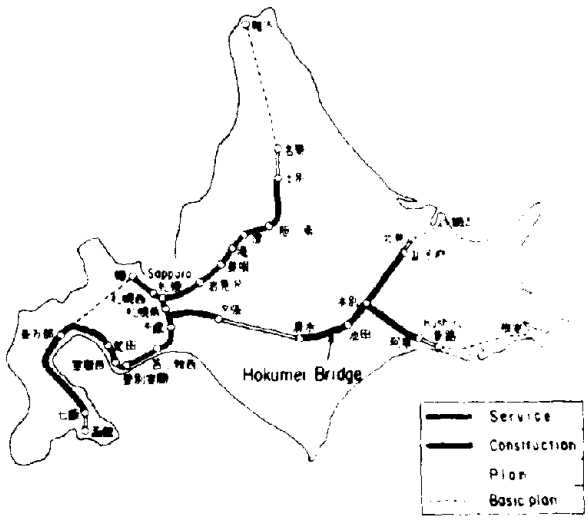

Fig.1 Highway Map in Hokkaido of Japan Highway Public Corp.

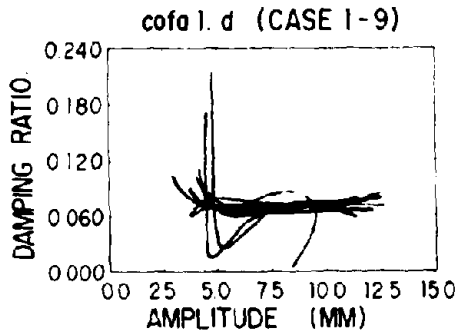

Fig.5 The damping ratio analyzed using deformation records on the A1 abutment

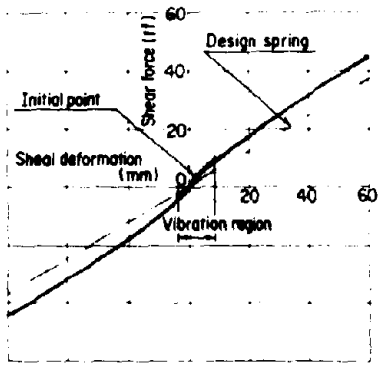

Fig.7 Load-Deformation Relation of a Rubber Bearing, showing the differet initial deformations

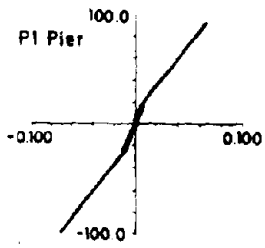

Fig.9 Oscillation Hysteresis Calculated (P1 pier)

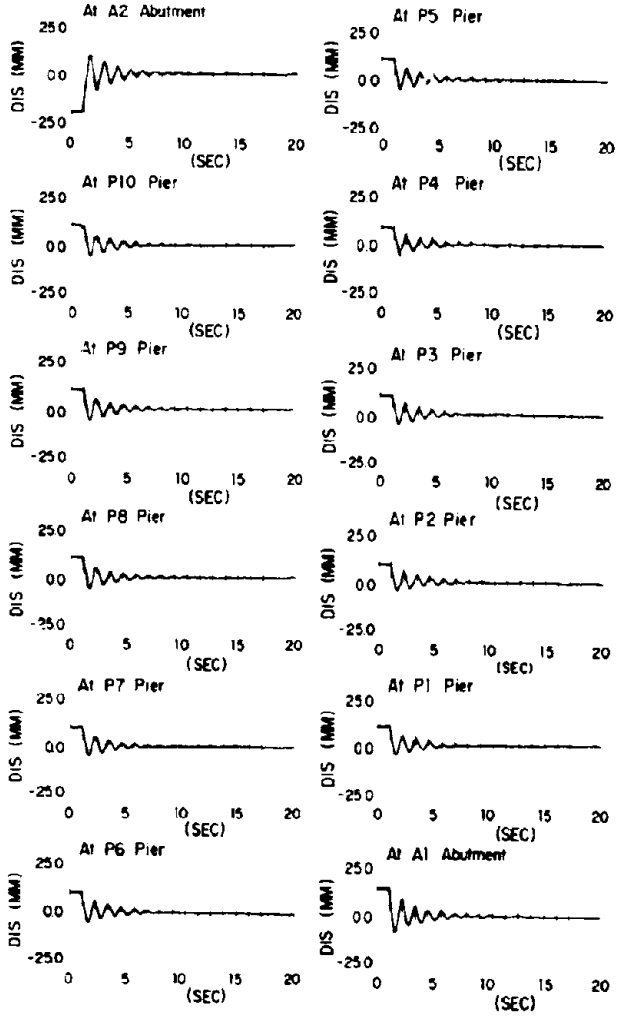

Fig.4 The deformation records observed in the first try in the vibration tests

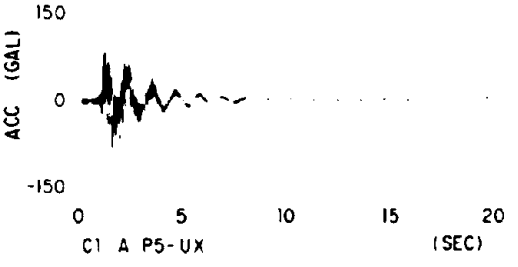

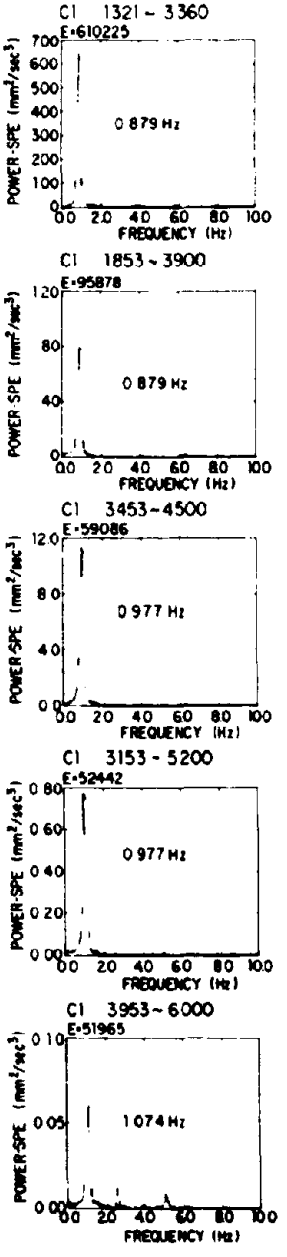

Fig.6 The Power Spectrums showing a transformation of it's dominant frequency

1 Static analysis under equivalent earthquake load (HOKUS4)

hokus4 (Rh 0.15)		P 1	P 2	P 3	P 4	P 5	P 6	P 7	P 8	P 9	P 1 0
Girder	cm	11.009	10.997	10.993	10.988	10.986	10.986	10.986	10.986	10.990	10.995
Pier Displacement	cm	3.452	4.322	4.487	3.035	2.635	4.518	4.346	2.774	3.480	4.843
(Pier/Girder)		.314	.393	.408	.280	.258	.411	.396	.254	.318	.358
Shear Force of Bearing	tf	91	80	73	111	92	68	90	106	88	86
(Shear force/ L)		.105	.090	.083	.126	.104	.077	.101	.119	.099	.097

2 Response Spectrum Method by the design shear springs (HOKUS4)

hokus4		P 1	P 2	P 3	P 4	P 5	P 6	P 7	P 8	P 9	P 1 0
Max. of Girder	cm	11.07	11.06	11.06	11.05	11.05	11.05	11.05	11.053	11.056	11.061
Max. of Pier	cm	2.95	3.65	3.79	2.63	2.43	3.73	3.75	2.406	2.740	3.278
(Pier/Girder)		.267	.330	.343	.238	.220	.338	.339	.218	.246	.296
Max. Shear Force of Bearing	tf	118	108	105	137	121	100	120	132	116	112
(Shear force/ L)		.161	.093	.090	.117	.104	.085	.102	.113	.099	.096

3 Response Spectrum Method by the shear springs in the small amplitude area. (HOKUS41)

hokus41		P 1	P 2	P 3	P 4	P 5	P 6	P 7	P 8	P 9	P 1 0
Max. of Girder	cm	9.65	9.65	9.64	9.63	9.63	9.63	9.63	9.63	9.64	9.64
Max. of Pier	cm	3.94	4.57	4.66	3.19	2.91	4.51	4.49	3.13	3.76	4.07
(Pier/Girder)		.408	.473	.483	.331	.302	.468	.465	.325	.390	.422
Max. Shear Force of Bearing	tf	158	133	130	167	149	122	144	125	151	141
(Shear force/ L)		.107	.091	.088	.113	.101	.083	.098	.119	.102	.096

4 Dynamic Response Analysis by a hysteresis rule (HOKUS42)

hokus42 β=0.0184		P 1	P 2	P 3	P 4	P 5	P 6	P 7	P 8	P 9	P 1 0
Max. of Girder	cm	9.70	9.69	9.69	9.68	9.68	9.68	9.68	9.68	9.69	9.69
Max. of Pier	cm	2.85	3.79	3.78	2.35	2.14	3.87	3.74	2.12	2.80	3.23
(Pier/Girder)		.294	.391	.390	.244	.221	.379	.386	.224	.289	.333
Max. Shear Force of Bearing	tf	116	115	106	126	111	103	122	123	114	113
(Shear force/ L)		.101	.100	.094	.109	.097	.089	.106	.107	.099	.098

5 Dynamic Response Analysis by de (HOKUS5)

hokus5		P 1	P 2	P 3	P 4	P 5	P 6	P 7	P 8	P 9	P 1 0
Max. of Girder	cm	10.16	10.16	10.15	10.15	10.15	10.15	10.15	10.15	10.15	10.16
Max. of Pier	cm	2.60	3.13	3.19	2.35	2.11	3.17	3.23	2.12	2.53	2.83
(Pier/Girder)		.256	.308	.314	.232	.208	.312	.318	.209	.249	.279
Max. Shear Force of Bearing	tf	104	95	90	120	104	84	103	114	101	99
(Shear force/ L)		.103	.093	.088	.118	.102	.084	.101	.112	.099	.097

Table. 3 The responses table calculated in the five methods.

1 Dynamic Response Analysis by a hysteresis rule using the acc. recorec for Type 1 of J. R. S. (MAX 102.24 gal)

HOKU42		P 1	P 2	P 3	P 4	P 5	P 6	P 7	P 8	P 9	P 1 0
Max. Dis. of Girder	cm	9.70	9.69	9.69	9.68	9.68	9.68	9.68	9.68	9.68	9.69
Max. Dis. of Pier	cm	2.85	3.79	3.78	2.35	2.14	3.87	3.74	2.12	2.80	3.23
(Pier/Girder)		.294	.391	.390	.244	.221	.379	.386	.224	.289	.333
Max. Shear Force of bearing	tf	116	115	106	126	111	103	122	123	114	113
(Shear force/ L)		.101	.100	.094	.109	.097	.089	.106	.107	.099	.098

2 Dynamic Response Analysis by a hysteresis rule using the Kushiro Earthquake record in the East West (MAX 922.20 gal)

KEW4		P 1	P 2	P 3	P 4	P 5	P 6	P 7	P 8	P 9	P 1 0
Max. Dis. of Girder	cm	12.86	12.85	12.84	12.83	12.82	12.80	12.79	12.78	12.78	12.78
Max. Dis. of Pier	cm	9.75	12.09	13.74	8.11	10.78	14.57	12.01	7.91	11.12	11.74
(Pier/Girder)		.758	.941	1.070	.632	.841	1.138	.939	.619	.870	.918
Max. Shear Force of bearing	tf	317	331	329	372	451	347	290	392	326	341
(Shear force/sum)		.089	.093	.092	.104	.126	.097	.081	.110	.091	.095

3 Dynamic Response Analysis by a hysteresis rule using the Kushiro Earthquake record

KNS84		P 1	P 2	P 3	P 4	P 5	P 6	P 7	P 8	P 9	P 1 0
Max. Dis. of Girder	cm	29.96	29.95	29.94	29.93	29.93	29.93	29.93	29.94	29.96	29.97
Max. Dis. of Pier	cm	10.52	14.37	14.47	9.09	9.66	15.91	14.29	8.30	11.66	11.64
(Pier/Girder)		.351	.480	.490	.304	.323	.532	.477	.277	.389	.388
Max. Shear Force of Bearing	tf	309	413	413	646	644	439	457	435	416	385
(Shear force/Sum)		.092	.098	.097	.105	.105	.104	.108	.103	.098	.091

Table 4 The response table calculated for the model with the hysteresis rule using the Kushiro Earthquake records by Meteorological Agency.

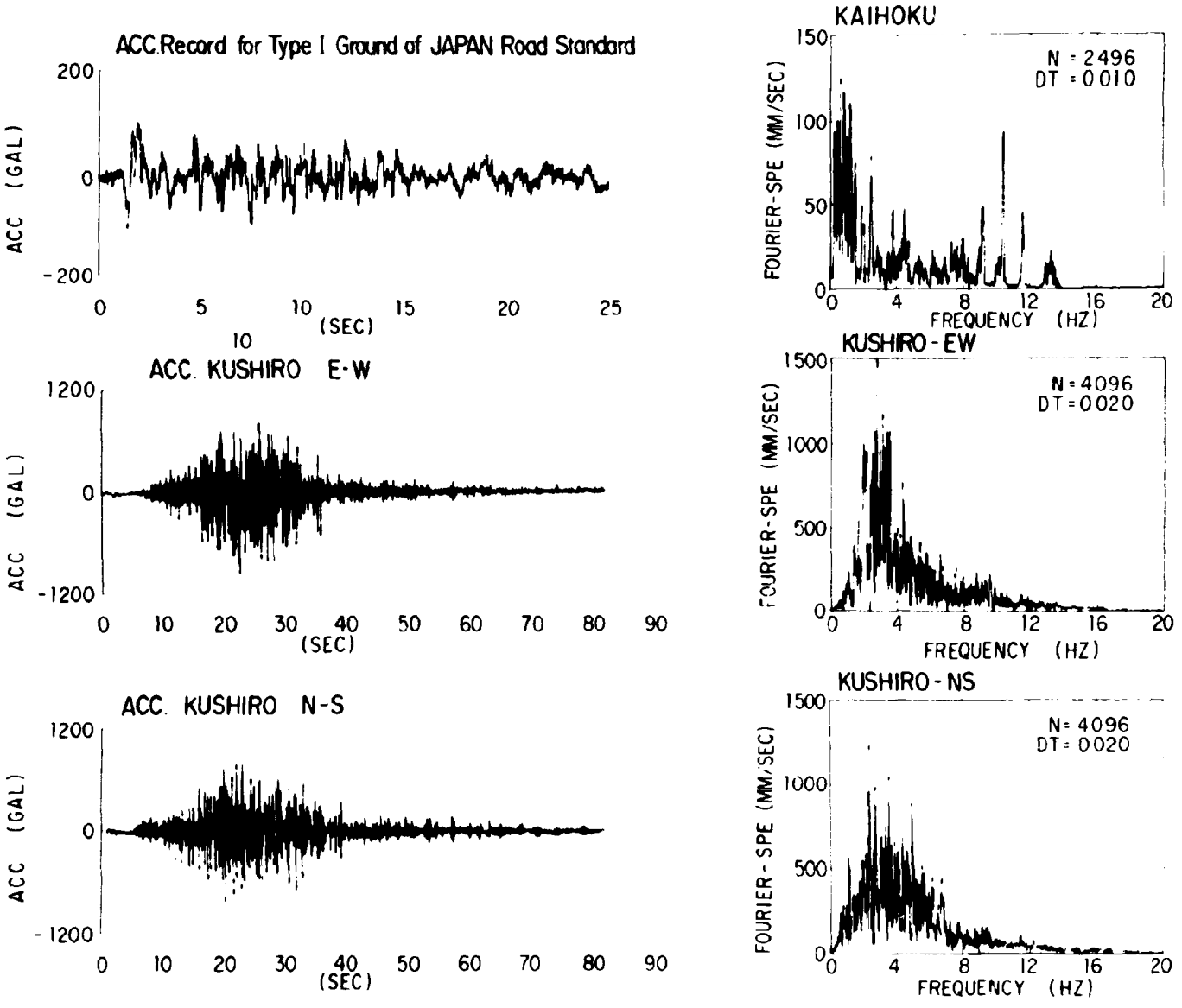

Fig.10 The oscillatory drawings and Fourier-Spectrums. of acceleration records used in these an alyses

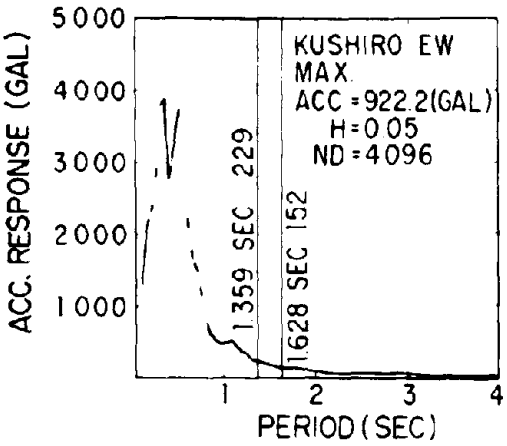

FIG.1-1 ACC. RESPONSE SPECTRUM

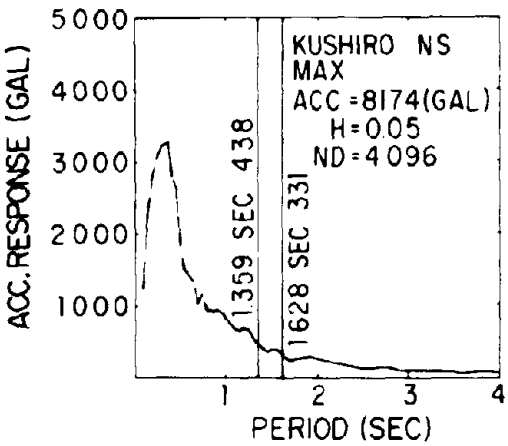

FIG.1-2 ACC.RESPONSE SPECTRUM

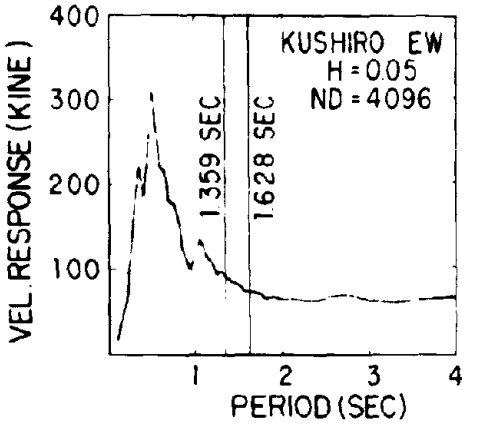

FIG.2-1 VEL.RESPONSE SPECTRUM

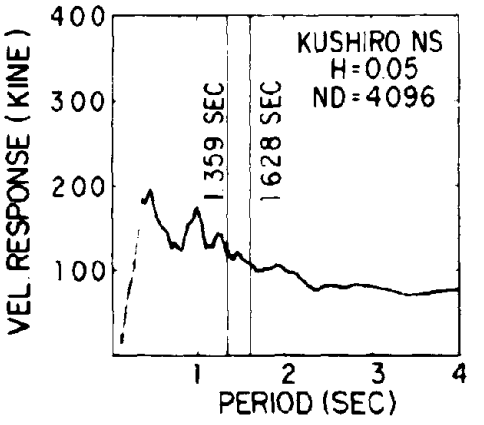

FIG.2-2 VEL.RESPONSE SPECTRUM

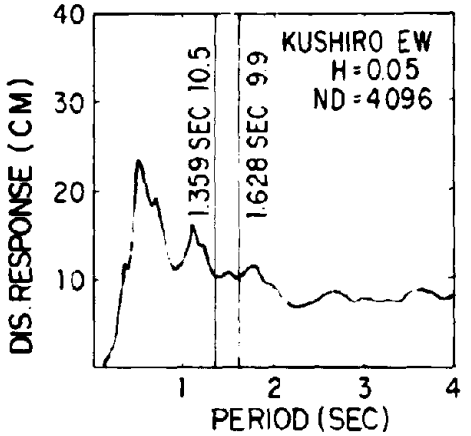

FIG.3-1 DIS. RESPONSE SPECTRUM

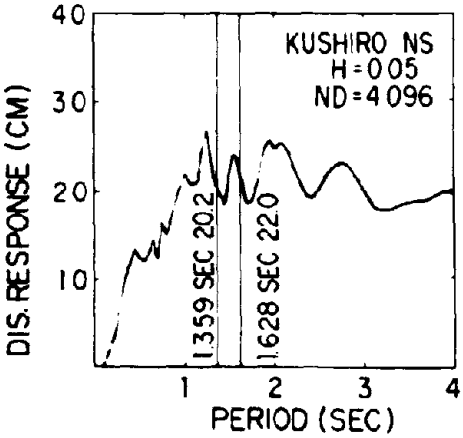

FIG.3-2 DIS.RESPONSE SPECTRUM

Fig. 11 The response spectrums of the Kushiro Earthquake records

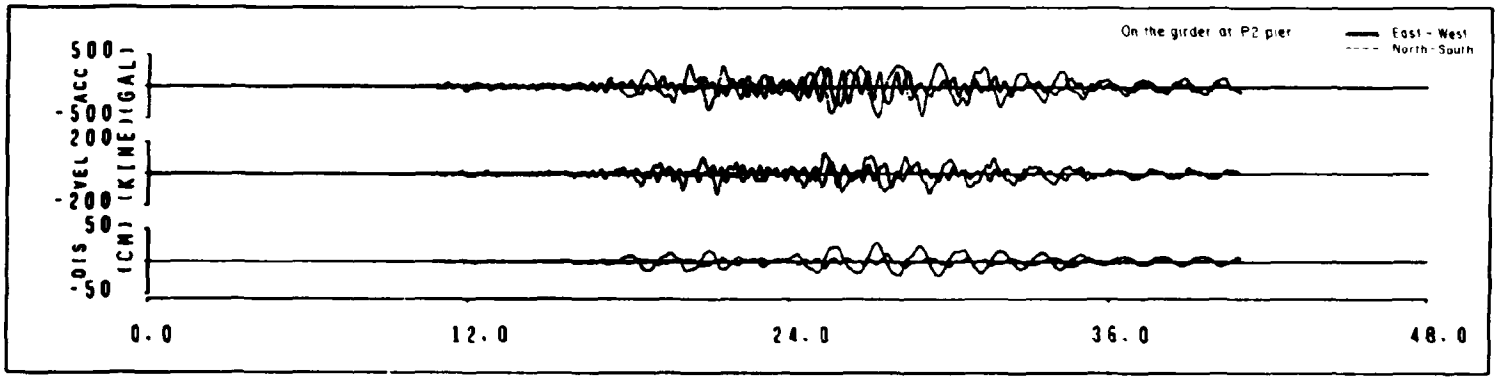

Fig.12 The response using the record from North-South was more than from East-West.

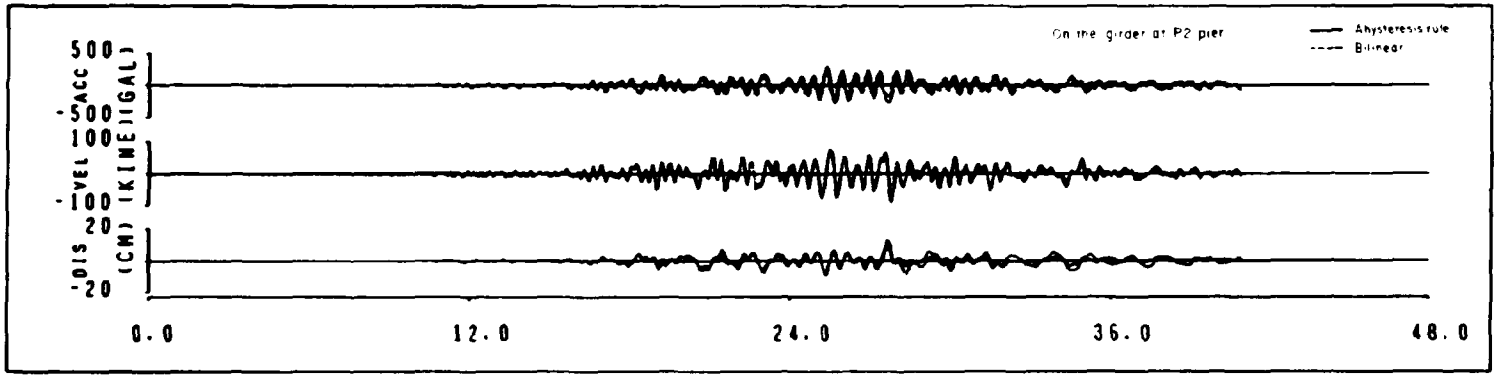

Fig.13 The phase angles were similar, and the maximum response displacement was reduced due to high damping rubber bearings.

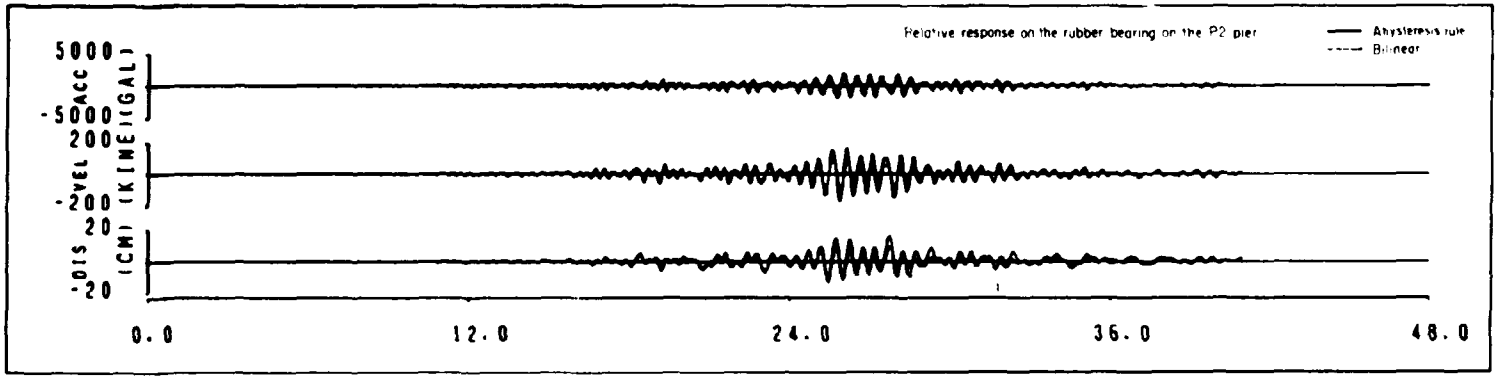

Fig.14 The phase angles were similar, and the maximum response deformation was reduced due to high damping rubber bearings.

GUIDELINES FOR PRE-QUALIFICATION, PROTOTYPE, AND QUALITY CONTROL TESTING OF SEISMIC ISOLATION SYSTEMS

Harry W. Shenton III[1]

ABSTRACT

At the present time, at least in the United States, seismic isolation systems are custom designed and built on a per project basis. As a result, testing has become an essential element in the design and construction of isolated structures. Currently, however, standards do not exist for conducting these much needed tests. The Building and Fire Research Laboratory of the National Institute of Standards and Technology is currently developing guidelines for testing of seismic isolation systems. Presented in the paper is a brief summary/outline of the guidelines. The guidelines address pre-qualification, prototype and quality control testing, are applicable to all types of isolation systems and are independent of the superstructure. The final guidelines will be developed after thorough review and evaluation of the draft guidelines. The guidelines are to serve as a resource document for voluntary standard/specification writing organizations, and for practitioners and researchers involved in the design, manufacture and testing of seismic isolation systems.

1. Introduction

Most isolation systems designed and built in the United States must undergo a series of tests prior to being placed in service, including systems for seismic isolation of bridges. The 1991 AASHTO *Guide Specifications for Seismic Isolation Design* (*Guide*, 1991) provide skeleton guidelines for conducting prototype tests (section 13 of *Guide*, 1991) and quality control (QC) tests (section 15 of *Guide*, 1991) of elastomeric seismic isolation bearings. Similar procedures are outlined in the 1991 *Uniform Building Code* (*Uniform*, 1991) for conducting prototype tests of isolation systems for buildings. At the present time, however, standards do not exist for conducting these much needed tests.

[1]Research Structural Engineer, Building and Fire Research Laboratory, National Institute of Standards and Technology, Gaithersburg, Maryland 20899, USA

Standard test procedures are needed to, (1) ensure the systematic characterization of isolation system properties, (2) provide a rational basis for demonstrating acceptable performance, and (3) facilitate the comparison of different isolation systems. The Building and Fire Research Laboratory (BFRL) of the National Institute of Standards and Technology (NIST) is currently developing guidelines for testing of seismic isolation systems. The guidelines, a pre-standard, are comprehensive and applicable to all types of isolation systems, whether they be elastomeric, sliding or hybrid, and are independent of the superstructure.

Although comprehensive in nature, the current guidelines are still considered "draft". The final guidelines will be published after thorough review and evaluation of the draft guidelines. The review process will involve broad industry input and a testing component. Presented in the paper is a brief overview of the draft guidelines for testing of seismic isolation systems.

2. Scope of the Guidelines

The guidelines incorporate three classes of tests: pre-qualification, prototype and quality control. The three are defined as follows:

> **Pre-Qualification tests** need not be project specific and are conducted in order to establish the fundamental properties and characteristics of the isolation system, and to determine the extent to which these properties and characteristics are dependent on load and environmental factors.
>
> **Prototype tests** are project specific and are conducted to verify the design properties of the isolation system prior to construction.
>
> **Quality Control tests** are project specific and are conducted to verify the quality of manufacture and as-built properties of the isolation system prior to installation.

Pre-qualification tests, as defined above, are formally not required by the codes (UBC, AASHTO), but are usually conducted in one form or another as a new system is developed.

The guidelines for pre-qualification and prototype testing are included in one report (Shenton 1994a), and are system independent. Quality control tests tend to be system specific, simply because production tests and some completed unit tests are unique to the design, materials and construction of the system. The guidelines for quality control testing of elastomeric systems are presented in a separate report (Shenton 1994b) as are the guidelines for quality control testing of sliding systems (Shenton 1994c).

The guidelines are intended for systems that isolate *in the horizontal plane only*, i.e , the system is assumed to be essentially rigid in the vertical direction. Guidelines for testing of vertical isolation systems are not specifically included. Furthermore, the guidelines are intended for *passive* isolation systems only. Although it is likely that many of the tests are applicable to components of active or semi-active systems, the test procedures were not written with these systems in mind.

The guidelines address with three major areas - rated capacity, general requirements and test schedule. Some test parameters are based on the rated capacity of the system, therefore, the capacity of the system must be rated before any tests are conducted. Detailed information pertaining to the test facility, instrumentation, calibration, data acquisition, data analysis and reporting of results are covered under general requirements. The individual test procedures are outlined in the test schedule. Included in the test procedures are performance criteria. Systems that do not meet or exceed the recommended criteria may not perform satisfactorily in service. Each of these major areas is discussed in more detail below.

3. Rated Capacity

Prior to any testing the capacity of the isolation system must be "rated". It is the responsibility of the supplier to report the fundamental properties of the isolation system. This includes the range of loads and environmental conditions in which the system can be expected to operate and function properly. The concept of rated capacity is fundamental to the guidelines and carries through from pre-qualification, to prototype, to quality control testing. Furthermore, details of the test procedures are based on the rated capacity of the system. A standard list of properties to be rated has been developed to cover all tests, and includes, among other properties: effective stiffness (horizontal, vertical and horizontal under wind load), design displacement, thermal displacement capacity, rotation capacity, operating vertical load range, tensile capacity and operating temperature range.

4. General Requirements

Most of tests procedures outlined in the guidelines fall under the general description of a cyclic lateral load test. In a typical test, a specimen is subject to a constant vertical load while, simultaneously, a cyclic lateral displacement or load is imposed on the specimen. The test is generally conducted for a specified vertical load, maximum lateral displacement, number of cycles and frequency of loading. Many of the tests procedures have similar equipment and data analysis requirements; therefore, rather than duplicate material, general requirements are outlined in one section of the guidelines and exceptions or special requirements are noted in the particular test description.

Test Facility

At a minimum, the test facility must be capable of subjecting a specimen to a combined compression/shear load. One pre-qualification test requires a bi-directional or bi-lateral shear load. The vertical load capacity of the facility is to be at least 10% greater than the largest vertical load to be applied during the test; the lateral load capacity is to be greater than the largest lateral load to be applied during the test. The lateral stroke must be at least twice the maximum displacement specified for the test.

The lateral load is to be applied under displacement control, such that the motion of the actuator is representative of a sinusoidal wave with specified frequency. The vertical load may

be applied under load control or displacement control, provided the load can be maintained within ±10% of that specified for the duration of the test. The guidelines recommend that the load systems be verified or calibrated periodically in accordance with accepted standards.

Instrumentation and Calibration

Transducers are to be in place to measure lateral load, lateral displacement, vertical load and vertical displacement. A thermometer is to be in place to record the temperature of the testing environment. Loads on the test specimen may be measured via the test machine read-out, load cells in the force train of the actuator or a force transducer between the specimen and reaction support. Transducers shall be such that loads are resolved to within 1% of the full load. Force transducers shall be calibrated periodically as described in ASTM E74 and shall have an uncertainty of not more than ±2.5% of force.

The recommended instrumentation setup is shown in Figure 1, for a single specimen under general bi-lateral loading. Vertical displacements are to be measured at 2 points on the lateral load plane at opposite sides of the specimen (δ_1 and δ_2 in Figure 1). Lateral displacements are to be measured at 2 points on the lateral load plane, at opposite sides of the specimen (Δ_{x1} and Δ_{x2}, or Δ_{y1} and Δ_{y2} in Figure 1). Displacement transducers are to be of sufficient precision to resolve the displacement to within 1% of the specified test displacement and have an uncertainty of not more than ±2.5% of displacement. The guidelines recommend that the transducers be calibrated periodically using accepted procedures.

Data Acquisition

The data is to be recorded using an analog or digital data acquisition system. The guidelines recommend digitizing or sampling at a rate of not less than 100 times the frequency of lateral loading (e.g., 50 samples/sec for a frequency of loading of 0.5 cyc/sec). At this rate a single hysteresis loop will be represented by approximately 100 data points. In some instances a faster rate may be needed in order to accurately resolve a complex or rapidly varying loop.

Data Analysis

The analysis of data from a cyclic lateral load test involves, (1) construction of hysteresis loops, (2) determination of the average effective stiffness and, (3) determination of the average energy dissipation. Effective stiffness and energy dissipation characterize the response of the isolation system, and, determine the magnitude of lateral load transmitted to the superstructure. The effective stiffness of a cycle, as typically defined elsewhere and in the guidelines, is the difference in maximum and minimum forces divided by the difference in maximum and minimum displacements. Energy dissipation is the area enclosed by the loop. These are illustrated in Figure 2.

For many systems effective stiffness represents the slope of the line that connects the points of maximum force (displacement) and minimum force (displacement), as shown in the example in Figure 2. The stiffness calculation in this case is intuitively obvious. In some cases, however, the maximum (minimum) force and maximum (minimum) displacement in a cycle are

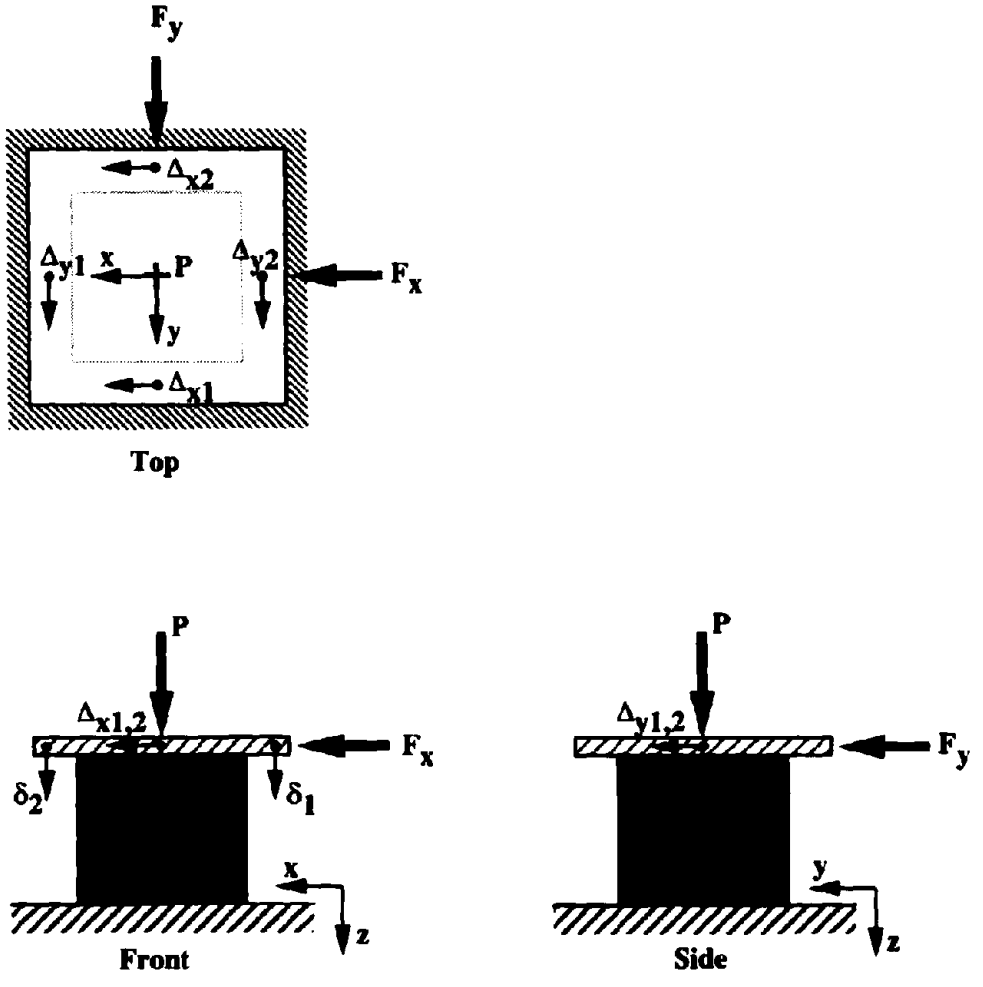

Figure 1. Definition Diagram

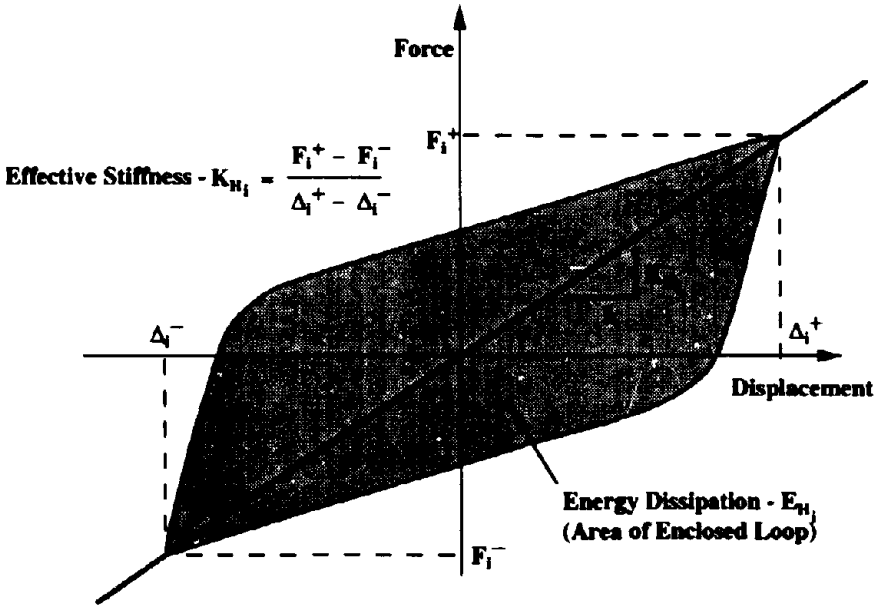

Figure 2. Hysteresis loop showing Effective Stiffness and Energy Dissipation calculation.

not coincident. This tends to occur, for example, when a hysteresis loop is very rounded. In this case, effective stiffness computed according to the procedure outlined in the guidelines is some average measure of the force-deflection behavior.

Effective stiffness and energy dissipation are computed for each complete cycle of the test. Average effective stiffness and average energy dissipation are then defined as the arithmetic mean of the stiffness and dissipation for the n cycles of the test.

Report of Results

The guidelines recommend reporting of results in a clear and concise format. The report is to include all pertinent data related to the test set-up and test procedure. Results to be reported include the effective stiffness and energy dissipation for each complete cycle, listed by cycle number in increasing order, and the average effective stiffness and average energy dissipation for the n cycles of the test. The report should include hysteresis plots for lateral deformation and vertical deformation for the specific test conditions.

4. Test Schedule

Pre-qualification Tests

A complete series of pre-qualification tests is to include all tests listed in Table 1, and a full series of prototype (Table 2) and quality control tests (Table 3). Each pre-qualification test is to be performed separately on two specimens; however, a sufficient number of specimens is to be used such that two independent data sets are obtained when testing in a multiple specimen configuration. Whenever possible, tests are to be conducted on full scale specimens. It is recognized, however, that facilities do not yet exist that have the load capacity to test full size specimens under some of the conditions outlined in the guidelines. In this case scale model specimens are acceptable, provided they are not less than 1/4 full scale and are representative of the full scale prototype.

Properly documented pre-qualification tests previously conducted on a system may be used to satisfy the requirements outlined in the guidelines, *provided the system to be tested is similar in design, materials and construction as that tested previously.*

Referring to Table 1, the pre-qualification test schedule is divided into two categories: Preliminary Characterization (category I) and Ultimate and Reserve Capacity (category II). Category I tests are designed to establish if, and the extent to which the properties and characteristics of a system are dependent on such things as virgin loading, frequency of load, load cycle history, vertical load, and load plane rotation. Note that the results of the Category I tests have a direct impact on the scope of prototype tests required for any given system. Category II tests are intended to establish the ultimate capacity, or demonstrate reserve capacity, of the system under various load conditions. Ideally, all Category II tests would be conducted to failure; however, there are still many uncertainties with regard to proof testing isolation systems under combined load conditions. This remains an immediate research need.

Table 1. Schedule of Pre-Qualification Tests[1]

Category	Test	Title/Purpose
I	I.1	Establish dependence on virgin loading
	I.2	Establish dependence on frequency of load
	I.3	Establish dependence on load cycle history
	I.4	Establish dependence on load cycling
	I.5	Establish dependence on vertical load
	I.6	Establish dependence on load direction
	I.7	Establish dependence on load plane rotation
	I.8	Establish dependence on bilateral load
	I.9	Establish dependence on temperature
	I.10	Establish dependence on creep
	I.11	Establish dependence on aging
II	II.1	Ultimate compression under zero lateral load
	II.2	Compression in displaced position
	II.3	Ultimate Tension under zero lateral load
	II.4	Tension in displaced position
	II.5	Lateral load and displacement capacity under design vertical load

[1]Pre-qualification shall also include a complete series of prototype tests (Table 2) and quality control tests (Table 3).

Prototype Tests

A complete series of prototype tests is to include all Category III tests and applicable Category IV tests listed in Table 2, as well as a full series of quality control tests (Table 3). Each prototype test is to be performed separately on two full-scale specimens of each type and size of isolation unit or component. Pre-qualification tests must have been conducted on a unit or component of similar design, material and construction prior to prototype testing.

The prototype schedule is divided into two categories: Seismic Loads (Category III) and Non-Seismic Loads (Category IV). Category III tests (seismic loads) are intended to establish the properties and characteristics of the system under seismic load conditions. Average Effective Stiffness and Average Energy Dissipation are evaluated for a range of displacements, under load and environmental conditions determined to be relevant based on the results of the Category I tests of the pre-qualification series. Stability of the system under extreme load conditions is also evaluated. Category IV tests (non-seismic loads) are intended to demonstrate the capacity of the system under non-seismic loads, such as wind load, thermal displacement, thermal cycling and braking/centrifugal forces. Only those Category IV tests relevant to the project or application are required in prototype testing.

The guidelines recommend that properly documented prototype tests previously conducted on a unit or component of similar size may be used to satisfy the prototype test requirement, provided:

(1) the unit or component is of similar design, material and construction;
(2) the largest overall dimension of the unit or component to be tested is within ± 10% of the same dimension of the unit or component previously tested;
(3) most other critical dimensions are within ±15% of the size previously tested.

Quality Control Tests

A full series of quality control tests for completed elastomeric isolation units is to include the three tests listed in Table 3. Similar tests for sliding systems are outlined in the respective guidelines for QC testing of sliding isolation systems. Referring to Table 3, it is recommended in the guidelines that all units manufactured undergo the sustained compression and effective stiffness and energy dissipation tests, and that 20% of all units manufactured undergo the compression stiffness test.

The purpose of the sustained compression test is to verify the integrity of the bond between the steel and elastomer layers. The test requires loading the specimen to 1.5 times the rated nominal vertical load capacity and maintaining that load for a minimum of 12 hours. The time may be reduced to 3 hours, however, if the supplier has documented results of a least 1000 consecutive tests without rejection.

Table 2. Schedule of Prototype Tests[1]

Category	Test	Title/Purpose
III	III.1	Effective Stiffness and Energy Dissipation
	III.2	Stability against degradation
	III.3	Stability at Maximum Lateral Displacement
IV	IV.1	Wind load
	IV.2	Thermal displacement
	IV.3	Stability with thermal cycling
	IV.4	Braking/Centrifugal force

[1]Prototype shall also include a complete series of quality control tests (Table 3).

Table 3. Schedule of Quality Control Tests of Elastomeric Systems

Test	Title/Purpose
1	Sustained Compression
2	Compression Stiffness
3	Effective Stiffness and Energy Dissipation

The guidelines for quality control testing, both elastomeric and sliding, also include recommended production tests. Production tests are conducted on materials or parts during fabrication and are recommended as part of the overall quality control program for the isolation system.

Example Test Procedure

Each test procedure is presented in a standard format that includes the following elements: test designation, purpose, sequence, procedure, criteria and exceptions (where applicable). Presented below is an example of a typical test description. The test is from Category I of the pre-qualification series and is intended to establish a dependence on vertical load.

Test Designation: I.5

Purpose: Establish dependence on vertical load.

Sequence: Three fully reversed cycles to peak displacements of $\pm D$. Tests shall be conducted for vertical loads corresponding to P_L, P_D, P_U. The frequency of loading shall be not less than f_L or 0.004 cyc/sec.

Procedure: Place the specimen in the test machine and secure to the supports and loading plate. Apply the full vertical load to the specimen and allow the load to stabilize. Apply the cyclic lateral load to the specimen for the required 3 fully reversed cycles of the test. Remove the vertical load. The test shall be run continuously without pause between cycles. The test shall be conducted at the vertical loads specified in the order P_L, P_D and P_U. Sufficient time shall be allowed between tests at the different vertical loads to dissipate any heat developed during the previous test.

Criteria: The System, Unit or Component response is considered to be independent of vertical load if:

(1.) the Average Effective Stiffnesses measured at vertical loads corresponding to P_L and P_U are within $\pm\alpha\%$ of the Average Effective Stiffness measured at the vertical load corresponding to P_D, i.e.,

$$\frac{\left| K_H^P - K_H \right|}{K_H} \leq 0.01\alpha \qquad (1)$$

where K_H is the reference Average Effective Stiffness measured at a vertical load corresponding to P_D, and K_H^P denotes the Average Effective Stiffness measured at vertical loads corresponding to P_L and P_U.

(2.) the Average Energy Dissipation measured at vertical loads corresponding to P_L and P_U are within $\pm\beta\%$ of the Average Energy Dissipation measured at the vertical load corresponding to P_D, i.e.,

$$\frac{\left| E_H^P - E_H \right|}{E_H} \leq 0.01\beta \qquad (2)$$

where E_H is the reference Average Energy Dissipation measured at a vertical load corresponding to P_D, and E_H^P denotes the Average Energy Dissipation measured at vertical loads corresponding to P_L and P_U.

Parameters D, P_L, P_D, and P_U correspond to the design displacement, lower, design and upper rated vertical load capacity, respectively. Parameter f_L is termed the "lower threshold frequency" and is defined as the minimum frequency that is less than the frequency of isolation, at which the measured response will be within a specified percentage of the response at the actual frequency of isolation. The lower threshold frequency is established in test I.3 (Table 1). The "draft" nature of the guidelines is evident in the performance criteria of this example: criteria have not been assigned "hard" numbers as of yet, but are instead expressed in terms of variables α and β. A recommendation is made in the guidelines as to the range of these parameters. In this case, α and β are likely to fall in the range of 10 to 30 (%).

5. Summary

Prototype and quality control tests are required of almost all seismic isolation systems designed and installed in the United States. Pre-qualification tests are formally not required by the codes, but are usually conducted in one form or another as a new system is developed. At the present time, however, standards do not exist for conducting these much needed tests.

Guidelines for pre-qualification, prototype and quality control testing are currently being developed at NIST. The draft guidelines are presented in three reports, one report addresses pre-qualification and prototype testing, the other two reports address quality control testing. The guidelines are applicable to all types of systems, whether they be elastomeric, sliding or hybrid, and are independent of the superstructure. The guidelines are still considered draft - the final guidelines will be developed after thorough review and evaluation of the draft guidelines. The review process will involve broad industry input and a testing component.

6. Acknowledgements

The author would like to gratefully acknowledge the NIST Oversight Committee for their guidance and assistance in developing the draft guidelines. The committee includes Dr. Ian Buckle, Dr. Charles Kircher, Professor James M. Kelly, Dr. Ronald Mayes and Dr. Victor A. Zayas. Their time and effort are greatly appreciated.

7. References

Guide Specifications for Seismic Isolation Design (1991), American Association of State Highway and Transportation Officials, Washington, D.C.

Shenton III, H.W., 1994a, "Draft Guidelines for Pre-qualification and Prototype Testing of Seismic Isolation Systems," NISTIR XXXX, in review, National Institute of Standards and Technology, Gaithersburg, Maryland.

Shenton III, H.W., 1994b, "Draft Guidelines for Quality Control Testing of Elastomeric Seismic Isolation Systems," NISTIR XXXX, in review, National Institute of Standards and Technology, Gaithersburg, Maryland.

Shenton III, H.W., 1994c, "Draft Guidelines for Quality Control Testing of Sliding Seismic Isolation Systems," NISTIR XXXX, in review, National Institute of Standards and Technology, Gaithersburg, Maryland.

Uniform Building Code (1991), International Conference of Building Officials, Whittier, California.

DESIGN EXAMPLES

Isolation System Design and Specification for the Olympic Boulevard Off-Ramp

Menshin Design Example of a Highway Bridge

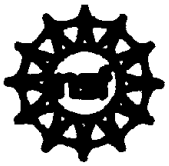

NIST

U.S. Department of Transportation
Federal Highway Administration

ISOLATION SYSTEM DESIGN AND SPECIFICATION FOR THE OLYMPIC BOULEVARD OFF-RAMP

David M. Jones[1], Deepak Choudhury[1]

INTRODUCTION

The design and specification of seismic isolation bearings for the first new bridge in California to use this technology forms the basis of this paper. This project is the first use of isolation bearings in a temporary structure followed by their reuse in a permanent structure. It is also the first use of a performance-type specification for isolation devices in California.

THE PROJECT

The Interstate 680 and State Highway 24 Interchange in Walnut Creek, California, is a busy component of the San Francisco Bay transportation network. It carries an average of 280,000 vehicles per day. A major reconstruction of the entire interchange, to increase capacity and improve safety, is underway. To minimize disruption to normal traffic during the construction period, a major, temporary detour ramp is under construction. This structure will be demolished in a subsequent construction phase. During the study for the reconstruction, a permanent segment of the final reconstruction for the Olympic Boulevard off-ramp separation was identified as very similar in width, vertical profile and horizontal geometry as a segment of the temporary ramp structure. This similarity would allow reuse of material from the temporary structure in the permanent one. Cost studies showed that a structure type normally considered uneconomical in California for a structure of this configuration, steel plate girders, was the best choice, provided they could be placed in the permanent Olympic Boulevard structure. Further cost comparison to a standard structure showed that a seismically isolated structure would be the most economical choice. Both the steel girders and the isolation bearings will be used, first in the temporary structure and then salvaged and placed in the permanent structure.

The Olympic Boulevard structure is four spans, 700 feet (213m) long, with a maximum span of 210 feet (64m). The cross section consists of three 7-foot (2.1m) deep plate girders. Single columns support the structure along with seat-type abutments. The bridge footings are supported on piles.

ISOLATION SYSTEM DESIGN

The isolation system assumed for the design was the lead-rubber isolation bearing. The design of the lead-rubber isolation bearing consists of two interrelated parts:

---

[1] Dynamic Isolation Systems, Inc., 2855 Telegraph Avenue, Suite 410, Berkeley, California 94705

1. The isolators must be designed for all nonseismic load cases.

    - The minimum plan size is governed by the dead and live load requirements.
    - The thickness of the internal rubber layers is determined by the vertical load, vertical stiffness and rotational capacity requirements.
    - The total rubber thickness in the bearing is generally governed by thermal loads, the desired earthquake force reduction and any force redistribution requirements. The minimum height of the elastomer is twice the R + S + T displacements.
    - The minimum diameter of the lead core is determined by the requirement to maintain elastic response under AASHTO prescribed combinations of wind, braking and centrifugal loads. The distribution of the lead cores throughout the system can be used to control the force levels transmitted to various substructures.

2. The bearings must be designed to safely support the vertical loads at seismic displacements and remain stable at those displacements. Typically, load capacity and stability are checked at 1.5 times the design seismic displacement. The seismic design forces transmitted by the isolators are a function of the seismic input, the vertical loads on the system and the strength and stiffness of the bearings.

The capacity of the elastomeric isolator to withstand vertical load is based on the limiting-strain criterion given in the *AASHTO Guide Specifications for Seismic Isolation Design*. This specification recognizes that shear strains are induced in reinforced elastomeric bearings by compression, rotation and shear deformations. The sum of the shear strains in the elastomer due to the combination of vertical load, rotation and horizontal deflection is limited to a fraction of the ultimate elongation-at-break of the elastomer, ϵ_u.

Bearings are also checked for the following limit states:

- critical (buckling) load
- stability (rollover)

The critical buckling load is taken from the classical theory for elastomeric isolators. The factor-of-safety (FS) against buckling is given by:

$$FS = P_{critical} \cdot (1 - \Delta/B)/P$$

where P_{cr} = critical load for the bearings.

A factor is included to allow for the reduction in effective plan area (footprint) of the isolator as it deflects horizontally.

The rollover displacement, Δ_{ro}, for systems with dowelled connections, may be computed from the overturning equilibrium equations for the isolator. The factor-of-safety against rollover is then given by:

$$FS = \Delta_{ro}/\Delta$$

where Δ_{ro} = rollover displacement.

The system was designed for the five AASHTO, nonseismic, lateral-load groups, plus the Caltrans seismic loading.

Factored AASHTO Lateral Load Groups

Group II	1.3 (W)
Group III	1.3 (CF + 0.3W + WL + LF)
Group IV	1.3 (CF + [R + S + T])
Group V	1.25 (W + [R + S + T])
Group VI	1.25 (CF + 0.3W + WL + LF + [R + S + T])
Seismic	1.0 (EQ)

For this bridge, the controlling, nonseismic lateral-load group was wind. The lateral yield level of the bearings was set to the factored wind load (1.3 × W). This insures that the lateral displacements due to all nonseismic loads will be small. The vertical dead plus live loads set the minimum plan sizes of the bearings. The seismic performance of these bearings was evaluated.

Seismic Performance

To evaluate the system seismic performance, nonlinear time-history analysis is used to prepare a nonlinear design spectrum. A single-degree-of-freedom model, incorporating the bilinear stiffness properties of the bearings, is prepared. The nonlinear spectrum used is generated as follows:

- Seven time histories are used as seeds.
- Each seed record is frequency-scaled so that its 5%-damped response spectrum closely matches the design spectrum. The average error on all frequencies is typically smaller than 5%. Figure 1 shows an example.
- The seed records are used as input for the single-degree-of-freedom, nonlinear, hysteretic model.
- The mean of the peak response of the nonlinear model to the seven scaled spectra forms the design spectrum.

For this project, the specified design spectrum was the Caltrans ARS B curve, 10 to 80 feet (3 to 24m) of alluvium, 0.6g peak ground acceleration. This is a maximum credible design spectrum corresponding to a 2500-year return period.

The seven time-history seeds used were:

1 - El Centro, 1940, NS
2 - Olympia, 1949, N04W
3 - Taft, Kern County, 1952, S69E
4 - El Centro, 1934, NS
5 - El Centro, 1940, EW
6 - Caltech Artificial A1
7 - Caltech Artificial B2

By first meeting all requirements for nonseismic load, constructing nonlinear spectra and evaluating the seismic performance of the initially designed bearings, a final bearing plan size and height is determined by iterating. Since the lateral yield level of the bearing is previously determined, bearing stiffness (area and rubber height) can be varied to obtain the most effective seismic performance within the vertical-load and lateral-displacement constraints. For this bridge, the bearings are bolted in place, eliminating the rollover-limit state.

The final bearing sizes selected were:

LOCATION	PLAN SIZE	HEIGHT	LEAD CORE SIZE
Abutments	23" × 23"	10"	5.75"
	580 mm × 580 mm	250mm	145mm
Piers	27" × 27"	10"	5.75"
	690 mm × 690 mm	250mm	145mm

The seismic performance for the single-mode, nonlinear spectrum analysis is:

Effective Period	1.8 sec	
F/W Lateral Force Coefficient	0.29g	290 gals
Maximum Displacement	9 in	230mm
Lateral Force	1700 kips	7600 kN

The bearings were incorporated into the conventional STRUDL model of the structure for seismic response-spectrum analysis. For this analysis, the elastic design spectrum is replaced with a composite spectrum. The composite spectrum is a combination of the nonlinear spectrum and the ARS design spectrum, shown in Figure 2. In the isolated period range, the nonlinear spectrum is used. At 80% of the isolated period and less, the elastic design spectrum is used. The bearing stiffness used in the response-spectrum analysis is the secant stiffness based on the maximum seismic displacement. From the STRUDL model:

First Mode	2.1 sec translation (transverse)
Second Mode	1.9 sec translation (longitudinal)
Third Mode	1.6 sec torsion

Table 1 shows the displacements and forces from the STRUDL analysis and the nonlinear spectrum, single-mode analysis. In the longitudinal direction, the difference in both the forces and displacements between STRUDL and the single-mode method are less than 10%.

In the transverse direction, the maximum difference in displacement in the two methods is 36%. The maximum difference in force is 50%. This is expected because the STRUDL model accounts for the mass distribution in the unequal spans and superstructure flexibility, while the single-mode method does not.

An ANSR-II, 3-dimensional stick model was also prepared for a step-by-step, time-integration analysis. This model incorporated the bilinear hysteretic properties of the bearings. Analysis was performed for three scaled records. The seed time histories used were El Centro, 1940 NS; Taft, 1952 S69E; and Olympia, 1949 N04W. Table 2 shows the displacements and forces obtained from this analysis. These are the maximum values of force and displacement at any time step at the locations listed for the three records. Note the scatter, typically a 20% to 30% difference between the lowest and highest values, even though the input records were scaled to produce the same elastic response spectrum.

Table 3 shows the forces and displacements for the single-mode, STRUDL and ANSR-II model. For ANSR-II, the values shown are the mean of the three sets of results from Table 2. The results are consistent, considering the difference between the SRSS modal combination and step-by-step, time-integration methods.

Code Checks

The *AASHTO Guide Specifications* uses a strain-limiting or rated-load method for determining bearing load capacity. In this method, the equivalent shear strain in the rubber must be less than some fraction of the minimum specified elongation-at-break (ϵ_u). The fraction of ϵ_u depends on the load case under consideration. The load combinations specified are as follows:

Dead load plus live load:

$$\tfrac{1}{3}\,\epsilon_u \geq \epsilon_{ac}$$

Dead load plus live load – with imposed rotation and nonseismic displacement:

$$\tfrac{1}{2}\,\epsilon_u \geq \epsilon_{ac} + \epsilon_{sh} + \epsilon_{sr}$$

Dead load with imposed rotation and seismic displacement:

$$\tfrac{3}{4}\,\epsilon_u > \epsilon_{ac} + \epsilon_{eq} + \epsilon_{sr}$$

The equivalent shear strain due to compression from vertical load, ϵ_{ac}, is defined as:

$$\epsilon_{ac} = 6S\frac{P}{A_b E(1+2kS^2)}\left[1-\frac{\Delta}{B}\right]$$

The shear strain due to rotation, ϵ_{sr}, is defined as:

$$\epsilon_{sr} = \frac{B^2\theta}{2t_i T}$$

The design conditions for the project are shown below:

	Units inches, kips		Units mm, kN	
Bearing Plan Size	**23**	**27**	**580**	**690**
Dead Load	160	600	710	2670
Dead Load + Live Load	250	800	1110	3560
Maximum R + S + T Displacement	1.6	0.9	41	23
Maximum Seismic Displacement	9	9	229	229
Imposed Rotation (radians)	0.007	0.007		

Bearing Load Capacity (kips)	Units inches, kips		Units mm, kN	
Bearing (Plan Size)	23	27	580	690
Vertical Load only	1174	1965	5220	8740
Vertical Load with Nonseismic Displacement	916	1639	4074	7290
Vertical Load with Seismic Displacement	770	1379	3425	6130

The capacities shown are for the design displacement, 9 inches. The controlling limit state is for vertical load at 1.5 times the design displacement, 13.5 inches (340mm).

Low Level Design

To examine the changes in the bearings if they were designed for a peak acceleration one half the original value, a design was performed for the same ARS spectrum (10 to 80 ft) alluvium, peak ground acceleration of 0.3g. The nonseismic loads remained the same. The factored wind load still controlled the lateral yield level of the bearings so the core size remains the same. The final bearing sizes are shown below:

Location	Plan Size	Height	Lead-Core Size	% of 0.6g by Design Volume
Abutment	17" × 17" 430mm × 430mm	7.5" 190mm	5.75" 145mm	41%
Piers	23" × 23" 580mm × 580mm	7.5" 190mm	5.75" 145mm	54%

The seismic performance is:

Effective Period	1.6 sec	
F/W Lateral Force Coefficient	0.18g	180 gals
Maximum Displacement	4.4 in	112mm
Lateral Force	1045 kips	4660 kN

The seismic strain-limit state, carrying the dead load at the seismic design displacement, is much less severe for this case (with the seismic displacement slightly less than one half of the 0.6g design). The design shear strain, due to seismic displacement, decreases from 150% to 117% and the [1 - Δ/B] term (effective plan area reduction) increases by a factor of 1.2. This allows the volume of the bearing to be reduced by roughly one half.

SPECIFICATIONS

Projects financed with public funds are built by contractors competing in an open bidding process. This process extends to all components of the project. Proprietary items are rarely allowed. For this project, the functional requirements of the isolation system were shown in the contract documents. Combined with the testing requirements in the specifications, this allowed competitive bidding for the isolation system components. The functional requirements are made up of two parts, the typical load-carrying requirements of a standard bearing and the additional requirements for seismic performance. Table 4 shows the bearing effective stiffness, yielded stiffness and energy dissipated per cycle with tolerances on these values. Table 5 shows the maximum seismic forces and displacements along with the maximum nonseismic lateral forces and displacements. The seismic forces and displacements are for the design spectrum, the ARS curve for 10 to 80 feet of alluvium, peak ground acceleration = 0.6g. The testing requirements are listed below. A single pair of each type of bearing was prototype tested. The quality control tests were performed on all bearings.

Prototype Tests

Prototype Test 1 - Twenty full-reversed cycles of loads at the lateral nonseismic force shown on the plans.

Prototype Test 2 - Three full-reversed cycles of loading at each of the following increments of the seismic displacements shown on the plans: 0.25, 0.50, 0.75, 1.0, and 1.1.

Prototype Test 3 - Ten full-reversed cycles of loading at the seismic displacements shown on the plans.

Prototype Test 4 - Three full-reversed cycles of loading at each of the following increments of the seismic displacement shown on the plans: 1.25 and 1.5.

Quality Control Tests

Proof Compression Test - The bearings shall be loaded for 12 hours at 1.5 times the sum of the dead load and live load shown on the plans.

Proof Combined Compression and Shear Tests - The bearings shall be tested at a vertical load of 1.0 times the total of dead load plus live load shown on the plans, and five full-reversed cycles of loading at 0.5 times the seismic displacement shown on the plans. The bearings may be tested in pairs. The test results shall be within ±10% of precalculated values.

For a successful prototype test, the following conditions were specified:

- The load-displacement plots of Prototype Tests 1, 2 and 3 shall have a positive incremental lateral stiffness (load divided by displacement).
- At each displacement increment specified in Prototype Test 2, there shall be less than ±10% change from the average value of effective stiffness of the given test specimen over the required three cycles of test.
- The effective stiffness (K_{eff}) of each test specimen shall not increase or decrease more than 15% over the test specified in Prototype Test 3.
- The energy dissipated per cycle (EDC) in Prototype Test 3 of each test specimen shall be within 10% of the value of EDC given on the plans.
- All specimens of seismic isolation bearings shall remain stable and without splits or fractures or other distress at all prototype loading conditions.

Test Results

Table 6 shows the results from Prototype Test 3. The force-displacement test loops are consistent and stable, with effective stiffness values remaining constant from the first through the tenth cycle. The energy dissipated per cycle (EDC) decreases less than 10% from the first to the tenth cycle. For both bearings, the effective stiffness is 10% below theoretical, while the EDC is about 10% higher. Figure 3 shows typical force-displacement test loops.

Tables 7 and 8 show the results of the quality control combined compression and shear tests for the small and large bearings, respectively. The effective stiffness values are within 5% of the theoretical values. The EDC is always greater than the specified value.
For these bearings with a rubber thickness of 6 inches (152mm), the maximum test shear strain was 225%.

FIELD TESTING

Engineers from the University of California's Richmond Field Station, in cooperation with Caltrans, are conducting a field test program on the temporary viaduct. This program includes snap-back tests of the bridge superstructure and bearings and the free-standing piers.

ACKNOWLEDGEMENTS

The assistance provided by Eric Thorkildsen of Caltrans and the staff of DIS is gratefully acknowledged.

Table 1: Comparison of STRUDL and Single-Mode Nonlinear Specification

	STRUDL Transverse	STRUDL Longitudinal	Single-Mode Nonlinear Spectrum Transverse and Longitudinal
DISPLACEMENTS (feet)			
Abutment 1	0.68	0.78	0.74
Pier 2 - Deck	0.89	0.78	0.74
- Bent	0.14	0.12	0.12
Pier 3 - Deck	1.01	0.78	0.74
- Bent	0.16	0.12	0.12
Pier 4 - Deck	0.75	0.78	0.74
- Bent	0.11	0.12	0.12
Abutment 2	0.55	0.78	0.74
FORCES (kips)			
Abutment 1	228	272	286
Pier 2	362	337	325
Pier 3	411	337	325
Pier 4	304	336	325
Abutment 2	192	269	286
TOTAL	**1497**	**1551**	**1547**

Table 2: Results from ANSR-II Analyses

		Transverse			Longitudinal		
		1	2	3	1	2	3
Displacements (feet)							
Abutment 1		0.59	0.56	0.85	0.81	0.69	0.89
Pier 2	Deck	0.98	0.84	1.13	0.81	0.69	0.89
	Pier	0.16	0.13	0.16	0.14	0.11	0.13
Pier 3	Deck	1.14	1.00	1.22	0.81	0.69	0.89
	Pier	0.18	0.15	0.17	0.14	0.11	0.14
Pier 4	Deck	0.91	0.84	1.10	0.81	0.69	0.89
	Pier	0.15	0.13	0.15	0.14	0.11	0.13
Abutment 2	Deck	0.44	0.38	0.62	0.81	0.69	0.89
Forces (kips)							
Abutment 1		207	213	268	288	256	307
Pier 2		405	348	438	352	309	372
Pier 3		464	398	473	345	308	371
Pier 4		374	342	425	356	311	376
Abutment 2		147	164	201	291	261	311
TOTALS		**1597**	**1465**	**1805**	**1632**	**1445**	**1737**

Table 3: Comparison of Results

		Displacement (ft)			Force (kips)		
		Single Mode	STRUDL	ANSR	Single Mode	STRUDL	ANSR
Longitudinal							
Abutment 1		0.74	0.78	0.80	286	272	284
Pier 2	Deck	0.74	0.78	0.80	325	337	344
	Pier	0.12	0.12	0.13			
Pier 3	Deck	0.74	0.78	0.80	325	337	341
	Pier	0.12	0.12	0.13			
Pier 4	Deck	0.74	0.78	0.80	325	336	348
	Pier	0.12	0.12	0.13			
Abutment 2		0.74	0.78	0.80	286	269	288
Transverse							
Abutment 1		0.74	0.68	0.67	286	228	229
Pier 2	Deck	0.74	0.89	0.98	325	362	397
	Pier	0.12	0.14	0.15			
Pier 3	Deck	0.74	1.01	1.12	325	411	445
	Pier	0.12	0.16	0.17			
Pier 4	Deck	0.74	0.75	0.95	325	304	380
	Pier	0.12	0.11	0.14			
Abutment 2		0.74	0.55	0.48	286	192	171

Table 4: Bearing Seismic Properties

	K_{eff} (kip/in)	K_r (kip/in)	EDC (kip/in)
Abutments 1 & 5	10.8	7.7	914
Bents 2, 3 and 4	14.0	10.9	914

Tolerance	K_{eff}	Prototype Test	± 10% K_{eff} in Table
	K_r	Prototype Test	≥ 90% K_r in Table
	EDC	Prototype Test	≥ 90% EDC in Table

Table 5: Maximum Specified Lateral Loads and Displacements

	SEISMIC		LATERAL NONSEISMIC	
	Forces (kip)	Displ. (in)	Forces (kip)	Displ. (in)
Abutment 1	100	9	28	½
Bent 2	135	9	28	½
Bent 3	135	9	28	½
Bent 4	135	9	28	½
Abutment 5	100	9	28	½

Table 6: Prototype Test G
Displacement = ±9.0"

Cycle	Prototype A		Prototype B	
	K_{eff} (kip/in)	EDC (kips-in)	K_{eff} (kip/in)	EDC (kips-in)
1	9.8	1007.6	12.8	1041.3
2	9.8	988.9	12.8	1021.0
3	9.7	978.5	12.8	1010.9
4	9.7	971.2	12.7	1005.5
5	9.7	963.8	12.7	1001.8
6	9.7	965.0	12.7	998.0
7	9.7	961.5	12.7	995.3
8	9.7	959.3	12.7	991.7
9	9.7	956.2	12.7	989.8
10	9.7	947.6	12.7	988.3
Maximum Value Minimum Value	9.8 9.7	1007.6 947.6	12.8 12.7	1041.3 988.3
Percent Change	-1.0%	-6.0%	-.7%	-5.1%
Allowable Change	±15%	NA	±15%	NA
Avg. Value	9.7	970.0	12.7	1004.4
Specification Value	10.8	908.3	14.0	916.2
Avg. Variance from Spec.	-10.2%	+6.8%	-9.3%	+9.6%
Allowable Variation from Spec.	NA	±10%	NA	±10%

Table 7: Force-Deflection Characteristics
Type A Isolators (S23-10.38-5.75)

Serial Number	K_{eff} (kips/in)	EDC (kip-in)
501	13.7	465.5
502	13.7	465.5
503	13.9	475.8
504	13.9	475.8
505	14.1	477.8
506	14.1	477.8
Mean Value	13.90	473.0
Measured Range	13.7 to 14.1	465.5 to 477.8
Theoretical Value	13.72	449.4
Percent Variation from Theoretical	-0.1% to +2.8%	+3.6% to +6.3%

Table 8: Force-Deflection Characteristics
Type B Isolators (S27-10.38-5.75)

Serial Number	K_{eff} (kips/in)	EDC (kip-in)
601	16.9	492.5
602	16.7	490.3
603	16.7	490.3
604	16.9	492.5
605	16.5	497.8
606	16.5	497.8
607	16.6	515.3
608	16.2	467.2
609	16.2	467.2
Mean Value	16.58	490.1
Measured Range	16.2 to 16.9	467.2 to 515.3
Theoretical Value	16.92	457.3
Percent Variation from Theoretical	-4.3% to -0.1%	+2.2% to 12.7%

DEFINITIONS

A_b	=	Bonded area of rubber
B	=	Plan dimension in loaded direction of rectangular bearing of diameter of circular bearing
d_i	=	Lateral displacement under earthquake loads
E	=	Modulus of elasticity of elastomer
K	=	Material constant
P	=	Maximum vertical load resulting from the combination of dead load plus live load (including seismic live load, if applicable) using a γ factor of 1
ϵ_{eq}	=	Shear strain due to d_i, the seismic design displacement
ϵ_{ac}	=	Shear strain due to vertical loads
ϵ_{sh}	=	Shear strain due to maximum horizontal displacement resulting from creep, post-tensioning, shrinkage, and thermal effects computed between the installation temperature and the least favorable extreme temperature
ϵ_{sr}	=	Shear strain due to imposed rotation
ϵ_c	=	Compression strain in bearing due to vertical loads
ϵ_u	=	Minimum elongation-at-break of rubber
θ	=	Rotation imposed on bearing
Δ	=	Shear deflection in the bearing

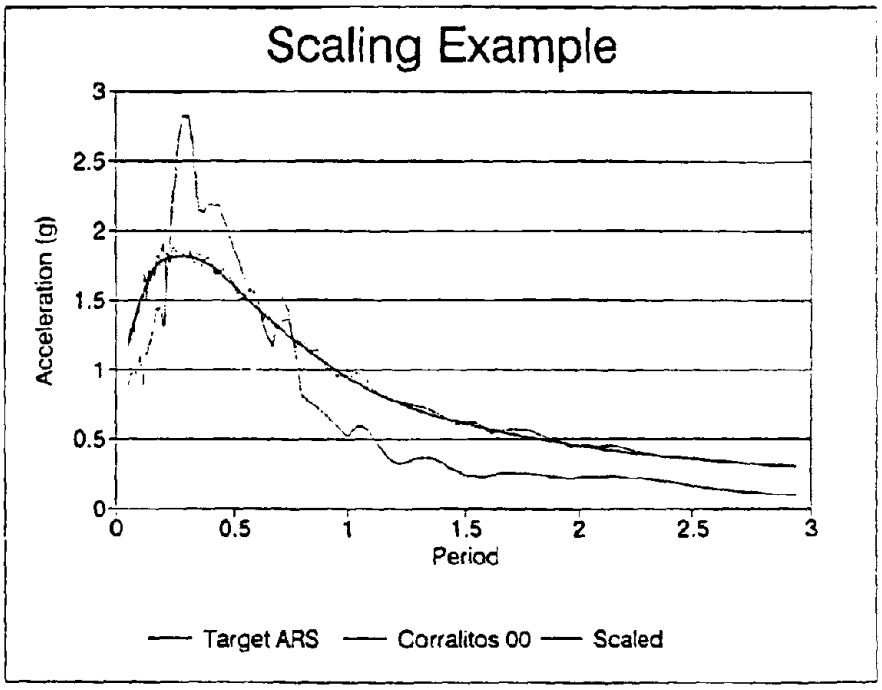

Figure 1

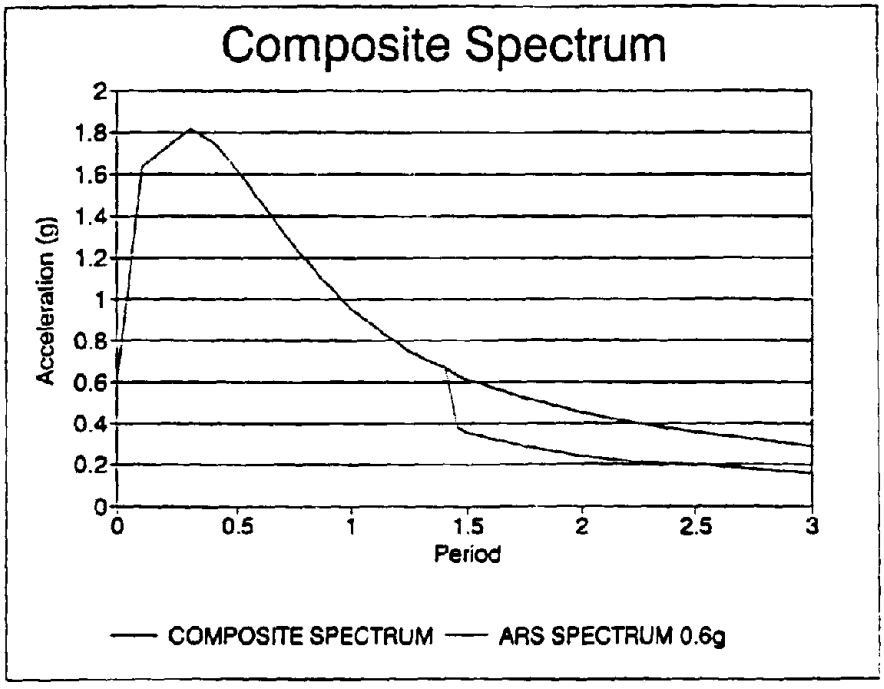

Figure 2

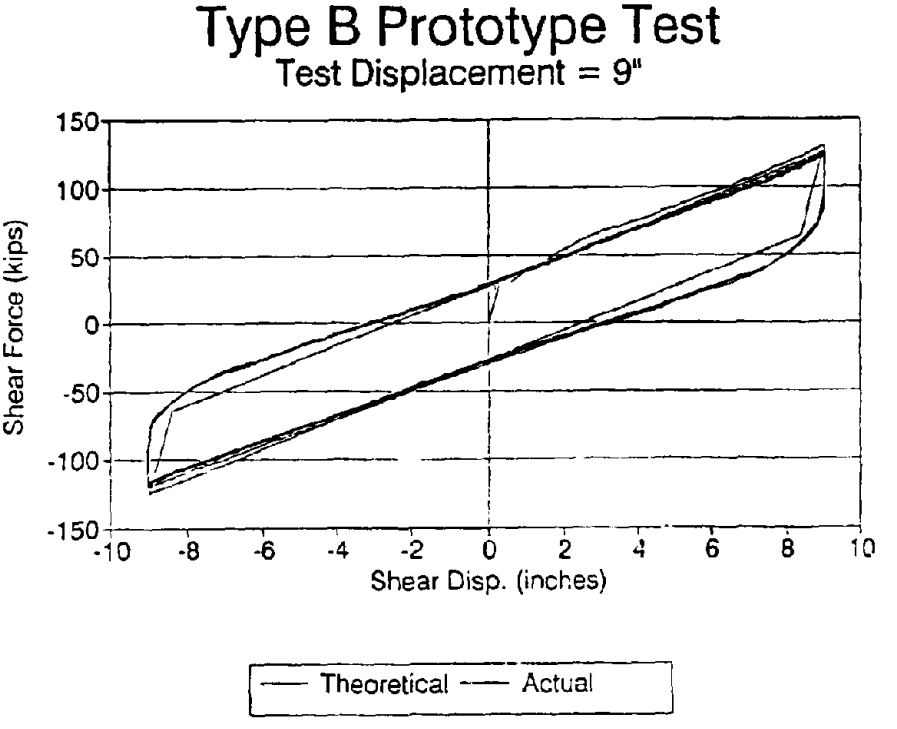
Type B Prototype Test
Test Displacement = 9"
Shear Force (kips)
150
100
50
0
-50
-100
-150
-10
-8
-6
-4
-2
0
2
4
6
8
10
Shear Disp. (inches)
Theoretical
Actual

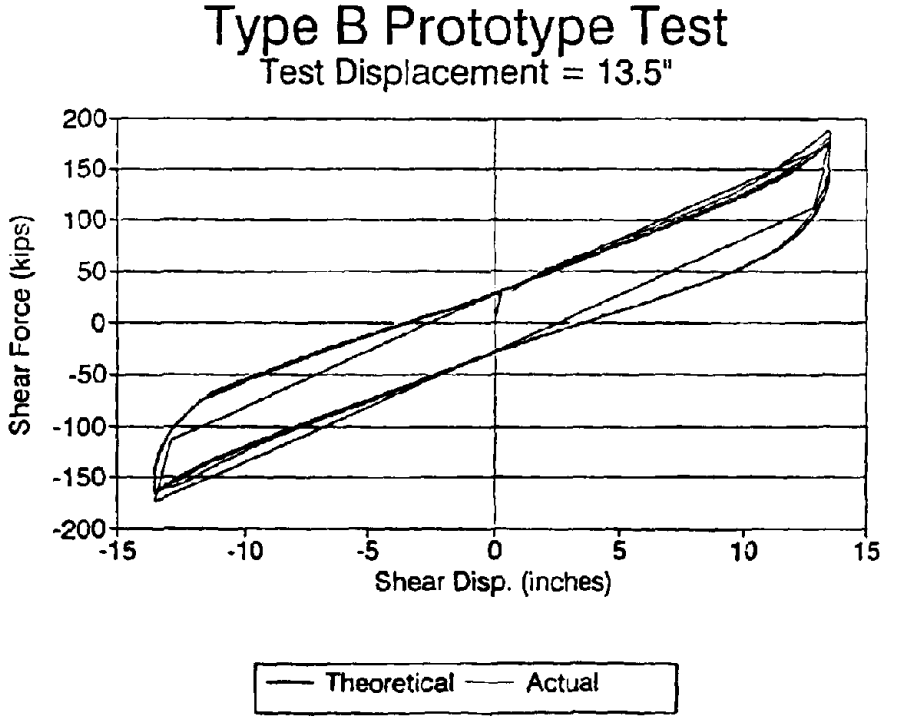
Type B Prototype Test
Test Displacement = 13.5"
Shear Force (kips)
200
150
100
50
0
-50
-100
-150
-200
-15
-10
-5
0
5
10
15
Shear Disp. (inches)
Theoretical
Actual

Figure 3

MENSHIN DESIGN EXAMPLE OF A HIGHWAY BRIDGE

Kazuhiko KAWASHIMA[1], Shigeki UNJOH[2], Tsuneo UZUKA[3]
Kazuhiko KAWAKAMI[4], Kazuomi KUMAKURA[5] and Hideo TANI[6]

1) Head, Earthquake Engineering Division, Public Works Research Institute, Ministry of Construction, Tsukuba Science City, Japan
2) Senior Research Engineer, ditto
3) Director, Road Construction Division, Department of Public Works, Tochigi Prefectural Government, Utsunomiya, Tochigi-ken, Japan
4) Section Chief, ditto
5) Senior Chief, ditto
6) Technical Staff, ditto

ABSTRACT

This paper presents a Menshin design example of a highway bridge based on the Japanese design specifications. The design of Yama-age Bridge which was completed in May 1993 in Tochigi Prefecture is presented as an example. The Yama-age bridge is of 6-span continuous concrete box girder with length of 246.3m. High damping rubber bearings were adopted as Menshin devices.

YAMA-AGE BRIDGE

Fig. 1 and **Photo 1** show the Yama-age bridge[1)-3)]. **Table 1** summarizes the design outlines of the Yama-age bridge. The superstructure is of 6-span continuous prestressed concrete two-cell box girder with length of 246.3m. The deck width ranging from 6.5m (standard section) to 8.0m (wide section). The abutment is of a inverted T-type reinforced concrete substructure and the piers are of reinforced concrete wall type with rectangular section. The foundations of all substructures are of direct foundation. High damping rubber (HDR) bearing is adopted for the bridge. Since Menshin design is applied only in longitudinal direction, the displacement in transverse direction is restrained by stoppers. Forced excitation test using an eccentric-mass shaker and quick-release jacks was also made for the bridge in December 1992 as shown in **Photo 2**[4)].

The ground condition of the Yama-age bridge consists of sand-gravel layers and slate layer. N-value by the standard penetration test for the sand-gravel layers is ranging from 30 to 50, and that of the slate layer is greater than 50. The ground condition is

classified as Class I.

MENSHIN DESIGN OF YAMA-AGE BRIDGE

Design Specifications

The Yama-age Bridge was designed in accordance with the regulations of the "Design Specifications for Highway Bridges[5]". "Guidelines for Design of Menshin Highway Bridges[6]" and "Manual for Menshin Design of Highway Bridges[7)-8)]" were also referred for the Menshin design issues. It should be noted that since the bridge was designed based on the Design Specifications for Highway Bridges, the design lateral force was not reduced in consideration of the damping effect of Menshin bearings.

Menshin Design

Fig. 2 shows the Menshin design flow used for the Yama-age Bridge. In the Menshin design of highway bridges, the Menshin devices are designed by the "Seismic Coefficient Method" and the "Bearing Capacity Method". In both methods, the lateral force is statically applied to the bridge, and the seismic safety is checked based on the allowable stress design approach in the Seismic Coefficient Method and bearing capacity basis considering ductility in the Bearing Capacity Method. Bridges are designed by the Seismic Coefficient Method, and then the ductility is checked for reinforced concrete piers by the Bearing Capacity Method.

Design of Menshin Bearing

The relation between shear modulus of elasticity $G(\gamma)$ and shear strain γ for HDR bearings adopted is shown in Fig. 3. The stiffness of the bearings shows the nonlinear characteristics depending on the strain of the bearing. The shear modulus of HDR is given by the following experimental equations.

$$\left.\begin{array}{ll} G(\gamma)=26.3-46.0\gamma+45.7\gamma^2-21.1\gamma^3+3.88\gamma^4 & (0<\gamma\leq 1.8) \\ G(\gamma)=0.31+6.89\gamma-1.08\gamma^2 & (\gamma>1.8) \end{array}\right\} \quad (1)$$

The design of HDR bearings was made according to the following procedure as :

1) Assume the design displacement of bearings for two levels of seismic lateral forces and compute the shear strain of bearings.

$$\gamma=\frac{u_B}{H_R} \quad (2)$$

where,

γ : shear strain

u_B : design displacement of bearing

H_R : thickness of rubber bearing

2) Compute the shear modulus of elasticity and the equivalent stiffness of bearings.

$$K_B = A_0 \times G(\gamma) \tag{3}$$

where,

$G(\gamma)$: shear modulus of elasticity

K_B : equivalent stiffness

A_0 : sectional area of bearing

3) Compute the natural period of the bridge and the horizontal design lateral force coefficient.

$$K_T = \sum K_B \tag{4}$$

$$T = \frac{2\pi \cdot R_d}{\sqrt{g \cdot K_T}} \tag{5}$$

where,

K_T : total stiffness of bearings

T : natural period

R_d : dead load of superstructure

g : gravity acceleration

4) Compute the displacement of bearings, and compare it with the assumed displacement.

$$u_s = \frac{R_d \cdot k_h}{K_B} \tag{6}$$

where,

k_h : lateral force coefficient

Tables 2 to 4 show the design of HDR bearings of the Yama-age bridge.

Design Lateral Force Coefficient

The bridge was designed based on the Seismic Coefficient Method. Since the seismic design structural unit of the Yama-age bridge is defined as the total bridge system, analytical idealization of the bridge is shown in Fig. 4. Bearings and foundations were modeled as equivalent linear spring elements. Natural period of the bridge is computed for the seismic design structural unit as :

$$T = 2.01 \cdot \sqrt{\delta} \tag{7}$$

$$\delta = \frac{\int w(s)\, u(s)^2 ds}{\int w(s)\, u(s) ds} \tag{8}$$

where,

T : natural period

$w(s)$: dead weight of the seismic design structural unit at point " s "

$u(s)$: lateral displacement at point " s " when subjected to $w(s)$ in the direction considered in design

Design seismic coefficient is computed as:

[Seismic Coefficient Method]

$$k_h = c_z \cdot c_G \cdot c_I \cdot c_T \cdot k_{h0} \quad (9)$$

$$c_T = 1.33 \cdot T^{-2/3} \text{ (Ground Condition : Class I)} \quad (10)$$

where,

k_h : lateral force coefficient
c_z : modification factor for zone (**Fig. 5**)
c_G : modification factor for ground condition (**Table 5**)
c_I : modification factor for importance (**Table 6**)
c_T : modification factor for structural response (**Table 7**)
k_{h0} : standard design horizontal seismic coefficient (=0.2)

[Bearing Capacity Method]

$$k_{he} = \frac{k_{hc}}{\sqrt{2 \cdot \mu - 1}} \quad (11)$$

$$k_{hc} = c_z \cdot c_I \cdot c_R \cdot k_{hc0} \quad (12)$$

$$c_R = 0.876 \cdot T^{-2/3} \text{ (Ground Condition : Class I)} \quad (13)$$

where,

k_{he} : equivalent lateral force coefficient for Bearing Capacity Method
k_{hc} : lateral force coefficient for Bearing Capacity Method
c_R : modification factor for structural response (**Table 8**)
μ : allowable ductility factor of reinforced concrete piers
k_{hc0} : standard design horizontal seismic coefficient (=1.0)

The natural period in longitudinal direction is 1.56sec, and that of the transverse direction is 0.194sec. Therefore, the lateral force coefficients are 0.16 and 0.20 in longitudinal and transverse directions, respectively. Since the natural period in longitudinal direction with usual design is 1.075sec, the lateral force coefficient is 0.20. Hence, by adopting the Menshin design, the lateral force is reduced by 20% than the usual design.

Table 9 shows the relative displacement of bearings by the Seismic Coefficient Method. **Table 10** shows the bending moment at the bottom of piers. The bending moment is compared between with and without the Menshin design. **Fig. 6** shows the cross section of pier (P1).

Check of Bearing Capacity for Lateral Force

To prevent a brittle failure such as falling-off of superstructure during large earthquakes, the bearing capacity of the reinforced concrete piers designed by the Seismic Coefficient Method was checked by the Bearing Capacity Method.

The natural period of the bridge is computed using the equivalent stiffness of bearings corresponding to the design displacement and equivalent yielding stiffness of substructures. Since it is 1.77 sec, the lateral force coefficient for the Bearing Capacity

Method k_{hc} is 0.60. **Tables 11 and 12** shows the check results of the bearing capacity of the reinforced concrete piers.

Dynamic Analysis

Dynamic Analysis was made to check the safety of the Yama-age Bridge. the response spectrum analysis and the time history analysis were made. The response spectrum and time history acceleration data of the earthquake ground motion corresponding to the Seismic Coefficient Method was used as an input acceleration. **Table 13** shows the equivalent stiffness and the equivalent damping ratio of HDR bearings.

Since the damping characteristics of the HDR bearings varies depending on the displacement, the following experimental equation on the damping ratio was used.

$$h_B = 0.172 - 0.00693\gamma + 0.00276\gamma^2 - 0.006924\gamma^3 \qquad (14)$$

where,

h_B : effective damping ratio

γ : shear strain of bearing

The damping ratio for the superstructure, substructures, and the foundations were assumed as 3%, 5%, and 10%, respectively. **Table 14** shows the natural period and the damping ratio of an each vibration mode. The 1st to 3rd vibration modes are shown in **Fig. 7**. The 1st mode is a sway mode of the superstructure and this is the most predominant mode in longitudinal direction. The damping ratio of the 1st mode is 14.3%.

Tables 15 and **16** shows the displacement of bearings and sectional forces of the pier bottom computed through the dynamic analyses in comparison with those by the Seismic Coefficient Method. The displacement of bearings and bending moment by the dynamic analyses are less than those by the Seismic Coefficient Method.

Fig. 8 shows the acceleration responses of deck and pier P1 computed through the time history analysis. It is found that the period of the deck response is elongated by adopting the Menshin design and that the deck acceleration is reduced comparing with that of the pier top.

It should be noted here that although the design lateral force was not reduced in consideration of the damping effect by Menshin devices in the design, it is found through the dynamic analyses that the response of the bridge is significantly reduced (by about 35 – 40% than those by the Seismic Coefficient Method) by adopting the Menshin design.

Design Details

According to the design specifications, the falling-off prevention devices are installed for the bridge. **Fig. 9** shows the stopper to prevent excessive displacement of the deck.

REFERENCES

1) Ikeda, T., Ozeki, k., Kumakura, K. and Abe, N. : Design of the Karasnyama No.1 Bridge

(Base Isolated Bridge), Bridge and Foundation Engineering, Vol.25, No.6, June 1991 (in Japanese)
2) Ikeda, T., Kumakura, K., Tani, H. and Abe, N. : Plan and Design of the Karasuyama No.1 Bridge, Bridge Engineering, Vol.27, No.6, June 1991 (in Japanese)
3) Uzuka, T., Kawakami, K., Kumakura, K. and Tani, H. : Menshin Design and Construction of Multi-span Continuous Prestressed Concrete Bridge, Proc. the 2nd U.S.-Japan Workshop on Earthquake Protective Systems for Bridges, December, 1992, Technical Memorandum of PWRI, No.3196
4) Kakinuma, T., Kawakami, K., Kumakura, K., Tani, H. and Abe, N. : Vibration Test of A Menshin Designed Multi-span Continuous Prestressed Concrete Bridge, Proc. the 3rd U.S.-Japan Workshop on Earthquake Protective Systems for Bridges, January, 1994, San Francisco
5) Japan Road Association : Design Specifications for Highway Bridges, Part I - V, February 1990 (in Japanese)
6) Technology Research Center for National Land Development : Guidelines for Base Isolation of Highway Bridges (Draft), March 1989 (in Japanese)
7) Public Works Research Institute : Development of Menshin Design of Highway Bridges, October, 1992, Technical Note of PWRI, Vol.60
8) Kawashima, K. : Manual for Menshin Design of Highway Bridges, Proc. the 2nd U.S.-Japan Workshop on Earthquake Protective Systems for Bridges, December, 1992, Technical Memorandum of PWRI, No.3196
9) Kawashima, K., Okado, M. and Horikawa, M. : Design Example of A Highway Bridge Based on The Manual for Menshin Design of Highway Bridges, Proc. the 2nd U.S.-Japan Workshop on Earthquake Protective Systems for Bridges, December, 1992, Technical Memorandum of PWRI, No.3196

Table 1 Design Outline of Yama-age Bridge

Bridge Type	Prestressed Concrete Post Tensioning
Structure	6-Span Continuous Box Girder
Road Class	Design Vehicle Speed : 60km/h
Bridge Length	246.3m
Span Length	$6 \times 40.8 = 244.8$m
Deck Width	Standard Section : 8.0m(roadway)+2.5m(sidewalk)=10.5m Widening section :11.0m(roadway)+2.5m(sidewalk)=13.5m
Live Load	TL-20
Impact Coefficient	$i = 1.0/(20+L)$
Alignment	R=∞ ~ A=240m
Vertical Gradient	1.0% ~ VCL=100m, R=2,500m ~ 5.0%
Cross Slope	1.5%(roadway), 2.0%(sidewalk)
Abutment Skew Angle	90° (A1), 90° 27' 43" (A2)
Ground Condition	Class : I
Design Lateral Force Coefficient	$k_h = 0.16$ (Longitudinal direction) $k_h = 0.20$ (Transverse direction)

Table 2 Dimension of HDR Bearings (unit:mm)

Item	A1	P1	P2	P3	P4	P5	A2
Dimension	700×855	950×1500	1030×1580	950×1500	950×1500	950×2500	700×855
Thickness of Rubber Layers	14.7×14 =205.8	21.0×6 =126.0	34.0×3 =102.0	24.0×5 =120.0	24.0×6 =144.0	18.7×8 =149.6	13.8×19 =262.2
Thickness of Insert Plates	4.2×13 =54.6	4.2×5 =21.0	4.2×2 =8.4	4.2×4 =16.8	4.2×5 =21.0	4.2×7 =29.4	4.2×18 =75.6
Height of bearing	260.4	147.0	110.4	136.8	165.0	179.0	337.8

Note)Dimension A×B represents the widths in longitudinal and transverse directions, respectively.

Table 3 Design of HDR Bearings by Seismic Coefficient Method

Item	[ ]:Unit	A1	P1	P2	P3	P4	P5	A2
Assumed Displacement	u_s [cm]	7.784						
Thickness of Rubber Bearing	H_R [cm]	20.58	12.60	10.20	12.00	14.40	14.96	26.22
Shear Strain	γ	0.378	0.618	0.763	0.649	0.541	0.520	0.297
Shear Modulus of Elasticity	$G(\gamma)$ [kgf/cm^2]	14.377	10.914	9.749	10.618	11.787	12.050	16.150
Area of Bearing	A_0 [cm^2]	5,872	14,137	16,161	14,137	14,137	14,137	5,872
Equivalent Stiffness	K_B [kgf/cm^2]	4,102	12,245	15,446	12,509	11,571	11,387	3,617
Number of Bearing on Each Substructure		2						
Sum of K_B	K_T [kgf/cm^2]	141,756						
Natural Period	T [sec]	1.337						
Dead load of Superstructure	R_d [kgf]	6,294,200						
Factor for Structural Response	c_T	1.096						
Design Lateral Force Coefficient	k_h	0.18						
Designed Displacement	u_s [cm]	7.770						

Table 4 Design of HDR Bearings by Bearing Capacity Method

Item	[ ]:Unit	A1	P1	P2	P3	P4	P5	A2
Assumed Displacement	u_s [cm]	32.69						
Thickness of Rubber Bearing	H_R [cm]	20.58	12.60	10.20	12.00	14.40	14.96	26.22
Shear Strain	γ	1.588	2.594	3.205	2.724	2.270	2.185	1.247
Shear Modulus of Elasticity	$G(\gamma)$ [kgf/cm^2]	8.674	10.916	11.299	11.064	10.385	10.208	8.469
Area of Bearing	A_0 [cm^2]	5,872	14,137	16,161	14,137	14,137	14,137	5,872
Equivalent Stiffness	K_B [kgf/cm^2]	2,475	12,247	17,902	13,035	10,195	9,647	1,896
Number of Bearing on Each Substructure		2						
Sum of K_B	K_T [kgf/cm^2]	134,794						
Natural Period	T [sec]	1.372						
Dead load of Superstructure	R_d [kgf]	6,294,200						
Factor for Structural Response	c_T	0.700						
Design Lateral Force Coefficient	k_h	0.70						
Designed Displacement	u_s [cm]	32.69						

Table 5 Modification Factor for Ground Condition c_G

Ground Group	I	II	III
c_G	0.8	1.0	1.2

Table 6 Modification Factor for Importance c_I

Group	c_I	Definition
1st class	1.0	Bridges on expressway (limited access highways), general national road and principal prefectural road. Important bridges on general prefectural road and municipal road.
2nd class	0.8	Other than the above

Table 7 Modification Factor for Structural Response c_T

Ground Group	Structural Response Coefficient c_T		
Group I	$T<0.1$ $c_T=2.69T^{1/3}\geq 1.00$	$0.1\leq T<1.1$ $c_T=1.25$	$1.1<T$ $c_T=1.33T^{-2/3}$
Group II	$T<0.2$ $c_T=2.15T^{1/3}\geq 1.00$	$0.2\leq T<1.5$ $c_T=1.25$	$1.3<T$ $c_T=1.49T^{-2/3}$
Group III	$T<0.34$ $c_T=1.80T^{1/3}\geq 1.00$	$0.34\leq T<1.5$ $c_T=1.25$	$1.5<T$ $c_T=1.64T^{-2/3}$

Table 8 Modification Factor for Structural Response c_R

Ground Group	Structural Response Coefficient c_R		
Group I	$T\leq 1.4$ $c_R=0.7$		$1.4<T$ $c_R=0.876T^{-2/3}$
Group II	$T<0.18$ $c_R=1.15T^{1/3}\geq 0.7$	$0.18\leq T\leq 1.6$ $c_R=0.85$	$1.6<T$ $c_R=1.16T^{-2/3}$
Group III	$T<0.29$ $c_R=1.15T^{1/3}\geq 0.7$	$0.29\leq T\leq 2.0$ $c_R=1.00$	$2.0<T$ $c_R=1.59T^{-2/3}$

Table 9 Relative Displacement of Bearings by Seismic Coefficient Method (unit:cm)

Item	A1	P1	P2	P3	P4	P5	A2
Relative Displacement of Bearings	10.04	8.31	5.65	6.33	6.62	7.22	9.75
Design Displacement of Bearings	7.77						

Table 10 Bending Moment at the Bottom of Piers (unit:tf·m)

Item	P1	P2	P3	P4	P5
Menshin Design	4,704.7	3,677.2	2,824.4	2,345.0	2,017.0
Usual Design	4,793.2	5,062.8	4,760.8	4,601.5	4,578.2

Table 11 Check of Bearing Capacity of Piers

Item		Unit	P1	P2	P3	P4	P5
Width of pier		m	8.0	8.0	6.5	6.5	6.5
Thickness of pier		m	2.5	2.2	2.2	2.0	2.0
Longitudinal Reinforcement	Main Reinforcement	mm cm^2	D32−ctc150 1.5 step 1,270.72	D32−ctc150 1.5 step 1,270.72	D29−ctc150 1.5 step 835.12	D29−ctc150 1.5 step 835.12	D29−ctc150 1.0 step 552.46
	Side Reinforcement	mm cm^2	D19−ctc150 138.03	D19−ctc150 126.57	D19−ctc150 114.42	D19−ctc150 108.69	D19−ctc150 108.69
Allowable Ductility Factor μ			4.739	3.683	5.393	4.991	4.984
Equivalent Horizontal Seismic Coefficient k_{h_e}			0.21	0.24	0.19	0.21	0.20
Bearing Capacity for Shear Failure P_s		tf	1,385.95	1,209.86	995.81	899.18	951.53
Bearing Capacity for Flexural force P_m		tf	378.60	347.17	285.88	278.04	269.70
Bearing Capacity for Lateral Force P_a		tf	378.60	347.17	285.88	278.04	269.70
Inertia Force $P = k_{h_e} \times w$		tf	348.20	346.58	239.58	245.54	250.82

Table 12 Relative Displacement of Bearings by Bearing Capacity Method (unit:cm)

	A1	P1	P2	P3	P4	P5	A2
Relative Displacement of Bearing	48.86	30.50	20.08	24.85	28.51	34.06	48.11
Design Displacement of Bearing	32.69						

Table 13 Equivalent Stiffness and Equivalent Damping Ratio of HDR Bearings

Item	[ ]:Unit	A1	P1	P2	P3	P4	P5	A2
Design Displacement	u [cm]	10.04	8.31	5.65	6.33	6.62	7.22	9.75
Area of Bearing	A [cm^2]	5,872	14,137	16,161	14,137	14,137	14,137	5,872
Thickness of Rubber Bearing	H_R [cm]	20.58	12.60	10.20	12.00	14.40	14.96	26.22
Shear Strain	γ	0.488	0.660	0.544	0.528	0.460	0.483	0.372
Shear Modulus of Elasticity	$G(\gamma)$ [kgf/cm^2]	12.505	10.512	11.621	11.955	12.943	12.583	14.503
Equivalent Stiffness	K_B [kgf/cm^2]	3,568	11,805	18,412	14,084	12,698	11,890	3,248
The Effective Damping Ratio	h_B	0.168	0.167	0.168	0.168	0.169	0.169	0.169

Table 14 Natural Period and Damping Ratio

Mode No.	Natural Period (sec)	Damping Ratio
1	1.546	0.143
2	0.451	0.030
3	0.419	0.030
4	0.357	0.030
5	0.302	0.092
6	0.299	0.056
7	0.273	0.115
8	0.259	0.031
9	0.253	0.114
10	0.236	0.031

Table 15 Displacement of Bearing computed by Dynamic Analysis Method (unit:mm)

	Seismic Coefficient Method	Dynamic Analysis	
		Response Spectrum Analysis	Time History Analysis
A1	100.42	65.76	68.72
P1	83.08	55.05	58.70
P2	77.84	36.85	38.82
P3	77.84	41.59	44.74
P4	77.84	43.60	47.14
P5	77.84	47.85	51.32
A2	97.51	63.47	67.77

Table 16 Sectional Forces at Pier Bottom computed by Dynamic Analysis Method

Item		Seismic Coefficient Method	Dynamic analysis	
			Response Spectrum Analysis	Time History Analysis
Bending Moment (tf·m)	A1	3,998.1	828.9	866.4
	P1	4,354.4	2,665.1	2,710.0
	P2	3,652.9	2,325.6	2,665.7
	P3	2,777.8	1,754.7	1,929.7
	P4	2,322.4	1,464.7	1,570.7
	P5	1,992.3	1,234.7	1,272.4
	A2	900.7	514.4	533.4
Shear stress (tf)	A1	426.6	47.3	49.4
	P1	345.1	200.0	186.2
	P2	286.5	165.0	206.9
	P3	238.5	140.8	162.6
	P4	218.3	129.5	146.1
	P5	218.6	128.2	138.2
	A2	146.8	101.6	90.8

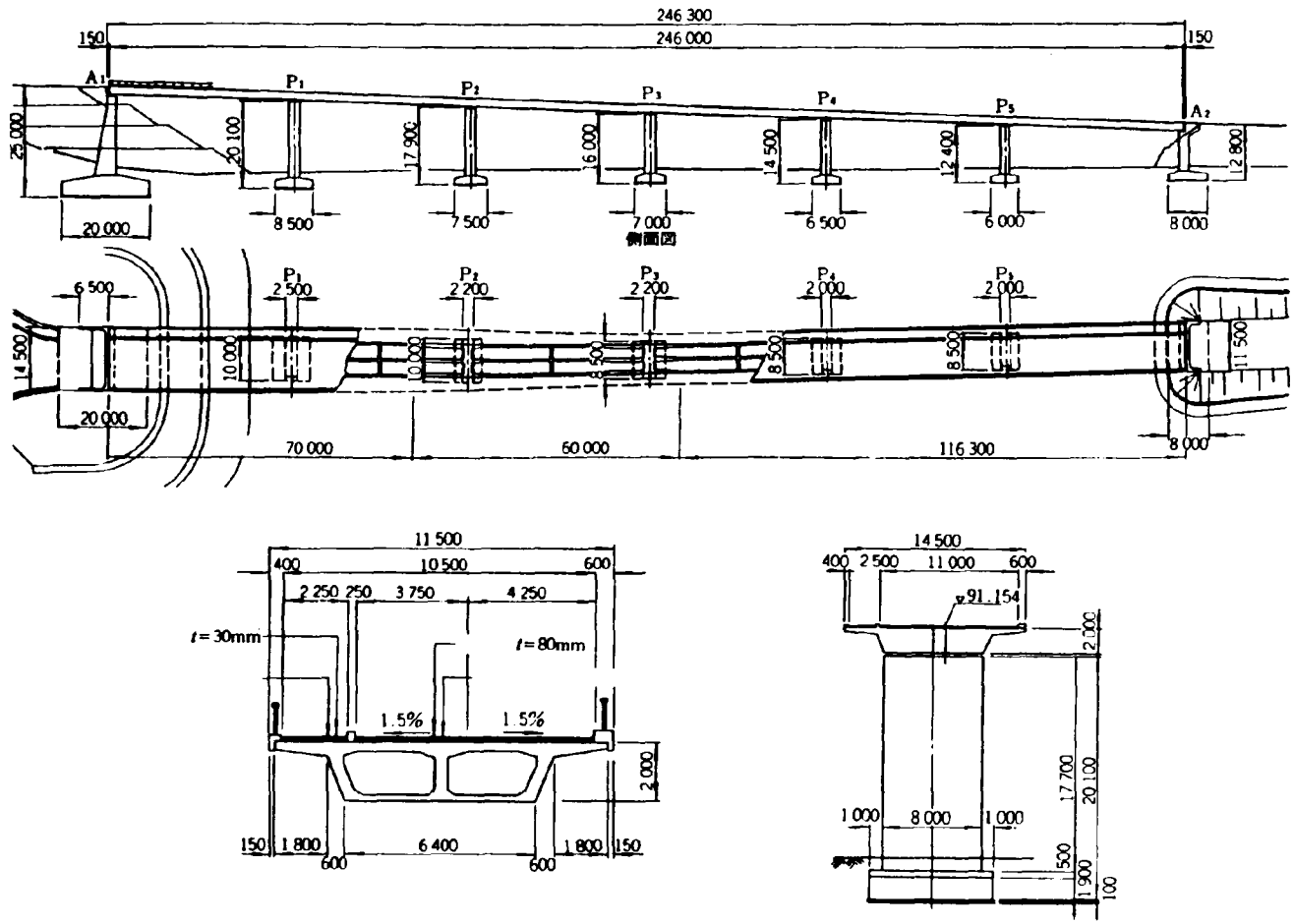

Fig. 1 General View of Yama-age Bridge

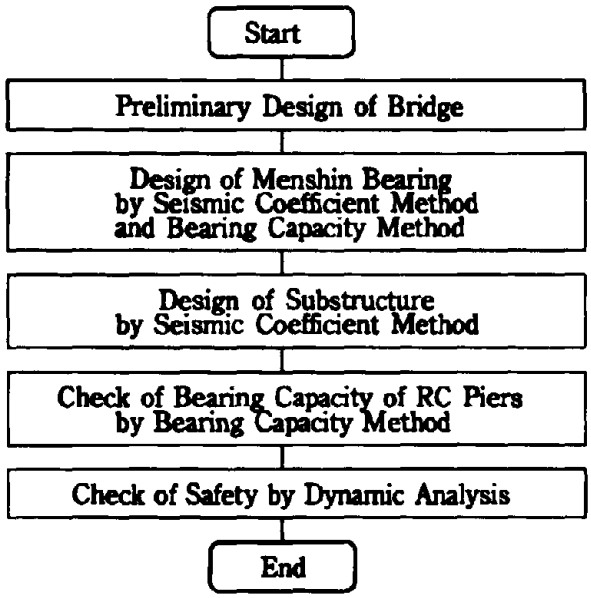

Fig. 2 Menshin Design Flow

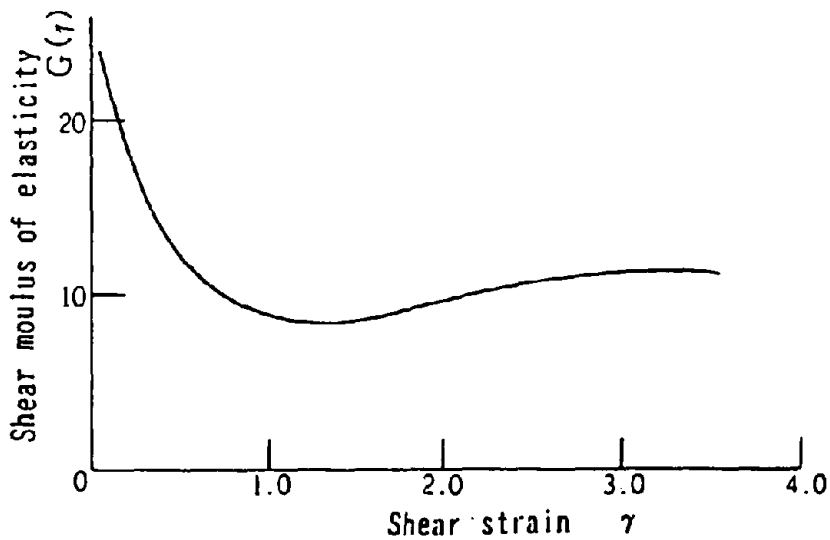

Fig. 3 $G(\gamma) \sim \gamma$ Relation of High Damping Rubber

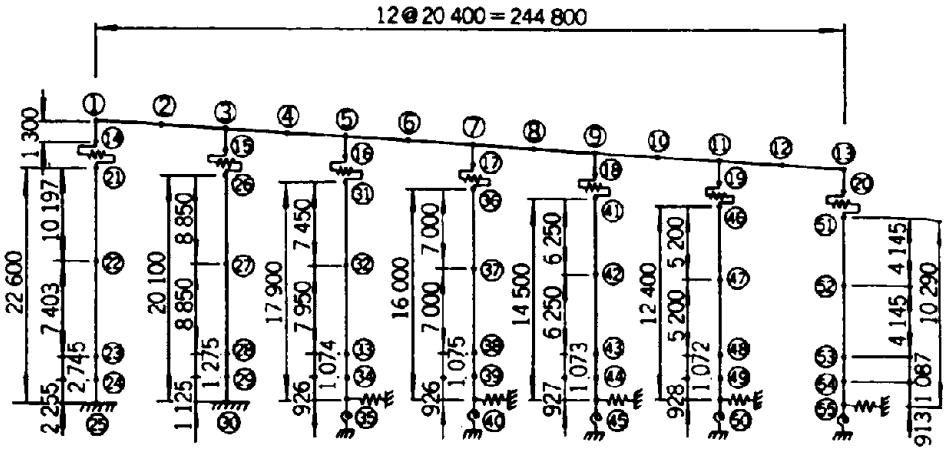

Fig. 4 Analytical Model

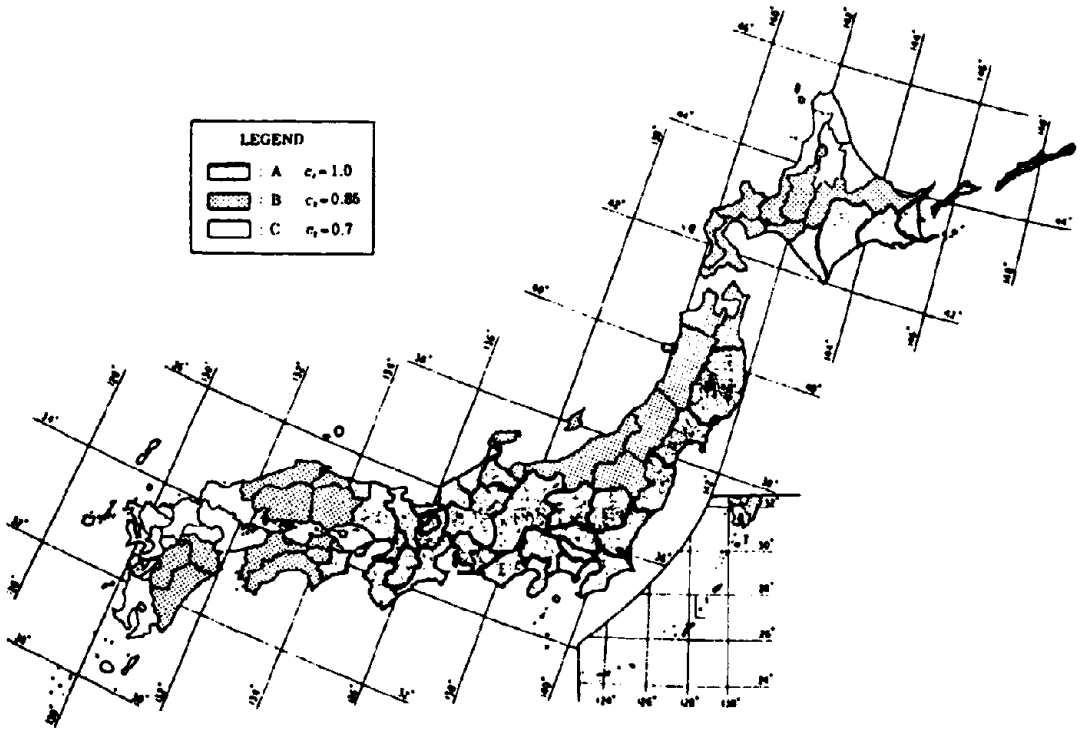

Fig. 5 Modification Factor for Zone c_z

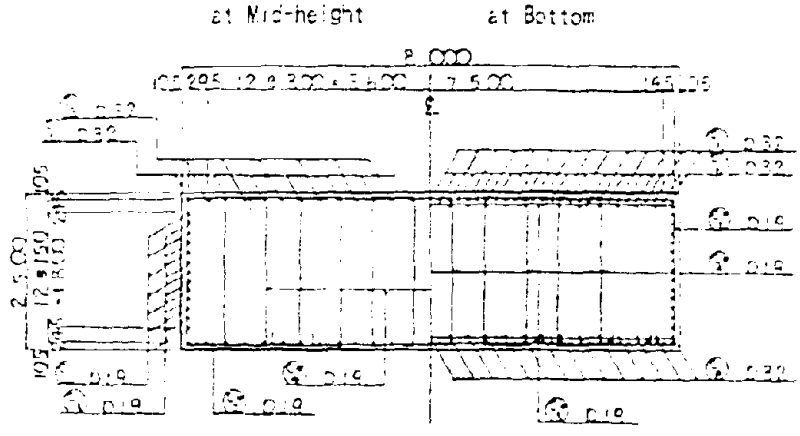

Fig. 6 Cross Section and Reinforcement of Pier (P1)

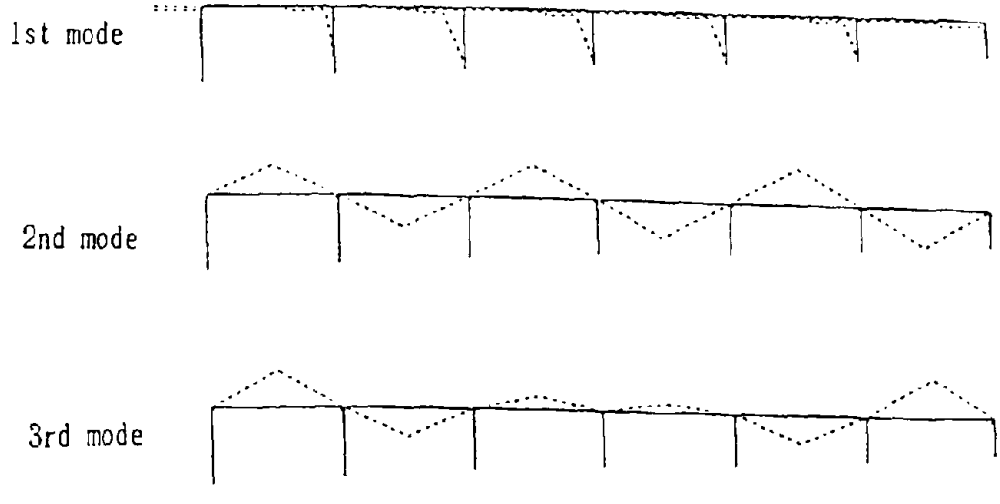

Fig. 7 Vibration Mode Shapes

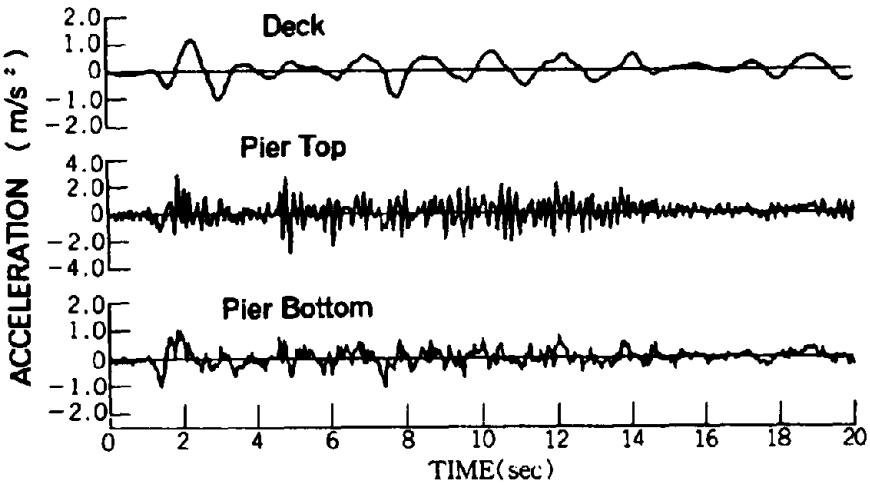

Fig. 8 Acceleration Response of Yama-age Bridge (Pier P1)

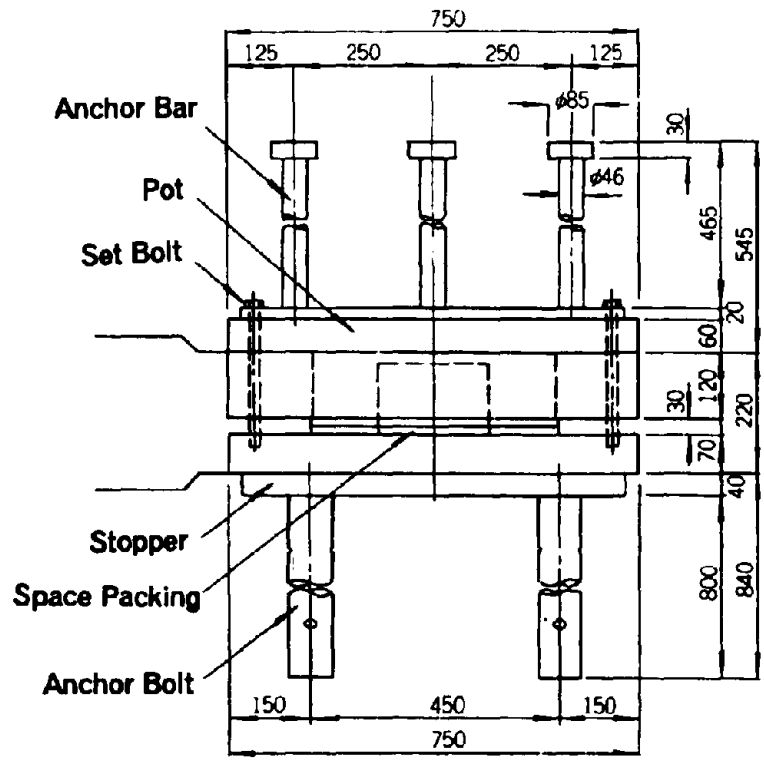

Fig. 9 Stopper

Photo 1 Yama-age Bridge

Photo 2 Forced Excitation Test using Quick-Release jacks

CONFERENCE INFORMATION

Workshop Program

U.S. Participants List

Japan Participants List

Order Information for Proceedings from the First and Second Workshops on Earthquake Protective Systems for Bridges

NIST

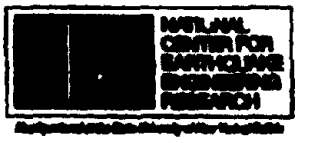

THIRD US-JAPAN WORKSHOP ON
EARTHQUAKE PROTECTIVE SYSTEMS FOR BRIDGES

January 24-25, 1994
Berkeley Marina Marriott Hotel
Berkeley, California

Workshop Program

Saturday, January 22, 1994

4:30 pm *Dinner Cruise Hosted by Japan Side*

Sunday, January 23, 1994

Study Tour

Monday, January 24, 1994

8:00 am REGISTRATION

8:15 am OPENING SESSION:

Co-chairmen: M. Shinozuka (US Side)
S. Unjoh (Japan Side)

US Side: S-C Liu — National Science Foundation
H.S. Lew — National Institute of Standards and Technology
J.D. Cooper — Federal Highway Administration

Japan Side: K. Toki — Kyoto University
K. Kawashima — Public Works Research Institute

US Workshop Committee: I.G. Buckle, State University of New York at Buffalo

8:45 am STATE-OF-THE-ART SESSION:

Co-chairmen: M. Shinozuka (US Side)
S. Unjoh (Japan Side)

J1: Menshin Design of Highway Bridges in Japan (Kawashima, K. and Unjoh, S.)
U1: Seismic Isolation of Bridges in the U.S.A. (Mayes, R.)

9:45 am *Break*

10:15 am

SESSION 1: **Passive Protective Systems**

Co-chairmen: S. Mahin (US Side)
K. Toki (Japan Side)

J2: Application of Base Isolation Bearings for Lateral Force Distribution (Takaku, T., Kimishima, T., Izuma, S. and Endou, K.)

U2: Shake Table Tests on Base-Isolated Bridge With Sliding System (Feng, M. and Okamoto, S.)

J3: Development of New Type Damper for Cable Stayed Bridge (Kitazawa, M., Iseki, J. and Shimoda, I.)

U3: Experimental Study of a Class of Bridge Sliding Seismic Isolation Systems (Constantinou, M., Tsopelas, P. and Okamoto, S.)

J4: Recovery Characteristics of Dynamic Properties of High Damping Rubber Bearings (Murota, N., Goda, K., Suzuki, S., Sudo, C. and Suizu, Y.)

U4: Effects of Pier Uplift and Sliding Isolation on Seismic Performance of Highway Bridges (Wang, X-F and Gould, P.)

12:15 pm

Lunch

1:30 pm

SESSION 2: **Hybrid Protective Systems - I**

Co-chairmen: I. Friedland (US Side)
M. Hoshiya (Japan Side)

J15: Seismic Response Control of Highway Bridges by Variable Stiffness Control (Kawashima, K., Unjoh, S. and Mukai, H.)

U7: Use of Hybrid Dampers for Vibration Control of Structures (Gordanineiad, F., Ray, A. and Wang, H.)

J5: Application of Electro-Rheological Fluid for Variable Damper (Kawashima, K., Unjoh, S. Suzuki, S. and Endoh, S.)

J16: Fuzzy Control of Bridge Vibration by Using Variable Dampers (Sun, L. and Goto, Y.)

2:50 pm

Break

3:05 pm — SESSION 3: **Hybrid Protective Systems - II**

Co-chairmen: R. Shepherd (US Side); W. Tanzo (Japan Side)

J17: Prediction Control of a SDOF System (Hoshiya, M. and Saito, Y.)

U5: Hybrid Protective Systems for Seismic-Excited Bridges (Yang, J., Li, Z., Wu, J., Kawashima, K. and Unjoh, S.)

J18: Closed-Open-Loop Control of Seismic Response of Structure With Active Mass Driver System (Toki, K., Sato, T., Mochizuki, T. and Yoshikawa, M.)

4:25 pm — *Break*

4:40 p.m. — SESSION 4: **Design Issues and Applications - I**

Co-chairmen: R. Mayes (US Side); Y. Yoshida (Japan Side)

J6: Extension of Equivalent Energy Method for Menshin Bridges (Hirai, T. and Sugimoto, M.)

U8: Current Caltrans Analysis Methods of Bridges Isolated With Bi-Linear Hysteresis Bearings (Sheng, L-H., Hwang, J-S. and Gates, J.)

J10: Design of a Menshin Bridge on Soft Ground (Hayashi, A.)

U9: Ultimate Restraint Considerations in Base-Isolated Bridges (Allred, B., Shepherd, R., and Billings, L.)

6:00 pm — *Break*

7:00 pm — *Reception and Dinner Hosted by U.S. Side*

Tuesday, January 25, 1994

8:15 am — SESSION 5: **Design Issues and Applications - II**

Co-chairmen: M. Sultan (US Side); Y. Goto (Japan Side)

J7: Design Plan of a Super Multi-span Continuous Menshin Bridge with Deck Length of 725m (Masumoto, H., Hara, K. and Yamashita, M.)

U10: Critical Loads of Elastomeric Isolators at High Shear Strain (Buckle, I. and Liu, H.)

J8: A Comparison Study on the Support Systems of a Multi-span Continuous Steel Bridge (Nanjoh, J., Nishibayashi, M. and Adachi, Y.)

U11: Base Isolation of the University Bridge (Koutsoukos, D. and Clark, J.)

J9: Seismic Design of a Continuous Steel Box Girder Bridge with Rubber Bearings for Trans-Tokyo Bay Highway Project (Shioi, Y., Yoshida, Y. and Takahashi, K.)

U12: Earthquake Protective Systems for the Seismic Upgrade of the Golden Gate Bridge (Rodriguez, S., Seim, C. and Ingham, T.)

10:15 am *Break*

10:45 am SESSION 6: **Experimental and Field Observations - I**

Co-chairmen: H. Shenton (US Side)
Y. Suizu (Japan Side)

J11: Vibration Test of a Meshin Designed Multi-span Continuous Prestressed Concrete Bridge (Kakinuma, T., Kawakami, K., Kumakura, K., Tani, H. and Abe, N.)

U13: Field Testing of Bridges Before and After Retrofitting with Seismic Isolation Bearings (Chen, S. and Mander, J.)

J12: Design of a Long Prestressed Concrete Continuous Girder Bridge Using Base Isolators (Hasegawa, K., Shikauchi, S., Ohsaki, H. and Fujiwara, Y.)

U14: Field Testing of the Seismically Isolated Walnut Creek Viaduct (Mahin, S., Aiken, I. and Gilani, A.)

12:15 pm *Lunch & Photo Session*

1:30 pm SESSION 7: **Experimental and Field Observations - II**

Co-chairmen: M. Constantinou (US Side)
T. Takaku (Japan Side)

J13: Response of On-netoh Bridge During Kushiro-oki Earthquake of January 1993 (Sato, M., Nishi, H., Kawashima, K. and Unjoh, S.)

U15: Caltrans/FHWA Program for Performance Testing of Seismic Isolation and Energy Dissipation Systems (Sultan, M. and Sheng, L-H.)

J14: Seismic Response Characteristics of the Hokumei Bridge Using Rubber Bearings (Kawamura, S., Tarumi, Y. and Kubo, A.)

U16: Guidelines for Pre-qualification, Prototype, and Quality Control Testing of Seismic Isolation Systems (Shenton, H.)

3:00 pm *Break*

3:30 pm	DESIGN EXAMPLE		
	Co-chairmen:	I. Buckle	(US Side)
		K. Kawashima	(Japan Side)
	US Presentation -	Isolation System Design and Specification for the Olympic Boulevard Off-Ramp (Jones, D. and Choudhury, D.)	
	Japan Presentation -	Menshin Design Example of a Highway Bridge (Kawashima, K., Unjoh, S., Uzuka, T., Kawakami, K., Kumakura, K. and Tani, H.)	
4:30 pm	DISCUSSION, RESOLUTIONS AND CLOSURE		
	Co-chairmen:	I. Buckle	(US Side)
		K. Kawashima	(Japan Side)
5:30 pm	*Workshop Adjourns*		

U.S. PARTICIPANTS LIST

Ian Aiken
Research Engineer
Earthquake Engineering Research Center
1301 S. 46th St., Bldg. 451
Richmond, CA 94804
Tel. 510-231-9556
Fax. 510-231-5696

Brian A. Allred
Department of Civil Engineering
University of California/Irvine
Irvine, CA 92717
Tel. 714-856-7393
Fax. 714-725-2117

Hanns U. Baumann, S.E.
Baumann Engineering
Consulting Structural Engineers
567 San Nicolas Drive
Suite 104
Newport Beach, CA 92660
Tel. 714-640-2880
Fax. 714-640-2520

Ian G. Buckle
Deputy Director
National Center for Earthquake
Engineering Research
105 Red Jacket Quadrangle
State University of New York at Buffalo
Buffalo, NY 14261
Tel. 716-645-3391
Fax. 716-645-3399

Deepak Choudhury
Dynamic Isolation Systems, Inc.
2855 Telegraph Avenue
Suite 410
Berkeley, CA 94705
Tel. 510-843-3576
Fax. 510-843-0366

John H. Clark
Andersen Bjornstad Kane Jacobs, Inc.
220 W. Harrison
Seattle, WA 98119
Tel. 206-285-1185
Fax. 206-285-8204

Peter Clark
Earthquake Engineering Research Center
1301 South 46th Street
Richmond, CA 94804
Tel. 510-231-9556
Fax. 510-231-5696

Michalakis C. Constantinou
Associate Professor
Department of Civil Engineering
State University of New York at Buffalo
132 Ketter Hall, North Campus
Buffalo, NY 14260
Tel. 716-645-2186
Fax. 716-645-3733

James D. Cooper, HNR-10
Chief, Structures Division
Turner-Fairbank Highway
Research Center
Federal Highway Administration
6300 Georgetown Pike
McLean, VA 22101
Tel. 703-285-2060
Fax. 703-285-2766

Tim Delis
California Department of Transportation
Division of Structures
P.O. Box 942874
Sacramento, CA 94274-0001
Tel. 916-227-8806
Fax. 916-227-8898

Saad El-Azazy
California Department of Transportation
Division of Structures
Seismic Retrofit/Seismic Technology
1801 30th Street West, M.S. 9
Sacramento, CA 95816
Tel. 916-227-8124
Fax. 916-227-8898

Maria Q. Feng
Department of Civil Engineering
University of California/Irvine
Irvine, CA 92717
Tel. 714-725-2162
Fax. 714-725-2162

Ian M. Friedland
Assistant Director for Bridges and Highways
National Center for Earthquake Engineering Research
102 Red Jacket Quadrangle
State University of New York at Buffalo
Buffalo, NY 14261
Tel. 716-645-3391
Fax. 716-645-3399

Faramarz Gordaninejad
Department of Mechanical Engineering
College of Engineering - 312
University of Nevada
Reno, NV 89557-0154
Tel. 702-784-6990
Fax. 702-784-1701

Masahiko Higashino
Visiting Scholar
University of California\Berkeley
Earthquake Engineering Research Center
1301 South 46th Street
Richmond, CA 94804
Tel. 510-231-9491

David Jones
Dynamic Isolation Systems, Inc.
2855 Telegraph Avenue
Suite 410
Berkeley, CA 94705
Tel. 510-843-3576
Fax. 510-843-0366

Dimitrios P. Koutsoukos
Andersen Bjornstad Kane Jacobs, Inc.
220 W. Harrison
Seattle, WA 98119
Tel. 206-285-1185
Fax. 206-285-8204

Roberto Lacalle
Senior Bridge Engineer
California Department of Transportation
1801 30th Street
Sacramento, CA 94274
Tel. 510-227-8070

H.S. Lew
Chief, Structures Division
National Institute of Standards and Technology
Building and Fire Research Laboratory
Building 226, Room B168
Gaithersburg, MD 20899
Tel. 301-975-6061
Fax. 301-869-6275

Helen Liu
Department of Civil Engineering
144 Ketter Hall
State University of New York at Buffalo
Buffalo, NY 14260
Tel. 716-645-3964
Fax. 716-645-3733

S-C Liu
Program Director
Division of Civil & Mechanical Systems
National Science Foundation
Room 545
4201 Wilson Blvd.
Arlington, VA 22230
Tel. 703-306-1362
Fax. 703-306-0312

James Macintyre
Associate Bridge Engineer
California Department of Transportation
Office of Structures Maintenance and Investigation
Toll Bridges Branch
1801 30th Street West, M.S. 9
Sacramento, CA 95816
Tel. 510-286-0628
Fax. 510-286-0893

Stephen Mahin
Department of Civil Engineering
771 Davis Hall
University of California
Berkeley, CA 94720
Tel. 510-642-4021
Fax. 510-643-5264

Ayaz Malik
Associate Civil Engineer (Structures)
New York State Department of
Transportation
Building 5, 6th Floor
1220 Washington Avenue
Albany, NY 12232
Tel. 518-457-6465
Fax. 518-485-7826

John Mander
Assistant Professor
Department of Civil Engineering
230 Ketter Hall
State University of New York at Buffalo
Buffalo, NY 14260
Tel. 716-645-2263
Fax. 716-645-3733

Ronald L. Mayes
Dynamic Isolation Systems, Inc.
2855 Telegraph Avenue
Suite 410
Berkeley, CA 94705
Tel. 510-843-3576
Fax. 510-843-0366

Roland B. Nimis
Regional Structural Engineer
Federal Highway Administration
211 Main Street, Room 1100
San Francisco, CA 94105
Tel. 415-744-2653
Fax. 415-744-2620

Deborah S. O'Rourke
Program Specialist
National Center for Earthquake
Engineering Research
101 Red Jacket Quadrangle
State University of New York at Buffalo
Buffalo, NY 14261
Tel. 716-645-3391
Fax. 716-645-3399

Santiago Rodriguez
Project Engineer
T.Y.LIN International
825 Battery Street
San Francisco, CA 94111
Tel. 415-291-3700
Fax. 415-433-0807

Li-Hong Sheng
Senior Bridge Engineer
California Department of Transportation
Division of Structures
P.O. Box 942874
Sacramento, CA 94274-0001
Tel. 916-227-8806
Fax. 916-227-8898

Harry Shenton
Research Structural Engineer
National Institute of
Standards and Technology
Building and Fire Research Laboratory
Building 226, Room B156
Gaithersburg, MD 20899
Tel. 301-975-6067
Fax. 301-869-6275

Robin Shepherd
Department of Civil Engineering
Room 245 Engineering Laboratory
University of California/Irvine
Irvine, CA 92717
Tel. 714-856-7393
Fax. 714-725-2117

Masanobu Shinozuka
Sollenberger Professor of
Civil Engineering
Department of Civil Engineering
E209 Engineering Quadrangle
Princeton University
Princeton, NJ 08544
Tel. 609-258-6757
Fax. 609-258-6759

Tony Smith, President
Jarret, Inc.
4050 Washington Road
McMurray, PA 15317
Tel. 412-942-0130
Fax. 412-942-0140

Mohsen Sultan
California Department of Transportation
Division of Structures
P.O. Box 942874
Sacramento, CA 94274-0001
Tel. 916-227-8806
Fax. 916-227-8898

Wendy Taniwangsa
Earthquake Engineering Research Center
1301 South 46th Street
Richmond, CA 94804
Tel. 510-231-9556
Fax. 510-231-5696

Panagiotis Tsopelas
Department of Civil Engineering
212 Ketter Hall
State University of New York at Buffalo
Buffalo, NY 14260
Tel. 716-645-2114
Fax. 716-645-3733

Umesh Vasishth
Exeltech, Consulting Engineers
2627 A Parkmont Lane SW
Olympia, WA 98502
Tel. 206-357-8289
Fax. 206-357-8225

Xiao-Feng Wang
School of Engineering & Applied Science
Department of Civil Engineering
Campus Box 1130
One Brookings Drive
Washington University in St. Louis
St. Louis, MO 63130-4899
Tel. 314-935-6350
Fax. 314-935-4338

Jann N. Yang
Department of Civil and Environmental Engineering
University of California/Irvine
Irvine, CA 92717
Tel. 714-856-4246
Fax. 714-856-5051

W. Phillip Yen
California Department of Transportation
Division of Structures
Design, 4th Floor
1801 30th Street, M.S. 9
Sacramento, CA 95816
Tel. 916-227-8815
Fax. 916-227-8379

Raymond Zelinski
Design Engineer
California Department of Transportation
Division of Structures
P.O. Box 942874
Sacramento, CA 94274-0001
Tel. 916-227-8806
Fax. 916-227-8898

NEW ZEALAND PARTICIPANT

William Henry Robinson
Materials Engineering Laboratories
New Zealand Institute for Industrial Research
P.O. Box 31 310,
Lower Hutt, New Zealand
Tel. 64 4 566 6919
Fax. 64 4 569 0117

TAIWAN PARTICIPANTS

Kuo-Chun Chang
National Taiwan University
Department of Civil Engineering
1, Roosevelt Road Sec. 4,
Taipei, Taiwan 106, 204
Tel. 886-2-363-8608
Fax. 886-2-362-2975

Jenn-Shin Hwang
National Taiwan Institute of Technology
Department of Construction Engineering
P.O. Box 90-130
Taipei, Taiwan
Tel. 886-2-737-6599
Fax. 886-2-737-6606

JAPAN PARTICIPANTS LIST

Mr. Yukio Adachi
Design Section
Engineering Division
Hanshin Expressway Public
Corporation
(Currently Graduate Student of
University of California
at Berkeley)
4-1-3 Kyutaro-cho Chuo-Ku,
Osaka, Japan, 541
Tel. 81-06-252-8121
Fax. 81-06-252-4583

Mr. Kazuo Endoh
Chief Engineer
Construction Materials Department
The Yokohama Rubber Co., Ltd.
36-11 Shinbashi, 5-Chome
Minatu-ko
Tokyo, Japan, 105
Tel. 81-0463-32-2700
Fax. 81-0463-32-1703

Mr. Yasuhisa Fujiwara
Section 2
Construction and Engineering Division
Civil Engineering Operations
Sumitomo Construction Co., Ltd.
13-4, Araki, Shinjyuku-ku
Tokyo, Japan, 160
Tel. 81-03-3225-5135
Fax. 81-03-3353-6656

Dr. Yozo Goto
Manager, The 5th Civil Engineering Division
Technical Research Institute
Obayashi Corporation
4-640, Shimokiyoto, Kiyose-shi,
Tokyo, Japan, 204
Tel. 81-0424-95-0951
Fax. 81-0424-95-0903

Mr. Koji Hara
Chief Technological Staff
Numazu Public Works Office
Construction Division No. 2
1-3, Takashima-honcho, Numazu-shi
Shizuoka, Japan, 410
Tel. 81-0559-20-2219
Fax. 81-0559-22-6684

Mr. Akio Hayashi
Consulting Engineer
General Research Institute
Pacific Consultants Co., Ltd.
1-7-5, Sekito, Tama-shi
Tokyo, Japan, 206
Tel. 81-0423-72-7293
Fax. 81-0423-72-4518

Mr. Takashi Hirai
Research Engineer
Applied Research and Development
Department
Takenaka Technical Research Institute
Takenaka Corporation
1-5, Ohstuka, Inzai-cho,
Chiba-ken, Japan, 270-13
Tel. 81-0476-47-1700
Fax. 81-0476-47-3070

Mr. Junichi Hoshikuma
Research Engineer
Earthquake Engineering Division
Earthquake Disaster Prevention
Department
Public Works Research Institute
Ministry of Construction
1, Asahi, Tsukuba-shi, Ibaraki,
Japan 305
Tel. 81-0298-64-2211
Fax. 81-0298-64-0598

Professor Masaru Hoshiya
Department of Civil Engineering
Musashi Institute of Technology
1-28-1, Tamatsutsumi, Setagaya-ku
Tokyo, Japan 158
Tel. 81-03-3703-3111
Fax. 81-03-3701-1853

Mr. Soichiro Kawahara
Manager, Design Section
Structural Equipment Division
Oiles Corporation
8, Kirihara-cho, Fujisawa-city
Kanagawa, Japan, 252
Tel. 81-0466-44-4818
Fax. 81-0466-43-6069

Dr. Kazuhiko Kawashima
Head, Earthquake Engineering Division
Earthquake Disaster Prevention Department
Public Works Research Institute
Ministry of Construction
1, Asahi, Tsukuba-shi, Ibaraki,
Japan 305
Tel. 81-0298-64-2211
Fax. 81-0298-64-0598

Mr. Akio Kimijima
Assistant General Manager
Development Department
Research and Development Center
Nippon Chuzo K K.
2-1, Shiroishi-Cho, Kawasaki-ku
Kawasaki-shi, Kanagawa, Japan, 210
Tel. 81-044-355-5033
Fax. 81-044-333-4575

Mr. Akihide Kubo
Chief Engineer
Civil Engineering and Research Department
P.S. Corporation
3-20-6, Minami-Ohtsuka, Toshima-ku
Tokyo, Japan, 170
Tel. 81-03-5391-6091
Fax. 81-03-5391-6095

Mr. H. Herb Kubota
Kubota & Associates
P.O. Box 210455
San Francisco, CA 94121-0455
Tel. 415-759-0470
Fax. 415-759-8547

Mr. Kazuomi Kumakura
Senior Officer
Road Construction Division
Department of Public Works
Tochigi Prefectural Government
1-1-20, Shimada, Utsunomiya-shi
Tochigi-ken, Japan, 3210
Tel. 81-0286-23-2414
Fax. 81-0286-23-2417

Mr. Yasuhito Morimoto
Consulting Engineer
Structural Second Division
Yokohama Branch
Pacific Consultants Co., Ltd.
3-8-8, Ohgi-machi, Naka-ku
Yokohama, Japan, 231
Tel. 81-045-664-4320
Fax. 81-045-651-5529

Mr. Nobuo Murota
Bridgestone Corporation
Kashio-cho 1, Totsuka-ku,
Yokohama-shi, Kanagawa-ken,
Japan
Tel. 045-825-7589
Fax. 045-825-7676

Mr. Norimichi Nakajima
Research and Development Division
Technical Research Institute
Mistui Construction Corporation
518-1, Komaki, Nagareyama-shi
Chiba, Japan, 270-01
Tel: 81-03-0471-40-5201
Fax: 81-03-0471-40-5216

Mr. Abe Nobora
No. 9 Chuo-Bldg.,
4-9-11, Nihonbashi Honcho
Chuo-ku, Tokyo 103
Japan
Tel. 03-3668-0451
Fax. 03-5695-1885

Mr. Keizo Ohtsuka
Maintenance Technology Division
Maintenance Facility Department
Metropolitan Expressway Public
Corporation
(Currently Graduate Student of
University of Texas)
1-4-1, Kasumigaseki, Chiyoda-ku
Tokyo, Japan, 100
Tel. 81-03-3502-7311
Fax. 81-03-3503-1806

Mr. Ikuo Shimoda
Manager, Technical Development Department
Oiles Corporation
8, Kirihara-cho, Fujisawa-shi
Kanagawa, Japan, 252
Tel. 81-0466-44-4818
Fax. 81-0466-43-6059

Mr. Hideki Sugita
Research Engineer
Earthquake Engineering Division
Earthquake Disaster Prevention Department
Public Works Research Institute
Ministry of Construction
(Currently Visiting Researcher at
University of California at Berkeley)
1, Asahi, Tsukuba-shi, Ibaraki,
Japan 305
Tel. 81-0298-64-2211
Fax. 81-0298-64-0598

Mr. Yoji Suizu
Manager, Research and Development
Bridgestone Corporation
3-1-1, Ogawa-higashi-machi
Kodaira-shi, Tokyo
Japan, 187
Tel. 81-0423-42-6272
Fax. 81-0423-43-6342

Mr. Yoshinori Tachibana
Research and Development
Oriental Consultants Co., Ltd.
3-5-7, Hisamoto, Tkatsu-ku
Kawasaki-shi
Japan, 213
Tel. 81-044-812-8815
Fax. 81-044-812-8825

Dr. Tatsumasa Takaku
General Manager
Bridge Construction and
Engineering Department
NKK Corporation
2-1, Suehiro-cho, Tsurumi-ku, Yokohama
Japan, 230
Tel. 81-045-505-7554
Fax. 81-045-505-7561

Mr. Isao Takatori
Director, Public Works Research Center
1-12-11, Daito, Daitoh-ku
Tokyo, Japan, 110
Tel. 81-03-3835-3609
Fax. 81-03-3832-7397

Dr. William Tanzo
Research Associate
Department of Civil and
Environmental Engineering
Saitama University
225, Shimo-Okubo, Urawa
Saitama, Japan 338
Tel. 81-048-858-3556
Fax. 81-048-855-9361

Professor Kenzo Toki
Department of Civil and
Traffic Engineering
Kyoto Univeraity
Yoshida-hon-machi, Sakyo-ku
Kyoto, Japan 606
Tel. 81-075-753-5131
Fax. 81-075-753-5131

Mr. Shigeki Unjoh
Senior Research Engineer
Earthquake Engineering Division
Earthquake Disaster Prevention Department
Public Works Research Institute
Ministry of Construction
1, Asahi, Tsukuba-shi, Ibaraki,
Japan 305
Tel. 81-0298-64-2211
Fax. 81-0298-64-0598

Mr. Mikio Yamashita
Director, Technical Department
Kaihatsu Consultant Co., Ltd.
9-4 Higashiueno, 2-Chome
Taito-ku, Tokyo, Japan, 110
Tel. 81-03-3831-0151
Fax. 81-03-3834-4297

Mr. Yoshitaka Yoshida
Manager, Bridge Design Division
Design Department
Trans-Tokyo Bay Highway Corp.
15-5 Ichibancho, Chiyoda-ku,
Tokyo, Japan, 102
Tel. 81-03-3239-6585
Fax. 81-03-3239-6586

Proceedings from the First and Second Workshops on Earthquake Protective Systems for Bridges

The Workshops

The National Center for Earthquake Engineering Research and the Public Works Research Institute of Japan have organized two previous workshops on Earthquake Protective Systems for Bridges. Proceedings from both workshops feature many state-of-the-art papers on U.S. and Japanese design methodologies. Both workshops were conducted under the auspices of Task Committee G on Passive, Active and Hybrid Control Systems and Task Committee J on Wind and Earthquake Engineering for Transportation Systems of the UJNR Panel on Wind and Seismic Effects.

Order Information

To order the ***Proceedings from the First U.S.-Japan Workshop on Earthquake Protective Systems for Bridges*** and/or ***The Second U.S.-Japan Workshop on Earthquake Protective Systems for Bridges***, please complete the form below and mail it to: *National Center for Earthquake Engineering Research, Publications Department, State University of New York at Buffalo, Red Jacket Quadrangle, Buffalo, NY 14261.*

Japanese participants should obtain ***The Second U.S.-Japan Workshop on Earthquake Protective Systems for Bridges*** from the Public Works Research Institute, Ministry of Construction, Government of Japan, 1, Asahi, Tskuba-shi, Ibaraki-ken, 305 Japan, Telephone: (0298) 64-2211; fax: (0298) 64-2840.

*Yes, I would like to order the **Proceedings from the First** and/or **Second U.S.-Japan Workshops on Earthquake Protective Systems for Bridges** as specified below:*

U.S. Orders:

_____ Copies of the ***First U.S.-Japan Workshop Proceedings*** (NCEER-92-0004) at $40.00 per copy.

_____ Copies of the ***Second U.S.-Japan Workshop Proceedings*** (ISSN 0386-5878;Technical Memorandum of PWRI No. 3196) at $5.00 per copy (to cover shipping and handling only).

International Orders:

_____ Copies of ***First U.S.-Japan Workshop Proceedings*** (NCEER-92-0004) at $50.00 per copy.

*Please pay by check or purchase order only. Make checks payable to the **Research Foundation**.*

All prices include postage and handling. Reports are sent either library rate, book rate or third class within the U.S. Allow 3-4 weeks for delivery.

Rush service is available. Add $7.00 U.S. or $15.00 international. Reports will be sent via first class mail or airmail.

Please ship to:

Name: _____

Organization: _____

Address: _____

_____

_____

City/State/Zip: _____

Country: _____

Telephone: _____

NATIONAL CENTER FOR EARTHQUAKE ENGINEERING RESEARCH
LIST OF TECHNICAL REPORTS

The National Center for Earthquake Engineering Research (NCEER) publishes technical reports on a variety of subjects related to earthquake engineering written by authors funded through NCEER. These reports are available from both NCEER's Publications Department and the National Technical Information Service (NTIS). Requests for reports should be directed to the Publications Department, National Center for Earthquake Engineering Research, State University of New York at Buffalo, Red Jacket Quadrangle, Buffalo, New York 14261. Reports can also be requested through NTIS, 5285 Port Royal Road, Springfield, Virginia 22161. NTIS accession numbers are shown in parenthesis, if available.

NCEER-87-0001 "First-Year Program in Research, Education and Technology Transfer," 3/5/87, (PB88-134275).

NCEER-87-0002 "Experimental Evaluation of Instantaneous Optimal Algorithms for Structural Control," by R.C. Lin, T.T. Soong and A.M. Reinhorn, 4/20/87, (PB88-134341).

NCEER-87-0003 "Experimentation Using the Earthquake Simulation Facilities at University at Buffalo," by A.M. Reinhorn and R.L. Ketter, to be published.

NCEER-87-0004 "The System Characteristics and Performance of a Shaking Table," by J.S. Hwang, K.C. Chang and G.C. Lee, 6/1/87, (PB88-134259). This report is available only through NTIS (see address given above).

NCEER-87-0005 "A Finite Element Formulation for Nonlinear Viscoplastic Material Using a Q Model," by O. Gyebi and G. Dasgupta, 11/2/87, (PB88-213764).

NCEER-87-0006 "Symbolic Manipulation Program (SMP) - Algebraic Codes for Two and Three Dimensional Finite Element Formulations," by X. Lee and G. Dasgupta, 11/9/87, (PB88-218522).

NCEER-87-0007 "Instantaneous Optimal Control Laws for Tall Buildings Under Seismic Excitations," by J.N. Yang, A. Akbarpour and P. Ghaemmaghami, 6/10/87, (PB88-134333). This report is only available through NTIS (see address given above).

NCEER-87-0008 "IDARC: Inelastic Damage Analysis of Reinforced Concrete Frame - Shear-Wall Structures," by Y.J. Park, A.M. Reinhorn and S.K. Kunnath, 7/20/87. (PB88-134325).

NCEER-87-0009 "Liquefaction Potential for New York State: A Preliminary Report on Sites in Manhattan and Buffalo," by M. Budhu, V. Vijayakumar, R.F. Giese and L. Baumgras, 8/31/87, (PB88-163704). This report is available only through NTIS (see address given above).

NCEER-87-0010 "Vertical and Torsional Vibration of Foundations in Inhomogeneous Media," by A.S. Veletsos and K.W. Dotson, 6/1/87, (PB88-134291).

NCEER-87-0011 "Seismic Probabilistic Risk Assessment and Seismic Margins Studies for Nuclear Power Plants," by Howard H.M. Hwang, 6/15/87, (PB88-134267).

NCEER-87-0012 "Parametric Studies of Frequency Response of Secondary Systems Under Ground-Acceleration Excitations," by Y. Yong and Y.K. Lin, 6/10/87, (PB88-134309).

NCEER-87-0013 "Frequency Response of Secondary Systems Under Seismic Excitation," by J.A. HoLung, J. Cai and Y.K. Lin, 7/31/87, (PB88-134317).

NCEER-87-0014 "Modelling Earthquake Ground Motions in Seismically Active Regions Using Parametric Time Series Methods," by G.W. Ellis and A.S. Cakmak, 8/25/87, (PB88-134283).

NCEER-87-0015 "Detection and Assessment of Seismic Structural Damage," by E. DiPasquale and A.S. Cakmak, 8/25/87, (PB88-163712).

NCEER-87-0016 "Pipeline Experiment at Parkfield, California," by J. Isenberg and E. Richardson, 9/15/87, (PB88-163720). This report is available only through NTIS (see address given above).

NCEER-87-0017 "Digital Simulation of Seismic Ground Motion," by M. Shinozuka, G. Deodatis and T. Harada, 8/31/87, (PB88-155197). This report is available only through NTIS (see address given above).

NCEER-87-0018 "Practical Considerations for Structural Control: System Uncertainty, System Time Delay and Truncation of Small Control Forces," J.N. Yang and A. Akbarpour, 8/10/87, (PB88-163738).

NCEER-87-0019 "Modal Analysis of Nonclassically Damped Structural Systems Using Canonical Transformation," by J.N. Yang, S. Sarkani and F.X. Long, 9/27/87, (PB88-187851).

NCEER-87-0020 "A Nonstationary Solution in Random Vibration Theory," by J.R. Red-Horse and P.D. Spanos, 11/3/87, (PB88-163746).

NCEER-87-0021 "Horizontal Impedances for Radially Inhomogeneous Viscoelastic Soil Layers," by A.S. Veletsos and K.W. Dotson, 10/15/87, (PB88-150859).

NCEER-87-0022 "Seismic Damage Assessment of Reinforced Concrete Members," by Y.S. Chung, C. Meyer and M. Shinozuka, 10/9/87, (PB88-150867). This report is available only through NTIS (see address given above).

NCEER-87-0023 "Active Structural Control in Civil Engineering," by T.T. Soong, 11/11/87, (PB88-187778).

NCEER-87-0024 "Vertical and Torsional Impedances for Radially Inhomogeneous Viscoelastic Soil Layers," by K.W. Dotson and A.S. Veletsos, 12/87, (PB88-187786).

NCEER-87-0025 "Proceedings from the Symposium on Seismic Hazards, Ground Motions, Soil-Liquefaction and Engineering Practice in Eastern North America," October 20-22, 1987, edited by K.H. Jacob, 12/87, (PB88-188115).

NCEER-87-0026 "Report on the Whittier-Narrows, California, Earthquake of October 1, 1987," by J. Pantelic and A. Reinhorn, 11/87, (PB88-187752). This report is available only through NTIS (see address given above).

NCEER-87-0027 "Design of a Modular Program for Transient Nonlinear Analysis of Large 3-D Building Structures," by S. Srivastav and J.F. Abel, 12/30/87, (PB88-187950).

NCEER-87-0028 "Second-Year Program in Research, Education and Technology Transfer," 3/8/88, (PB88-219480).

NCEER-88-0001 "Workshop on Seismic Computer Analysis and Design of Buildings With Interactive Graphics," by W. McGuire, J.F. Abel and C.H. Conley, 1/18/88, (PB88-187760).

NCEER-88-0002 "Optimal Control of Nonlinear Flexible Structures," by J.N. Yang, F.X. Long and D. Wong, 1/22/88, (PB88-213772).

NCEER-88-0003 "Substructuring Techniques in the Time Domain for Primary-Secondary Structural Systems," by G.D. Manolis and G. Juhn, 2/10/88, (PB88-213780).

NCEER-88-0004 "Iterative Seismic Analysis of Primary-Secondary Systems," by A. Singhal, L.D. Lutes and P.D. Spanos, 2/23/88, (PB88-213798).

NCEER-88-0005 "Stochastic Finite Element Expansion for Random Media," by P.D. Spanos and R. Ghanem, 3/14/88, (PB88-213806).

NCEER-88-0006 "Combining Structural Optimization and Structural Control," by F.Y. Cheng and C.P. Pantelides, 1/10/88, (PB88-213814).

NCEER-88-0007 "Seismic Performance Assessment of Code-Designed Structures," by H.H-M. Hwang, J-W. Jaw and H-J. Shau, 3/20/88, (PB88-219423).

NCEER-88-0008 "Reliability Analysis of Code-Designed Structures Under Natural Hazards," by H.H-M. Hwang, H. Ushiba and M. Shinozuka, 2/29/88, (PB88-229471).

NCEER-88-0009 "Seismic Fragility Analysis of Shear Wall Structures," by J-W Jaw and H.H-M. Hwang, 4/30/88, (PB89-102867).

NCEER-88-0010 "Base Isolation of a Multi-Story Building Under a Harmonic Ground Motion - A Comparison of Performances of Various Systems," by F-G Fan, G. Ahmadi and I.G. Tadjbakhsh, 5/18/88, (PB89-122238).

NCEER-88-0011 "Seismic Floor Response Spectra for a Combined System by Green's Functions," by F.M. Lavelle, L.A. Bergman and P.D. Spanos, 5/1/88, (PB89-102875).

NCEER-88-0012 "A New Solution Technique for Randomly Excited Hysteretic Structures," by G.Q. Cai and Y.K. Lin, 5/16/88, (PB89-102883).

NCEER-88-0013 "A Study of Radiation Damping and Soil-Structure Interaction Effects in the Centrifuge," by K. Weissman, supervised by J.H. Prevost, 5/24/88, (PB89-144703).

NCEER-88-0014 "Parameter Identification and Implementation of a Kinematic Plasticity Model for Frictional Soils," by J.H. Prevost and D.V. Griffiths, to be published.

NCEER-88-0015 "Two- and Three- Dimensional Dynamic Finite Element Analyses of the Long Valley Dam," by D.V. Griffiths and J.H. Prevost, 6/17/88, (PB89-144711).

NCEER-88-0016 "Damage Assessment of Reinforced Concrete Structures in Eastern United States," by A.M. Reinhorn, M.J. Seidel, S.K. Kunnath and Y.J. Park, 6/15/88, (PB89-122220).

NCEER-88-0017 "Dynamic Compliance of Vertically Loaded Strip Foundations in Multilayered Viscoelastic Soils," by S. Ahmad and A.S.M. Israil, 6/17/88, (PB89-102891).

NCEER-88-0018 "An Experimental Study of Seismic Structural Response With Added Viscoelastic Dampers," by R.C. Lin, Z. Liang, T.T. Soong and R.H. Zhang, 6/30/88, (PB89-122212). This report is available only through NTIS (see address given above).

NCEER-88-0019 "Experimental Investigation of Primary - Secondary System Interaction," by G.D. Manolis, G. Juhn and A.M. Reinhorn, 5/27/88, (PB89-122204).

NCEER-88-0020 "A Response Spectrum Approach For Analysis of Nonclassically Damped Structures," by J.N. Yang, S. Sarkani and F.X. Long, 4/22/88, (PB89-102909).

NCEER-88-0021 "Seismic Interaction of Structures and Soils: Stochastic Approach," by A.S. Veletsos and A.M. Prasad, 7/21/88, (PB89-122196).

NCEER-88-0022 "Identification of the Serviceability Limit State and Detection of Seismic Structural Damage," by E. DiPasquale and A.S. Cakmak, 6/15/88, (PB89-122188). This report is available only through NTIS (see address given above).

NCEER-88-0023 "Multi-Hazard Risk Analysis: Case of a Simple Offshore Structure," by B.K. Bhartia and E.H. Vanmarcke, 7/21/88, (PB89-145213).

NCEER-88-0024 "Automated Seismic Design of Reinforced Concrete Buildings," by Y.S. Chung, C. Meyer and M. Shinozuka, 7/5/88, (PB89-122170). This report is available only through NTIS (see address given above).

NCEER-88-0025 "Experimental Study of Active Control of MDOF Structures Under Seismic Excitations," by L.L. Chung, R.C. Lin, T.T. Soong and A.M. Reinhorn, 7/10/88, (PB89-122600).

NCEER-88-0026 "Earthquake Simulation Tests of a Low-Rise Metal Structure," by J.S. Hwang, K.C. Chang, G.C. Lee and R.L. Ketter, 8/1/88, (PB89-102917).

NCEER-88-0027 "Systems Study of Urban Response and Reconstruction Due to Catastrophic Earthquakes," by F. Kozin and H.K. Zhou, 9/22/88, (PB90-162348).

NCEER-88-0028 "Seismic Fragility Analysis of Plane Frame Structures," by H.H-M. Hwang and Y.K. Low, 7/31/88, (PB89-131445).

NCEER-88-0029 "Response Analysis of Stochastic Structures," by A. Kardara, C. Bucher and M. Shinozuka, 9/22/88, (PB89-174429).

NCEER-88-0030 "Nonnormal Accelerations Due to Yielding in a Primary Structure," by D.C.K. Chen and L.D. Lutes, 9/19/88, (PB89-131437).

NCEER-88-0031 "Design Approaches for Soil-Structure Interaction," by A.S. Veletsos, A.M. Prasad and Y. Tang, 12/30/88, (PB89-174437). This report is available only through NTIS (see address given above).

NCEER-88-0032 "A Re-evaluation of Design Spectra for Seismic Damage Control," by C.J. Turkstra and A.G. Tallin, 11/7/88, (PB89-145221).

NCEER-88-0033 "The Behavior and Design of Noncontact Lap Splices Subjected to Repeated Inelastic Tensile Loading," by V.E. Sagan, P. Gergely and R.N. White, 12/8/88, (PB89-163737).

NCEER-88-0034 "Seismic Response of Pile Foundations," by S.M. Mamoon, P.K. Banerjee and S. Ahmad, 11/1/88, (PB89-145239).

NCEER-88-0035 "Modeling of R/C Building Structures With Flexible Floor Diaphragms (IDARC2)," by A.M. Reinhorn, S.K. Kunnath and N. Panahshahi, 9/7/88, (PB89-207153).

NCEER-88-0036 "Solution of the Dam-Reservoir Interaction Problem Using a Combination of FEM, BEM with Particular Integrals, Modal Analysis, and Substructuring," by C-S. Tsai, G.C. Lee and R.L. Ketter, 12/31/88, (PB89-207146).

NCEER-88-0037 "Optimal Placement of Actuators for Structural Control," by F.Y. Cheng and C.P. Pantelides, 8/15/88, (PB89-162846).

NCEER-88-0038 "Teflon Bearings in Aseismic Base Isolation: Experimental Studies and Mathematical Modeling," by A. Mokha, M.C. Constantinou and A.M. Reinhorn, 12/5/88, (PB89-218457). This report is available only through NTIS (see address given above).

NCEER-88-0039 "Seismic Behavior of Flat Slab High-Rise Buildings in the New York City Area," by P. Weidlinger and M. Ettouney, 10/15/88, (PB90-145681).

NCEER-88-0040 "Evaluation of the Earthquake Resistance of Existing Buildings in New York City," by P. Weidlinger and M. Ettouney, 10/15/88, to be published.

NCEER-88-0041 "Small-Scale Modeling Techniques for Reinforced Concrete Structures Subjected to Seismic Loads," by W. Kim, A. El-Attar and R.N. White, 11/22/88, (PB89-189625).

NCEER-88-0042 "Modeling Strong Ground Motion from Multiple Event Earthquakes," by G.W. Ellis and A.S. Cakmak, 10/15/88, (PB89-174445).

NCEER-88-0043 "Nonstationary Models of Seismic Ground Acceleration," by M. Grigoriu, S.E. Ruiz and E. Rosenblueth, 7/15/88, (PB89-189617).

NCEER-88-0044 "SARCF User's Guide: Seismic Analysis of Reinforced Concrete Frames," by Y.S. Chung, C. Meyer and M. Shinozuka, 11/9/88, (PB89-174452).

NCEER-88-0045 "First Expert Panel Meeting on Disaster Research and Planning," edited by J. Pantelic and J. Stoyle, 9/15/88, (PB89-174460).

NCEER-88-0046 "Preliminary Studies of the Effect of Degrading Infill Walls on the Nonlinear Seismic Response of Steel Frames," by C.Z. Chrysostomou, P. Gergely and J.F. Abel, 12/19/88, (PB89-208383).

NCEER-88-0047 "Reinforced Concrete Frame Component Testing Facility - Design, Construction, Instrumentation and Operation," by S.P. Pessiki, C. Conley, T. Bond, P. Gergely and R.N. White, 12/16/88, (PB89-174478).

NCEER-89-0001 "Effects of Protective Cushion and Soil Compliancy on the Response of Equipment Within a Seismically Excited Building," by J.A. HoLung, 2/16/89, (PB89-207179).

NCEER-89-0002 "Statistical Evaluation of Response Modification Factors for Reinforced Concrete Structures," by H.H-M. Hwang and J-W. Jaw, 2/17/89, (PB89-207187).

NCEER-89-0003 "Hysteretic Columns Under Random Excitation," by G-Q. Cai and Y.K. Lin, 1/9/89, (PB89-196513).

NCEER-89-0004 "Experimental Study of 'Elephant Foot Bulge' Instability of Thin-Walled Metal Tanks," by Z-H. Jia and R.L. Ketter, 2/22/89, (PB89-207195).

NCEER-89-0005 "Experiment on Performance of Buried Pipelines Across San Andreas Fault," by J. Isenberg, E. Richardson and T.D. O'Rourke, 3/10/89, (PB89-218440). This report is available only through NTIS (see address given above).

NCEER-89-0006 "A Knowledge-Based Approach to Structural Design of Earthquake-Resistant Buildings," by M. Subramani, P. Gergely, C.H. Conley, J.F. Abel and A.H. Zaghw, 1/15/89, (PB89-218465).

NCEER-89-0007 "Liquefaction Hazards and Their Effects on Buried Pipelines," by T.D. O'Rourke and P.A. Lane, 2/1/89, (PB89-218481).

NCEER-89-0008 "Fundamentals of System Identification in Structural Dynamics," by H. Imai, C-B. Yun, O. Maruyama and M. Shinozuka, 1/26/89, (PB89-207211).

NCEER-89-0009 "Effects of the 1985 Michoacan Earthquake on Water Systems and Other Buried Lifelines in Mexico," by A.G. Ayala and M.J. O'Rourke, 3/8/89, (PB89-207229).

NCEER-89-R010 "NCEER Bibliography of Earthquake Education Materials," by K.E.K. Ross, Second Revision, 9/1/89, (PB90-125352).

NCEER-89-0011 "Inelastic Three-Dimensional Response Analysis of Reinforced Concrete Building Structures (IDARC-3D), Part I - Modeling," by S.K. Kunnath and A.M. Reinhorn, 4/17/89, (PB90-114612).

NCEER-89-0012 "Recommended Modifications to ATC-14," by C.D. Poland and J.O. Malley, 4/12/89, (PB90-108648).

NCEER-89-0013 "Repair and Strengthening of Beam-to-Column Connections Subjected to Earthquake Loading," by M. Corazao and A.J. Durrani, 2/28/89, (PB90-109885).

NCEER-89-0014 "Program EXKAL2 for Identification of Structural Dynamic Systems," by O. Maruyama, C-B. Yun, M. Hoshiya and M. Shinozuka, 5/19/89, (PB90-109877).

NCEER-89-0015 "Response of Frames With Bolted Semi-Rigid Connections, Part I - Experimental Study and Analytical Predictions," by P.J. DiCorso, A.M. Reinhorn, J.R. Dickerson, J.B. Radziminski and W.L. Harper, 6/1/89, to be published.

NCEER-89-0016 "ARMA Monte Carlo Simulation in Probabilistic Structural Analysis," by P.D. Spanos and M.P. Mignolet, 7/10/89, (PB90-109893).

NCEER-89-P017 "Preliminary Proceedings from the Conference on Disaster Preparedness - The Place of Earthquake Education in Our Schools," Edited by K.E.K. Ross, 6/23/89, (PB90-108606).

NCEER-89-0017 "Proceedings from the Conference on Disaster Preparedness - The Place of Earthquake Education in Our Schools," Edited by K.E.K. Ross, 12/31/89, (PB90-207895). This report is available only through NTIS (see address given above).

NCEER-89-0018 "Multidimensional Models of Hysteretic Material Behavior for Vibration Analysis of Shape Memory Energy Absorbing Devices, by E.J. Graesser and F.A. Cozzarelli, 6/7/89, (PB90-164146).

NCEER-89-0019 "Nonlinear Dynamic Analysis of Three-Dimensional Base Isolated Structures (3D-BASIS)," by S. Nagarajaiah, A.M. Reinhorn and M.C. Constantinou, 8/3/89, (PB90-161936). This report is available only through NTIS (see address given above).

NCEER-89-0020 "Structural Control Considering Time-Rate of Control Forces and Control Rate Constraints," by F.Y. Cheng and C.P. Pantelides, 8/3/89, (PB90-120445).

NCEER-89-0021 "Subsurface Conditions of Memphis and Shelby County," by K.W. Ng, T-S. Chang and H-H.M. Hwang, 7/26/89, (PB90-120437).

NCEER-89-0022 "Seismic Wave Propagation Effects on Straight Jointed Buried Pipelines," by K. Elhmadi and M.J. O'Rourke, 8/24/89, (PB90-162322).

NCEER-89-0023 "Workshop on Serviceability Analysis of Water Delivery Systems," edited by M. Grigoriu, 3/6/89, (PB90-127424).

NCEER-89-0024 "Shaking Table Study of a 1/5 Scale Steel Frame Composed of Tapered Members," by K.C. Chang, J.S. Hwang and G.C. Lee, 9/18/89, (PB90-160169).

NCEER-89-0025 "DYNAID: A Computer Program for Nonlinear Seismic Site Response Analysis - Technical Documentation," by Jean H. Prevost, 9/14/89, (PB90-161944). This report is available only through NTIS (see address given above).

NCEER-89-0026 "1:4 Scale Model Studies of Active Tendon Systems and Active Mass Dampers for Aseismic Protection," by A.M. Reinhorn, T.T. Soong, R.C. Lin, Y.P. Yang, Y. Fukao, H. Abe and M. Nakai, 9/15/89, (PB90-173246).

NCEER-89-0027 "Scattering of Waves by Inclusions in a Nonhomogeneous Elastic Half Space Solved by Boundary Element Methods," by P.K. Hadley, A. Askar and A.S. Cakmak, 6/15/89, (PB90-145699).

NCEER-89-0028 "Statistical Evaluation of Deflection Amplification Factors for Reinforced Concrete Structures," by H.H.M. Hwang, J-W. Jaw and A.L. Ch'ng, 8/31/89, (PB90-164633).

NCEER-89-0029 "Bedrock Accelerations in Memphis Area Due to Large New Madrid Earthquakes," by H.H.M. Hwang, C.H.S. Chen and G. Yu, 11/7/89, (PB90-162330).

NCEER-89-0030 "Seismic Behavior and Response Sensitivity of Secondary Structural Systems," by Y.Q. Chen and T.T. Soong, 10/23/89, (PB90-164658).

NCEER-89-0031 "Random Vibration and Reliability Analysis of Primary-Secondary Structural Systems," by Y. Ibrahim, M. Grigoriu and T.T. Soong, 11/10/89, (PB90-161951).

NCEER-89-0032 "Proceedings from the Second U.S. - Japan Workshop on Liquefaction, Large Ground Deformation and Their Effects on Lifelines, September 26-29, 1989," Edited by T.D. O'Rourke and M. Hamada, 12/1/89, (PB90-209388).

NCEER-89-0033 "Deterministic Model for Seismic Damage Evaluation of Reinforced Concrete Structures," by J.M. Bracci, A.M. Reinhorn, J.B. Mander and S.K. Kunnath, 9/27/89.

NCEER-89-0034 "On the Relation Between Local and Global Damage Indices," by E. DiPasquale and A.S. Cakmak, 8/15/89, (PB90-173865).

NCEER-89-0035 "Cyclic Undrained Behavior of Nonplastic and Low Plasticity Silts," by A.J. Walker and H.E. Stewart, 7/26/89, (PB90-183518).

NCEER-89-0036 "Liquefaction Potential of Surficial Deposits in the City of Buffalo, New York," by M. Budhu, R. Giese and L. Baumgrass, 1/17/89, (PB90-208455).

NCEER-89-0037 "A Deterministic Assessment of Effects of Ground Motion Incoherence," by A.S. Veletsos and Y. Tang, 7/15/89, (PB90-164294).

NCEER-89-0038 "Workshop on Ground Motion Parameters for Seismic Hazard Mapping," July 17-18, 1989, edited by R.V. Whitman, 12/1/89, (PB90-173923).

NCEER-89-0039 "Seismic Effects on Elevated Transit Lines of the New York City Transit Authority," by C.J. Costantino, C.A. Miller and E. Heymsfield, 12/26/89, (PB90-207887).

NCEER-89-0040 "Centrifugal Modeling of Dynamic Soil-Structure Interaction," by K. Weissman, Supervised by J.H. Prevost, 5/10/89, (PB90-207879).

NCEER-89-0041 "Linearized Identification of Buildings With Cores for Seismic Vulnerability Assessment," by I-K. Ho and A.E. Aktan, 11/1/89, (PB90-251943).

NCEER-90-0001 "Geotechnical and Lifeline Aspects of the October 17, 1989 Loma Prieta Earthquake in San Francisco," by T.D. O'Rourke, H.E. Stewart, F.T. Blackburn and T.S. Dickerman, 1/90, (PB90-208596).

NCEER-90-0002 "Nonnormal Secondary Response Due to Yielding in a Primary Structure," by D.C.K. Chen and L.D. Lutes, 2/28/90, (PB90-251976).

NCEER-90-0003 "Earthquake Education Materials for Grades K-12," by K.E.K. Ross, 4/16/90, (PB91-251984).

NCEER-90-0004 "Catalog of Strong Motion Stations in Eastern North America," by R.W. Busby, 4/3/90, (PB90-251984).

NCEER-90-0005 "NCEER Strong-Motion Data Base: A User Manual for the GeoBase Release (Version 1.0 for the Sun3)," by P. Friberg and K. Jacob, 3/31/90 (PB90-258062).

NCEER-90-0006 "Seismic Hazard Along a Crude Oil Pipeline in the Event of an 1811-1812 Type New Madrid Earthquake," by H.H.M. Hwang and C-H.S. Chen, 4/16/90(PB90-258054).

NCEER-90-0007 "Site-Specific Response Spectra for Memphis Sheahan Pumping Station," by H.H.M. Hwang and C.S. Lee, 5/15/90, (PB91-108811).

NCEER-90-0008 "Pilot Study on Seismic Vulnerability of Crude Oil Transmission Systems," by T. Ariman, R. Dobry, M. Grigoriu, F. Kozin, M. O'Rourke, T. O'Rourke and M. Shinozuka, 5/25/90, (PB91-108837).

NCEER-90-0009 "A Program to Generate Site Dependent Time Histories: EQGEN," by G.W. Ellis, M. Srinivasan and A.S. Cakmak, 1/30/90, (PB91-108829).

NCEER-90-0010 "Active Isolation for Seismic Protection of Operating Rooms," by M.E. Talbott, Supervised by M. Shinozuka, 6/8/9, (PB91-110205).

NCEER-90-0011 "Program LINEARID for Identification of Linear Structural Dynamic Systems," by C-B. Yun and M. Shinozuka, 6/25/90, (PB91-110312).

NCEER-90-0012 "Two-Dimensional Two-Phase Elasto-Plastic Seismic Response of Earth Dams," by A.N. Yiagos, Supervised by J.H. Prevost, 6/20/90, (PB91-110197).

NCEER-90-0013 "Secondary Systems in Base-Isolated Structures: Experimental Investigation, Stochastic Response and Stochastic Sensitivity," by G.D. Manolis, G. Juhn, M.C. Constantinou and A.M. Reinhorn, 7/1/90, (PB91-110320).

NCEER-90-0014 "Seismic Behavior of Lightly-Reinforced Concrete Column and Beam-Column Joint Details," by S.P. Pessiki, C.H. Conley, P. Gergely and R.N. White, 8/22/90, (PB91-108795).

NCEER-90-0015 "Two Hybrid Control Systems for Building Structures Under Strong Earthquakes," by J.N. Yang and A. Danielians, 6/29/90, (PB91-125393).

NCEER-90-0016 "Instantaneous Optimal Control with Acceleration and Velocity Feedback," by J.N. Yang and Z. Li, 6/29/90, (PB91-125401).

NCEER-90-0017 "Reconnaissance Report on the Northern Iran Earthquake of June 21, 1990," by M. Mehrain, 10/4/90, (PB91-125377).

NCEER-90-0018 "Evaluation of Liquefaction Potential in Memphis and Shelby County," by T.S. Chang, P.S. Tang, C.S. Lee and H. Hwang, 8/10/90, (PB91-125427).

NCEER-90-0019 "Experimental and Analytical Study of a Combined Sliding Disc Bearing and Helical Steel Spring Isolation System," by M.C. Constantinou, A.S. Mokha and A.M. Reinhorn, 10/4/90, (PB91-125385).

NCEER-90-0020 "Experimental Study and Analytical Prediction of Earthquake Response of a Sliding Isolation System with a Spherical Surface," by A.S. Mokha, M.C. Constantinou and A.M. Reinhorn, 10/11/90, (PB91-125419).

NCEER-90-0021 "Dynamic Interaction Factors for Floating Pile Groups," by G. Gazetas, K. Fan, A. Kaynia and E. Kausel, 9/10/90, (PB91-170381).

NCEER-90-0022 "Evaluation of Seismic Damage Indices for Reinforced Concrete Structures," by S. Rodriguez-Gomez and A.S. Cakmak, 9/30/90, PB91-171322).

NCEER-90-0023 "Study of Site Response at a Selected Memphis Site," by H. Desai, S. Ahmad, E.S. Gazetas and M.R. Oh, 10/11/90, (PB91-196857).

NCEER-90-0024 "A User's Guide to Strongmo: Version 1.0 of NCEER's Strong-Motion Data Access Tool for PCs and Terminals," by P.A. Friberg and C.A.T. Susch, 11/15/90, (PB91-171272).

NCEER-90-0025 "A Three-Dimensional Analytical Study of Spatial Variability of Seismic Ground Motions," by L-L. Hong and A.H.-S. Ang, 10/30/90, (PB91-170399).

NCEER-90-0026 "MUMOID User's Guide - A Program for the Identification of Modal Parameters," by S. Rodri guez-Go mez and E. DiPasquale, 9/30/90, (PB91-171298).

NCEER-90-0027 "SARCF-II User's Guide - Seismic Analysis of Reinforced Concrete Frames," by S. Rodri guez-Go mez, Y.S. Chung and C. Meyer, 9/30/90, (PB91-171280).

NCEER-90-0028 "Viscous Dampers: Testing, Modeling and Application in Vibration and Seismic Isolation," by N. Makris and M.C. Constantinou, 12/20/90 (PB91-190561).

NCEER-90-0029 "Soil Effects on Earthquake Ground Motions in the Memphis Area," by H. Hwang, C.S. Lee, K.W. Ng and T.S. Chang, 8/2/90, (PB91-190751).

NCEER-91-0001 "Proceedings from the Third Japan-U.S. Workshop on Earthquake Resistant Design of Lifeline Facilities and Countermeasures for Soil Liquefaction, December 17-19, 1990," edited by T.D. O'Rourke and M. Hamada, 2/1/91, (PB91-179259).

NCEER-91-0002 "Physical Space Solutions of Non-Proportionally Damped Systems," by M. Tong, Z. Liang and G.C. Lee, 1/15/91, (PB91-179242).

NCEER-91-0003 "Seismic Response of Single Piles and Pile Groups," by K. Fan and G. Gazetas, 1/10/91, (PB92-174994).

NCEER-91-0004 "Damping of Structures: Part 1 - Theory of Complex Damping," by Z. Liang and G. Lee, 10/10/91, (PB92-197235).

NCEER-91-0005 "3D-BASIS - Nonlinear Dynamic Analysis of Three Dimensional Base Isolated Structures: Part II," by S. Nagarajaiah, A.M. Reinhorn and M.C. Constantinou, 2/28/91, (PB91-190553).

NCEER-91-0006 "A Multidimensional Hysteretic Model for Plasticity Deforming Metals in Energy Absorbing Devices," by E.J. Graesser and F.A. Cozzarelli, 4/9/91, (PB92-108364).

NCEER-91-0007 "A Framework for Customizable Knowledge-Based Expert Systems with an Application to a KBES for Evaluating the Seismic Resistance of Existing Buildings," by E.G. Ibarra-Anaya and S.J. Fenves, 4/9/91, (PB91-210930).

NCEER-91-0008 "Nonlinear Analysis of Steel Frames with Semi-Rigid Connections Using the Capacity Spectrum Method," by G.G. Deierlein, S-H. Hsieh, Y-J. Shen and J.F. Abel, 7/2/91, (PB92-113828).

NCEER-91-0009 "Earthquake Education Materials for Grades K-12," by K.E.K. Ross, 4/30/91, (PB91-212142).

NCEER-91-0010 "Phase Wave Velocities and Displacement Phase Differences in a Harmonically Oscillating Pile," by N. Makris and G. Gazetas, 7/8/91, (PB92-108356).

NCEER-91-0011 "Dynamic Characteristics of a Full-Size Five-Story Steel Structure and a 2/5 Scale Model," by K.C. Chang, G.C. Yao, G.C. Lee, D.S. Hao and Y.C. Yeh," 7/2/91, (PB93-116648).

NCEER-91-0012 "Seismic Response of a 2/5 Scale Steel Structure with Added Viscoelastic Dampers," by K.C. Chang, T.T. Soong, S-T. Oh and M.L. Lai, 5/17/91, (PB92-110816).

NCEER-91-0013 "Earthquake Response of Retaining Walls; Full-Scale Testing and Computational Modeling," by S. Alampalli and A-W.M. Elgamal, 6/20/91, to be published.

NCEER-91-0014 "3D-BASIS-M: Nonlinear Dynamic Analysis of Multiple Building Base Isolated Structures," by P.C. Tsopelas, S. Nagarajaiah, M.C. Constantinou and A.M. Reinhorn, 5/28/91, (PB92-113885).

NCEER-91-0015 "Evaluation of SEAOC Design Requirements for Sliding Isolated Structures," by D. Theodossiou and M.C. Constantinou, 6/10/91, (PB92-114602).

NCEER-91-0016 "Closed-Loop Modal Testing of a 27-Story Reinforced Concrete Flat Plate-Core Building," by H.R. Somaprasad, T. Toksoy, H. Yoshiyuki and A.E. Aktan, 7/15/91, (PB92-129980).

NCEER-91-0017 "Shake Table Test of a 1/6 Scale Two-Story Lightly Reinforced Concrete Building," by A.G. El-Attar, R.N. White and P. Gergely, 2/28/91, (PB92-222447).

NCEER-91-0018 "Shake Table Test of a 1/8 Scale Three-Story Lightly Reinforced Concrete Building," by A.G. El-Attar, R.N. White and P. Gergely, 2/28/91, (PB93-116630).

NCEER-91-0019 "Transfer Functions for Rigid Rectangular Foundations," by A.S. Veletsos, A.M. Prasad and W.H. Wu, 7/31/91.

NCEER-91-0020 "Hybrid Control of Seismic-Excited Nonlinear and Inelastic Structural Systems," by J.N. Yang, Z. Li and A. Danielians, 8/1/91, (PB92-143171).

NCEER-91-0021 "The NCEER-91 Earthquake Catalog: Improved Intensity-Based Magnitudes and Recurrence Relations for U.S. Earthquakes East of New Madrid," by L. Seeber and J.G. Armbruster, 8/28/91, (PB92-176742).

NCEER-91-0022 "Proceedings from the Implementation of Earthquake Planning and Education in Schools: The Need for Change - The Roles of the Changemakers," by K.E.K. Ross and F. Winslow, 7/23/91, (PB92-129998).

NCEER-91-0023 "A Study of Reliability-Based Criteria for Seismic Design of Reinforced Concrete Frame Buildings," by H.H.M. Hwang and H-M. Hsu, 8/10/91, (PB92-140235).

NCEER-91-0024 "Experimental Verification of a Number of Structural System Identification Algorithms," by R.G. Ghanem, H. Gavin and M. Shinozuka, 9/18/91, (PB92-176577).

NCEER-91-0025 "Probabilistic Evaluation of Liquefaction Potential," by H.H.M. Hwang and C.S. Lee," 11/25/91, (PB92-143429).

NCEER-91-0026 "Instantaneous Optimal Control for Linear, Nonlinear and Hysteretic Structures - Stable Controllers," by J.N. Yang and Z. Li, 11/15/91, (PB92-163807).

NCEER-91-0027 "Experimental and Theoretical Study of a Sliding Isolation System for Bridges," by M.C. Constantinou, A. Kartoum, A.M. Reinhorn and P. Bradford, 11/15/91, (PB92-176973).

NCEER-92-0001 "Case Studies of Liquefaction and Lifeline Performance During Past Earthquakes, Volume 1: Japanese Case Studies," Edited by M. Hamada and T. O'Rourke, 2/17/92, (PB92-197243).

NCEER-92-0002 "Case Studies of Liquefaction and Lifeline Performance During Past Earthquakes, Volume 2: United States Case Studies," Edited by T. O'Rourke and M. Hamada, 2/17/92, (PB92-197250).

NCEER-92-0003 "Issues in Earthquake Education," Edited by K. Ross, 2/3/92, (PB92-222389).

NCEER-92-0004 "Proceedings from the First U.S. - Japan Workshop on Earthquake Protective Systems for Bridges," Edited by I.G. Buckle, 2/4/92, (PB94-142239, A99, MF-A06).

NCEER-92-0005 "Seismic Ground Motion from a Haskell-Type Source in a Multiple-Layered Half-Space," A.P. Theoharis, G. Deodatis and M. Shinozuka, 1/2/92, to be published.

NCEER-92-0006 "Proceedings from the Site Effects Workshop," Edited by R. Whitman, 2/29/92, (PB92-197201).

NCEER-92-0007 "Engineering Evaluation of Permanent Ground Deformations Due to Seismically-Induced Liquefaction," by M.H. Baziar, R. Dobry and A-W.M. Elgamal, 3/24/92, (PB92-222421).

NCEER-92-0008 "A Procedure for the Seismic Evaluation of Buildings in the Central and Eastern United States," by C.D. Poland and J.O. Malley, 4/2/92, (PB92-222439).

NCEER-92-0009 "Experimental and Analytical Study of a Hybrid Isolation System Using Friction Controllable Sliding Bearings," by M.Q. Feng, S. Fujii and M. Shinozuka, 5/15/92, (PB93-150282).

NCEER-92-0010 "Seismic Resistance of Slab-Column Connections in Existing Non-Ductile Flat-Plate Buildings," by A.J. Durrani and Y. Du, 5/18/92.

NCEER-92-0011 "The Hysteretic and Dynamic Behavior of Brick Masonry Walls Upgraded by Ferrocement Coatings Under Cyclic Loading and Strong Simulated Ground Motion," by H. Lee and S.P. Prawel, 5/11/92, to be published.

NCEER-92-0012 "Study of Wire Rope Systems for Seismic Protection of Equipment in Buildings," by G.F. Demetriades, M.C. Constantinou and A.M. Reinhorn, 5/20/92.

NCEER-92-0013 "Shape Memory Structural Dampers: Material Properties, Design and Seismic Testing," by P.R. Witting and F.A. Cozzarelli, 5/26/92.

NCEER-92-0014 "Longitudinal Permanent Ground Deformation Effects on Buried Continuous Pipelines," by M.J. O'Rourke, and C. Nordberg, 6/15/92.

NCEER-92-0015 "A Simulation Method for Stationary Gaussian Random Functions Based on the Sampling Theorem," by M. Grigoriu and S. Balopoulou, 6/11/92, (PB93-127496).

NCEER-92-0016 "Gravity-Load-Designed Reinforced Concrete Buildings: Seismic Evaluation of Existing Construction and Detailing Strategies for Improved Seismic Resistance," by G.W. Hoffmann, S.K. Kunnath, A.M. Reinhorn and J.B. Mander, 7/15/92, (PB94-142007, A08, MF-A02).

NCEER-92-0017 "Observations on Water System and Pipeline Performance in the Limón Area of Costa Rica Due to the April 22, 1991 Earthquake," by M. O'Rourke and D. Ballantyne, 6/30/92, (PB93-126811).

NCEER-92-0018 "Fourth Edition of Earthquake Education Materials for Grades K-12," Edited by K.E.K. Ross, 8/10/92.

NCEER-92-0019 "Proceedings from the Fourth Japan-U.S. Workshop on Earthquake Resistant Design of Lifeline Facilities and Countermeasures for Soil Liquefaction," Edited by M. Hamada and T.D. O'Rourke, 8/12/92, (PB93-163939).

NCEER-92-0020 "Active Bracing System: A Full Scale Implementation of Active Control," by A.M. Reinhorn, T.T. Soong, R.C. Lin, M.A. Riley, Y.P. Wang, S. Aizawa and M. Higashino, 8/14/92, (PB93-127512).

NCEER-92-0021 "Empirical Analysis of Horizontal Ground Displacement Generated by Liquefaction-Induced Lateral Spreads," by S.F. Bartlett and T.L. Youd, 8/17/92, (PB93-188241).

NCEER-92-0022 "IDARC Version 3.0: Inelastic Damage Analysis of Reinforced Concrete Structures," by S.K. Kunnath, A.M. Reinhorn and R.F. Lobo, 8/31/92, (PB93-227502, A07, MF-A02).

NCEER-92-0023 "A Semi-Empirical Analysis of Strong-Motion Peaks in Terms of Seismic Source, Propagation Path and Local Site Conditions, by M. Kamiyama, M.J. O'Rourke and R. Flores-Berrones, 9/9/92, (PB93-150266).

NCEER-92-0024 "Seismic Behavior of Reinforced Concrete Frame Structures with Nonductile Details, Part I: Summary of Experimental Findings of Full Scale Beam-Column Joint Tests," by A. Beres, R.N. White and P. Gergely, 9/30/92, (PB93-227783, A05, MF-A01).

NCEER-92-0025 "Experimental Results of Repaired and Retrofitted Beam-Column Joint Tests in Lightly Reinforced Concrete Frame Buildings," by A. Beres, S. El-Borgi, R.N. White and P. Gergely, 10/29/92, (PB93-227791, A05, MF-A01).

NCEER-92-0026 "A Generalization of Optimal Control Theory: Linear and Nonlinear Structures," by J.N. Yang, Z. Li and S. Vongchavalitkul, 11/2/92, (PB93-188621).

NCEER-92-0027 "Seismic Resistance of Reinforced Concrete Frame Structures Designed Only for Gravity Loads: Part I - Design and Properties of a One-Third Scale Model Structure," by J.M. Bracci, A.M. Reinhorn and J.B. Mander, 12/1/92, (PB94-104502, A08, MF-A02).

NCEER-92-0028 "Seismic Resistance of Reinforced Concrete Frame Structures Designed Only for Gravity Loads: Part II - Experimental Performance of Subassemblages," by L.E. Aycardi, J.B. Mander and A.M. Reinhorn, 12/1/92, (PB94-104510, A08, MF-A02).

NCEER-92-0029 "Seismic Resistance of Reinforced Concrete Frame Structures Designed Only for Gravity Loads: Part III - Experimental Performance and Analytical Study of a Structural Model," by J.M. Bracci, A.M. Reinhorn and J.B. Mander, 12/1/92, (PB93-227528, A09, MF-A01).

NCEER-92-0030 "Evaluation of Seismic Retrofit of Reinforced Concrete Frame Structures: Part I - Experimental Performance of Retrofitted Subassemblages," by D. Choudhuri, J.B. Mander and A.M. Reinhorn, 12/8/92, (PB93-198307, A07, MF-A02).

NCEER-92-0031 "Evaluation of Seismic Retrofit of Reinforced Concrete Frame Structures: Part II - Experimental Performance and Analytical Study of a Retrofitted Structural Model," by J.M. Bracci, A.M. Reinhorn and J.B. Mander, 12/8/92, (PB93-198315, A09, MF-A03).

NCEER-92-0032 "Experimental and Analytical Investigation of Seismic Response of Structures with Supplemental Fluid Viscous Dampers," by M.C. Constantinou and M.D. Symans, 12/21/92, (PB93-191435).

NCEER-92-0033 "Reconnaissance Report on the Cairo, Egypt Earthquake of October 12, 1992," by M. Khater, 12/23/92, (PB93-188621).

NCEER-92-0034 "Low-Level Dynamic Characteristics of Four Tall Flat-Plate Buildings in New York City," by H. Gavin, S. Yuan, J. Grossman, E. Pekelis and K. Jacob, 12/28/92, (PB93-188217).

NCEER-93-0001 "An Experimental Study on the Seismic Performance of Brick-Infilled Steel Frames With and Without Retrofit," by J.B. Mander, B. Nair, K. Wojtkowski and J. Ma, 1/29/93, (PB93-227510, A07, MF-A02).

NCEER-93-0002 "Social Accounting for Disaster Preparedness and Recovery Planning," by S. Cole, E. Pantoja and V. Razak, 2/22/93, to be published.

NCEER-93-0003 "Assessment of 1991 NEHRP Provisions for Nonstructural Components and Recommended Revisions," by T.T. Soong, G. Chen, Z. Wu, R-H. Zhang and M. Grigoriu, 3/1/93, (PB93-188639).

NCEER-93-0004 "Evaluation of Static and Response Spectrum Analysis Procedures of SEAOC/UBC for Seismic Isolated Structures," by C.W. Winters and M.C. Constantinou, 3/23/93, (PB93-198299).

NCEER-93-0005 "Earthquakes in the Northeast - Are We Ignoring the Hazard? A Workshop on Earthquake Science and Safety for Educators," edited by K.E.K. Ross, 4/2/93, (PB94-103066, A09, MF-A02).

NCEER-93-0006 "Inelastic Response of Reinforced Concrete Structures with Viscoelastic Braces," by R.F. Lobo, J.M. Bracci, K.L. Shen, A.M. Reinhorn and T.T. Soong, 4/5/93, (PB93-227486, A05, MF-A02).

NCEER-93-0007 "Seismic Testing of Installation Methods for Computers and Data Processing Equipment," by K. Kosar, T.T. Soong, K.L. Shen, J.A. HoLung and Y.K. Lin, 4/12/93, (PB93-198299).

NCEER-93-0008 "Retrofit of Reinforced Concrete Frames Using Added Dampers," by A. Reinhorn, M. Constantinou and C. Li, to be published.

NCEER-93-0009 "Seismic Behavior and Design Guidelines for Steel Frame Structures with Added Viscoelastic Dampers," by K.C. Chang, M.L. Lai, T.T. Soong, D.S. Hao and Y.C. Yeh, 5/1/93, (PB94-141959, A07, MF-A02).

NCEER-93-0010 "Seismic Performance of Shear-Critical Reinforced Concrete Bridge Piers," by J.B. Mander, S.M. Waheed, M.T.A. Chaudhary and S.S. Chen, 5/12/93, (PB93-227494, A08, MF-A02).

NCEER-93-0011 "3D-BASIS-TABS: Computer Program for Nonlinear Dynamic Analysis of Three Dimensional Base Isolated Structures," by S. Nagarajaiah, C. Li, A.M. Reinhorn and M.C. Constantinou, 8/2/93, (PB94-141819, A09, MF-A02).

NCEER-93-0012 "Effects of Hydrocarbon Spills from an Oil Pipeline Break on Ground Water," by O.J. Helweg and H.H.M. Hwang, 8/3/93, (PB94-141942, A06, MF-A02).

NCEER-93-0013 "Simplified Procedures for Seismic Design of Nonstructural Components and Assessment of Current Code Provisions," by M.P. Singh, L.E. Suarez, E.E. Matheu and G.O. Maldonado, 8/4/93, (PB94-141827, A09, MF-A02).

NCEER-93-0014 "An Energy Approach to Seismic Analysis and Design of Secondary Systems," by G. Chen and T.T. Soong, 8/6/93, (PB94-142767, A11, MF-A03).

NCEER-93-0015 "Proceedings from School Sites: Becoming Prepared for Earthquakes - Commemorating the Third Anniversary of the Loma Prieta Earthquake," Edited by F.E. Winslow and K.E.K. Ross, 8/16/93.

NCEER-93-0016 "Reconnaissance Report of Damage to Historic Monuments in Cairo, Egypt Following the October 12, 1992 Dahshur Earthquake," by D. Sykora, D. Look, G. Croci, E. Karaesmen and E. Karaesmen, 8/19/93, (PB94-142221, A08, MF-A02).

NCEER-93-0017 "The Island of Guam Earthquake of August 8, 1993," by S.W. Swan and S.K. Harris, 9/30/93, (PB94-141843, A04, MF-A01).

NCEER-93-0018 "Engineering Aspects of the October 12, 1992 Egyptian Earthquake," by A.W. Elgamal, M. Amer, K. Adalier and A. Abul-Fadl, 10/7/93, (PB94-141983, A05, MF-A01).

NCEER-93-0019 "Development of an Earthquake Motion Simulator and its Application in Dynamic Centrifuge Testing," by I. Krstelj, Supervised by J.H. Prevost, 10/23/93.

NCEER-93-0020 "NCEER-Taisei Corporation Research Program on Sliding Seismic Isolation Systems for Bridges: Experimental and Analytical Study of a Friction Pendulum System (FPS)," by M.C. Constantinou, P. Tsopelas, Y-S. Kim and S. Okamoto, 11/1/93, (PB94-142775, A08, MF-A02).

NCEER-93-0021 "Finite Element Modeling of Elastomeric Seismic Isolation Bearings," by L.I. Billings, Supervised by R. Shepherd, 11/8/93, to be published.

NCEER-93-0022 "Seismic Vulnerability of Equipment in Critical Facilities: Life-Safety and Operational Consequences," by K. Porter, G.S. Johnson, M.M. Zadeh, C. Scawthorn and S. Eder, 11/24/93.

NCEER-93-0023 "Hokkaido Nansei-oki, Japan Earthquake of July 12, 1993, by P.I. Yanev and C.R. Scawthorn, 12/23/93.

NCEER-94-0001 "Seismic Serviceability of Water Supply Networks with Application to San Francisco Auxiliary Water Supply System," by I. Markov, Supervised by M. Grigoriu and T. O'Rourke, 1/21/94, to be published.

NCEER-94-0002 "NCEER-Taisei Corporation Research Program on Sliding Seismic Isolation Systems for Bridges: Experimental and Analytical Study of Systems Consisting of Sliding Bearings, Rubber Restoring Force Devices and Fluid Dampers," Volumes I and II, by P. Tsopelas, S. Okamoto, M.C. Constantinou, D. Ozaki and S. Fujii, 2/4/94.

NCEER-94-0003 "A Markov Model for Local and Global Damage Indices in Seismic Analysis," by S. Rahman and M. Grigoriu, 2/18/94, to be published.

NCEER-94-0004 "Proceedings from the NCEER Workshop on Seismic Response of Masonry Infills," edited by D.P. Abrams, 3/1/94.

NCEER-94-0005 "The Northridge, California Earthquake of January 17, 1994: General Overview," edited by J.D. Goltz, 3/11/94.

NCEER-94-0006 "Seismic Energy Based Fatigue Damage Analysis of Bridge Columns: Part I - Evaluation of Seismic Capacity," by G.A. Chang and J.B. Mander, 3/14/94, to be published.

NCEER-94-0007 "Seismic Isolation of Multi-Story Frame Structures Using Spherical Sliding Isolation Systems," by T.M. Al-Hussaini, V.A. Zayas and M.C. Constantinou, 3/17/94.

NCEER-94-0008 "The Northridge, California Earthquake of January 17, 1994: Bridge Reconnaissance Report," by I.G. Buckle, B. Douglas, R. Mayes, R. Nutt and S. Thoman, 3/24/94.

NCEER-94-0009 "Proceedings of the Third U.S.-Japan Workshop on Earthquake Protective Systems for Bridges," edited by I. Buckle and I. Friedland, 3/31/94.